Steady State Response of Thin-walled Members under Harmonic Forces

By

Mohammed Ali Hjaji

A Thesis submitted to the
Faculty of Graduate and Postdoctoral Studies
in partial fulfillment of the requirements for the degree of

DOCTOR OF PHILOSOPHY

in Civil Engineering

Department of Civil Engineering
Faculty of Engineering
University of Ottawa
Ottawa, Ontario, Canada
March 2013

The Ph.D in Civil Engineering is a joint program with the
Carleton University, administrated by the Ottawa-Carleton Institute for Civil Engineering

Acknowledgement

The author would like to express his deepest gratitude and appreciation to his supervisor, Dr. Magdi Mohareb, for his guidance, assistance, advice, support and continued encouragement throughout the course of this work.

The author also would like to thank the members of his thesis proposal committee Dr. Khoo, Dr. Martin-Perez and Dr. Palermo for their valuable comments, suggestions and encouragement.

Finally, the author would like to dedicate his dissertation to his beloved wife, Sohir Ghaffar, his lovely children, Ali, Raghad, Owais and Abdulrahman, and his brothers and sisters and all his friends for their invaluable support during his study. Without their love, support and understanding, the author could not complete his work and achieve his goals.

Mohammed Ali Hjaji

March 2013

Abstract

The steady state response of thin-walled members subjected to harmonic forces is investigated in the present study. The governing differential equations of motion and associated boundary conditions are derived from the Hamilton variational principle. The harmonic form of the applied forces is exploited to eliminate the need to discretize the problem in the time domain, resulting in computational efficiency.

The formulation is based on a generalization of the Timoshenko-Vlasov beam theory and accounts for warping effects, shear deformation effects due to bending and non-uniform warping, translational and rotary inertial effects and captures flexural-torsional coupling arising in asymmetric cross-sections.

Six of the resulting seven field equations are observed to be fully coupled for asymmetric cross-sections while the equation of longitudinal motion is observed to be uncoupled. Separate closed form solutions are provided for the cases of (i) doubly symmetric cross sections, (ii) monosymmetric cross-sections, and (iii) asymmetric cross-sections. The closed-form solutions are provided for cantilever and simply-supported boundary conditions.

A family of shape functions is then developed based on the exact solution of the homogeneous field equations and then used to formulate a series of super-convergent finite beam elements. The resulting two-noded beam elements are shown to successfully capture the static and dynamic responses of thin-walled members. The finite elements developed involve no special discretization errors normally encountered in other finite element formulations and provide results in excellent agreement with those based on other established finite elements with a minimal number of degrees of freedom. The formulation is also capable to predict the natural frequencies and mode-shapes of the structural members.

Comparisons with non-shear deformable beam solutions demonstrate the importance of shear deformation effects within short-span members subjected to harmonic loads with higher

exciting frequencies. Comparisons with shell element solution results demonstrate that distortional effects are more pronounced in cantilevers with short spans.

A generalized stress extraction scheme from the finite element formulation is then developed. Also, a generalization of the analysis procedure to accommodate multiple loads with distinct exciting frequencies is established. The study is concluded with design examples which illustrate the applicability of the formulation, in conjunction with established principles of fatigue design, in determining the fatigue life of steel members subjected to multiple harmonic forces.

Table of Contents

List of Figures

List of Tables

CHAPTER (1)

INTRODUCTION AND SCOPE

Chapter 1 - Introduction and Scope

1.1 Introduction and Motivation

Thin-walled members are structural components widely used in various engineering fields, e.g., as stiffeners in aircraft structures, vehicles axles, compressor and turbine blades, ship and marine structures, steel building structures, bridge decks, etc. In these applications, thin-walled members are frequently subjected to cyclic loading (e.g. harmonic excitation) caused by machinery, aerodynamics forces, wind loading, fluid flows, waves motion, etc. For example, harmonic forces can arise from unbalance in rotating machinery and propellants, and forces produced by reciprocating machines, traffic motion and hydrodynamic loads. In such applications, members under harmonic loads are prone to fatigue failures. Therefore, the steady state dynamic response of thin-walled members due to effect of repetitive harmonic forces is of particular importance to fatigue design. In contrast, the transient component of the response occurs initially and quickly dampens out and thus is of no importance in fatigue design.

Under harmonic excitations, open thin-walled members can experience complex coupled deformations, i.e. flexural deformation modes can be coupled with torsional modes. In order to reliably predict the response of such members, the model needs to account for shear deformation, warping and translational and rotary inertia effects. The neglect of any of these aspects can lead to inaccurate results particularly when the structure is subjected to exciting forces with high frequencies.

1.2 Objectives of the Research

In the above context, the present study aims at developing a theory capable of capturing shear deformation and warping effects as well as in translational and rotational inertia effects and at providing two types of solutions for the steady state response of thin-walled members subject to harmonic forces:

(1) Determining analytical closed-form solutions for the problem to provide closed form solutions for simple problems.

(2) Developing a family of accurate and efficient finite elements to expand the solution for more complex problems.

1.3 Outline of the Thesis

Chapter 2 provides a comprehensive review of common energy and variational principles in elastodynamics analysis and dynamic analysis methods. A survey of the studies for free and forced vibrations for thin-walled open members under general harmonic forces is also provided.

In Chapter 3, the formulation of the governing field equations and possibly boundary conditions derived based on the Hamiltonian variational principle is developed.

The first part of Chapter 4 starts with the governing differential equations and boundary conditions derived in Chapter 3 and provides closed form solutions for the special case of doubly symmetric sections. The complete steady state responses, homogeneous and particular solutions, for longitudinal, transverse, lateral and torsional vibrations of the system are obtained by exactly solving the coupled differential equations obtained. The second part of Chapter 4 develops a finite element formulation for doubly symmetric sections under general harmonic loads. The numerical solutions are presented and compared with closed-form solutions and ABAQUS's shell element in order to assess and demonstrate the validity and accuracy of the present closed-form and finite element solutions.

In Chapter 5, closed form solutions of the governing coupled field equations are developed for monosymmetric cross-sections. The solution successfully captures bending-torsional coupling effects due to the cross-sectional monosymmetry. A finite element formulation is then developed by adopting the shape functions which satisfy the homogeneous form of the coupled field equations for monosymmetric sections.

In Chapter 6, the governing coupled field equations derived in Chapter 3 are exactly solved for the cased of asymmetric cross-sections. A general closed-form solution was developed for the triply coupled lateral-transverse-torsional-warping response of thin-walled members. Closed-form solutions were obtained for cantilever and simply-supported boundary

conditions. A family of shape functions was then developed based on the exact solution of the coupled field equations and then used to formulate a super-convergent finite element.

Chapter 7 derives generalized normal and shearing stress expressions based on the theory and finite element developed in Chapters (3-6). A procedure for generalizing the solutions developed for the case of multiple applied harmonic forces with distinct exciting frequency is also presented and compared to results of conventional transient analysis solutions. Design techniques for fatigue design of steel structures are briefly reviewed and design examples are then provided to illustrate the suitability of the finite element formulation in efficiently predicting the fatigue life of steel structures under harmonic loads.

CHAPTER (2)

BACKGROUND AND LITERATURE REVIEW

Chapter 2 - Background and Literature Review

2.1 Introduction and Background

Dynamic response analysis of thin-walled open members has been extensively studied. Most of studies are based on classical Bernoulli-Euler beam or the Timoshenko beam. A few studies have taken into account rotary inertia. However, most of these studies deal with free vibrations, and were aimed at determining the natural frequencies and mode shapes, while only a few focused on forced vibration analysis under harmonic excitations.

Coupled bending-torsional free and forced vibrations of open cross-sections thin-walled beams with various (doubly symmetric, monosymmetric and asymmetric) cross-sections have been studied using a variety of approaches:

- The exact dynamic stiffness matrix method,
- The Rayleigh-Ritz method,
- The dynamic transfer matrix method, and
- Finite element method

Studies dealing with the dynamic behaviour of thin-walled beams with open cross-sections were carried out in the early works of Vlasov (1961) and Timoshenko and Gere (1961). The present review focuses on three aspects related to dynamic analysis of beams. These are (1) Variational principles related to displacement formulations in dynamic analyses, (2) Kinematic assumptions in thin-walled beam theories, and (3) Studies related to free and forced vibrations of thin-walled beams.

2.2 Variational Principles in Elasto-dynamics

Variational principles are powerful tools for the analysis of elastic structures. The variational principles are concerned with the stationary value of the integral function for the description of the behaviour of dynamical systems. There are several variational principles in elasto-dynamics that can be classified into two types, differential and integral variational principles. The differential principles such as d'Alembert principle and Lagrange's equations describe

the motion at every time instant, while the integral principles such as Hamilton's principle describe the motion in a finite time interval [Tabarrok and Rimrott 1994].

Among various energy principles, two types of principles form the basis of variational formulations. These principles are based on the variation of displacements which can lead to theorem of stationary potential energy and the variation of stresses which can lead to theorem of stationary complementary energy. The first type of principles deals with stresses or forces undergoing virtual displacements. In the second set of principles, a system of virtual stresses or forces undergoes displacements [Wallerstein 2002].

2.2.1 Hamilton's Variational Principle

Hamilton's principle is one of the most powerful variational principle techniques for deriving the dynamic equations of motion and the associated boundary conditions for continuous systems. Hamilton's principle states that the sum of variations of the difference in kinetic and potential energies over any time interval t_1 to t_2 is zero. Thus, the variational form of Hamilton principle is given as [Humar 2002]:

$$\int_{t_1}^{t_2} \delta\left(T - \Pi\right)dt = \int_{t_1}^{t_2} \delta\left(T - U\right)dt + \int_{t_1}^{t_2} \delta W \; dt = 0 \tag{2.1}$$

where T is the total kinetic energy of the system, $\Pi = U - W$ is the total potential energy of the system including the internal strain energy U and the work done W by external forces. The difference between the kinetic and total potential energies is often called the Lagrangian function and is denoted by $L = T - \Pi$.

2.2.2 Lagrange Equations

The equations of motion of a structural or mechanical system also called Lagrange's equations are expressed in terms of generalized coordinates $\bar{q}_1, \bar{q}_2, ..., \bar{q}_n$. For a dynamic system, the equations of motion are given as [e.g. Virgin 2007]:

$$\frac{d}{dt}\left(\frac{\partial L}{\partial \dot{\bar{q}}_i}\right) - \frac{\partial L}{\partial \bar{q}_i} = \bar{Q}_i \quad , \quad \text{for } i = 1, 2, 3, ..., \text{n} \tag{2.2}$$

in which the Lagrange equations of motion are expressed in terms of the generalized coordinates and their time derivatives. In Equation (2.2), $\dot{\bar{q}}_1$ are the generalized velocities and $\bar{Q}_i$ are the generalized forces. From a variational principle view point, the Lagrange equations of motion arise as conditions of extremum from Hamilton's principle.

2.3 Potential and Kinetic Energy Expressions

The total potential energy, i.e. internal strain energy and potential energy by external forces, and kinetic energy expressions are used to derive the governing equations of motion and the associated boundary conditions for conservative and nonconservative systems. These expressions are:

2.3.1 Total Potential Energy

The total potential energy of the structural member Π comprises of the internal strain energy U and the potential energy gained by the external loads V and is given by:

$$\Pi = U + V \tag{2.3}$$

In its most general form, the internal strain energy of a linear elastic system is expressed as [Timoshenko and Goodier 1970];

$$U = \frac{1}{2}\int_0^{\ell}\int_A \left[\sigma_{xx}\,\varepsilon_{xx} + \sigma_{yy}\,\varepsilon_{yy} + \sigma_{zz}\,\varepsilon_{zz} + \tau_{xy}\,\gamma_{xy} + \tau_{xz}\,\gamma_{xz} + \tau_{yz}\,\gamma_{yz}\right] dA\,dz \tag{2.4}$$

The potential energy gained by the applied forces V is the negative of the work done W by the external dynamic forces, i.e.

$$V = -W = -\int_{\ell} q_i\,\bar{u}_i\,dz - \sum_{i=1} P_i\,\bar{u}_i \tag{2.5}$$

in which $\bar{u}_i$ are the displacements through which are acting the distributed dynamic loads q_i and the concentrated dynamic loads P_i .

2.3.2 Kinetic Energy

The kinetic energy is stored in the mass by virtue of its velocity. The kinetic energy T stored in a linear elastic beam of length ℓ is given by [Craig and Kurdila 2006]:

$$T = \frac{1}{2}\int_0^{\ell}\int_A \rho\left[(\dot{u})^2 + (\dot{v})^2 + (\dot{w})^2\right] dA\,dz \tag{2.6}$$

where u,v,w are displacements in the principal X,Y,Z directions, and ρ is the mass density of the material per unit length and the dot represents the time derivative.

2.4 Dynamic Analysis Methods

The most commonly dynamic methods used to determine the dynamic characteristic (natural frequencies, mode shapes, and transient and steady state responses) of structural members are: (1) Modal Superposition Method (MSM), (2) Direct Integration Methods, (3) Finite Element Method (FEM), (4) Dynamic Transfer Matrix Method (DTMM), and (5) Dynamic Stiffness Matrix Method (DSMM). These methods are given in brief details.

2.4.1 Modal Superposition Method (MSM)

The modal superposition method (or normal mode method) is a general approach for analyzing the dynamic response of linear multi-degree-of-freedom structural systems. It describes the response of the system in terms of the modes of free vibration whose orthogonality facilitates the solution [Humar 2002]. In this analytical approach, the orthogonal modes can be used to uncouple the governing equations of motion. In other words, if the orthogonal (natural) modes of the vibration for a Multi-Degree-Of-Freedom (MDOF) system are used as generalized coordinates for defining the system response, the n coupled equations of motion become uncoupled and can be solved independently as if each equation pertained to an independent system with only a single degree of freedom [Humar 2002]. As a result, the dynamic response of the MDOF system by mode superposition is defined as the summation of the individual responses of the n uncoupled equations. The drawback of the solution is the necessity of conducting a free vibration eigenvalue analysis to extract the natural modes of vibration. The method is only valid for linear systems, and is applied to undamped systems or systems where damping can be mathematically represented by a linear combination of scaled mass and stiffness matrices [Dukkipati 2006].

The dynamic equations of motion for general forced vibrations of an n-degree freedom linear system without considering damping effects can be written as:

$$[m]_{n\times n}\{\ddot{U}(t)\}_{n\times 1}+[k]_{n\times n}\{U(t)\}_{n\times 1}=\{F(t)\}_{n\times 1} \tag{2.7}$$

in which $[k]_{n\times n}$ and $[m]_{n\times n}$ are the stiffness and mass matrices for the system, $\{F(t)\}_{n\times 1}$ is the applied force vector, $\{U(t)\}_{n\times 1}$ and $\{\ddot{U}(t)\}_{n\times 1}$ refer to the displacement and acceleration vectors of the system in original coordinates. The mode superposition method employed uncouples the above differential equations by applying the linear transformation:

$$\{U(t)\}_{n\times 1}=[\Phi]_{n\times n}\{Y(t)\}_{n\times 1} \tag{2.8}$$

where $\langle U(t)\rangle_{1\times n}^{T}=\langle u_1\ \ u_2\ \ u_3\ ....\ u_n\rangle_{1\times n}^{T}$, $[\Phi]_{n\times n}=\left[\{\phi\}_1\ \{\phi\}_2\ \{\phi\}_3\ .....\ \{\phi\}_n\right]_{n\times n}$ is the modal shape matrix consisting of n modal vectors $\{\phi\}_n$, and $\{Y(t)\}_{n\times 1}$ is the vector of orthogonal coordinates.

From Equation (2.8), by substituting $\{U(t)\}_{n\times 1}$ and $\{\ddot{U}(t)\}_{n\times 1}$ into Equation (2.7), and pre-multiplying by $[\Phi]_{n\times n}^{T}$, the following system of uncoupled equations of motion is recovered:

$$[\hat{M}]_{n\times n}\{\ddot{Y}(t)\}_{n\times 1}+[\hat{K}]_{n\times n}\{Y(t)\}_{n\times 1}=\{\hat{F}(t)\}_{n\times 1} \tag{2.9}$$

where the modal mass matrix is defined by $[\hat{M}]_{n\times n}=[\Phi]_{n\times n}^{T}[m]_{n\times n}[\Phi]_{n\times n}$, the modal stiffness matrix is defined by $[\hat{K}]_{n\times n}=[\Phi]_{n\times n}^{T}[k]_{n\times n}[\Phi]_{n\times n}$, and $\{\hat{F}(t)\}_{n\times 1}=[\Phi]_{n\times n}^{T}\{F(t)\}_{n\times 1}$ is the modal force vector.

Based on the orthogonality conditions, i.e. $\{\phi\}_r^{T}[m]\{\phi\}_s=\{\phi\}_r^{T}[k]\{\phi\}_s=0$ for $r\neq s$. Matrices $[\hat{M}]_{n\times n}$ and $[\hat{K}]_{n\times n}$ are diagonal matrices. Thus, the equations of motion in modal coordinates (2.9) can be written as n uncoupled (independent) equations, i.e.

$$M_r\ddot{q}_r(t)+K_r q_r(t)=P_r(t)\quad ,\quad \text{for } r=1,2,3,...,n \tag{2.10}$$

with $M_r = \langle \phi \rangle_{1\times r}^T [m]_{r\times r} \{\phi\}_{r\times 1}$, $K_r = \langle \phi \rangle_{1\times r}^T [k]_{r\times r} \{\phi\}_{r\times 1}$, $P_r(t) = \langle \phi \rangle_{1\times r}^T \{\hat{F}(t)\}_{r\times 1}$ and $q_r(t)$ is the response for the r - th mode in orthogonal coordinates and can be determined for general time-dependent loads by one of the direct integration methods, for example the Duhamel integral method [Humar 2002]. Finally, the dynamic response of the system in physical coordinates is obtained by superimposing the individual modal solutions in normal coordinates as:

$$\{U(t)\}_{r\times 1} = \sum_{r=1}^{n} [\Phi]_{r\times r} \{q_r(t)\}_{r\times 1} \tag{2.11}$$

A few studies are focused on the mode superposition to the dynamic analysis of thin-walled beams. This includes Eslimy-Isfahany et al (1996a), who developed an analytical solution to investigate the response of coupled bending–torsion behaviour of thin-walled beams subjected to harmonic and random excitations using the normal mode method, in which the effects of shear deformation, warping stiffness and rotary inertia were not included in the formulation. Eslimy-Isfahany et al (1996b) extended their previous study in (1996a) to include the influence of axial force on the dynamic response. Li et al (2004b) used the mode superposition method to study the influence of axial loads and warping deformation on the coupled flexural-torsional vibration of thin-walled members with monosymmetric open cross-sections, in which the effects of shear deformation and rotary inertia were ignored in their formulation.

2.4.2 Direct Time-Integration Methods

Several numerical direct integration methods are available to numerically integrate the dynamic equations of motion of a structural system. The dynamic equations of motion are integrated by using a step-by-step numerical procedure at discrete time intervals $\Delta t, 2\Delta t, 3\Delta t, ..., \bar{n}\Delta t$, in which the total time span T_d is divided into "$\bar{n}$" equal time intervals, i.e. $\Delta t = T_d / \bar{n}$. Direct integration methods widely used for linear and nonlinear dynamic analyses can be classified as either implicit (e.g. Houbolt method, Wilson-θ method and Newmark - β method) or explicit schemes (e.g. central difference method, two cycle iteration with trapezoidal rule and Runge-Kutta method). In implicit integration methods, the dynamic difference equations are combined with the equations of motion, and the displacements are

determined directly by solving the equations. In explicit approaches, the response is expressed in terms of previously determined values of displacement, velocity and acceleration. The stability and computational efficiency are the most important differences between the implicit (unconditionally stable) and explicit integration (conditionally stable) schemes. When the selected time step Δt is larger than the threshold value, explicit integration methods becomes unstable. In other words, typically small time intervals are required to make the solution useful in explicit methods, while in implicit methods the solution remains stable even with large time steps Δt . Therefore, a proper time interval Δt is required to satisfy the conditional stability of explicit methods. Detailed descriptions of these methods can be found in the texts by Humar 2002, Craig and Kurdila 2006, and Chopra 2007. For example Chen and Tamma (1994) used the finite element method in combination with an implicit self-starting method, second-order accurate unconditionally stable, to analyze the dynamic forced response of open thin-walled structures with arbitrary open cross-section subjected to transverse loads. The formulation was based on Vlasov's assumptions and both warping deformation and rotary inertia effects were incorporated. Results obtained for cantilever and simply-supported beams with asymmetric, monosymmetric and doubly symmetric cross-sections were used to investigate the effects of various forms of coupling and rotary inertia on the dynamic behaviour of thin-walled beams.

2.4.3 Finite Element Method

The finite element method is well recognized as a powerful numerical technique based on the variational methods. It is used to solve problems that may be difficult to solve analytically. The accuracy of the solution depends on the element size and the selected interpolation functions. Three different types of variational principles can form the basis of finite element formulations: displacement based, force based, and hybrid-mixed. Displacement-based finite element solutions start with the Hamiltonian functional or the principle of virtual work, in which the compatibility and geometric boundary conditions of the field are satisfied a-priori while the equilibrium is satisfied in a weak sense. The principles of complementary energy or complementary virtual work exactly satisfy the equilibrium equations and the force boundary conditions a-priori, while in the case of hybrid-mixed principles are expressed in terms of both displacements and stresses. Among the numerous mixed variational principles the one

developed by Reissner is widely used. Reissner functional allows variations of both displacements and stresses (Washizu 1982).

In the literature survey relating to the dynamic analysis of thin-walled members, Mei (1970) developed a finite element for the coupled free vibrations analysis of thin-walled beams. The formulation incorporated warping effects and was based on shape functions derived based on the solution of static equilibrium equations. Hu et al. (1996) developed a finite element formulation for the coupled bending-torsional dynamic behavior of thin-walled beams of asymmetric cross-sections. The interpolation functions adopted were based on the homogenous solutions of static differential equations of equilibrium and were used to derive the stiffness and mass matrices of the beam element in the finite element formulation.

Chen and Tamma (1994) developed a finite element for the analysis of thin-walled open members under constant transverse loads. Their formulation was based on assumed linear and cubic displacement shape functions, in conjunction with an implicit self-starting unconditionally stable integration scheme. Tanaka and Bercin (1997) developed a bending-torsional coupled free vibration finite element for thin-walled members with asymmetric cross-sections. Similar to the study by Chen and Tamma (1994), the stiffness and mass matrices of the beam element were determined based on linear and cubic Hermitian shape functions in which the warping stiffness and rotary inertia are included. Hashemi and Richard (2000a and b) developed a dynamic finite element for the coupled bending–torsional vibration analysis of thin-walled beams with/without axial loads effect. Their solution can be regarded as an intermediate method between the finite element method and the dynamic stiffness matrix method. The exact solutions of the governing dynamic equations of equilibrium were obtained and subsequently frequency-dependent hyperbolic interpolation functions were adopted to formulate the stiffness and mass matrices of the structure. Lee and Kim (2002a,b) developed a finite element for the coupled free vibration of thin-walled composite beams with doubly symmetric and channel-shaped cross-sections in which the displacements are interpolated through linear shape functions for the longitudinal displacement and cubic Hermitian functions for the lateral displacements and angle of twist. Kim and Kim (2005) developed a finite element formulation for the coupled bending-

torsional free vibration of asymmetric thin-walled shear deformable beams by using an isoparametric beam element with two nodes and seven nodal degrees of freedom.

Voros (2008, 2009) formulated an element for the coupled bending-torsional free vibration and mode shapes of thin-walled open members induced by lateral loads. Recently, Vo and Lee (2009a,b,2010a,b), and Vo et al. (2009, 2010 and 2011) studied the coupled flexural-torsional coupled free vibrations of thin-walled composite members including/excluding axial loads and shear deformation effects. The finite element formulations were implemented via a displacement-based one-dimensional beam element with two nodes and seven degrees of freedom per node, i.e. the axial, vertical, lateral and rotational displacements are interpolated using linear and cubic Hermite shape functions.

To date no publication exists in which the finite element formation based on the analytical closed–form solutions of the dynamic field equation is used for investigating the dynamic analysis of thin-walled open members under harmonic forces. The present study attempts to fill this gap. A particular objective of the present study is to develop a finite element formulation for steady state dynamic response of thin-walled open members with asymmetric cross-sections under general harmonic excitations. The formulations will be based on a generalized Vlasov-Timoshenko beam theory, in which the shear deformation, warping deformation, and translational and rotary inertias are captured.

2.4.4 Dynamic Transfer Matrix Method (DTMM)

The dynamic transfer matrix method (DTMM) is a structural analysis technique which is extensively used for one-dimensional structures. In this method, the structural member is modeled by a series of elements linked together like a chain. Each element is considered as a space beam. At each point along the beam, the state variables such as displacements, rotations, shear forces and moments exist on each side of the element as shown in Figure (2.1). The displacements and forces at both ends are transferred between two adjacent elements by applying the force equilibrium equations and displacement compatibility across the element interface [Harris 2002]. To derive dynamic transfer matrix for the entire beam

structure, the beam is divided into m elements, as shown in Figure (2.1), the transfer matrix for beam element *"a"* can be expressed as:

$$\{\chi_2\}_{12\times1} = \left[\bar{T_a}\right]_{12\times12}\{\chi_1\}_{12\times1} \tag{2.12}$$

in which $\langle\chi_1\rangle^{\mathrm{T}}_{1\times12} = \langle\chi_{d_1} \vdots \chi_{f_1}\rangle^{\mathrm{T}}_{1\times12}$ and $\langle\chi_2\rangle^{\mathrm{T}}_{1\times12} = \langle\chi_{d_2} \vdots \chi_{f_2}\rangle^{\mathrm{T}}_{1\times12}$ are the state vectors at end 1 (or the left end of the beam denoted by subscript ℓ) and end 2 of beam element *"a"*, where $\langle\chi_{d_i}\rangle^{T}_{1\times6} = \langle u_i \;\; v_i \;\; w_i \;\; \theta_{x_i} \;\; \theta_{y_i} \;\; \theta_{z_i}\rangle^{T}_{1\times6}$, $\langle\chi_{f_i}\rangle^{T}_{1\times6} = \langle V_{x_i} \;\; V_{y_i} \;\; V_{z_i} \;\; M_{x_i} \;\; M_{y_i} \;\; M_{z_i}\rangle^{T}_{1\times6}$, for $(i = 1 \text{ and } 2)$. These vectors are composed of the displacements, rotations and forces at ends of the element *"a"*, and $\left[\bar{T_a}\right]_{12\times12}$ is the transfer matrix for beam element *"a"*.

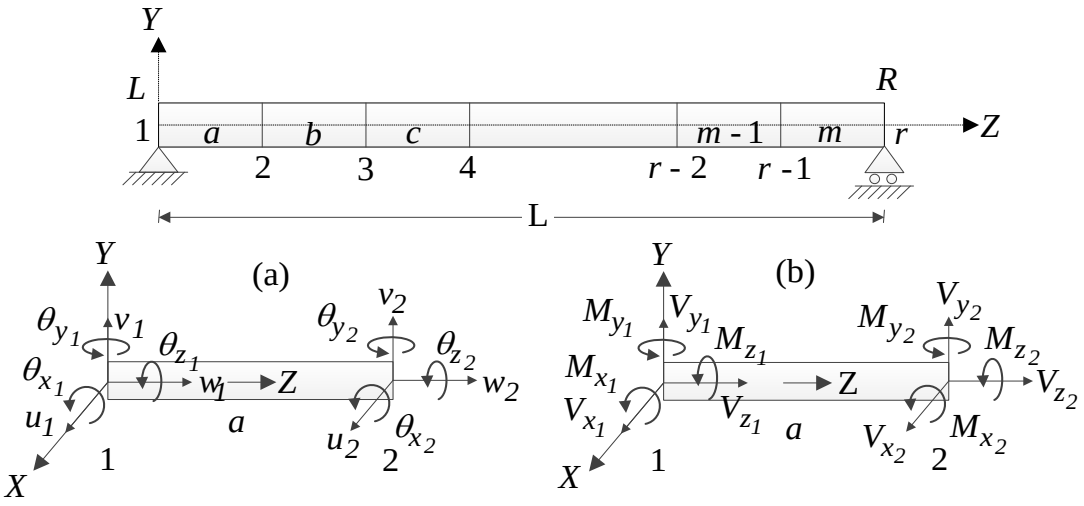

Figure (2.1): Schematic diagram for actual beam: (a) end displacements, (b) end forces

In a similar manner, the remaining elements transfer matrices at stations $2,3,4,.....,r$ are:

$\{\chi_3\}_{12\times1} = \left[\bar{T_b}\right]_{12\times12}\{\chi_2\}_{12\times1}$,

$\{\chi_4\}_{12\times1} = \left[\bar{T_c}\right]_{12\times12}\{\chi_3\}_{12\times1}$, …….…. , and

$$\{\chi_r\}_{12\times1} = \left[\bar{T_m}\right]_{12\times12}\{\chi_{r-1}\}_{12\times1} \tag{2.13}$$

On substitution, the global dynamic transfer matrix for the entire system is given by:

$$\{\chi_R\}_{12\times1} = \left[\bar{T}_G\right]_{12\times12}\{\chi_L\}_{12\times1} \tag{2.14}$$

in which $\langle\chi_L\rangle^{\mathrm{T}}_{1\times12} = \langle\chi_{d_L} \vdots \chi_{f_L}\rangle^{\mathrm{T}}_{1\times12}$ and $\langle\chi_R\rangle^{\mathrm{T}}_{1\times12} = \langle\chi_{d_R} \vdots \chi_{f_R}\rangle^{\mathrm{T}}_{1\times12}$ are the state vectors composed of the displacements, rotations and forces at left and right ends of the entire beam, where $\langle\chi_{d_j}\rangle^{\mathrm{T}}_{1\times6} = \langle u_j \;\; v_j \;\; w_j \;\; \theta_{x_j} \;\; \theta_{y_j} \;\; \theta_{z_j}\rangle^{\mathrm{T}}_{1\times6}$, $\langle\chi_{f_j}\rangle^{\mathrm{T}}_{1\times6} = \langle V_{x_j} \;\; V_{y_j} \;\; V_{z_j} \;\; M_{x_j} \;\; M_{y_j} \;\; M_{z_j}\rangle^{\mathrm{T}}_{1\times6}$, for $(j = R \text{ and } L)$, and $\left[\bar{T}_G\right]_{12\times12} = \left[\bar{T}_a\right]\left[\bar{T}_b\right]\left[\bar{T}_c\right].....\left[\bar{T}_{m\text{-}1}\right]\left[\bar{T}_m\right]$ is the dynamic transfer matrix for whole system. For dynamic analysis, the transfer matrix includes the elastic material properties, geometric and inertial properties of the structural system, and exciting frequency Ω. The natural frequencies of the system are those which satisfy Equation (2.14) when the boundary conditions on the left and right boundaries are specified.

The dynamic transfer matrix method has many advantages; elements of the matrix are based on the closed form solution of the governing differential equations of the structural member. It is an efficient and easily computerized method. Also it provides a fast and practical solution since the dimensions of the matrix for the elements of the system never change, i.e. the size of the system of equations does not depend on the complexity of the structural system, but it is related only to the number of displacements and forces on the boundaries of the structure. It also provides better accuracy in the prediction of higher frequencies when compared with classical finite element or other approximate methods [Li et al. 2004c].

Using the dynamic transfer matrix method, Ohga et al. (1995) studied the free vibration analysis of thin-walled members with closed and open cross-sections. Li et al. (2004a) employed the method to determine the natural frequencies and mode shapes of Euler-Bernoulli members under the effect of axial force. Li et al. (2004c) improved the formulation to include the effects of warping stiffness and axial forces on the coupled bending-torsional natural frequencies and vibration mode shapes. The inclusion of shear deformation effect on free vibration analysis of thin-walled members with monosymmetric cross-sections was also investigated by Li et al. (2004e).

2.4.5 Dynamic Stiffness Matrix Method (DSMM)

The dynamic stiffness matrix method (DSMM) is a powerful matrix method widely used for studying the natural and forced vibrations of a structural member, i.e. used to compute the natural frequencies and response analysis. The main idea is to adopt frequency dependent shape functions based on the exact solution of the governing differential equations of the system. The dynamic stiffness matrix eliminates the discretization errors in time and space and is capable of predicting an infinite number of natural frequencies by means of an infinite number of degrees of freedom [Leung 1991]. The dynamic stiffness matrix is derived for each element in a discretized structure and then assembled into global dynamic stiffness matrix $D(\Omega)$ of the system. The dynamic stiffness matrix $D(\Omega)$ of a harmonically vibrating system at a frequency Ω relates the amplitudes of the response displacements $\{\bar{u}_i\}$ to those of exciting forces $\{\bar{Q}_i\}$ and is given by:

$$\left[D(\Omega)\right]\{\bar{u}_i\} = \{\bar{Q}_i\} \tag{2.15}$$

in which $\left[D(\Omega)\right] = \left[K(\Omega)\right] - \Omega^2\left[M(\Omega)\right]$, where $\left[K(\Omega)\right]$ and $\left[M(\Omega)\right]$ are the global stiffness and mass matrices, and $\{\bar{u}_i\}$ is the nodal displacement vector.

For free vibrations $\{\bar{Q}_i\} = 0$ and one has:

$$\left[D(\Omega)\right]\{\bar{u}_i\} = \{0\} \tag{2.16}$$

Moreover, the dynamic stiffness matrix method in vibration analysis of structural members has certain advantages over the conventional finite element method, especially when higher frequencies and higher accuracy of results are desired. This is due to the fact that individual stiffness matrices are derived based on approximate shape functions, while those based on the dynamic stiffness matrix method are derived from the exact shape functions on the closed-form solution of the governing differential equations of the system elements [Banerjee 1997]. The derivation of the dynamic stiffness matrix for coupled bending-torsion behaviour of beams has been developed by several researchers. Friberg (1983) developed the exact dynamic stiffness matrix to study the coupled bending-torsion vibrations of thin-walled open Euler-Bernoulli beams. His solution neglects warping deformation. Later, Friberg (1985) extended his previous work to modify the dynamic stiffness matrix to include the effects of

warping deformation, rotary inertia and axial forces. Leung (1985) presented the dynamic stiffness matrix method for damped and undamped structural members subjected to harmonic excitations excluding the shear deformation, warping and rotary inertia effects. Based on Vlasov beam theory, Leung (1991) developed the dynamic stiffness matrix of a thin-walled open beam by neglecting the shear deformation effects. Leung (1992) expanded his previous study for the dynamic stiffness matrix to take into account the effect of constant axial force and moments about the strong axis. Banerjee (1989 and 1991) adopted the dynamic stiffness matrices to investigate the free vibration characteristics of thin-walled composite beams excluding the effects of shear deformation, warping stiffness as well as rotary inertia. Banerjee and Williams (1992 and 1994) developed the analytical expressions for the coupled bending-torsional dynamic stiffness matrix of thin-walled beam elements. Their solution included shear deformation effects and investigated the effect of axial loads. Using power series expressions for displacement fields, Bin and Leung (2006) formulated the dynamic stiffness matrix including the effects of warping stiffness, rotary inertia and axial force on the free vibration characteristics of thin-walled members using the power series expressions for displacement fields. Kim et al. (2003a and 2007) developed a dynamic stiffness matrix for the free vibration analysis of thin-walled members with asymmetric open cross-sections taking into account the warping stiffness, rotary inertia and axial force effects. Their formulations, i.e. equations of motion and force-deformation relations, are derived from the total potential energy of the beam under initial stress resultants based on finite semitangential rotations and semitangential moments. In a subsequent paper (Kim et al. 2003b), they extended their formulation for the dynamic stiffness matrix to capture the effect of shear deformation.

2.5 Kinematics for Beams

The objective of this section is to review common flexural and torsional beam theories since they form the foundation of the proposed research. Beam theories are based on kinematics assumptions aimed at simplifying the 3D nature of the problem into a simplified one-dimensional problem. Depending on the kinematics assumptions made, different levels of approximations are achieved. This reviews key flexure theories (i.e. Euler-Bernoulli and Timoshenko beam) and torsional theories for solid beam and thin-walled members. In the following, emphasis is placed on the kinematics assumptions made in each theory.

2.5.1 Beam Flexural Theories

In order to describe the kinematics of beam theories, a rectangular Cartesian coordinate system (x, y, z) is chosen such that axes x and y coincide with the principal axes of the cross-section, and the z axis coincides with the longitudinal centroidal axis of the member. Displacement u acting along the x axis is the lateral displacement, displacement v, acting along the y axis, is the transverse displacement, while displacement w oriented along the z axis is the longitudinal displacement. Angles $\theta_x, \theta_y, \theta_z$ denote the angles of rotation of planes about the X, Y, Z axes, respectively.

2.5.1.1 Euler-Bernoulli Bending Beam Theory

The Euler-Bernoulli beam theory is based on the kinematics assumptions that (i) the cross section of the beam (open or closed) remains undeformed in its own plane throughout deformation, (ii) the cross-section is assumed to remain plane and normal to the centroidal axis of the beam throughout deformation as illustrated in Figure (2.2). In other words, the deformations associated with the transverse shear are neglected. Based on the normality assumption, the cross-sectional rotation is equal to the derivative of the displacement, i.e. $\theta_x = dv/dz$.

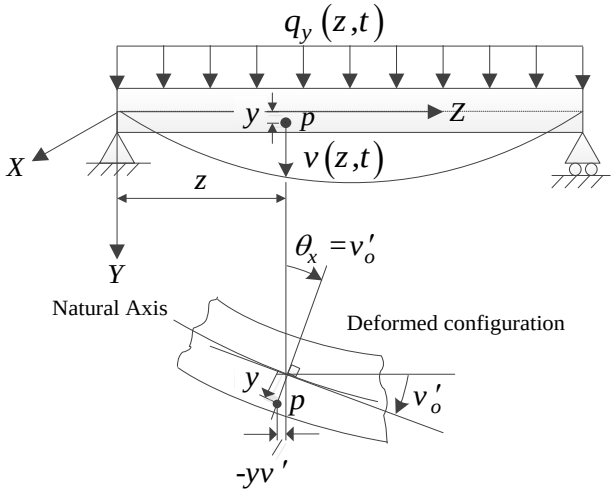

Figure (2.2): Deformation of Euler-Bernoulli Beam.

Kinematics and Strains

The displacement components u,v,w for any point $p(x,y,z)$ of height y from the neutral axis of the beam are given as [Bottega 2006]:

$$\begin{Bmatrix} u(x,y,z,t) \\ v(x,y,z,t) \\ w(x,y,z,t) \end{Bmatrix} = \begin{Bmatrix} 0 \\ v_o(z,t) \\ -y\, v_o'(z,t) \end{Bmatrix} \tag{2.17}$$

where $v_o(z,t)$ is the transverse displacement of the centroidal axis of the beam. The normal strain ε_{zz} and shear strains γ_{xz}, γ_{yz} are related to the displacements by:

$$\begin{Bmatrix} \gamma_{xz} \\ \gamma_{yz} \\ \varepsilon_{zz} \end{Bmatrix} = \begin{Bmatrix} \frac{1}{2}\left(\frac{\partial u}{\partial z} + \frac{\partial w}{\partial x}\right) \\ \frac{1}{2}\left(\frac{\partial v}{\partial z} + \frac{\partial w}{\partial y}\right) \\ \frac{\partial w}{\partial z} \end{Bmatrix} = \begin{Bmatrix} 0 \\ 0 \\ -y\, v_o''(z,t) \end{Bmatrix} \tag{2.18}$$

where all primes denote differentiation with respect to z .

Moment-Stress Relations

The normal stresses σ_{zz} acting at a point z on the cross-section is given as:

$$\sigma_{zz}(z,t) = E\,\varepsilon_{zz}(z,t) = -Ey\,v_o''(z,t) \tag{2.19}$$

The total bending moment M_x is given by the area integral of the moments of the normal stresses about the section centroid, i.e.,

$$M_x(z,t) = \int_A y\,\sigma_{zz}(z,t)\,dA = -\int_A Ey^2 v_o''(z,t)\,dA = -EI_{xx}v_o''(z,t) \tag{2.20}$$

From Equations (2.19) and (2.20), the bending stresses can be obtained as:

$$\sigma_{zz}(z,t) = M_x(z,t)\,y\,/I_{xx} \tag{2.21}$$

where E is modulus of elasticity and $I_{xx} = \int_A y^2 dA$ is the moment of inertia about the X axis.

Potential and Kinetic Energy Expressions

The strain energy U_e of the whole beam due to bending is found by integrating the strain energy density throughout the beam as:

$$U_e = \frac{1}{2}\int_V \sigma_{zz}\,\varepsilon_{zz}\,dV = \frac{1}{2}\int_0^{\ell} EI_{xx}\left[v_o''(z,t)\right]^2 dz \tag{2.22}$$

where U_e is the internal strain energy induced by the normal stress σ_{zz} .

The work done W_e by the applied distributed transverse force $q_y(z,t)$ is given by:

$$W_e = \int_0^{\ell} q_y(z,t)\,v_o(z,t)\,dz \tag{2.23}$$

and, the total potential strain energy Π_e is obtained by:

$$\Pi_e = U_e - W_e = \frac{1}{2}\int_0^{\ell} EI_{xx}\left[v_o''(z,t)\right]^2 dz - \int_0^{\ell} q_y(z,t)\,v_o(z,t)\,dz \tag{2.24}$$

The kinetic energy of the beam consists of two parts; one account for the motion due to the transverse displacement *v* and the other one account for the longitudinal displacement *w* induced by the rotation of the section. The kinetic energy T_e for an Euler-Bernoulli beam is then given by:

$$T_e = \frac{1}{2}\int_V \left(\left[\dot{v}(z,t)\right]^2 + \left[\dot{w}(z,t)\right]^2\right)dV = \frac{1}{2}\int_0^{\ell}\rho A\left[\dot{v}_o(z,t)\right]^2 dz + \frac{1}{2}\int_0^{\ell}\rho I_{xx}\left[\dot{v}_o(z,t)\right]^2 dz \tag{2.25}$$

where $A = \int_A dA$ is the cross sectional area of the beam.

Equations of Motion for Euler-Bernoulli Beam

The detailed derivations for the Euler-Bernoulli beam can be found in Inman (2001), Rao (2004), Thomson (2005) and Bottega (2006). The equation of motion can be either derived by using Newton's second law or the Hamilton's variational principle. Using the variational form of the Hamilton principle, one obtains:

$$\int_0^{\ell}\int_{t_1}^{t_2}\left[\rho A\dot{v}_o(z,t)\delta\dot{v}_o(z,t)+\rho I_{xx}\dot{v}_o'(z,t)\delta\dot{v}_o'(z,t)-EI_{xx}v_o''(z,t)\delta v_o''(z,t)\right.$$
$$\left.+q_y(z,t)\delta v_o(z,t)\right]dtdz=0 \tag{2.26}$$

Integrating by parts, the governing differential equation of motion and the boundary conditions are obtained as:

$$\rho A\ddot{v}_o(z,t)-\rho I_{xx}\ddot{v}_o''(z,t)+EI_{xx}v_o^{iv}(z,t)=q_y(z,t) \tag{2.27}$$

and the associated boundary conditions are:

$$\left[EI_{xx}v_o''(z,t)\delta v_o'(z,t)\right]_0^{\ell}=0$$

$$\left[EI_{xx}v_o'''(z,t)\delta v_o(z,t)\right]_0^{\ell}=0 \tag{2.28}$$

Equations (2.28) provide the possible essential and natural boundary conditions for the problem.

2.5.1.2 Timoshenko Beam Theory

The Timoshenko beam theory can be conceived as an extension of the Euler-Bernoulli beam theory which captures the transverse shear deformation effects. The Timoshenko beam theory retains the first Euler-Bernoulli assumption regarding planar deformation, while relaxing the second one regarding the normality of the plane relative to the centroidal axis. The relaxation of the second assumption allows for an angle of rotation of the plane θ_x that is distinct from the slope of centreline $dv/dz \neq \theta_x$, and thus provides a nonzero transverse shear strain.

Kinematics and Strains

The kinematics of deformation of the Timoshenko beam is illustrated in Figure (2.3). As shown, the cross-section remains planar but does not remain perpendicular to the centroidal axis of the beam. This leads to an angle of rotation $\theta_x(z,t)$ of the cross section at z, which is generally distinct from the slope, i.e., $\theta_x(z,t)\neq v_o'(z,t)$.

The displacement components u,v,w are expressed as:

$$\begin{Bmatrix} u(x,y,z,t) \\ v(x,y,z,t) \\ w(x,y,z,t) \end{Bmatrix} = \begin{Bmatrix} 0 \\ v_o(z,t) \\ y\,\theta_x(z,t) \end{Bmatrix} \tag{2.29}$$

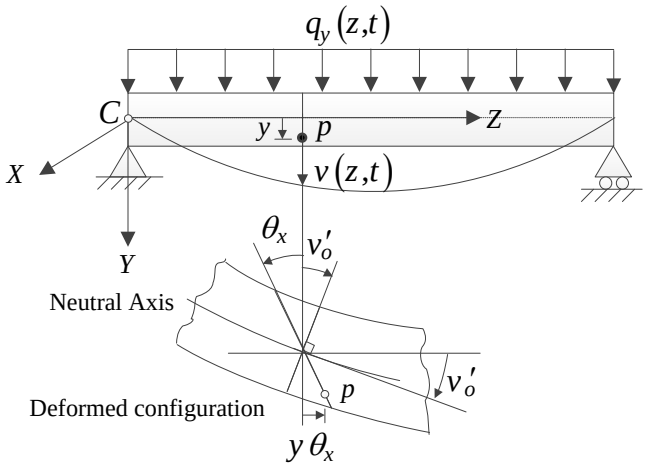

Figure (2.3): Timoshenko Beam Theory.

The corresponding strains field expressions are given by:

$$\begin{Bmatrix} \gamma_{xz} \\ \gamma_{yz} \\ \varepsilon_{zz} \end{Bmatrix} = \begin{Bmatrix} \frac{1}{2}\left(\frac{\partial u}{\partial z} + \frac{\partial w}{\partial x}\right) \\ \frac{1}{2}\left(\frac{\partial v}{\partial z} + \frac{\partial w}{\partial y}\right) \\ \frac{\partial w}{\partial z} \end{Bmatrix} = \begin{Bmatrix} 0 \\ \frac{1}{2}\left[v_o'(z,t) + \theta_x(z,t)\right] \\ y\,\theta_x'(z,t) \end{Bmatrix} \tag{2.30}$$

Moment-Stress Relations

The bending moment $M_x(z,t)$ and shear force $V_y(z,t)$ are:

$$M_x(z,t) = \int_A y\,\sigma_{zz}(z,t)\,dA = EI_{xx}\,\theta_x'(z,t) \quad \text{, and} \tag{2.31}$$

$$V_y(z,t) = \int_A \tau_{zy}(z,t)\,dA = GA\,\gamma_{zy}(z,t) = GA\left[v_o'(z,t) + \theta_x(z,t)\right] \tag{2.32}$$

where G is the shear rigidity.

Potential and Kinetic Energy Expressions

The internal strain energy U_t due to bending and shear deformations is given as:

$$U_t = \frac{1}{2}\int_V E\,\sigma_{zz}^2\,dV + \frac{1}{2}\int_V G\,\gamma_{yz}^2\,dV = \frac{1}{2}\int_0^\ell EI_{xx}\left[\theta_x'(z,t)\right]^2 dz + \frac{1}{2}\int_0^\ell GA\left[v_o'((z,t)+\theta_x(z,t)\right]^2 dz \quad (2.33)$$

For a beam under distributed transverse load $q_y(z,t)$, the work done by this force is given by Equation (2.23). The kinetic energy T_t of the Timoshenko beam is given as:

$$T_t = \frac{1}{2}\int_0^\ell \rho A\left[\dot{v}_o(z,t)\right]^2 dz + \frac{1}{2}\int_0^\ell \rho I_{xx}\left[\dot{q}_x(z,t)\right]^2 dz \quad (2.34)$$

where the first term in Equation (2.34) is the kinetic energy due to translation while the second term is the rotary inertia.

Dynamic Equations of Motion for Timoshenko Beam

Using the variational form of Hamilton principle; $\int_{t_1}^{t_2}\delta(T_t - \Pi_t)\,dt = 0$, one obtains:

$$\int_{t_1}^{t_2}\int_0^\ell \left\{\rho A\dot{v}_o(z,t)\delta\dot{v}_o(z,t) + \rho I_{xx}\,\dot{\theta}_x(z,t)\delta\dot{\theta}_x(z,t) - EI_{xx}\,\theta_x'(z,t)\delta\theta_x'(z,t) - GA\left[v_o'(z,t) + \theta_x(z,t)\right]\delta v_o'(z,t) - GA\left[v_o'(z,t)+\theta_x(z,t)\right]\delta\theta_x(z,t) + \theta_y(z,t)\delta v_o(z,t)\right\} dz\,dt = 0$$

Integrating by parts, the equations of motion are given as [Hurty 1964]:

$$\rho A\ddot{v}_o(z,t) - GA\left[v_o''(z,t) + \theta_x'(z,t)\right] = q_y(z,t) \quad (2.35)$$

$$\rho I_{xx}\ddot{\theta}_x(z,t) - EI_{xx}\,\theta_x''(z,t) + GA\left[v_o'(z,t) + q_x(z,t)\right] = 0 \quad (2.36)$$

and the associated boundary conditions are obtained as:

$$\begin{aligned} &EI_{xx}\,\theta_x'(z,t)\,\delta\theta_x(z,t)\Big|_0^\ell = 0 \\ &GA\left[v_o'(z,t)+\theta_x(z,t)\right]\delta v_o(z,t)\Big|_0^\ell = 0 \end{aligned} \quad (2.37)$$

It is possible to eliminate $\theta_x(z,t)$ from the two field equations (2.35) and (2.36) and obtain a single equation in terms of the transverse deflection $v_o(z,t)$ and its derivatives as:

$$\left[EI_{xx}\frac{\partial^4 v_o(z,t)}{\partial z^4}+\rho A\frac{\partial^2 v_o(z,t)}{\partial t^2}-q_y(z,t)\right]-\rho I_{xx}\frac{\partial^4 v_o(z,t)}{\partial t^2\partial z^2}+\frac{\rho I_{xx}}{GA}\frac{\partial^2}{\partial z^2}\left[q_y(z,t)-\rho A\frac{\partial^2 v_o(z,t)}{\partial t^2}\right]-\frac{EI_{xx}}{GA}\frac{\partial^2}{\partial t^2}\left[q_y(z,t)-\rho A\frac{\partial^2 v_o(z,t)}{\partial t^2}\right]=0 \quad (2.38)$$

2.5.2 Torsional Theories for Thin-walled Beams

Consider a uniform beam with open cross section subjected to torsional moments M_z applied at the ends of the beam as illustrated in Figure (2.4a). Under the applied torsional moments, two types of deformations can take place, (1) uniform torsion (or Saint-Venant torsion) and nonuniform torsion (or warping torsion). In uniform torsion, the rate of change of the angle of twist (and thus the associated longitudinal warping deformations) is constant along the member or (2) Non-uniform torsion, in which the rate of change of the angle of twist (and thus the longitudinal warping deformations) varies along the member. If the structural member is allowed to warp freely (i.e., longitudinal displacements are unrestrained), the applied torsional moment is resisted only by the torsional shear stresses or St. Venant shearing stresses. The analysis of non-uniform torsional deformation of thin-walled beams with open cross-sections is presented in different theories such as Vlasov (1961) and Gjelsvik (1981).

Figure (2.4b) shows that the shear stress distribution across the thickness of the open section is linear and the maximum stress is located at the edge and zero at the middle surface. On the other hand, when the warping deformations are restrained, the torsion is non-uniform. In this case, additional normal stresses σ_w are induced in addition to shear stress τ_w and the applied torsion is resisted by two simultaneous actions: St. Venant action and the warping restraint (Figure 2.5). Thus, the total twisting moment M_z is the sum of the St. Venant torsion $M_{z_{sv}}$ and the warping torsion M_{z_w}, i.e., $M_z = M_{z_{sv}} + M_{z_w}$.

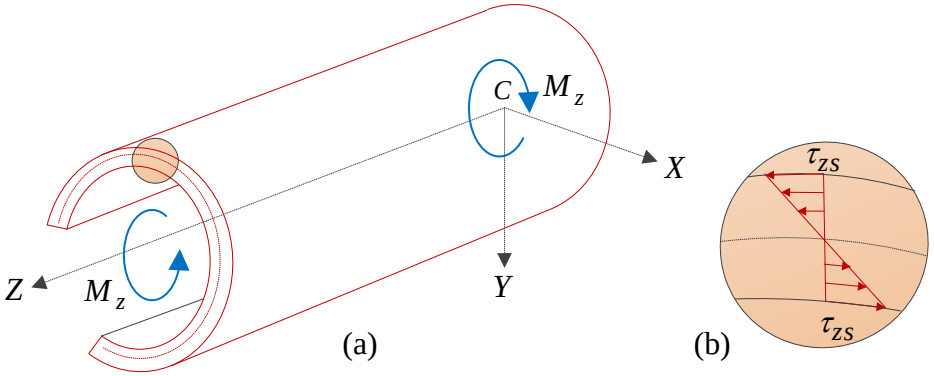

Figure (2.4): (a) A thin-walled beam subjected to twisting moments
(b) Shear stress distribution

Several theories were devised to describe the static and dynamic torsional analysis of members. Most common are the Saint-Venant torsion theory and the Vlasov theory. These are reviewed in the following sections.

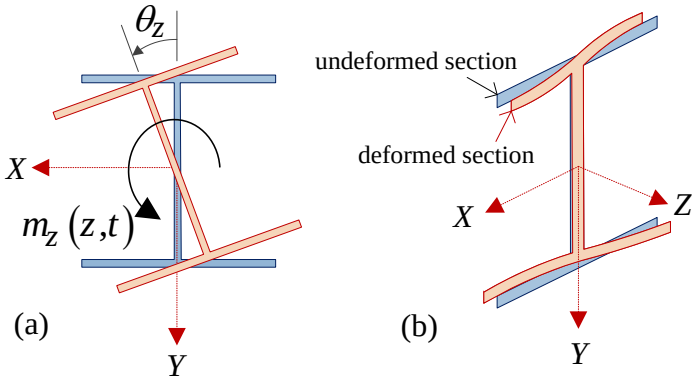

Figure (2.5): (a) Twisted thin-walled I-beam, (b) warping deformation of the cross-section

2.5.2.1 Saint-Venant Torsion Theory

A thin-walled member of open cross section is assumed to be subjected to uniformly distributed dynamic torsion $m_z(z,t)$, in which both ends are assumed to warp freely (Figure 2.5a). In St. Venant theory, the rate of angle of twist is assumed constant along the beam.

Kinematics and Strains

The member cross section is assumed to rotate by a small angle $\theta_z(z,t)$ about the *Z*-axis, as illustrated in Figure (2.6). The corresponding small displacements *u,v,w* of a point *p* located on the mid-surface of the section are given [Timoshenko 1970]:

$$\begin{Bmatrix} u(x,y,z,t) \\ v(x,y,z,t) \\ w(x,y,z,t) \end{Bmatrix} = \begin{Bmatrix} -(y-y_s)\theta_z(z,t) \\ (x-x_s)\theta_z(z,t) \\ -w(z,t)\theta_z'(z,t) \end{Bmatrix} \tag{2.39}$$

where (x_s, y_s) are the coordinates of the shear centre and $\omega(x,y)$ is the warping function. According to Saint-Venant assumptions, the warping function is constant along the longitudinal axis and the twist rotation varies linearly along the beam, so that the rate of the angle of twist is constant, i.e. $\theta_z'(z,t) = \text{constant}$.

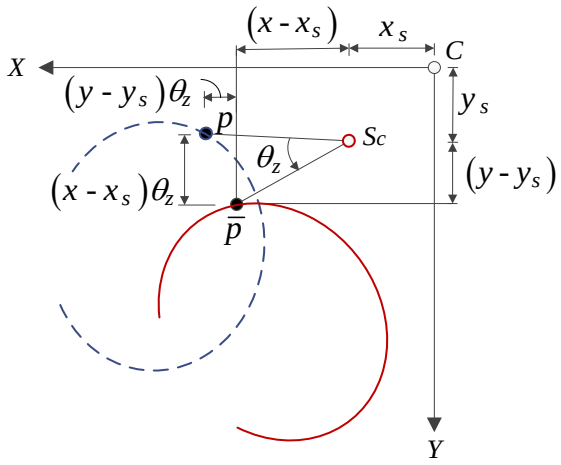

Figure (2.6): Deformations of open thin-walled member.

The corresponding strain-displacement relations can be expressed as follows [Saade 2004]:

$$\begin{Bmatrix} \varepsilon_{zz} \\ \gamma_{xz} \\ \gamma_{yz} \end{Bmatrix} = \begin{Bmatrix} \dfrac{\partial w}{\partial z} \\ \dfrac{\partial u}{\partial z} + \dfrac{\partial w}{\partial x} \\ \dfrac{\partial v}{\partial z} + \dfrac{\partial w}{\partial y} \end{Bmatrix} = \begin{Bmatrix} 0 \\ -\left(y - y_s + \dfrac{\partial \omega}{\partial x} \right)\theta_z' \\ \left(x - x_s - \dfrac{\partial \omega}{\partial y} \right)\theta_z' \end{Bmatrix} \tag{2.40}$$

Moment-Stress Relations

For a homogeneous, isotropic and linearly elastic material, by applying the generalized Hooke's law the normal and shear stresses are expressed in terms of strains as:

$$\begin{Bmatrix} \sigma_{zz} \\ \tau_{xz} \\ \tau_{yz} \end{Bmatrix} = \begin{Bmatrix} E\,\varepsilon_{zz} \\ G\,\gamma_{xz} \\ G\,\gamma_{yz} \end{Bmatrix} = \begin{Bmatrix} 0 \\ -G\left(y - y_S + \dfrac{\partial \omega}{\partial x} \right)\theta_z' \\ G\left(x - x_S - \dfrac{\partial \omega}{\partial y} \right)\theta_z' \end{Bmatrix} \tag{2.41}$$

The St. Venant twisting moment can be determined by integrating the moments of in-plane shear stresses about the section shear centre:

$$M_{z_{sv}}(z,t) = \int_A \left[\tau_{yz}(x - x_S) - \tau_{xz}(y - y_S) \right] dA = GJ_{sv}\,\theta_z'(z,t) \tag{2.42}$$

where the St. Venant Torsional Constant J_{sv} is defined as:

$$J_{sv} = \int_A \left[(x - x_S)^2 + (y - y_S)^2 - (x - x_S)\frac{\partial \omega}{\partial y} + (y - y_S)\frac{\partial \omega}{\partial x} \right] dA \tag{2.43}$$

Potential and Kinetic Energy Expressions

The increment of strain energy stored in an element dz of a twisted thin-walled member due to Saint-Venant torsion is:

$$dU_{sv} = \frac{1}{2} M_{z_{sv}}\, d\theta_z \tag{2.44}$$

in which $d\theta_z = \dfrac{1}{GJ_{sv}} M_{z_{sv}}\, dz$ (2.45)

From Equations (2.44) and (2.45), and integrating over the length gives the strain energy in the entire member due to Saint-Venant torsion as:

$$U_{sv} = \frac{1}{2}\int_0^{\ell} GJ_{sv}\left[\theta_z'(z,t) \right]^2 dz \tag{2.46}$$

The work done by the distributed torsion $m_z(z,t)$ is:

$$W_{sv} = \int_0^{\ell} m_z(z,t)\theta_z(z,t)dz \tag{2.47}$$

and the total potential energy of the beam is:

$$\Pi_{sv} = \frac{1}{2}\int_0^{\ell}\left(GJ_{sv}\left[\theta_z'(z,t)\right]^2 - m_z(z,t)\theta_z(z,t)\right)dz \tag{2.48}$$

By substituting Equation (2.39) into Equation (2.6) and by ignoring the second order terms, then the kinetic energy T_{sv} can be expressed as:

$$T_{sv} = \frac{1}{2}\int_0^{\ell}\rho r_o\left[\dot{\theta}_z(z,t)\right]^2 dz \tag{2.49}$$

in which the polar moment of inertia is defined as $r_o = \int_A\left[(x - x_s)^2 + (y - y_s)^2\right]dA$.

Dynamic Equations of Torsional motion

The application of Hamilton's variational principle; $\int_{t_1}^{t_2}\delta(T_{sv} - \Pi_{sv})dt = 0$, yields:

$$\int_{t_1}^{t_2}\int_0^{\ell}\left[\rho r_o\,\dot{\theta}_z(z,t)\delta\dot{\theta}_z(z,t) - GJ_{sv}\,\theta_z'(z,t)\delta\theta_z'(z,t) + m_z(z,t)\delta\theta_z(z,t)\right]dzdt = 0$$

By integrating by parts, and noting that $\delta\theta_z(z,t_1) = 0$ and $\delta\theta_z(z,t_2) = 0$, the dynamic equation of motion of the torsion member is given as:

$$\rho r_o\,\ddot{\theta}_z(z,t) - GJ_{sv}\,\theta_z''(z,t) = m_z(z,t) \tag{2.50}$$

and the relevant boundary conditions are:

$$GJ_{sv}\,\theta_z'(z,t)\,\delta\theta_z(z,t)\Big|_0^{\ell} = 0 \tag{2.51}$$

2.5.2.2 Vlasov Non-Uniform Torsion Theory

When a thin-walled member with open cross-section is subjected to twisting moments, its cross-sections undergo longitudinal displacements and a plane section before deformation

generally does not remain plane (Figure 2.7a). This phenomenon is called warping. The Saint Venant torsion theory assumes warping to be completely unrestrained. In reality, many support details can prevent member ends from warping freely. This causes an increase of the member torsional stiffness and introduces longitudinal stresses especially nearby the member ends. These effects can be often ignored for solid and thin-wall closed sections, while these effects can lead to significant longitudinal stresses for open sections restrained warping.

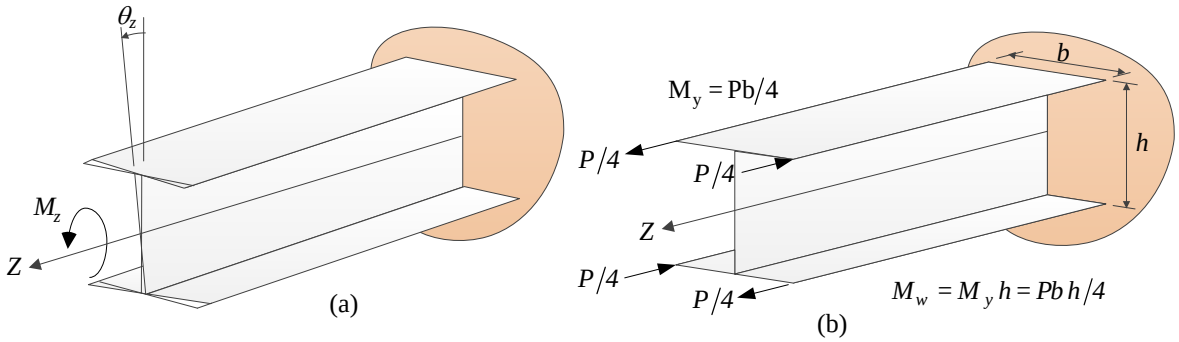

Figure (2.7): (a) Warping deformation of cantilever I-beam, (b) Bimoment in I-section

Thin-walled beam theories which capture warping effects include the works of Vlasov (1961), Timoshenko (1960) and Gjelsvik (1981). Vlasov (1961) suggests treating the cylindrical shells as thin-walled beams when their dimensions satisfy the following relations; their thickness to characteristic section width $t_i/d \le 0.1$ and when their section width to span $d/\ell \le 0.1$ (Figure 2.8). He developed a general theory for isotropic thin-walled beams with open and closed sections which captures warping effects. Compared to the typical convential Euler-Bernoulli beam theory, the Vlasov theory introduced the rate of change of the angle of twist as a measure of warping deformation, which leads to an additional straining action, the bimoment B (Figure 2.7b). Timoshenko (1960) independently developed a similar theory for isotropic beams with open cross-sections in which the primary warping effects are included.

Gjelsvik (1981) extended the Vlasov's theory to account for the additional through-thickness secondary warping for beams with open and closed cross-sections.

The Vlasov theory is applicable for combined non-uniform torsion and flexure. His theory is based on the following main assumptions: (i) the cross section does not deform in its own plane. (ii) shear strains on the middle surface of the cross section are negligible. It implies that the normal strain in the contour direction is small compared to the longitudinal strain in the longitudinal direction.

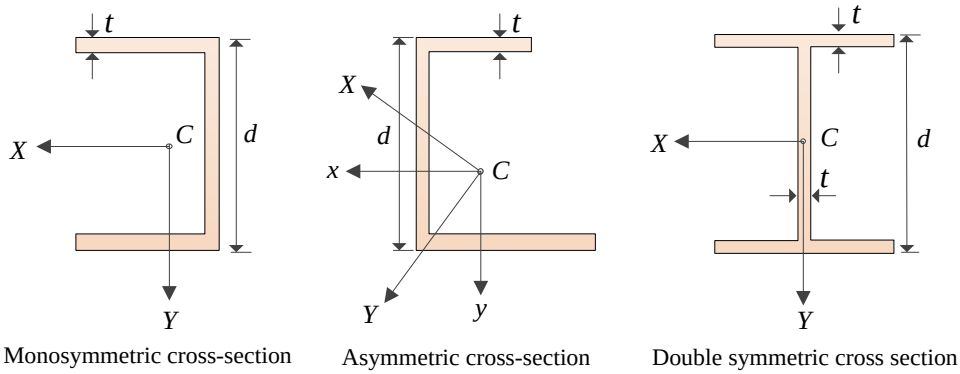

Figure (2.8): Open Thin-walled Cross sections.

Kinematics and Strains

A thin-walled beam with arbitrary open cross section (Figure 2.9) has a fixed right-handed Cartesian coordinate system (x, y, z) with the z - axis parallel to the longitudinal axis of the beam used to describe the geometry and displacements. In addition to the coordinate system (x, y, z), a local coordinate system (n, s, z) is positioned on the contour. Coordinate s is oriented along the tangent to the middle surface in a contour at a point of interest, while n is the coordinate in the normal direction to the s coordinate with the origin of the (n, s) system lying on the section contour at the point of interest, and s is oriented such that the axes system (n, s, z) is a right-handed coordinate system.

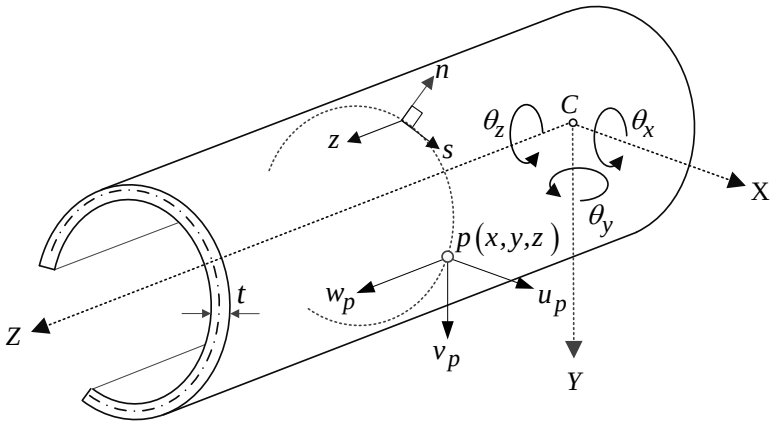

Figure (2.9): Geometry of a thin-walled Beam

According to the first Vlasov's assumption, the cross-section is undeformed in its own plane and the only possible motion of the section in its own plane is a rigid body motion (Figure 2.10) characterized by two orthogonal displacements u and v at an arbitrary point (selected as the shear centre S_c for mathematical convenience) and an angle of twist θ_z. This implies that the horizontal and vertical displacements $u_p(z,s,t)$ and $v_p(z,s,t)$ of an arbitrary point $p(x,y)$ located on the mid-surface of the cross-section along the principal X and Y directions can be described in terms of displacements u and v of the shear centre S_c and the angle of rotation θ_z of the cross section about the shear centre.

Thus, for a small angle of twist, the displacement components $u_p(z,s,t)$ and $v_p(z,s,t)$ of the arbitrary point $p(x,y)$ are expressed as:

$$u_p(z,s,t) = u(z,t) - \left[y(s) - y_s\right]\theta_z(z,t) \tag{2.52}$$

$$v_p(z,s,t) = v(z,t) + \left[x(s) - x_s\right]\theta_z(z,t) \tag{2.53}$$

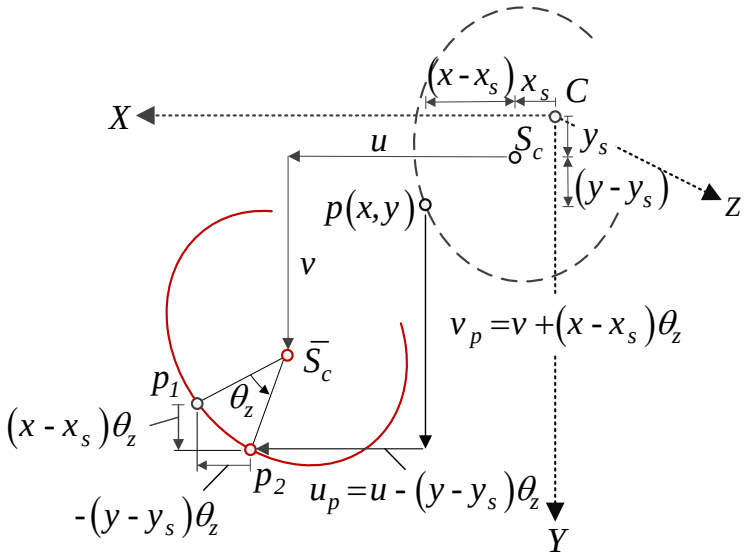

Figure (2.10): Displacements in the Plane of the Cross-section.

The tangential and normal displacement components $\xi(z,s,t)$ and $\eta(z,s,t)$ of a point $p(x,y)$ along s and n directions can be expressed in terms of transverse and lateral displacements $u_p(z,s,t)$ and $v_p(z,s,t)$ of the point $p(x,y)$ as:

$$\xi(z,s,t) = u_p(z,s,t)\cos\hat{\alpha}(s) + v_p(z,s,t)\sin\hat{\alpha}(s) \tag{2.54}$$

$$\eta(z,s,t) = v_p(z,s,t)\cos\hat{\alpha}(s) - u_p(z,s,t)\sin\hat{\alpha}(s) \tag{2.55}$$

in which $\hat{\alpha}(s)$ is the angle between the tangent of the cross section at point $p(x,y)$ and the positive direction of the X axis, as illustrated in Figure (2.11). From Equations (2.52) and (2.53), by substituting into Equations (2.54) and (2.55), one obtains:

$$\xi(z,s,t) = u(z,s)\cos\hat{\alpha}(s) + v(z,s)\sin\hat{\alpha}(s) + h(s)\theta_z(z,t) \tag{2.56}$$

$$\eta(z,s,t) = v(z,s)\cos\hat{\alpha}(s) - u(z,s)\sin\hat{\alpha}(s) + r(s)\theta_z(z,t) \tag{2.57}$$

From Figure (2.11) it is seen that:

$$h(s) = [x(s) - x_s]\sin\hat{\alpha}(s) - [y(s) - y_s]\cos\hat{\alpha}(s) \tag{2.58}$$

$$r(s) = [x(s) - x_s]\cos\hat{\alpha}(s) + [y(s) - y_s]\sin\hat{\alpha}(s) \tag{2.59}$$

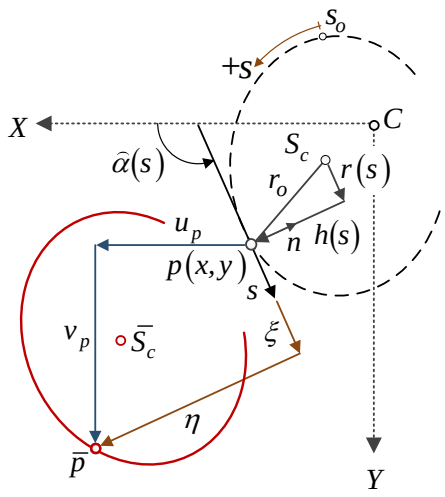

Figure (2.11): Local Coordinate System and Displacement Components of a point $p(x,y)$ on the Cross-section.

in which the geometric relations are considered: $\cos\bar{\alpha}(s)=dx/ds$ and $\sin\bar{\alpha}(s)=dy/ds$, where $h(s)$ is the perpendicular distance from the shear centre to the mid-thickness tangent at an arbitrary point $p(x,y)$, $r(s)$ represents the magnitude of the perpendicular distance from the shear centre to the normal of the profile line at point $p(x,y)$, ds is the arc element of the profile line, and dx,dy are the projections of ds along the global Cartesian coordinates corresponding to the arc element ds.

The longitudinal displacement $w_p(z,s,t)$ of point $\bar{p}$ located on the centreline of the open cross-section can be described in terms of displacements $\xi(z,s,t)$, $\eta(z,s,t)$ and angle $\bar{\alpha}(s)$. Based on the second Vlasov's assumption, the shear strain γ_{zs} vanishes at the middle surface of the cross-section. i.e.,

$$\gamma_{zs}=\frac{\partial w_p}{\partial s}+\frac{\partial \xi}{\partial z}=0 \qquad (2.60)$$

By integrating Equation (2.60) with respect to coordinate s and using Equations (2.56) and (2.58), the longitudinal displacement $w_p(z,s,t)$ of point $p(x,y)$ is:

$$w_p(z,s,t) = w(z,t) - x(s)u'(z,t) - y(s)v'(z,t) - \omega(s)\theta_z'(z,t) \tag{2.61}$$

in which $w(z,t)$ is an integration function that represents the average longitudinal displacement and $\omega(s)$ is the warping function (also termed as sectorial area) of the cross-section and can be determined [Vlasov 1961] by:

$$\omega(s) = \int_0^s h(s)\,ds \tag{2.62}$$

The sectorial area at point $p(x,y)$ is geometrically equal (Figure 2.11) to twice the area enclosed between the arc pS_o of the cross section and the two lines $S_c p$ and $S_o S_c$ which join the ends of the arc, i.e. $\omega = 2Area(S_c p S_o)$. The sectorial area is taken positive when radius $h(s)$ rotates in the counter-clockwise direction. The sectorial origin S_o is chosen so that the sectorial statical moment S_ω vanishes, i.e.,

$$S_\omega = \int_A \omega(s)\,dA = 0 \tag{2.63}$$

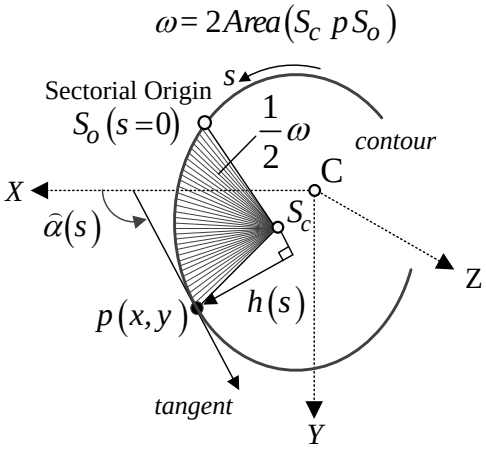

Figure (2.11): Sectorial area.

The last term in Equation (2.61) is responsible for warping of the middle surface of the cross section, also known as primary warping. In addition to primary warping, a secondary warping (or through thickness warping) arises. Secondary warping is proportional to the normal distance of a point from the corresponding point on the middle surface and thus gains

significance for thicker sections. The additional effect due to through thickness warping is accounted for in the theory of Gjelsvik (1981). The resulting governing differential equations based on Vlasov and Gjelsvik theories are identical. The only difference between both theories lies in the expressions of the warping constants.

Moment-Stress Relations

In Vlasov beam theory, three types of stresses are induced in the thin-walled member:

(i) longitudinal stresses σ_w due to bimoments, (ii) warping shear stress τ_w due to bimoments and (iii) St. Venant shear stress τ_{sv} due to twisting.

Longitudinal Normal Strain

The longitudinal normal strain at point $p(x,y)$ is ε_{zz} and can be obtained by differentiating Equation (2.61) with respect to z, yields:

$$\varepsilon_{zz} = \frac{\partial w_p}{\partial z} = w'(z,t) - x(s)u''(z,t) - y(s)v''(z,t) - \omega(s)\theta_z''(z,t) \tag{2.64}$$

Longitudinal Normal Stresses

The total normal stress $\sigma_{zz}(z,s,t)$ at the point $p(x,y)$ in the cross-section is given by:

$$\sigma_{zz}(z,s,t) = E\varepsilon_{zz} = E\left[w'(z,t) - x(s)u''(z,t) - y(s)v''(z,t) - \omega(s)\theta_z''(z,t)\right] \tag{2.65}$$

From Vlasov's beam theory (1961), the longitudinal stress $\sigma_w(z,s,t)$ induced by the warping restraint is:

$$\sigma_{zz}(z,s,t) = -E\omega(s)\theta_z''(z,t) \tag{2.66}$$

These normal stresses lead to the generalized force commonly referred to as the "bimoment" of the member [Vlasov 1961]:

$$M_w(z,s,t) = -\int_A \sigma_w(z,s,t)\omega(s)dA = EC_w\theta_z''(z,t) \tag{2.67}$$

in which the warping constant of the cross-section is defined as $C_w = \int_A [\omega(s)]^2 dA$. Combining Equations (2.66) and (2.67), the warping normal stress σ_w is obtained as:

$$\sigma_w(z,s,t) = -\frac{M_w(z,t)\omega(s)}{C_w} \tag{2.68}$$

The warping normal stress can be added to other stresses caused by shear forces and bending moments about the principal axes of the section. Then the total normal stresses caused by longitudinal force $N_z(z,t)$, bending moments $M_x(z,t), M_y(z,t)$ about X and Y principal axes and bimoments $M_w(z,t)$ at a point on the mid-line of the beam are:

$$\sigma_{zz}(z,s,t) = \frac{N_z(z,t)}{A} - \frac{M_y(z,t)}{I_{yy}}x(s) - \frac{M_x(z,t)}{I_{xx}}y(s) - \frac{M_w(z,t)}{C_w}\omega(s) \tag{2.69}$$

which $N_z(z,t) = \int_A \sigma_{zz}(z,s,t)dA$, $M_x(z,t) = -\int_A \sigma_{zz}(z,s,t)y(s)dA$, $M_y(z,t) = -\int_A \sigma_{zz}(z,s,t)x(s)dA$, $M_w(z,t) = -\int_A \sigma_{zz}(z,s,t)\omega(s)dA$, and $I_{yy} = \int_A x^2 dA$ is the second moment of inertia with respect to principal Y axis.

Orthogonality Conditions

In conventional solutions (e.g. Vlasov 1961), it is convenient to select an orthogonal system of coordinates to simplify the solution by enforcing the following conditions or integrals to zero:

$$S_x, S_y, S_{xy}, S_{\omega x}, S_{\omega y}, S_\omega = \int_A [x(s), y(s), x(s)y(s), x(s)\omega(s), y(s)\omega(s), \omega(s)]dA = 0 \tag{2.70}$$

where the first three integrals for S_x, S_y, S_{xy} are zero when the origin of the coordinate system is located at the centroid of the cross section and the axes *OX* and *OY* are the principal axes. Integrals given by $S_{\omega x}, S_{\omega y}$ can be satisfied by selecting the arbitrary point (pole) to be the shear centre of the cross-section. The sectorial origin S_o can be selected so that the last integral given by S_ω is satisfied. More details can be found in Erkmen (2006).

Internal Strain Energy, Kinetic Energy and Load Potential Energy

The internal strain energy U_v of the member has two contributions: one due to the normal stresses σ_{zz} and the other are due to St. Venant torsional shear stress τ_{zs}, and it is given by:

$$U_v = \frac{1}{2}\int_V E\,\varepsilon_{zz}^2\,dV + \frac{1}{2}\int_0^\ell GJ\left[\theta_z'\left(z,t\right)\right]^2 dz \tag{2.71}$$

By substituting the longitudinal strain expression in Equation (2.64) into Equation (2.71) and enforcing the orthogonality conditions (represented by Equation 2.70), leads to:

$$\delta U_v = \int_0^\ell \left[Ew'\delta w' + EI_{yy}u''\delta u'' + EI_{xx}v''\delta v'' + EC_w\theta_z''\delta\theta_z'' \right] dz \tag{2.72}$$

The variation of the work done by the applied distributed line loads per unit length acting along the member, (i) a longitudinal load $q_z\left(z,t\right)$, (ii) a transverse force $q_y\left(z,t\right)$, (iii) lateral force $q_x\left(z,t\right)$ and (iv) twisting moment $m_z\left(z,t\right)$ is:

$$\delta W_v = \int_0^\ell \left[q_z\left(z,t\right)\delta w\left(z,t\right) + q_x\left(z,t\right)\delta u\left(z,t\right) + q_y\left(z,t\right)\delta v\left(z,t\right) + m_z\left(z,t\right)\delta\theta_z\left(z,t\right) \right] dz \tag{2.73}$$

Therefore, the total potential strain energy $\delta\Pi_v$ is:

$$\begin{aligned}\delta\Pi_v = \int_0^\ell \big[& Ew'\delta w' + EI_{yy}u''\delta u'' + EI_{xx}v''\delta v'' + EC_w\theta_z''\delta\theta_z'' + GJ\theta_z'\delta\theta_z' - q_z\delta w \\ & - q_x\delta u - q_y\delta v - m_z\delta\theta_z \big] dz\end{aligned} \tag{2.74}$$

The kinetic energy T_v of the thin-walled member is given by:

$$T_v = \frac{1}{2}\int_0^\ell \int_A \rho\left[\left(\dot{\xi}\right)^2 + \left(\dot{\eta}\right)^2 + \left(\dot{w}_p\right)^2\right] dA\,dz \tag{2.75}$$

Substituting Equations (2.56), (2.57) and (2.61) into the kinetic energy Equation (2.75) and by performing the area integrals in the resulting equation and applying the orthogonality conditions represented by Equation (2.70), the variation of kinetic energy δT_v is given as:

$$\begin{aligned}\delta T_v = \int_0^\ell \rho\big[& A\dot{w}\,\delta\dot{w} + I_{yy}\dot{u}'\,\delta\dot{u}' + I_{xx}\dot{v}'\delta\dot{v}' + C_w\dot{\theta}_z'\delta\,\dot{\theta}_z' + A\left(\dot{u} + y_s\dot{\theta}_z\right)\delta\dot{u} + A\left(\dot{v} - x_s\dot{\theta}_z\right)\delta\dot{v} \\ & + A\left(y_s\dot{u} - x_s\dot{v} + r_o^2\dot{\theta}_z\right)\delta\dot{\theta}_z \big] dz\end{aligned} \tag{2.76}$$

in which $r_o^2 = \frac{1}{A}\int_A \left(h^2 + r^2\right) dA = \frac{\left(I_{xx} + I_{yy}\right)}{A} + \left(x_s^2 + y_s^2\right)$.

Dynamic Equations of Motion for Vlasov Thin-walled Beam

After performing integration by parts, the governing differential equations for dynamic equilibrium are obtained as:

$$EAw'' - \rho A\ddot{w} = q_z(z,t) \tag{2.77}$$

$$EI_{yy}u^{iv} - \rho I_{yy}\ddot{u}'' + \rho A\left[\ddot{u} + y_s\ddot{q}_z\right] = q_x(z,t) \tag{2.78}$$

$$EI_{xx}v^{iv} - \rho I_{xx}\ddot{v}'' + \rho A\left[\ddot{v} - x_s\ddot{q}_z\right] = q_y(z,t) \tag{2.79}$$

$$EC_w\theta_z^{iv} - \rho C_w\ddot{\theta}_z'' - GJ\theta_z'' + \rho A\left[y_s\ddot{u} - x_s\ddot{v} + r_o^2\ddot{\theta}_z\right] = m_z(z,t) \tag{2.80}$$

The associated boundary conditions are:

$$EAw'\delta w\Big|_0^\ell = 0 \tag{2.81}$$

$$EI_{yy}u''\delta u'\Big|_0^\ell = 0 \quad , \quad EI_{yy}u'''\delta u\Big|_0^\ell = 0 \tag{2.82}$$

$$EI_{xx}v''\delta v'\Big|_0^\ell = 0 \quad , \quad EI_{xx}v'''\delta v\Big|_0^\ell = 0 \tag{2.83}$$

$$EC_w\theta_z\delta\theta_z'\Big|_0^\ell = 0 \quad , \quad \left(EC_w\theta_z''' - GJ\theta_z'\right)\delta\theta_z\Big|_0^\ell = 0 \tag{2.84}$$

2.6 Review of Thin-walled Theories without Shear Deformation Effects

Friberg (1983) formulated the exact dynamic stiffness matrix finite element formulation of thin-walled beams for angle-sections. The coupled bending-torsion vibrations are studied under the effect of harmonic end excitation. The bending formulation used is based on Euler-Bernoulli beam theory and the torsion theory is that of the Saint-Venant theory and thus the warping of the cross-section is not considered in the analysis. Complex algebra is employed for developing the exact expressions for the displacement fields. The eigenfrequencies were developed for simply supported and clamped-clamped beams with an axis of symmetry, using the Wittrick and Williams's algorithm (1970). Leung (1985) applied the dynamic stiffness method to analyze the damped and undamped structural members subjected to exponentially varying harmonic excitations. In his formulation, single degree of freedom, i.e. flexural displacement, of a damped and undamped Euler-Bernoulli beam member are used and solved

to investigate the complete steady state response of nodal harmonically excited systems. The forced dynamic total response is directly determined without the need to extract the natural modes. Dokumaci (1987) derived the governing equations for free bending-torsion coupled equations for thin-walled members with cross-sections having a single axis of symmetry. In his study, he combined the flexural Euler-Bernoulli theory with the St. Venant torsional theory. The coupled natural frequencies for cantilever beams were determined and the influence of shear centre offset on natural frequencies and mode shapes were studied as well. Banarjee (1989) studied the free vibration behaviour of the bending-torsional coupled beam using the dynamic stiffness matrix method with focus on the behaviour of aircraft wings. Their dynamic stiffness matrix did not include the effects of shear deformation, rotatory inertia nor warping deformation. Their formulation is limited to monosymmetric sections. In a subsequent study, Banarjee (1991) extended his work in (1991) to investigate the bending-torsional coupled vibration for asymmetric thin-walled open beams. Based on his formulation, Banerjee developed a FORTRAN subroutine for computing the dynamic stiffness matrix of bending-torsion coupled beam. He used the subroutine to determine the natural frequencies and mode shapes for a cantilever beam with substantial coupling between the bending and torsional modes. Banarjee and Fisher (1992) extended the work of Banarjee (1989, 1991) to incorporate the effect of axial forces on the natural frequencies and mode shapes. In their study, the closed form explicit analytical expression for the dynamic stiffness matrix elements of a bending-torsional coupled vibration were formulated by solving the governing differential equations of motion. Numerical results were provided for examples of a cantilever and simply-supported beams of monosymmetric semi-circular cross sections. They investigated the influence of axial force on coupled bending-torsional frequencies of thin-walled beams. Based on the dynamic transfer matrix method (DTMM) and a 2D assembly model, Ohga et. al (1995) developed a procedure to predict the natural frequencies and mode shapes of thin-walled members. They applied their study for C-sections, I-sections and box-section. Eslimy-Isfahany et al. (1996a) and (1996b) developed a theory to investigate the response of a torsional-flexural behaviour of beams under deterministic and random excitations by using the normal mode method. The deterministic load on the beam was assumed to vary harmonically, whereas the random load was assumed to be Gaussian with stationary and ergodic properties. The effects of shear deformation, warping deformation and

rotatory inertia were neglected in their analysis. The influence of axial load on the dynamic response is taken into account in their first paper (1996a), while this effect is neglected in the second paper (1996). The analysis was applied to a cantilever aircraft wing. Significant coupling between bending and torsional modes of deformation was reported in their study. Based on the formulations in Banarjee (1989) and (1991), Banerjee (1999) derived the exact analytical expressions for the frequency equation and the corresponding mode shapes of coupled bending-torsion beam with cantilever end conditions using a symbolic Algebraic computation package "REDUCE". The results based on explicit expressions based on the Euler-Bernoulli beam hypothesis and St. Venant torsion theory are compared with the exact published results to verify the exactness and accuracy of the expressions. A new Dynamic Finite Element method (DFEM) for the free vibration analysis of coupled bending-torsional vibrations was presented by Hashemi and Richard (2000a). In their approach, the classical finite element method was combined with dynamic stiffness method to develop a superior finite element model. Based on the Euler-Bernoulli and Saint-Venant beam theories, the exact solutions of the governing differential equations of uncoupled motions were utilized to formulate shape functions. The shape functions are frequency dependent and were employed to evaluate the stiffness and mass matrices. The warping rigidity of the beam cross-section, shear deformation, and rotary inertia are neglected in the analysis. The theory is applied to free vibration analysis of members of open section and closed sections. The numerical results obtained by using the dynamic finite element were in very good agreement with those obtained in the literature by using the exact dynamic stiffness matrix approach. In a subsequent paper, Hashemi and Richard (2000b) developed a dynamic finite element formulation for coupled bending-torsional vibration of axially loaded members with asymmetric cross-sections based on the Bernoulli-Euler and St. Venant beam theories. The shear deformation and the warping stiffness of the beam cross section were neglected. Based on the exact solution of the differential equations governing the uncoupled vibrations, they formulated the frequency dependent shape functions. Consequently, exploiting the principle of virtual work and interpolating the variables based on dynamic trigonometric shape functions, the exact dynamic finite element formulations for uniform beams are derived. The applicability of the DFEM is demonstrated for a beam with semi-circular cross- section. Also, the effect of the axial force on the natural frequencies for coupled bending-torsional thin-

walled beams is also studied in this paper. By using the dynamic stiffness matrix method, Banerjee and Su (2006) analyzed the free vibration of coupled bending-torsional coupled beams. The governing differential equations of motion for free vibration were derived based on the Hamilton's principle and then solved under the applicable boundary conditions to obtain the analytical expressions for generalized displacements, internal forces, and moments, which were obtained in exact sense. These expressions were then recast in the form of the dynamic stiffness matrix.

Table (2.1) provides a comparative summary of free vibration of thin-walled beam theories which do not include the effects of shear deformation, warping deformation and rotary inertia.

Table (2.1): Summary of comparative review for studies of free vibration analysis of Euler-Bernoulli-St. Venant beam theories which neglect shear deformation, warping and rotary inertia effects

No	Author	Cross Section	Method of Solution			Field variables	Static Load effect included	Remarks
			Dynamic stiffness matrix	Closed form solution	Finite element solution			
1	Hallauer and Liu (1982)	Mono-symmetric Closed	√	√	-	v,θ_z	-	- Coupled bending-torsion vibration - Cantilever three beam wing
2	Friberg (1983)	Asymmetric L-shape	√	√	-	w,v,u,θ_z	-	- Coupled bending-torsional vibration - Clamped and simply supported beams
3	Dokumaci (1987)	Mono-symmetric Closed	×	√	-	v,θ_z	-	- Coupled bending-torsion vibration - Clamped beam
4	Banerjee (1989)	Mono-symmetric Closed	√	√	-	v,θ_z	-	- Coupled bending-torsional vibration - -Cantilever open box beam
5	Banerjee (1991)	Asymmetric C-shaped	√	√	-	v,θ_z	-	- Coupled bending-torsional vibration - Cantilever wing beam
6	Banerjee and Fisher (1992)	Mono-symmetric Closed	√	√	-	v,θ_z	axial force	-Coupled bending-torsion vibration -Cantilever and hinged-hinged beams
7	Banerjee and Butler (1994)	Doubly symmetric Closed	√	√	-	w,θ_z	-	-Coupled extension-torsion vibration - Composite beam theory - Cantilever box section beam

Cont. Table (2.1): Summary of comparative review for studies of free vibration analysis of Euler-Bernoulli-St. Venant beam theories which neglect shear deformation, warping and rotary inertia effects

No	Author	Cross Section	Method of Solution			Field variables	Static Load effect included	Remarks
			Dynamic stiffness matrix	Closed form solution	Finite element solution			
8	Banerjee (1999)	Mono-symmetric Closed	-		-	v, θ_z	-	-Coupled bending-torsional vibration - Cantilever wing beam
9	Hashemi and Richard (2000a)	Mono-symmetric Closed	√	√	√	v, θ_z	-	-Finite element method combined with dynamic stiffness method to develop a dynamic finite element -Cantilever beams
10	Hashemi and Richard (2000b)	Mono-symmetric Closed	√	√	√	v, θ_z	axial force	-Coupled bending-torsion vibration -Cantilever beams
11	Banerjee and Su (2006)	Asymmetric Closed	√	√	×	u, v, θ_z	-	- Coupled bending-torsional vibration -Cantilever aircraft wings - Wittrick-Williams algorithm.

2.7 Review of Thin-Walled Theories with Shear Deformation Effects

Shear deformation plays an important factor in dynamic problems where higher modes of vibrations are to be determined or where the beam is subjected to harmonic forces with high frequencies. Because of this, the effect of shear deformation has been well studied in dynamic analysis of beams. The Timoshenko beam theory [Timoshenko 1937] is based on the assumption that the plane normal to the beam axis before deformation remains plane but not normal to the beam axis after deformation. Thus, unlike the Euler-Bernoulli beam and the Vlasov theories, it incorporates the effect of shear deformation. Banerjee and Williams (1992) derived the exact dynamic stiffness matrix of a thin-walled beam element taking into account the effects of shear deformation and rotary inertia, by solving the governing equations of motion of the free vibration of the beam. The natural frequencies and mode shapes of the beam are numerically computed based on the explicit expressions for the dynamic stiffness matrix. By incorporating the effect of axial force on the free vibration, Banerjee and Williams (1994) formulated the analytical expressions for coupled flexural-torsional dynamic stiffness matrix of an axially loaded uniform Timoshenko beam based on the Hamilton variational principle. An exact solution of the governing partial differential equations of motion was developed. The effect of warping deformation was neglected in the formulation. Numerical results demonstrate the influences of axial force, shear deformation and rotary inertia on the natural frequencies of the coupled bending-torsion behaviour for cantilever beams with semi-circular thin-walled sections. Banerjee (2000) derived the exact expressions for the frequency equation and mode shapes for coupled bending and torsion vibrations of uniform Timoshenko beams with cantilever end conditions. The effect of axial force together with the effect of shear deformation and rotary inertia was taken into account in the formulation. The method is demonstrated by an illustrative example of a coupled bending-torsion cantilever beam with semi-circular cross-section for which published results are available [Friberg 1985]. The results for frequencies and mode shapes agreed well with those published in Friberg (1985) and Banerjee and Williams (1994) based on the exact dynamic stiffness matrix method.

A comparative summary for thin-walled beam theories including the shear deformation and rotary inertia effects are presented in Table (2.2).

Table (2.2): Summary of comparative review for studies of free vibration analysis of thin-walled beam theories which include shear deformation and rotary inertia effects

No.	Author	Cross Section	Method of Solution		Static load effect included	Remarks
			Dynamic stiffness matrix	Closed form solution		
1	Banerjee and Williams (1992)	Mono-symmetric Closed	√	√	-	-Coupled bending and torsional vibration -Formulation captured shear deformation due to bending
2	Banerjee and Williams (1994)	Mono-symmetric Closed	√	√	axial force	-Coupled bending and torsional vibration -Cantilever end conditions -Symbolic computing package REDUC
3	Banerjee (2000)	T-section	×	√	axial force	-Bending-torsion coupled vibration -Cantilever beam

2.8 Review of Thin-Walled Beam Theories involving Warping Deformation Effects

The torsional response of most thin-walled beams of open cross-sections is significantly influenced by constraining the cross-section's ability to warp. The warping deformation of thin-walled open-sections generally consist of two parts; the contour or section profile warping (also known as primary warping), and the through-thickness warping (called as the secondary warping). Vlasov (1961) and many other authors considered only the contour warping deformation, while Gjelsvik (1981) added the secondary warping function to the formulation.

2.8.1 Thin-Walled Beam Theories excluding Shear Deformation

The Vlasov thin-walled beam theory (Vlasov 1961) is based on two assumptions, these are; (i) the cross section of a beam remains undeformed (or rigid) after deformation, and (ii) the shear strain in the middle surface is neglected. In other words, Vlasov torsion theory for thin-walled beams considers the warping stiffness of the beam cross section but neglects the shear deformation effects at the middle surface. The theory formulated by Vlasov (1961) is extensively used in the dynamic analysis of thin-walled, open section beams, as exemplified by the studies of Friberg (1985), Leung (1991), Chen and Tamma (1994), and others, all discussed in the following: Friberg (1985) formulated the exact dynamic stiffness matrix for a thin-walled beam in coupled flexural and torsion vibrations. He accounted for the effects of warping deformation, rotary inertia and axial load by using Vlasov's theory and numerically developed the 14x14 dynamic stiffness matrix. A FORTRAN program and a numerical example are presented to evaluate the eigenfrequencies of a uniform beam with general open section and with various boundary conditions. The eigenfrequencies results for a free-clamped beam with semicircular cross section are evaluated by using the well-established Wittrick-Williams algorithm [Wittrick and Williams 1971]. Bishop et al. (1989) extended the study of Dokumaci (1987) by including the effect of warping of the beam cross section. They concluded that the neglect of warping deformation effect can lead to significant errors in estimating the natural frequencies of thin-walled members. Leung (1991) presented a numerical procedure for developing the exact dynamic stiffness matrix of a thin-walled beam based on Vlasov theory. The effect of shear deformation is neglected in the formulation, while the effects of warping deformation and rotary inertia are taken into account. The homogeneous form of the governing equations for static equilibrium were solved exactly and the transverse, lateral and rotational

displacement functions, all coupled due to the presence of the axial force, were developed in the study. Leung developed a Vlasov finite element based on the exact static shape functions. The results were observed to rapidly converge to the eigen-frequencies in free vibration analysis. In a subsequent study, Leung (1992) developed the dynamic stiffness matrix method (DSMM) to analyze a thin-walled beam of open section subjected to constant axial compressive force and in-plane moments. The dynamic stiffness matrix is formulated by frequency-dependent shape functions which satisfy the exact solutions of the governing differential equations. The effects of rotary inertia, warping stiffness and axial force are accounted for in the analysis. The dynamic stiffness method is extended to analyze the lateral buckling of monosymmetric open thin-walled beams under the influence of axial force and in-plane moments. Numerical results for a clamped-free thin-walled beam representing a semi-circular tube are presented and demonstrated that the constant in-plane moment softens the flexural modes while preventing the torsional modes. Chen and Tamma (1994) employed the finite element method in conjunction with an implicit – starting unconditionally stable numeric integration methodology for the coupled vibrations of an elastic thin-walled member of arbitrary open cross-section subjected to constant axial force. The governing equations of motion for thin-walled beam are derived using the principle of virtual work. The formulations are based on Vlasov's assumptions and rotary inertia effects were included in the formulation. Three examples dealing with triple coupling (L-shaped cross-section), double coupling (C-shaped cross section) and no coupling (I-shaped cross-section) were provided to demonstrate the coupling effects and rotary inertia on the forced vibrations characteristics of thin-walled beams. The dynamic response, displacements and rotation, of both simply supported and cantilever beams with and without rotary inertia effects are obtained in graphical forms. Numerical results indicated that, the effect of rotary inertia on displacement and rotation angle is insignificant. Li and Smith (1994) formulated expressions for calculating the torsional vibration frequencies and mode shapes of open thin-walled beams. The theoretical expressions are obtained for three boundary conditions: clamped-clamped, hinged-hinged, and free-free end conditions. The effect of warping rigidity on torsional natural frequencies for a beam with I-shaped cross-section is demonstrated via numerical examples. Results for beams with free-free and hinged-hinged end conditions showed that torsional natural frequencies of beams with high width to depth ratio are more sensitive to the effects of warping rigidity. Banerjee et. al (1996) extended the previous theory (Banerjee 1989) to develop the dynamic

stiffness matrix of coupled bending-torsion beams with monosymmetric open cross-sections to include the effect of warping deformation. They studied the effect of warping deformation on the natural frequencies of thin-walled beams with monosymmetric C-sections and various boundary conditions. Based on their results, the warping deformation has a profound significant influence on the natural frequencies of the beam. They concluded that the warping deformation effect induced large errors when ignored. By using the finite element method, Tanaka and Bercin (1997) studied the coupled bending and torsional free vibration of thin-walled beams of asymmetric open cross-section. The study accounts for the warping deformation and rotary inertia effects. The stiffness and mass matrices for coupled bending-torsion beam elements were determined by employing the linear interpolation for longitudinal displacements and cubic Hermitian shape functions for transverse, lateral displacements and angle of twist. The coupled natural frequencies for thin-walled open beam with asymmetric and mono-symmetric cross sections are computed for various boundary conditions. Tanaka and Bercin (1999) studied the triple coupling free vibration behaviour of thin-walled beam with asymmetric open sections. The governing equations for the coupled bending and torsional vibrations of beams capturing the warping deformation effects are solved in an exact sense. Results for free vibration of beams with various boundary conditions were developed in the study. Arpaci and Bozdag (2002) developed the governing differential equations of motion based on non-orthogonal coordinates derived by Tanaka and Bercin (1999) by including the product of inertia terms in the formulation of bending deformations. They investigated the triply coupled vibrations of thin-walled beams with asymmetric open cross sections. The governing differential equations for coupled bending and torsional vibrations are derived using the d'Alembert principle and solved exactly. The natural frequencies and mode shapes of thin-walled beams with asymmetric channel and Z cross sections are provided under various boundary conditions. Arpaci et. al (2003) extended their work (Arpaci and Bozdag 2002) to include the effect of rotary inertia on the triply coupled vibration analysis of thin-walled beams of open asymmetric cross section. They presented the exact analytical solution of the system of equations for predicting the undamped natural frequencies. The influences of rotary inertia and warping stiffness were included in the analysis. Based on the results obtained, the effect of rotary inertia was observed to lead to the decrease of the natural frequencies predicted. Kim et. al (2003a) conducted a free vibration analysis for the flexural–torsional behaviour of uniform thin-walled beams with asymmetric sections under

eccentric axial loads. The effect of rotary inertia was taken into account in the analysis. The resulting high-order ordinary simultaneous differential equations were transformed into first-order simultaneous differential equations by introducing a displacement state vector consisting of 14 displacement parameters. The associated linear eigen-value problem with non-symmetric matrices was obtained. The displacement functions were exactly obtained and the dynamic exact stiffness matrices evaluated using force-deformation relationships. Comparison with finite element solutions using ABAQUS's shell element were conducted. Voros (2004) analyzed the free coupled vibration of thin-walled beams with asymmetric open cross sections. The formulation captured the warping deformation effect. In this study, 14-degrees of freedom finite element model for the free vibration is developed, in which the kinetic energy expression is obtained based on the lumped and consistent mass matrices. The derivation of the element stiffness matrix, lumped and consistent mass matrices are based on the assumed linear interpolation functions for longitudinal displacement and cubic interpolation functions for transverse, lateral displacements and the angle of twist. The influence of warping stiffness and the lumped mass matrix on the natural frequencies was investigated for cantilever and simply-supported beams with I and U sections. Li et. al (2004a) derived the dynamic transfer matrix by solving the governing differential equations of motion for coupled bending-torsion vibration for uniform axially loaded members with mono-symmetric open cross sections. The method takes into account the effects of axial load and warping deformation while neglecting the rotary inertia. Numerical results of natural frequencies and mode shapes were presented and compared with the available results in the literature. Using the modal superposition method (MSM), Li et al. (2004b) investigated the dynamic flexure-torsion coupled vibrations of axially loaded mono-symmetric thin-walled beams. The influence of axial force and cross-sectional warping deformation on the coupled bending-torsional frequencies and mode shapes are studied. Li et al (2004c) extended their previous work to develop the dynamic transfer matrix to compute the natural frequencies and mode shapes of axially loaded thin-walled beams with asymmetric opened cross sections, in which the effect of warping deformation of the cross section is included. The transfer matrix is derived from the differential equations of motion for beams under axial force using d'Alembert principle. The application of the dynamic transfer matrix is illustrated by numerical results for natural frequencies and mode shapes of the beams with various boundary conditions. The influences of axial force and warping stiffness on the coupled

bending-torsional frequencies are also studied. Mohri et. al (2004) investigated the dynamic behavior of pre-buckled and post-buckled thin-walled composite open sections. Using Hamilton's principle, they formulated the governing differential equations of motion based on Vlasov's assumptions and a non-linear model that accounts for the non-linear warping and bending-torsion couplings. The Galerkin's approach is employed to reduce the developed differential equations to a non-linear coupled differential system in the time domain. The model is used for the vibration analysis in pre-buckling and post-buckling analyses under axial compression and transverse loads. Analytical solutions are derived for the eigen-frequencies of doubly symmetric I-sections, and mono-symmetric T-sections are developed for general cross sections. Numerical results are obtained for the free vibrations of pre-buckled and post-buckled simply-supported thin-walled elements under axial and transverse loads for doubly symmetric and monosymmetric sections. Prokic (2005) derived a system of equations for triply coupled free vibrations of thin-walled beams with general open cross sections including the effects of rotary inertia and warping deformation. The governing differential equations for coupled bending-torsion vibrations are performed using the principle of virtual work. The closed-form solutions are derived for the natural frequencies for free vibration of simply-supported thin-walled of asymmetric cross-sections. Comparisons were made between solutions including and excluding the warping deformations and rotary inertia effects. In Bin and Leung (2006), the dynamic stiffness matrix of open thin-walled beams is explicitly derived by employing frequency dependent shape functions obtained based on the exact solutions of the governing differential equations for free vibration of beams. The effects of warping deformation, rotary inertia and axial force were modelled using power series expansions. The influence of axial force on the natural frequencies and flexural and torsional modes of the thin-walled beam was studied. Chen and Hsiao (2007) analyzed the coupled axial-torsional vibration of the thin-walled beam of Z-section. The governing differential equations for linear axial and torsional vibration of thin-walled Z-section members based on Vlasov beam theory are derived using the d'Alembert principle and the principle of virtual work. The natural frequencies of axial and torsional vibration were obtained by solving the homogeneous equations using the bisection method. The influence of the warping function is studied on the natural frequencies and mode shapes. Kim et. al (2007) developed new static and dynamic stiffness matrices for spatially coupled flexural-torsional stability analysis and free vibration analysis of thin-walled beam with asymmetric

cross-section subjected to linearly varying axial force. Their theory is developed based on Vlasov's kinematics assumptions and the static and dynamic stiffness matrices are derived based on the power series method. Additionally, the authors derived the static stiffness matrix for the lateral buckling analysis of asymmetric thin-walled beams. The governing equations of motion and force-deformation relations are derived from the principle of stationary total potential energy by including in the formulation the second order terms of the rotations. Explicit expressions for displacement parameters are derived based on power series expansions of the displacement fields. The effects of constant and linearly variable axial compressive force on the buckling behaviour and vibration response of asymmetric thin-walled beam are investigated. The accuracy and validity of the proposed study are assessed via illustrative numerical examples and then compared with the finite element solutions based on Hermtian interpolations and ABAQUS's shell solution. The numerical examples demonstrated that results based on their study using a single element showed excellent agreement with the finite element solutions using multiple Hermitian beam elements and ABAQUS's shell solution. Voros (2008 and 2009) investigated the bending-torsional coupled vibration of thin-walled beams of arbitrary open cross-section subjected to vertical loads. In these papers, the formulation accounts for large rotations and is based on Euler-Bernoulli beam theory for bending and Vlasov thin-walled beam theory for torsion. The governing differential equations of motion are derived using the principle of virtual work. The closed-form solutions for free vibration analysis were developed for the coupled bending-torsional frequencies of thin-walled beams of doubly symmetric and monosymmetric I-sections under uniform bending moment for simply-supported beams. In order to solve the governing equations, a finite element with two nodes and fourteen degrees of freedom is developed, in which the shape functions were linear and third-order Hermitian polynomials are adopted to interpolate the displacements. Altintas (2010) derived the governing equations of motion of asymmetric axially loaded thin-walled beam including the warping stiffness effect using d'Alembert's principle. The model solution of the field equations for the triply coupled vibrations is based on the finite difference method. The effect of material properties (i.e. shear modulus, elasticity modulus, Poisson' ratio and mass density) on the coupled bending-torsion natural frequencies of an unloaded beam are investigated. Further results illustrate the effect of axial force on the natural frequencies. Lately, Prokic and Lukic (2012) studied the bending-torsional coupled vibrations analysis of thin-walled beam of arbitrary open cross-section. Using

the principle of virtual displacements, the governing field equations of motion based on Vlasov beam theory were derived. The effects of axial force, warping deformation and rotary inertia were incorporated in their formulation. The solution for the coupled natural frequencies of free harmonic vibrations was derived and exactly solved for simply-supported thin-walled beams.
The summary of comparative review for studies of free vibration analysis of thin-walled theories involving warping deformation effect and excluding the effect of shear deformation is provided in Table (2.3).

2.8.2 Thin-walled Beam Theory Including Shear Deformation Effects

Although the Vlasov theory for thin-walled members of open cross-sections is well established, it presents limitations in the dynamic analysis of thin-walled open members when the higher natural frequencies are required or when the member is subject to high exciting frequencies. The range of applicability of the Vlasov's beam theory can be extended by taking into consideration shear deformation effects. Towards this goal, a number of studies dealing with coupled vibrations of thin-walled open members based on generalized Vlasov-Timoshenko beam theories were developed. Rao (1974) studied the free torsional vibration of thin-walled open members of doubly symmetric I-sections. His study incorporated the effects of longitudinal inertia and shear deformation. The solutions of the frequency equations are numerically solved and the first two torsional vibration modes for various boundary conditions are presented in his study. Bishop and Price (1985) studied the free vibration of thin-walled members with channel sections using two beam theories, the modified Timoshenko-Vlasov beam theory and the conventional Vlasov beam theory. A comparison of the mathematical models for both beam theories illustrates that both theoretical models contain warping terms, but the modified Timoshenko model has extra shear rigidity terms. Their predictions of the natural frequencies and mode shapes obtained under both theories show that lower natural frequencies and modes of the beams for various end conditions are generally in reasonable agreement with each other and with measured results. Laudiero and Savoia (1991) studied the flexural-torsional vibrations of thin-walled beams with open and closed cross-sections. Their study accounted for the effect of the shear strains due to non-uniform bending and torsion. The effect of secondary warping deformation and shear lag are also included in the formulation. By using the Hamilton variational principle, a system of nine differential equations was derived for the dynamic equilibrium of the beam subjected to non-

Table (2.3): Summary of comparative review for studies of free vibration analysis of thin-walled theories which capture warping effect and ignore shear deformation effect

No.	Author	Cross Section	Method of Solution			Field variables	Rotary Inertia effect included	Static load effect included	Remarks
			Dynamic stiffness matrix	Closed form solution	Finite element solution				
1	Friberg (1985)	Asymmetric C-shaped	√	√	-	w,u,v,θ_z	√	Axial force	-Coupled bending-torsion vibration -FORTRAN program used to solve the generalized linear eigen-value problem -Clamped-free beam
2	Bishop et. al (1989)	Mono-symmetric C-shaped	-	√	-	v,θ_z	-	-	-Coupled bending-torsion vibration -Closed form solution for beam with free-free end conditions
3	Zhang and Chen (1990)	Doubly symmetric	-	√	√	θ_z	-	-	-Torsional vibration for thin-walled open/closed sections -Dynamic finite element method used based on the homogeneous solution of the field equation
4	Leung (1991)	Asymmetric C-shaped	-	√	√	u,v,θ_z	√	Axial force	-Finite element formulation used shape functions based on the static solution of the governing equations
5	Leung (1992)	Asymmetric C-shaped	√	√	-	u,v,θ_z	√	Axial force and in-plane moments	-Coupled bending-torsion vibration

Cont. Table (2.3): Summary of comparative review for studies of free vibration analysis of thin-walled theories which capture warping effect and ignore shear deformation effect

No.	Author	Cross Section	Method of Solution			Field variables	Rotary Inertia effect	Static load effect included	Remarks
			Dynamic stiffness matrix	Closed form solution	Finite element solution				
6	Chen and Tamma (1994)	Asymmetric Opened	-	-	√	w,u,v,θ_z	√	-	-Finite element formulation used in conjunction with an numerical implicit method -General dynamic loads -Dynamic response for simply-supported and cantilever beams
7	Li et. al (1994)	Doubly symmetric I-shaped	-	√	-	θ_z	-	-	-Torsional vibration -Closed form solutions obtained for various boundary conditions
8	Banerjee et. al (1996)	Mono-symmetric C-section	√	√	-	v,θ_z	-	-	-Coupled bending-torsion vibration -Various boundary conditions
9	Tanaka and Bercin (1997)	Asymmetric opened	-	-	√	u,v,θ_z	√	-	-Finite element formulation based on Hermite shape functions -Coupled bending-torsion vibration -Various boundary conditions
10	Tanaka and Bercin (1999)	Asymmetric C-shaped	-	√	-	u,v,θ_z	√	-	-Closed form solutions for various boundary conditions -Various boundary conditions

Cont. Table (2.3): Summary of comparative review for studies of free vibration analysis of thin-walled theories which capture warping effect and ignore shear deformation effect

No.	Author	Cross Section	Method of Solution			Field variables	Rotary Inertia effect included	Static load effect included	Remarks
			Dynamic stiffness matrix	Closed form solution	Finite element solution				
11	Arpaci and Bozdag (2002)	Asymmetric C-shaped	-	√	-	u,v,θ_z	√	-	-Coupled bending-torsion equations -General coordinate system -Product of inertia included
12	Arpaci and Bozdag (2003)	Asymmetric C-shaped	-	√	-	u,v,θ_z	√	-	-Coupled bending-torsion vibrations -Principal coordinate system
13	Kim et. al (2003a)	Asymmetric Open section	√	√	-	w,u,v,θ_z	√	-	-Equations of motion and force-displacement relations based on semitangential rotations and semitangential moments.
14	Li et al. (2004a)	Mono-symmetric C-section	-	√	-	v,θ_z	-	Axial force	-Dynamic transfer matrix method -Coupled bending-torsional vibrations
15	Voros (2004)	Asymmetric Opened	-	-	√	w,u,v,θ_z	√	-	-Consistent and lumped mass matrices -Hermitian functions used in the finite element formulation

Cont. Table (2.3): Summary of comparative review for studies of free vibration analysis of thin-walled theories which capture warping effect and ignore shear deformation effect

No.	Author	Cross Section	Method of Solution			Field variables	Rotary Inertia effect included	Static load effect included	Remarks
			Dynamic stiffness matrix	Closed form solution	Finite element solution				
16	Li et al. (2004b)	Mono-symmetric C-section	-	√	-	v,θ_z	-	-	-Damping effect included -Forced dynamic bending-torsion coupled vibrations -Normal mode method -Monosymmetric cantilever beam
17	Li et al. (2004c)	Asymmetric Opened	-	√	-	u,v,θ_z	-	Axial force	-Dynamic transfer matrix -Coupled bending-torsional vibrations -Asymmetric cantilever beam
18	Mohri et al. (2004)	Asymmetric Opened	-	-	-	u,v,θ_z	√	Axial and in-plane bending	-Large rotation -The vibration behaviour of pre- and post-buckled
19	Prokic (2005)	Asymmetric Opened	-	√	-	w,u,v,θ_z	√	-	-Coupled bending-torsional vibrations -Principle of virtual displacements -Simply-supported beam
20	Bin and Leung (2006)	Asymmetric section	√	√	-	u,v,θ_z	√	Axial force and biaxial moments	-Power series used to solve the governing coupled bending-torsion equations

Cont. Table (2.3): Summary of comparative review for studies of free vibration analysis of thin-walled theories which capture warping effect and ignore shear deformation effect

No.	Author	Cross Section	Method of Solution			Field variables	Rotary Inertia effect included	Type of applied Load	Remarks
			Dynamic stiffness matrix	Closed form solution	Finite element solution				
21	Chen and Hsiao (2007)	Asymmetric Z-shaped	-	√	-	w,θ_z	-	-	-Uncoupled longitudinal-torsional vibrations -d'Alembert and virtual work principles
22	Kim et al. (2007)	Asymmetric Opened	√	√	√	u,v,θ_z	√	-	-Field equations and force-displacement relations based on semitangential rotations -Closed form solution derived using power series -Hermitian functions used for finite element formulation
23	Voros (2008 and 2009)	Asymmetric Opened	-	√	√	w,u,v,θ_z	√	Vertical force	-Virtual work principle - Account for large rotations -Hermitian functions used in finite element formulation
24	Altintas (2010)	Asymmetric Opened	-	√	-	u,v,θ_z	-	Axial force	-Coupled bending-torsion vibration -Finite difference method
25	Prokic (2012)	Asymmetric Opened	-	√	-	w,u,v,θ_z	√	Axial force	-Coupled bending-torsion vibration -Principle of virtual displacements -Simply-supported beam

uniform bending and torsion. The formulation retains the first Vlasov assumption while incorporating shear deformation effects through a generalized Timoshenko hypothesis. A discrete approach based on trigonometric series expansions was developed for the general of coupled flexural-torsional vibrations of beams subject to general boundary conditions. The coupled bending-torsion natural frequencies are obtained for simply supported and cantilever beams and compared with previously published results. The study demonstrates the significant influence of warping effect and shear lag on the behaviour of thin-walled beams. Hu et al (1996) derived a fourth order governing equations for thin-walled beams with asymmetric sections under coupled bending and torsion. The governing equations of motion are formulated according to the Vlasov assumption of rigid body cross-section and the Kollbrunner-Hajdin assumption for the warping displacement, in which the axial displacement *w* due to warping of a point within the cross-section is the product of the warping function $\hat{\chi}(z)$ and the sectorial coordinate $\omega(s)$, i.e., $w = -\hat{\chi}(z)\omega(s)$, where $\omega(s) = \int_0^s \left[h(s) - \left(\hat{\Psi}/t\right) \right] ds$, and $\hat{\Psi} = \tau_B t / G\theta_z'$ is the torsional function, which determines the distribution of Bredt stress over the cross-section and is dependent only on the geometry of the cross-section. The stiffness matrix and consistent mass matrix were developed based on interpolation functions based on the homogeneous solutions to the fourth order governing differential equations. The shear deformation effect and the coupling between bending and torsion are fully taken into account in the finite element developed. Bercin and Tanaka (1997) studied the coupled flexural-torsional free vibrations of thin-walled members of monosymmetric open cross-sections. The effects of warping stiffness, shear deformation and rotatory inertia were taken into account in the formulations. The warping and shear deformation effects on natural frequencies and mode shapes for cantilever beams were reported in the study. Results obtained demonstrate that the natural frequencies increase when warping effects are included and decrease if shear deformation effects are included. Tanaka and Bercin (1998) employed the symbolic computation package "Mathematica" for the determination of coupled frequencies of asymmetric cross-section thin-walled beams including the effects of shear deformation, warping stiffness and rotary inertia. The natural frequencies of asymmetric thin-walled beams are determined for a variety of boundary conditions. Kim et al. (2003b) developed the theory by Kim et al (2003a) to obtain the exact dynamic and static stiffness matrices for the free vibration and stability analysis of thin-walled shear-deformable beams with

asymmetric cross-sections. Their study included shear deformation effects due to the shear forces and the warping torsion and captures the coupled effects between both effects. Also incorporated were the rotary inertia effects and the flexural-torsional coupling effects due to the asymmetry of the cross-sections. Comparison were conducted for cantilever, simply supported, and fixed end beams under an axial load against previous analytical results and finite element solutions using thin-walled beam elements and ABAQUS's shell element. The numerical results for spatially coupled natural frequencies and buckling loads of thin-walled beam-columns have shown good agreement with other numerical solutions available in the literature. The influences of the shear deformation and axial load on the vibration behaviour and stability of asymmetric thin-walled beams are investigated in the study. Referring to their previous studies [Li et al. 2004a, b, c], Li et. al (2004e) extended their study to improve the dynamic transfer matrix method for the dynamic coupled vibrations of uniform shear deformable thin-walled beam with mono-symmetric cross-section subjected to uniform axial force. The dynamic transfer method is employed to evaluate the natural frequencies and mode shapes. Based on a continuous beam model, the influences of shear deformation, warping deformation, rotary inertia, and axial force are included in the formulation. The bending-torsion coupled differential equations of motion are derived using d'Alembert principle and the dynamic transfer matrix is directly formulated by solving these equations. The method is applied to a semi-circular and channel cross-sections and the effects of bending-torsion coupling, axial force, shear deformation, warping deformation, and rotary inertia is investigated. The numerical results obtained showed good agreement with the results in Friberg (1985) and Bercin and Tanaka (1997). Based on their previous work (2003a, b), Kim and Kim (2005) adopted an improved method to evaluate the exact static element stiffness matrix for the flexural-torsional buckling analysis of asymmetric shear-deformable thin-walled beams and exact dynamic stiffness matrix for flexural-torsional free vibration analysis. In their analysis, they included the influence of: (i) shear deformations due to bending and warping torsion, (ii) coupled shear deformation (CSD) effects between shear forces and restrained warping, (iii) rotary inertia and, (iii) the flexural-torsional coupling due to the cross-section asymmetry. By applying the Hellinger-Reissner Principle, the governing equations of motion for coupled vibration responses of thin-walled beams with asymmetric cross-sections and the force-deformation relations are derived. They developed an isoparametric finite element with two-nodes and seven nodal degrees of freedom per a node. Numerical results for frequencies and the

lateral-torsional displacements of thin-walled beams with open and closed cross-sections and different boundary conditions are determined and compared with other analytical solutions results available in the literature. Prokic (2006) analyzed the fivefold coupled vibration of thin-walled beams of asymmetric open cross sections including the effects of shear deformation, warping stiffness and rotary inertia. The governing differential equations of motions for coupled bending-torsional-shearing vibrations are formulated using the virtual work principle. The closed-form solutions for the natural frequencies of free harmonic vibrations are derived for simply-supported thin-walled beams. The analytical expressions for natural frequencies are determined using the symbolic computing package Mathcad. The natural frequencies of simply supported asymmetric thin-walled beams with coupled deformation modes are computed for various cross sections. Ambrosini (2009) presented a general theory of coupled flexure and torsion free vibrations of thin-walled beams of asymmetric open cross sections. The governing differential equations of motion derived are based on Vlasov's thin-walled beam theory and are modified to capture the effect of shear deformation. The free vibration results for asymmetric thin-walled beams are numerically and experimentally obtained for various boundary conditions. Comparison with the finite element solutions were also provided in the study. The experimental studies showed very good agreement with the results obtained by the present theory. De Borbon and Ambrosini (2010) extended the theory for coupled flexure and torsion vibrations of thin-walled beams presented by Ambrosini (2009) to include influence of the axial forces. Numerical results based on the system of equations developed are presented and the influence of the constant axial force on the free vibration results is investigated. In Ambrosini (2010), an experimental study for free vibration of thin-walled beams with asymmetric open cross section is presented in order to provide experimental data to be used for checking the accuracy of different theoretical approaches. In this study, the system of equations based on Vlasov's theory of thin-walled beams is modeled to capture the effects of rotary inertia and shear deformation. Numerical results for natural frequencies of the open asymmetric thin-walled cantilever beams based on theoretical solution are given for comparison with measured natural frequencies results as well as those based on the finite element software SAP2000. Table (2.4) presents the summary of comparative review for studies of free vibration analysis of thin-walled theories involving warping deformation effect and shear deformation effect.

Table (2.4): Summary of comparative review for studies of free vibration analysis of thin-walled theories which capture warping and shear deformation effects

No.	Author	Cross Section	Method of Solution			Field variables	Rotary inertia effect included	Static load effect included	Remarks
			Dynamic stiffness matrix	Closed form solution	Finite element solution				
1	Rao et. al (1974)	I- Double symmetric	-	√	-	θ_z ,ψ	-	-	-Longitudinal inertia captured in the formulation - Torsional vibration analysis
2	Laudiero and Savoia (1991)	Asymmetric closed-open section	-	-	-	w,u,v,θ_x θ_y ,θ_z ,ψ χ_x ,χ_y ,χ_o	√	-	-Coupled equations derived using Hamilton's principle -General dynamic forces -Formulation captured shear lag and secondary warping
3	Kim et. al (1994)	Asymmetric Opened	-	√	-	w,u,v,θ_x θ_y ,θ_z ,ψ	√	-	-Governing coupled equations obtained from Hellinger-Reissner principle -Formulation account for finite rotation
4	Bercin and Tanaka (1997)	Mono-symmetric C-shaped	-	√	-	v,θ_x ,θ_z	√	-	-Coupled bending-torsional vibrations -Cantilever beam
5	Tanaka and Bercin (1998)	Asymmetric C-shaped	-	√	-	u,v,θ_x θ_y ,θ_z	√	-	-Closed form solutions derived using symbolic computational package Mathematica -Coupled bending-torsion vibration

Cont. Table (2.4): Summary of comparative review for studies of free vibration analysis of thin-walled theories which capture warping and shear deformation effects

No.	Author	Cross Section	Method of Solution			Field variables	Rotary inertia effect included	Static load effect included	Remarks
			Dynamic stiffness matrix	Closed form solution	Finite element solution				
6	Cortinez and Piovan (2002)	Asymmetric Open-closed	-	√	-	w,u,v,θ_x θ_y,θ_z,ψ	√	Initial stresses	-Coupled bending-torsional equations -Hellinger-Reissner principle -Secondary warping -Composite beams
7	Kim et. al (2003b)	Asymmetric Opened	√	√	-	w,u,v,θ_x θ_y,θ_z,ψ	√	Axial force	-Displacement field based on semitangential rotations -Governing equations and force-displacement relations derived from energy principle
8	Li et al. (2004e)	Mono-symmetric C-shaped	-	√	-	v,θ_x,θ_z	√	-	-Dynamic transfer matrix method -Bending-torsion coupled vibrations
9	Kim and Kim (2005)	Asymmetric Opened/ Closed	√	√	√	w,u,v,θ_x θ_y,θ_z,ψ	√	Vertical force and torque	-Hellinger-Reissner principle -Isoparametric beam element used in finite element procedure
10	Prokic (2006)	Asymmetric Opened	-	√	-	w,u,v $\theta_x,\theta_y,\theta_z$	√	-	- Coupled bending-torsion -Virtual work principle -Shear deformation due to warping not captured

Cont. Table (2.4): Summary of comparative review for studies of free vibration analysis of thin-walled theories which capture warping and shear deformation effects

No.	Author	Cross Section	Method of Solution			Field variables	Rotary inertia effect included	Static load effect included	Remarks
			Dynamic stiffness matrix	Closed form solution	Finite element solution				
11	Machado (2007)	Asymmetric Opened-Closed	-	√	-	w,u,v,θ_x θ_y,θ_z,ψ	√	Initial stresses	-Formulation captured Initial deformation -Nonlinear filed equations obtained using principle of virtual work -Composite beam theory
12	Vo et. al (2009)	Doubly symmetric Closed	-	-	√	w,u,v,θ_x θ_y,θ_z,ψ	√	-	--Coupled bending-torsion vibrations - Hamilton's principle -Secondary warping included -Composite beam theory. -1D Lagrange interpolation functions used in finite element formulation
13	Vo and Lee (2009a, 2010b)	Asymmetric Composite section	-	-	√	w,u,v,θ_x θ_y,θ_z,ψ	√	Axial force and end moment	-Governing equations obtained from Hamilton's principle -Secondary warping included -Composite beam theory. -1D Lagrange interpolation functions were used in finite element formulation

2.9 Thin-walled Solutions for Composite Members

Several investigations have been presented in the literature to study the free vibration analysis of thin-walled composite members. Among them, Banerjee and Butler (1994) used the dynamic composite beams. The exact expression for the dynamic stiffness matrix elements is derived from the governing differential equations of motion. The derived dynamic stiffness matrix was used to determine the natural frequencies of the coupled extensional-torsional vibrations of composite beams. Banerjee and Williams (1996) developed the exact dynamic stiffness matrix of composite beams. The formulation is then used to investigate the free vibration characteristics taking into account the effects of shear deformation and rotary inertia. The theory accounts for the bending-torsional coupling effects that arise from the ply orientation and stacking sequence in laminated fibrous composites. Natural frequencies for the bending-torsion coupled vibrations were computed by Wittrick and Williams (1971) algorithm. The free vibration results including/excluding the effects of shear deformation and rotary inertia are discussed and compared with published ones. Banerjee (1998) extended previous theories (Banerjee and Williams 1996) to incorporate the effect of axial force. He developed the dynamic stiffness matrices of composite beams with and without including shear deformation effect. The governing partial differential equations of motion for the coupled bending-torsional free vibration of axially loaded composite beam, which exhibits bending-torsion coupling, were derived using the Hamilton variational principle. By ignoring the warping deformation effect, the theory accounted for the effects of shear deformation, rotary inertia and axial force. Explicit analytical expressions for the dynamic stiffness matrices are derived by applying symbolic algebra. The dynamic stiffness matrix is then used in conjunction with the Wittrick-Williams algorithm to determine the coupled bending-torsional natural frequencies and the corresponding mode shapes of axially loaded composite beams. The effects of axial force, shear deformation and rotatory inertia effects on the natural frequencies are investigated in the study. Kollar (2001) presented the free vibration analysis of thin-walled open section composite beams. The governing differential equations including both the transverse shear deformation and warping deformation were developed. Closed-form solutions for the coupled flexural-torsional natural frequencies were derived for simply-supported beams. Cortinez and Piovan (2002) developed a linear theory for the dynamic and stability analyses of thin-walled composite beams of open and closed cross-section with initial stresses. The governing differential equations were derived

using the Hellinger-Reissner principle. In their study, the effects of shear deformations due to bending and non-uniform warping were incorporated. The analytical solution of the present governing equations is performed for thin-walled composite beams with simply-supported end conditions. Numerical results are performed to study the effects of shear deformation on the natural frequencies and buckling loads of the composite beams for various cross-sectional shapes and laminate schemes. Lee and Kim (2002a) developed an analytical model to study the coupled flexural-torsional free vibration of a thin-walled composite laminated beam of doubly symmetric I-section. Starting from Vlasov beam theory, the governing differential equations of motion are derived using the Hamilton's principle. To formulate the problem, a one-dimensional displacement-based finite element method is employed to predict the natural frequencies and the corresponding vibration mode shapes for a thin-walled composite I-beam. The numerical results investigated the effects of coupling, fibre angle and modulus ratio on the natural frequencies and mode shapes for thin-walled laminated composite beams with clamped and simply-supported boundary conditions. Lee and Kim (2002b) extended their previous work in Lee and Kim (2002a) to investigate the coupled flexural-torsional free vibrations for the thin-walled composite laminated beams with channel cross-sections. The theory is based on the classical lamination theory and neglected shear deformation and rotary inertia effects. The coupling of flexural and torsional modes for arbitrary laminate stacking sequence configuration is incorporated in the formulation. They developed a displacement-based one dimensional finite element model for the free vibration analysis of channel-section composite beams based on Vlasov's thin-walled beam theory. In their study, the generalized displacements are expressed over each element as a linear combination of one-dimensional Lagrange interpolation functions for the longitudinal displacement and cubic Hermite interpolation functions for the lateral displacements and angle of twist. Investigated in the study were the effects of fibre angle, modulus ratio, and boundary conditions on the free vibration frequencies and mode shapes of the thin-walled composites beams with channel-sections. Piovan and Cortinez (2005) investigated the dynamic analysis of thin-walled composite beams with arbitrary open and closed cross-sections. Their study incorporated the effect of shear deformation effects due to bending and non-uniform warping. The governing differential equations of motion for thin-walled composite beams were derived using the Hellinger-Reissner principle. The natural frequencies for coupled flexural and torsional vibrations of thin-walled composite beams are

obtained for simply-supported and cantilever boundary conditions. Machado and Cortinez (2007) investigated the vibration analysis of thin-walled composite beams of doubly symmetric I-section in which the effects of the initial deformations (induced by the action of static external loads) and shear deformation are included. The formulations were based on a geometrically non-linear shear deformable theory based on large displacements and rotations. The governing differential equations of motion are derived using the virtual work principle. Ritz method is employed to solve the governing differential equations by reducing the variational problem to an algebraic equation to compute the free vibration characteristics. The natural frequencies of thin-walled I-beams subjected to concentrated and distributed vertical forces are evaluated for cantilever and simply-supported boundary conditions. The effect of the initial deformations due to geometric non-linearity on the dynamic response of thin-walled beams of doubly symmetric I-sections subjected to concentrated forces, end moments or uniformly distributed loads is investigated. The influence of shear deformation is studied as well for different load conditions and stacking sequence. By using a geometrically higher-order non-linear beam theory, Machado (2007) extended the previous work in Machado and Cortinez (2007) to investigate analytically and numerically the effect of large rotation on the lateral buckling and free vibration behaviour of thin-walled composite open beams subjected to static vertical loads. The beam model is strictly valid for symmetrically balanced and orthotropic laminates and accounts for the effects of shear deformation (bending and warping shear). The non-linear governing differential equations were derived using the principle of virtual work and solved by employing the Ritz variational approach in order to investigate the dynamic and buckling behaviours in which the initial deformations were generated by the applied static loads. Numerical results were obtained to study the effects of large rotations on the lateral buckling and free vibration behaviour of the thin-walled composite beams. The buckling loads and natural frequencies of composite I-beams subjected to constant concentrated and distributed vertical loads were determined for cantilever and simply-supported boundary conditions. The numerical results obtained were in good agreement when compared with those obtained by the Abaqus shell finite element model. Vo and Lee (2009a) developed a general analytical method for the dynamic and buckling analyses of thin-walled composite members of open cross-sections. The formulation is based on shear-deformable beam theory, accounts for warping deformation, rotary inertia and structural coupling due to material anisotropy. Using the Hamilton principle,

the governing differential equations for the coupled flexural-torsional-shearing vibrations are derived, and a one-dimensional finite element model is developed. Numerical results investigated the influence of shear deformation and axial compressive force on the flexural-torsional coupled natural frequencies and corresponding mode shapes. Load-frequency interaction curves were presented graphically for various boundary conditions and fibre orientations. In a subsequent study, Vo et. al (2009) extended the theory developed by Vo and Lee (2009a) to study the coupled flexural-torsional free vibration of thin-walled composite box beams with arbitrary laminate lay-ups. Starting with the Hamilton variational principle, the seven differential equations of motion governing the axial-flexural-torsional shearing vibrations of the thin-walled composite box beams are derived, which accounts for structural and material coupling, shear deformation, warping deformation and rotary inertia effects. The influences of including or excluding shear deformation and warping deformation are investigated on the coupled natural frequencies and associating vibration mode shapes. Vo and Lee (2009b) extended their previous works to study the flexural-torsional coupled vibration of thin-walled composite closed members subjected to a constant axial force. Their formulation was based on the classical lamination theory in which shear deformation is not included. The effects of axial force on the flexural-torsional coupled natural frequencies and related mode shapes of thin-walled composite box beams are presented in a graphical form for cantilever and simply-supported end conditions. In another paper, Vo and Lee (2010) developed a general model to analyze the flexural-torsional coupled free vibration and stability of thin-walled composite box members subjected to constant axial loads and end moments. The explicit form of governing equations of motion for flexural-torsional coupled vibration of the member is formulated using the Hamilton principle, in which the shear deformation effects are not captured in the model. The formulation is implemented using a displacement-based finite element model with seven degrees of freedom at each node, a linear shape function for the axial displacement and Hermite-cubic shape functions for lateral, transverse displacements and angle of twist. By ignoring the effects of all the coupling of the material anisotropy, the analytical closed-form solutions for flexural-torsional vibration and buckling under axial loads and equal end moments are presented for doubly symmetric cross-sections. Numerical results investigated the effects of axial forces, bending moments, fibre orientation and modulus ratio on the buckling loads, natural frequencies, corresponding mode shapes and axial-moment-frequency interaction

relations. Vo et. al (2010) studied the coupled flexural-torsional free vibration of thin-walled open composite beams with arbitrary lay-ups subjected to constant axial compressive force excluding shear deformation effects. The theory was based on classical lamination theory and accounts for warping stiffness, rotary inertia and material anisotropy couplings. The dynamic equations of motion governing the coupled flexural-torsional vibrations were derived from the Hamilton principle. The resulting equations are implemented through a displacement-based one-dimensional finite element with seven degrees of freedom, i.e. the axial displacement is interpolated using linear shape functions while the transverse, lateral displacements and angle of twist were interpolated using Hermite-cubic shape functions. Numerical results were evaluated for thin-walled composites members for various boundary conditions to investigate the effects of axial force, fiber orientations and modulus ratio on the free vibration frequencies and corresponding vibration mode shapes. Load-frequency interaction curves were also developed. Most recently, Vo et al. (2011) developed an analytical model to study the free vibration analysis of thin-walled composite beams with I-cross-sections subjected to combined constant axial forces and bending moments. This model is based on the classical lamination theory and accounts for the material coupling for arbitrary laminate stacking sequence configurations. A displacement-based one dimensional finite element model with seven degrees of freedom is developed to predict the natural frequencies and corresponding vibration modes for thin-walled composite I-beams with various boundary conditions. Numerical results investigated the effects of axial forces, bending moments, fiber orientation on the natural frequencies and corresponding vibration modes as well as the load-frequency interaction curves.

2.10 Forced Vibrations of Thin-walled Open Members

A few studies dealing with coupled vibrations of thin-walled open members subjected to cyclic (i.e., harmonic) loads were developed. Rao (1976) studied the forced torsional vibrations of doubly symmetric beams of thin-walled open cross section for which the centroid and shear centre coincide. The two coupled differential equations for torsional vibrations in terms of twisting angle and warping deformation were derived. This study included the effects of longitudinal inertia and shear deformation with viscous damping. The numerical results, natural frequencies and mode shapes, are evaluated for a beam with both ends simply supported

subjected to uniformly distributed torque over the span, which varies sinusoidally in time. The amplitudes of torsional deformation obtained including both effects are found larger than those based on the classical beam theory. Yaman (1997) investigated the triply coupled forced vibration behaviour of thin-walled beams with open channel cross sections by using the wave propagation approach. His formulation incorporates the effect of warping deformation of the cross-section. The excitation source is taken as a single-point harmonic force. Various frequency response curves, wave numbers and the mode shapes of coupled vibrations were developed for structurally damped and undamped beams for a variety of different end boundary conditions. Adam (1999) analyzed the coupled bending-torsional vibrations of open thin-walled monosymmetric beams. The effect of warping deformation is included in the formulation. The dynamic response of the governing coupled differential equations was assumed to consist of two parts; quasi-static and complementary dynamic parts, i.e. $u(z,t)=u_{\hat{s}}(z,t)+u_{\hat{d}}(z,t)$ and $\theta_z(z,t)=\theta_{z_{\hat{s}}}(z,t)+\theta_{z_{\hat{d}}}(z,t)$, where $u(z,t)$ is the lateral displacement of the shear centre axis and $\theta_z(z,t)$ is the angle of twist of the cross-section. The quasi-static portion of the solution denoted by a superscript $\hat{S}$ may contain singularities or discontinuities due to sudden load changes whereas the complementary dynamic part, denoted by a superscript $\hat{d}$, is non-singular and can be approximated by a finite modal series for accelerated convergence. The solution of the resulting generalized decoupled SDOF equations is given by the Duhamel's convolution integral. The results obtained by using Adam's approach suggest a significant improvement when compared to the classical modal analysis approach. Yaman (2002) extended his work in Yaman (1997) to develop an exact analytical method for the determination of triply coupled forced vibrations of elastically supported, single and multi-bay open cross-section. The beam ends and the periodic intermediate supports are modeled as springs with finite flexural and torsional stiffness. He also studied the effects of a variety of end conditions on the vibration characteristics of a thin-walled beam.

2.11 References

[2.1] Adam, C. (1999), Forced vibrations of elastic bending-torsion coupled beams, J. of Sound and Vibration, 221, p 273-287.

[2.2] Arpaci, A. and Bozdag, E. (2002), On free vibration analysis of thin-walled beams with non-symmetrical open cross-sections, Computers and Structures, 80, p 691–695.

[2.3] Arpaci, A. et al. (2003), Triply coupled vibrations of thin-walled open cross-section beams including rotary inertia effects, Journal of Sound and Vibration, 260(5), p 889-900.

[2.4] Ambrosini, D. (2009), On free vibration of nonsymmetrical thin-walled beams, Thin-Walled Structures, 47(6-7), p 629-636.

[2.5] Ambrosini, D. (2010), Experimental validation of free vibrations from nonsymmetrical thin walled beams, Engineering Structures, 32(5), p 1324-1332.

[2.6] Altintas, G. (2010), Effect of material properties on vibrations of non-symmetrical axially loaded thin-walled Euler-Bernoulli beams, Mathematical and Computational Applications, 15, p 96-107.

[2.7] Banerjee, J. R. (1989), Coupled bending-torsional dynamic stiffness matrix for beam elements. International Journal for Numerical Methods in Engineering, 28, p. 1283–1289.

[2.8] Banerjee, J. R. (1991), A FORTRAN routine for the computation of coupled bending-torsional dynamic stiffness matrix of beam elements, Advances in Engineering Software, 13, p 17-24.

[2.9] Banerjee, J. R. and Williams, F. W. (1992), Coupled bending-torsional dynamic stiffness matrix for Timoshenko beam elements, Computers and Structures, 42, p 301-310.

[2.10] Banerjee, J. R. and Fisher, S. A. (1992), Coupled bending-torsional dynamic stiffness matrix for axially loaded beam elements. International Journal for Numerical Methods in Engineering, 33, p 739–751.

[2.11] Banerjee, J. R. and Williams, F. W. (1994), Coupled bending-torsional dynamic stiffness matrix of an axially loaded Timoshenko beam element, Int. J. Solids Structures, 31(6), p 749-762.

[2.12] Banerjee, J. R. and Butler, R., (1994), Coupled Extensional-torsional vibration of composite beams – An exact method, AIAA, p 147-154.

[2.13] Banerjee, J. R., Guo, S. and Howson, W.P., (1996), Exact dynamic stiffness matrix of a bending-torsion coupled beam including warping, Computers and Structures, 59(4), p 613-621.

[2.14] Banerjee, J. R. (1997), Dynamic Stiffness Formulation for Structural Elements, A General Approach, Computers and Structures, 63, p 101-103.

[2.15] Banerjee, J. R. (1998), Free vibration of axially loaded composite Timoshenko beam using the dynamic stiffness matrix method, Computers and Structures, 69, p 197-208.

[2.16] Banerjee, J. R. (1999), Explicit frequency equation and mode shapes of a cantilever beam coupled in bending and torsion. Journal of Sound and Vibration, 224(2), p 267-281.

[2.17] Banerjee, J. R. (2000), Explicit Modal Analysis of an Axially Loaded Timoshenko Beam with Bending-Torsion Coupling, J. of Applied Mechanics, 67, p 307-313.

[2.18] Banerjee, J. R. and Su, H. (2006), Free Transverse and Lateral Vibration of Beams with Torsional Coupling, Journal of Aerospace Engineering, 19(1), p 13-20.

[2.19] Bercin A. N., Tanaka M. (1997), Coupled flexural-torsional vibrations of Timoshenko beams, Journal of Sound and vibration, 207(1), p 47-59.

[2.20] Bin, Z. and Leung, A. Y. T. (2006), Dynamic stiffness for thin-walled structures by power series, Journal of Zhejiang University SCIENCE A, 7(8), p 1351-1357.

[2.21] Bishop, R. E. and Price, W. G. (1985), A note on the dynamical behavior of uniform beams having open channel section, Journal of Sound and Vibration, 99(2), p 155-167.

[2.22] Bishop, R. E. et al. (1989), On coupled bending and torsional vibration of uniform beams, Journal of Sound and Vibration, 131(3), p 457-464.

[2.23] Bottega, W. (2006), Engineering Vibrations, CRC Taylor and Francis Group, NY, USA.

[2.24] Chen, X.; Tamma, K. K. (1994), Dynamic response of elastic thin-walled structures influenced by coupling effects, Computers and Structures, 51(1), p 91-105.

[2.25] Chen, H. H. and Hsiao, K. M. (2007), Coupled Axial-torsional Vibration of Thin-walled Z-section Beam Induced by Boundary Conditions, Thin-walled Structures, 45(6), p 573-583.

[2.26] Craig, R. R. and Kurdila, A., (2006), Fundamentals of Structural Dynamics, John Willey and Sons, New Jersey, USA.

[2.27] Chopra, A. K., (2007), Dynamics of Structures, Theory and Applications to Earthquake Engineering, Third edition, Pearson Prentice Hall, USA.

[2.28] Cortinez, V. H. and Piovan, M. T. (2002), Vibration and buckling of composite thin-walled beams with shear deformability, Journal of Sound and Vibration, 258(4-5), p 701–723.

[2.29] De Bordon, F. and Ambrosini, D. (2010), On free vibration analysis of thin-walled beams axially loaded, Thin-Walled Structures, 48(12), p 915-920.

[2.30] Dokumaci, E. (1987), An exact solution for coupled bending and torsion vibrations of uniform beams having single cross-sectional symmetry, Journal of Sound and Vibration, 119(3), p 443–449.

[2.31] Dukkipati, R. V. (2006), Advanced Mechanical Vibrations, Alpha Science International Ltd., Oxford, U. K.

[2.32] Erkmen, R. E., (2006), Finite element formulations for thin-walled members, Ph.D. thesis, University of Ottawa, Ottawa, Canada.

[2.33] Eslimy-Isfahany S. H. and Banerjee J. R. (1996a), Dynamic response of an axially loaded bending-torsion coupled beam, Journal of Aircraft, May-June, 33 (3), p 601-607.

[2.34] Eslimy-Isfahany S. H. Banerjee J. R. (1996b), Response of bending-torsion coupled beam to deterministic and random loads, J. of Sound and vibration, 195(2), p 267-283

[2.35] Friberg, P.O. (1983), Coupled vibration of beams - An exact dynamic element stiffness matrix. International Journal for Numerical Methods in Engineering, 19, p 479-493.

[2.36] Friberg, P.O. (1985), Beam element matrices derived from Vlasov's theory of open thin-walled elastic beams. International Journal for Numerical Methods in Engineering 21, p 1205-1228.

[2.37] Gjelsvik, A. (1981), The Theory of Thin-Walled Bars, John Wiley and Sons, NY, USA.

[2.38] Harris, C. M., (2002), Shock and Vibration Handbook, Fifth edition, McGraw-Hill.

[2.39] Hashemi S. M., Richard M. J. (2000a), A Dynamic Finite Element Method for Free Vibrations of Bending -Torsion Coupled Beams, Aerospace Sci. Technology, 4, p 41-55.

[2.40] Hashemi S. M., and Richard M. J. (2000b), Free vibrational analysis of axially Bending-Torsion Coupled Beams-A dynamic finite element, Computers and structures, 77, p711-724.

[2.41] Humar, J. L., (2002), Dynamics of Structures, second edition, A. Balkima Publisher, Netherlands.

[2.42] Hurty, W. C. and Rubintein, M. F., (1964), Dynamics of Structures, Prentice-Hall, INC, New Jersey.

[2.43] Hu Y. et al (1996), A finite element model for static and dynamic analysis of thin-walled beam with asymmetric cross-sections, Computers and Structures, 61(5), p 897-908.

[2.44] Inman, D., (2001), Engineering Vibrations, second edition, Prentice Hall. Upper Saddle river, N. J.

[2.45] Kim, N. et al (2003a), Exact dynamic and static stiffness matrices of nonsymmetric thin-walled beam-columns, Computers and Structures, 81, p 1425-1448.

[2.46] Kim, M. Y. et al (2003b), Exact dynamic and static stiffness matrices of shear deformable thin-walled beam-columns, Journal of Sound and Vibration, 267, p 29–55.

[2.47] Kim, N. et al (2005), Exact Dynamic Stiffness Matrix of Non-Symmetric Thin-Walled Beams on Elastic Foundation using Power Series Method, Advances in Engineering Software, 6, p 518-532.

[2.48] Kim, N. I. and Kim, M. N. (2005), Exact Dynamic/Static Stiffness Matrices of Non-Symmetric Thin-Walled Beams considering coupled shear deformation effects, Thin-walled Structures, 43, p 701-734.

[2.49] Kim, N. et al. (2007), Stiffness matrices for flexural–torsional/lateral buckling and vibration analysis of thin-walled beam, Journal of Sound and Vibration, 299(4-5), p 739-756.

[2.50] Kollar, J. P. (2001), Flexural-torsional vibration of open section composite columns with shear deformation, International Journal of Solids and Structures, 38(42-43), p 7543-7558.

[2.51] Laudiero, F. and Savoia, M. (1991), The shear strain influence on the dynamics of thin-walled beams, Thin-walled structures, 11, p 375-407.

[2.52] Leung, A.Y.T. (1985), Dynamic stiffness method for exponentially varying harmonic excitation of continuous systems, Journal of Sound and Vibration, 98, p 337-347

[2.53] Leung, A. Y. T. (1991), Natural shape functions of a compresses Vlasov element, Thin-walled Structures, 11, p 431-438.

[2.54] Leung, A.Y.T. (1992), Dynamic stiffness analysis of thin-walled structures, Thin-walled Structures, 14, p 209-222.

[2.55] Lee, J. and Kim, S. E. (2002a), Free Vibration of Thin-walled Composite Beams with I-Shaped cross-sections, Composite Structures, 55(2), p 205-215.

[2.56] Lee, J. and Kim, S. E. (2002b), Flexural–torsional coupled vibration of thin-walled composite beams with channel sections, Computers and Structures 80, p 133–144.

[2.57] Li D. B. et al (1994), Effect of warping on torsional vibration of members with open cross-sections, Journal of Sound and vibration, Vol 170 (2), p.270-275.

[2.58] Li, J, Shen, R., Hua, H., Jin, X. (2004a), Coupled bending and torsional vibration of axially loaded Bernoulli-Euler beams including warping effects, Applied Acoustics, 65, p 153-170.

[2.59] Li, J, Hua, H, Shen, R, Jin, X. (2004b), Dynamic response of axially loaded monosymmetrical thin-walled Bernoulli-Euler beams, Thin-walled Structures, 42, p 1689-1707.

[2.60] Li, J, Li, W., Shen, R., Hua, H. (2004c), Coupled bending and torsional vibration of nonsymmetrical axially loaded thin-walled Bernoulli-Euler beams, Mechanics Research Communications, 31, p 697-711.

[2.61] Li, J, Shen, R, Hua, H, Jin, X (2004d), Response of mono-symmetric thin-walled Timoshenko beams to random excitations, Int. J. of Solids and Structures, 41, p 6023-6040.

[2.62] Li, J, Li, W., Shen, R., Hua, H. (2004e), Coupled bending and torsional vibration of axially loaded thin-walled Timoshenko beams, Mechanics International Journal of Mechanical Sciences, 46, p 299-320.

[2.63] Librescu, L and Song, O. (2006), Thin-walled composite beams: theory and application, Springer, The Netherlands.

[2.64] Machado, S. P. (2007), Geometrically non-linear approximations on stability and free vibration of composite beams, Engineering Structures, 29(12), p 3567-3578.

[2.65] Machado, S. P. and Cortinez, V. (2007), Free vibration of thin-walled composite beams with static initial stresses and deformations, Engineering Structures, 29(3), p 372-382.

[2.66] Mei, C. (1970), Coupled vibrations of thin-walled beams of open section using the finite element method, International Journal of Mechanical Sciences, 12(10), p 883-891.

[2.67] Mohri, F. et al (2004), Vibration analysis of buckled thin-walled beams with open sections, Journal of Sound and Vibration, 275, p 434-446.

[2.68] Ohga, M. et al. (1995), Natural frequencies and mode shapes of thin-walled members, Computers and Structures, 55(6), p 971-978.

[2.69] Piovan, M. T. and Cortinez, V. H. (2005), Transverse shear deformability in the dynamics of thin-walled composite beams: consistency of different approaches, Journal of Sound and Vibration, 285(3), p 721-733.

[2.70] Prokic, A. (2005), On fivefold coupled vibrations of Timoshenko thin-walled beams, Engineering Structures, 28, p 54-62.

[2.71] Prokic, A. (2006), On fivefold coupled vibrations of Timoshenko thin-walled beams, Engineering Structures, 28, p 54-62.

[2.72] Prokic, A. and Lukic, D. (2012), Flexural-torsional vibration analysis of axially loaded thin-walled beam, Journal of Braz. Soc. Of Mech. Sci. and Eng., Vol XXXIV (3), p 262-268.

[2.73] Rao, C. K. et al (1974), Effect of longitudinal inertia and of shear deformation on the torsional frequency and normal modes of thin-walled open section beams, Journal of the Aeronautical Society of India, 26(1-2), p 32-41.

[2.74] Rao, C. K. (1976), Forced vibrations of thin-walled beams of open section with longitudinal inertia, shear deformation and viscous damping, J. of Aero. Soc. of India, 28(4), p 405-412.

[2.75] Rao, S. S. (2004), Mechanical Vibrations, 4th edition, Pearson Education, Delhi, India.

[2.76] Tabarrok, B and Rimrott, F.P (1994), Variational Methods and Complementary Formulations in Dynamics, Kluwer Academic Publishers, Netherlands

[2.77] Tanaka, M. and Bercin, A. N. (1997), Finite element modeling of the coupled bending and torsional free vibration of uniform beams with an arbitrary cross-section, Applied Mathematical Modelling, 21(6), p 339-344.

[2.78] Tanaka, M. and Bercin, A.N. (1998), Free vibration solution for uniform beams of nonsymmetrical cross section using Mathematica, Computes and Structures, 71 , p 1–8.

[2.79] Thomson, W. T. and Dahleh, M. D. (2005), Theory of vibration with applications, fifth edition, Pearson Education, Delhi, India.

[2.80] Timoshenko, S.P. and Gere, J.M. (1961), Theory of elastic stability, 2nd edition, McGraw-Hill, New York, USA.

[2.81] Timoshenko, S.P. and Goodier, J.N. (1970), Theory of elasticity, McGraw-Hill company, New York, USA.

[2.82] Yaman, Y. (1997), Vibrations of open-section channels: a coupled flexural and torsional wave analysis, J. of Sound and Vibration, 204(1), p 131-158.

[2.83] Yaman, Y.(2002), Forced vibrations of triply coupled, periodically and elastically supported, finite, open-section channels, J. of Sound and Structures, 250(4), p 649-673.

[2.84] Virgin, L. N. (2007), Vibration of Axially Loaded Structures, 1st edition, Cambridge University Press, New York, USA.

[2.85] Vlasov, V. Z. (1961), Thin-walled elastic beams, 2nd edition, Israel Program for Scientific Translation, Jerusalem.

[2.86] Voros, G. M. (2004), Free vibration of thin-walled beams, Periodica Polytechnica Ser. Mech. Eng. 48(1), p 99–110.

[2.87] Voros, G. M. (2008), On Coupled vibrations of beams with lateral loads, Journal of Computational and Applied Mechanics, 9(2), p 1-14.

[2.88] Voros, G. M. (2009), On Coupled bending-torsional vibrations of beams with initial loads, Mechanics Research Communications, 36, p 603-611.

[2.89] Vo, T. P. and Lee, J. (2009a), Flexural-torsional coupled vibration and buckling of thin-walled open section composite beams using shear-deformable beam theory, International Journal of Mechanics Sciences, 51, p 631-641.

[2.90] Vo, T. P. and Lee, J. (2009b), Free vibration of axially thin-walled composite box beams, Composite Structures, 90, p 233-241.

[2.91] Vo, T. P. et al. (2009), On six-fold coupled vibrations of thin-walled composite box beams, Composite Structures, 89, p 524-535.

[2.92] Vo, T. P. and Lee, J. (2010a), Interaction curves for vibration and buckling of thin-walled composite box beams under axial loads and end moments, Applied Mathematical Modelling, 34, p 3142-3157.

[2.93] Vo, T. P. and Lee, J. (2010b), Free vibration of axially thin-walled composite Timoshenko beams, Archive of Applied Mechanics.

[2.94] Vo, T. P. et al. (2010), On triply coupled vibrations of axially loaded thin-walled composite beams, Computers and Structures, 88(3-4), p 144-153.

[2.95] Vo, T. P. et al. (2011), Vibration analysis of thin-walled composite beams with I-shaped cross-sections, Composite Structures, 93(3-4), p 812-820.

[2.96] Wallerstein, D.V. (2002), A variational approach to structural analysis, John Willey and Sons, New York, USA.

[2.97] Washizu, K. (1982), Variational Methods in Elasticity and Plasticity, third edition, Pergamon Press, New York, USA.

List of Symbols

A	Cross-section area
b_i	Length of i-th rectangular element
C	Centroid of the cross-section
C_w	Warping constant
d	Height of beam cross-section (see Figure 2.7)
$\left[D(\omega)\right]$	Dynamic stiffness matrix
E	Modulus of elasticity
$\{F(t)\}_{n\times 1}$	Force vector in original coordinates
$\langle \widehat{F}(t)\rangle^T_{1\times n}$	Modal forces vector
G	Shear modulus
$h(s)$	Normal distance between the shear centre and the tangent to mid-surface
I_{xx} , I_{yy}	Moment of inertia of the cross-section about the principal X and Y axes
r_o	Polar moment of inertia of the cross section
J	Torsional constant
$[k]_{n\times n}$	Elastic stiffness matrix ($n \times n$ are the total degrees of freedom)
$\left[K(\omega)\right]$	Global stiffness matrix
$\left[\widehat{K}\right]_{\mathrm{n\times n}}$	Modal stiffness matrix
ℓ	Length of the member
L, L^*	Lagrangian function
$M_j(z,t)$	Moments about X ,Y ,Z axes (where $j = x, y, z$)
$M_w(z,t)$	Bimoment
$m_j(z,t)$	Distributed dynamic moments about X ,Y ,Z axes (where $j = x, y, z$)
$M_{z_{sv}}(z,t)$	Saint-Venant twisting moment
$m_w(z,t)$	Distributed warping twisting moment

$[m]_{n\times n}$	Mass matrix
$\left[\hat{M}\right]_{n\times n}$	Modal mass matrix
$\left[M\ (\omega)\right]$	Global mass matrix
n	Axis along the normal direction at a point on the mid-surface
$\bar{n}$	Equal time intervals
n,s,z	Local curvilinear coordinate system
P_i	Concentrated dynamic forces (for i =1,2,3,.....,n)
$\bar{q}_i$	Generalized coordinates (for i =1,2,3,.....,n)
$\dot{\bar{q}}_i$	Generalized velocities (for i =1,2,3,.....,n)
$\bar{Q}_i$	Generalized forces (for i =1,2,3,.....,n)
$q_j\ (z,t)$	Applied distributed dynamic forces along X ,Y ,Z directions
$\langle q \rangle^T$	Nodal displacement vector
$\{q_r\ (t)\}_{r\times 1}$	Response vector for the r-th mode
$\langle Q \rangle^T$	Nodal Force vector
$r\ (s)$	Normal distance between the shear centre to the normal to mid-surface
r_o	Radius of gyration
s	Curvilinear coordinate along mid-surface of the section
S_c	Shear centre of the cross-section
S_o	Sectorial origin
S_x ,S_y ,S_ω	First moments of the area of coordinates X,Y and ω
S_{xy}	Product moment of the area
$S_{x\omega}$,$S_{y\omega}$	Section products of inertia
t	Time in seconds
t_1 ,t_2	Time intervals
Δt	Time interval in seconds

T,T^*	Kinetic energy
T_e,T_t	Kinetic energy
T_d	Total time in seconds
T_{sv},T_v	Kinetic energy for St. Venant and Vlasov beam theories
$\left[\bar{T_i}\right]_{12\times12}$	Transfer matrices for beam elements (for $i=a,b,c,.....,m$)
$\left[\bar{T_G}\right]_{12\times12}$	Dynamic transfer matrix for whole member
$\bar{u}_i$	Displacements (for $i=1,2,3,.....,\mathrm{n}$)
u,v	Displacements of the shear centre along the principal X,Y axes
u_p,v_p,w_p	Displacements of a point on the mid-surface of the section along X,Y,Z axes
$\dot{u},\dot{v},\dot{w}$	Velocities along the principal axes X,Y,Z
u',v',w'	Derivative of displacements u,v,w with respect to z
u'',v'',w''	Second derivative of displacements u,v,w with respect to z
U,U^*	Internal strain energy
U_e,U_t	Internal strain energy for Euler-Bernoulli and Timoshenko beam theories
U_{sv},U_v	Internal strain energy for St. Venant torsion and Vlasov beam theories
$\{\bar{u}_k\}_{k\times1}$	Nodal displacement vector (for $k=1,2,3,.....,\mathrm{n}$)
$\{U(t)\}_{n\times1}$	Displacement vector in original coordinates
$\{\ddot{U}(t)\}_{n\times1}$	Acceleration vector in original coordinates
v_o	Displacement of a point along Y axis and located on the centriodal axis
$\dot{v}_o$	Velocity of a point along Y axis and located on the centriodal axis
V	Volume of the element
v,V^*	Potential energy by the external forces
$V_y(z,t)$	Shear force along Y axis
w	Average longitudinal displacement along Z axis
W,W^*	Work done by applied forces

W_e ,W_t	Work done by applied forces for Euler-Bernoulli and Timoshenko theories
W_{sv} ,W_v	Work done by applied forces for St. Venant and Vlasov beam theories
x, y, z	Cartesian coordinate system
X, Y, Z	Principal coordinate system
$x(s), y(s)$	Coordinate of arbitrary point on mid-surface of the contour along the principal X and Y axes
x_s , y_s	Coordinates of the shear centre along X and Y axes
$\{Y(t)\}_{n\times 1}$	Displacement vector in normal coordinates
z	Longitudinal coordinate
Π, Π^*	Total potential energy
Π_e, Π_t	Total potential energy for Euler-Bernoulli and Timoshenko beam theories
Π_{sv}	Total potential energy related to St. Venant torsion
σ_{ii}	Normal stresses (for $i = x, y, z$)
σ_w	Warping normal stress due to bimoment
τ_{ij}	Shear stresses (for $i, j = x, y, z$)
τ_{zs}	Shear stress at the mid-surface of the cross-section
τ_{sv}	Shear stress due to Saint-Venant torsion
τ_{w}	Warping shear stress due to bimoment
τ_{B}	Bredt shear stress over the cross-section
ε_{ii}	Normal strains (for $i = x, y, z$)
γ_{ij}	Shear strains (for $i, j = x, y, z$ and $i \neq j$)
γ_{zs}	Shear strain at the mid-surface of the cross-section
ρ	Density of the material
ξ, η	Tangential and normal displacements of a point p along s and n directions
θ_x , θ_y , θ_z	Rotations angles around the X, Y, Z axes

$\hat{\alpha}(s)$	Angle between the tangent to the cross-section and the principal X axis
$\psi(z,t)$	Warping deformation function
$\hat{\Psi}$	Product of the warping function
Ω	Eigen-frequency
$\omega(s)$	Warping function of the cross-section
$[\Phi]_{n\times n}$	Modal shape matrix
$\{\chi_i\}_{12\times 1}$	State vector composed of displacements and forces at element ends (for $i=1,2,3,.....,r$)
$\left\{\chi_{d_j}\right\}_{12\times 1}$	State vectors composed of displacements at element ends (for $j=1,2$)
$\left\{\chi_{f_j}\right\}_{12\times 1}$	State vectors composed of forces at element ends (for $j=1,2$)
$\{\chi_R\}_{12\times 1}$	Global state vector composed of forces at right end of the member
$\{\chi_L\}_{12\times 1}$	Global state vector composed of forces at left end of the member

CHAPTER (3)

ANALYSIS OF THIN-WALLED MEMBERS UNDER DYNAMIC FORCES

FORMULATING FIELD EQUATIONS

Chapter 3- Analysis of Thin-walled Members under Harmonic Forces

Formulating Field Equations

3.1 Introduction

This chapter deals with dynamic analysis of thin-walled beams of open cross-section subjected to applied dynamic excitations. The derivation is based on a generalized Timoshenko-Vlasov thin-walled beam theory. The Hamilton's variational principle is used to formulate the governing differential coupled equations and associated boundary conditions. The formulation incorporates shear deformation, warping deformation effects and the effects of translational and rotary inertia.

3.2 Basic Assumptions

The basic assumptions used in the formulation are:

(1) The thin-walled beam is prismatic.

(2) Material is assumed to deform within the elastic range of the material.

(3) The cross-section of the thin-walled member is assumed to remain undistorted (rigid) in its own plane (i.e. consistent with Vlasov's first assumption) [Vlasov 1961]; but free to undergo warping.

(4) The strains and rotations are assumed small.

(5) A planar cross-section originally normal to the centroidal axis is assumed, in general, not remain perpendicular to the cross-section after deformation, i.e. the transverse shear deformations of the middle-surface of the cross-section are incorporated in the assumed kinematics (analogous to the Timoshenko beam theory). The assumption is further generalized to warping deformation (i.e. the shear strains induced by warping at the middle surface are non-zero and characterized by a generalized displacement function multiplied by the sectorial coordinate).

The assumed kinematics can be conceived as a combination of Vlasov-Generalized and Timoshenko theory. Similar kinematics have been assumed in Laudiero and Savoia (1991),

Back and Will (1998), Cortinez and Piovan (2002), Li et. al (2004), Kim et. al (2003) , Kim and Kim (2005), Prokic (2006), Machado and Cortinez (2007), Machado (2007), Vo and Lee (2009) and (2011), and Liping and Mohareb (2011).

3.3 Displacement Fields For Thin-walled Member

According to the first Vlasov assumption, the section is assumed un-deformable in its own plane. As a result, the in-plane displacements $u_p(z,s,t)$ and $v_p(z,s,t)$ of an arbitrary point $p(x(s),y(s))$ on the cross-section can be related to the displacement components of the shear centre $u(z,t)$, $v(z,t)$ and the angle of twist of the cross section $\theta_z(z,t)$ through:

$$u_p(z,s,t)=u(z,t)-(y-y_s)\theta_z(z,t) \tag{3.1}$$

$$v_p(z,s,t)=v(z,t)+(x-x_s)\theta_z(z,t) \tag{3.2}$$

According to Timoshenko assumption (fourth assumption), the longitudinal displacement $w_p(z,s,t)$ of the general point $p(x,y)$ of the cross-section can be obtained as [e.g. Back and Will 1998]:

$$w_p(z,s,t)=w(z,t)-x(s)\theta_y(z,t)+y(s)\theta_x(z,t)+\omega(s)\psi(z,t) \tag{3.3}$$

in which $\theta_x(z,t)$ and $\theta_y(z,t)$ denote the rotations of the cross-section about X and Y axes, respectively, the term $\omega(s)\psi(z,t)$ represents the axial displacement of point $p(x,y)$ due to warping deformation, where $\psi(z,t)$ is a function which characterizes the magnitude of the warping deformation. Figure (3.1) shows the rotations $\theta_x(z,t)$ and $\theta_y(z,t)$ of the cross-section about X and Y axes and their contribution to the longitudinal displacement.

3.4 Tangential and Normal Displacements

The tangential and normal displacements $\xi(z,s,t)$ and $\eta(z,s,t)$ of point $p(x,y)$ along the tangential t and normal n local coordinates are obtained as:

$$\begin{Bmatrix}\xi(z,s,t)\\ \eta(z,s,t)\end{Bmatrix}=\begin{bmatrix}dy/ds & dx/ds\\ dx/ds & -dy/ds\end{bmatrix}\begin{Bmatrix}v(z,t)\\ u(z,t)\end{Bmatrix}+\begin{Bmatrix}h(s)\theta_z(z,t)\\ r(s)\theta_z(z,t)\end{Bmatrix} \tag{3.4}$$

in which:

$$h(s)=\left[x(s)-x_s\right]\left(\frac{dy}{ds}\right)-\left[y(s)-y_s\right]\left(\frac{dx}{ds}\right) \tag{3.5}$$

$$r(s)=\left[x(s)-x_s\right]\left(\frac{dx}{ds}\right)+\left[y(s)-y_s\right]\left(\frac{dy}{ds}\right) \tag{3.6}$$

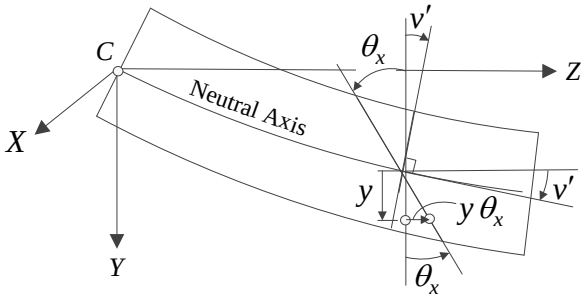

(i) Rotation of the Cross-Section about *X*-Axis.

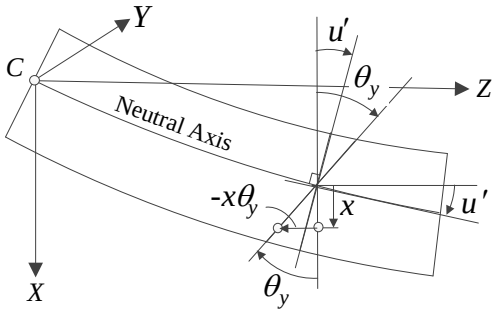

(ii) Rotation of the Cross-Section about *Y*-Axis.

Figure (3.1): Rotations of the Cross-Section about *X* and *Y* Axes.

3.5 Linear Strain-Displacement Relations

Based on the small strain assumption (Assumption 4), the strains associated with the linear small displacement theory of elasticity are adopted.

3.5.1 Longitudinal Normal Strain

The longitudinal normal strain ε_{zz} is:

$$\varepsilon_{zz} \approx \frac{\partial w_p}{\partial z} \tag{3.7}$$

From equation (3.3) by substituting into equation (3.7), one obtains:

$$\varepsilon_{zz} = w'(z,t) - x(s)\theta_y'(z,t) + y(s)\theta_x'(z,t) + \omega(s)\psi'(z,t) \tag{3.8}$$

3.5.2 Transverse Shear Strain

The transverse shear strain of the point $p(x,y)$ is:

$$\gamma_{zs} \approx \frac{\partial \xi}{\partial z} + \frac{\partial w_p}{\partial s} \tag{3.9}$$

From equations (3.3) and (3.4) by substituting into equation (3.9), one obtains

$$\gamma_{zs} = (v' + \theta_x)\frac{dy}{ds} + (u' - \theta_y)\frac{dx}{ds} + (\theta_z' + \psi)\frac{d\omega}{ds} \tag{3.10}$$

3.6 Variational Formulation

In order to derive the equations of motion and the boundary conditions of a linear thin-walled member, the variational form of Hamilton's variational principle is used as [e.g. Craig 1981]:

$$\delta \int_{t_1}^{t_2} (T - U + W)\,dt = 0 \tag{3.11}$$

in which T is the kinetic energy, U is the internal strain energy and W is the virtual work of the externally applied end and member traction loads.

3.6.1 Internal Strain Energy

The internal strain energy U is the sum of contributions of the normal stresses, associated shear stresses and St. Venant stresses, and is given by:

$$U = \frac{1}{2}\int_0^\ell \int_A E\,\varepsilon_{zz}^2\,dA\,dz + \frac{1}{2}\int_0^\ell \int_A G\,\gamma_{zs}^2\,dA\,dz + \frac{1}{2}\int_0^\ell GJ\,(\theta_z')^2 dz \tag{3.12}$$

By substituting Equations (3.8) and (3.10) into Equation (3.12), one obtains:

$$\begin{aligned}\delta U = &\int_0^\ell \int_A E\,(w' + y\,\theta_x' - x\,\theta_y' + \omega\psi')(\delta w' + y\,\delta\theta_x' - x\,\delta\theta_y' + \omega\delta\psi')\,dA\,dz \\ &+ \int_0^\ell \int_A G\left((v' + \theta_x)\frac{dy}{ds} + (u' - \theta_y)\frac{dx}{ds} + (\theta_z' + \psi)\frac{d\omega}{ds}\right)\left((\delta v' + \delta\theta_x)\frac{dy}{ds}\right. \\ &\left. + (\delta u' - \delta\theta_y)\frac{dx}{ds} + (\delta\theta_z' + \delta\psi)\frac{d\omega}{ds}\right)dA\,dz + \int_0^\ell GJ\,\theta_z'\,\delta\theta_z'\,dz\end{aligned} \tag{3.13}$$

By performing the area integrals in equation (3.13) and recalling that the axes chosen are principal centroidal, and that the pole is chosen to coincide with the shear centre and the sectorial origin is principal, i.e. the following orthogonality conditions are satisfied

$$S_x, S_y, S_{xy}, S_{\omega x}, S_{\omega y}, S_\omega = \int_A \left[x(s), y(s), x(s)y(s), x(s)\omega(s), y(s)\omega(s), \omega(s) \right] dA = 0 \tag{3.14}$$

The internal strain energy U expression becomes

$$\begin{aligned}
\delta U = \int_0^\ell & \left[EAw'\delta w' + EI_{xx}\,\theta_x'\,\delta\theta_x' + EI_{yy}\,\theta_y'\,\delta\theta_y' + GJ\,\theta_z'\,\delta\theta_z' + EC_w\,\psi'\delta\psi' \right] dz \\
& + \int_0^\ell G\left[D_{xx}\left(u' - \theta_y\right) + D_{xy}\left(v' + \theta_x\right) + D_{hx}\left(\theta_z' + \psi\right) \right] \delta u'\, dz \\
& + \int_0^\ell G\left[D_{xy}\left(u' - \theta_y\right) + D_{yy}\left(v' + \theta_x\right) + D_{hy}\left(\theta_z' + \psi\right) \right] \delta v'\, dz \\
& + \int_0^\ell G\left[D_{hx}\left(u' - \theta_y\right) + D_{hy}\left(v' + \theta_x\right) + D_{ww}\left(\theta_z' + \psi\right) \right] \delta\theta_z'\, dz \\
& + \int_0^\ell G\left[D_{xy}\left(u' - \theta_y\right) + D_{yy}\left(v' + \theta_x\right) + D_{hy}\left(\theta_z' + \psi\right) \right] \delta\theta_x\, dz \\
& - \int_0^\ell G\left[D_{xx}\left(u' - \theta_y\right) + D_{xy}\left(v' + \theta_x\right) + D_{hx}\left(\theta_z' + \psi\right) \right] \delta\theta_y\, dz \\
& + \int_0^\ell G\left[D_{hx}\left(u' - \theta_y\right) + D_{hy}\left(v' + \theta_x\right) + D_{\omega\omega}\left(\theta_z' + \psi\right) \right] \delta\psi\, dz
\end{aligned} \tag{3.15}$$

in which the following cross section properties were defined:

$$D_{xx}, D_{yy}, D_{xy}, D_{hx}, D_{hy}, D_{\omega\omega} = \int_A \left[\left(\frac{dx}{ds}\right)^2, \left(\frac{dy}{ds}\right)^2, \left(\frac{dx}{ds}\right)\left(\frac{dy}{ds}\right), \left(\frac{d\omega}{ds}\right)\left(\frac{dx}{ds}\right), \left(\frac{d\omega}{ds}\right)\left(\frac{dy}{ds}\right), \left(\frac{d\omega}{ds}\right)^2 \right] dA \tag{3.16}$$

Similar relations for section properties to the expressions given in equation (3.16) are available in the literature by Laudiero and Savoia (1991).

3.6.2 Potential Energy for External Loads

A prismatic straight thin-walled member element of arbitrary open cross-section is considered as shown in the Figure (3.2). The beam element is subjected to two kinds of dynamic forces: (1) member surface tractions $p_x(z,s,t)$, $p_y(z,s,t)$ and $p_z(z,s,t)$ per unit

area of the undeformed middle surface and acting along the X,Y and Z directions, respectively, and (2) external applied tractions acting at the member ends. The normal stress and shear resultants $\bar{\sigma}_o(0,s,t)=\bar{\sigma}_{zz}(0,s,n,t)$ and $\bar{\tau}_o(0,s,t)=\bar{\tau}_{zs}(0,s,n,t)$ are acting at member end $z=0$, $\bar{\sigma}_\ell(\ell,s,t)=\bar{\sigma}_{zz}(\ell,s,n,t)$ and $\bar{\tau}_\ell(\ell,s,t)=\bar{\tau}_{zs}(\ell,s,n,t)$ are acting at the other end $z=\ell$ [Erkmen 2006]. The positive directions of stress and force resultants $\bar{\sigma}_o,\bar{\sigma}_\ell,\bar{\tau}_o,\bar{\tau}_\ell,N_{zo},N_{z\ell},V_{xo},V_{x\ell},V_{yo},V_{y\ell},M_{xo},M_{x\ell},M_{yo},M_{y\ell},M_{zo}$ and $M_{z\ell}$ are illustrated in Figure (3.2).

The variation of the potential energy δW due to the external applied forces is obtained by taking the external virtual work done δW_1 due to the external applied tractions $\bar{\sigma}_o,\bar{\sigma}_\ell,\bar{\tau}_o,\bar{\tau}_\ell$ and the external virtual work done δW_2 induced by the member tractions $p_x(z,s,t)$, $p_y(z,s,t)$ and $p_z(z,s,t)$ acting along X,Y and Z axes, respectively [Erkmen 2006]. This yield:

$$\delta W=\delta W_1+\delta W_2 \tag{3.17}$$

The external virtual work done δW_1 due to applied end tractions is:

$$\begin{aligned}\delta W_1=&-\int_A \bar{\sigma}_o\delta w_p(0,s,t)\,dA-\int_A \bar{\tau}_o\cos\hat{\alpha}(s)\,\delta u_p(0,s,t)dA-\int_A \bar{\tau}_o\sin\hat{\alpha}(s)\,\delta v_p(0,s,t)dA\\&+\int_A \bar{\sigma}_\ell\delta w_p(\ell,s,t)dA+\int_A \bar{\tau}_\ell\cos\hat{\alpha}(s)\,\delta u_p(\ell,s,t)dA+\int_A \bar{\tau}_\ell\sin\hat{\alpha}(s)\,\delta v_p(\ell,s,t)dA\end{aligned}$$

By substituting the expressions for displacements, equations (3.1) to (3.3), and leads to:

$$\begin{aligned}\delta W_1=&-\int_A\Big[\bar{\sigma}_o\Big[\delta w(0,t)+y(s)\delta\theta_x(0,t)-x(s)\delta\theta_y(0,t)+\omega(s)\delta\psi(0,t)\Big]dA\\&-\int_A\bar{\tau}_o\cos\hat{\alpha}(s)\Big[\delta u(0,t)-(y(s)-y_s)\delta\theta_z(0,t)\Big]dA\\&-\int_A\bar{\tau}_o\sin\hat{\alpha}(s)\Big[\delta v(0,t)+(x(s)-x_s)\delta\theta_z(0,t)\Big]dA\\&+\int_A\bar{\sigma}_\ell\Big[\delta w(\ell,t)+y(s)\,\delta\theta_x(\ell,t)-x(s)\delta\theta_y(\ell,t)+\omega(s)\delta\psi(\ell,t)\Big]dA\\&+\int_A\bar{\tau}_\ell\cos\hat{\alpha}(s)\Big[\delta u(\ell,t)-(y(s)-y_s)\delta\theta_z(\ell,t)\Big]dA\\&+\int_A\bar{\tau}_\ell\sin\hat{\alpha}(s)\Big[\delta v(\ell,t)+(x(s)-x_s)\delta\theta_z(\ell,t)\Big]dA\end{aligned}\tag{3.18}$$

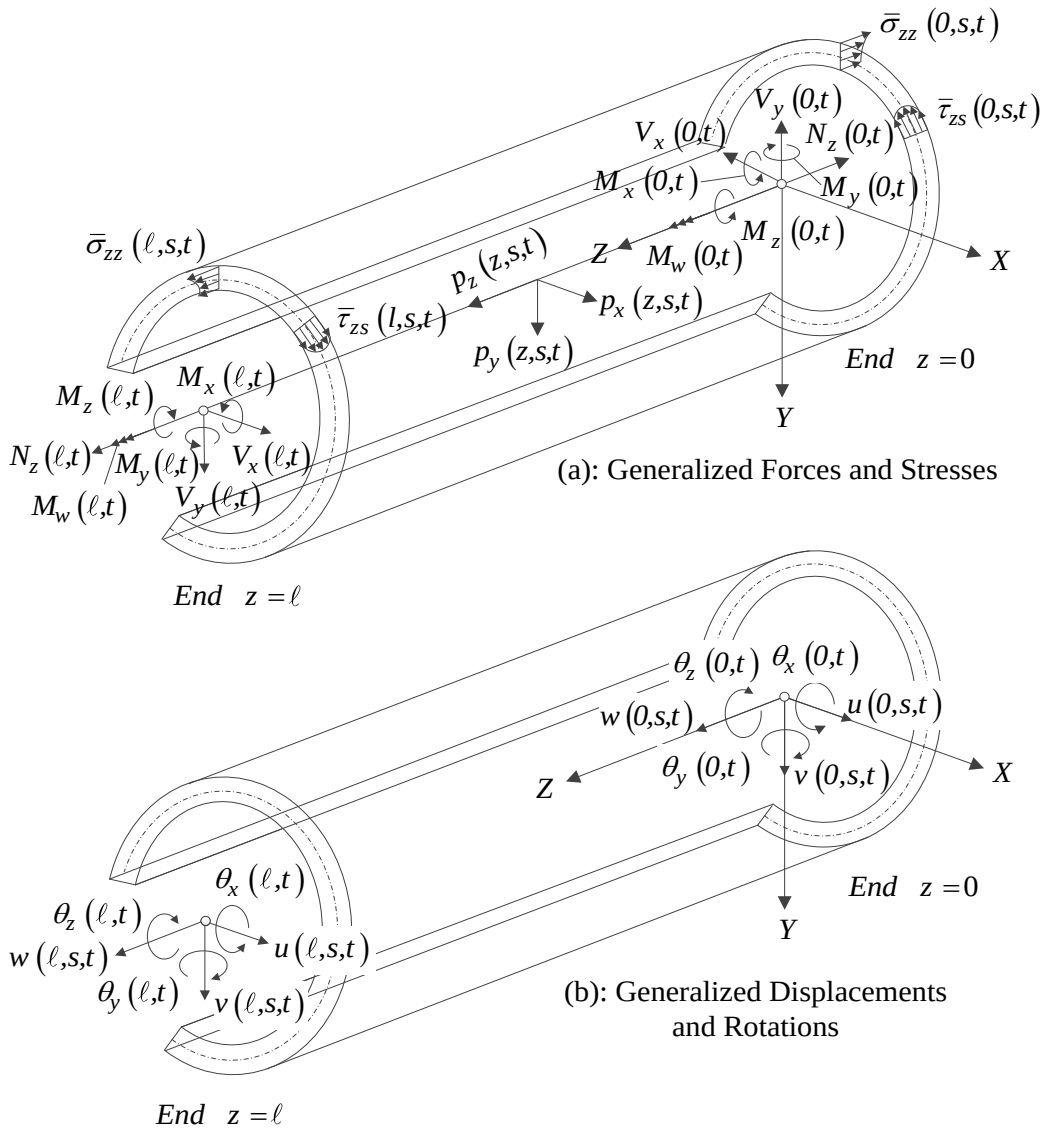

Figure (3.2): Thin-walled Beam Element Geometry [Erkmen 2006].

By regrouping terms, equation (3.18) takes the form:

$$\begin{aligned}\delta W_1 = &-N_z(0,t)\delta w(0,t) - V_x(0,t)\delta u(0,t) - V_y(0,t)\delta v(0,t) + M_x(0,t)\delta\theta_x(0,t)\\ &- M_y(0,t)\delta\theta_y(0,t) - M_z(0,t)\delta\theta_z(0,t) + M_w(0,t)\delta\psi(0,t) + N_z(\ell,t)\delta w(\ell,t)\\ &+ V_x(\ell,t)\delta u(\ell,t) + V_y(\ell,t)\delta v(\ell,t) - M_x(\ell,t)\delta\theta_x(\ell,t) + M_y(\ell,t)\delta\theta_y(\ell,t)\\ &+ M_z(\ell,t)\delta\theta_z(\ell,t) - M_w(\ell,t)\delta\psi(\ell,t)\end{aligned} \tag{3.19}$$

in which the energy conjugate stress resultants are defined by:

$$N_z(j,t) = \int_A \bar{\sigma}_j dA\ ,\ V_x(j,t) = \int_A \bar{\tau}_j \cos\hat{\alpha}(s) dA\ ,\ V_y(j,t) = \int_A \bar{\tau}_j \sin\hat{\alpha}(s) dA$$

$M_x(j,t) = -\int_A \bar{\sigma}_j\, y(s)\, dA$, $M_y(j,t) = -\int_A \bar{\sigma}_j\, x(s)\, dA$, $M_w(j,t) = -\int_A \bar{\sigma}_j\, \omega(s)\, dA$

$M_z(j,t) = \int_A \left[-\bar{\tau}_j(j,s,t,n)\cos\hat{\alpha}(s)\left(y(s) - y_s\right) + \bar{\tau}_j(j,s,t,n)\sin\hat{\alpha}(s)\left(x(s) - x_s\right)\right] dA$, for $j = 0, \ell$.

where $N_z(z,t)$ is the normal force acting along the centroidal axis, $V_x(z,t), V_y(z,t)$ are the shear forces acting at the end shear centre, $M_x(z,t), M_y(z,t)$ are the bending moments about the principal axes acting at the end cross-sections and $M_w(z,t)$ is the bimoment, at the end cross-sections, related to a Sectorial origin S_o defined by the orthogonality condition $S_\omega = 0$, and $M_z(z,t)$ is the twisting moment of the tractions tangent, all acting at the end cross-sections $z = 0$ and $z = \ell$.

The external virtual work done δW_2 induced by the surface member tractions $p_x(z,s,t)$, $p_y(z,s,t)$ and $p_z(z,s,t)$ is given as:

$$\delta W_2 = \int_0^\ell \int_s \left[p_x(z,s,t)\, \delta u_p(z,s,t) + p_y(z,s,t)\, \delta v_p(z,s,t) + p_z(z,s,t)\, \delta w_p(z,s,t)\right] ds\, dz \qquad (3.20)$$

Substituting the expressions for virtual displacements $\delta u_p(z,s,t), \delta v_p(z,s,t), \delta w_p(z,s,t)$ of the general point $p(x,y)$ into equation (3.20), yields:

$$\delta W_2 = \int_0^\ell \left[q_x(z,t)\delta u + q_y(z,t)\delta v + q_z(z,t)\delta w + m_z(z,t)\delta\theta_z + m_x(z,t)\delta\theta_x + m_y(z,t)\delta\theta_y + m_w(z,t)\delta\psi \right] dz \qquad (3.21)$$

where the resultant forces and moments per unit length are defined, respectively, as:

$q_x(z,t), q_y(z,t), q_z(z,t) = \int_s \left[p_x(z,s,t), p_y(z,s,t), p_z(z,s,t)\right] ds$

$m_x(z,t), m_y(z,t), m_w(z,t) = \int_s p_z(z,s,t)\left[y(s), -x(s), \omega(s)\right] ds$

while the resultant twisting moments $m_z(z,t)$ per unit length induced by the action of traction components $p_x(z,s,t)$, $p_y(z,s,t)$ acting in the plane of the cross-section about the shear centre is given by:

$$m_z(z,t) = \int_s \left(p_y(z,s,t)\left[x(s) - x_s\right] - p_x(z,s,t)\left[y(s) - y_s\right] \right) ds$$

Adding equations (3.19) and (3.21) to equation (3.15), the variation of the total potential energy $\delta\Pi$ is expressed as:

$$\begin{aligned}
\delta\Pi = & \left[N_z(z,t)\,\delta w(z,t)\right]_0^\ell + \left[V_x(z,t)\delta u(z,t)\right]_0^\ell + \left[V_y(z,t)\delta v(z,t)\right]_0^\ell \\
& - \left[M_x(z,t)\delta\theta_x(z,t)\right]_0^\ell + \left[M_y(z,t)\delta\theta_y(z,t)\right]_0^\ell \\
& + \left[M_z(z,t)\delta\theta_z(z,t)\right]_0^\ell - \left[M_w(z,t)\delta\psi(z,t)\right]_0^\ell \\
& + \int_0^\ell G\left[D_{xx}\left(u' - \theta_y\right) + D_{xy}\left(v' + \theta_x\right) + D_{hx}\left(\theta_z' + \psi\right)\right]\delta u'\,dz \\
& + \int_0^\ell G\left[D_{xy}\left(u' - \theta_y\right) + D_{yy}\left(v' + \theta_x\right) + D_{hy}\left(q_z' + \psi\right)\right]\delta v'\,dz \\
& + \int_0^\ell G\left[D_{hx}\left(u' - \theta_y\right) + D_{hy}\left(v' + \theta_x\right) + D_{ww}\left(\theta_z' + \psi\right)\right]\delta\theta_z'\,dz \\
& + \int_0^\ell G\left[D_{xy}\left(u' - \theta_y\right) + D_{yy}\left(v' + \theta_x\right) + D_{hy}\left(\theta_z' + \psi\right)\right]\delta\theta_x\,dz \\
& - \int_0^\ell G\left[D_{xx}\left(u' - \theta_y\right) + D_{xy}\left(v' + \theta_x\right) + D_{hx}\left(\theta_z' + \psi\right)\right]\delta\theta_y\,dz \\
& + \int_0^\ell G\left[D_{hx}\left(u' - \theta_y\right) + D_{hy}\left(v' + \theta_x\right) + D_{\omega\omega}\left(\theta_z' + \psi\right)\right]\delta\psi\,dz \\
& + \int_0^\ell \left[EAw'\delta w' + EI_{xx}\,\theta_x'\delta\theta_x' + EI_{yy}\,\theta_y'\,\delta\theta_y' + GJ\,\theta_z'\,\delta\theta_z' + EC_w\,\psi'\delta\psi'\right]dz \\
& - \int_0^\ell \left[q_x(z,t)\delta u + q_y(z,t)\delta v - q_z(z,t)\delta w - m_z(z,t)\delta\theta_z - m_x(z,t)\delta\theta_x\right. \\
& \left. - m_y(z,t)\delta\theta_y - m_w(z,t)\delta\psi\right]dz
\end{aligned} \tag{3.22}$$

3.6.3 The Kinetic Energy

The variation of the kinetic energy δT [e.g. Librescu and Song 2006] is:

$$\delta T = \int_0^\ell \int_A \rho\left(\dot{\xi}\delta\dot{\xi} + \dot{\eta}\,\delta\dot{\eta} + \dot{w}_p\,\delta\dot{w}_p\right)dA\,dz \tag{3.23}$$

Substituting equations (3.3) and (3.4) into equation (3.23), and by performing the area integrals in the resulting equation and applying the orthogonality conditions $S_x = S_y = S_{xy} = S_{\omega x} = S_{\omega y} = S_\omega = 0$, the variation of kinetic energy is expressed as:

$$\begin{aligned}\delta T = \rho \int_0^{\ell} \Big(& A\dot{w}\, d\dot{w} + \Big[\left(D_{yy} + D_{xx}\right)\dot{u} + \left(D_{hx} - D_{ry}\right)\dot{\theta}_z \Big]\delta\dot{u} + \Big[\left(D_{yy} + D_{xx}\right)\dot{v} + \left(D_{hy} + D_{rx}\right)\dot{\theta}_z \Big]\delta\dot{v} \\ & + I_{xx}\,\dot{\theta}_x\,\delta\dot{\theta}_x + I_{yy}\,\dot{\theta}_y\,\delta\dot{\theta}_y + \Big[\left(D_{hx} - D_{ry}\right)\dot{u} + \left(D_{hy} + D_{rx}\right)\dot{v} + A r_o^2 \dot{\theta}_z \Big]\delta\dot{\theta}_z + C_w\,\dot{\psi}\delta\dot{\psi} \Big) dz\end{aligned} \tag{3.24}$$

in which

$$D_{rx}, D_{ry} = \int_A \left[r\left(\frac{dx}{ds}\right), r\left(\frac{dy}{ds}\right) \right] dA, \quad r_o^2 = \frac{1}{A}\int_A \left(h^2 + r^2\right) dA = \frac{\left(I_{xx} + I_{yy}\right)}{A} + \left(x_s^2 + y_s^2\right) \tag{3.25}$$

where r_o is the polar distance of arbitrary point $p(x, y)$ measured from the shear centre of the cross-section (as shown in Fig. 2.11). Substituting expressions of $h(s)$ and $r(s)$ represented in equations (3.5) and (3.6) into equation (3.24), the resulting equation is simplified to:

$$\begin{aligned}\delta T = \rho \int_0^{\ell} \Big(& A\dot{w}\, d\dot{w} + A\left(\dot{u} + y_s\dot{\theta}_z\right)\delta\dot{u} + A\left(\dot{v} - x_s\dot{\theta}_z\right)\delta\dot{v} + I_{xx}\,\dot{\theta}_x\,\delta\,\dot{\theta}_x + I_{yy}\,\dot{\theta}_y\,\delta\dot{\theta}_y \\ & + A\left[\left(y_s\dot{u} - x_s\dot{v}\right) + r_o^2\dot{\theta}_z \right]\delta\dot{\theta}_z + C_w\,\dot{\psi}\delta\dot{\psi} \Big) dz\end{aligned} \tag{3.26}$$

where the following expressions are newly arising from the formulation as:

$$D_{hx} - D_{ry} = y_s A \quad \text{and} \quad D_{hy} + D_{rx} = -x_s A \tag{3.27}$$

3.7 Dynamic Equations of Motion

The equations of motion are given by substituting the variational expressions for total potential energy $\delta\Pi$ and kinetic energy δT into Hamilton's principle, equation (3.11). After performing integration by parts, governing differential equations for dynamic equilibrium are recovered:

$$\rho A\ddot{w} - EAw'' = q_z(z,t) \tag{3.28}$$

$$\rho A\left[\ddot{u}+y_s\ddot{\theta}_z\right]-G\left[D_{xx}\left(u''-\theta_y'\right)+D_{xy}\left(v''+\theta_x'\right)+D_{hx}\left(\theta_z''+\psi'\right)\right]=q_x\left(z,t\right) \tag{3.29}$$

$$\rho A\left[\ddot{v}-x_s\ddot{\theta}_z\right]-G\left[D_{xy}\left(u''-\theta_y'\right)+D_{yy}\left(v''+\theta_x'\right)+D_{hy}\left(\theta_z''+\psi'\right)\right]=q_y\left(z,t\right) \tag{3.30}$$

$$\rho A\left[\left(y_s\ddot{u}-x_s\ddot{v}\right)+r_o^2\ddot{\theta}_z\right]-GJ\theta_z''-G\left[D_{hx}\left(u''-\theta_y'\right)+D_{hy}\left(v''+\theta_x'\right)+D_{ww}\left(\theta_z''+\psi'\right)\right]=m_z\left(z,t\right) \tag{3.31}$$

$$\rho I_{xx}\ddot{\theta}_x-EI_{xx}\theta_x''+G\left[D_{xy}\left(u'-\theta_y\right)+D_{yy}\left(v'+\theta_x\right)+D_{hy}\left(\theta_z'+\psi\right)\right]=m_x\left(z,t\right) \tag{3.32}$$

$$\rho I_{yy}\ddot{\theta}_y-EI_{yy}\theta_y''-G\left[D_{xx}\left(u'-\theta_y\right)+D_{xy}\left(v'+\theta_x\right)+D_{hx}\left(\theta_z'+\psi\right)\right]=m_y\left(z,t\right) \tag{3.33}$$

$$-\rho C_w\ddot{\psi}+EC_w\psi''-G\left[D_{hx}\left(u'-\theta_y\right)+D_{hy}\left(v'+\theta_x\right)+D_{\omega\omega}\left(\theta_z'+\psi\right)\right]=m_w\left(z,t\right) \tag{3.34}$$

The associated boundary conditions are

$$\left[EAw'\left(z,t\right)-N_z\left(z,t\right)\right]\delta w\left(z,t\right)\Big|_0^\ell=0 \tag{3.35}$$

$$\left[G\left\{D_{xx}\left(u'-\theta_y\right)+D_{xy}\left(v'+\theta_x\right)+D_{hx}\left(\theta_z'+\psi\right)\right\}-V_x\left(z,t\right)\right]\delta u\left(z,t\right)\Big|_0^\ell=0 \tag{3.36}$$

$$\left[G\left\{D_{xy}\left(u'-\theta_y\right)+D_{yy}\left(v'+\theta_x\right)+D_{hy}\left(\theta_z'+\psi\right)\right\}-V_y\left(z,t\right)\right]\delta v\left(z,t\right)\Big|_0^\ell=0 \tag{3.37}$$

$$\left[GJ\theta_z'+G\left\{D_{hx}\left(u'-\theta_y\right)+D_{hy}\left(v'+\theta_x\right)+D_{ww}\left(\theta_z'+\psi\right)\right\}-M_z\left(z,t\right)\right]\delta\theta_z\left(z,t\right)\Big|_0^\ell=0 \tag{3.38}$$

$$\left[EI_{xx}\theta_x'+M_x\left(z,t\right)\right]\delta\theta_x\left(z,t\right)\Big|_0^\ell=0 \tag{3.39}$$

$$\left[EI_{yy}\theta_y'-M_y\left(z,t\right)\right]\delta\theta_y\left(z,t\right)\Big|_0^\ell=0 \tag{3.40}$$

$$\left[EC_w\psi'+M_w\left(z,t\right)\right]\delta\psi\left(z,t\right)\Big|_0^\ell=0 \tag{3.41}$$

The first equation represents the longitudinal displacement equilibrium equation and involves a single field variable, the longitudinal displacement w . This equation is observed to be uncoupled from the remaining differential equations, which are found to be coupled in the field variables $u,v,\theta_x,\theta_y,\theta_z,\psi$.

3.7.1 Special Case: Field Equations without Shear Deformations

When one ignores the shear deformation, i.e. by setting the shear strain expressed in equation (3.10) to zero, the following conditions are obtained

$$\theta_x = -v' \,,\ \theta_y = u' \ \text{ and } \ \psi = -\theta_z' = -\phi' \tag{3.42}$$

Substituting equation (3.42) into equation (3.22), the governing differential equations simplify to:

$$\rho A\ddot{w} - EAw'' = q_z(z,t) \tag{3.43}$$

$$EI_{xx}v^{iv} - \rho I_{xx}\ddot{v}'' + \rho A\left(\ddot{v} - x_s\ddot{\phi}\right) = q_y(z,t) - \frac{\partial m_x(z,t)}{\partial z} \tag{3.44}$$

$$EI_{yy}u^{iv} - \rho I_{yy}\ddot{u}'' + \rho A\left(\ddot{u} + y_s\ddot{\phi}\right) = q_x(z,t) + \frac{\partial m_y(z,t)}{\partial z} \tag{3.45}$$

$$EC_w\phi^{iv} - \rho C_w\ddot{\phi}'' - GJ\phi'' + \rho A\left(y_s\ddot{u} - x_s\ddot{v} + r_o^2\ddot{\phi}\right) = m_z(z,t) + \frac{\partial m_w(z,t)}{\partial z} \tag{3.46}$$

and the associated boundary conditions are

$$\left[EAw'(z,t) - N_z(z,t)\right]\delta w(z,t)\Big|_0^\ell = 0 \tag{3.47}$$

$$\left[\rho I_{yy}\ddot{u}' - EI_{yy}u''' - V_x(z,t)\right]\delta u(z,t)\Big|_0^\ell = 0 \tag{3.48}$$

$$\left[\rho I_{xx}\ddot{v}' - EI_{xx}v''' - V_y(z,t)\right]\delta v(z,t)\Big|_0^\ell = 0 \tag{3.49}$$

$$\left[\rho C_w\ddot{\phi}' - EC_w\phi''' + GJ\phi' - M_z(z,t)\right]\delta\phi(z,t)\Big|_0^\ell = 0 \tag{3.50}$$

$$\left[EI_{xx}v'' - M_x(z,t)\right]\delta v'(z,t)\Big|_0^\ell = 0 \tag{3.51}$$

$$\left[EI_{yy}u'' - M_y(z,t)\right]\delta u'(z,t)\Big|_0^\ell = 0 \tag{3.52}$$

$$\left[EC_w\phi'' - M_w(z,t)\right]\delta\phi'(z,t)\Big|_0^\ell = 0 \tag{3.53}$$

The linear differential equations (3.43) to (3.46) with the boundary conditions (3.47) to (3.53) governing the coupled flexural-torsional vibrations are the familiar Vlasov's dynamic equations [Vlasov 1961].

3.7.2 Static Case: Including Shear Deformation Effects

To investigate the behaviour of the open thin-walled elastic beam subjected to static loads, the terms derived from the kinetic energy expression cannot be included in the differential equations (3.28) to (3.34) and the associated boundary conditions (3.35) to (3.41), i.e. the

terms containing time derivation in the differential equations and the associated boundary conditions can be omitted, then, the resulting differential equations governing the static behaviour of the open thin-walled shear deformable member are given as:

$$EAw'' = -q_z(z,t) \tag{3.54}$$

$$-G\left[D_{xx}\left(u''-\theta_y'\right)+D_{xy}\left(v''+\theta_x'\right)+D_{hx}\left(\theta_z''+\psi'\right)\right]=q_x(z,t) \tag{3.55}$$

$$-G\left[D_{xy}\left(u''-\theta_y'\right)+D_{yy}\left(v''+\theta_x'\right)+D_{hy}\left(\theta_z''+\psi'\right)\right]=q_y(z,t) \tag{3.56}$$

$$-GJ\theta_z''-G\left[D_{hx}\left(u''-\theta_y'\right)+D_{hy}\left(v''+\theta_x'\right)+D_{\omega\omega}\left(\theta_z''+\psi'\right)\right]=m_z(z,t) \tag{3.57}$$

$$-EI_{xx}\theta_x''+G\left[D_{xy}\left(u'-\theta_y\right)+D_{yy}\left(v'+\theta_x\right)+D_{hy}\left(\theta_z'+\psi\right)\right]=m_x(z,t) \tag{3.58}$$

$$-EI_{yy}\theta_y''-G\left[D_{xx}\left(u'-\theta_y\right)+D_{xy}\left(v'+\theta_x\right)+D_{hx}\left(\theta_z'+\psi\right)\right]=m_y(z,t) \tag{3.59}$$

$$EC_w\psi''-G\left[D_{hx}\left(u'-\theta_y\right)+D_{hy}\left(v'+\theta_x\right)+D_{\omega\omega}\left(\theta_z'+\psi\right)\right]=m_w(z,t) \tag{3.60}$$

Corresponding boundary conditions are:

$$\left[EAw'(z)-N_z(z)\right]\delta w(z)\Big|_0^\ell = 0 \tag{3.61}$$

$$\left[G\left\{D_{xx}\left(u'-\theta_y\right)+D_{xy}\left(v'+\theta_x\right)+D_{hx}\left(\theta_z'+\psi\right)\right\}-V_x(z)\right]\delta u(z)\Big|_0^\ell = 0 \tag{3.62}$$

$$\left[G\left\{D_{xy}\left(u'-\theta_y\right)+D_{yy}\left(v'+\theta_x\right)+D_{hy}\left(\theta_z'+\psi\right)\right\}-V_y(z)\right]\delta v(z)\Big|_0^\ell = 0 \tag{3.63}$$

$$\left[GJ\theta_z'+G\left\{D_{hx}\left(u'-\theta_y\right)+D_{hy}\left(v'+\theta_x\right)+D_{ww}\left(\theta_z'+\psi\right)\right\}-M_z(z)\right]\delta\theta_z(z)\Big|_0^\ell = 0 \tag{3.64}$$

$$\left[EI_{xx}\theta_x'+M_x(z)\right]\delta\theta_x(z)\Big|_0^\ell = 0 \tag{3.65}$$

$$\left[EI_{yy}\theta_y'-M_y(z)\right]\delta\theta_y(z)\Big|_0^\ell = 0 \tag{3.66}$$

$$\left[EC_w\psi'+M_w(z)\right]\delta\psi(z)\Big|_0^\ell = 0 \tag{3.67}$$

The above differential equations (3.54) to (3.60) with the boundary conditions, equations (3.61) to (3.67), are the general form linear differential equations governing the behaviour of thin-walled shear deformable member of general open cross-section subjected to general static loads.

3.7.3 Static Solution - Ignoring Shear Deformation

The most comprehensive theory of combined flexure and torsion of thin-walled open members was developed by Vlasov (1961) in which the shearing deformations of the middle surface of the member were assumed to vanish (Vlasov assumption). Vlasov equations are enforced by neglecting the shear deformations of the middle surface of the member in the above differential equations (3.54) to (3.60) and the associated boundary conditions (3.61) to (3.67), i.e. $\theta_x = -v'$, $\theta_y = u'$ and $\psi = -\theta_z' = -\phi'$ (see Figure 3.1), which results in:

$$EAw'' + q_z(z) = 0 \tag{3.68}$$

$$EI_{xx}u^{iv} = q_x(z) + \frac{\partial m_y(z)}{\partial z} \tag{3.69}$$

$$EI_{xx}v^{iv} = q_y(z) - \frac{\partial m_x(z)}{\partial z} \tag{3.70}$$

$$EC_w\phi^{iv} - GJ\phi'' = m_z(z) + \frac{\partial m_w(z)}{\partial z} \tag{3.71}$$

According to Vlasov beam theory, the associated boundary conditions are reduced to:

$$\left[EAw'(z) - N_z(z)\right]\delta w(z)\Big|_0^\ell = 0 \tag{3.72}$$

$$\left[EI_{yy}u''' + V_x(z)\right]\delta u(z)\Big|_0^\ell = 0 \tag{3.73}$$

$$\left[EI_{xx}v''' + V_y(z)\right]\delta v(z)\Big|_0^\ell = 0 \tag{3.74}$$

$$\left[EC_w\phi''' - GJ\phi' + M_z(z)\right]\delta\phi(z)\Big|_0^\ell = 0 \tag{3.75}$$

$$\left[EI_{xx}v'' - M_x(z)\right]\delta v'(z)\Big|_0^\ell = 0 \tag{3.76}$$

$$\left[EI_{yy}u'' - M_y(z)\right]\delta u'(z)\Big|_0^\ell = 0 \tag{3.77}$$

$$\left[EC_w\phi'' - M_w(z)\right]\delta\phi'(z)\Big|_0^\ell = 0 \tag{3.78}$$

Equations (3.68) to (3.71) with the boundary conditions (3.72) to (3.78) governing the behaviour of thin-walled open members of arbitrary sections without shear deformations are identical to those of Vlasov (1961). It is noted that the seven differential equations are reduced to four differential equations for the case of negligible shear deformations.

3.8 Field Equations for General Cross-Section

The resulting field equations (3.37) to (3.43) are the general differential equations governing the extension and coupled bending-torsion dynamic behaviour of thin-walled members of arbitrary open sections, which incorporates shear deformation, warping deformation and translational and rotary inertia effects, subjected to general dynamic excitations. The time variable in equations (3.37-3.43) can be eliminated by assuming the solution to be harmonic.

3.8.1 Expressions for Applied Forces

The thin-walled member is assumed to be subjected to general applied harmonic forces within the member;

$$\begin{aligned} &q_x(z,t), q_y(z,t), q_z(z,t), m_x(z,t), m_y(z,t), m_z(z,t), m_w(z,t) \\ &\qquad = \left[\bar{q}_x(z), \bar{q}_y(z), \bar{q}_z(z), \bar{m}_x(z), \bar{m}_y(z), \bar{m}_z(z), \bar{m}_w(z)\right] e^{i\Omega t} \end{aligned} \tag{3.79}$$

and the end harmonic forces are;

$$\begin{aligned} &N_z(z_e,t), V_x(z_e,t), V_y(z_e,t), M_x(z_e,t), M_y(z_e,t), M_z(z_e,t), M_w(z_e,t) \\ &\qquad = \left[\bar{N}_z(z_e), \bar{V}_x(z_e), \bar{V}_y(z_e), \bar{M}_x(z_e), \bar{M}_y(z_e), \bar{M}_z(z_e), \bar{M}_w(z_e)\right] e^{i\Omega t} \end{aligned} \tag{3.80}$$

in which Ω is the circular frequency of the applied loads, $i = \sqrt{-1}$ is the imaginary constant, $q_x(z,t)$, $q_y(z,t)$, $q_z(z,t)$ are the distributed harmonic forces, $m_x(z,t)$, $m_y(z,t)$, $m_z(z,t)$ are the distributed harmonic moments, $m_w(z,t)$ is the distributed harmonic bimoment, $N_z(z_e,t)$, $V_x(z_e,t)$, $V_y(z_e,t)$ are the longitudinal, transverse and lateral harmonic forces at member ends $(z_e = 0, \ell)$, $M_x(z_e,t)$, $M_y(z_e,t)$, $M_z(z_e,t)$ are the harmonic end moments and $M_w(z_e,t)$ is the harmonic end bimoments. The applied forces are assumed to have the same sign convention as those of the end displacement components (Figure 2.9).

3.8.2 Steady State Displacement Functions

Under the above applied harmonic forces, the steady state component of the response is assumed to take the form:

$$w(z,t),u(z,t),v(z,t),\theta_x(z,t),\theta_y(z,t),\theta_z(z,t),\psi(z,t) = \left[\bar{w}(z),\bar{u}(z),\bar{v}(z),\bar{\theta}_x(z),\bar{\theta}_y(z),\bar{\theta}_z(z),\bar{\psi}(z)\right]e^{i\Omega t} \tag{3.81}$$

where $\bar{w}(z),\bar{u}(z),\bar{v}(z),\bar{\theta}_x(z),\bar{\theta}_y(z),\bar{\theta}_z(z)$ and $\bar{\psi}(z)$ are space functions for longitudinal translation, bending translations, bending rotations, torsional rotation and warping deformation, respectively. In line with the objective of the present study, the displacement fields postulated in Equation (3.81) neglect the transient response.

3.8.3 Equilibrium Field Equations for Harmonic Vibration

Substituting equations (3.79) to (3.81) into governing field equations (3.37) to (3.43), gives the seven differential equations for space functions $\bar{w}(z),\bar{u}(z),\bar{v}(z),\bar{\theta}_x(z),\bar{\theta}_y(z),\bar{\theta}_z(z)$ and $\bar{\psi}(z)$ as:

$$\left(\rho A\,\Omega^2 + EA\mathcal{D}^2\right)\bar{w}(z) = -\bar{q}_z(z) \tag{3.82}$$

$$-\left(\rho A\,\Omega^2 + GD_{xx}\mathcal{D}^2\right)\bar{u}(z) - \left(GD_{xy}\,\mathcal{D}^2\right)\bar{v}(z) - \left(GD_{xy}\mathcal{D}\right)\bar{\theta}_x(z) + \left(GD_{xx}\mathcal{D}\right)\bar{\theta}_y(z) - \left(\rho A\Omega^2 y_s + GD_{hx}\mathcal{D}^2\right)\bar{\theta}_z(z) - \left(GD_{hx}\mathcal{D}\right)\bar{\psi}(z) = \bar{q}_x(z) \tag{3.83}$$

$$\left(-GD_{xy}\mathcal{D}^2\right)\bar{u}(z) - \left(\rho A\,\Omega^2 + GD_{yy}\mathcal{D}^2\right)\bar{v}(z) - \left(GD_{yy}\mathcal{D}\right)\bar{\theta}_x(z) + \left(GD_{xy}\mathcal{D}\right)\bar{\theta}_y(z) + \left(\rho A\,\Omega^2 x_s - GD_{hy}\mathcal{D}^2\right)\bar{\theta}_z(z) - \left(GD_{hy}\mathcal{D}\right)\bar{\psi}(z) = \bar{q}_y(z) \tag{3.84}$$

$$-\left(GD_{xy}\mathcal{D}\right)\bar{u}(z) - \left(GD_{yy}\mathcal{D}\right)\bar{v}(z) + \left(\rho I_{xx}\Omega^2 - GD_{yy} + EI_{xx}\mathcal{D}^2\right)\bar{\theta}_x(z) + GD_{xy}\bar{\theta}_y(z) - \left(GD_{hy}\mathcal{D}\right)\bar{\theta}_z(z) - GD_{hy}\bar{\psi}(z) = \bar{m}_x(z) \tag{3.85}$$

$$\left(GD_{xx}\mathcal{D}\right)\bar{u}(z) + \left(GD_{xy}\mathcal{D}\right)\bar{v}(z) + GD_{xy}\bar{\theta}_x(z) - \left(GD_{xx} - \rho I_{yy}\Omega^2 - EI_{yy}\mathcal{D}^2\right)\bar{\theta}_y(z) + \left(GD_{hx}\mathcal{D}\right)\bar{\theta}_z(z) + GD_{hx}\bar{\psi}(z) = \bar{m}_y(z) \tag{3.86}$$

$$-\left(\rho A\Omega^2 y_s + GD_{hx}\mathcal{D}^2\right)\bar{u}(z) + \left(\rho A\Omega^2 x_s - GD_{hy}\mathcal{D}^2\right)\bar{v}(z) - \left(GD_{hy}\mathcal{D}\right)\bar{\theta}_x(z) + \left(GD_{hx}\mathcal{D}\right)\bar{\theta}_y(z) - \left[\rho A\,\Omega^2 r_o^2 + G\left(J + D_{\omega\omega}\right)\mathcal{D}^2\right]\bar{\theta}_z(z) - \left(GD_{\omega\omega}\mathcal{D}\right)\bar{\psi}(z) = \bar{m}_z(z) \tag{3.87}$$

$$-\left(GD_{hx}\mathcal{D}\right)\bar{u}\left(z\right)-\left(GD_{hy}\mathcal{D}\right)\bar{v}\left(z\right)-GD_{hy}\bar{\theta}_x\left(z\right)+GD_{hx}\bar{\theta}_y\left(z\right)-\left(GD_{\omega\omega}\mathcal{D}\right)\bar{\theta}_z\left(z\right)$$
$$+\left(\rho C_w\,\Omega^2-GD_{\omega\omega}+EC_w\mathcal{D}^2\right)\bar{\psi}\left(z\right)=\bar{m}_w\left(z\right) \tag{3.88}$$

In the above equations, $\mathcal{D}$ and $\mathcal{D}^2$ denotes the first and second differentiation with respect to z, i.e. $\mathcal{D}\equiv d/dz$ and $\mathcal{D}^2\equiv d^2/dz^2$.

The boundary conditions corresponding to the governing field equations in (3.82) to (3.88) are adapted by substituting the expressions in (3.79) and (3.81) into equations (3.35) to (3.41), give

$$\left[EA\bar{w}'-\bar{N}_z\left(z\right)\right]\delta\bar{w}\left(z\right)\Big|_0^\ell=0 \tag{3.89}$$

$$\left[GD_{xx}\left(\bar{u}'-\bar{\theta}_y\right)+GD_{xy}\left(\bar{v}'+\bar{\theta}_x\right)+GD_{hx}\left(\bar{\theta}_z'+\bar{\psi}\right)-\bar{V}_x\left(z\right)\right]\delta\bar{u}\left(z\right)\Big|_0^\ell=0 \tag{3.90}$$

$$\left[GD_{xy}\left(\bar{u}'-\bar{\theta}_y\right)+GD_{yy}\left(\bar{v}'+\bar{\theta}_x\right)+GD_{hy}\left(\bar{\theta}_z'+\bar{\psi}\right)-\bar{V}_y\left(z\right)\right]\delta\bar{v}\left(z\right)\Big|_0^\ell=0 \tag{3.91}$$

$$\left[EI_{xx}\,\bar{\theta}_x'+\bar{M}_x\left(z\right)\right]\delta\bar{\theta}_x\left(z\right)\Big|_0^\ell=0 \tag{3.92}$$

$$\left[EI_{yy}\,\bar{\theta}_y'-\bar{M}_y\left(z\right)\right]\delta\bar{\theta}_y\left(z\right)\Big|_0^\ell=0 \tag{3.93}$$

$$\left[GD_{hx}\left(\bar{u}'-\bar{\theta}_y\right)+GD_{hy}\left(\bar{v}'+\bar{\theta}_x\right)+GD_{\omega\omega}\left(\bar{\theta}_z'+\bar{\psi}\right)+GJ\,\bar{\theta}_z'-\bar{M}_z\left(z\right)\right]\delta\bar{\theta}_z\left(z\right)\Big|_0^\ell=0 \tag{3.94}$$

$$\left[EC_w\,\bar{\psi}'+\bar{M}_w\left(z\right)\right]\delta\bar{\psi}\left(z\right)\Big|_0^\ell=0 \tag{3.95}$$

The system of equations (3.82) to (3.88) and boundary conditions (3.89) to (3.95) are a set of coupled partial differential equations in the variable z governing the behaviour of thin-walled members of asymmetric open cross-section under applied harmonic loads. The coupled field equations (3.82) to (3.88) are rewritten in matrix form as

$$
\begin{bmatrix}
\left(\rho A\Omega^2 + EA\mathcal{D}^2\right) & 0 & 0 & 0 & 0 & 0 & 0 \\
 & -\left(\rho A\Omega^2 + GD_{xx}\mathcal{D}^2\right) & -GD_{yy}\mathcal{D} & -GD_{xy}\mathcal{D}^2 & GD_{xy}\mathcal{D} & \left(x_s\rho A\Omega^2 - GD_{hy}\mathcal{D}^2\right) & -GD_{hy}\mathcal{D} \\
 & & \left(\rho I_{xx}\Omega^2 - GD_{yy} + EI_{xx}\mathcal{D}^2\right) & -GD_{xy}\mathcal{D} & GD_{xy}\mathcal{D} & -GD_{hy}\mathcal{D} & -GD_{hy} \\
 & & & -\left(\rho A\Omega^2 + GD_{xx}\mathcal{D}^2\right) & GD_{xx}\mathcal{D} & -\left(y_s\rho A\Omega^2 + GD_{hx}\mathcal{D}^2\right) & -GD_{hx}\mathcal{D} \\
 & & Symm & & \left(\rho I_{yy}\Omega^2 + EI_{yy}\mathcal{D}^2 - GD_{xx}\right) & GD_{hx}\mathcal{D} & GD_{hx} \\
 & & & & & -\left(\rho A\Omega^2 r_o^2 + G\left[J + D_{ww}\right]\mathcal{D}^2\right) & -GD_{ww}\mathcal{D} \\
 & & & & & & \left(\rho C_w\Omega^2 - GD_{ww} + EC_w\mathcal{D}^2\right)
\end{bmatrix}
\times
\begin{Bmatrix}
\bar{w} \\ \bar{v} \\ \bar{\theta}_x \\ \bar{u} \\ \bar{\theta}_y \\ \bar{\theta}_z \\ \bar{\psi}
\end{Bmatrix}
=
\begin{Bmatrix}
-\bar{q}_z(z) \\ \bar{q}_y(z) \\ -\bar{m}_x(z) \\ \bar{q}_x(z) \\ \bar{m}_y(z) \\ \bar{m}_z(z) \\ \bar{m}_w(z)
\end{Bmatrix}
\tag{3.96}
$$

In the above field equations (3.96), the first equation represents the longitudinal response of the system and it is uncoupled from the remaining set of equations. The remaining partition consists of six coupled equations in the displacements $\left(\bar{u},\bar{v},\bar{\theta}_y,\bar{\theta}_x,\bar{\theta}_z,\bar{\psi}\right)$. For asymmetric cross-sections, the 6×6 matrix of coefficients is full, signifying that the system is fully

coupled. This system of equation is solved in Chapter (6) for the case of asymmetric sections. In this case, the characteristic equation is observed to have twelve distinct roots. The solution in chapter 6 is thus valid only if all roots are distinct.

For the cases of doubly symmetric and mono-symmetric sections, some of roots of the characteristic polynomial will be repeated zeros and the solution in Chapter (6) cannot be applied. A special treatment which accounts for repeated roots is thus provided in Chapter (4) for the case of doubly symmetric sections. Also, for the case of mono-symmetric section is treated separately in Chapter (5).

3.9 A comparative study between present theory and similar theories

Among the numerous studies presented in Chapter 2, two are particularly relevant to the present research work (Table 3.1) and are given in more details in order to illustrate the differences between their work and the present research work. The comparison focuses on three main aspects: (i) method used to derive the governing equations of motion, (ii) the analytical closed form solutions of these equations, and (iii) shape functions used to formulate finite element formulations.

3.9.1 Theory Developed by Laudiero and Savoia (1991)

Laudiero and Savoia (1991) developed a dynamic analysis solution for thin-walled beams with open and closed cross-sections under general dynamic forces. Their theory is based on Vlasov-Timoshenko beam theory, i.e. it accounts for shear deformation, warping deformation and rotary inertia effects. In addition, the influences of the shear lag in the closed section are also included in the formulation. Based on Vlasov-Timoshenko assumptions, the in-plane displacement components of a point p are:

$$u_p(z,s,t) = u(z,t) - (y - y_s)\theta_z(z,t) \tag{3.97}$$

$$v_p(z,s,t) = v(z,t) + (x - x_s)\theta_z(z,t) \tag{3.98}$$

The longitudinal displacement w_p is expressed as:

$$\begin{aligned} w_p(z,s,t) = w(z,t) - y(s)\theta_x(z,t) - x(s)\theta_y(z,t) - \bar{\omega}(s)\psi(z,t) \\ + \chi_x(z,t)\psi_x(s) + \chi_y(z,t)\psi_y(s) + \chi_o(z,t)\psi_o(s) \end{aligned} \tag{3.99}$$

in which the terms $\chi_x(z,t)\psi_x(s)$, $\chi_y(z,t)\psi_y(s)$ represent the warping deformation related to shear strains induced by shear forces while $\chi_o(z,t)\psi_o(s)$ represents the secondary warping due to non-uniform torsion, the warping function $\bar{\omega}(s)$ for hybrid thin-walled section is taken as $\bar{\omega}(s)=\int_0^s\left[h(s)-\left(f_s/t(s)\right)\right]ds$, where f_s is the shear flow constant for each branch of the closed contour and $t(s)$ is the wall thickness. Equations (3.97) and (3.98) are identical to equations (3.1) and (3.2), whereas equation (3.99) is different from equation (3.3) due to the last three warping terms presented in equation (3.99). Laudiero and Savoia (1991) derived the equations of motion from the Hamilton variational principle as:

$$\rho A\ddot{w} - EAw'' - q_z(z,t) = 0 \tag{3.100}$$

$$\rho A\left[\ddot{u} + y_s\ddot{\theta}_z\right] - G\left[D_{xx}\left(u'' - \theta_y'\right) + D_{xy}\left(v'' - \theta_x'\right) + D_{hx}\left(\theta_z'' - \psi'\right)\right] \underline{- GD_{x\psi_x}\chi_x' - GD_{x\psi_y}\chi_y' - GD_{x\psi_o}\chi_o'} = q_x(z,t) \tag{3.101}$$

$$\rho A\left[\ddot{v} - x_s\ddot{\theta}_z\right] - G\left[D_{xy}\left(u'' - \theta_y'\right) + D_{yy}\left(v'' - \theta_x'\right) + D_{hy}\left(\theta_z'' - \psi'\right)\right] \underline{- GD_{y\psi_x}\chi_x' - GD_{y\psi_y}\chi_y' - GD_{y\psi_o}\chi_o'} = q_y(z,t) \tag{3.102}$$

$$\rho A\left[\left(y_s\ddot{u} - x_s\ddot{v}\right) + r_o^2\ddot{\theta}_z\right] - GJ\theta_z'' - G\left[D_{hx}\left(u'' - \theta_y'\right) + D_{hy}\left(v'' - \theta_x'\right) + D_{\omega\omega}\left(\theta_z'' - \psi'\right)\right] \underline{- GD_{\omega\psi_x}\chi_x' - GD_{\omega\psi_y}\chi_y' - GD_{\omega\psi_o}\chi_o'} = m_z(z,t) \tag{3.103}$$

$$\rho I_{xx}\ddot{\theta}_x - EI_{xx}\theta_x'' - G\left[D_{xy}\left(u' - \theta_y\right) + D_{yy}\left(v' - \theta_x\right) + D_{hy}\left(\theta_z' - \psi\right)\right] \underline{- GD_{y\psi_x}\chi_x - GD_{y\psi_y}\chi_y - GD_{y\psi_o}\chi_o} = m_x(z,t) \tag{3.104}$$

$$\rho I_{yy}\ddot{\theta}_y - EI_{yy}\theta_y'' - G\left[D_{xx}\left(u' - \theta_y\right) + D_{xy}\left(v' - \theta_x\right) + D_{hx}\left(\theta_z' - \psi\right)\right] \underline{- GD_{x\psi_x}\chi_x - GD_{x\psi_y}\chi_y - GD_{x\psi_o}\chi_o} = m_y(z,t) \tag{3.105}$$

$$-\rho C_w\ddot{\psi} + EC_w\psi'' + G\left[D_{hx}\left(u' - \theta_y\right) + D_{hy}\left(v' - \theta_x\right) + D_{\omega\omega}\left(\theta_z' - \psi\right)\right] \underline{- GD_{\omega\psi_x}\chi_x - GD_{\omega\psi_y}\chi_y - GD_{\omega\psi_o}\chi_o} = 0 \tag{3.106}$$

$$-\rho I_{\psi_x}\ddot{\chi}_x + EI_{\psi_x}\chi_x'' - G\left[D_{x\psi_x}\left(u'' - \theta_y'\right) + D_{y\psi_x}\left(v'' - \theta_x'\right) + D_{\omega\psi_x}\left(\theta_z'' - \psi'\right)\right] \underline{- GD_{\psi_x}\chi_x - GD_{\psi_x\psi_y}\chi_y - GD_{\psi_x\psi_o}\chi_o} = 0 \tag{3.107}$$

$$-\rho I_{\psi_y}\ddot{\chi}_y + EI_{\psi_y}\chi_y'' - G\left[D_{x\psi_y}\left(u'' - \theta_y'\right) + D_{y\psi_y}\left(v'' - \theta_x'\right) + D_{\omega\psi_y}\left(\theta_z'' - \psi'\right)\right] \underline{- GD_{\psi_x\psi_y}\chi_x - GD_{\psi_y}\chi_y - GD_{\psi_y\psi_o}\chi_o} = 0 \tag{3.108}$$

$$-\rho I_{\psi_o}\ddot{\chi}_o + EI_{\psi_o}\chi_o'' - G\left[D_{x\psi_o}\left(u'' - \theta_y'\right) + D_{y\psi_o}\left(v'' - \theta_x'\right) + D_{\omega\psi_o}\left(\theta_z'' - \psi'\right)\right] \underline{- GD_{\psi_x\psi_o}\chi_x - GD_{\psi_y\psi_o}\chi_y - GD_{\psi_o}\chi_o} = 0 \tag{3.109}$$

where $D_{ij} = \int_A \frac{di}{ds}\frac{dj}{ds}dA$, for $i, j = x, y, \omega, \psi_x, \psi_y, \psi_o$, the repeated subscripts are reported once only, $\frac{d\psi_o}{ds} = -\frac{D_{\omega\omega}S_\omega}{C_w t} - c_{ox}\frac{dx}{ds} - c_{oy}\frac{dy}{ds} - c_{o\omega}\frac{d\omega}{ds}$, $\frac{d\psi_y}{ds} = -\frac{D_{yy}S_x}{I_{xx}t} - c_{yx}\frac{dx}{ds} - c_{yy}\frac{dy}{ds} - c_{y\omega}\frac{d\omega}{ds}$,

$D_{y\psi_y} = -D_{x\psi_x} = -D_{\omega\psi_o} = 0, D_{xy} = -D_{x\psi_y} = -D_{y\psi_x}, D_{\omega w} = -D_{x\psi_o} = -D_{\omega\psi_x}, D_{y\omega} = -D_{y\psi_o} = -D_{\omega\psi_y}$,

$D_{\psi_x\psi_y} = \frac{D_{xx}D_{yy}}{I_{xx}I_{yy}}\int_A \frac{S_x S_y}{t^2}dA + D_{xy}$, $D_{\psi_x\psi_o} = \frac{D_{xx}D_{\omega\omega}}{I_{xx}C_w}\int_A \frac{S_x S_\omega}{t^2}dA + D_{x\omega}, D_{\psi_y\psi_o} = \frac{D_{yy}D_{\omega\omega}}{I_{yy}C_w}\int_A \frac{S_y S_\omega}{t^2}dA + D_{y\omega}$

and c_{ij} are constants that can be determined by imposing the orthogonality conditions S_x, S_y represent the first area moments and S_ω is the first sectorial moment.

It is noted that the governing field equations (3.28) to (3.34) derived in this study are a subset of those of (3.100) to (3.109). The underlined terms capture the shear lag effects and secondary warping effects. The study provided in the present research differs from that in Laudiero and Savoia (1991) in several respects:

(1) Laudiero and Savoia (1991) formulations are more general than those presented in this work. Their formulations accounted for shear lag effects and secondary warping. This leads to the increase in the number of field variables from seven to ten variables.

(2) Laudiero and Savoia (1991) developed an approximate solution based on trigonometric series expansions for the field equations. In contrast, the present theory explicitly solves the coupled differential equations for general closed form solutions (Chapters 4-6).

(3) Laudiero and Savoia (1991) investigated the free vibration analysis. In contrast, the current developed theory provides the steady state dynamic response under general harmonic forces. In addition, the present solution is able to predict the natural frequencies, mode shapes and static response.

(4) In the current study, the closed form solutions derived are used to formulate exact shape functions and to develop super-convergence finite elements, while Laudiero and Savoia (1991) did not provide a finite element solution.

3.9.2 Theory Developed by Kim et al (2003, 2005)

Kim et al (2003) developed a general theory to investigate the exact dynamic and static stiffness matrices for free vibration and stability analyses of asymmetric thin-walled open members. The formulation accounts for the effects of shear deformation due to bending and warping torsion and captures the coupled effects between them. Their theory is based on the averaging concept of shear flows and coupled shear effects due to shear forces and warping torsion. The inclusion of rotary inertia effect is also incorporated in their study. The displacement fields including the high order terms of the finite semi-tangential rotation are obtained. They derived the governing equations of motion and force-deformation relations by introducing the displacement fields based on finite semi-tangential rotations and semi-tangential moments and applying the variational principle of the total potential energy. The second order simultaneous ordinary differential equations are transformed into simultaneous first-order differential equations with constant coefficients by introducing a displacement state vector consisting of 14 displacement parameters ($\bar{w}, \bar{w}', \bar{u}, \bar{u}', \bar{v}, \bar{v}', \bar{\theta}_x, \bar{\theta}_x', \bar{\theta}_y, \bar{\theta}_y', \bar{\theta}_z, \bar{\theta}_z', \bar{\psi}, \bar{\psi}'$) to transform the system into a linear eigenvalue problem with non-symmetric matrices. By solving the eigenvalue problem, the displacement functions are exactly derived and the dynamic stiffness matrices are formulated using member force-displacement relations.

In a subsequent study, Kim and Kim (2005) adopted the theory in Kim et al. (2003b) to investigate the dynamic stiffness matrix element for the coupled flexural-torsion vibration analysis of asymmetric thin-walled shear-deformable beams. For asymmetric thin-walled

cross-section, the displacement components of an arbitrary point p on the middle-surface of the section are determined in a manner similar to Equations (3.1) and (3.2), except that the longitudinal displacement is based on a normalized warping function $\Psi(x,y)$ defined at the shear centre of the cross-section. The governing equations of motion and the force-deformation relations considering the coupled shear deformation effect due to the asymmetric cross-section are derived by applying the Hellinger-Reissner Principle for general vibrating harmonic motion as:

$$\rho A\Omega^2\bar{u}+EA\bar{w}''=0 \tag{3.110}$$

$$\rho A\Omega^2\left[\bar{u}+y_s\bar{\theta}_z\right]+Gk_{11}\left(\bar{u}''-\bar{\theta}_y'\right)+Gk_{12}\left(\bar{v}''+\bar{\theta}_x'\right)+Gk_{13}\left(\bar{\theta}_z''+\bar{\Psi}'\right)=0 \tag{3.111}$$

$$\rho A\Omega^2\left[\bar{v}-x_s\bar{\theta}_z\right]+Gk_{12}\left(\bar{u}''-\bar{\theta}_y'\right)+Gk_{22}\left(\bar{v}''+\bar{\theta}_x'\right)+Gk_{23}\left(\bar{\theta}_z''+\bar{\Psi}'\right)=0 \tag{3.112}$$

$$\rho A\Omega^2\left[x_s\bar{v}-y_s\bar{u}+r_o^2\bar{\theta}_z\right]+GJ\bar{\theta}_z''+Gk_{13}\left(\bar{u}''-\bar{\theta}_y'\right)+Gk_{23}\left(\bar{v}''+\bar{\theta}_x'\right)+Gk_{33}\left(\bar{\theta}_z''+\bar{\Psi}'\right)=0 \tag{3.113}$$

$$\rho I_{yy}\Omega^2\bar{\theta}_y+EI_{yy}\bar{\theta}_y''+Gk_{11}\left(\bar{u}'-\bar{\theta}_y\right)+Gk_{12}\left(\bar{v}'+\bar{\theta}_x\right)+Gk_{13}\left(\bar{\theta}_z'+\bar{\Psi}\right)=0 \tag{3.114}$$

$$\rho I_{xx}\Omega^2\bar{\theta}_x+EI_{xx}\bar{\theta}_x''+Gk_{12}\left(\bar{u}'-\bar{\theta}_y\right)+Gk_{22}\left(\bar{v}'+\bar{\theta}_x\right)+Gk_{23}\left(\bar{\theta}_z'+\bar{\Psi}\right)=0 \tag{3.115}$$

$$\rho C_w\Omega^2\bar{\Psi}+EC_w\bar{\Psi}''-Gk_{13}\left(\bar{u}'-\bar{\theta}_y\right)-Gk_{23}\left(\bar{v}'+\bar{\theta}_x\right)-Gk_{33}\left(\bar{\theta}_z'+\bar{\Psi}\right)=0 \tag{3.116}$$

These equations are similar to Equations (3.28-3.34) derived in this chapter. The difference between both formulations lies in the definition of the cross-section constants k_{ij} for $i,j=1,2,3$, which are given by:

$$\begin{bmatrix} k_{11} & k_{12} & k_{13} \\ k_{12} & k_{22} & k_{23} \\ k_{13} & k_{23} & k_{33} \end{bmatrix}_{3\times3}\begin{bmatrix} 1/A_2 & 1/A_{23} & 1/A_{2r} \\ 1/A_{23} & 1/A_3 & 1/A_{3r} \\ 1/A_{2r} & 1/A_{3r} & 1/A_r \end{bmatrix}_{3\times3}=\left[I_3\right]_{3\times3} \tag{3.117}$$

where A_2, A_3 are the effective shear areas due to shear forces, A_{23}, A_{2r}, A_{3r} are the effective shear areas due to flexural-warping torsional coupling effects, A_r is the effective shear area due to restraint warping torsion, and $\left[I_3\right]$ is the 3×3 identity matrix. The A 's constants are obtained from the following relations:

$$\left(\frac{1}{A_2},\frac{1}{A_3},\frac{1}{A_{\mathrm{r}}},\frac{1}{A_{23}},\frac{1}{A_{2\mathrm{r}}},\frac{1}{A_{3\mathrm{r}}}\right)=\int_S\left(\frac{S_{\mathrm{y}}^2}{I_{\mathrm{yy}}^2},\frac{S_{\mathrm{x}}^2}{I_{\mathrm{xx}}^2},\frac{S_{\mathrm{r}}^2}{C_{\mathrm{w}}^2},\frac{S_xS_y}{I_{\mathrm{xx}}I_{\mathrm{yy}}},\frac{S_yS_r}{I_{\mathrm{yy}}C_w},\frac{S_xS_r}{I_{\mathrm{xx}}C_w}\right)\frac{ds}{t}$$

with the statical moments S_x, S_y of area about the X, Y axes and the statical warping moment S_r are defined as $S_xS_y, S_r=\int_S(x,y,\omega)tds$.

In addition, they developed an approximate finite element model by using an isoparametric beam element with two-nodes and seven nodal degrees of freedom per node.

Even though the coupled governing equations of motion were derived by considering the effects of shear deformation due to bending and warping torsion, coupled shear deformation effects between them and rotary inertia effect, and the analytical procedure developed to obtain the exact displacement fields of the homogeneous field equations, the following important points can be summarized to demonstrate the difference between the theory developed in the present research and that of Kim et al. (2005):

1. Two different variational principles are used. Kim et al. applied the Hellinger-Reissner principle to derive the equations of motion and force-displacement relations while in the first part of the present study Hamilton variational principle is employed to derive the governing equations of motion of the system.

2. In their numerical procedure, the second-order ordinary differential equations are transformed to first-order simultaneous ordinary differential equations by introducing 14 displacement parameters in order to obtain a system of linear eigenvalue problem. In contrast, the governing ordinary differential equations derived in the present study are solved by introducing seven displacement functions in order to obtain a quadratic eigenvalue problem which expands analytically to yield a generalized eigenvalue expression.

3. Kim et al. (2005) and the present study developed the dynamic stiffness matrices based on the exact displacement solutions of the governing differential equations. Kim et al. (2005) developed the dynamic stiffness matrix using the force-displacement relationships and it is only used for free vibration analysis in order to determine the natural frequencies

Table (3.1): Summary of comparative review of the most relevant studies

No.	Author	Cross Section Type	Method of Solution			Effect included		Field variables	Type of analysis	Remarks
			Dynamic stiffness matrix	Closed form solution	Finite element solution	Shear deformation due to warping	Secondary warping			
1	Laudiero and Savoia (1991)	Asymmetric combined closed-open		√		√	√	w,u,v,θ_x θ_y,θ_z,ψ χ_x,χ_y,χ_o	Free vibration	-Hamilton's principle -Shear lag effects -Trigonometric series solution -Simply-supported and cantilever beams
2	Kim et al. (2003b, 2005)	Asymmetric Open	√	√	√	√		w,u,v,θ_x θ_y,θ_z,ψ	Free vibration	-Hellinger-Reissner Principle -Semi-tangential rotations and moments -Finite element based on assumed shape functions
3	Present study	Asymmetric Open	√	√	√	√		w,u,v,θ_x θ_y,θ_z,ψ	Steady state dynamic response	-Hamilton's principle -Finite element based on Exact shape functions -General harmonic loads

and corresponding mode shapes of the system. In contrast, in the present solution, the dynamic stiffness matrix formed by frequency-dependent shape functions (which are the exact solutions of the field equations) captures forced vibration response under general harmonic forces. Moreover, the current dynamic stiffness matrix is capable to predict the natural frequencies and mode shapes of the structural member.

4. They developed a finite element formulation based on isoparametric beam element. In contrast, in the present research study, the finite element is formulated based on exact displacement functions of the homogeneous form of the governing differential equations.

3.10 References

[3.1] Back, S. Y. and Will, K. M., (1998), A shear flexible element with warping for thin-walled open beams, Int. Journal Numerical Methods in Engineering, 43, p 1173-1191.

[3.2] Craig, R.R. and Kurdila, A. (2006), Fundamentals of Structural Dynamics, John Willey and Sons, New Jersey, USA.

[3.3] Cortinez, V. H. and Piovan, M. T. (2002), Vibration and buckling of composite thin-walled beams with shear deformability, Journal of Sound and Vibration, 258(4-5), p 701–723.

[3.4] Erkmen, R. E. (2006), Finite element formulations for thin-walled members, Ph.D thesis, University of Ottawa, Ottawa, Canada.

[3.5] Kim, M. Y. et al (2003), Exact dynamic and static stiffness matrices of shear deformable thin-walled beam-columns, Journal of Sound and Vibration, 267, p 29–55.

[3.6] Kim, N. I. and Kim, M. N. (2005), Exact Dynamic/Static Stiffness Matrices of Non-Symmetric Thin-Walled Beams considering coupled shear deformation effects, Thin-walled Structures, 43, p 701-734.

[3.7] Laudiero, F. and Savoia, M. (1991), The shear strain influence on the dynamics of thin-walled beams, Thin-walled structures, 11, p 375-407.

[3.8] Li, J, Li, W., Shen, R., Hua, H. (2004), Coupled bending and torsional vibration of axially loaded thin-walled Timoshenko beams, Mechanics International Journal of Mechanical Sciences, 46, p 299-320.

[3.9] Librescu, L. and Song, O., (2006), Thin-walled composite beams- theory and application, Springer, Netherland.

[3.10] Machado, S. P. (2007), Geometrically non-linear approximations on stability and free vibration of composite beams, Engineering Structures, 29(12), p 3567-3578.

[3.11] Machado, S. P. and Cortinez, V. H. (2007), Free vibration of thin-walled composite beams with static initial stresses and deformations, Engineering Structures, 29(3), p 372-382.

[3.12] Prokic, A. (2006), On fivefold coupled vibrations of Timoshenko thin-walled beams, Engineering Structures, 28, p 54-62.

[3.13] Vlasov, V. Z. (1961), Thin-walled elastic beams, 2nd edition, Israel Program for Scientific Translation, Jerusalem.

[3.14] Vo, T. P. and Lee, J. (2009), Flexural-torsional coupled vibration and buckling of thin-walled open section composite beams using shear-deformable beam theory, International Journal of Mechanics Sciences, 51, p 631-641.

[3.15] Vo, T. P. and Lee, J. (2011), Free vibration of axially loaded thin-walled composite Timoshenko beams, Archive of Applied Mechanics, 81, p 1165–1180.

[3.16] Wu, L. and Mohareb, M., (2011), Buckling of shear deformable thin-walled members: I-Variational principle and analytical solutions, Thin-walled Structures, 49 (1), p 197-207.

List of Symbols

A	Cross-section area
C_w	Warping constant
D_{xx}, D_{yy}, D_{xy} $D_{hx}, D_{hy}, D_{\omega\omega}$	Cross-sectional properties defined by equation (3.16)
D_{rx}, D_{ry}	Cross-sectional properties defined by equation (3.35)
E	Modulus of elasticity
G	Shear modulus
$h(s)$	Normal distance between the shear centre and the tangent to mid-surface
I_{xx}, I_{yy}	Moment of inertia of the cross-section about the principal X and Y axes
J	Torsional constant
ℓ	Length of the member
k_x, k_y	Shear factor coefficients
$M_j(z,t)$	Moments about X, Y, Z axes (where $j = x, y, z$)
$M_w(z,t)$	Warping dynamic twisting moment
$m_j(z,t)$	Member dynamic moments about X, Y, Z axes (where $j = x, y, z$)
$m_w(z,t)$	Member warping dynamic twisting moment
$p_j(z,s,t)$	Surface member tractions along X, Y, Z axes (where $j = x, y, z$)
$q_j(z,t)$	Applied distributed dynamic forces along X, Y, Z directions (where $j = x, y, z$)
$r(s)$	Normal distance between the shear centre to the normal to mid-surface
r_o	Radius of gyration
s	Curvilinear coordinate along mid-surface of the section
S_x, S_y, S_ω	First moments of the area of coordinates X, Y and ω
S_{xy}	Product moment of the area
$S_{x\omega}, S_{y\omega}$	Section products of inertia

t	Time in seconds
t_1, t_2	Time intervals
δT	Variation of kinetic energy
u,v	Displacements of the shear centre along the principal X,Y axes
u_p, v_p, w_p	Displacements of a point on the mid-surface of the section along X,Y,Z axes
δU	Variation of internal strain energy
$V_i(z,t)$	Shear force along X and Y axes (where $i = x, y$)
w	Average longitudinal displacement along Z axis
δW	Variation of the work done by applied forces
x,y,z	Cartesian coordinate system
X,Y,Z	Principal coordinate system
$x(s), y(s)$	Coordinate of arbitrary point p on mid-surface along the principal X and Y axes
x_s, y_s	Coordinates of the shear centre along the principal X and Y axes
$\delta \Pi$	Variation of the total potential energy
σ_{zz}	Normal stress in the longitudinal direction
τ_{zs}	Shear stress at the mid-surface of the cross-section
ε_{zz}	Normal strain in the longitudinal direction
γ_{zs}	Shear strain at the mid-surface of the cross-section
ρ	Density of the material
ξ, η	Tangential and normal displacements of a point p along s and n directions
$\theta_x, \theta_y, \theta_z$	Rotations angles around the X,Y,Z axes
$\hat{\alpha}(s)$	Angle between the tangent to the cross-section and the principal X axis
$\psi(z,t)$	Warping deformation function
Ω	Eigen-frequency
$\omega(s)$	Warping function of the cross-section

CHAPTER (4)

ANALYSIS OF THIN-WALLED MEMBERS OF DOUBLY SYMMETRIC CROSS-SECTIONS

Closed-Form Solution and Finite Element Formulation

Chapter (4) - Analysis of Thin-walled Members of Doubly Symmetric Cross-Sections

Closed-Form Solution and Finite Element Formulation

Abstract

This chapter investigates the dynamic behaviour of thin-walled members of open sections with doubly symmetric cross-sections under external harmonic forces. The governing equilibrium equations and associated boundary conditions for general cross-section developed in Chapter 3 are specialized in this chapter for the case of doubly symmetric cross-sections. In the first part of this chapter, the closed-form solutions are obtained. In the second chapter, a finite element formulation based on exact shape functions is then formulated. The exact shape functions developed are based on the closed form expressions obtained in the first part for the displacement fields and are subsequently employed to derive the stiffness and mass matrices of the element. The applicability of the present solutions is demonstrated via several examples. In order to assess the validity of the solutions, comparisons are made against other established beam and shell finite element solutions. Additional comparisons are made against solutions based on non-shear deformable theories and the effect of shear deformation is quantified.

4.1 Introduction and Scope

The present study aims at (1) developing an analytical solution for the analysis of thin-walled open members subjected to harmonic excitations, in which the time dependency of the response is eliminated. The analytical solution developed is obtained in a closed-form and, unlike some conventional solutions; it eliminates the need of extracting the eigenmodes to obtain the steady state response of the member. In addition, the current analytical method is able to predict the natural frequencies and modes of the structural member. (2) Developing an efficient finite element formulation. The closed form displacement expressions developed

in the first part of the study are employed to formulate the stiffness and mass matrices as well as the load potential vector.

4.2 Literature review on analytical solutions

The Vlasov theory (1961) is widely used in the analysis of thin-walled members of open section. The Vlasov formulation is based on two kinematic assumptions; (i) the beam cross-section is assumed to be rigid in its own plane, and (ii) the transverse shear strains along the section mid-surface are neglected. Based on Vlasov theory, Friberg (1983), Leung (1991) and (1992), Chen and Tamma (1994), Li et al. (2004a) and Kim et al. (2007) developed the dynamic stiffness matrix of Vlasov beam in which shear deformation is entirely ignored. Many researchers modified the Vlasov theory for the analysis of elastic thin-walled members to capture the transverse shear deformations. Among them, Bercin and Tanaka (1997) studied the coupled flexural-torsional free vibrations of monosymmetric beams. Cortinez and Piovan (2002) developed an analytical solution for free vibration analysis of composite thin-walled beams of open and closed cross-section. Using the dynamic transfer matrix method, Li et al. (2004b) derived an analytical method for determining the coupled bending-torsion response of thin-walled monosymmetric beams under external random excitations. Based on the virtual work principle, Prokic (2006) derived the differential equations for the coupled vibrations of members of general thin-walled cross-sections. The closed-form solution for the natural frequencies was derived for the case of simply supported beams. Vo and Lee (2009) developed a general analytical solution for the study of flexural-torsional buckling and vibration analysis of open thin-walled composite beams. Features common to the above studies are the fact they capture shear deformation effect, warping deformation and rotatory inertia.

4.3 Literature review on finite element formulations

The current review focuses on the dynamic analysis of thin-walled members of open cross-sections by applying finite element formulations. Among them, Mei (1970) employed a finite element method to investigate the solution of the coupled vibrations of the thin-walled open beams which included the effect of warping stiffness effects. Chen and Tamma (1994) used

the finite element method in conjunction with an implicit-starting unconditionally stable methodology for the dynamic analysis of thin-walled open members under deterministic loads. Hu et al. (1996) derived the fourth order differential equations governing the coupled bending-torsional dynamic behavior of thin-walled beams of asymmetric cross-sections. The homogenous solutions of these fourth order equations in static state were used as the interpolation functions in deriving the stiffness and mass matrices of the thin-walled beam element. Voros (2008) analyzed the coupled bending-torsional free vibration and mode shapes of thin-walled open members induced by steady state lateral loads using a finite element formulation. The derivation of the stiffness matrices was based on assumed displacement fields in which the linear interpolation and cubic Hermitian functions are adopted for the axial and lateral displacements and twist. Vo and Lee (2009) developed an analytical model based on shear deformable beam theory developed to study the flexural-torsional coupled vibrations of thin-walled composite columns under compressive force. Their finite element model was based on a one-dimensional Lagrange interpolation function.

4.4 Governing Field Equations for Doubly Symmetric Cross-Sections

The general field equations obtained in Eqs. (3.82-3.88) governing the dynamic behaviour of thin-walled member of arbitrary section can be specialized for the case of doubly symmetrical cross-section. It is known that, for doubly symmetrical section such as the one illustrated in Figure (4.1), that the shear centre S_c coincides with the centroid C , i.e.,

$$x_s = y_s = 0 \tag{4.1}$$

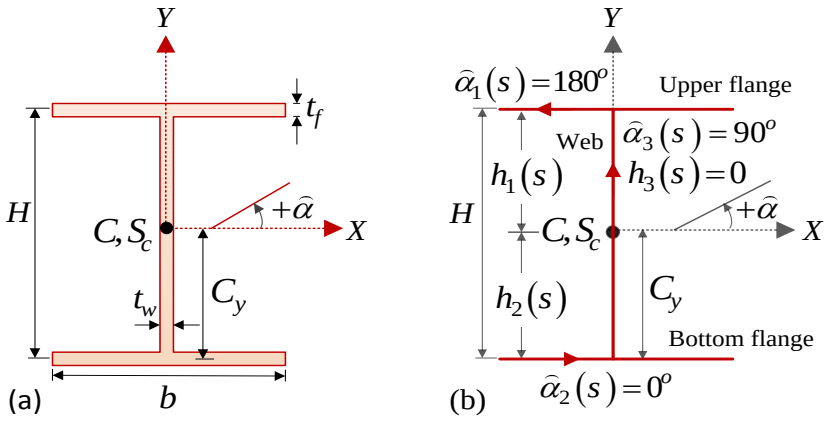

Figure (4.1): Doubly Symmetric I-section

The cross-sectional properties D_{xx} ,D_{yy} ,D_{xy} ,D_{hx} ,D_{hy} and $D_{\omega\omega}$ for doubly symmetric I-section (Figure 4.1) can be determined from the following expressions

$$D_{xx} = \sum_{i=1}^{3} \int_{A_i} \left(\frac{dx_i(s)}{ds} \right)^2 dA_i = \sum_{i=1}^{3} \int_{A_i} \left[\cos\hat{\alpha}_i(s) \right]^2 dA_i = A_f \tag{4.2}$$

$$D_{yy} = \sum_{i=1}^{3} \int_{A_i} \left(\frac{dy_i(s)}{ds} \right)^2 dA_i = \sum_{i=1}^{3} \int_{A_i} \left[\sin\hat{\alpha}_i(s) \right]^2 dA_i = A_w \tag{4.3}$$

$$D_{xy} = \sum_{i=1}^{3} \int_{A_i} \left(\frac{dx_i(s)}{ds} \right) \left(\frac{dy_i(s)}{ds} \right) dA_i = \sum_{i=1}^{3} \int_{A_i} \cos\hat{\alpha}_i(s) \sin\hat{\alpha}_i(s) dA_i = 0 \tag{4.4}$$

$$D_{hx} = \sum_{i=1}^{3} \int_{A_i} h_i(s) \left(\frac{dx_i(s)}{ds} \right) dA_i = \sum_{i=1}^{3} \int_{A_i} h_i(s) \cos\hat{\alpha}_i(s) dA_i = 0 \tag{4.5}$$

$$D_{hy} = \sum_{i=1}^{3} \int_{A_i} h_i(s) \left(\frac{dy_i(s)}{ds} \right) dA_i = \sum_{i=1}^{3} \int_{A_i} h_i(s) \sin\hat{\alpha}_i(s) dA_i = 0 \tag{4.6}$$

$$D_{\omega\omega} = \sum_{i=1}^{3} \int_{A_i} \left[h_i(s) \right]^2 dA_i = (H/2)^2 A_f \tag{4.7}$$

in which, as illustrated from Figure (4.1b) that $\hat{\alpha}_1(s) = 180^o$ and $h_1(s) = C_y$ for the top flange, $\hat{\alpha}_2(s) = 0^o$ and $h_1(s) = -C_y$ for and bottom flange, while $\hat{\alpha}_3(s) = 90^o$ and $h_3(s) = 0$, and $A_f = 2bt_f$ is the area of both flanges, $A_w = Ht_w$ is the area of the web.

Introducing Equations (4.1) to (4.8) into the governing field equations of motion (3.82) to (3.88), the uncoupled equations for doubly symmetric cross-section are then given in terms of space displacement functions $\bar{w}(z), \bar{v}(z), \bar{\theta}_x(z), \bar{u}(z), \bar{\theta}_y(z), \bar{\theta}_z(z)$ and $\bar{\psi}(z)$ as

$$\begin{bmatrix}
\left(\rho A\,\Omega^2 + EA\,\mathcal{D}^2\right) & 0 & 0 & 0 & 0 & 0 & 0 \\
0 & -\left(\rho A\,\Omega^2 + GA_w\,\mathcal{D}^2\right) & -GA_w\,\mathcal{D} & 0 & 0 & 0 & 0 \\
0 & -GA_w\,\mathcal{D} & \left(\rho I_{xx}\,\Omega^2 - GA_w + EI_{xx}\,\mathcal{D}^2\right) & 0 & 0 & 0 & 0 \\
0 & 0 & 0 & -\left(\rho A\,\Omega^2 + GA_f\,\mathcal{D}^2\right) & GA_f\,\mathcal{D} & 0 & 0 \\
0 & 0 & 0 & GA_f\,\mathcal{D} & -\left(GA_f - \rho I_{yy}\,\Omega^2 - EI_{yy}\,\mathcal{D}^2\right) & 0 & 0 \\
0 & 0 & 0 & 0 & 0 & -\left(\rho A\,\Omega^2 r_o^2 + \left[GJ + A_f\left(\frac{H}{2}\right)^2\right]\right)\mathcal{D}^2 & -GA_f\left(\frac{H}{2}\right)^2\mathcal{D} \\
0 & 0 & 0 & 0 & 0 & -GA_f\left(\frac{H}{2}\right)^2\mathcal{D} & \left(\rho C_w\,\Omega^2 - GA_f\left(\frac{H}{2}\right)^2 + EC_w\,\mathcal{D}^2\right)
\end{bmatrix}_{7\times 7}$$

$$\times\begin{Bmatrix}
\bar{w}(z) \\ \bar{v}(z) \\ \bar{\theta}_x(z) \\ \bar{u}(z) \\ \bar{\theta}_y(z) \\ \bar{\theta}_z(z) \\ \bar{\psi}(z)
\end{Bmatrix}_{7\times 1} = \begin{Bmatrix}
-\bar{q}_z(z) \\ \bar{q}_y(z) \\ \bar{m}_x(z) \\ \bar{q}_x(z) \\ \bar{m}_y(z) \\ \bar{m}_z(z) \\ \bar{m}_w(z)
\end{Bmatrix}_{7\times 1}$$

The above partitioned system of equations consists of four systems. The first system describes the longitudinal motion and consists of a single differential equation in the longitudinal displacement $w(z,t)$. The second system describes the transverse motion and

consists of two coupled differential equations which involve the transverse motion $v(z,t)$ and associated angle of rotation $\theta_x(z,t)$. The third system describes the lateral motion $u(z,t)$ and related angle of rotation $\theta_y(z,t)$, while the fourth system provides the torsional motion $\theta_z(z,t)$ and associated warping deformation $\psi(z,t)$.

The general boundary conditions in Eq. (3.89-3.95) are adapted for the case of doubly symmetric cross sections by setting $x_s = y_s = 0$ and $D_{xy} = D_{hx} = D_{hy} = 0$. The resulting boundary conditions related to the longitudinal dynamic response are

$$\left[EA\bar{w}' - \bar{N}_z(z)\right]\delta\bar{w}(z)\Big|_0^\ell = 0 \tag{4.9}$$

those related to the transverse motion are

$$\left[GA_w\left(\bar{v}' + \bar{\theta}_x\right) - \bar{V}_y(z)\right]\delta\bar{v}(z)\Big|_0^\ell = 0 \tag{4.10}$$

$$\left[EI_{xx}\,\bar{\theta}_x' + \bar{M}_x(z)\right]\delta\bar{\theta}_x(z)\Big|_0^\ell = 0, \tag{4.11}$$

those related to lateral motion are

$$\left[GA_f\left(\bar{u}' - \bar{\theta}_y\right) - \bar{V}_x(z)\right]\delta\bar{u}(z)\Big|_0^\ell = 0 \tag{4.12}$$

$$\left[EI_{yy}\,\bar{\theta}_y' - \bar{M}_y(z)\right]\delta\bar{\theta}_y(z)\Big|_0^\ell = 0 \tag{4.13}$$

and those related to the torsional-warping motion are

$$\left[GA_f(H/2)^2\left(\bar{\theta}_z' + \bar{\psi}\right) + GJ\bar{\theta}_z' - \bar{M}_z(z)\right]\delta\bar{\theta}_z(z)\Big|_0^\ell = 0 \tag{4.14}$$

$$\left[EC_w\,\bar{\psi}' + \bar{M}_w(z)\right]\delta\bar{\psi}(z)\Big|_0^\ell = 0 \tag{4.15}$$

4.5 Homogeneous Solutions for the Field Equations

The homogeneous part of the solution for the governing differential equations (4.8) can be obtained by setting the right hand side of the field equations to zero. The solutions of the unknown displacement functions $\langle\bar{U}_S(z)\rangle_{1\times7}^T = \langle\bar{w}(z)\ \bar{v}(z)\ \bar{\theta}_x(z)\ \bar{u}(z)\ \bar{\theta}_y(z)\ \bar{\theta}_z(z)\ \bar{\psi}(z)\rangle_{1\times7}^T$ are then assumed to take the exponential form

$$\left\langle \bar{U}_S\left(z\right)\right\rangle_{1\times 7}^{T} = \left\langle A_i \right\rangle_{1\times 7}^{T} e^{m_i z} \quad \text{, for } i = 1,2,3,...,7 \tag{4.16}$$

in which $\left\{\bar{U}_S\left(z\right)\right\}_{7\times 1}$ is the space displacement vector, and $\left\{A_i\right\}_{7\times 1}$ is the vector of unknown integration constants. The resulting closed form steady state solutions are provided in Section (4.6) while a finite element formulation for the problem is provided in Section (4.7).

4.6 Closed Form Solutions

In the following sub-section (4.6.1) provides the solution for longitudinal displacement. Sub-sections (4.6.2) and (4.6.3) provide the steady state solutions of the transverse displacement and associated rotation and lateral displacements and associate rotation, respectively. The solution for twist and warping is provided in Sub-section (4.6.4).

4.6.1 Solution for Longitudinal displacement

The first uncoupled equation in Eq. (4.8) governing the longitudinal response of thin-walled member of double symmetric section is

$$\rho A\,\Omega^2 w\left(z\right) + EAw''\left(z\right) = \bar{q}_z\left(z\right) \tag{4.17}$$

4.6.1.1 General Solution for Longitudinal Displacement

The general steady state solution for the longitudinal equation (4.17) is obtained as the sum of the homogeneous and particular solutions, i.e.,

$$\bar{w}_L\left(z\right) = \bar{w}_H\left(z\right) + \bar{w}_P\left(z\right) = A_{1,1}e^{\bar{\lambda}_1 z} + A_{1,2}e^{\bar{\lambda}_2 z} - \frac{\bar{q}_z}{\rho A\,\Omega^2} \tag{4.18}$$

in which $\bar{\lambda}_{1,2} = \pm i\sqrt{\rho\Omega^2/E}$ are the roots obtained from the characteristic equation $\rho A\Omega^2 + EAm_i^2 = 0$, where $i = \sqrt{-1}$ is the imaginary constant, and $A_{1,1}$, $A_{1,2}$ are the unknown integration constants to be determined from the problem boundary conditions.

4.6.1.2 Example - Cantilever under uniform axial load and end load

For a cantilever beam fixed at the end $z=0$ and subjected to a uniform distributed longitudinal harmonic force $q_z(z,t)=\bar{q}_z e^{i\Omega t}$ and concentrated harmonic force $N_z(\ell,t)=\bar{N}_z(\ell)e^{i\Omega t}$ at the free end $z=\ell$ (Figure 4.2).

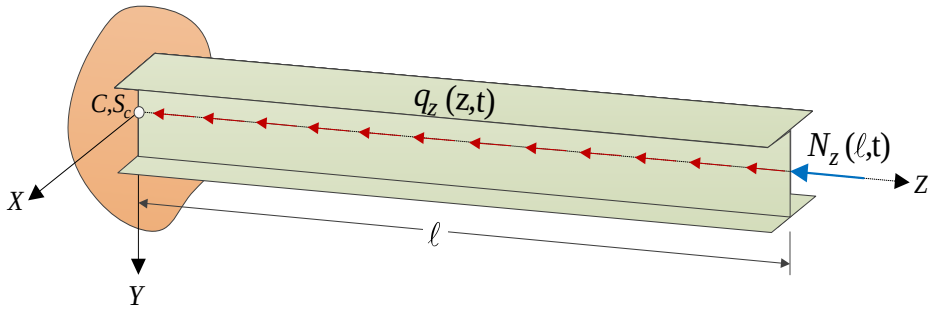

Figure (4.2): Cantilever member of doubly symmetric I-section subjected to longitudinal compressive harmonic forces

Noting that the cantilever boundary conditions are:

$$\bar{w}(0)=0 \text{ , and } EA\bar{w}'(\ell)=\bar{N}_z(\ell) \tag{4.19}$$

The unknown integration constants $A_{1,1}$ and $A_{1,2}$ can determined by enforcing the boundary conditions in (4.19) yielding

$$\bar{w}_t(z)=\left\langle e^{\bar{\lambda}_1 z} \quad e^{\bar{\lambda}_2 z}\right\rangle_{1\times 2}^{T}\begin{bmatrix}1 & 1\\ \bar{\lambda}_1 e^{\bar{\lambda}_1 \ell} & \bar{\lambda}_2 e^{\bar{\lambda}_2 \ell}\end{bmatrix}_{2\times 2}^{-1}\begin{Bmatrix}\dfrac{\bar{q}_z}{\rho A\Omega^2}\\ \dfrac{\bar{N}_z(\ell)}{EA}\end{Bmatrix}_{2\times 1}-\frac{\bar{q}_z}{\rho A\Omega^2} \tag{4.20}$$

4.6.2 Solution for Transverse Displacement

In this section, the general solution of the governing transverse equations (i.e., second system of equations in 4.8) for a thin-walled member of double symmetric section subjected to transverse harmonic force $q_y(z,t)=\bar{q}_y e^{i\Omega t}$ and bending moment $m_x(z,t)=\bar{m}_x e^{i\Omega t}$ is determined.

4.6.2.1 Homogeneous Solution

The homogeneous form of the field equations for transverse response is obtained by setting the applied harmonic forces $\bar{q}_y(z)=\bar{m}_x(z)=0$ in the second set of equations in (4.8) yielding

$$-\rho A\Omega^2\bar{v}(z)-GA_w\bar{v}''(z)-GA_w\bar{\theta}_x'(z)=0 \tag{4.21}$$

$$-GA_w\bar{v}'(z)+\left(\rho I_{xx}\Omega^2-GA_w\right)\bar{\theta}_x(z)+EI_{xx}\bar{\theta}_x''(z)=0 \tag{4.22}$$

Assuming exponential solution for the displacement functions $\bar{v}(z)$ and $\bar{\theta}_x(z)$ in Eq. (4.16) yields

$$\left[\begin{matrix}-\left(\rho A\Omega^2+GA_w m_i^2\right) & -GA_w m_i\\ -GA_w m_i & \left(\rho I_{xx}\Omega^2-GA_w+EI_{xx}m_i^2\right)\end{matrix}\right]_{2\times2}\left\{\begin{matrix}A_{2,i}\\ A_{3,i}\end{matrix}\right\}_{2\times1}e^{m_i z}=0$$

The non-trivial solution of the above equation can be solved by setting the determinant of the unknown coefficients to zero, yielding the following characteristic equation

$$m_i^4+\frac{\Omega^2\rho}{E}\left(\frac{EA}{GA_w}+1\right)m_i^2-\frac{\rho A\Omega^2}{EI_{xx}}\left(1-\frac{\rho I_{xx}\Omega^2}{GA_w}\right)=0 \tag{4.23}$$

The roots of equation (4.30) are

$$m_{1,2}=\bar{\beta}_{1,2}=\pm\sqrt{\frac{1}{2}\left\{\frac{-\Omega^2\rho}{E}\left(\frac{EA}{GD_{yy}}+1\right)+\sqrt{\left[\frac{\Omega^2\rho}{E}\left(\frac{EA}{GD_{yy}}+1\right)\right]^2+\frac{4\rho A\Omega^2}{EI_{xx}}\left(1-\frac{\rho I_{xx}\Omega^2}{GD_{yy}}\right)}\right\}}$$

$$m_{3,4}=\bar{\beta}_{3,4}=\pm i\sqrt{\frac{1}{2}\left\{\frac{\Omega^2\rho}{E}\left(\frac{EA}{GD_{yy}}+1\right)+\sqrt{\left[\frac{\Omega^2\rho}{E}\left(\frac{EA}{GD_{yy}}+1\right)\right]^2+\frac{4\rho A\Omega^2}{EI_{xx}}\left(1-\frac{\rho I_{xx}\Omega^2}{GD_{yy}}\right)}\right\}}$$

It is noted that, the four roots are distinct and the homogeneous solutions for in-plane transverse deformation functions $\bar{v}_h(z)$ and $\bar{\theta}_{x_h}(z)$ are obtained as

$$\bar{v}_h(z)=\sum_i^4 A_{2,i}\,e^{\bar{\beta}_i z}=A_{2,1}e^{\bar{\beta}_1 z}+A_{2,2}\,e^{\bar{\beta}_2 z}+A_{2,3}e^{\bar{\beta}_3 z}+A_{2,4}\,e^{\bar{\beta}_4 z} \tag{4.24}$$

$$\bar{\theta}_{x_h}(z)=\sum_i^4 A_{3,i}\,e^{\bar{\beta}_i z}=A_{3,1}e^{\bar{\beta}_1 z}+A_{3,2}\,e^{\bar{\beta}_2 z}+A_{3,3}e^{\bar{\beta}_3 z}+A_{3,4}\,e^{\bar{\beta}_4 z} \tag{4.25}$$

The displacement functions $\bar{v}_h(z)$ and $\bar{\theta}_{x_h}(z)$ provided in equations (4.31) and (4.32) are only valid if roots $\hat{\beta}_i$ for $i=1,2,3,4$ are distinct. It is observed that the roots are not distinct when $\frac{\rho A\Omega^2}{EI_{xx}}\left[1-\left(\rho I_{xx}\Omega^2/GD_{yy}\right)\right]=0$, i.e., $\hat{\beta}_1=\hat{\beta}_2=0$, this leads to the condition $\Omega=\sqrt{GA_w/\rho I_{xx}}$. Thus, only for the case where the exciting frequency is $\Omega=\sqrt{GA_w/\rho I_{xx}}$ the equations given in this study become invalid.

To obtain the homogeneous solution of in-plane transverse displacement functions $\bar{v}_h(z)$ and $\bar{\theta}_{x_h}(z)$, it is necessary to reduce the eight unknown integration constants $A_{2,i}$ and $A_{3,i}$ for $i=1,2,3,4$ to four independent integration constants. By substituting the displacement expressions in Equations (4.24) and (4.25) into Equations (4.20) and (4.21), and solving for unknown constants (see appendix 4.A for more details), one obtains

$$\bar{v}_h(z)=\sum_i^4 A_{2,i}\,e^{\hat{\beta}_i z}=A_{2,1}e^{\hat{\beta}_1 z}+A_{2,2}\,e^{\hat{\beta}_2 z}+A_{2,3}e^{\hat{\beta}_3 z}+A_{2,4}\,e^{\hat{\beta}_4 z} \tag{4.26}$$

$$\bar{\theta}_{x_h}(z)=\sum_i^4 A_{2,i}\bar{A}_i\,e^{\hat{\beta}_i z}=A_{2,1}\bar{A}_1e^{\hat{\beta}_1 z}+A_{2,2}\,\bar{A}_2e^{\hat{\beta}_2 z}+A_{2,3}\bar{A}_3e^{\hat{\beta}_3 z}+A_{2,4}\bar{A}_4\,e^{\hat{\beta}_4 z} \tag{4.27}$$

where $\bar{A}_i=-\left(\frac{GA_w\hat{\beta}_i^2+\rho A\Omega^2}{GA_w\hat{\beta}_i}\right)=\left(\frac{GA_w\hat{\beta}_i}{\rho I_{xx}\Omega^2-GA_w+EI_{xx}\hat{\beta}_i^2}\right)$, for $i=1,2,3,4$.

The homogeneous solution for displacement and rotation functions $\bar{v}_h(z)$ and $\bar{\theta}_{x_h}(z)$ can be rewritten in matrix form as

$$\left\{\bar{V}_h(z)\right\}_{2\times1}=\left[L_b\right]_{2\times4}\left[E_b(z)\right]_{4\times4}\left\{A_{2,i}(z)\right\}_{4\times1} \tag{4.28}$$

where $\left\langle\bar{V}_h(z)\right\rangle_{1\times2}^T=\left\langle\bar{v}_h(z)\quad\bar{\theta}_{x_h}(z)\right\rangle_{1\times2}^T$, $\left[L_b\right]_{2\times4}=\begin{bmatrix}1&1&1&1\\ \bar{A}_1&\bar{A}_2&\bar{A}_3&\bar{A}_4\end{bmatrix}_{2\times4}$,

$\left[E_b(z)\right]_{4\times4}=diag\left[e^{\hat{\beta}_1 z}\;\vdots\;e^{\hat{\beta}_2 z}\;\vdots\;e^{\hat{\beta}_3 z}\;\vdots\;e^{\hat{\beta}_4 z}\right]_{4\times4}$, and

$\left\langle A_{2,i}\right\rangle_{1\times4}^T=\left\langle A_{2,1}\quad A_{2,2}\quad A_{2,3}\quad A_{2,4}\right\rangle_{1\times4}^T$.

Equation (4.28) represents the homogenous solution of the space component of the displacement $\bar{v}_h(z)$ and rotation $\bar{\theta}_{x_h}(z)$ functions undergoing transverse bending. The unknown integration constants $\langle A_{2,i} \rangle_{1\times 4}^T$, for $i = 1,2,3,4$ can be evaluated by enforcing the boundary conditions associated with the problem.

4.6.2.2 Particular Solution for Uniform Loads

For a member under uniform transverse load and uniform moment

$$\left[\bar{q}_y(z), \bar{m}_x(z)\right] e^{i\Omega t} = \left(\bar{q}_y, \bar{m}_x\right) e^{i\Omega t}$$

The corresponding particular solution for the transverse response equations can be evaluated by considering the inplane displacement functions as

$$\bar{v}_p(z) = A_{o1} + A_{o2} z \quad \text{and} \quad \bar{\theta}_{x_p}(z) = B_{o1} + B_{o2} z \tag{4.29}$$

From Eq. (4.29), by substituting into the second system of equations in Eq. (4.8), the unknown constants are obtained as: $A_{o1} = -\bar{q}_y / \rho A \Omega^2$, $B_{o1} = -\bar{m}_x / \left(\rho I_{xx} \Omega^2 - G A_w\right)$, $A_{o2} = B_{o2} = 0$. Consequently, one obtains

$$\langle \bar{V}_p \rangle_{2\times 1} = \langle \bar{v}_p \quad \bar{\theta}_{x_p} \rangle_{2\times 1} = \langle -\bar{q}_y / \rho A \Omega^2 \quad -\bar{m}_x / \left(\rho I_{xx} \Omega^2 - G A_w\right) \rangle_{2\times 1} \tag{4.30}$$

The complete steady state solution $\langle \bar{V}_b(z) \rangle_{1\times 2}^T = \langle \bar{v}(z) \quad \bar{\theta}_x(z) \rangle_{1\times 2}^T$ for transverse response is obtained by adding the homogeneous solution (4.28) to the particular solution (4.30), i.e.,

$$\{ \bar{V}_b(z) \}_{2\times 1} = [L_b]_{2\times 4} [E_b(z)]_{4\times 4} \{ A_{2,i} \}_{4\times 1} + \{ \bar{V}_p \}_{2\times 1} \tag{4.31}$$

Equation (4.31) represents the complete steady state solution of inplane transverse displacements for thin-walled beam of doubly symmetric sections under uniformly distributed harmonic forces. Again, the integration constants $\{A_{2,i}\}_{4\times 1}$ are determined from the relevant boundary conditions.

4.6.2.3 Example - Cantilever under Transverse Forces

A thin walled cantilever of doubly symmetric open section (Figure 4.3) is subjected to uniformly distributed harmonic force $\bar{q}_y(z)e^{i\Omega t}$, concentrated harmonic vertical load $\bar{V}_y(\ell)e^{i\Omega t}$ and bending moment $\bar{M}_x(\ell)e^{i\Omega t}$, both acting at the free end $(z=\ell)$ of the cantilever beam.

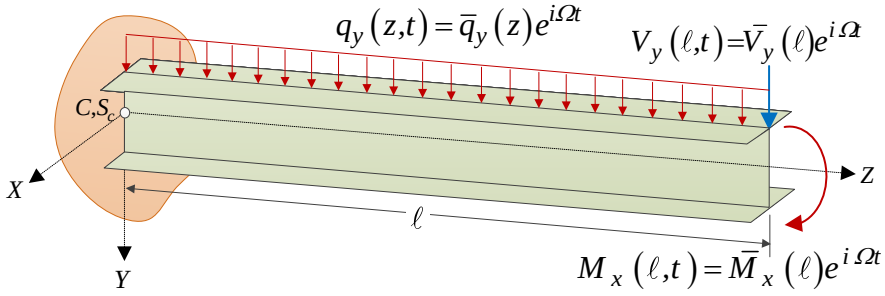

Figure (4.3): Cantilever I-beam under Inplane harmonic forces

Knowing that the boundary conditions at the fixed end $z=0$ are

$$\bar{v}(0)=0,\quad \bar{\theta}_x(0)=0 \tag{4.32-33}$$

and at the free end $z=0$ one has

$$GA_w\left[\bar{v}'(\ell)+\bar{\theta}_x(\ell)\right]=\bar{V}_y(\ell) \text{ and } EI_{xx}\bar{\theta}_x'(\ell)+\bar{M}_x(\ell)=0 \tag{4.34-35}$$

and substituting Equation (4.31) into Equations (4.32) to (4.35), the unknown integration constants $\{A_{2,i}\}_{4\times1}$ are then obtained as

$$\{A_{2,i}\}_{4\times1}=[\Phi_b]^{-1}_{4\times4}\{Q_b\}_{4\times1} \tag{4.36}$$

where $[\Phi_b]_{4\times4}=\begin{bmatrix} 1 & 1 & 1 & 1 \\ \bar{A}_1 & \bar{A}_2 & \bar{A}_3 & \bar{A}_4 \\ \left(\hat{\beta}_1+\bar{A}_1\right)e^{\hat{\beta}_1\ell} & \left(\hat{\beta}_2+\bar{A}_2\right)e^{\hat{\beta}_2\ell} & \left(\hat{\beta}_3+\bar{A}_3\right)e^{\hat{\beta}_3\ell} & \left(\hat{\beta}_4+\bar{A}_4\right)e^{\hat{\beta}_4\ell} \\ \hat{\beta}_1\bar{A}_1\,e^{\hat{\beta}_1\ell} & \hat{\beta}_2\,\bar{A}_2\,e^{\hat{\beta}_2\ell} & \hat{\beta}_3\bar{A}_3\,e^{\hat{\beta}_3\ell} & \hat{\beta}_4\bar{A}_4\,e^{\hat{\beta}_4\ell} \end{bmatrix}_{4\times4}$

and $\langle Q_b\rangle^T_{1\times4}=\left\langle \dfrac{\bar{q}_y}{\rho A\Omega^2} \quad \dfrac{\bar{m}_x}{\left(\rho I_{xx}\Omega^2-GA_w\right)} \quad \left(\dfrac{\bar{V}_y(\ell)}{GA_w}+\dfrac{\bar{m}_x}{\left(\rho I_{xx}\Omega^2-GA_w\right)}\right) \quad -\dfrac{\bar{M}_x(\ell)}{EI_{xx}} \right\rangle^T_{1\times4}$.

From Eq. (4.36), by substituting into Eq. (4.31), the closed-form solution of the displacement and rotation functions $\bar{v}(z)$ and rotation $\bar{\theta}_x(z)$ for transverse response are determined as:

$$\left\{\bar{V}_b(z)\right\}_{2\times1} = \left[L_b\right]_{2\times4}\left[E_b(z)\right]_{4\times4}\left[\Phi_b\right]^{-1}_{4\times4}\left\{Q_b\right\}_{4\times1} + \left\{\bar{V}_p\right\}_{2\times1} \tag{4.37}$$

4.6.2.4 Example - Simply Supported Beam under Transverse Forces

This section formulates the displacement field functions for a simply-supported doubly symmetric I-beam subjected to inplane transverse harmonic forces. A simply supported beam with doubly symmetric cross-section under distributed transverse force $q_y(z,t)=\bar{q}_y e^{i\Omega t}$ and bending moments $M_x(z_e,t)=\bar{M}_x(z_e)e^{i\Omega t}$ at both ends $(z_e=0,\ell)$ is considered (Figure 4.4).

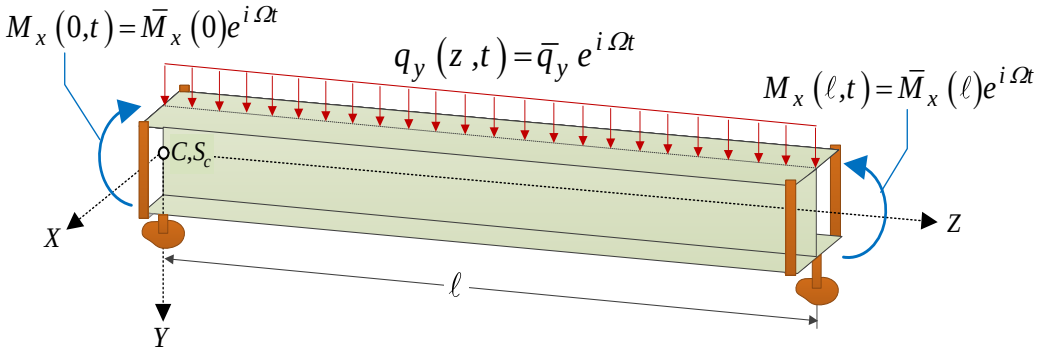

Figure (4.4): Simply supported I-beam under inplane transverse harmonic forces

The fork supports allow the beam end-sections to warp freely and to rotate about X and Y axes. Then, the following simply supported boundary conditions at beam ends $z=0$ and $z=\ell$ are:

$$\bar{v}(0)=0, \quad EI_{xx}\bar{\theta}'_x(0) = -\bar{M}_x(0) \text{ , and} \tag{4.38-39}$$

$$\bar{v}(\ell)=0, \quad EI_{xx}\bar{\theta}'_x(\ell) = \bar{M}_x(\ell) \tag{4.40-41}$$

By substituting the transverse displacement and related rotation in equation (4.37) into equations (4.39) to (4.42), the general steady state solution for simply supported I-beam under transverse harmonic loads is determined from

$$\left\{\bar{V}_S(z)\right\}_{2\times1} = \left[L_b\right]_{2\times4}\left[E_b(z)\right]_{4\times4}\left[\Phi_S\right]^{-1}_{4\times4}\left\{\bar{Q}_S\right\}_{4\times1} + \left\{\bar{V}_p\right\}_{2\times1} \tag{4.42}$$

in which the unknown integration constants $\{A_{2,i}\}_{4\times1}$ are obtained from the above set of boundary conditions, where

$$[\Phi_S]_{4\times4}=\begin{bmatrix} 1 & 1 & 1 & 1 \\ \bar{A}_1\hat{\beta}_1 & \bar{A}_2\hat{\beta}_2 & \bar{A}_3\hat{\beta}_3 & \bar{A}_4\hat{\beta}_4 \\ e^{\hat{\beta}_1\ell} & e^{\hat{\beta}_2\ell} & e^{\hat{\beta}_3\ell} & e^{\hat{\beta}_4\ell} \\ \hat{\beta}_1\bar{A}_1 e^{\hat{\beta}_1\ell} & \hat{\beta}_2\bar{A}_2 e^{\hat{\beta}_2\ell} & \hat{\beta}_3\bar{A}_3 e^{\hat{\beta}_3\ell} & \hat{\beta}_4\bar{A}_4 e^{\hat{\beta}_4\ell} \end{bmatrix}_{4\times4}, \text{ and}$$

$$\langle \bar{Q}_S \rangle_{1\times4}^T=\left\langle \frac{\bar{q}_y}{\rho A\Omega^2} \quad \frac{-\bar{M}_x(0)}{EI_{xx}} \quad \frac{\bar{q}_y}{\rho A\Omega^2} \quad \frac{\bar{M}_x(\ell)}{EI_{xx}} \right\rangle_{1\times4}^T.$$

4.6.3 Solution for Lateral Displacement

The coupled field equations that govern the lateral response of thin-walled beam of doubly symmetric cross-section subjected to distributed lateral harmonic force $q_x(z,t)=\bar{q}_x e^{i\Omega t}$ and bending moment $m_y(z,t)=\bar{m}_y e^{i\Omega t}$ are represented by the third system of equations in (4.8) as

$$-\rho A\Omega^2\bar{u}(z)-GA_f\bar{u}''(z)+GA_f\bar{\theta}_y'(z)=\bar{q}_x(z) \tag{4.43}$$

$$GA_f\bar{u}'(z)-\left(GA_f-\rho I_{yy}\Omega^2\right)\bar{\theta}_y(z)+EI_{yy}\bar{\theta}_y''(z)=\bar{m}_y(z) \tag{4.44}$$

And the relevant boundary conditions are given as:

$$\left[GA_f\left(\bar{u}'-\bar{\theta}_y\right)-\bar{V}_x(z)\right]\delta\bar{u}(z)\Big|_0^\ell=0 \tag{4.45}$$

$$\left[EI_{yy}\bar{\theta}_y'-\bar{M}_y(z)\right]\delta\bar{\theta}_y(z)\Big|_0^\ell=0 \tag{4.46}$$

4.6.3.1 Homogeneous Solution

The homogeneous solutions for lateral displacement and related rotation are evaluated by using two steps; (i) substituting the lateral displacement $\bar{u}_h(z)$ and rotation $\bar{\theta}_y(z)$ expressions in equation (4.16) into the homogeneous form of equations (4.43) and (4.44), one obtains

$$\bar{u}_h(z)=\sum_{i=1}^{4}A_{4,i}\,e^{\bar{\eta}_i z}\quad\text{and}\quad\bar{\theta}_{y_h}(z)=\sum_{i=1}^{4}A_{5,i}\,e^{\bar{\eta}_i z}\quad,\ for\ \ i=1,2,3,4 \tag{4.47}$$

in which $\bar{\eta}_i$ *for* $i=1,2,3,4$ are the distinct roots of the quartic algebraic equation given as:

$$\bar{\eta}_{1,2}=\pm\sqrt{\frac{1}{2}\left[-\frac{\Omega^2\rho}{E}\left(\frac{EA}{GA_f}+1\right)+\sqrt{\left[\frac{\Omega^2\rho}{E}\left(\frac{EA}{GA_f}+1\right)\right]^2+\frac{4\rho A\,\Omega^2}{EI_{yy}}\left(1-\frac{\rho I_{yy}\Omega^2}{GA_f}\right)}\right]}$$

$$\bar{\eta}_{3,4}=\pm i\sqrt{\frac{1}{2}\left[\frac{\Omega^2\rho}{E}\left(\frac{EA}{GA_f}+1\right)+\sqrt{\left[\frac{\Omega^2\rho}{E}\left(\frac{EA}{GA_f}+1\right)\right]^2+\frac{4\rho A\,\Omega^2}{EI_{yy}}\left(1-\frac{\rho I_{yy}\Omega^2}{GA_f}\right)}\right]}$$

(ii) the eight integration constants $A_{4,i}$ and $A_{5,i}$ are reduced to only four constants by substituting Eq. (4.47) into the homogeneous form of Eqs. (4.43) and (4.44) to approach the homogenous solution for the lateral bending vibration of the member

$$\left\{\bar{U}_h(z)\right\}_{2\times1}=\left[L_\ell\right]_{2\times4}\left[E_\ell(z)\right]_{4\times4}\left\{A_{4,i}\right\}_{4\times1} \tag{4.48}$$

in which $\left\langle\bar{U}_h(z)\right\rangle_{1\times2}^T=\left\langle\bar{u}_h(z)\quad\bar{\theta}_{y_h}(z)\right\rangle_{1\times2}^T$, $\left[E_\ell(z)\right]_{4\times4}=diag\left[e^{\bar{\eta}_1 z}\ \vdots\ e^{\bar{\eta}_2 z}\ \vdots\ e^{\bar{\eta}_3 z}\ \vdots\ e^{\bar{\eta}_4 z}\right]_{4\times4}$

$\left[L_\ell\right]_{2\times4}=\begin{bmatrix}1&1&1&1\\ \bar{B}_1&\bar{B}_2&\bar{B}_3&\bar{B}_4\end{bmatrix}_{2\times4}$, $\left\langle A_{4,i}\right\rangle_{1\times4}^T=\left\langle A_{4,1}\quad A_{4,2}\quad A_{4,3}\quad A_{4,4}\right\rangle_{1\times4}^T$, where

$\bar{B}_i=\left(\dfrac{\rho A\ \Omega^2+GA_f\,\bar{\eta}_i^2}{GA_f\,\bar{\eta}_i}\right)=\left(\dfrac{GA_f\,\bar{\eta}_i}{GA_f\ -\rho I_{yy}\,\Omega^2-\ EI_{yy}\,\bar{\eta}_i^2}\right)$, for $i=1,2,3,4$ is an expression obtained by using the same procedures given in Appendix (4.A) used for reducing the integration constants $A_{4,i}$ and $A_{5,i}$, i.e., $A_{5,i}=\bar{B}_i A_{4,i}$, for $i=1,2,3,4$.

4.6.3.2 Particular Solution for Uniform Lateral Forces

In a similar way, the particular solution for lateral bending vibration equations (4.43) and (4.44) is obtained as

$$\left\langle\bar{U}_p\right\rangle_{1\times2}^T=\left\langle\left(-\bar{q}_x(z)/\rho A\Omega^2\right)\quad-\bar{m}_y/\left(GA_f-\rho I_{yy}\Omega^2\right)\right\rangle_{1\times2}^T \tag{4.49}$$

The complete solution is obtained by adding Equation (4.48) to Equation (4.49), yields

$$\left\{\bar{U}_h(z)\right\}_{2\times1} = \left[L_\ell\right]_{2\times4}\left[E_\ell(z)\right]_{4\times4}\left\{A_{4,i}\right\}_{4\times1} + \left\{\bar{U}_p(z)\right\}_{2\times1} \tag{4.50}$$

Equation (4.50) represents the complete steady state solution for the lateral bending vibration of thin-walled doubly symmetric members under lateral harmonic loads. By imposing the problem boundary conditions, the vector of unknown integration constants $\left\{A_{4,i}\right\}_{4\times1}$ can be evaluated.

4.6.3.3 Example - Cantilever Beam under Lateral Forces

A Cantilever thin walled I-section member subjected to lateral harmonic loads, uniformly distributed load $\bar{q}_x(z)e^{i\Omega t}$, end moment $\bar{M}_y(\ell)e^{i\Omega t}$ about Y axis and end lateral load $\bar{V}_x(\ell)e^{i\Omega t}$ at the free end $(z=\ell)$, as shown in Figure (4.5), is considered.

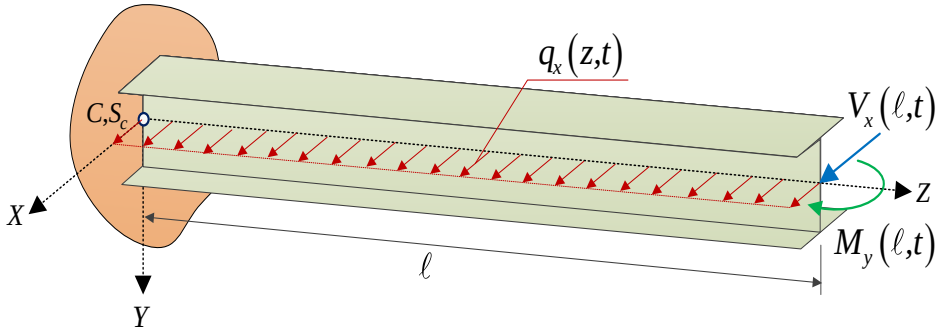

Figure (4.5): Cantilever beam with doubly symmetric I-section under lateral forces

The cantilever boundary conditions at fixed $(z=0)$ and free ends $(z=\ell)$ are given as:

$$\bar{u}(0)=0,\ \bar{\theta}_y(0)=0 \ \text{ and } \ GA_f\left[\bar{u}'(\ell)-\bar{\theta}_y(\ell)\right]=\bar{V}_x(\ell),\ EI_{yy}\bar{\theta}_y'(\ell)=\bar{M}_y(\ell) \tag{4.51-54}$$

From Equation (4.50), by substituting into Equations (4.51) to (4.54), leads to

$$\left\{A_{4,i}\right\}_{2\times1} = \left[\Phi_\ell\right]_{4\times4}\left\{Q_\ell\right\}_{4\times1} \tag{4.55}$$

where $\left\langle Q_\ell\right\rangle^T_{1\times4} = \left\langle \dfrac{\bar{q}_x}{\rho A\Omega^2} \quad \dfrac{\bar{m}_y}{\left(GA_f-\rho I_{yy}\Omega^2\right)} \quad \dfrac{\bar{V}_x(\ell)}{GA_f} \quad \dfrac{\bar{M}_y(\ell)}{EI_{yy}} \right\rangle^T_{1\times4}$ and

$$\left[\Phi_L\right]_{4\times4}=\begin{bmatrix} 1 & 1 & 1 & 1 \\ \bar{B}_1 & \bar{B}_2 & \bar{B}_3 & \bar{B}_4 \\ \left(\hat{\eta}_1-\bar{B}_1\right)e^{\hat{\eta}_1\ell} & \left(\hat{\eta}_2-\bar{B}_2\right)e^{\hat{\eta}_2\ell} & \left(\hat{\eta}_3-\bar{B}_3\right)e^{\hat{\eta}_3\ell} & \left(\hat{\eta}_4-\bar{B}_4\right)e^{\hat{\eta}_4\ell} \\ \hat{\eta}_1\bar{B}_1e^{\hat{\eta}_1\ell} & \hat{\eta}_2\bar{B}_2e^{\hat{\eta}_2\ell} & \hat{\eta}_3\bar{B}_3e^{\hat{\eta}_3\ell} & \hat{\eta}_4\bar{B}_4e^{\hat{\eta}_4\ell} \end{bmatrix}_{4\times4}.$$

From Eq. (4.55), by substituting into Eq. (4.50), the complete steady state lateral response is then evaluated as:

$$\left\{\bar{U}(z)\right\}_{2\times1}=\left[L_\ell\right]_{2\times4}\left[E_\ell(z)\right]_{4\times4}\left[\Phi_\ell\right]^{-1}_{4\times4}\left\{Q_\ell\right\}_{4\times1}+\left\{\bar{U}_p(z)\right\}_{2\times1} \tag{4.56}$$

4.6.4 Solution for Torsion and Warping

The governing differential equations provided in the fourth partition in Equation (4.8) and the associated boundary equations in (4.14) and (4.15) are

$$-\rho A\,\Omega^2 r_o^2\bar{\theta}_z(z)-\left[GJ+GA_f\,(H/2)^2\right]\bar{\theta}_z''(z)-GA_f\,(H/2)^2\,\bar{\psi}'(z)=\bar{m}_z(z) \tag{4.57}$$

$$-GA_h\bar{\theta}_z'(z)+\left[\rho C_w\,\Omega^2-GA_f\,(H/2)^2\right]\bar{\psi}(z)+EC_w\,\bar{\psi}''(z)=\bar{m}_w(z)$$

(4.58)

and the boundary conditions are

$$\left[\left(GJ+GA_f\,(H/2)^2\right)\bar{\theta}_z'(z)+GA_f\,(H/2)^2\,\bar{\psi}(z)-\bar{M}_z(z)\right]\delta\bar{\theta}_z(z)\Big|_0^\ell=0 \tag{4.59}$$

$$\left[EC_w\,\bar{\psi}'(z)+\bar{M}_w(z)\right]\delta\bar{\psi}(z)\Big|_0^\ell=0 \tag{4.60}$$

In a similar manner to the lateral displacement solution, the solution for the coupled torsional-warping equations is the sum of the homogeneous and particular solutions, i.e.,

$$\left\{\bar{\theta}_{z_T}(z)\right\}_{2\times1}=\left[L_T\right]_{2\times4}\left[E_T(z)\right]_{4\times4}\left\{A_{6,i}\right\}_{4\times1}+\left\{\bar{\theta}_{z_P}\right\}_{2\times1} \tag{4.61}$$

where $\left\langle\bar{\theta}_{z_T}(z)\right\rangle^{\mathrm{T}}_{1\times2}=\left\langle\bar{\theta}_z(z)\quad\bar{\psi}(z)\right\rangle^{\mathrm{T}}_{1\times2}$, $\left\langle\bar{\theta}_{z_P}\right\rangle^{T}_{1\times2}=\left\langle\dfrac{-\bar{m}_z}{r_o^2\rho A\Omega^2}\quad\dfrac{\bar{m}_w}{\left(\rho C_w\,\Omega^2-G(H/2)^2A_f\right)}\right\rangle^{T}_{1\times2}$.

In Equation (4.61), matrices $[E_T(z)]_{4\times4}$ and $[L_T]_{2\times4}$ are similar to those of $[E_b(z)]_{4\times4}$ and $[L_b]_{2\times4}$ can be obtained by replacing the set of constants $\bar{A}_i$ and $\hat{\beta}_i$ (for $i=1,2,3,4$) by constants $\bar{C}_i$ and $\hat{\mu}_i$, in which $\hat{\mu}_i$ are determined by replacing q_1 and q_2 by α_1 and α_2 in the expression for $\hat{\beta}_i$, where $\alpha_1=\left(\dfrac{\rho\Omega^2C_w\left[EAr_o^2+GJ+GA_f\left(H/2\right)^2\right]-G^2JA_f\left(H/2\right)^2}{EC_wG\left(J+A_f\left(H/2\right)^2\right)}\right)$ and

$\alpha_2=\left(\dfrac{\rho A\Omega^2r_o^2\left(GA_f\left(H/2\right)^2-\rho C_w\Omega^2\right)}{EC_wG\left(J+A_f\left(H/2\right)^2\right)}\right)$, and the constants

$\bar{C}_i=\dfrac{-\left[\left(GJ+GA_f\left(H/2\right)^2\right)\hat{\eta}_i^2+\rho A\Omega^2r_o^2\right]}{GA_f\left(H/2\right)^2\hat{\eta}_i}=\dfrac{GA_f\left(H/2\right)^2\hat{\eta}_i}{\left(\rho C_w\Omega^2-GA_f\left(H/2\right)^2+EC_w\hat{\eta}_i^2\right)}$ are obtained

by using the same procedures given in Appendix (4.A) to reduce the unknown integration constants, i.e., $A_{7,i}=\bar{C}_iA_{6,i}$, *for* $i=1,2,3,4$.

4.6.4.1 Example - Cantilever under Torsion and Bimoments

In a similar way, the general solution for a cantilever subjected to harmonic forces (i) uniformly distributed torsion $\bar{m}_z(z)e^{i\Omega t}$, bimoment $\bar{m}_w(z)e^{i\Omega t}$, (ii) end twisting moment $\bar{M}_z(\ell)e^{i\Omega t}$ and end bimoment $\bar{M}_w(\ell)e^{i\Omega t}$ is obtained (Figure 4.6) by:

$$\left\{\bar{\theta}_{z_T}(z)\right\}_{2\times1}=[L_T]_{2\times4}\left[E_T(z)\right]_{4\times4}[\Phi_T]^{-1}_{4\times4}\{Q_T\}_{4\times1}+\left\{\bar{\theta}_{z_P}\right\}_{2\times1} \tag{4.62}$$

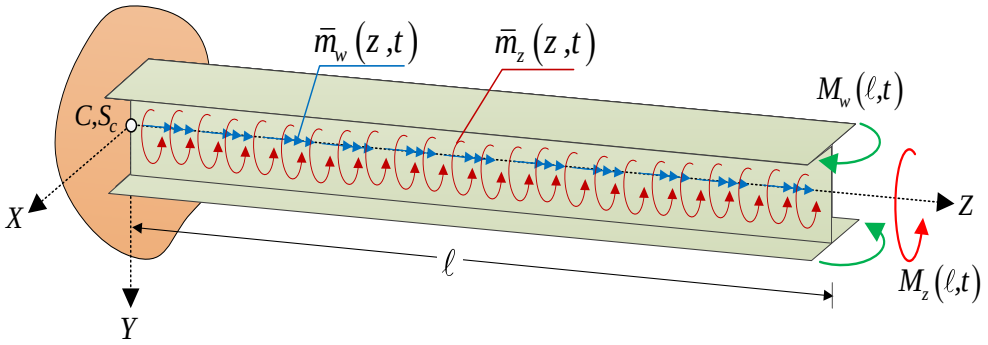

Figure (4.6): Cantilever I-beam under distributed harmonic torsion and bimoment

In Equation (4.61), the integration constants $\left\{A_{6,i}\right\}_{4\times1}$ are evaluated by enforcing the cantilever boundary conditions at both ends;

$$\bar{\theta}_z(0)=0, \quad \bar{\psi}(0)=0$$

$$G\left[\left(A_f\left(H/2\right)^2+J\right)\bar{\theta}_z'(\ell)+A_f\left(H/2\right)^2\bar{\psi}(\ell)\right]=\bar{M}_z(\ell), \quad EC_w\,\bar{\psi}(\ell)=\bar{M}_w(\ell)$$

where

$$\left[\Phi_T\right]_{4\times4}=\begin{bmatrix} 1 & 1 & 1 & 1 \\ \bar{G}_1 & \bar{G}_2 & \bar{G}_3 & \bar{G}_4 \\ G_{3,1} & G_{3,2} & G_{3,3} & G_{3,4} \\ \hat{\mu}_1\bar{G}_1 e^{\hat{\mu}_1 l} & \hat{\mu}_2\bar{G}_2 e^{\hat{\mu}_2 l} & \hat{\mu}_3\bar{G}_3 e^{\hat{\mu}_3 l} & \hat{\mu}_4\bar{G}_4 e^{\hat{\mu}_4 l} \end{bmatrix}_{4\times4},$$

$$G_{3,i}=\left[\hat{\mu}_i\left(1+\left(J/A_h\right)\right)+\bar{G}_i\right]e^{i\Omega t}$$

$$\bar{G}_i=-\left(\frac{\rho A\Omega^2 r_o^2+G\left(J+A_f\left(H/2\right)^2\right)\hat{\mu}_i^2}{GA_f\left(H/2\right)^2\hat{\mu}_i}\right)=\left(\frac{GA_f\left(H/2\right)^2\hat{\mu}_i}{\rho C_w\Omega^2-GA_f\left(H/2\right)^2+EC_w\,\hat{\mu}_i^2}\right), \text{ for } i=1,2,3,4 \text{ and}$$

$$\left\langle Q_T\right\rangle_{4\times1}^{\mathrm{T}}=\left\langle \frac{\bar{m}_z}{\rho A\Omega^2 r_0^2} \quad \frac{-\bar{m}_w}{\left(\rho C_w\Omega^2-GA_f\left(H/2\right)^2\right)} \quad \left(\frac{\bar{M}_z(\ell)}{GA_f\left(H/2\right)^2}-\frac{\bar{m}_w}{\left(\rho C_w\Omega^2-GA_f\left(H/2\right)^2\right)}\right) \quad \frac{\bar{M}_w(\ell)}{EC_w}\right\rangle_{4\times1}^{\mathrm{T}}.$$

4.7 Finite Element Formulation

The finite element to be derived has two nodes and seven degrees of freedom per node. The exact homogeneous displacement fields are used to formulate the exact stiffness and mass matrices as well as the load potential vector.

4.7.1 Displacement Fields in Terms of Nodal Displacements

The displacement fields $\left\langle\bar{U}_S(z)\right\rangle_{1\times7}^T=\left\langle\bar{w}_h(z)\;\bar{v}_h(z)\;\bar{\theta}_{x_h}(z)\;\bar{u}_h(z)\;\bar{\theta}_{y_h}(z)\;\bar{\theta}_{z_h}(z)\;\bar{\psi}_h(z)\right\rangle_{1\times7}^T$ which exactly satisfy the homogeneous solution of the uncoupled field equations derived in this study can be expressed as

$$\left\{\bar{U}_S(z)\right\}_{7\times1}=\left[\bar{\chi}\right]_{7\times14}\left[E(z)\right]_{14\times14}\left\{A_i\right\}_{14\times1} \tag{4.63}$$

In Equation (4.63), $\langle A_i \rangle_{1\times4}^T = \langle A_1 \quad A_2 \quad A_3 \quad ..... \quad A_{14} \rangle_{1\times4}^T$ is the vector of unknown integration constants, $[\,\bar{\chi}\,]_{7\times14}$ is the matrix of eigenvectors of the homogeneous solution of the governing field equations, $\left[E(z)\right]_{14\times14} = diag\left[e^{m_1 z} \;\vdots\; e^{m_2 z} \;\vdots\; e^{m_2 z} \;\vdots\; e^{m_3 z} \;\vdots\; e^{m_4 z} \;\vdots\; ..... \;\vdots\; e^{m_{14} z}\right]_{14\times14}$, and $m_i\,(for\ i = 1,2,3,....,14)$ are the roots of the characteristic polynomial equations for longitudinal, transverse, lateral and torsional-warping responses (i.e., $m_{1,2} = \bar{\lambda}_{1,2}$, $m_{3,4} = \bar{\beta}_{1,2}$, $m_{5,6} = \bar{\beta}_{3,4}$, $m_{7,8} = \bar{\eta}_{1,2}$, $m_{9,10} = \bar{\eta}_{3,4}$, $m_{11,12} = \bar{\mu}_{1,2}$ and $m_{13,14} = \bar{\mu}_{3,4}$). In the present formulation, the vector of nodal displacements $\{U_N\}_{14\times1}$ can be written as

$$\begin{aligned}\langle U_N \rangle_{1\times14}^T &= \langle w_1 \;\vdots\; v_1 \;\vdots\; \theta_{x_1} \;\vdots\; u_1 \;\vdots\; \theta_{y_1} \;\vdots\; \theta_{z_1} \;\vdots\; \psi_1 \;\vdots\; w_2 \;\vdots\; v_2 \;\vdots\; \theta_{x_1} \;\vdots\; u_2 \;\vdots\; \theta_{y_2} \;\vdots\; \theta_{z_2} \;\vdots\; \psi_2 \rangle_{1\times14}^T \\ &= \left\langle \langle \bar{U}_S(0) \rangle_{1\times7}^T \;\vdots\; \langle \bar{U}_S(\ell) \rangle_{1\times7}^T \right\rangle_{1\times14}^T \end{aligned} \tag{4.64}$$

From Equation (4.63), one obtains

$$\{U_N\}_{14\times1} = \left[\begin{array}{c} [\bar{\chi}]_{7\times14}\left[E(0)\right]_{14\times14} \\ \hdashline [\bar{\chi}]_{7\times14}\left[E(\ell)\right]_{14\times14} \end{array}\right]_{14\times14} \{A\}_{14\times1} = \left[\bar{\Phi}\right]_{14\times14}\{A\}_{14\times1} \tag{4.65}$$

From Equations (4.64) and (4.65), the displacement functions are written in terms of nodal displacements as

$$\{\bar{U}_S(z)\}_{7\times1} = \left[H(z)\right]_{7\times14}\{U_N\}_{14\times1} \tag{4.66}$$

in which $\left[H(z)\right]_{7\times14} = [\,\chi]_{7\times14}\left[E(z)\right]_{14\times14}\left[\bar{\Phi}\right]_{14\times14}^{-1}$ is the matrix of exact shape functions, and

$$\begin{aligned}\left[H(z)\right]_{14\times7}^T = \Big[&\{H_{1,j}(z)\}_{14\times1} \;\vdots\; \{H_{2,j}(z)\}_{14\times1} \;\vdots\; \{H_{3,j}(z)\}_{14\times1} \;\vdots\; \{H_{4,j}(z)\}_{14\times1} \\ &\vdots\; \{H_{5,j}(z)\}_{14\times1} \;\vdots\; \{H_{6,j}(z)\}_{14\times1} \;\vdots\; \{H_{7,j}(z)\}_{14\times1}\Big]_{14\times7}^T \end{aligned}$$

It is noted that the interpolation shape functions provided in Equation (4.66) exactly satisfy the homogeneous form of the governing field Equations.

4.7.2 Energy Expressions in Terms of Nodal Displacements

From the forces and displacements expressions presented in (3.80) to (3.81), by substituting into the energy expressions (3.15), (3.17) and (3.21) and by adapting the resulting equations to the case of doubly symmetric section (i.e., setting $x_s = y_s = 0$ and the section properties D_{xy}, D_{hx}, D_{hy} are vanished), the variations of the energy equations are then obtained in terms of nodal degrees of freedom by using Equation (4.66).

4.7.2.1 Discretization of kinetic energy

The variation of the kinetic energy δT^* is written in terms of nodal displacements as:

$$\begin{aligned}\delta T^* &= -\int_{t_1}^{t_2}\left(\Omega^2\int_0^{\ell}\left\langle\delta\bar{\dot{U}}_S(z)\right\rangle_{1\times7}^T\left[X_m\right]_{7\times7}\left\{\bar{\dot{U}}_S(z)\right\}_{7\times1}dz\right)e^{i\Omega t}\,dt \\ &= -\int_{t_1}^{t_2}\left(\Omega^2\int_0^{\ell}\left\langle\delta U_N\right\rangle_{1\times14}^T\left[H(z)\right]_{14\times7}^T\left[X_m\right]_{7\times7}\left[H(z)\right]_{7\times14}\left\{U_N\right\}_{14\times1}dz\right)e^{i\Omega t}dt\end{aligned} \tag{4.67}$$

in which $\left[X_m\right]_{7\times7} = diag\left[\rho A \;\vdots\; \rho A \;\vdots\; \rho I_{xx} \;\vdots\; \rho A \;\vdots\; \rho I_{yy} \;\vdots\; \rho A r_o^2 \;\vdots\; \rho C_w\right]_{7\times7}$, r_o is the polar radius of the gyration and is defined in the case of doubly symmetric cross-section by $r_o^2 = (1/A)\int_A\left(x^2+y^2\right)dA = \left(I_{xx}+I_{yy}\right)/A$.

4.7.2.2 Discretization of Internal Strain Energy

The variation of the internal stain energy δU^* for doubly symmetric thin-walled member is:

$$\begin{aligned}&\delta U^* \\ &= \int_{t_1}^{t_2}\left(\int_0^{\ell}\left[\left\langle\delta\bar{U}_S'(z)\right\rangle_{1\times7}^T\left[Z_a\right]_{7\times7}\left\{\bar{U}_S'(z)\right\}_{7\times1} + \left\langle\delta\bar{U}_d(z)\right\rangle_{1\times7}^T\left[Z_d\right]_{7\times7}\left\{\bar{U}_d(z)\right\}_{7\times1}\right]dz\right)e^{i\Omega t}dt \\ &= \int_{t_1}^{t_2}\left(\int_0^{\ell}\left[\left\langle\delta U_N\right\rangle_{1\times14}^T\left[H'(z)\right]_{14\times7}^T\left[Z_a\right]_{7\times7}\left[H'(z)\right]_{7\times14}\left\{U_N\right\}_{14\times1}\right.\right. \\ &\qquad \left.\left. + \left[\left\langle\delta U_N\right\rangle_{1\times14}^T\left[H_d(z)\right]_{14\times7}^T\left[Z_d\right]_{7\times7}\left[H_d(z)\right]_{7\times14}\left\{U_N\right\}_{14\times1}\right]dz\right)e^{i\Omega t}dt\end{aligned} \tag{4.68}$$

where

$$\left[Z_a\right]_{7\times7} = E\int_A\left\{Y_m\right\}_{7\times1}\left\langle Y_m\right\rangle_{1\times7}^T dA + GJ = diag\left[EA \;\vdots\; 0 \;\vdots\; EI_{xx} \;\vdots\; 0 \;\vdots\; EI_{yy} \;\vdots\; GJ \;\vdots\; EC_w\right]_{7\times7},$$

in which $\langle Y_m \rangle_{1\times7}^T = \langle 1 \quad 0 \quad y(s) \quad 0 \quad -x(s) \quad 0 \quad \omega(s) \rangle_{1\times7}^T$,

$$[Z_d]_{7\times7} = G\int_A \{Y_s\}_{7\times1}\langle Y_s\rangle_{1\times7}^{\mathrm{T}} dA = \begin{bmatrix} 0 & 0 & 0 & 0 & 0 & 0 & 0 \\ & GD_{yy} & GD_{yy} & 0 & 0 & 0 & 0 \\ & & GD_{yy} & 0 & 0 & 0 & 0 \\ & & & GD_{xx} & -GD_{xx} & 0 & 0 \\ & & Symm & & GD_{xx} & 0 & 0 \\ & & & & & GD_{\omega\omega} & GD_{\omega\omega} \\ & & & & & & GD_{\omega\omega} \end{bmatrix}_{7\times7},$$

$$\langle Y_s \rangle_{1\times7}^T = \left\langle 0 \quad \frac{dy(s)}{ds} \quad \frac{dy(s)}{ds} \quad \frac{dx(s)}{ds} \quad -\frac{dx(s)}{ds} \quad \frac{d\omega(s)}{ds} \quad \frac{d\omega(s)}{ds} \right\rangle_{1\times7}^T, \text{ and}$$

$$\left[H_d(z)\right]_{14\times7}^T = \Big[\{H_{1,\mathrm{j}}(z)\}_{14\times1} \;\Big|\; \{H'_{2,\mathrm{j}}(z)\}_{14\times1} \;\Big|\; \{H_{3,\mathrm{j}}(z)\}_{14\times1} \;\Big|\; \{H'_{4,\mathrm{j}}(z)\}_{14\times1} \;\Big|\; \{H_{5,\mathrm{j}}(z)\}_{14\times1} \;\Big|\; \{H'_{6,\mathrm{j}}(z)\}_{14\times1} \;\Big|\; \{H_{7,\mathrm{j}}(z)\}_{14\times1}\Big]_{14\times7}^T.$$

4.7.2.3 Work Done by External Harmonic Forces

The variation of the work done δW^* due to applied harmonic forces is obtained:

$$\begin{aligned}\delta W^* &= \int_{t_1}^{t_2}\left(\int_0^{\ell}\langle \delta\bar{U}_s(z)\rangle_{1\times7}^T\{\bar{P}(z)\}_{7\times1}dz + \langle \delta\bar{U}_s(\ell)\rangle_{1\times7}^T\{\bar{F}_\ell(\ell)\}_{7\times1} - \langle \delta\bar{U}_s(0)\rangle_{1\times7}^T\{\bar{F}_0(0)\}_{7\times1}\right)e^{i\Omega t}dt \\ &= \int_{t_1}^{t_2}\langle \delta U_N\rangle_{1\times14}^T\left(\int_0^{\ell}[H(z)]_{14\times7}^T\{\bar{P}(z)\}_{7\times1}dz + [H(\ell)]_{14\times7}^T\{\bar{F}_\ell(\ell)\}_{7\times1} - [H(0)]_{14\times7}^T\{\bar{F}_0(0)\}_{7\times1}\right)e^{i\Omega t}dt\end{aligned} \tag{4.69}$$

in which $\langle \bar{P}(z)\rangle_{1\times7}^T = \langle \bar{q}_z(z) \;|\; \bar{q}_y(z) \;|\; \bar{m}_x(z) \;|\; \bar{q}_x(z) \;|\; \bar{m}_y(z) \;|\; \bar{m}_z(z) \;|\; \bar{m}_w(z)\rangle_{1\times7}^T$ and $\langle \bar{F}_j(j)\rangle_{1\times7}^T = \langle \bar{N}_z(j) \;\; \bar{V}_y(j) \;\; \bar{M}_x(j) \;\; \bar{V}_x(j) \;\; \bar{M}_y(j) \;\; \bar{M}_z(j) \;\; \bar{M}_w(j)\rangle_{1\times7}^T$, for $z_e = 0, \ell$.

4.7.2.4 Finite Element Formulation of Dynamic Field Equations

Substituting the energy expressions (4.67) to (4.69) into the variational form of Hamilton's principle, $\int_{t_1}^{t_2}\left(\delta T^* - \delta U^* + \delta W^*\right)dt = 0$, leads to the finite element model of a typical element as

$$\left(\left[K_e\right]_{14\times14}-\Omega^2\left[M_e\right]_{14\times14}\right)_{14\times14}\left\{U_N\right\}_{14\times1}=\left\{F_e\right\}_{14\times1} \tag{4.70}$$

in which $\left[K_e\right]_{14\times14}=\int_0^{\ell}\left(\left[H'(z)\right]_{14\times7}^{\mathrm{T}}\left[Z_a\right]_{7\times7}\left[H'(z)\right]_{7\times14}+\left[H_d(z)\right]_{14\times7}^{\mathrm{T}}\left[Z_d\right]_{7\times7}\left[H_d(z)\right]_{7\times14}\right)dz$ is the element stiffness matrix, $\left[M_e\right]_{14\times14}=\int_0^{\ell}\left[H(z)\right]_{14\times7}^{\mathrm{T}}\left[X_m\right]_{7\times7}\left[H(z)\right]_{7\times14}dz$ is the element mass matrix, evaluated by considering the combination effects of translational and rotational inertias, and

$\left\{F_e(z)\right\}_{14\times1}=\int_0^{\ell}\left(\left[H(z)\right]_{14\times7}^{\mathrm{T}}\left\{\bar{P}(z)\right\}_{7\times1}\right)dz+\left[H(\ell)\right]_{14\times7}^{\mathrm{T}}\left\{\bar{F}_{\ell}(\ell)\right\}_{7\times1}-\left[H(0)\right]_{14\times7}^{\mathrm{T}}\left\{\bar{F}_0(0)\right\}_{7\times1}$ is the element load vector of the harmonic forces.

For a thin-walled structural beam consisting of n nodes, the total number of degrees of freedom is $7n$, i.e., each node has seven degrees of freedom. Figure (4.7) shows the degrees of freedom for the present finite beam element. The stiffness, mass matrices and load vector are evaluated by using the exact interpolation shape functions.

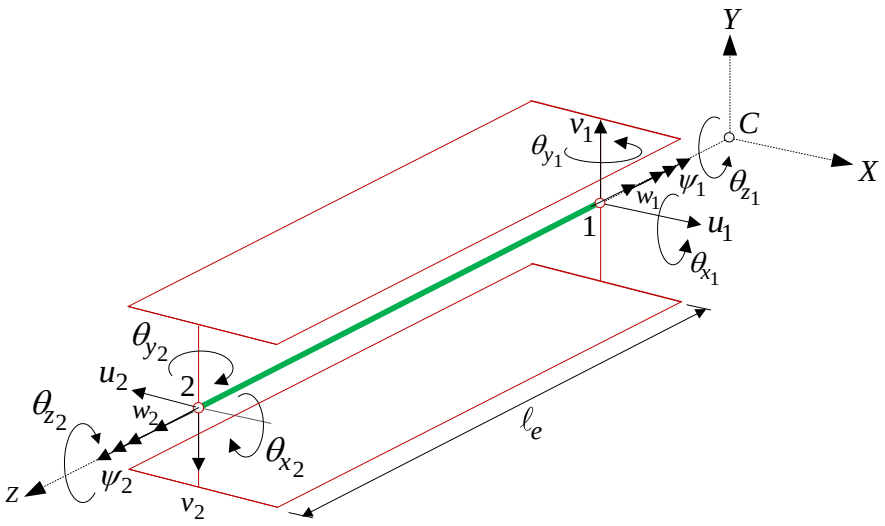

Figure (4.7): Degrees of freedom for present finite beam element.

4.8 Numerical Examples and Discussion

The analytical solutions developed in the current study are applied to compute the dynamic response of cantilever thin-walled members of doubly symmetric I-section subjected to

harmonic excitations, i.e., concentrated and distributed loads. For each problem, one numerical example with two loading cases will demonstrate the validity and accuracy of the present solutions, closed-form and finite element formulation using a single beam element. The results based on the present formulations are compared against the following solutions:

(1) Euler-Bernoulli beam solution which neglects the shear deformation effects due to bending and restrained warping torsion, and distortional effects as well.

(2) A Vlasov beam theory solution which ignores shear deformation and distortional effects.

(3) An Abaqus two-noded B31OS beam element (Figure 4.8a) with seven degrees of freedom per node (i.e. three translations, three rotations and warping deformation) which (i) captures only the shear deformations due to bending but ignores these effects due to restrained warping, and (ii) omits the distortional effects of the cross-section.

(4) An Abaqus S4R shell element solution (shell element with four nodes with six degrees of freedom per node (Figure 4.8b), i.e., three translation and three rotations, and reduced integration) which captures the shear deformation and distortional effects.

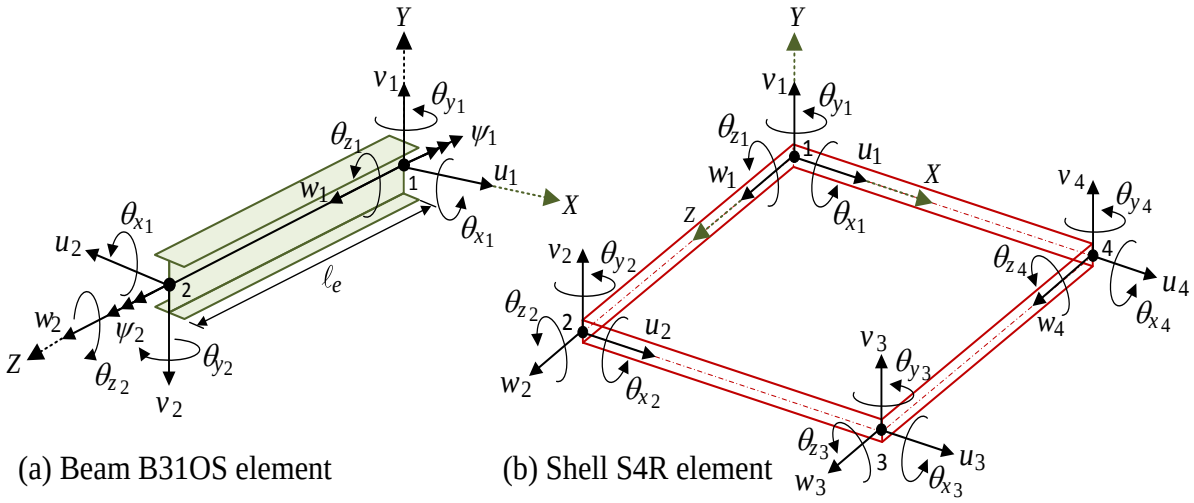

(a) Beam B31OS element (b) Shell S4R element

Figure (4.8): Abaqus beam B31OS and shell S4R elements

The S4R shell element with reduced integration and large strain formulation is sufficient and consistent and widely used by many authors to model steel structural members [e.g. Mohareb and Dabbas (2003), Zinoviev and Mohareb (2004)]. The advantages of the reduced integration are; (1) it avoids shear locking and (2) it makes the solution computationally less

expensive and reduces the CPU time compared to fully integrated elements. Previous studies Mohareb and Dabbas (2003) demonstrated that the S4R element yields most accurate results when the element aspect ratio is close to unity.

In the Abaqus shell element model solutions, a total of 3,120 S4R shell elements are used for the analysis of transverse bending response (Example 1). The member is subdivided into 120 shell S4R elements along the longitudinal axis of the beam, 8 elements per each flange and 10 elements along the web height. In the case of torsional response analysis (Example 2) and in-plane transverse response (Example 3) for short beams, the number of elements along the member axis is 50 shell S4R elements, i.e., a 1,300 shell element is used for transverse and torsional models. Figure (4.9) illustrates the Abaqus finite shell S4R element model mesh adopted for the thin-walled member with doubly symmetric I-section. In the Abaqus beam B31OS element models, 100 elements are used to approach the accurate results. In Abaqus solutions, the bending and torsional displacements are interpolated using linear and cubic Hermite shape functions. In contrast, the present study develops an efficient finite element

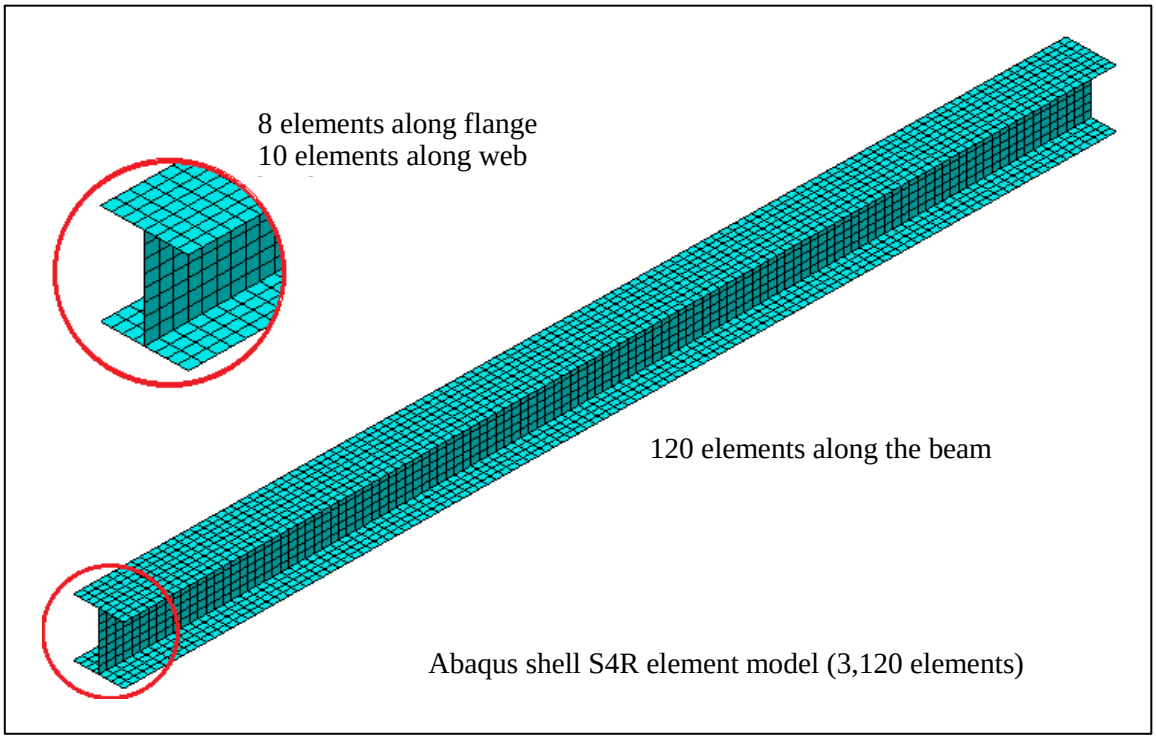

Figure (4.9): View for uniform Abaqus shell S4R element mesh adopted for doubly symmetric thin-walled I-beam

based on the exact shape functions that exactly satisfy the homogeneous form of the resulting coupled differential equations of motion. The new two-noded beam element is free from shear locking and converges to the exact result with a minimal number of degrees of freedom. The exact shape functions developed are dependent on (1) the exciting frequency, (2) type of response (longitudinal, transverse, lateral or torsional/warping), (3) sectional properties, and (4) the length of the element.

4.8.1 Example 1- Transverse Displacement

A cantilever thin-walled doubly symmetric I-beam of a 4m span is considered as shown in Figure (4.10). It is required to determine the static and dynamic responses of the beam under the given vertical harmonic loads: (a) concentrated $P_y\left(\ell,t\right)=10.0e^{i\Omega t}kN$ and (b) distributed $q_y\left(z,t\right)=5.0e^{i\Omega t}kN/m$ loads. Two values of exciting frequencies are used; (i) $\Omega=0.01\bar{\omega}_1$ to capture the static response and (ii) $\Omega=1.80\bar{\omega}_1$ to establish the dynamic response.

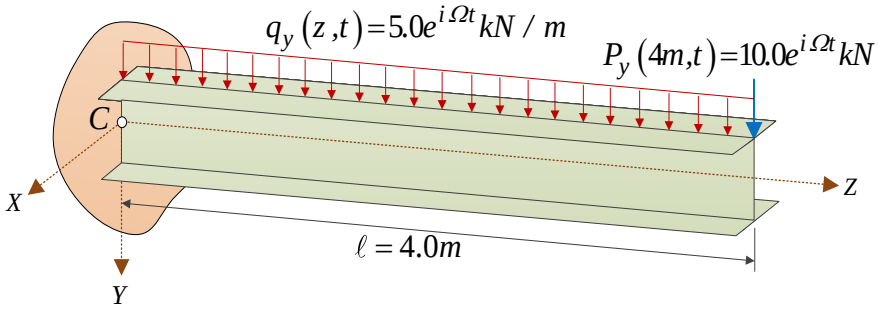

Figure (4.10): Cantilever I-beam under inplane transverse harmonic forces

The material and geometric properties for I-beam (W250×58) are used in all examples; $E=200GPa$, $G=77GPa$, $\rho=7800kg/m^3$, width of each flange $b=203mm$, height of middle surface $H=238.5mm$, flange thickness $t_f=13.5mm$ and web thickness $t_w=8mm$, while the cross-sectional properties for the doubly symmetric section are: $A=7420mm^2$, $I_{xx}=87.30\times10^6mm^4$, $I_{yy}=18.80\times10^6mm^4$, $J=409.0\times10^6mm^4$, $C_w=268.0\times10^9mm^6$, $D_{xx}=54.81\times10^4mm^2$, $D_{yy}=19.08\times10^4mm^2$ and $D_{\omega\omega}=77.94\times10^6mm^4$.

4.8.1.1 Static Solution

In order to approach the static response, the exciting frequency Ω should be taken significantly lower than the first eigen-frequency of the system. Since the first natural frequency of $4.0m$ cantilever I-beam is $\bar{\omega}_1 = 55.37 rad/\sec$. The harmonic forces with exciting frequency of $\Omega = 0.01\bar{\omega}_1 \approx 0.554 rad/\sec$ should approach that of the static response of the beam. The static results for maximum transverse displacement $\bar{v}_{\max}$ and related rotation $\bar{\theta}_{x_{\max}}$ of the cantilever under transverse harmonic loads are given in Table (4.1).

Table (4.1): Static Analysis results for cantilever I-beam under transverse harmonic loads

Type of Load	Variable	Abaqus S4R Solution [1]	Present Solution [2]	Abaqus B31OS Solution [3]	Euler Bernoulli Solution [4]	Present Difference =[1-2]/1	B31OS Difference =[1-3]/1	EB Difference =[1-4]/1
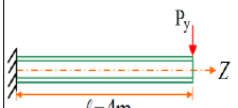	$\bar{v}_{\max}$ (mm)	12.55	12.53	12.33	12.26	0.16%	1.75%	2.31%
	$\bar{\theta}_{x_{\max}}$ (10^{-3}rad)	-4.599	-4.598	-4.598	-4.598	0.02%	0.02%	0.02%
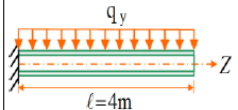	$\bar{v}_{\max}$ (mm)	9.486	9.469	9.282	9.197	0.18%	2.15%	3.05%
	$\bar{\theta}_{x_{\max}}$ (10^{-3}rad)	-3.073	-3.069	-3.070	-3.066	0.13%	0.10%	0.23%

In the present finite element solution, the results obtained using only single beam element based on the exact shape functions related to the transverse response. Figures (4.11a-b) demonstrates the exact shape functions used to capture the transverse static response of the cantilever doubly symmetric I-beam. The static results obtained for two loading cases demonstrated that, although the maximum rotation angle exactly match in all four solutions, the maximum transverse displacement based on the present study is greater than the one based on non-shear deformable beam theory but agrees well with Abaqus beam B31OS and shell S4R model solutions. The difference between the present closed-form solution and Bernoulli-Euler beam theory is due to the transverse shear deformation effects which are captured in the present solution.

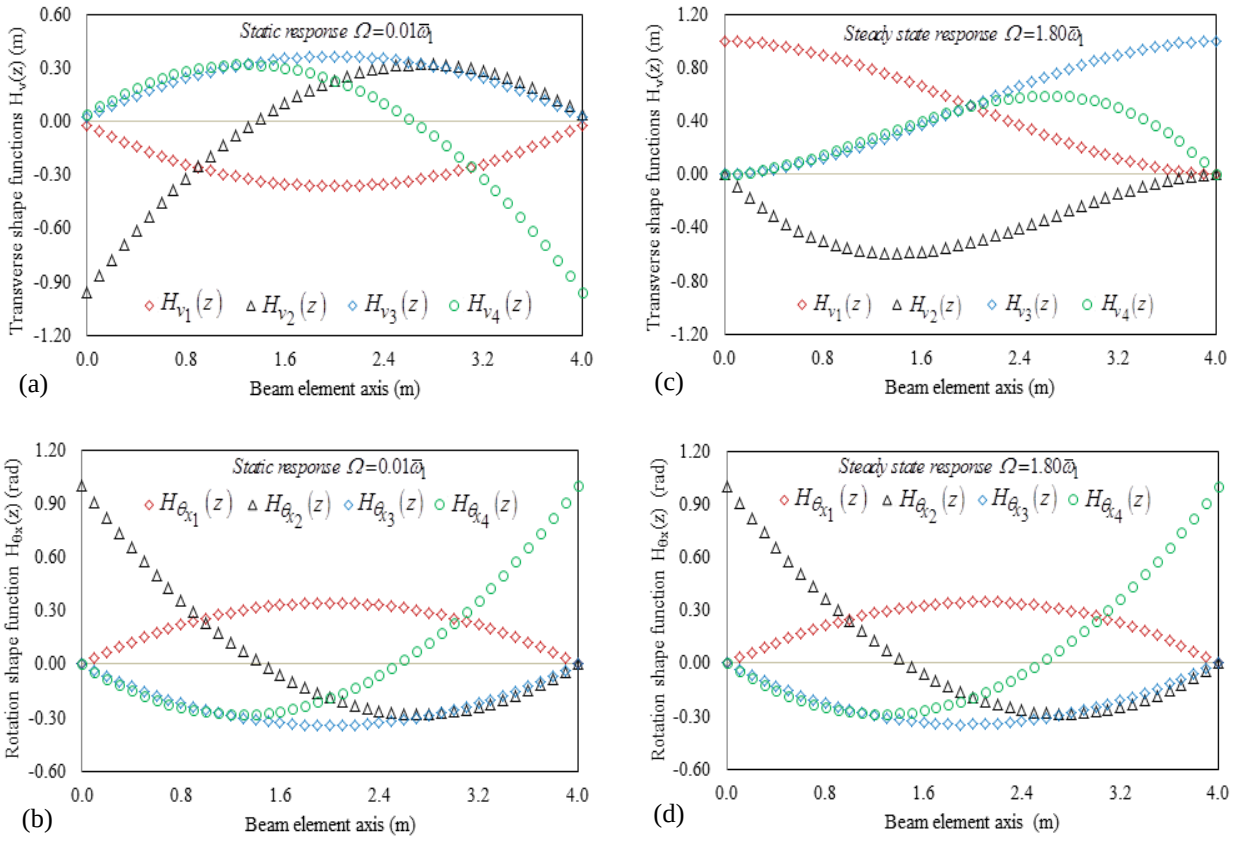

Figure (4.11): Exact shape functions for the static and dynamic transverse responses of cantilever I-beam under end concentrated transverse harmonic force

4.8.1.2 Dynamic Analysis

The amplitudes of steady state responses for transverse displacement $\bar{v}(z)$ and rotation angle $\bar{\theta}_x(z)$ under given end concentrated and distributed harmonic loads with exciting frequency $\Omega = 1.80\bar{\omega}_1 \approx 99.67 rad/\sec$ are shown in Figures (4.12a-d). Results obtained by the present closed-form solution and finite element formulation, using one element based on the exact shape functions illustrated in Figure (4.12c and 4.12d), are in excellent agreement with those based on Abaqus shell S4R and beam B31OS solutions, while, due to shear deformation effects, the displacements and rotations based on the present formulation are higher than those based on Bernoulli-Euler solution.

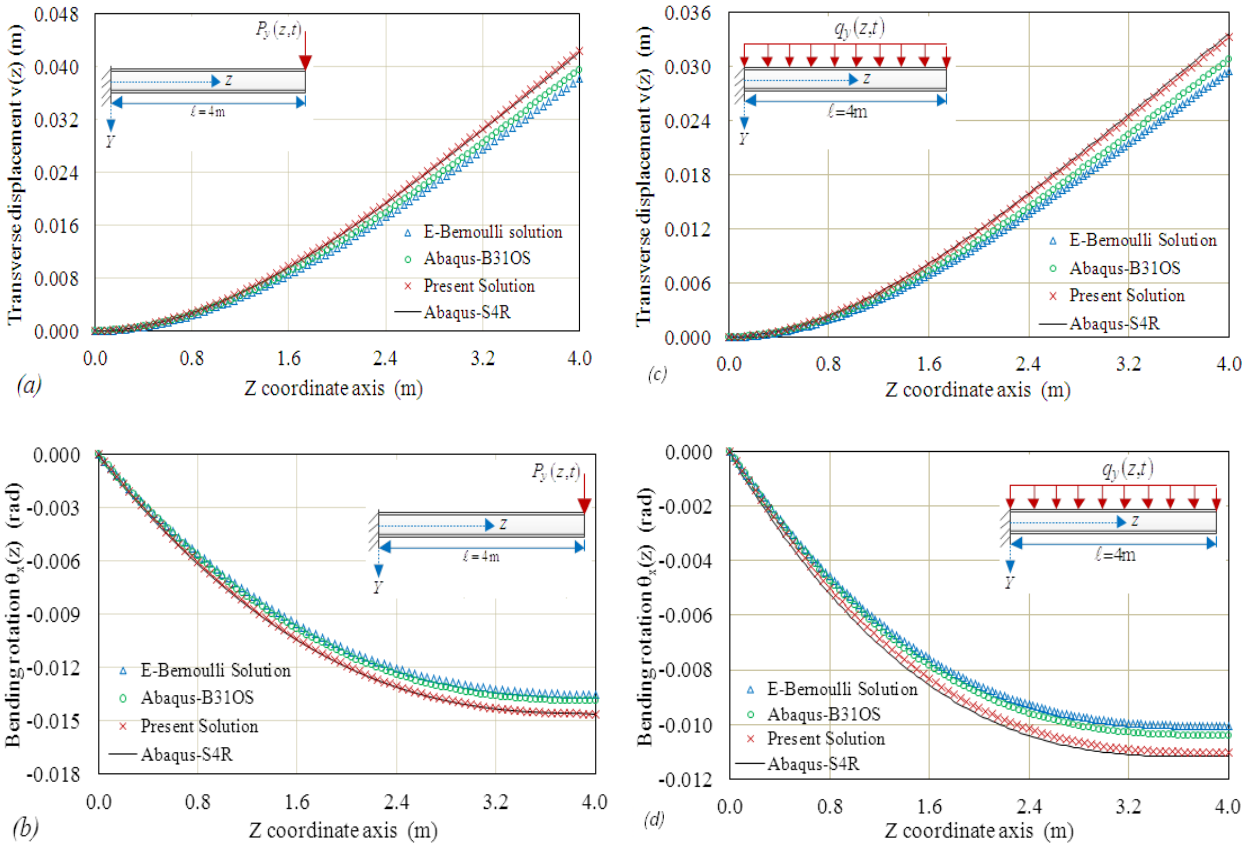

Figure (4.12): Dynamic transverse response of cantilever I-beam under concentrated and distributed transverse harmonic forces.

4.8.2 Example 2 - Torsional analysis

A 1.0m span cantilever with the same cross-section as given in Example 1 is subjected to two harmonic torsional loading cases; (a) concentrated torsion $M_z\left(1.0m,t\right)=1.50e^{i\,\Omega t}\,kNm$ at the free end, and (b) uniformly distributed torsion $m_z\left(z,t\right)=2.0e^{i\,\Omega t}\,kNm/m$ as illustrated in Figure (4.13). In order to validate the computed results, Example 2 is solved for two values of exciting frequencies $\Omega=0.01\bar{\omega}_{t1}$ and $\Omega=0.80\,\bar{\omega}_{t1}$. Results are compared with Vlasov beam theory and Abaqus beam B31OS and shell S4R solutions. The first torsional natural frequency of the cantilever I-beam of 1.0m span is $\bar{\omega}_{t1}=135.4Hz$.

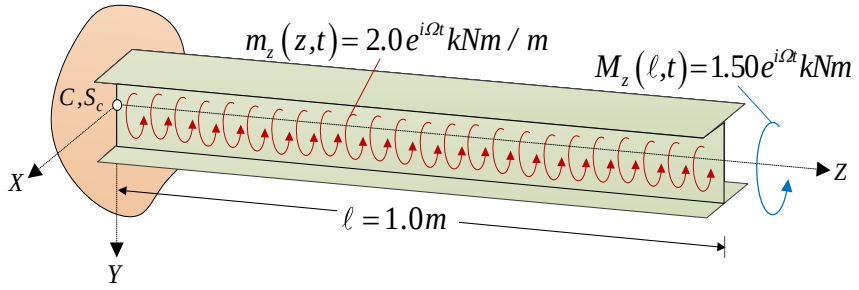

Figure (4.13): Cantilever I-beam under concentrated and distributed harmonic torsion

4.8.2.1 Static torsional response

Figures (4.14a-b) and (4.15c-d) are plotted for static torsional analysis of the cantilever beam under effects of the end concentrated torsion $M_z(1.0m,t)=1.50e^{i\Omega t}kNm$ and uniformly distributed torsion $m_z(z,t)=2.0e^{i\Omega t}kNm/m$, respectively, where the exciting frequency

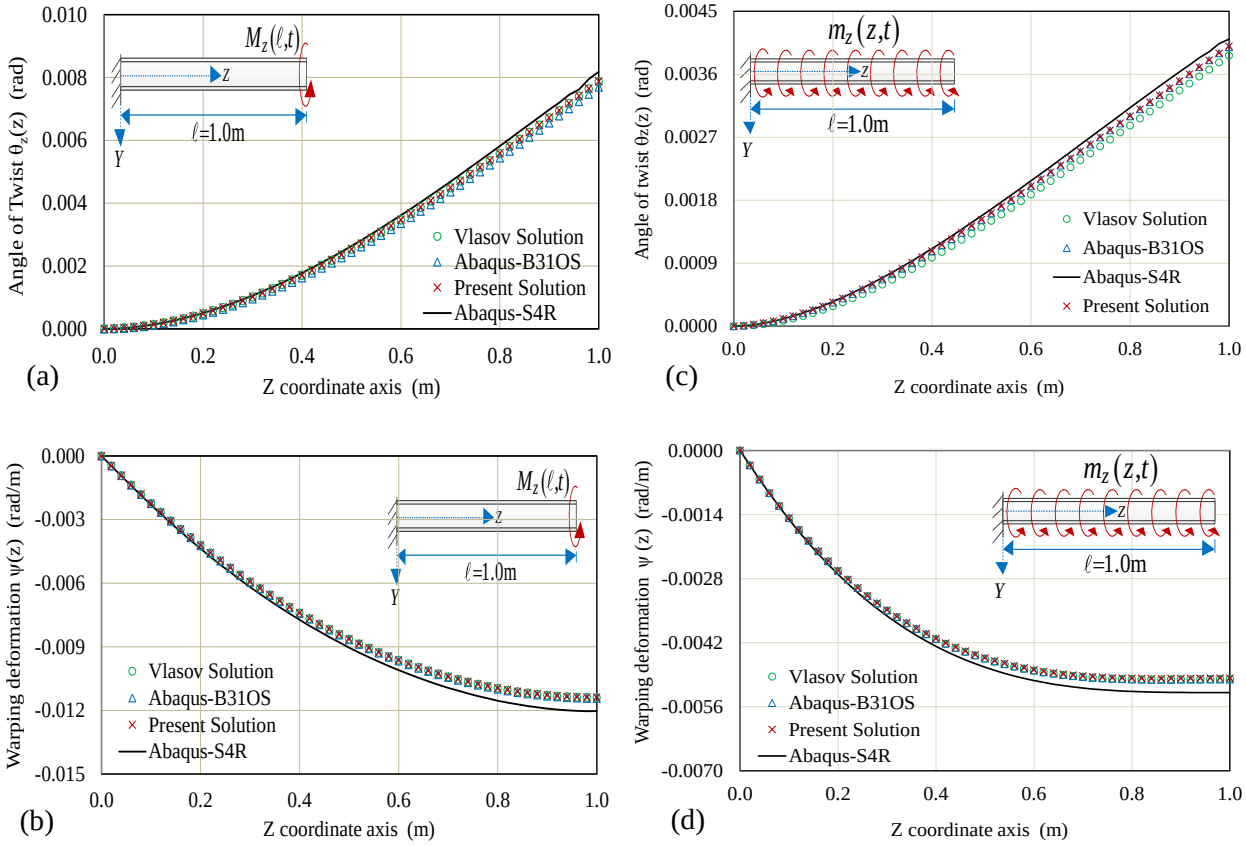

Figure (4.14): Torsional static analysis of cantilever I-beam under concentrated and distributed harmonic twisting moments.

ratio is $\Omega/\bar{\omega}_{t1} = 0.001$. It is noted that, the twist angle $\bar{\theta}_z(z)$ and warping deformation $\bar{\psi}(z)$ results based on the present solutions (closed-form solution and finite element formulation using one element with four degrees of freedom) are in excellent agreement with those based on Vlasov beam theory and Abaqus beam model but slightly deviates from those based on the Abaqus shell solution. The difference between them is due to the distortional effects which are captured in the Abaqus shell model solution but not in the present solution.

For comparison, the static response of the cantilever doubly symmetric I-beam under torsional loading is depicted in Figure (4.15). Figure (4.15a) shows the deformed configuration based on the Abaqus shell S4R model which captures distortional effect while Figure (4.15b) illustrates the deformed configuration based on the present solution which does not capture distortional effects.

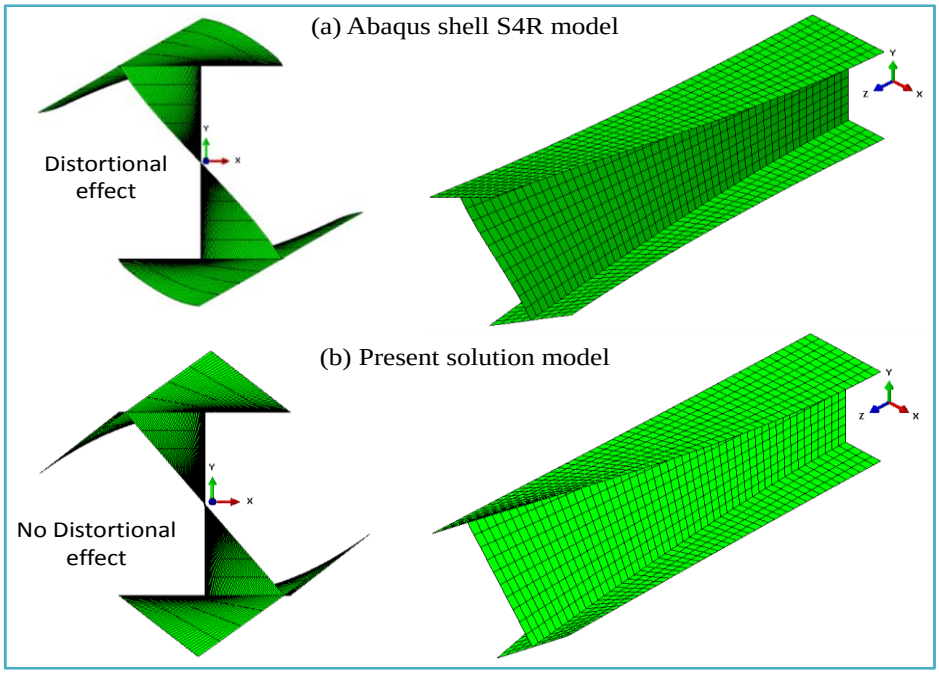

Figure (4.15): Distortional effect of the torsional response of the cantilever I-beam

4.8.2.2 Dynamic torsional steady state response

The steady state amplitudes $\bar{\theta}_z(z)$ and $\bar{\psi}(z)$ of the torsional vibration, as given by Equation (4.53), of a cantilever I-beam under end concentrated torsion $M_z(\ell,t) = 1.50e^{i\Omega t}kNm$ and

distributed twisting moment $m_z(z,t) = 2.0e^{i\Omega t} kNm/m$, in which the exciting frequency is taken as $\Omega = 0.80\bar{\omega}_1 \approx 108.3 rad/\sec$ are calculated. The distributions of angle of twist $\bar{\theta}_z(z)$ and warping deformation $\bar{\psi}(z)$ along the beam span are plotted in Figures (4.16a, 4.16b) and (4.16c, 4.16d) for concentrated and distributed harmonic torsion, respectively. It is observed that, the angle of twist and warping deformation based on the current study are smaller than that based on Abaqus shell model solution but agrees well with the Vlasov beam solution and Abaqus beam model. The difference between the present and Abaqus solutions is likely introduced by distortional effects of the cross-section as in case of static response. It is noted that the Vlasov solution neglects shear deformation effects and this provides a less flexible solution than the present formulation study which includes shear deformation effects.

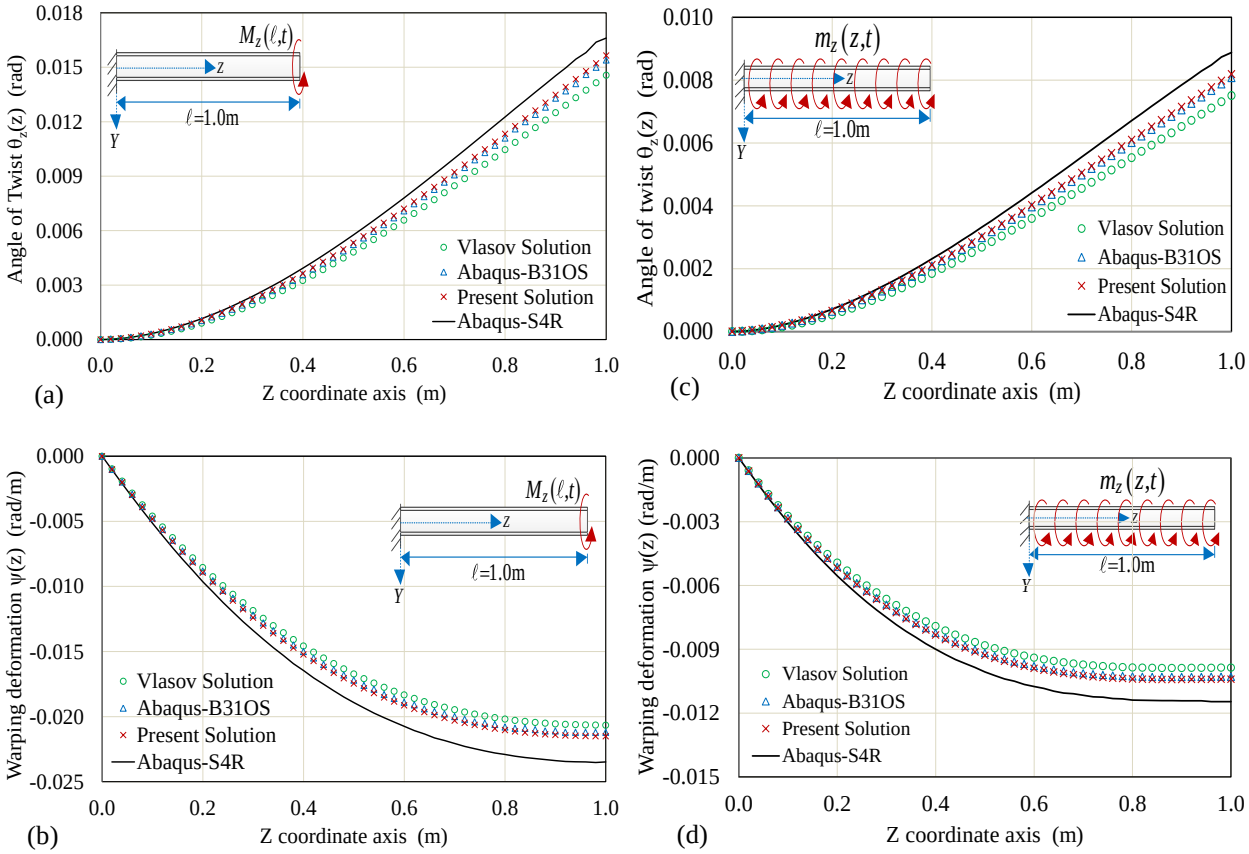

Figure (4.16): Torsional steady state response of cantilever I-beam under concentrated and distributed harmonic twisting moments.

4.8.2.3 Extraction of natural frequencies and modes

The steady state dynamic responses for the transverse and torsional vibrations of 4m cantilever I-beam with the same cross-section properties as given in example 1 are shown in Figure (4.17) for different values of ratio of the applied load frequency to the first natural frequency $\left(\Omega_i / \bar{\omega}_1\right)$, i.e., varied from 0.0 to 35.0Hz, where the first exciting frequency is 8.812Hz. Under concentrated transverse harmonic load $P_y\left(\ell,t\right)=10.0e^{i\Omega t}kN$ acting at the cantilever tip, the natural frequencies related to in-plane transverse vibration, transverse displacement $\bar{v}\left(z\right)$ and bending rotation angle $\bar{\theta}_x\left(z\right)$, are provided in Figures (4.17a-b). Figures (4.17e-f) represent the steady state transverse response of a cantilever I-beam subjected to given transverse harmonic load for four values of exciting frequencies, $\Omega_1=0.6\bar{\omega}_1$, $\Omega_2=6.6\bar{\omega}_1$, $\Omega_3=14.6\bar{\omega}_1$ and $\Omega_4=32.6\bar{\omega}_1$, which are indicated on curves by numbers 1,2,3 and 4, respectively. Similar curves for torsional response, angle of twist $\bar{\theta}_z\left(z\right)$ and warping deformation function $\bar{\psi}\left(z\right)$, of the cantilever I-beam under end harmonic twisting moment $M_z\left(\ell,t\right)=1.50e^{i\Omega t}kNm$ are plotted in Figures (4.17c), (4.17d), (4.17g) and (4.17h) for frequencies $\Omega_1=0.6\bar{\omega}_1$, $\Omega_2=4.6\bar{\omega}_1$, $\Omega_3=8.6\bar{\omega}_1$ and $\Omega_4=20.6\bar{\omega}_1$, respectively. The variations of angle of twist and warping deformation against the exciting frequencies are depicted in Figures (4.17g-e), respectively.

Figures (4.17a-b) and (4.17c-d) show the frequency-response curves obtained by analyzing the cantilever I-beam subjected to concentrated transverse and torsional harmonic loads, respectively. The steady state inplane transverse and torsional response curves are similar, both having three peaks, but the relative heights and locations of the peaks are different. Each peak is being at the natural frequency of a vibrational mode of the member. In other words, the three peaks in Figures (4.17a-b) are labeled as the first three natural frequencies for transverse vibration while Figures (4.17c-d) present the first three torsional natural frequencies at the peaks of the response curves. Table (4.2) presents the first three transverse and torsional natural frequencies values extracted from the steady state response of the cantilever I-beam subjected to given harmonic forces. In addition, a comparison of the natural frequency predictions obtained by the present solution, and those obtained based on

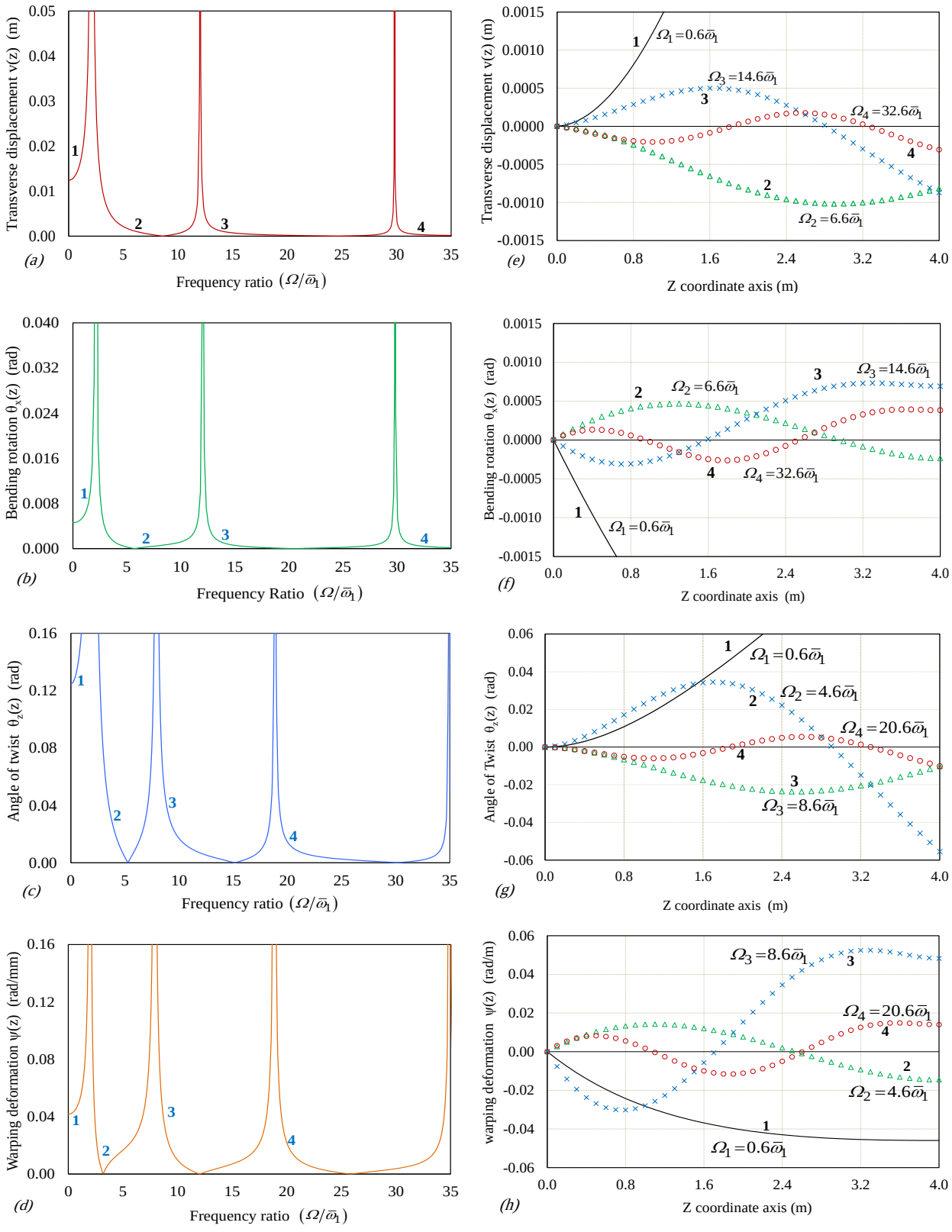

Figure (4.17): Natural frequencies, transverse and torsional responses for cantilever I-beam

Vlasov beam theory and Abaqus beam and shell models is presented in Table (4.2). It is noded that, close agreement is obtained between all four solutions especially at the lower natural frequencies. Moreover, the transverse and torsional frequencies predicted by the present solution provide the closest agreement with the Abaqus shell model solution. Due to the inclusion of shear deformation and distortional effects, Abaqus shell S4R model solution provides the most flexible solution. In contrast, the Euler - Bernoulli beam and Vlasov beam theories, in which the shear deformation and distortional effects are ignored, predict the highest transverse and torsional frequencies, respectively, and then both theories provide the stiffest representation of the cantilever beam. Moreover, the frequencies obtained by Abaqus beam B31OS element, in which the shear deformation due to bending is only captured, predicts the frequency results greater than the results based on the present solution but less than the Euler-Bernoulli and Vlasov beam solutions. It is seen that the effects of shear deformation on the transverse and torsional natural frequencies are significant, particularly at the higher transverse natural frequencies. The percentage differences due to omission of shear deformation effects are shown in columns seven and eight in Table (4.2).

Table (4.2): Transverse and torsional Natural frequencies of cantilever I-beam

No	Abaqus S4R [1]	Present solution [2]	Abaqus B31OS [3]	Vlasov Solution [4]	Present Difference =[1-2]/1	B31OS Difference =[1-3]/1	Vlasov Difference =[1-4]/1	Mode Type
1	18.85	18.86	19.10	19.22	-0.05%	-1.33%	-1.96%	Transverse mode 1
2	106.4	107.1	115.6	119.8	-0.66%	-8.65%	-12.59%	Transverse mode 2
3	259.8	265.6	295.6	331.6	-2.23%	-13.78%	-27.64%	Transverse mode 3
1	16.92	17.23	17.24	17.27	-1.83%	-1.89%	-2.07%	Torsional mode 1
2	67.73	69.04	69.24	69.64	-1.93%	-2.23%	-2.82%	Torsional mode 2
3	162.7	165.2	166.4	168.7	-1.54%	-2.27%	-3.69%	Torsional mode 3

Figures (4.18a) through (4.18d) show the first three transverse and torsional vibration eigenmodes of doubly symmetric cantilever I-beam obtained by the present solution.

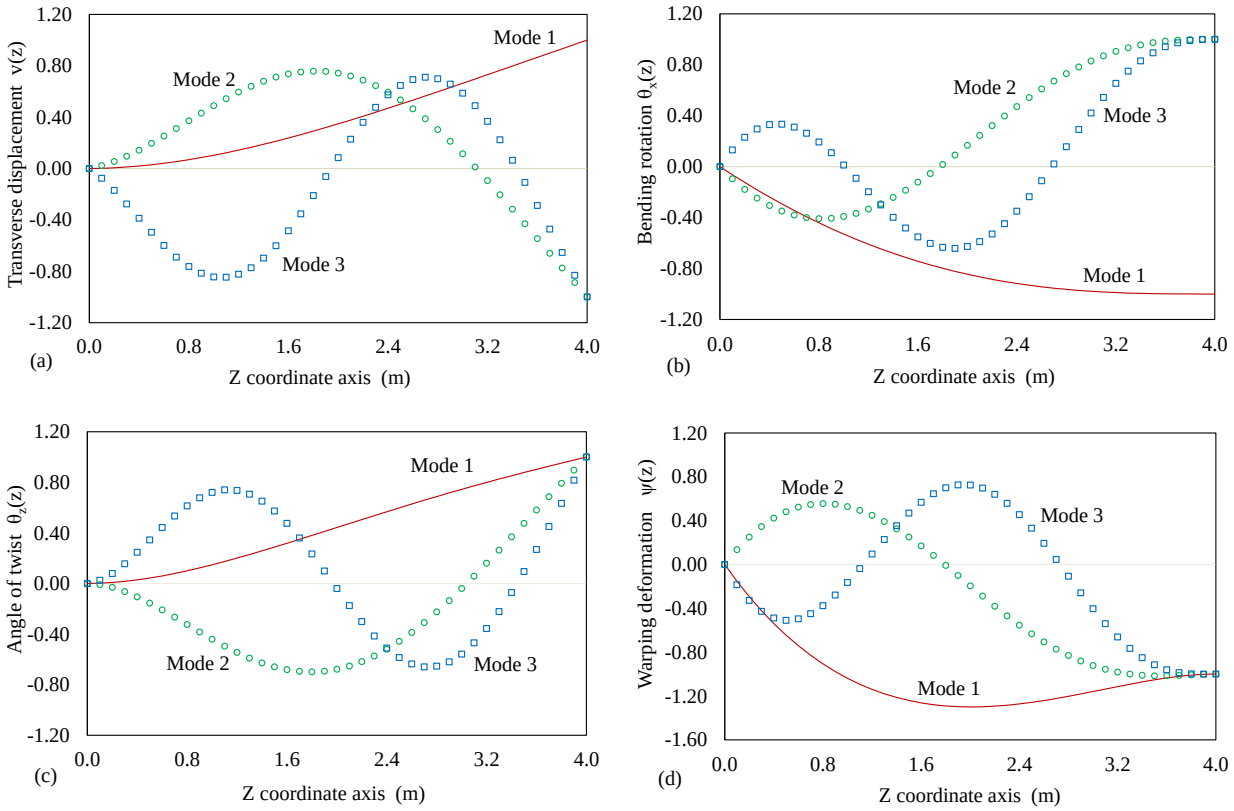

Figure (4.18): The first three transverse and torsional mode shapes for cantilever I-beam

4.8.3 Example 3 – Effect of shear deformation

A doubly symmetric cantilever I-beam of short span ($\ell = 1.0m$) with the same cross-section as given in Example (1) subjected to concentrated transverse harmonic force $P_y(\ell,t) = 80.0e^{i\Omega t}\,kN$ is analyzed to study the influence of shear deformation as illustrated in Figure (4.19).

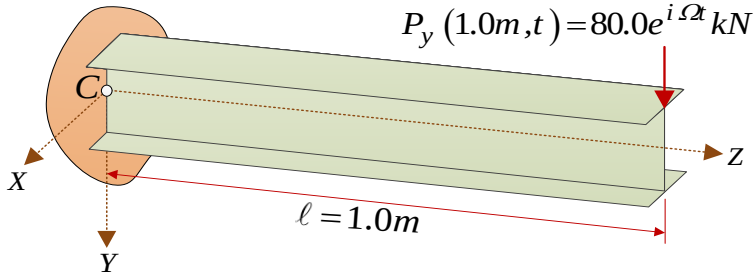

Figure (4.19): Cantilever I-beam subjected to end transverse harmonic force

An exciting frequency Ω=1.20$\bar{\omega}_1$ of the harmonic force is given for the steady state dynamic analysis, where the first natural frequency of the beam is $\bar{\omega}_1$=135.4Hz. The response curves of the transverse displacement $\bar{v}(z)$ and related bending rotation $\bar{\theta}_x(z)$ are plotted against the beam axis z as shown in Figures (4.20a) and (4.20b), respectively. It is observed that the maximum transverse displacement and bending rotation obtained from the present formulation are 42.16% and 19.39% greater than those based on the Euler-Bernoulli beam theory. The differences are due to the effect of shear deformation, which is captured in the present closed-form and finite element solutions, in which the finite element formulation is based on nine beam elements with eighteen degrees of freedom, but it is not captured in Euler-Bernoulli beam theory.

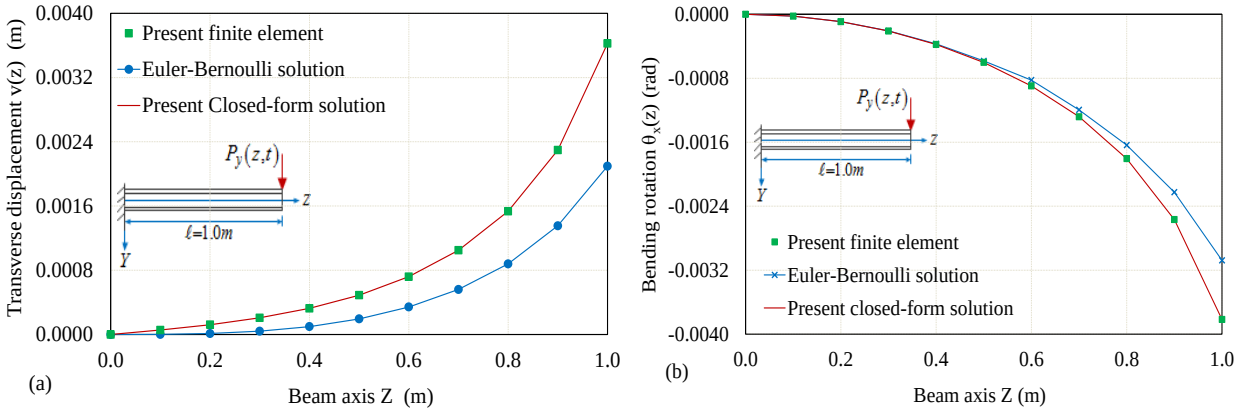

Figure (4.20): Transverse displacement and rotation angle for short cantilever I-beam

4.8.4 Example 4 -Three-span continuous beam - Finite Element Solution

In this example, a three-span continuous beam with doubly symmetric section subjected to transverse harmonic forces $P_{y_1}(2m,t)$=10.0$e^{i\Omega t}$ kN and $P_{y_2}(10m,t)$=10.0$e^{i\Omega t}$ kN is considered as shown in Figure (4.21). The geometric and material properties of the doubly symmetric I-section are identical to Example 1.

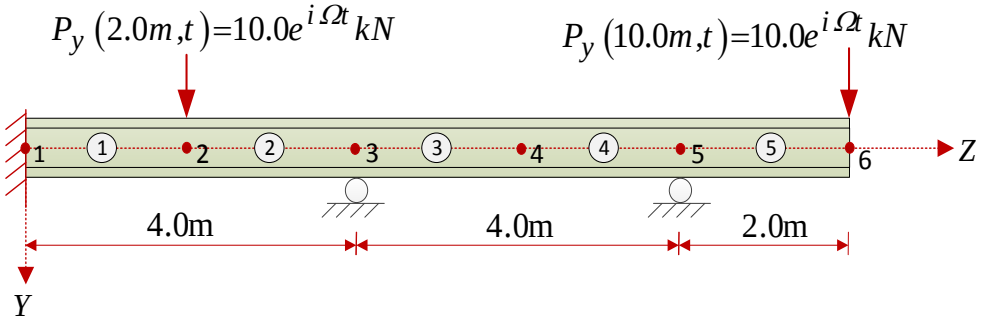

Figure (4.21): Continuous Beam under concentrated transverse harmonic loads

Given that the previous three examples have shown that Abaqus S4R solution and Abaqus B31OS solution and present solution provide results in excellent agreement for large spans, comparisons of the present solution in this example are limited to Abaqus S4R shell solution. The vertical displacement $\bar{v}\left(z\right)$ and associated rotation angle $\bar{\theta}_x\left(z\right)$ are plotted in Figures (4.22a) and (4.22b), in which the static response is captured by using a very low exciting frequency compared to the first natural frequency, i.e., $\Omega=0.01\bar{\omega}_1$, and the steady state dynamic response is given for exciting frequency $\Omega=1.825\bar{\omega}_1\approx 200.0\,rad/\sec$, where the first natural frequency for the beam is $\bar{\omega}_1=109.6\,rad/\sec$. It is noted that the current finite element formulation (FES) results based on five elements with ten degrees of freedom are very close to those obtained by using Abaqus shell model using 4,000 shell S4R elements, i.e., six elements per upper and bottom flanges, eight elements along web height and 200 elements along 10m beam.

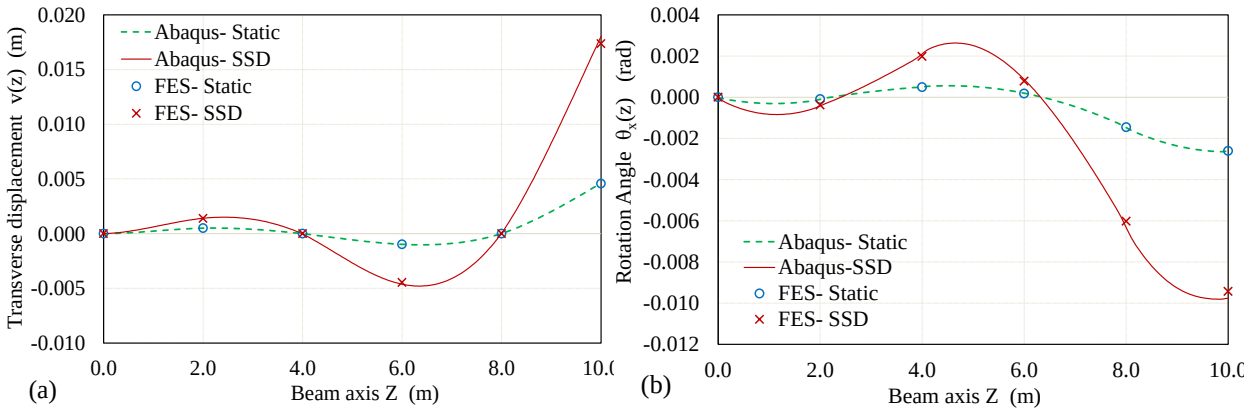

Figure (4.22): Transverse displacement and rotation angle for three-Span I-beam

4.9 Summary and conclusions

The governing differential dynamic equations based on a generalized Vlasov-Timoshenko beam theory derived in Chapter 3 were specialized for the case of doubly symmetric cross-sections in this chapter. The system of equations shows that the longitudinal, transverse, lateral and torsional motions are uncoupled. Closed-form and finite element solutions for the longitudinal, transverse, lateral and torsional steady state dynamic responses were developed. The finite element derived is based on shape functions which exactly satisfy the homogeneous form of the field equations. The finite element formulation developed does not involve time discretization and thus eliminates the need to extract eigenmodes as in other methods based on mode superposition. Closed-form solutions for transverse and torsional were derived for clamped end and simply supported conditions. Numerical results were presented and compared with the analytical solutions and Abaqus shell and beam element solutions. The comparison demonstrates that the present closed-form solutions are in close agreement with other established solutions, and the new finite element gives excellent agreement with Abaqus beam and shell models while keeping the number of DOFs to a minimum. In addition, the new finite element efficiently and accurately predicts results at a fraction of the computational and modeling costs. The modelling effort involved in the present solution is also significantly smaller than that needed in Abaqus shell solution.

4.10 References

[4.1] Bercin A. N., Tanaka M. (1997), Coupled flexural-torsional vibrations of Timoshenko beams, Journal of Sound and vibration, 207(1), p 47-59.

[4.2] Chen, X. and Tamma, K. (1994), Dynamic Response of Elastic Thin-walled Structures Influenced by Coupling Effects, Computers and Structures, 51(1): 91-105.

[4.3] Cortinez, V. H. and Piovan, M. T. (2002), Vibration and buckling of composite thin-walled beams with shear deformability, Journal of Sound and Vibration, 258(4-5), p 701–723.

[4.4] Friberg, P.O. (1983), Coupled vibration of beams - An exact dynamic element stiffness matrix. International Journal for Numerical Methods in Engineering, 19, p 479-493.

[4.5] Hjaji, M. A. and Mohareb, M. (2011), Steady State Response of Doubly symmetric Thin-Walled Members under Harmonic Loads - Closed-Form Solution, Second International Engineering Mechanics and Materials Specialty Conference, Ottawa, Canada, EM-115.

[4.6] Hjaji, M. A. and Mohareb, M. (2011), Steady State Response of Doubly symmetric Thin-Walled Members-Under Harmonic Loads-Closed-Form Solution, Second International Engineering Mechanics and Materials Specialty Conference, Ottawa, Canada, EM-115.

[4.7] Hu, Y. et al. (1996), A Finite Element Model for Static and Dynamic Analysis of Thin-walled Beams with Asymmetric Cross-Sections, Computers and Structures, 61: 897-908.

[4.8] Humar, J. (2005), Dynamics of Structures, second edition, Taylor and Francis, London, U.K.

[4.9] Librescu, L. and Song, O. 2006, Thin-walled Composite Beams-Theory and Application, Springer, Netherlands.

[4.10] Kim, N. et al. (2007), Stiffness matrices for flexural–torsional/lateral buckling and vibration analysis of thin-walled beam, Journal of Sound and Vibration, 299, p 739-756.

[4.11] Leung, A. Y. T. (1991), Natural shape functions of a compresses Vlasov element, Thin-walled Structures, 11, p 431-438.

[4.12] Leung, A.Y.T. (1992), Dynamic stiffness analysis of thin-walled structures, Thin-walled Structures, 14, p 209-222.

[4.13] Li, J, Shen, R., Hua, H., Jin, X. (2004a), Coupled bending and torsional vibration of axially loaded Bernoulli-Euler beams including warping effects, Applied Acoustics, 65, p 153-170.

[4.14] Li, J, Hua, H, Shen, R, Jin, X. (2004b), Dynamic response of axially loaded mono-symmetrical thin-walled Bernoulli-Euler beams, Thin-walled Structures, 42, p 1689-1707.

[4.15] Mei, C. (1970), Coupled Vibrations of Thin-walled Beams of Open Section Using the Finite Element Method, International journal of mechanical science, 12: 883-891.

[4.16] Mohareb, M., and Dabbas, A. (2003), Lateral Stability of Partially Restrained Cantilever Supports, Proceedings of the Annual Technical Session and Meeting, Baltimore, MD, Structural Stability Research Council, April, 671-694.

[4.17] Prokic, A. (2006), On fivefold coupled vibrations of Timoshenko thin-walled beams, Engineering Structures, 28, p 54-62.

[4.18] Vlasov, V. Z. (1961), Thin-walled elastic beams, 2nd edition, Israel Program for Scientific Translation, Jerusalem.

[4.19] Voros, G. (2008), On Coupled Vibrations of Beams with Lateral Loads, Journal of computational and Applied Mechanics, 9 (2): 1-14.

[4.20] Vo, T.P. and Lee, J. (2009), On Six-Fold Coupled Buckling of Thin-walled Composite Beams, Composite Structures, 90: 295-303.

[4.21] Zinoviev, I. and Mohareb, M. (2004), Analysis and design of laterally unsupported frames for out-of-plane stability", Canadian Journal of Civil Engineering, 31(3): 440-452.

Appendix (4A): Reducing Unknown Integration Constants for Transverse Response of Doubly Symmetric Thin-walled Members

The homogeneous solutions for transverse response, transverse displacement $\bar{v}_h(z)$ and bending rotation $\bar{\theta}_{x_h}(z)$ given by equations (4.24) and (4.25) have eight unknown integration constants $A_{2,i}$ and $A_{3,i}$ for $i=1,2,3,4$, but only four boundary conditions related to $\bar{v}_h(z)$ and $\bar{\theta}_{x_h}(z)$ which are provided in equations (4.10) and (4.11). It is thus necessary to reduce the integration constants to only eight independent integration constants which can be obtained from the eight boundary conditions. In this appendix, the two sets of integration constants $A_{2,i}$ and $A_{3,i}$ can be related to reduce to the number of constants to four. These integration constants can then be determined from the four boundary conditions.

Substituting the transverse displacement and bending rotation $\bar{v}_h(z)$ and $\bar{\theta}_{x_h}(z)$ in equations (4.24) and (4.25) into equations (4.21) and (4.22), yields

$$\left[\left(\rho A\Omega^2+GA_w m_1^2\right)A_{2,1}+GA_w m_1 A_{3,1}\right]e^{m_1 z}+\left[\left(\rho A\Omega^2+GA_w m_2^2\right)A_{2,2}+GA_w m_2 A_{3,2}\right]e^{m_2 z}$$
$$+\left[\left(\rho A\Omega^2+GA_w m_3^2\right)A_{2,3}+GA_w m_3 A_{3,3}\right]e^{m_3 z}+\left[\left(\rho A\Omega^2+GA_w m_4^2\right)A_{2,4}+GA_w m_4 A_{3,4}\right]e^{m_4 z}=0 \tag{4A.1}$$

Equation (4A.1) must be applicable for any value of variable z leading to

$$\left(\rho A\Omega^2+GA_w m_i^2\right)A_{2,i}+GA_w m_i A_{3,i}=0 \ , \ for\ i=1,2,3,4 \tag{4A.2}$$

The constant set $A_{2,i}$ can be expressed in terms of $A_{3,i}$ as

$$A_{3,i}=\frac{-\left(\rho A\Omega^2+GA_w m_i^2\right)}{GA_w m_i}A_{2,i} \ , \ for\ i=1,2,3,4 \tag{4A.3}$$

Performing a similar substitution into equation (4.28) for $A_{2,i}$, given by equation (4A.3), one obtains

$$A_{3,i}=\frac{GA_w m_i}{\left(\rho I_{xx}\Omega^2-GA_w+EI_{xx}m_i^2\right)}A_{2,i} \quad , \quad for\ \ i=1,\ 2,\ 3,\ 4 \tag{4A.4}$$

The two expressions given in equations (4A.3) and (4A.4) are used as a check for the four roots obtained from equations (4.30). By equating both equations one obtains

$$\left(\rho A\Omega^2 + GA_w m_i^2\right)\left[\rho I_{xx}\Omega^2 - GA_w + EI_{xx} m_i^2\right] + G^2 A_w^2 m_i^2 = 0 \tag{4A.5}$$

Expanding equation (4A.5) one obtains to the fourth-order algebraic equation

$$m_i^4 + \frac{\rho\Omega^2}{E}\left(\frac{EA}{GA_w} + 1\right)m_i^2 + \frac{\rho A\Omega^2}{EI_{xx}}\left(\frac{\rho I_{xx}\Omega^2}{GA_w} - 1\right) = 0 \tag{4A.6}$$

Equation (4A.6) is identical to equation (4.23), and thus will yield the same expressions for the four roots. Therefore, both equations (4A.3) and (4A.4) are valid relationships between $A_{2,i}$ and $A_{3,i}$. The eight integration constants are reduced to four independent integration constants by using

$$A_{3,i} = \bar{A}_i A_{2,i} \ , \quad for \ i = 1,2,3,4 \tag{4A.7}$$

in which $\bar{A}_i = \dfrac{-GA_w m_i}{\left(\rho A\Omega^2 + GA_w m_i^2\right)} = \dfrac{\left(\rho I_{xx}\Omega^2 - GA_w + EI_{xx} m_i^2\right)}{GA_w m_i}$, $for\ i = 1,2,3,4$.

Finally, the homogeneous solutions for the transverse displacement $\bar{v}_h(z)$ and bending rotation and $\bar{\theta}_{x_h}(z)$ given in equations (4.26) and (4.27) are obtained by substituting equation (4A.7) into equations (4.24) and (4.25).

List of Symbols

A	Cross-sectional area
A_f ,A_w	Areas of flanges and web
b	Length of the flange
C	Centroid of the cross-section
C_w	Warping constant
D_{xx} ,D_{yy} D_{xy} ,D_{hx} D_{hy} ,$D_{\omega\omega}$	Section properties defined by Equations (4.2-7)
E	Modulus of elasticity
G	Shear modulus
$h(s)$	Normal distance between the shear centre and the tangent to mid-surface
H	Height of beam cross-section from the flanges mid-surfaces
I_{xx} ,I_{yy}	Moment of inertias of the cross-section about the principal X and Y axes
J	Torsional constant
ℓ	Length of the member
$M_j(z,t)$	Concentrated harmonic moment about j -th direction (for $j=x,y,z$)
$M_w(z,t)$	Concentrated bimoment
$m_j(z,t)$	Distributed harmonic moments about j -th direction (for $j=x,y,z$)
$m_w(z,t)$	Distributed harmonic bimoment
$N_z(z,t)$	Concentrated harmonic end forces along longitudinal axis
n,s,z	Local curvilinear coordinate system
$q_j(z,t)$	Distributed harmonic forces along x,y,z directions (for $j=x,y,z$)
s	Curvilinear coordinate along mid-surface of the section
S_c	Shear centre of the cross-section
t	Time in seconds

t_1, t_2	Time intervals
t_f , t_w	Flange and web thicknesses
T^*	Kinetic energy
u, v	Displacements of the shear centre along the principal X ,Y axes
u_p, v_p, w_p	Displacements of a point p on the mid-surface of the section along X ,Y ,Z axes
U^*	Internal strain energy
$V_j(z,t)$	Shear forces along x ,y axes (for $j = x, y$)
w	Average longitudinal displacement along the Z axis
W^*	Work done by applied forces
x, y, z	Cartesian coordinate system
X ,Y ,Z	Principal coordinate system
$x(s), y(s)$	Coordinate of arbitrary point on mid-surface of the section
x_s, y_s	Coordinates of the shear centre
Z	Longitudinal coordinate
ρ	Density of the material
r_o	Polar radius of gyration
$\theta_x, \theta_y, \theta_z$	Rotation angles around the X ,Y ,Z axes, respectively
$\bar{\alpha}(s)$	Angle between the tangent to the cross-section and the principal X axis
$\psi(z,t)$	Warping deformation function
Ω	Exciting frequency
$\omega(s)$	Warping function of the cross-section

CHAPTER (5)

ANALYSIS OF THIN-WALLED MEMBERS WITH MONOSYMMETRIC CROSS-SECTIONS UNDER HARMONIC FORCES

Analytical Solution and Finite Element Formulation

Chapter (5) - Analysis of Thin-walled Members with Monosymmetric Sections under Harmonic Forces

Abstract

Starting with Hamilton's variational principle, the governing field equations for the steady state response of thin-walled beams under harmonic forces are derived. The formulation captures shear deformation effects due to bending and warping, translational and rotary inertia effects and as well as torsional flexural coupling effects due to the cross section mono-symmetry. The equations of motion consist of four coupled differential equations in the unknown displacement field variables. A general closed form solution is then developed for the coupled system of equations. The solution is subsequently used to develop a family of shape functions which exactly satisfy the homogeneous form of the governing field equations. A super-convergent finite element is then formulated based on the exact shape functions. Key features of the element developed include its ability to (a) isolate the steady state response component of the response to make the solution amenable to fatigue design, (b) capture coupling effects arising as a result of section mono-symmetry, (c) eliminate spatial discretization arising in commonly used finite elements, (d) avoiding shear locking phenomena, and (e) eliminate the need for time discretization. The results based on the present solution are found to be in excellent agreement with those based on finite element solutions at a small fraction of the computational and modelling cost involved.

5.1 Introduction and Scope

Thin-walled structural members are used as stiffeners in aircraft structures, propellant and turbine blades, steel structures, ships, marine structures and vehicle axles. In these applications, they are commonly subjected to harmonic loading. Sources of harmonic loads include aerodynamics forces, hydro-dynamic wave motion and forces arising from unbalance in rotating machinery, propellants and reciprocating machines. In such applications, thin-walled members are prone to fatigue failures. Under harmonic forces, member response has two components; (1) a transient component which is induced at the

beginning of the excitation, and (2) a steady state component which is sustained for a long time. The transient response attenuates quickly due to damping and is thus of no importance for fatigue design. In contrast, the sustained steady state component of the response is of key for fatigue design, and is the prime focus of the present study.

Thus, the present study aims at developing an efficient solution which isolates the steady state response of thin-walled beams when subjected to harmonic forces. For doubly-symmetric cross-sections, the longitudinal, transverse, lateral and torsional vibrations are uncoupled and have resolved recently [e.g., Hjaji and Mohareb (2011a, b)]. In contrast, for mono-symmetric cross-sections (e.g., I-section with unequal flanges, channel section), the flexural response in the direction normal to the axis of symmetry is found to be coupled with the torsional response. The challenges associated with coupling are resolved in the present work while developing an efficient finite element for the analysis of beams of mono-symmetric sections under harmonic forces.

5.2 Literature review

Methods of analysis of thin walled beams under dynamic loads consist of analytical solutions and summarized in Section (5.2.1) and those based on finite element analysis as summarized in Section (5.2.2).

5.2.1 Literature Review on Analytical Solutions

The classical thin-walled beam theory developed by Vlasov (1961) assumes that the beam cross-section does not deform in its own plane, and the transverse shear strains at the middle surface are negligible. The theory has been extensively used in dynamic analysis of thin-walled beams as exemplified by the studies of Friberg(1985), Bishop et al. (1989), Leung (1991), Chen and Tamma (1994), Banerjee et al. (1996), Li et al. (2004a) and Kim et al. (2007). Bishop and Price (1985) studied the free vibration of thin-walled members with channel-shaped sections. More advanced theories capturing shear deformation effects were also developed by several authors. This includes the work of Dokumaci (1987) who studied the coupled flexural–torsional vibration of thin-walled beams whose study captured warping effects. Tanaka and Bercin (1997) studied the coupled flexural-torsional free vibrations of thin-walled open members. Their solution captured rotatory inertia effects. Using the dynamic transfer matrix method, and the mode superposition

technique, Li et al. (2004a) formulated a solution for determining the coupled bending-torsion response of thin-walled beams under external random excitations. Their solution accounts for warping and rotary inertia. In a subsequent study, Li et al. (2004b) extended their formulations to include the influence of uniform axial forces. Laudiero and Savoia (1991) studied the flexural-torsional vibrations of thin-walled beams with open and closed cross-sections. Their study accounted for the effect of bending and non-uniform torsion, secondary warping and shear lag effects. Tanaka and Bercin (1998) extended their former work (Tanaka and Bercin 1997) to asymmetric sections. Kollar (2001) developed a theory of free vibration analysis of thin-walled open section composite beams including closed-form solutions for the coupled flexural-torsional natural frequencies for simply-supported beams. Cortinez and Piovan (2001) developed an analytical solution for the free vibration analysis of composite thin-walled beams of open and closed cross-sections. Kim et al. (2003) formulated the exact dynamic and static stiffness matrices for the free vibration and stability analysis of thin-walled beams. Their theory accounts for shear deformation effects due to bending and warping torsion and captures the coupling effects between both effects. Also, they incorporated the rotary inertia effects and the flexural-torsional coupling effects due to the asymmetry of the cross-sections. In a subsequent study, Kim and Kim (2005) adopted the theory in Kim et al. (2003) to develop the dynamic stiffness matrix element for the flexural-torsional free vibration of asymmetric thin-walled beams. By applying the Hellinger-Reissner variational principle, the governing equations of motion were derived for the coupled vibration response of thin-walled beams with asymmetric cross-sections and the force-deformation relations. Using the principle of virtual work, Prokic (2006) derived the differential equations for the coupled vibrations of a general thin-walled beam theory capturing shear deformation effects due to bending based on multiple degrees of freedom to express the warping deformation. Closed-form solution for the natural frequencies was derived for the case of simply supported beams. Vo and Lee (2009b) developed a solution based on a shear deformable beam theory for the study of flexural-torsional buckling and vibration analysis of open thin-walled composite beams. Based on a modified Vlasov theory which accounts for shear deformation, Ambrosini (2004) presented a general theory for the coupled flexural-torsional vibration of thin-walled beams of open cross-sections. De Borbon and Ambrosini (2010) extended the theory of Ambrosini (2004) to incorporate the effect of the axial forces.

5.2.2 Literature Review on Finite Element Formulations

Most finite elements for the dynamic analysis of thin-walled members are based on two approaches. In the first approach, formulations are based on approximate shape functions such as the work of Tanaka and Bercin (1997), Lee and Kim (2002a, b) and Voros (2008, 2009), etc. In the second approach, shape functions are based on the solution of the homogeneous solution of the static equilibrium equations, such as the work of Mei (1970), Chen and Tamma (1994) and Hu et al. (1996). Finite element formulations which omit shear deformation effects includes the work of Mei (1970), Chen and Tamma (1994), Hu et al. (1996), Tanaka and Bercin (1998), Hashemi and Richard (2000a, b), Lee and Kim (2002a, b), Voros (2008, 2009). Based on exact shape functions, Mei (1970) developed a finite element for the coupled free vibration analysis of thin-walled beams which incorporated warping effects. Chen and Tamma (1994) formulated a finite element to study the dynamic coupled vibrations of thin-walled open members with arbitrary cross-sections including the influence of constant transverse loads. Their formulation was based on assumed linear and cubic displacement shape functions in conjunction with an implicit self-starting unconditionally stable integration scheme. Hu et al. (1996) studied the coupled bending-torsional dynamic behavior of thin-walled beams of asymmetric cross-sections. The shear deformation and bending-torsional coupling effects due to the cross-section non-symmetry were fully incorporated in the solution. Hashemi and Richard (2000a) studied the coupled bending–torsional vibration analysis of thin-walled beams by developing a dynamic finite element. The exact solutions of the governing dynamic equations of equilibrium were obtained and, subsequently, frequency-dependent hyperbolic interpolation functions were adopted to formulate the stiffness and mass matrices of the structure. Later on, Hashemi and Richard (2000b) extended their work to include the effect of axial force. By using linear and cubic Hermitian shape functions, Lee and Kim (2002a, b) investigated the coupled free vibration of thin-walled composite beams with doubly symmetric and channel-shaped cross-sections. The influence of lateral forces on the coupled bending-torsional free vibration of thin-walled open members was studied by Voros (2008, 2009) who formulated a two-noded beam element with fourteen degrees of freedom. Recently, Vo and Lee (2009a, 2010) and Vo et al. (2010, 2011)

studied the coupled flexural-torsional free vibration of thin-walled open composite beams under constant axial forces and end moments by developing a displacement-based one dimensional finite element model. Finite element formulations including shear deformation effects include the work of Kim and Kim (2005) who formulated an isoparametric element to capture the coupled flexural-torsional free vibration of asymmetric thin-walled shear deformable beams. Recently, Vo and Lee (2009c), and Vo et al. (2009) extended their previous studies for the coupled flexural-torsional coupled composite members to incorporate the shear deformation effects in the finite element formulation developed based on a displacement-based one-dimensional shear-deformable finite beam element using linear and cubic Hermite shape functions.

A feature common to the above studies is use of approximate shape functions involving spatial discretization errors, and thus requiring fine meshes to converge to the actual solution. In contrast, the present study avoids discretization errors by formulating shape functions which exactly satisfy the homogeneous form of the dynamic equilibrium equations. Another commonality between the above studies is the fact they focus on extracting the free vibration characteristics including extracting the natural frequencies and mode shapes. In contrast, the present study aims at directly extracting the steady state response without the need to extracting the natural frequencies and mode shapes.

5.3 Field Differential Equations for Mono-symmetric Sections

For a mono-symmetric channel-section shown in Figure (5.1), it is found that, the shear centre coordinate normal to axis of symmetry is zero, i.e.,

$$y_s = 0 \tag{5.1}$$

The section properties D_{xx} ,D_{yy} ,D_{xy} ,D_{hx} ,D_{hy} and $D_{\omega\omega}$ for mono-symmetric cross-sections are determined from the expressions given in Equation (3.16). From Figure (5.1), it can be shown that, $\left[\cos\hat{\alpha}_1(s), \sin\hat{\alpha}_1(s)\right]=(1,0)$, $h_1(s)=C_y$ at the top flange, $\left[\cos\hat{\alpha}_2(s),\sin\hat{\alpha}_2(s)\right]=(-1,0)$, $h_2(s)=-C_y$ at the bottom flange. For the web, $\left[\cos\hat{\alpha}_3(s),\sin\hat{\alpha}_3(s)\right]=(0,1)$ and $h_3(s)=-(C_x+x_s)$. Thus, one has

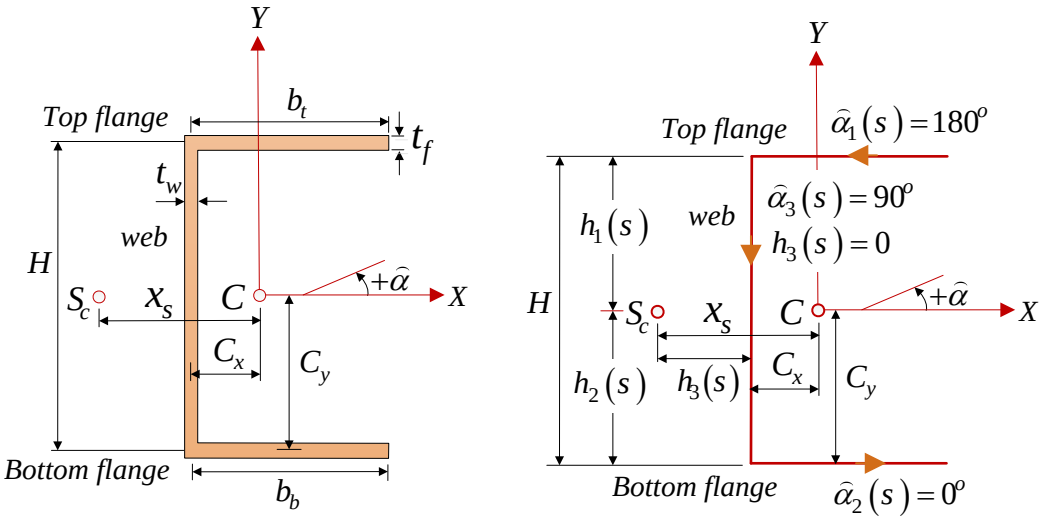

Figure (5.1): Mono-symmetric channel-section

$$D_{xx}=\sum_{i=1}^{3}\int_{A_i}\left(\frac{dx_i(s)}{ds}\right)^2 dA_i=\sum_{i=1}^{3}\int_{A_i}\left[\cos\hat{\alpha}_i(s)\right]^2 dA_i=A_{tf}+A_{bf}=A_f \tag{5.2}$$

$$D_{yy}=\sum_{i=1}^{3}\int_{A_i}\left(\frac{dy_i(s)}{ds}\right)^2 dA_i=\sum_{i=1}^{3}\int_{A_i}\left[\sin\hat{\alpha}_i(s)\right]^2 dA_i=A_w \tag{5.3}$$

$$D_{xy}=D_{yy}=\sum_{i=1}^{3}\int_{A_i}\left(\frac{dx_i(s)}{ds}\right)\left(\frac{dy_i(s)}{ds}\right)dA_i=\sum_{i=1}^{3}\int_{A_i}\cos\hat{\alpha}_i(s)\sin\hat{\alpha}_i(s)\,dA_i=0 \tag{5.4}$$

$$D_{hx}=\sum_{i=1}^{3}\int_{A_i}h_i(s)\left(\frac{dx_i(s)}{ds}\right)dA_i=\sum_{i=1}^{3}\int_{A_i}h_i(s)\cos\hat{\alpha}_i(s)\,dA_i=0 \tag{5.5}$$

$$D_{hy}=\sum_{i=1}^{3}\int_{A_i}h_i(s)\left(\frac{dy_i(s)}{ds}\right)dA_i=\sum_{i=1}^{3}\int_{A_i}h_i(s)\sin\hat{\alpha}_i(s)\,dA_i=-(C_x+x_s)A_w \tag{5.6}$$

$$D_{\omega\omega}=\sum_{i=1}^{3}\int_{A_i}\left[h_i(s)\right]^2 dA_i=C_y^2A_f+(C_x+x_s)^2A_w \tag{5.7}$$

in which the area of the two flanges $A_f=A_{tf}+A_{bf}$ is the sum of the area of the top flange $A_{tf}=b_u t_f$ and that of the bottom flange $A_{bf}=b_\ell t_f$. The area $A_w=Ht_w$ is that of the web. It is found that the properties D_{xy} and D_{hx} for thin-walled members of monosymmetric channel-section, in which X is the axis of symmetry, vanish, i.e.,

$$D_{xy}=D_{hx}=0 \tag{5.8}$$

Similar results for the sectional properties of a mono-symmetric I section are provided in appendix (5B). From Equations (5.1) and (5.8), by substituting into governing field equations (3.82) to (3.88) and into relevant boundary conditions (3.89) to (3.95), then the governing differential equations for monosymmetric thin-walled beams under dynamic loads are considerably simplified as:

$$\rho A\Omega^2\bar{w}(z)+EA\bar{w}''(z)=-\bar{q}_z(z) \tag{5.9}$$

$$-\rho A\Omega^2\bar{u}(z)-GD_{xx}\left[\bar{u}''(z)+\bar{\theta}_y'(z)\right]=\bar{q}_x(z) \tag{5.10}$$

$$-\rho I_{yy}\Omega^2\bar{\theta}_y(z)-EI_{yy}\bar{\theta}_y''(z)+GD_{xx}\left[\bar{u}'(z)+\bar{\theta}_y(z)\right]=\bar{m}_y(z) \tag{5.11}$$

$$-\rho A\Omega^2\left[\bar{v}(z)-x_s\bar{\theta}_z(z)\right]-G\left(D_{yy}\left[\bar{v}''(z)-\bar{\theta}_x'(z)\right]+D_{hy}\left[\bar{\theta}_z''(z)+\bar{\psi}'(z)\right]\right)=\bar{q}_y(z) \tag{5.12}$$

$$-\rho I_{xx}\Omega^2\bar{\theta}_x(z)-EI_{xx}\bar{\theta}_x''(z)-G\left(D_{yy}\left[\bar{v}'(z)-\bar{\theta}_x(z)\right]+D_{hy}\left[\bar{\theta}_z'(z)+\bar{\psi}(z)\right]\right)=\bar{m}_x(z) \tag{5.13}$$

$$\begin{aligned}-\rho A\Omega^2\left[-x_s\bar{v}(z)+r_o^2\bar{\theta}_z(z)\right]-G\Big[&D_{hy}\left(\bar{v}''(z)-\bar{\theta}_x'(z)\right)\\&+\left(D_{\omega\omega}+J\right)\bar{\theta}_z''(z)+D_{\omega\omega}\bar{\psi}'(z)\Big]=\bar{m}_z(z)\end{aligned} \tag{5.14}$$

$$-\rho C_w\Omega^2\bar{\psi}(z)-EC_w\bar{\psi}''(z)+G\left(D_{hy}\left[\bar{v}'(z)-\bar{\theta}_x(z)\right]+D_{\omega\omega}\left[\bar{\theta}_z'(z)+\bar{\psi}(z)\right]\right)=\bar{m}_w(z) \tag{5.15}$$

The related boundary conditions are

$$\left[EA\bar{w}'(z)-\bar{N}_z(z)\right]\delta\bar{w}(z)\Big|_0^\ell=0 \tag{5.16}$$

$$\left(GD_{xx}\left[\bar{u}'(z)+\bar{\theta}_y(z)\right]-\bar{V}_x(z)\right)\delta\bar{u}(z)\Big|_0^\ell=0 \tag{5.17}$$

$$\left[EI_{yy}\bar{\theta}_y'(z)+\bar{M}_y(z)\right]\delta\bar{\theta}_y(z)\Big|_0^\ell=0 \tag{5.18}$$

$$\left(GD_{yy}\left[\bar{v}'(z)-\bar{\theta}_x(z)\right]+GD_{hy}\left[\bar{\theta}_z'(z)+\bar{\psi}(z)\right]-\bar{V}_y(z)\right)\delta\bar{v}(z)\Big|_0^\ell=0 \tag{5.19}$$

$$\left[EI_{xx}\bar{\theta}_x'(z)-\bar{M}_x(z)\right]\delta\bar{\theta}_x(z)\Big|_0^\ell=0 \tag{5.20}$$

$$\left(GD_{hy}\left[\bar{v}'(z)-\bar{\theta}_x(z)\right]+GD_{\omega\omega}\left[\bar{\theta}_z'(z)+\bar{\psi}(z)\right]+GJ\bar{\theta}_z'(z)-\bar{M}_z(z)\right)\delta\bar{\theta}_z(z)\Big|_0^\ell=0 \tag{5.21}$$

$$\left[EC_w\bar{\psi}'(z)+\bar{M}_w(z)\right]\delta\bar{\psi}(z)\Big|_0^\ell=0 \tag{5.22}$$

The seven linear differential equations (5.5) to (5.15) for space displacement functions $\bar{w}(z),\bar{u}(z),\bar{\theta}_y(z),\bar{v}(z),\bar{\theta}_x(z),\bar{\theta}_z(z)$ and $\bar{\psi}(z)$ are rewritten in matrix form as

$$\begin{bmatrix} \left[\bar{Z}_{11}\right]_{1\times1} & \left[0\right]_{1\times2} & \left[0\right]_{1\times4} \\ \left[0\right]_{2\times1} & \left[\bar{Z}_{22}\right]_{2\times2} & \left[0\right]_{2\times4} \\ \left[0\right]_{4\times1} & \left[0\right]_{4\times2} & \left[\bar{Z}_{33}\right]_{4\times4} \end{bmatrix} \begin{Bmatrix} \left\{\bar{U}_1(z)\right\}_{1\times1} \\ \left\{\bar{U}_2(z)\right\}_{2\times1} \\ \left\{\bar{U}_3(z)\right\}_{4\times1} \end{Bmatrix} = \begin{Bmatrix} \left\{\bar{Q}_1(z)\right\}_{1\times1} \\ \left\{\bar{Q}_2(z)\right\}_{2\times1} \\ \left\{\bar{Q}_3(z)\right\}_{4\times1} \end{Bmatrix} \tag{5.23-25}$$

where

$$\left\langle \left\langle \bar{U}_1(z)\right\rangle^T \left\langle \bar{U}_2(z)\right\rangle^T \left\langle \bar{U}_3(z)\right\rangle^T \right\rangle = \left\langle \bar{w}(z)\ \bar{u}(z)\ \bar{\theta}_y(z)\ \bar{v}(z)\ \bar{\theta}_x(z)\ \bar{\theta}_z(z)\ \bar{\psi}(z)\right\rangle,$$

$$\left\langle \left\langle \overline{Q_1}(z)\right\rangle^T \left\langle \overline{Q_2}(z)\right\rangle^T \left\langle \overline{Q_3}(z)\right\rangle^T \right\rangle = \left\langle \bar{q}_z(z)\ \bar{q}_x(z)\ \bar{m}_y(z)\ \bar{q}_y(z)\ -\bar{m}_x(z)\ \bar{m}_z(z)\ \bar{m}_w(z)\right\rangle,$$

$$\left[\bar{Z}_{11}\right]_{1\times1} = \left[\rho A\Omega^2 - EA\mathcal{D}^2\right],\ \left[\bar{Z}_{22}\right]_{2\times2} = \begin{bmatrix} -\left(\rho A\Omega^2 + GD_{xx}\mathcal{D}^2\right) & -GD_{xx}\mathcal{D} \\ -GD_{xx}\mathcal{D} & \left(EI_{yy}\Omega^2 - GD_{xx} + EI_{yy}\mathcal{D}^2\right) \end{bmatrix},$$

and

$$\left[\bar{Z}_{33}\right]_{4\times4} = \begin{bmatrix} -\rho A\Omega^2 - GD_{yy}\mathcal{D}^2 & -GD_{yy}\mathcal{D} & \rho A\Omega^2 x_s - GD_{hy}\mathcal{D}^2 & -GD_{hy}\mathcal{D} \\ & \rho I_{xx}\Omega^2 - GD_{yy} + EI_{xx}\mathcal{D}^2 & -GD_{hy}\mathcal{D} & -GD_{hy} \\ & Symm & -\rho A\Omega^2 r_o^2 - G\left(J + D_{\omega\omega}\right)\mathcal{D}^2 & -GD_{\omega\omega}\mathcal{D} \\ & & & \rho C_w\Omega^2 - GD_{\omega\omega} + EC_w\mathcal{D}^2 \end{bmatrix} \tag{5.26}$$

Equation (5.23) provides the governing equation for longitudinal deformation of the member, which is uncoupled from the remaining field equations and can be solved independently. Equation (5.24) governs the lateral deflection and associated angle of rotation while Equation (5.25) consists of four coupled equation which govern torsional-flexural response and associated angle of rotation and warping deformations. Equations (5.23) and (5.24) are observed to be identical to those of the case of doubly symmetric section presented in chapter 4 and the reader is referred to chapter 4 for the solution of such systems. The present study focuses on developing the solution for response governed by the four coupled torsional-flexural equations provided in Equation (5.25) $\left[\bar{Z}_{33}\right]\left\{\bar{U}_3(z)\right\} = \left\{\bar{Q}_3(z)\right\}$.

5.4 Closed Form Solution

5.4.1 Homogeneous Solution

The homogeneous solution of the system $\left[\bar{Z}_{33}\right]\left\{\bar{U}_3(z)\right\}=\left\{\bar{Q}_3(z)\right\}$ is obtained by setting the right hand side to zero, i.e., $\left\{\bar{Q}_3(z)\right\}=\{0\}$. The homogeneous solution of the space displacement functions $\left\{\bar{U}_{3H}(z)\right\}$ is then assumed to take the exponential form

$$\left\{\bar{U}_{3H}(z)\right\}=\begin{Bmatrix}\bar{v}_h(z)\\ \bar{\theta}_{xh}(z)\\ \bar{\theta}_{zh}(z)\\ \bar{\psi}_h(z)\end{Bmatrix}=\begin{Bmatrix}b_1\\ b_2\\ b_3\\ b_4\end{Bmatrix}_i e^{m_i z} \tag{5.27}$$

From Equation (5.27), by substituting into $\left[\bar{Z}_{33}\right]_{4\times4}\left\{\bar{U}_{3H}(z)\right\}_{4\times1}=\{0\}_{4\times1}$, one obtains

$$\begin{bmatrix} -\rho A\Omega^2 - GD_{yy}m_i^2 & -GD_{yy}m_i & \rho A\Omega^2 x_s - GD_{hy}m_i^2 & -GD_{hy}m_i \\ & \rho I_{xx}\Omega^2 - GD_{yy} + EI_{xx}m_i^2 & -GD_{hy}m_i & -GD_{hy} \\ & Symm & -\rho A\Omega^2 r_o^2 - G(J+D_{\omega\omega})m_i^2 & -GD_{\omega\omega}m_i \\ & & & \rho C_w\Omega^2 - GD_{\omega\omega} + EC_w m_i^2 \end{bmatrix} \begin{Bmatrix} b_1 \\ b_2 \\ b_3 \\ b_4 \end{Bmatrix}_i = \{0\}_{4\times1} \tag{5.28}$$

in which $\langle b\rangle_i^T=\langle b_1 \quad b_2 \quad b_3 \quad b_4\rangle_i$ is a vector of unknown constants corresponding to root m_i. For a non-trivial solution $\{b\}_i$, the determinant of the bracketed matrix in Equation (5.28) is set to vanish leading to the bi-quartic equation of the form

$$p_4 m_i^8 + p_3 m_i^6 + p_2 m_i^4 + p_1 m_i^2 + p_0 = 0 \tag{5.29}$$

in which p_o through p_4 are constants arising from the expansion of the determinant of the 4x4 matrix in Equation (5.28) and depend upon cross-sectional properties, material constants, and the exciting frequency and are

$$p_4 = E^2 I_{xx} C_w G^2\left[D_{yy}(J+D_{\omega\omega}) - D_{hy}^2\right],$$

$$p_3=\Big[G\left(J+D_{\omega\omega}\right)\Big\{EI_{xx}GD_{yy}\left(\rho C_w\,\Omega^2-GD_{\omega\omega}\right)+EI_{xx}G^2D_{hy}^2\Big\}+EG^3D_{yy}\left(I_{xx}D_{\omega\omega}^2+C_wD_{hy}^2\right)$$
$$+\rho\Omega^2EI_{xx}C_w\left\{EAG\left(r_o^2D_{yy}+2x_sD_{hy}\right)+\left(GD_{yy}+EA\right)\right\}$$
$$-EG^2D_{hy}^2\left\{G\left(D_{\omega\omega}I_{xx}-C_wD_{yy}\right)+2\rho I_{xx}C_w\,\Omega^2\right\}\Big],$$

$$p_2=GD_{yy}\Big[\left(\rho C_w\,\Omega^2-GD_{\omega\omega}\right)\Big\{\rho A\Omega^2r_o^2EI_{xx}+G\left(J+D_{\omega\omega}\right)\left(\rho I_{xx}\,\Omega^2-GD_{yy}\right)$$
$$+G^2\left(D_{yy}J+D_{yy}D_{\omega\omega}\right)-\rho I_{xx}\,\Omega^2\left(D_{hy}/D_{yy}\right)\left(GD_{hy}-2EAx_s\right)\Big\}$$
$$+\left(\rho I_{xx}\,\Omega^2-GD_{yy}\right)\Big\{\rho A\Omega^2r_o^2EC_w+G^2D_{\omega\omega}^2\Big\}+G^3D_{hy}^2\left(D_{\omega\omega}-J\right)\Big]$$
$$+\left(\rho I_{xx}\,\Omega^2-GD_{yy}\right)\Big[G^3D_{hy}^2\left(J-D_{\omega\omega}\right)+2\rho A\Omega^2x_sEC_wGD_{hy}\Big]$$
$$+\rho A\Omega^2\Big[G\left(J+D_{\omega\omega}\right)\Big\{EI_{xx}\left(\rho C_w\,\Omega^2-GD_{\omega\omega}\right)+EC_w\left(\rho I_{xx}\,\Omega^2-GD_{yy}\right)\Big\},$$
$$+EG^2\Big\{I_{xx}D_{\omega\omega}^2+C_wD_{hy}^2\Big\}+\rho A\Omega^2E^2I_{xx}C_w\left(r_o^2-x_s^2\right)$$
$$+EG^2r_o^2\left(I_{xx}D_{hy}^2+C_wD_{yy}^2\right)+2x_sEG^2D_{hy}\left(C_wD_{yy}+I_{xx}D_{\omega\omega}\right)\Big]$$
$$+G^2D_{yy}\Big[G^2D_{yy}D_{\omega\omega}^2+2D_{hy}^2\left(G^2\left\{J-D_{\omega\omega}\right\}-EC_w\right)\Big]$$

$$p_1=\rho A\Omega^2\Big[\Big[\Big[GD_{yy}r_o^2\Big\{\left(\rho I_{xx}\,\Omega^2-GD_{yy}\right)\left(\rho C_w\,\Omega^2-GD_{\omega\omega}\right)-G^2D_{hy}^2\Big\}$$
$$+G^2D_{hy}\Big\{2x_s\left(GD_{yy}D_{\omega\omega}+D_{hy}\right)+2GD_{hy}\left(r_o^2D_{yy}-x_sD_{hy}\right)\Big\}$$
$$+\Big[\left(\rho C_w\,\Omega^2-GD_{\omega\omega}\right)\Big\{\rho A\Omega^2EI_{xx}\left(r_o^2-x_s^2\right)+G\left(J+D_{\omega\omega}\right)\left(\rho I_{xx}\,\Omega^2-GD_{yy}\right)$$
$$+G^2D_{hy}^2\left(r_o^2+1\right)+2x_sG^2D_{yy}D_{hy}\Big\}+\left(\rho I_{xx}\,\Omega^2-GD_{yy}\right)\Big\{\rho A\Omega^2r_o^2EC_w+G^2D_{\omega\omega}^2\Big\}$$
$$+G^3D_{hy}^2\left(D_{\omega\omega}-J\right)+\left(\rho I_{xx}\,\Omega^2-GD_{yy}\right)\Big\{r_o^2G^2D_{hy}^2+\rho\Omega^2C_wx_s\left(2GD_{hy}-EAx_s\right)\Big\}\Big]\Big]\Big]$$

and $p_o=\left(\rho A\Omega^2\right)^2\left(r_o^2-x_s^2\right)\Big[\left(\rho I_{xx}\,\Omega^2-GD_{yy}\right)\left(\rho C_w\,\Omega^2-GD_{\omega\omega}\right)-G^2D_{hy}^2\Big]$ (5.30a-e)

The above characteristic equation has eight distinct roots m_i $(i=1,2,3,.....,8)$. For each root m_i, there corresponds a set of constants $\langle b\rangle_i^T=\langle b_1\ b_2\ b_3\ b_4\rangle_i^T$. By back-substitution into the original system of equations $\left[\bar{Z}_{33}\right]_{4\times4}\left\{\bar{U}_{3H}(z)\right\}_{4\times1}=\{0\}_{4\times1}$, one can relate constants $(b_1,b_2,b_3)_i$ to constant b_{4i} through

$$\begin{Bmatrix}b_1\\b_2\\b_3\end{Bmatrix}_i=\begin{Bmatrix}\bar{G}_1\\\bar{G}_2\\\bar{G}_3\end{Bmatrix}_i b_{4,i} \tag{5.31}$$

in which

$$\bar{G}_{1,i}=\frac{Gm_i}{\beta_w}\Big[G^2D_{hy}m_i^2\left(D_{yy}D_{\omega\omega}-D_{hy}^2\right)-D_{hy}\beta_1\left(\rho I_{xx}\Omega^2+EI_{xx}m_i^2\right)+\left(\rho A\Omega^2x_s-GD_{hy}m_i^2\right)\left(D_{yy}D_{\omega\omega}-EI_{xx}D_{\omega\omega}m_i^2-G\rho I_{xx}D_{\omega\omega}\Omega^2-GD_{hy}^2\right)\Big] \tag{5.32}$$

$$\bar{G}_{2,i}=\frac{G}{\beta_w}\Big[\left(\rho A\Omega^2x_s-GD_{hy}m_i^2\right)\left(D_{hy}+Gm_i^2\left[D_{hy}^2+D_{yy}D_{\omega\omega}\right]\right)+GD_{hy}D_{\omega\omega}m_i^2\left(\rho A\Omega^2+GD_{yy}m_i^2\right)-\rho A\Omega^2D_{hy}\beta_1\Big] \tag{5.33}$$

$$\bar{G}_{3,i}=\frac{Gm_i}{\beta_w}\Big[G^2D_{yy}m_i^2\left(D_{hy}^2-D_{yy}D_{\omega\omega}\right)-\left(\rho A\Omega^2+GD_{yy}m_i^2\right)\left(D_{\omega\omega}\beta_o+GD_{hy}^2\right)-D_{hy}\left(\rho I_{xx}\Omega^2+EI_{xx}m_i^2\right)\left(\rho A\Omega^2x_s-GD_{hy}m_i^2\right)\Big] \tag{5.34}$$

where

$\beta_o=\rho I_{xx}\Omega^2+EI_{xx}m_i^2-GD_{yy}$, $\beta_1=\rho A\Omega^2r_o^2+G\left(J+D_{\omega\omega}\right)m_i^2$, and

$$\beta_w=\left(\rho A\Omega^2x_s-GD_{hy}m_i^2\right)\left(2G^2D_{hy}D_{yy}m_i^2-\beta_o\rho A\Omega^2x_s+G\beta_oD_{hy}m_i^2\right)+\left(\rho A\Omega^2+GD_{yy}m_i^2\right)\left[G^2D_{hy}^2m_i^2+\beta_o\beta_1\right]+\beta_1\left(GD_{yy}m_i\right)^2 .$$

Equation (5.31) reduces the number of unknown constants from 32 to 8 independent constants. From Equation (5.31) by substituting into Equation (5.27), the homogeneous solution is obtained as

$$\left\{\bar{U}_{3H}(z)\right\}_{4\times1}=\left[\bar{G}\right]_{4\times8}\left[\bar{E}(z)\right]_{8\times8}\left\{\bar{B}\right\}_{8\times1}=\left[\chi(z)\right]_{4\times8}\left\{\bar{B}\right\}_{8\times1} \tag{5.35}$$

in which

$$\left[\bar{G}\right]_{4\times8}=\left[\begin{Bmatrix}\bar{G}_{1,1}\\ \bar{G}_{2,1}\\ \bar{G}_{3,1}\\ 1\end{Bmatrix}_{4\times1}\ \begin{Bmatrix}\bar{G}_{1,2}\\ \bar{G}_{2,2}\\ \bar{G}_{3,2}\\ 1\end{Bmatrix}_{4\times1}\ \begin{Bmatrix}\bar{G}_{1,3}\\ \bar{G}_{2,3}\\ \bar{G}_{3,3}\\ 1\end{Bmatrix}_{4\times1}\ \cdots\cdots\ \begin{Bmatrix}\bar{G}_{1,8}\\ \bar{G}_{2,8}\\ \bar{G}_{3,8}\\ 1\end{Bmatrix}_{4\times1}\right]_{4\times8},$$

matrix $\left[\bar{E}(z)\right]_{8\times8}$ is a diagonal matrix consisting of the exponential functions e^{m_iz} (for $i=1,2,3,.....,8$), the vector of constants $\left\langle\bar{B}\right\rangle_{1\times8}^T=\left\langle b_{4,1}\ b_{4,2}\ b_{4,3}\ .....\ b_{4,8}\right\rangle_{1\times8}^T$ is to be determined from the boundary conditions of the problem, and the matrix $\left[\chi(z)\right]_{4\times8}=\left[\bar{G}\right]_{4\times8}\left[\bar{E}(z)\right]_{8\times8}$ relating the homogeneous solution to the integration constants has been introduced.

5.4.2 Special Case: Particular Solution for Uniform Member Loads

For a member under uniform distributed loads, $\left[\bar{q}_y(z),\bar{m}_x(z),\bar{m}_z(z),\bar{m}_w(z)\right]e^{i\Omega t}=\left[\bar{q}_y,\bar{m}_x,\bar{m}_z,\bar{m}_w\right]e^{i\Omega t}$, the corresponding particular solution $\left\{\bar{U}_{3P}(z)\right\}_{4\times1}$ is given as

$$\left\{\bar{U}_{3P}\right\}_{4\times1}=\begin{Bmatrix}\bar{v}_p\\ \bar{\theta}_{xp}\\ \bar{\theta}_{zp}\\ \bar{\psi}_p\end{Bmatrix}_{4\times1}=\begin{Bmatrix}\dfrac{r_o^2\bar{q}_y+x_s\bar{m}_z}{\rho A\Omega^2\left(x_s^2-r_o^2\right)}\\ \dfrac{\left(\rho C_w\Omega^2-GD_{\omega\omega}\right)\bar{m}_x-GD_{hy}\bar{m}_w}{G^2D_{hy}^2-\left(\rho I_{xx}\Omega^2-GD_{yy}\right)\left(\rho C_w\Omega^2-GD_{\omega\omega}\right)}\\ \dfrac{x_s\bar{q}_y+\bar{m}_z}{\rho A\Omega^2\left(x_s^2-r_o^2\right)}\\ \dfrac{GD_{hy}\bar{m}_x-\left(\rho I_{xx}\Omega^2-GD_{yy}\right)\bar{m}_w}{G^2D_{hy}^2-\left(\rho I_{xx}\Omega^2-GD_{yy}\right)\left(\rho C_w\Omega^2-GD_{\omega\omega}\right)}\end{Bmatrix}_{4\times1} \tag{5.36}$$

5.4.3 Total Solution for Uniform Member Loads

The total steady state response is obtained by adding the homogeneous solution in Equation (5.35) to the particular solution in Equation (5.36), yielding

$$\left\{\bar{U}_3(z)\right\}_{4\times1}=\left[\chi(z)\right]_{4\times8}\left\{\bar{B}\right\}_{8\times1}+\left\{\bar{U}_{3P}\right\}_{4\times1} \tag{5.37}$$

Integration constants $\left\{\bar{B}\right\}$ appearing in Equation (5.37) are determined from the boundary conditions leading to the closed-form solutions. Two examples of closed-form solutions are provided in the following sections for a cantilever and simply-supported beams. The above treatment provides a formulized closed-form solution for thin-walled members of monosymmetric cross-sections under harmonic loads. Closed-form solutions for displacement fields are applicable for general harmonic loads and cantilever and simply-supported boundary conditions (closed-form solutions for members with different boundary conditions can be derived). Although the formulations are developed towards determining the steady state response, they are able to capture the static response and natural frequencies. In addition, closed-form solutions can be developed for members of multiple spans.

5.4.4 Example-Cantilever under Member and End Forces

A cantilever beam with monosymmetric section subjected to: (1) distributed harmonic forces: transverse force $\bar{q}_y(z)e^{i\Omega t}$, bending moment $\bar{m}_x(z)e^{i\Omega t}$, twisting moment $\bar{m}_z(z)e^{i\Omega t}$ and bimoment $\bar{m}_w(z)e^{i\Omega t}$, (2) concentrated harmonic forces: transverse force $\bar{P}_y(\ell)e^{i\Omega t}$, bending moment $\bar{M}_x(\ell)e^{i\Omega t}$, twisting moment $\bar{M}_z(\ell)e^{i\Omega t}$ and bimoment $\bar{M}_w(\ell)e^{i\Omega t}$ is considered as illustrated in Figure (5.2).

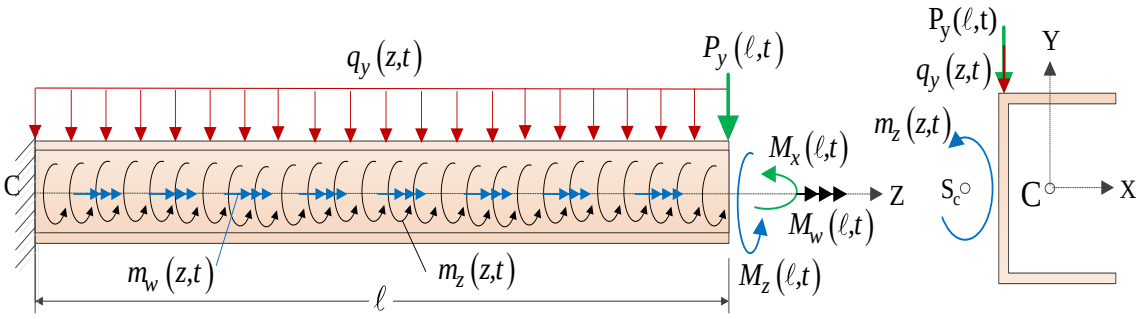

Figure (5.2): Cantilever C-beam under general harmonic forces

It is required to determine the integration constants $\{\bar{B}\}_{8\times1}$ from the associated boundary conditions. At the fixed end $z=0$, the boundary conditions are given as

$$\bar{v}(0)=\bar{\theta}_x(0)=\bar{\theta}_z(0)=\bar{\psi}(0)=0 \tag{5.38-41}$$

and at the free end $z=\ell$

$$GD_{yy}\left[\bar{v}'(\ell)+\bar{\theta}_x(\ell)\right]+GD_{hy}\left[\bar{\theta}_z'(\ell)+\bar{\psi}(\ell)\right]=\bar{V}_y(\ell) \tag{5.42}$$

$$EI_{xx}\,\bar{\theta}_x'(\ell)=\bar{M}_x(\ell) \tag{5.43}$$

$$GD_{hy}\left[\bar{v}'(\ell)+\bar{\theta}_x(\ell)\right]+\left(GD_{\omega\omega}+GJ\right)\bar{\theta}_z'(\ell)+GD_{\omega\omega}\bar{\psi}(\ell)=\bar{M}_z(\ell) \tag{5.44}$$

$$EC_w\,\bar{\psi}'(\ell)=\bar{M}_w(\ell) \tag{5.45}$$

Substituting the expressions for displacement fields presented in Equation (5.37) into above boundary conditions (5.38) to (5.45), one obtains

$$\{B_{4,i}\}_{8\times1}=[\,\Phi_c\,]^{-1}_{8\times8}\{\,\bar{Q}_c\,\}_{8\times1} \tag{5.46}$$

From Equation (5.46) and by substituting into Equation (5.37), the total steady state solution is then obtained as

$$\{\bar{U}_{3C}(z)\}_{4\times1}=[\bar{\chi}(z)]_{4\times8}[\,\Phi_c\,]^{-1}_{8\times8}\{\,\bar{Q}_c\,\}_{8\times1}+\{\bar{U}_{3p}\}_{4\times1} \tag{5.47}$$

where

$$\left[\Phi_c\right]^{\mathrm{T}}_{8\times 8}=\left[\left\{\bar{G}_{1,\mathrm{i}}\right\}_{8\times 1}\ \left\{\bar{G}_{2,\mathrm{i}}\right\}_{8\times 1}\ \left\{\bar{G}_{3,\mathrm{i}}\right\}_{8\times 1}\ \left\{1\right\}_{8\times 1}\ \left\{\bar{E}_{1,\mathrm{i}}\right\}_{8\times 1}\ \left\{\bar{E}_{2,\mathrm{i}}\right\}_{8\times 1}\ \left\{\bar{E}_{3,\mathrm{i}}\right\}_{8\times 1}\ \left\{\bar{E}_{4,\mathrm{i}}\right\}_{8\times 1}\right]^{\mathrm{T}}_{8\times 8},$$

$$\left\langle\bar{Q}_c\right\rangle^{\mathrm{T}}_{1\times 8}=\left\langle -\bar{v}_p\ \middle|\ -\bar{\theta}_{x_p}\ \middle|\ -\bar{\theta}_{z_p}\ \middle|\ -\bar{\psi}_p\ \middle|\ \left[\frac{\bar{P}_y(\ell)}{GD_{yy}}+\bar{\theta}_{x_p}-\left(\frac{D_{hy}}{D_{yy}}\right)\bar{\psi}_p\right]\ \middle|\ \frac{\bar{M}_x(\ell)}{GD_{hy}}\ \middle|\ \left[\frac{\bar{M}_z(\ell)}{GD_{hy}}+\bar{\theta}_{x_p}-\left(\frac{D_{\omega\omega}}{D_{hy}}\right)\bar{\psi}_p\right]\ \middle|\ \frac{\bar{M}_w(\ell)}{EC_w}\right\rangle^{\mathrm{T}}_{1\times 8},$$

$$\bar{E}_{1,\mathrm{i}}=\left[m_i\bar{G}_{1,\mathrm{i}}-\bar{G}_{2,\mathrm{i}}+\frac{D_{hy}}{D_{yy}}\left(m_i\bar{G}_{3,\mathrm{i}}+1\right)\right]e^{m_i\ell},\quad \bar{E}_{2,\mathrm{i}}=m_i\bar{G}_{2,\mathrm{i}}e^{m_i\ell}$$

$$\bar{E}_{3,\mathrm{i}}=\left[m_i\bar{G}_{1,\mathrm{i}}-\bar{G}_{2,\mathrm{i}}+\frac{\left(D_{\omega\omega}+J\right)}{D_{hy}}m_i\bar{G}_{3,\mathrm{i}}+\frac{D_{\omega\omega}}{D_{hy}}\right]e^{m_i\ell}\ \text{and}\ \bar{E}_{4,\mathrm{i}}=m_ie^{m_i\ell},\ (\text{for } i=1,2,3,...,8).$$

5.4.5 Example- Simply-supported under Member and End Forces

A simply supported beam of monosymmetric cross-section under general distributed harmonic forces; transverse force $\bar{q}_y(z)e^{i\Omega t}$, twisting moment $\bar{m}_z(z)e^{i\Omega t}$, bending moment $\bar{m}_x(z)e^{i\Omega t}$, bimoment $\bar{m}_w(z)e^{i\Omega t}$, and concentrated harmonic forces: bending moments $\bar{M}_x(z_e)e^{i\Omega t}$ and bimoments $\bar{M}_w(z_e)e^{i\Omega t}$ at both ends $(z_e=0,\ell)$ as shown in Figure (5.3).

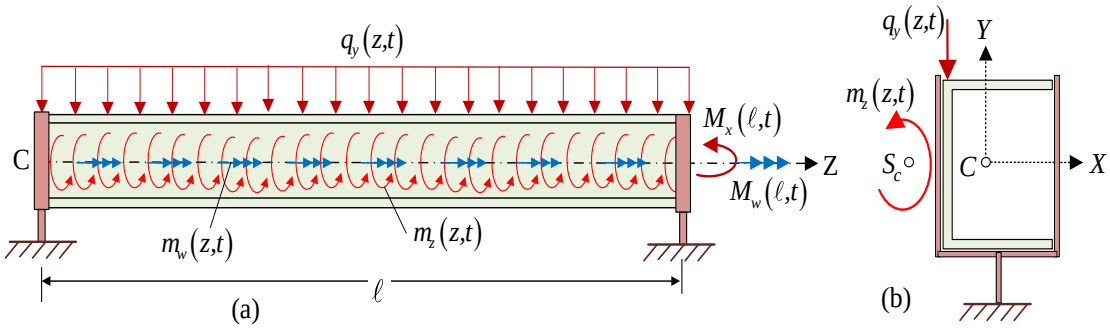

Figure (5.3): Simply-supported C-beam under general harmonic forces (a) elevation, and (b) cross-section at the support

The fork support keeps the end-sections free to warp and to rotate about x and y axes. Imposing the following simply supported boundary conditions at member both ends $z=0$ and $z=\ell$ yields

$$\bar{v}(0)=0\ ,\quad EI_{xx}\bar{\theta}'_x(0)=-\bar{M}_x(0) \qquad (5.48\text{-}49)$$

$$\bar{\theta}_z(0)=0\ , \qquad EC_w\,\bar{\psi}'(0)=\bar{M}_w(0) \tag{5.50-51}$$

$$\bar{v}(\ell)=0\ , \qquad EI_{xx}\,\bar{\theta}_x'(\ell)=\bar{M}_x(\ell) \tag{5.52-53}$$

$$\bar{\theta}_z(\ell)=0, \qquad EC_w\,\bar{\psi}'(\ell)=-\bar{M}_w(\ell) \tag{5.54-55}$$

The general steady state solution for simply supported monosymmetric beam under is obtained as

$$\left\{\bar{U}_{3S}(z)\right\}_{4\times1}=\left[\chi(z)\right]_{4\times8}\left[\Phi_S\right]^{-1}_{8\times8}\left\{\bar{Q}_S\right\}_{8\times1}+\left\{\bar{U}_{3P}\right\}_{4\times1} \tag{5.56}$$

in which the unknown integration constants $\left\{\bar{B}\right\}_{8\times1}=\left[\Phi_s\right]^{-1}_{8\times8}\left\{\bar{Q}_s\right\}_{8\times1}$ are determined from the set of boundary conditions in Equations (5.48) to (5.55), yielding

$$\left[\Phi_S\right]^{\mathrm{T}}_{8\times8}=\left[\left\{\bar{G}_{1,\mathrm{i}}\right\}_{8\times1}\ \left\{\bar{C}_{1,\mathrm{i}}\right\}_{8\times1}\ \left\{\bar{G}_{3,\mathrm{i}}\right\}_{8\times1}\ \left\{m_i\right\}_{8\times1}\ \left\{\bar{C}_{2,\mathrm{i}}\right\}_{8\times1}\ \left\{\bar{C}_{3,\mathrm{i}}\right\}_{8\times1}\ \left\{\bar{C}_{4,\mathrm{i}}\right\}_{8\times1}\ \left\{\bar{C}_{5,\mathrm{i}}\right\}_{8\times1}\right]^{\mathrm{T}}_{8\times8},$$

$$\left\langle\bar{Q}_S\right\rangle^{\mathrm{T}}_{1\times8}=\left\langle-\bar{v}_p\ \middle|\ \frac{-\bar{M}_x(0)}{EI_{xx}}\ \middle|\ -\bar{\theta}_{z_p}\ \middle|\ \frac{\bar{M}_w(0)}{EC_w}\ \middle|\ -\bar{v}_p\ \middle|\ \frac{\bar{M}_x(\ell)}{EI_{xx}}\ \middle|\ -\bar{\theta}_{z_p}\ \middle|\ \frac{-\bar{M}_w(\ell)}{EC_w}\right\rangle^{\mathrm{T}}_{1\times8},$$

$\bar{C}_{1,\mathrm{i}}=m_i\bar{G}_{2,\mathrm{i}}$, $\bar{C}_{2,\mathrm{i}}=\bar{G}_{1,\mathrm{i}}e^{m_i\ell}$, $\bar{C}_{3,\mathrm{i}}=m_i\bar{G}_{2,\mathrm{i}}e^{m_i\ell}$, $\bar{C}_{4,\mathrm{i}}=\bar{C}_{1,\mathrm{i}}e^{m_i\ell}$, and

$\bar{C}_{5,\mathrm{i}}=m_ie^{m_i\ell}$, for $i=1,2,3,....,8$.

5.5 Finite Element Formulation

The finite element sought has two nodes with four degrees of freedom per node as illustrated in Fig. (5.4). Displacement fields $\left\langle\bar{U}_{3H}(z)\right\rangle^T_{1\times4}=\left\langle\bar{v}_h(z)\ \bar{\theta}_{xh}(z)\ \bar{\theta}_{zh}(z)\ \bar{\psi}_h(z)\right\rangle^T_{1\times4}$ are thus to be expressed in terms of nodal displacements

$$\left\langle U_N\right\rangle^T_{1\times8}=\left\langle v_1\ \middle|\ \theta_{x1}\ \middle|\ \theta_{z1}\ \middle|\ \psi_1\ \middle|\ v_2\ \middle|\ \theta_{x2}\ \middle|\ \theta_{z2}\ \middle|\ \psi_2\right\rangle^T_{1\times8}.$$

5.5.1 Formulating Shape Functions

Shape functions which exactly satisfy the homogeneous part of the coupled field equations are formulated through

$$\left\{U_N\right\}_{8\times1}=\left\{\begin{array}{c}\left\{\bar{U}_{3H}(0)\right\}_{4\times1}\\ \hdashline \left\{\bar{U}_{3H}(l)\right\}_{4\times1}\end{array}\right\}=\left[\begin{array}{c}\left[\chi(0)\right]_{4\times8}\\ \hdashline \left[\chi(\ell)\right]_{4\times8}\end{array}\right]\left\{\bar{B}\right\}_{8\times1}=\left[L\right]_{8\times8}\left\{\bar{B}\right\}_{8\times1} \tag{5.57}$$

Equation (5.57) is solved for vector $\left\{\bar{B}\right\}_{8\times1}$ and then substituted into Eq. (5.37), yielding

$$\left\{ \bar{U}_{3H}(z) \right\}_{4\times1} = \left[\chi(z) \right]_{4\times8} \left[L \right]^{-1}_{8\times8} \left\{ U_N \right\}_{8\times1} = \left[H(z) \right]_{4\times8} \left\{ U_N \right\}_{8\times1} \tag{5.58}$$

in which $\left[H(z) \right]_{4\times8} = \left[\chi(z) \right]_{4\times8} \left[L \right]^{-1}_{8\times8}$ is a matrix of shape functions which exactly satisfy the homogeneous form of the equilibrium equations. Such shape functions will be shown to avoid mesh discretization errors appearing in most finite elements. Also, it yields an element that is free of shear locking.

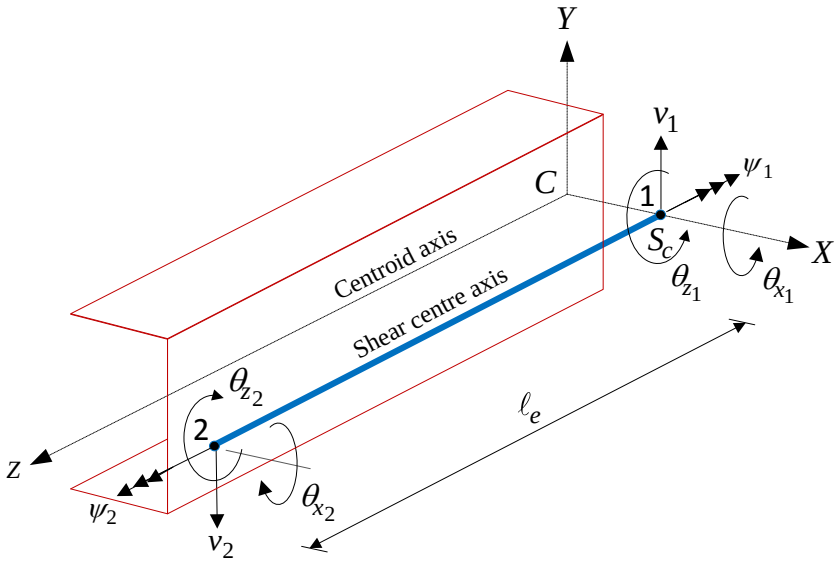

Figure (5.4): Thin-walled two-noded C-beam element

5.5.2 Dynamic Equilibrium Equations of Motion

From the steady state displacements and forces in Equations (3.79) to (3.81), substituting into displacement expressions in Equations (3.1) to (3.4), and then substituting the resulting expressions with Equations (3.8) and (3.10) are then substituted into the energy expressions (given in Chapter 3 as Equations 3.15, 3.22 and 3.26), the resulting energy equations are substituted into the variational form of Hamilton's principle, $\int_{t_1}^{t_2} \delta\left(T^* - U^*\right) dt + \int_{t_1}^{t_2} \delta W^* dt = 0$. By (1) imposing the orthogonality conditions and performing integration by parts with respect to t, (2) evoking the stationary condition of the Hamilton's functional, and by (3) noting that all the variations of the coefficients at the time limits t_1 and t_2 are zero, i.e., $\delta v(z,t)\big|_{t_1}^{t_2} = 0$, $\delta\theta_x(z,t)\big|_{t_1}^{t_2} = 0$, $\delta\theta_z(z,t)\big|_{t_1}^{t_2} = 0$, $\delta\psi(z,t)\big|_{t_1}^{t_2} = 0$, one recovers the discretized form of the equilibrium equation

$$\int_{t_1}^{t_2}\left\{\int_0^{\ell}\left(\left[\left\langle\delta\bar{U}_3'(z)\right\rangle_{1\times4}^T\left[Y_a\right]_{4\times4}\left\{\bar{U}_3'(z)\right\}_{4\times1}+\left\langle\delta\bar{U}_S(z)\right\rangle_{1\times4}^T\left[Y_S\right]_{4\times4}\left\{\bar{U}_S(z)\right\}_{4\times1}\right]\right.\right.$$
$$\left.-\Omega^2\left\langle\delta\bar{U}_3(z)\right\rangle_{1\times4}^T\left[X_m\right]_{4\times4}\left\{\bar{U}_3(z)\right\}_{4\times1}+\left\langle\delta\bar{U}_3(z)\right\rangle_{1\times4}^T\left\{\bar{P}_H(z)\right\}_{4\times1}\right)dz \qquad (5.59)$$
$$\left.\left.-\left\langle\delta\bar{U}_3(z)\right\rangle_{1\times4}^T\left\{\bar{F}_H(z)\right\}_{4\times1}\right|_0^{\ell}\right\}dt=0$$

in which the variation of kinetic energy is given as

$$\int_{t_1}^{t_2}\delta T^*dt=\int_{t_1}^{t_2}\left[-\Omega^2\int_0^{\ell}\left\langle\delta\bar{U}_3(z)\right\rangle_{1\times4}^T\left[X_m\right]_{4\times4}\left\{\bar{U}_3(z)\right\}_{4\times1}dz\right]e^{i\Omega t}dt$$

where $\left[X_m\right]_{4\times4}=\begin{bmatrix}\rho A & 0 & -x_s & 0\\ & \rho I_{xx} & 0 & 0\\ & Symm & \rho A r_o^2 & 0\\ & & & \rho C_w\end{bmatrix}_{4\times4}$.

The variation of the internal strain energy is

$$\int_{t_1}^{t_2}\delta U^*dt=\int_{t_1}^{t_2}\left[\int_0^{\ell}\left[\left\langle\delta\bar{U}_3'(z)\right\rangle_{1\times4}^T\left[Y_a\right]_{4\times4}\left\{\bar{U}_3'(z)\right\}_{4\times1}+\left\langle\delta\bar{U}_S(z)\right\rangle_{1\times4}^T\left[Y_S\right]_{4\times4}\left\{\bar{U}_S(z)\right\}_{4\times1}\right]dz\right]e^{i\Omega t}dt$$

where

$$\left\langle\bar{U}_S(z)\right\rangle_{1\times4}^T=\left\langle\bar{v}'(z)\quad\bar{\theta}_x(z)\quad\bar{\theta}_z'(z)\quad\bar{\psi}(z)\right\rangle_{1\times4}^T,$$

$$\left[Y_a\right]_{4\times4}=diag\left[0\;\middle|\;EI_{xx}\;\middle|\;GJ\;\middle|\;EC_w\right]_{4\times4},\quad\left[Y_s\right]_{4\times4}=\begin{bmatrix}GD_{yy} & GD_{yy} & GD_{hy} & GD_{hy}\\ & GD_{yy} & GD_{hy} & GD_{hy}\\ & Symm & GD_{\omega\omega} & GD_{\omega\omega}\\ & & & GD_{\omega\omega}\end{bmatrix}_{4\times4}$$

and the variation of the work done δW^* by the applied harmonic forces is given as

$$\int_{t_1}^{t_2}\delta W^*dt=\int_{t_1}^{t_2}\left[\left\langle\delta\bar{U}_3(z)\right\rangle_{1\times4}^T\left\{\bar{F}_H(z)\right\}_{4\times1}\Big|_0^{\ell}+\int_0^{\ell}\left\langle\delta\bar{U}_3(z)\right\rangle_{1\times4}^T\left\{\bar{P}_H(z)\right\}_{4\times1}dz\right]e^{i\Omega t}dt$$

where

$$\left\langle\bar{P}_H(z)\right\rangle_{1\times4}^T=\left\langle\bar{q}_y(z)\quad\bar{m}_x(z)\quad\bar{m}_z(z)\quad\bar{m}_w(z)\right\rangle_{1\times4}^T,\text{ and}$$

$$\left\langle\bar{F}_H(z)\right\rangle_{1\times4}^T=\left\langle\bar{V}_y(z)\quad\bar{M}_x(z)\quad\bar{M}_z(z)\quad\bar{M}_w(z)\right\rangle_{1\times4}^T.$$

5.5.3 Matrix Formulation

Equation (5.59) can now be rewritten leading to the following discrete form for the finite beam element

$$\left(\left[K_e\right]_{8\times8} - \Omega^2\left[M_e\right]_{8\times8}\right)\left\{U_N\right\}_{8\times1} = \left\{F_e\right\}_{8\times1} \tag{5.60}$$

in which the element stiffness matrix $\left[K_e\right]_{8\times8}$ is given by:

$$\left[K_e\right]_{8\times8} = \int_0^{\ell}\left(\left[H'(z)\right]_{8\times4}^{\mathrm{T}}\left[Y_a\right]_{4\times4}\left[H'(z)\right]_{4\times8} + \left[H_S(z)\right]_{8\times4}^{\mathrm{T}}\left[Y_s\right]_{4\times4}\left[H_S(z)\right]_{4\times8}\right)dz \ ,$$

where

$$\left[H(z)\right]_{8\times4}^{\mathrm{T}} = \left[\left\{H_{1,\mathrm{j}}(z)\right\}_{8\times1} \ \vdots \ \left\{H_{2,\mathrm{j}}(z)\right\}_{8\times1} \ \vdots \ \left\{H_{3,\mathrm{j}}(z)\right\}_{8\times1} \ \vdots \ \left\{H_{4,\mathrm{j}}(z)\right\}_{8\times1}\right]_{8\times4}^{\mathrm{T}}, \text{ and}$$

$$\left[H_S(z)\right]_{8\times4}^{\mathrm{T}} = \left[\left\{H'_{1,\mathrm{j}}(z)\right\}_{8\times1} \ \vdots \ \left\{H_{2,\mathrm{j}}(z)\right\}_{8\times1} \ \vdots \ \left\{H'_{3,\mathrm{j}}(z)\right\}_{8\times1} \ \vdots \ \left\{H_{4,\mathrm{j}}(z)\right\}_{8\times1}\right]_{8\times4}^{\mathrm{T}}.$$

Also, in Equation (5.60), the element mass matrix $\left[M_e\right]_{8\times8}$ that is determined by considering the translational and rotational inertias is given by

$$\left[M_e\right]_{8\times8} = \int_0^{\ell}\left[H(z)\right]_{8\times4}^{\mathrm{T}}\left[X_m\right]_{4\times4}\left[H(z)\right]_{4\times8}dz$$

and the energy equivalent element load vector $\left\{F_e(z)\right\}_{8\times1}$ is given by:

$$\left\{F_e(z)\right\}_{8\times1} = \int_0^{\ell}\left[H(z)\right]_{8\times4}^{\mathrm{T}}\left\{\bar{Q}_3(z)\right\}_{4\times1}dz$$

For a thin-walled structural beam consisting of n nodes, the total number of degrees of freedom is 4n, i.e., each node has four degrees of freedom for coupled transverse-torsional deformation problems,

$$\left(\left[K_G\right]_{4n\times4n} - \Omega^2\left[M_G\right]_{4n\times4n}\right)\left\{U_{N_G}\right\}_{4n\times1} = \left\{F_G\right\}_{4n\times1} \tag{5.61}$$

in which the global stiffness matrix $\left[K_G\right]_{4n\times4n}$, global mass matrix $\left[M_G\right]_{4n\times4n}$ and global load vector $\left\{F_G\right\}_{4n\times1}$ are computed by using the exact shape functions. Even though the finite element formulation developed in this study is applied to determine the steady state dynamic response of thin-walled members of monosymmetric cross-sections under harmonic excitations, the static response for the system under harmonic excitations can be approached by using very low exciting frequency compared to the first natural frequency of the system. Also the present formulation can predict the natural frequencies and mode shapes of the structural member.

5.6 Examples and Discussion

While the above closed-form and finite element formulations provide the response under harmonic loads, it can also approach the response under static loads when adopting a very low exciting frequency Ω compared to the first natural frequency $\bar{\omega}_1$ of the system (i.e., $\Omega \approx 0.01\bar{\omega}_1$). In order to demonstrate the validity, accuracy and applicability of the present closed-form solution and finite element formulation, several examples are conducted for monosymmetric beams with a variety of cross-sections, loading and boundary conditions. Material is assumed to be steel with $E = 200GPa$, $G = 77GPa$ and $\rho = 7850kg/m^3$. The finite element solution developed in the present study based on the exact shape functions which exactly satisfy the homogeneous form of the governing field coupled equations are conducted using a finite beam element with four degrees of freedom per node. This treatment eliminates mesh discretization errors in conventional finite element solutions based on polynomial shape functions. As a result, it was observed that solutions based on a single finite element per span yielded results which exactly matched those based on closed-from solution up to five significant digits. Additional solutions were provided for comparison. These solutions are:

(1) A Vlasov beam theory solution (Appendix 5C formulates the closed-form solution for Vlasov beam theory), which neglects shear deformation and distortional effects,
(2) An Abaqus two-noded B31OS beam element with seven degrees of freedom per node (i.e. three translation, three rotations and warping deformation) which accounts for shear deformation for only bending but omits (a) shear deformation effects due to warping deformation and (b) distortional effects, and
(3) An Abaqus S4R shell element solution (shell element with four nodes with six degrees of freedom per node, i.e., three translation and three rotations, and reduced integration) which captures for shear deformation and distortional effects.

5.6.1 Example 1- Long cantilever under Uniformly Distributed Torsion

A 4m span cantilever beam with monosymmetric I-section is subjected to uniformly distributed harmonic torsion $m_z(z) = 1.80e^{i\Omega t}kNm/m$ is considered (Figure 5.5). The dimensions of the cross-section are; flange thickness $t_f = 20mm$, web thickness $t_w = 15mm$, upper flange width $b_u = 100mm$, lower flange width $b_\ell = 200mm$ and a

middle surface height $H = 200mm$. It is required to (a) conduct a steady state analysis and extract the natural frequencies, (b) conduct a quasi-state analysis by adopting an exciting frequency $\Omega \approx 0.01\bar{\omega}_1 = 0.4415 rad/\sec$, and (c) conducting a steady state dynamic response $\Omega = 1.423\bar{\omega}_1 \approx 62.83 rad/\sec$.

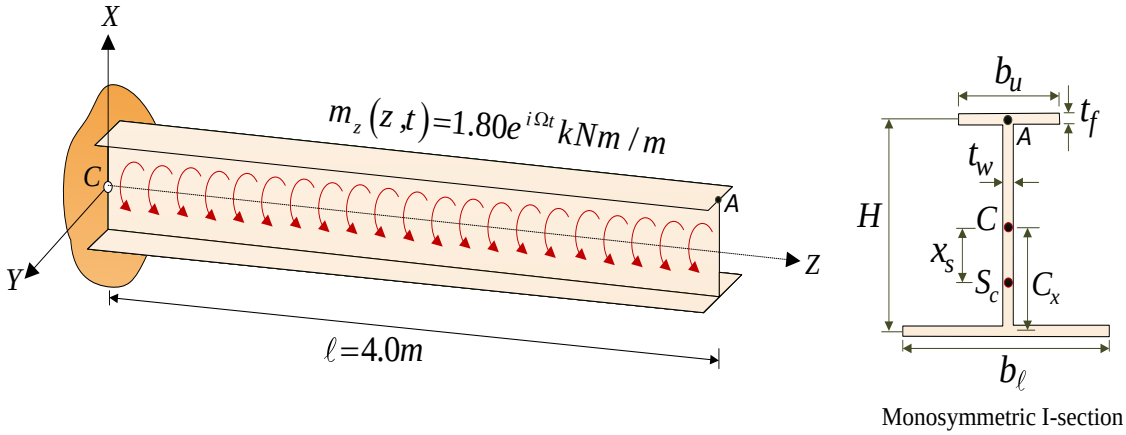

Figure (5.5): Cantilever mono-symmetric I-section under distributed harmonic torsion

The shear centre S_c coordinate along the axis of symmetry is $x_s = -55.56mm$, and the coordinate of the centroid C in the direction of the principle axis of symmetry is $C_x = 77.78mm$. The sectional properties are; $A = 0.56\times10^4 mm^2$, $I_{xx} = 15.0\times10^6 mm^4$, $I_{yy} = 65.56\times10^6 mm^4$, $J = 1.025\times10^6 mm^4$, $C_w = 59.26\times10^9 mm^6$, $D_{xx} = 0.30\times10^4 mm^2$, $D_{yy} = 0.60\times10^4 mm^2$, $D_{hy} = 26.67\times10^3 mm^3$ and $D_{\omega\omega} = 65.19\times10^6 mm^4$.

In the Abaqus shell model (Figure 5.6), a total of 3,520 S4R shell elements (≈22,200 degrees of freedom) are used (i.e., 4 elements per upper flange, 8 elements per bottom flange, 10 elements along the web height and 160 elements along the longitudinal axis), while in the case of Abaqus B31OS beam element, a total of 100 elements (700 degrees of freedom) along the cantilever axis are used to achieve the accuracy in this example. In contrast, the present finite element uses a single beam element with eight degrees of freedom to capture the exact solution.

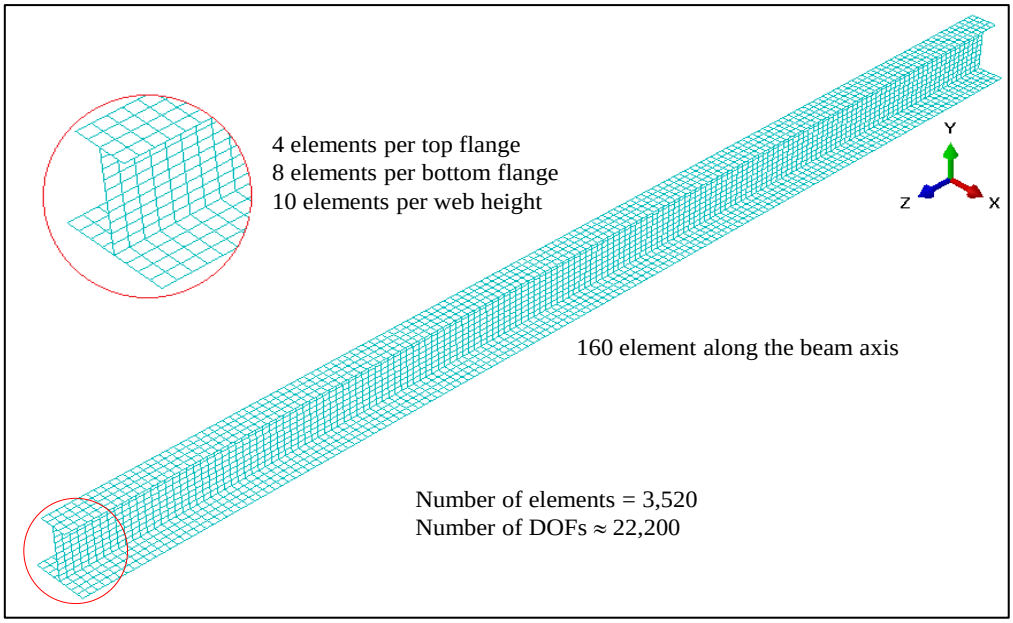

Figure (5.6): Finite element Abaqus model for monosymmetric I-beam using shell S4R element

5.6.1.1 Extracting Natural Frequencies

Under uniformly distributed harmonic twisting moment, $m_z(z,t) = 1.80\, e^{i\Omega t}\, kNm/m$, the natural frequencies related to coupled lateral-torsional response can be extracted from the steady state response analysis as illustrated in Figures (5.7a-d). Figures (5.7a-d) show the peak lateral displacement $\bar{v}$, related bending moment $\bar{\theta}_x$, angle of twist and warping deformation at the cantilever tip as a function of the exciting frequency. The solution is based on the element developed in the present study. Overlaid on the same plots are solutions based on (1) the Vlasov beam theory, (2) Abaqus B31OS beam element using 100 elements and (3) Abaqus S4R shell element using 3,520 elements for comparison.

The exciting frequency Ω was varied from nearly zero to 200*Hz*. Peaks on both diagrams indicate resonance and are thus indicators of the natural frequencies of the beam. It is noted that lateral displacement, bending angle peaks are synchronized with the twist angle $\bar{\theta}_z$ and warping deformation $\bar{\psi}$ peaks indicating that the mode shapes are indeed coupled lateral-torsional. Excellent agreement is obtained between all solutions.

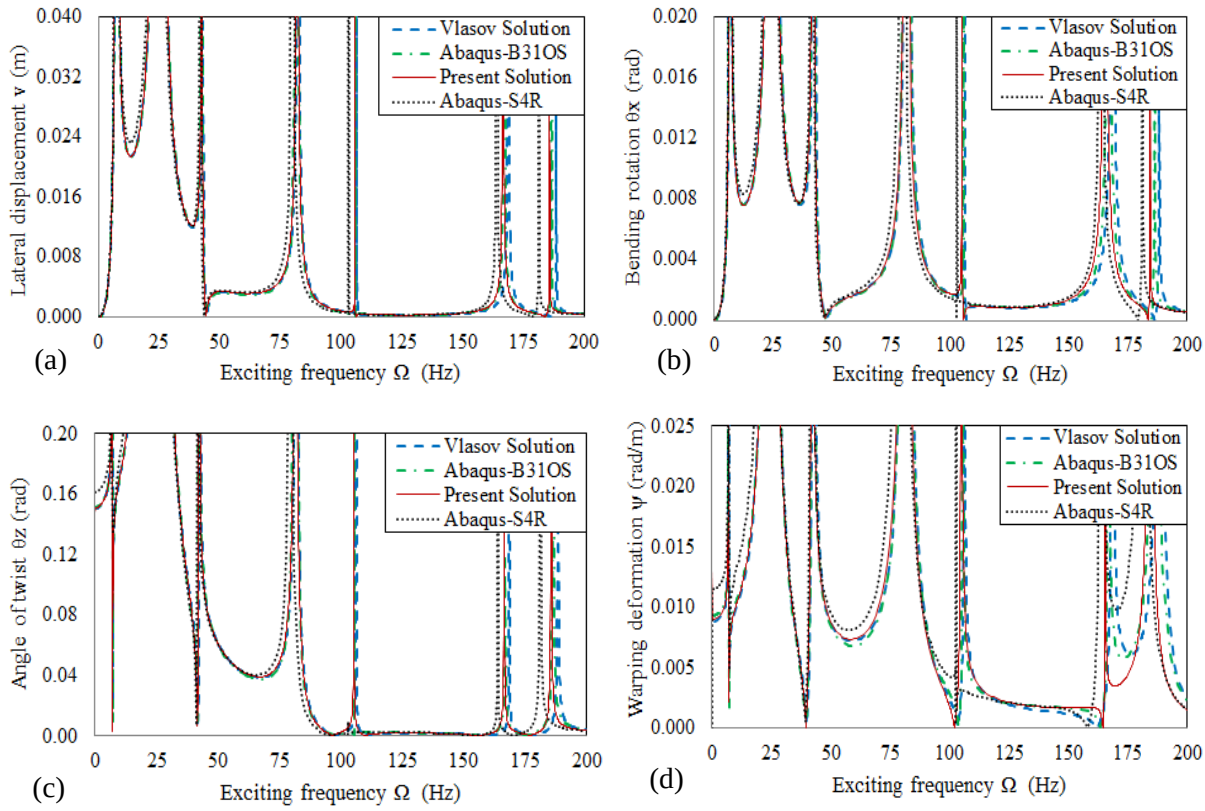

Figure (5.7): Natural frequencies of monosymmetric cantilever under member torsion

Table (5.1) provides the first seven natural frequencies extracted from the steady state response analysis of the cantilever under distributed harmonic torsion. Close agreement is observed between all four solutions, particularly at lower natural frequencies. For higher natural frequencies, predictions by the Vlasov closed form solution were the highest followed by the B31OS solution, followed by the present solution, while the frequencies predicted by the Abaqus shell S4R element were the lowest. This is a natural outcome of the fact that the Vlasov beams provides the stiffest representation of the beam (since it ignores shear deformation and distortional effects) while that based on ABAQUS shell analysis provides the most flexible one. The frequencies predicted by the present solution differed from 0.58% to 2.43% from those based on Abaqus shell element and the present solution provides the closest agreement with the shell solution.

Figure (5.8) shows the first six mode shapes of the response of cantilever with mono-symmetric I-section under distributed harmonic torsion $m_z(z,t) = 1.80\, e^{i\Omega t}\, kNm/m$. These modes obtained using the present solution are (normalized to be one at their

maximums) plotted using magnification scale factor=0.5 for different exciting frequencies (i.e., at peaks as illustrated in Figure 5.7); $7.082Hz$, $24.69Hz$, $42.28Hz$, $81.50Hz$, $105.2Hz$ and $165.8Hz$, respectively.

Table (5.1): Natural frequencies of cantilever beam of monosymmetric I-section

Mode	Abaqus S4R [1] (22,200DOF)	Present Finite element [2] (8DOF)	Abaqus B31OS [3] (700DOF)	Vlasov Solution [4] (Closed-form)	Present Finite element Difference =[1-2]/1	B31OS Difference =[1-3]/1	Vlasov solution Difference =[1-4]/1
1	7.041	7.082	7.093	7.098	-0.58%	-0.74%	-0.81%
2	24.02	24.69	24.70	24.73	-2.79%	-2.83%	-2.96%
3	41.95	42.28	42.56	42.69	-0.79%	-1.45%	-1.76%
4	79.93	81.51	81.70	82.05	-1.98%	-2.21%	-2.65%
5	103.1	105.2	105.7	106.5	-2.04%	-2.52%	-3.30%
6	164.0	165.8	167.1	168.8	-1.10%	-1.89%	-2.93%
7	181.4	185.8	186.5	188.6	-2.43%	-2.81%	-3.97%

In generating the 3D deformed configuration in Figure (5.8), the deformed coordinates of the structure were calculated based on the displacement fields $\left(\bar{u},\bar{v},\bar{\theta}_z\right)$ as computed by the FORTRAN program developed in the present study. The displacement components at a point s on the contour are then calculated from Equations (3.1) and (3.2). The procedure is implemented for a rectangular mesh on the web and flanges and the deformed nodal coordinates at the mesh points were computed, and input into Abaqus. Connectivity between the various nodes was also defined in order to build a model within Abaqus which represents the deformed configuration as predicted by the FORTRAN program implemented in the present study. This allowed the use of Abaqus features displaying the 3D deformed shape as predicted by the present formulation.

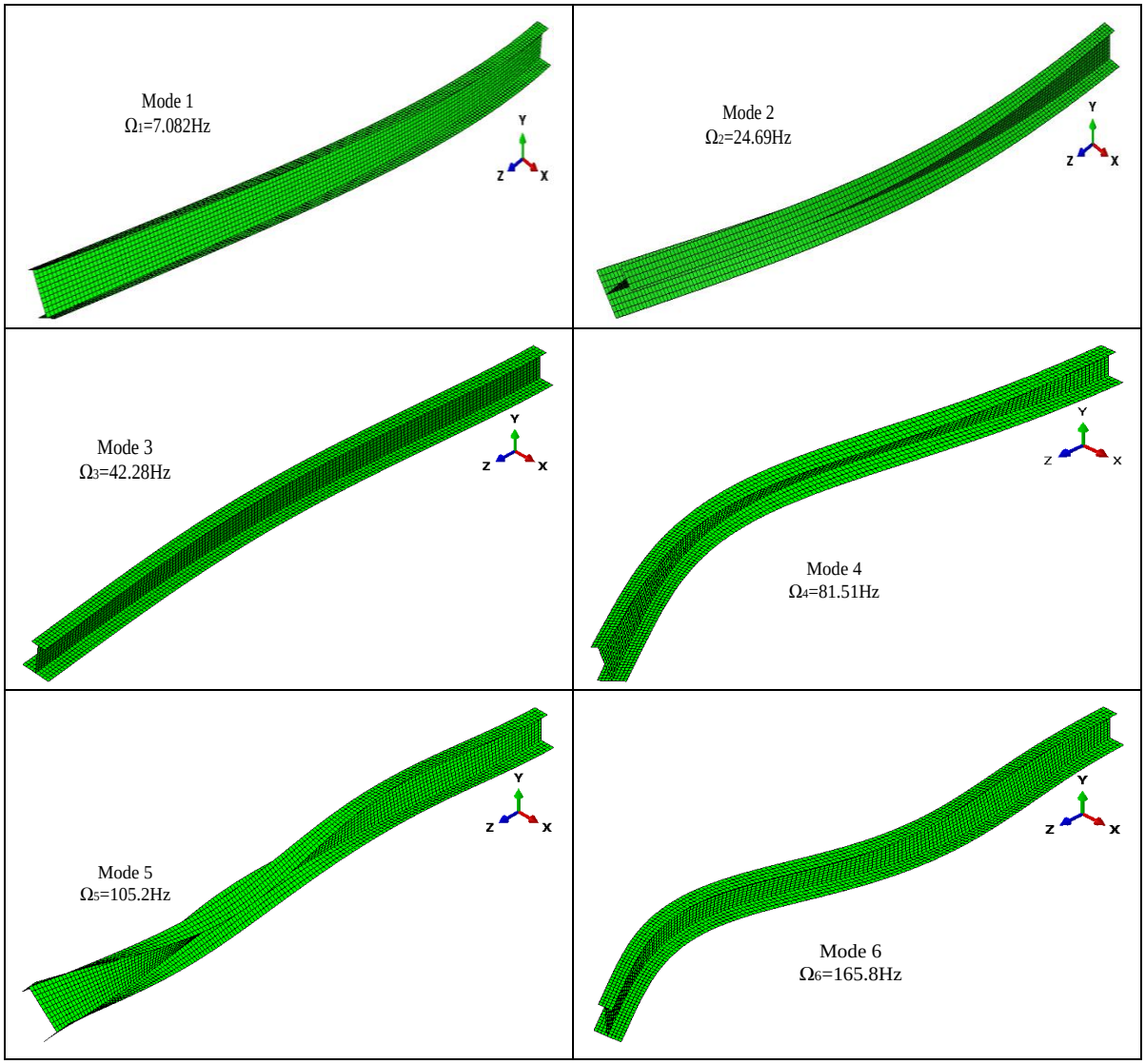

Figure (5.8): The first six steady state mode shapes based on present solution.

5.6.1.2 Quasi-Static Solution

Table (5.2) shows the quasi-static response results for maximum lateral displacement $\bar{v}_A$ of point A (Figure 5.5), twist angle $\bar{\theta}_z$ and the warping deformation function $\bar{\psi}$. Due to the mono-symmetry of the cross-section, the lateral response $\bar{u}(z)$ and $\bar{\theta}_y(z)$ is fully coupled with torsional-warping response $\bar{\theta}_z(z)$ and $\bar{\psi}(z)$ but in the case of quasi-static response, it is observed that the bending rotation $\bar{\theta}_y(z)$ vanishes in all four solutions (see Appendix 5A for more details). This leads to conclude that the coupling terms in quasi-static response become weak couplings. Results are based on (a) the solutions (closed form and finite element) developed in the present study, (b) Vlasov beam theory and (c) Abaqus B31OS-beam and S4R-shell elements. Results based on the present study are

observed to nearly coincide with those based on the Vlasov beam theory and Abaqus B31OS beam element, but slightly depart from the Abaqus shell element. The lateral displacement $\bar{v}_A$, and twist angle $\bar{\theta}_z$ were respectively found 5.82% , 4.96% lower than those based on Abaqus S4R-shell model. The differences are attributed to distortional effects of the cross-section, as illustrated in Figure (5.9), which are captured in Abaqus shell element solution but not in the other three solutions.

Table (5.2): Quasi-static analysis of cantilever with monosymmetric I-section

Variable	Abaqus S4R [1]	Present Solution [2]	Abaqus B31OS [3]	Vlasov Solution [4]	Present Difference =[1-2]/1	B31OS Difference =[1-3]/1	Vlasov Difference =[1-4]/1
$\bar{v}_A$ (mm)	-28.53	-26.87	-26.85	-26.77	5.82%	5.89%	6.17%
$\bar{\theta}_z$ (10^{-3}rad)	159.3	151.4	151.2	150.1	4.96%	5.08%	5.78%
$\bar{\psi}$ (10^{-4} rad/mm)	11.03	9.061	8.954	8.796	17.85%	18.82%	20.25%

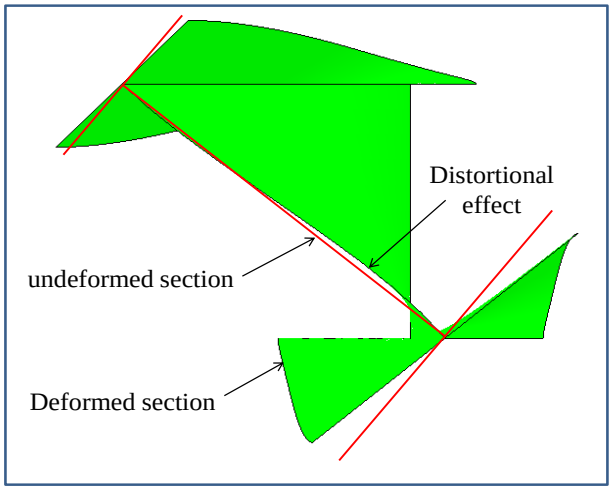

Figure (5.9): Distortional effect of monosymmetric I-section in Abaqus shell model

In order to extract the bending rotation $\bar{\theta}_x(z)$ and warping deformation $\bar{\psi}(z)$ from the finite shell model at a given section z , the top flange rotation $\bar{\theta}_t(z)$ and bottom flange rotation $\bar{\theta}_b(z)$ about the X axis were extracted from the model. Equation (3.3) is then applied at the bottom flange (by setting $x = h_b$, h_b being the distance from the shear centre to the bottom flange), leading to

$w_b(z,y,t)=w(z,t)+y\,\theta_x(z,t)-h_b\,\theta_y(z,t)+h_b\,y\,\psi(z,t)$. Equation (3.81) is then used to express the steady state component of the displacement response leading to $\bar{w}_b(z,x)=\bar{w}(z)+y\,\bar{\theta}_x(z)-h_b\,\bar{\theta}_y(z)+h_b\,y\,\bar{\psi}(z)$. The rotation of the bottom flange is then obtained by differentiation with respect to coordinate *y* yielding $\bar{\theta}_b(z)=\partial\bar{w}_b/\partial y=\bar{\theta}_x(z)+h_b\bar{\psi}(z)$. A similar treatment for the top flange yields $\bar{\theta}_t(z)=\partial\bar{w}_t/\partial x=\bar{\theta}_x(z)-h_t\,\bar{\psi}(z)$, h_t being the distance from the shear centre to the top flange. Knowing $\bar{\theta}_t(z)$ and $\bar{\theta}_b(z)$ from the finite element model and the distances h_t and h_b , one can calculate the angle of rotation $\bar{\theta}_x(z)$ and the warping deformation $\bar{\psi}(z)$ for the section of interest z as predicted by finite element.

The above procedure has led to the warping deformation entry $\bar{\psi}$ in the last row of column [1] which is subsequently used as a basis to compare the warping deformations obtained in other beam solutions. Again, the closest prediction is that based on the present study which underestimated the warping deformation $\bar{\psi}$ with 17.85%. This compares to 20.25% for the Vlasov theory. Under the applied quasi-static loading, $\bar{\theta}_x(z)$ was observed to vanish in all four solution solutions.

Under the Vlasov and the B31OS solutions subject to static twisting moments, $\bar{\theta}_x(z)$ are expected to vanish since there is no coupling between the flexural and twisting mode. Under the present theory, the presence of non-zero terms on the off-diagonal terms of the field equations (Equation 5.28) suggest that, in principle, coupling should exist between twist and lateral deformation. The coupling is due to two factors: (1) shear deformation effects (evidence by the presence of the term GD_{hy} in the off-diagonal term), and (2) the presence of harmonic forces (given the dependence of the off-diagonal terms on the exciting frequency). As a general observation, the present solution is successful at capturing the static response of the system.

5.6.1.3 Steady State Dynamic Response

For the exciting frequency $\Omega = 1.423\bar{\omega}_1 \approx 62.83 rad/sec$, Figures (5.10a-d) show the lateral displacement $\bar{v}_A(z)$, associated bending rotation $\bar{\theta}_x(z)$, angle of twist $\bar{\theta}_z(z)$ and warping deformation $\bar{\psi}(z)$. Results are in excellent agreement with the Vlasov beam theory and Abaqus B31OS but slightly differ from Abaqus S4R shell model which exhibits a slightly more flexible response. Again the difference is attributed to cross-sectional distortional effects.

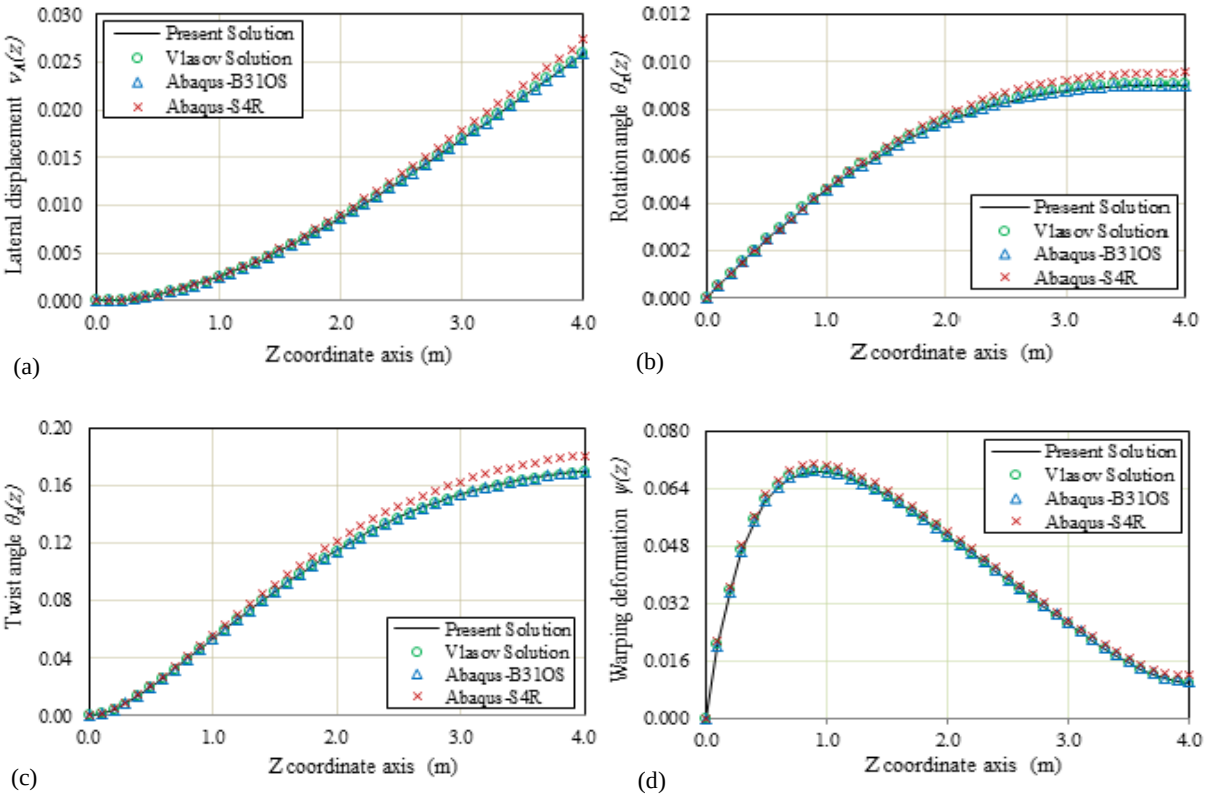

Figure (5.10): Steady state response for cantilever monosymmetric I-section under distributed harmonic torsion

The peak displacement responses corresponding to three frequencies $\Omega_1 = 1.10\bar{\omega}_1$, $\Omega_2 = 0.5(\bar{\omega}_1 + \bar{\omega}_2)$ and $\Omega_3 = 1.10\bar{\omega}_2$ are plotted in Figure (5.11). Given the proximity of the exciting frequencies Ω_1 to the first natural frequency and Ω_3 to the third natural frequency, the corresponding deformation responses assume a shape close to the first two natural modes of vibration. The exciting frequency $\Omega_2 = 0.5(\bar{\omega}_1 + \bar{\omega}_2)$ lies between both

natural frequencies. Thus, the corresponding deformation response can be conceived as a linear combination of the first and second modes of vibrations. Also, since the exciting frequency Ω_2 is far from both natural frequencies $\bar{\omega}_1, \bar{\omega}_2$, resonance does not take place and the magnitude of the displacements are generally smaller than those based on the exciting frequencies $\Omega_1 = 1.10\bar{\omega}_1$ and $\Omega_3 = 1.10\bar{\omega}_2$.

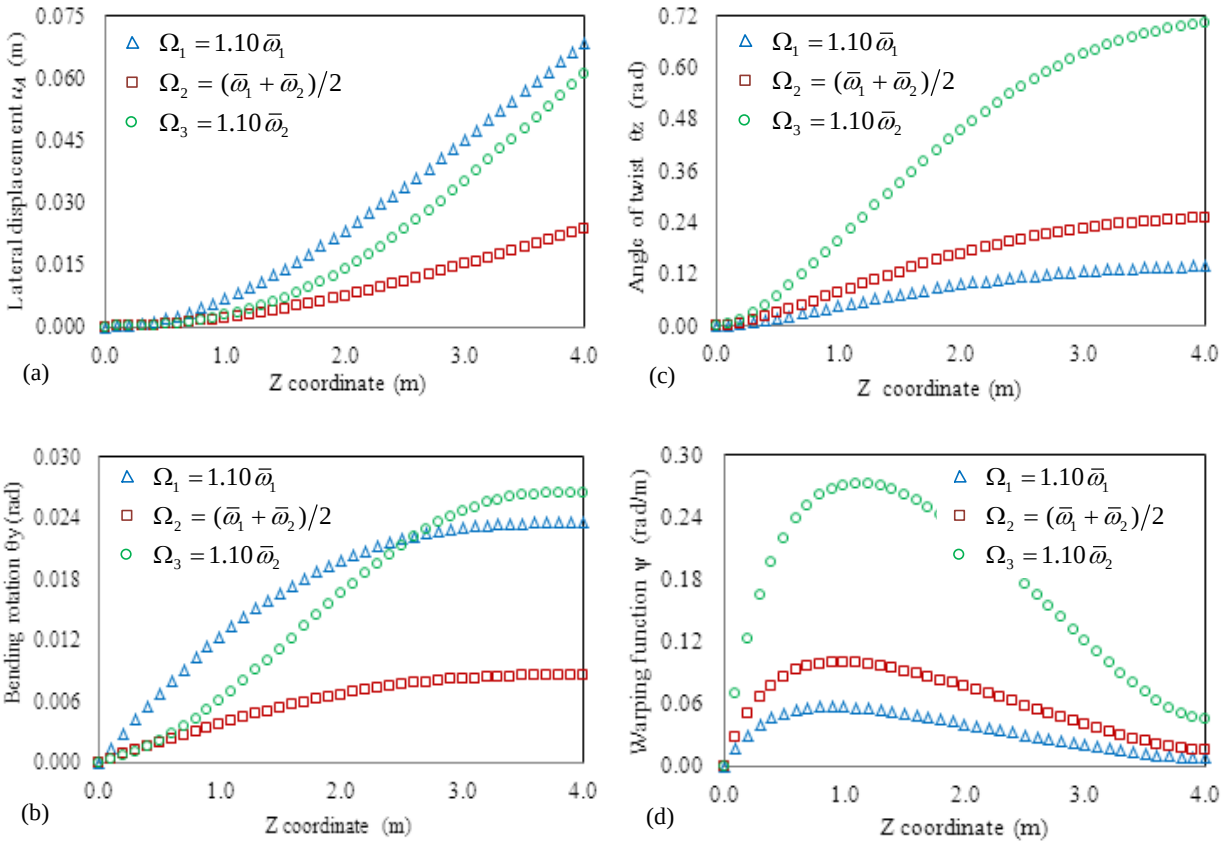

Figure (5.11): (a) Lateral displacement, (b) bending rotation, (c) twist angle, (d) warping deformation responses for cantilever monosymmetric I-section

5.6.2 Example 2 - Effect of Shear Deformation

The purpose of this example is to illustrate the ability of the element developed in the present study to capture shear deformation effects on the coupled lateral-torsional behavior of short cantilever spanning 0.8m. The cantilever has the same cross-section as that given in Example 1 and is subjected to a uniformly distributed harmonic torsion $m_z(z,t) = 15.0e^{i\Omega t}\, kNm/m$ acting along the beam axis as shown in Figure (5.12).

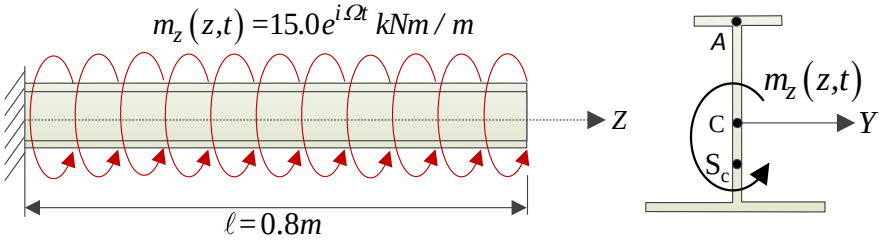

Figure (5.12): Cantilever with monosymmetric I-section under member torsion

Two exciting frequencies $\Omega = 0.001\bar{\omega}_1\ rad/\sec$ and $\Omega \approx 1.37\,\bar{\omega}_1\ rad/sec$ are considered to investigate the quasi-static and steady state dynamic analyses of the short beam. The first natural frequency of the short cantilever is $\bar{\omega}_1 = 131.4Hz$. In order to validate the validity of the present solutions (i.e. closed-form solution and finite element formulation based on a single element), Abaqus model solutions based on B31OS-beam and S4R-shell elements are presented while the influence of shear deformation is exhibited by comparison with classical Vlasov beam solution.

5.6.2.1 Natural Frequency Extraction

A steady state analysis is conducted based on the present solution (with a single element). Results based on Vlasov theory, the Abaqus B31OS model (with 40 beam elements) and shell element (with 880 S4R elements) are provided for comparison. It is known that, due to the monosymmetry of the cross-section, the bending deformation response in the perpendicular direction to the axis of symmetry is coupled with the torsional response of the beam. Therefore, the variations of lateral displacement and twist angle with the exciting frequency Ω are presented to demonstrate the influence of the shear deformation on the coupled response of the cantilever. The lateral displacement $\bar{u}_A$ at the cantilever tip is plotted versus the exciting frequency Ω in Figure (5.13a). Also, the angle of twist $\bar{\theta}_z$ versus the exciting frequency is plotted in Figure (5.13b). Again, since the response is coupled, the peak lateral displacements are observed to be synchronized with those of values at the natural frequencies of the structure (Table 5.3). All four solutions closely predict the location the first peak corresponding to the fundamental frequency. For higher frequencies, some discrepancy in the location of the peak response becomes apparent between the four solutions. For the third mode of vibration, the Abaqus shell model predicts the lowest natural frequency, followed by the present solution, followed by

Abaqus B31OS while the highest frequency is predicted by Vlasov solution. This is expected since (a) for higher modes, shear deformation is known to have a higher influence [Chen and Lui 2005], and (b) distortional effects become more prominent. Compared to the shell solution, the present solution overpredicts the third natural frequency by 7.59%, followed by B31OS by 9.54% since both do not capture distortional effects, while the Vlasov solution overpredicts the solution by 12.91% since it captures neither distortion nor shear deformation.

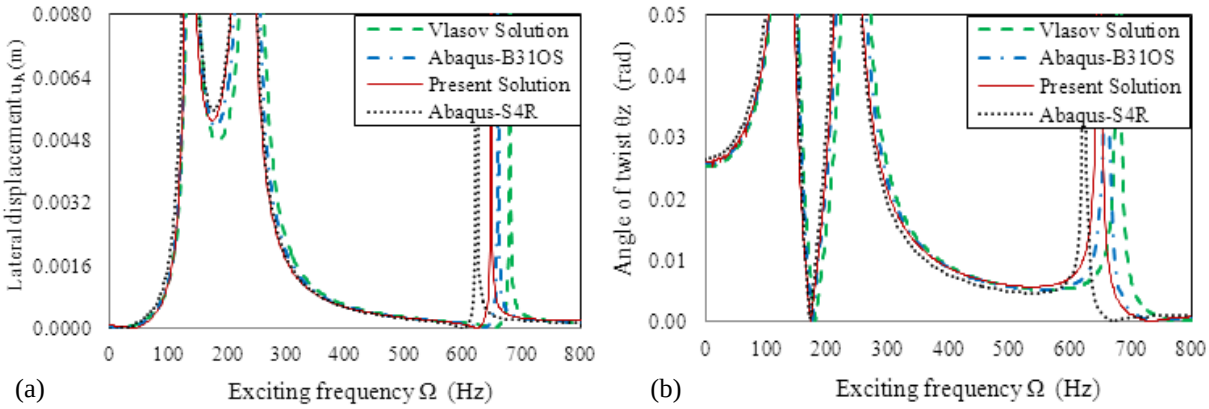

Figure (5.13): Natural frequency analysis of short cantilever monosymmetric I-section; (a) Lateral displacement $\bar{u}_A$ and (b) angle of twist $\bar{\theta}_z$.

Table (5.3): Natural frequencies of cantilever monosymmetric I-section under torsion

Mode	Abaqus S4R [1]	Present Solutions [2]	Abaqus B31OS [3]	Vlasov Solution [4]	Present Difference =[1-2]/1	B31OS Difference =[1-3]/1	Vlasov Difference =[1-4]/1
1	131.4	136.6	137.3	138.5	-3.96%	-4.49%	-5.40%
2	229.3	230.1	236.5	244.6	-0.35%	-3.14%	-6.67%
3	602.5	648.2	660.0	680.3	-7.59%	-9.54%	-12.91%

5.6.2.2 Comparison of Displacement Responses

A comparison between the displacement responses of all four solutions is provided in Table (5.4) for the quasi-static case and Table (5.5) for the dynamic case. In both cases, the best agreement with the Abaqus shell solution is obtained in the case of the present solution. For the static case, the difference is 12.15% for the lateral displacement, 4.86% for the angle of twist, and 5.43% for the warping deformation. Again, the bending rotation $\bar{\theta}_y$ nearly vanished in all four solutions.

For the steady state dynamic case, the present study predicts displacement $\bar{u}_A$, bending rotation $\bar{\theta}_y$, angle of twist $\bar{\theta}_z$ and warping deformation $\bar{\psi}$ that are respectively 3.09%, 0.36%, 5.09% and 3.97% lower than those based on the Abaqus shell element model. These percentages respectively correspond to 17.00%, 8.08%, 18.64% and 24.09% for the Vlasov theory (as listed in the last column of the table). Thus, the present theory provides a significantly more accurate response compared to that of Abaqus. The differences are due to the effects of shear deformation which are incorporated in the present theory but not in Vlasov theory. The results provided in Tables (5.4) and (5.5) show that shear deformation effects are more important in the steady state dynamic response analysis than they are for static analysis.

Table (5.4): Static response of short cantilever monosymmetric I-section under torsion

Variable	Abaqus S4R [1]	Present solution [2]	Abaqus B31OS [3]	Vlasov solution [4]	Present Difference =[1-2]/1	B31OS Difference =[1-3]/1	Vlasov Difference =[1-4]/1
$\bar{u}_A$ (mm)	5.299	4.655	4.557	4.462	12.15%	14.00%	15.80%
$\bar{\theta}_z$ (10^{-3} rad)	27.15	25.97	25.77	25.19	4.86%	5.08%	7.26%
$\bar{\psi}$ (10^{-6} rad/mm)	35.72	33.78	33.85	33.34	5.43%	5.24%	6.66%

Table (5.5): Steady State Response of cantilever monosymmetric I-section under

Variable	Abaqus S4R [1]	Present solution [2]	Abaqus B31OS [3]	Vlasov solution [4]	Present Difference =[1-2]/1	B31OS Difference =[1-3]/1	Vlasov Difference =[1-4]/1
$\bar{u}_A$ (mm)	5.784	5.605	5.421	4.801	3.09%	6.28%	17.00%
$\bar{\theta}_y$ (10^{-3} rad)	8.995	8.963	8.822	8.268	0.36%	1.92%	8.08%
$\bar{\theta}_z$ (10^{-3} rad)	4.693	4.454	4.375	3.818	5.09%	6.78%	18.64%
$\bar{\psi}$ (10^{-6} rad/mm)	-6.406	-6.152	-5.470	-4.863	3.97%	14.61%	24.09%

Figure (5.14) shows the displacement response for the case of harmonic loading. The present theory/finite element is observed to be in excellent agreement with the Abaqus S4R shell solution. The omission of shear deformation effects in the other two solutions (either fully in the Vlasov theory or partially in the Abaqus B31OS) results in some discrepancy in the predicted displacement response. This was observed to particularly be the case of short beams under harmonic forces.

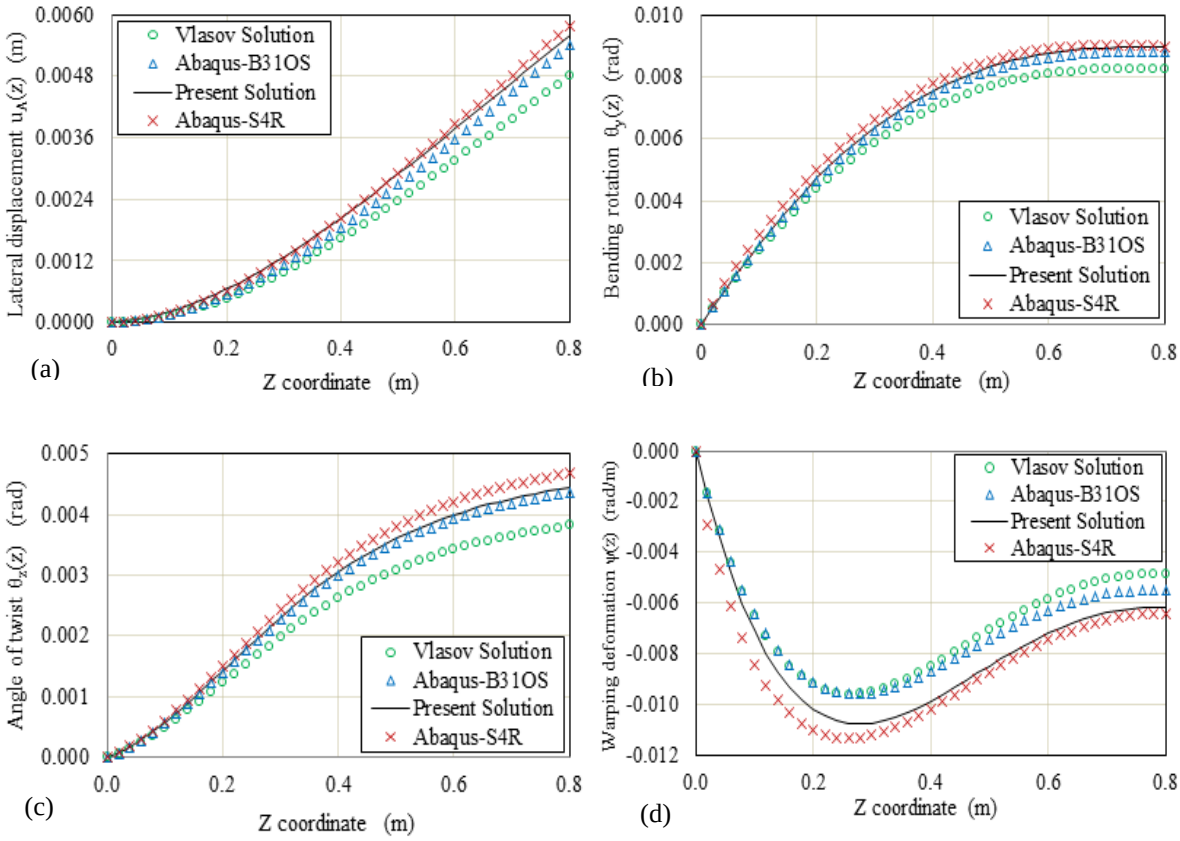

Figure (5.14): Dynamic analysis of short cantilever under harmonic torsion; (a) lateral displacement, (b) bending rotation, (c) twist angle, and (d) warping deformation.

5.6.3 Example 3 – Distortional effects

In order to study the influence of the cross-sectional distortion on the static and steady state dynamic responses, a 1.0m cantilever thin-walled beam with monosymmetric channel cross-section as illustrated in Figure (5.15) is analyzed. The cantilever is subjected to transverse harmonic force $P_y = 40.0e^{i\Omega t}kN$ acting at the corner point A at the tip. Two values of exciting frequencies $\Omega = 0.001\bar{\omega}_1$ and $\Omega \approx 1.803\bar{\omega}_1$ are considered to investigate the quasi-static response and steady state response, respectively, where the first transverse-torsional natural frequency for the cantilever channel-section is $\bar{\omega}_1 = 77.65Hz$.

The dimensions of the channel section are $t_f = 12mm$, $t_w = 8mm$, $b = 80mm$ and $H = 200mm$. The coordinates of the centroid are $C_x = 21.82mm$, $C_y = 100mm$ and the coordinate of the shear centre along the axis of symmetry is $x_s = -53.12mm$. The section properties are provided in Table (5.6).

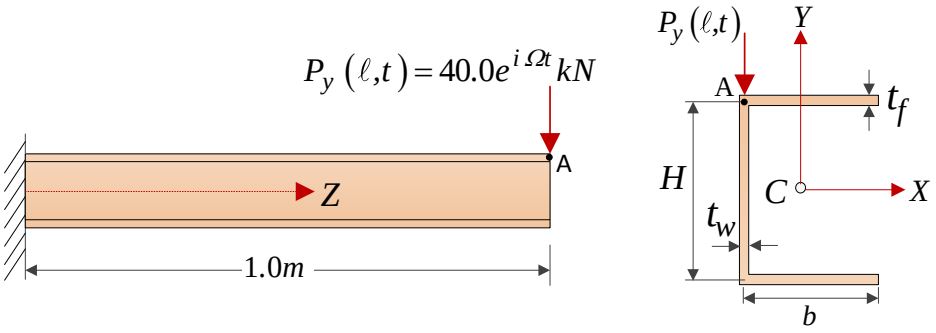

Figure (5.15): Cantilever monosymmetric C-section under transverse harmonic load

Table (5.6): Sectional properties for monosymmetric Channel-section

$A = 35.2\times10^{6}\,mm^{2}$	$J = 0.1263\times10^{6}\,mm^{4}$	$D_{yy} = 0.16\times10^{4}\,mm^{2}$
$I_{xx} = 24.53\times10^{6}\,mm^{4}$	$C_w = 16.92\times10^{9}\,mm^{6}$	$D_{hy} = 5.10\times10^{4}\,mm^{3}$
$I_{yy} = 2.420\times10^{6}\,mm^{4}$	$D_{xx} = 0.192\times10^{4}\,mm^{2}$	$D_{\omega\omega} = 20.77\times10^{6}\,mm^{4}$

The static and dynamic results for coupled transverse-torsional dynamic response, i.e., the transverse displacement $\bar{v}_A(z)$, bending rotation $\bar{\theta}_x(z)$, twist angle $\bar{\theta}_z(z)$ and warping deformation $\bar{\psi}(z)$, computed by the present solution are compared with the Abaqus beam and shell element solutions. In the Abaqus shell model, the cantilever beam of 1.0m span is subdivided into 50 shell elements along the longitudinal direction, 5 elements per flange and 10 elements along the web height. Thus a total of 1,000 shell S4R elements are used to conduct the analysis (Fig. 5.16). In the Abaqus beam element model, a total of 100 beam B31OS element is used.

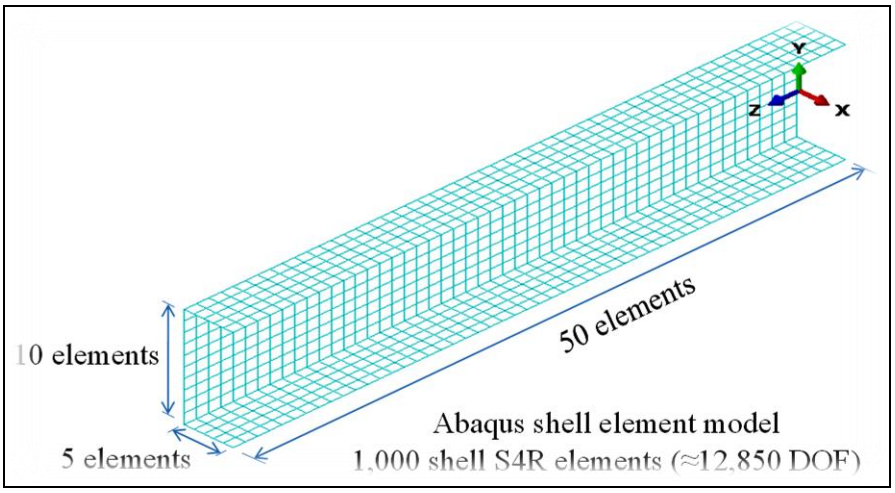

Figure (5.16): Abaqus shell element model for monosymmetric C-section

5.6.3.1 Static Analysis

The static response results based on an exciting frequency ratio $\Omega/\bar{\omega}_1 = 0.001$ are provided in Table (5.7). Results based on the present closed-form and finite element solutions based on a single beam element with four degrees of freedom per node, are in excellent agreements with those obtained by Abaqus B31OS-beam model but slightly differ from those based on Abaqus S4R shell element due to distortional effects of the cross-section (Figure 5.17) that are captured in shell element solution but not in other beam solutions. The results for transverse displacement, related rotation and angle of twist based on Abaqus shell element are 6.95%, 2.42% and 4.24% higher than those obtained by the present study, while the percentage difference in the warping deformation caused by distortional effects of the cross-section is 16.43%.

Table (5.7): Static Analysis of Cantilever C-beam under end transverse harmonic load

Variable	Abaqus S4R [1] (≈12,850 DOF)	Present Solutions [2] (8DOF)	Abaqus B31OS [3] (700DOF)	Present Difference =[1-2]/1	B31OS Difference =[1-3]/1
$\bar{v}_{A_{\max}}$ (10^{-3} m)	-5.221	-4.858	-4.706	6.95%	9.86%
$\bar{\theta}_{x\max}$ (10^{-3} rad)	4.177	4.076	4.076	2.42%	2.42%
$\bar{\theta}_{z\max}$ (10^{-3} rad)	-59.88	-57.61	-57.34	3.79%	4.24%
$\bar{\psi}_{\max}$ (10^{-6} rad/m)	99.78	83.39	83.70	16.43%	16.12%

In order to demonstrate the cross-sectional distortion of the beam, Figure (5.17) illustrates the cross-sectional distortion deformation for static response. A comparison with the Abaqus shell is also provided in Figure (5.17). It is observed from the Abaqus model deformed configuration depicted in the upper part of the diagram that it exhibits some distortional deformation while in the case of the present solution model depicted in the lower part of the diagram, this deformational effect is not captured.

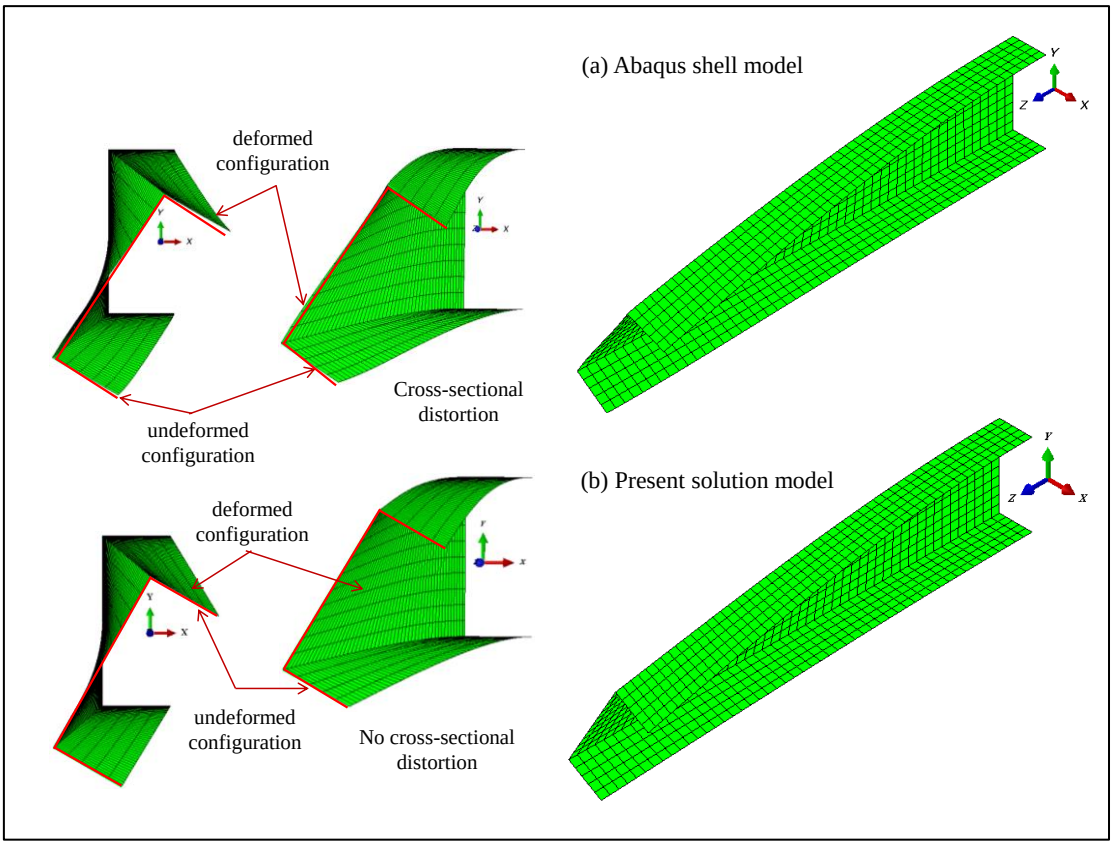

Figure (5.17): Cross-sectional distortion of cantilever monosymmetric channel-section under concentrated transverse harmonic force - Static response

5.6.3.2 Steady State Response

The steady state results are provided in Table (5.8). Excellent agreement is observed based on the formulations developed in the present study with those based on the Abaqus B31OS-beam model. The transverse displacement and associated rotation based on the present solutions agree to a lesser extent with those based on the Abaqus S4R-shell solution which is 4.18% higher than those based on the present solution.

Table (5.8): Steady state response of monosymmetric cantilever under transverse load

Variable	Abaqus S4R [1] (≈12,850 DOF)	Present Solutions [2] (8DOF)	Abaqus B31OS [3] (700DOF)	Present Difference =[1-2]/1	B31OS Difference =[1-3]/1
$\bar{v}_{A_{max}}$ (10^{-3} m)	-1.752	-1.606	-1.575	8.33%	10.10%
$\bar{\theta}_{x\,max}$ (10^{-3} rad)	4.317	4.219	4.100	2.27%	5.03%
$\bar{\theta}_{z\,max}$ (10^{-3} rad)	52.83	50.78	50.40	3.88%	4.60%
$\bar{\psi}_{max}$ (10^{-6} rad/m)	-51.01	-48.88	-43.19	4.18%	15.33%

Again, the difference is attributed to distortional effects (Figure 5.18).

Tables (5.7) and (5.8) suggest that distortional effects for transverse-torsional coupled deformation in static response are more significant than for the case of dynamic response.

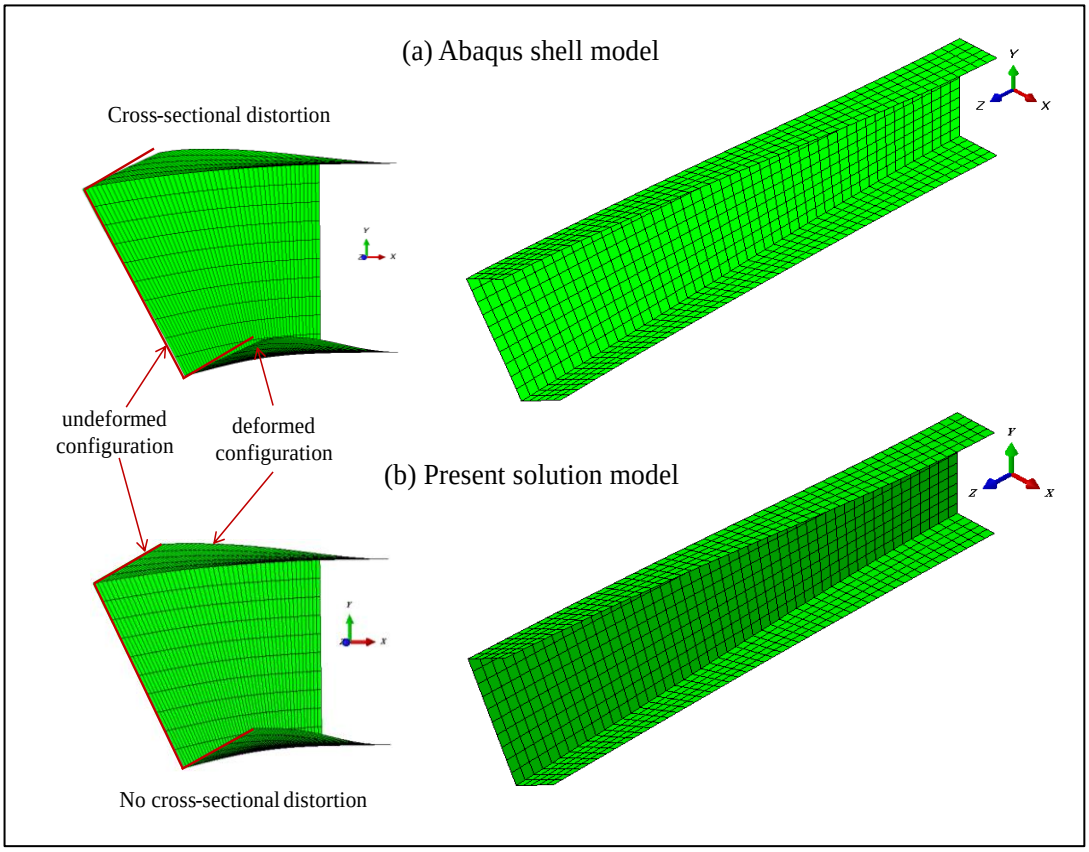

Figure (5.18): Cross-sectional distortion of cantilever monosymmetric C-section under concentrated transverse harmonic force – dynamic response

5.6.5 Example 5 – Three-span continuous beam

A three-span continuous beam with channel-section subjected to three harmonic forces; distributed transverse force $q_y\left(z,t\right)=8.0e^{i\Omega t}kN/m$, concentrated twisting moment $M_z\left(6m,t\right)=15.4e^{i\Omega t}kNm$ and concentrated transverse force $P_y\left(10m,t\right)=16.0e^{i\Omega t}kN$ and is considered as shown in Figure (5.19).

The dimensions of the channel section the cross-sectional properties are: flange thickness $t_f=20mm$, web thickness $t_w=12mm$, flange width $b=80mm$, middle surface height $H=200mm$, coordinate of shear centre along axis of symmetry $x_s=-54.86mm$,

coordinates of centroid along the principle axes $C_x = 22.86mm$, $C_y = 100mm$, while the C-section properties are: $A = 0.56\times10^4 mm^2$, $I_{xx} = 40.0\times10^6 mm^4$, $I_{yy} = 3.90\times10^6 mm^4$, $J = 0.54\times10^6 mm^4$, $C_w = 27.31\times10^9 mm^9$, $D_{xx} = 0.32\times10^4 mm^2$, $D_{yy} = 0.24\times10^4 mm^2$, $D_{hy} = 76.60\times10^3 mm^3$ and $D_{\omega\omega} = 34.46\times10^6 mm^4$.

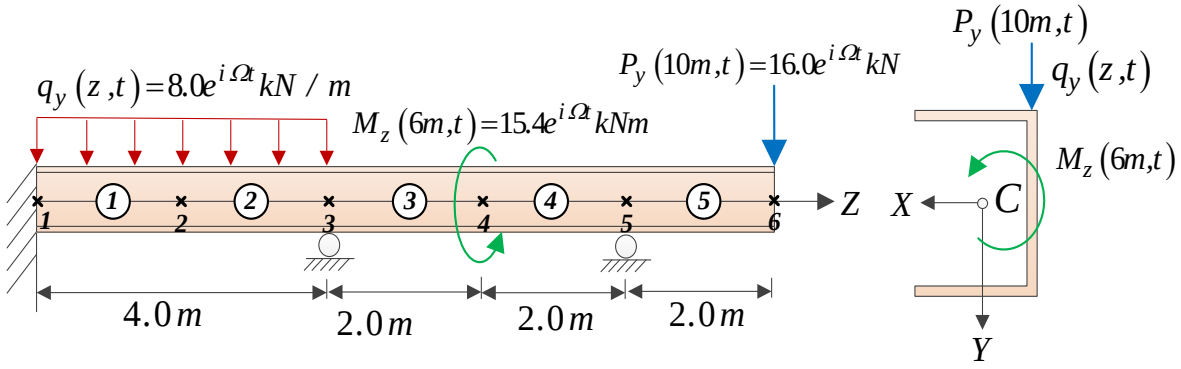

Figure (5.19): Continuous beam with channel-section under harmonic forces

The exciting frequency is assumed to take two values $\Omega = 0.001\bar{\omega}_1$ (quasi-static) and $\Omega = 2.38\bar{\omega}_1$, where the first natural frequency for the three-span continuous beam is $\bar{\omega}_1 \approx 58.06 rad/\sec$ in the present problem. It is required to compare the static and steady state dynamic responses based on the finite element with the beam solution.

In order to demonstrate the validity and capability of the present finite element that captures the shear deformation effects, the nodal degrees of freedom results for static response (SR) and steady state dynamic response (SSR) are obtained and compared against the results based on established finite element Abaqus. Under the present finite element solution, five elements with twenty degrees of freedom are used while in Abaqus analysis, the model is consisted of one-hundred beam B31OS elements with seven-hundred degrees of freedom along the beam axis.

This example is presented in order to demonstrate the capability and the accuracy of the present finite element formulation that captures the shear deformation effects due to bending and warping. The transverse displacement $\bar{v}(z)$, relevant rotation $\bar{\theta}_x(z)$, twist angle $\bar{\theta}_z(z)$ and warping deformation function $\bar{\psi}(z)$ are plotted against the coordinate axis z as shown in Figures (5.20a-d), in which the static response (SR) is captured by

using a very low exciting frequency compared to the first natural frequency, i.e., $\Omega \approx 0.001\bar{\omega}_1$, and the steady state response (SSR) is given for exciting frequency $\Omega = 2.38\bar{\omega}_1$. It is observed that the developed finite element formulation results based on five elements shows excellent agreement with those based on the Abaqus solution using one-hundred beam elements.

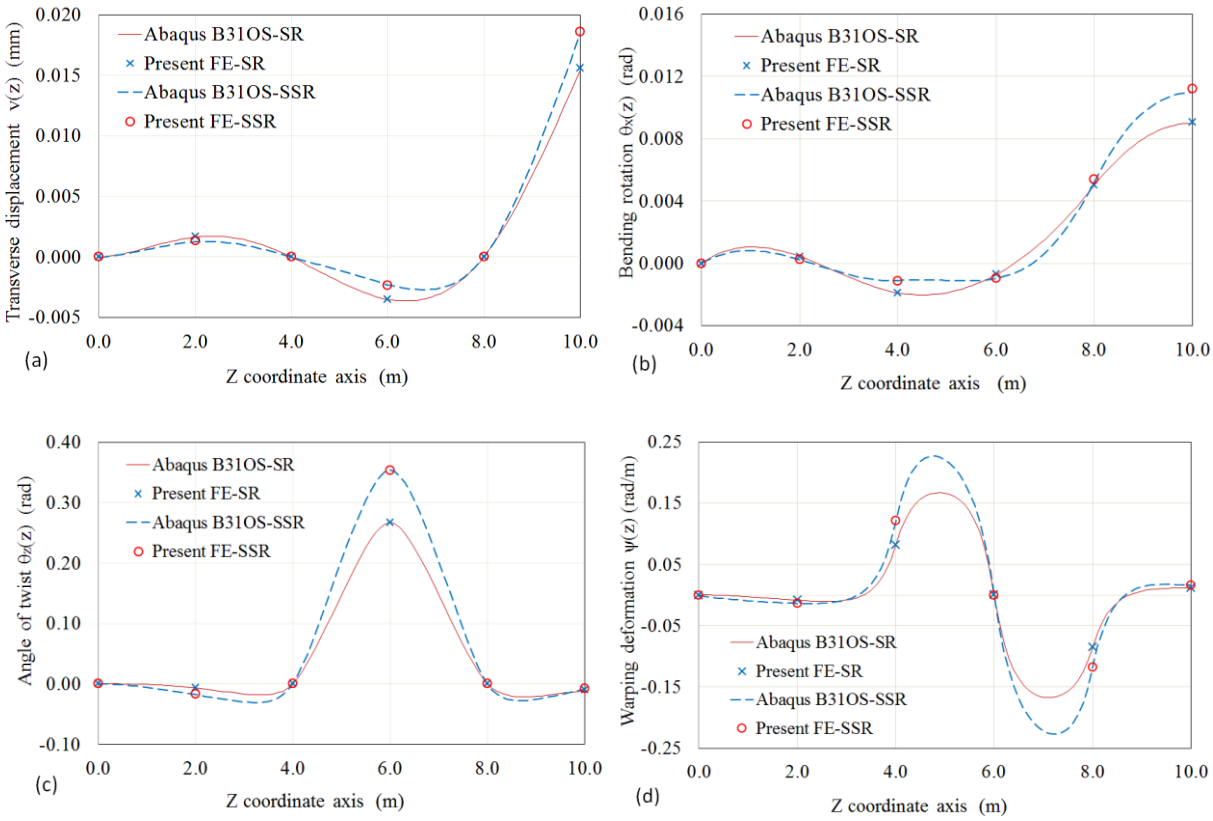

Figure (5.20): Static and Steady state dynamic analysis of three-span channel-shaped beam under harmonic forces

5.7 Summary and Conclusions

The main conclusions provided from this chapter can be summarized as follows:

1. A super-convergent finite element formulation has been developed for beams with monosymmetric sections. The element is based on shape functions which exactly satisfy the homogeneous form of the equilibrium equations and thus eliminates the discretization errors encountered under other interpolation schemes. The solution captures shear deformation effects, warping, translational and rotary inertial effects.

2. The solution is able to efficiently capture the static and steady state response of beams under harmonic loads. The steady state response is obtained without the need to extract the eigen-modes. The solution is also able to capture the eigen-frequencies and eigen-modes, when needed.
3. The formulation successfully captures the coupled lateral-torsional response of monosymmetric cross-sections.
4. It was shown that shear deformation effects are influential when predicting the response of short span cantilevers. They were also found to be important when predicting the response under steady state analyses.
5. The solution provides excellent agreement with shell finite elements at a fraction of the computational and modeling cost.
6. The finite element provides superior response predictions to Abaqus B31OS and Vlasov solution with a significantly smaller number of degrees of freedom.

5.8 References

[5.1] Ambrosini, D. (2004), On free vibration of nonsymmetrical thin-walled beams, Thin-Walled Structures, 47(6-7): 629-636.

[5.2] Back, S.Y. and Will, K.M. (1998), A shear-flexible element with warping for thin-walled open beams, Int. J Numerical Methods in Engineering, 43:1173–1191.

[5.3] Banerjee J. R., Guo S. Howson W.P. (1996), Exact dynamic stiffness matrix of a bending–torsion coupled beam including warping, Computers and Structures, 59: 613–621.

[5.4] Bercin, A. N. and Tanaka, M. (1997), Finite element modeling of the coupled bending and torsional free vibration of uniform beams with an arbitrary cross-section, Applied Mathematical Modelling, 21:6: 339-344.

[5.5] Bishop, R. E. et al. (1989), On coupled bending and torsional vibration of uniform beams, Journal of Sound and Vibration, 131 (3): 457-464.

[5.6] Bishop, R. E. and Price, W. G. (1985), A note on the dynamical behavior of uniform beams having open channel section, Journal of Sound and Vibration, 99(2):155-167.

[5.7] Chen, X. and Tamma, K. (1994), Dynamic response of elastic thin-walled structures influenced by coupling effects, Computers and Structures, 51(1): 91-105.

[5.8] Cortinez, V. H. and Piovan, M. T. (2002), Vibration and buckling of composite thin-walled beams with shear deformability, Journal of Sound and Vibration, 258: 701–723.

[5.9] De Bordon, F. and Ambrosini, D. (2010), On free vibration analysis of thin-walled beams axially loaded, Thin-Walled Structures, 48(12): 915-920.

[5.10] Dokumaci, E. (1987), An exact solution for coupled flexural and torsional vibrations of uniform beams having single cross-sectional symmetry, Journal of Sound and Vibration, 119: 443–449.

[5.11] Friberg, P.O. (1985), Beam element matrices derived from Vlasov's theory of open thin-walled elastic beams. International Journal for Numerical Methods in Engineering, 21:1205-28.

[5.12] Hashemi S. M., Richard M. J. (2000a), A Dynamic Finite Element Method for Free Vibrations of Bending-Torsion Coupled Beams, Aerospace Sci. Technology, 4: 41-55.

[5.13] Hashemi S. M., and Richard M. J. (2000b), Free vibrational analysis of axially Bending-Torsion Coupled Beams-A dynamic finite element, Computers and structures, 77: 711-724.

[5.14] Hjaji, M. A. and Mohareb, M. (2011a), Steady state response of doubly symmetric thin-walled members under harmonic excitations- Closed-Form solution, second International Engineering Mechanics and Materials Specialty Conference, Ottawa, Ontario, Canada.

[5.15] Hjaji, M. A. and Mohareb, M. (2011b), Steady state response of doubly symmetric thin-walled members under harmonic excitations–Finite element formulation, second International Engineering Mechanics and Materials Specialty Conference, Ottawa, Ontario, Canada.

[5.16] Hu, Y. et al. (1996), A Finite Element Model for Static and Dynamic Analysis of Thin-walled Beams with Asymmetric Cross-Sections, Computers and Structures, 61: 897-908.

[5.17] Vlasov, V. (1961), Thin-walled elastic beams, second edition, Jerusalem, Israel Prog. for Scientific Translation.

[5.18] Kim, M. et al. (2003), Exact dynamic and static stiffness matrices of shear deformable thin-walled beam-columns, Journal of Sound and Vibration, 267: 29–55.

[5.19] Kim, N. I. and Kim, M. N. (2005), Exact Dynamic/Static Stiffness Matrices of Non-Symmetric Thin-Walled Beams considering coupled shear deformation effects, Thin-walled Structures, 43: 701-734.

[5.20] Kim, N. et al. (2007), Stiffness matrices for flexural-torsional/lateral buckling and vibration analysis of thin-walled beam, Journal of Sound and Vibration, 299: 739-756.

[5.21] Kollar, J. P. (2001), Flexural-torsional vibration of open section composite columns with shear deformation, International Journal of Solids and Structures, 38 (42-43):7543-7558.

[5.22] Laudiero, F. and Savoia, M. (1991), The shear strain influence on the dynamics of thin-walled beams, Thin-walled Structures, 11: 375-407.

[5.23] Leung, A., (1991), Natural shape functions of a compressed Vlasov element, Thin-walled Structures, 11: 431-38.

[5.24] Li, Jun et al. (2004a), Dynamic response of axially loaded monosymmetrical thin-walled Bernoulli-Euler beams, Thin-walled Structures, 42(12): 1689-1707.

[5.25] Li, Jun et al. (2004b), Response of monosymmetric thin-walled Timoshenko beams to random excitations, International Journal of Solids and Structures, 41:6023-40.

[5.26] Li, J, et al. (2004c), Coupled bending and torsional vibration of axially loaded thin-walled Timoshenko beams, Mechanics International Journal of Mechanical Sciences, 46: 299-320.

[5.27] Lee, J. and Kim, S. E. (2002a), Free Vibration of Thin-walled Composite Beams with I-Shaped cross-sections, Composite Structures, 55(2): 205-215.

[5.28] Lee, J. and Kim, S. E. (2002b), Flexural–torsional coupled vibration of thin-walled composite beams with channel sections, Computers and Structures, 80: 133–144.

[5.29] Machado, S. P. (2007), Geometrically non-linear approximations on stability and free vibration of composite beams, Engineering Structures, 29(12): 3567-3578.

[5.30] Machado, S. P. and Cortinez, V. H. (2007), Free vibration of thin-walled composite beams with static initial stresses and deformations, Engineering Structures, 29(3): 372-382.

[5.31] Mei, C., (1970), Coupled vibrations of thin-walled beams of open section using the finite element method, International journal of mechanical science, 12: 883-891.

[5.32] Prokic, A. (2006), On fivefold coupled vibrations of Timoshenko thin-walled beams, Engineering Structures, 28: 54-62.

[5.34] Saad, Y., (1992), Numerical methods for large eigenvalue problems, John Wiley and Sons Inc., New York, USA.

[5.35] Tanaka, M. and Bercin, A.N., (1998), Free vibration solution for uniform beams of nonsymmetrical cross section using Mathematica, Computes and Structures,71:1–8.

[5.36] Voros, G. (2008), On Coupled Vibrations of Beams with Lateral Loads, Journal of computational and Applied Mechanics, 9 (2): 1-14.

[5.37] Voros, G. M. (2009), On Coupled bending-torsional vibrations of beams with initial loads, Mechanics Research Communications, 36: 603-611.

[5.38] Vo, T.P. and Lee, J. (2009), On six-fold coupled buckling of thin-walled composite beams, Composite Structures, 90: 295-303.

[5.39] Vo, T. P. and Lee, J. (2009a), Flexural-torsional coupled vibration and buckling of thin-walled open section composite beams using shear-deformable beam theory, International Journal of Mechanics Sciences, 51: 631-641.

[5.40] Vo, T. P. and Lee, J. (2009b), Free vibration of axially thin-walled composite box beams, Composite Structures, 90: 233-241.

[5.41] Vo, T. P. et al. (2009), On six-fold coupled vibrations of thin-walled composite box beams, Composite Structures, 89: 524-535.

[5.42] Vo, T. P. and Lee, J. (2010a), Interaction curves for vibration and buckling of thin-walled composite box beams under axial loads and end moments, Applied Mathematical Modelling, 34: 3142-3157.

[5.43] Vo, T. P. and Lee, J. (2010b), Free vibration of axially thin-walled composite Timoshenko beams, Archive of Applied Mechanics.

[5.44] Vo, T. P. et al. (2010), On triply coupled vibrations of axially loaded thin-walled composite beams, Computers and Structures, 88(3-4): 144-153.

[5.45] Vo, T. P. et al. (2011), Vibration analysis of thin-walled composite beams with I-shaped cross-sections, Composite Structures, 93(3-4): 812-820.

[5.46] Wu, L. and Mohareb, M. (2011), Buckling of shear deformable thin-walled members–I. Variational principle and analytical solutions, Thin-walled Structures, 49(1): 197-207.

Appendix (5A): Proof that Bending Rotation vanishes for a Cantilever under Concentrated End Forces

When no distributed lateral force $\bar{q}_y$ nor distributed moment $\bar{m}_x$ are applied, the right hand side of the following two static equilibrium equations (Equations 5.12 and 5.13) vanish, i.e.,

$$G\left(D_{yy}\left[\bar{v}'(z)-\bar{\theta}_x(z)\right]-D_{hy}\left[\bar{\theta}_z'(z)+\bar{\psi}(z)\right]\right)'=0 \tag{5A.1}$$

$$EI_{xx}\,\bar{\theta}_x''(z)+G\left(D_{yy}\left[\bar{v}'(z)-\bar{\theta}_x(z)\right]+D_{hy}\left[\bar{\theta}_z'(z)+\bar{\psi}(z)\right]\right)=0 \tag{5A.2}$$

Subject to the relevant boundary conditions

$$\left(GD_{yy}\left[\bar{v}'(z)-\bar{\theta}_x(z)\right]+GD_{hy}\left[\bar{\theta}_z'(z)+\bar{\psi}(z)\right]-\bar{V}_y(z)\right)\delta\bar{v}(z)\Big|_0^{\ell}=0 \tag{5A.3}$$

$$\left[EI_{xx}\,\bar{\theta}_x'(z)-\bar{M}_x(z)\right]\delta\bar{\theta}_x(z)\Big|_0^{\ell}=0 \tag{5A.4}$$

For simplicity, the bracket in Equation (5A.1), $G\left(D_{yy}\left[\bar{v}'(z)-\bar{\theta}_x(z)\right]-D_{hy}\left[\bar{\theta}_z'(z)+\bar{\psi}(z)\right]\right)$ can be written as $\zeta(z)$, which allowing to re-write the simplified equation (5A.1) as:

$$\zeta'(z)=0 \quad \text{gives} \quad \zeta(z)=C_1 \tag{5A.5}$$

Then, Equation (5A.2) is written as:

$$EI_{xx}\,\bar{\theta}_x''(z)+\zeta(z)=0 \tag{5A.6}$$

For the cantilever problem with no external forces, at the cantilever root ($z=0$):

$$\bar{v}(0)=0 \quad \text{and} \quad \bar{\theta}_x(0)=0 \tag{5A.7}$$

and at the cantilever tip ($z=\ell$), noting that no external bending moments nor shears are applied, one has:

$$\left(GD_{yy}\left[\bar{v}'(\ell)-\bar{\theta}_x(\ell)\right]+GD_{hy}\left[\bar{\theta}_z'(\ell)+\bar{\psi}(\ell)\right]\right)=0 \tag{5A.8}$$

$$EI_{xx}\,\bar{\theta}_x'(\ell)=0 \tag{5A.9}$$

From Equation (5A.8), the above equation can be written simply as:

$$\zeta(\ell)=0 \tag{5A.10}$$

From Equation (5A.5), one can conclude that:

$$\zeta(z)=\zeta(\ell)=\boxed{C_1=0} \tag{5A.11}$$

Now integrating Equation (5A.6) to have:

$$\bar{\theta}_x(z) = C_2 z + C_3 \tag{5A.12}$$

Enforcing the boundary condition in Equation (5A.7)

$$\bar{\theta}_x(0) = C_2(0) + C_3 = 0 \quad \Rightarrow \quad \boxed{C_3 = 0} \tag{5A.13}$$

Enforcing the boundary condition in Equation (5A.9):

$$\bar{\theta}'_x(\ell) = C_2 \ell = 0 \;\Rightarrow\; \boxed{C_2 = 0} \tag{5A.14}$$

In summary, by substituting Equations (5A.13) and (5A.14) into Eq. (5A.12), leads to:

$$\boxed{\bar{\theta}_x(z) = 0} \tag{5A.15}$$

Equation (5A.15) shows that in the case of quasi-static response, the bending rotation for a cantilever beam with no external forces is vanished. This leads to conclude that the coupling terms are weak in quasi-static response of the cantilever monosymmetric beam.

Appendix (5B): Section properties for monosymmetric I-section

The section properties D_{xx} ,D_{yy} ,D_{xy} ,D_{hx} ,D_{hy} and $D_{\omega\omega}$ for mono-symmetric I-section are obtained as:

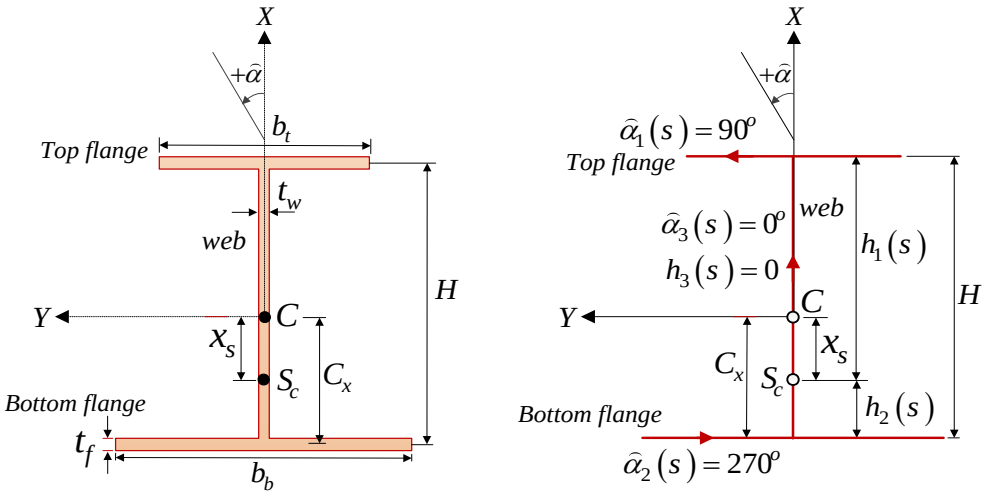

Figure (5B): Mono-symmetric I-section

From Figure (5B), it can be illustrated that, the angles between the X axis and the mid-surface at top, bottom flanges and web are $\hat{\alpha}_1(s)=90^o$, $\hat{\alpha}_2(s)=270^o$ and $\hat{\alpha}_3(s)=0^o$, while the distances from the shear centre to the mid-surfaces of upper, bottom flanges and web are $h_1(s)=(H-C_x)-x_s$, $h_2(s)=-(C_x+x_s)$ and $h_3(s)=0$. Then, one obtains

$$D_{xx}=\sum_{i=1}^{3}\int_{A_i}\left[\cos\hat{\alpha}_i(s)\right]^2 dA_i=A_w \tag{5B.1}$$

$$D_{yy}=\sum_{i=1}^{3}\int_{A_i}\left[\sin\hat{\alpha}_i(s)\right]^2 dA_i=A_{tf}+A_{bf}=A_f \tag{5B.2}$$

$$D_{xy}=\sum_{i=1}^{3}\int_{A_i}\cos\hat{\alpha}_i(s)\sin\hat{\alpha}_i(s)\,dA_i=0 \tag{5B.3}$$

$$D_{hx}=\sum_{i=1}^{3}\int_{A_i}h_i(s)\cos\hat{\alpha}_i(s)\,dA_i=0 \tag{5B.4}$$

$$D_{hy}=\sum_{i=1}^{3}\int_{A_i}h_i(s)\sin\hat{\alpha}_i(s)\,dA_i=HA_{tf}-(C_x+x_s)(A_{tf}-A_b) \tag{5B.5}$$

$$D_{\omega\omega}=\sum_{i=1}^{3}\int_{A_i}\left[h_i(s)\right]^2 dA_i=\left[(H-C_x)-x_s\right]^2+(C_x+x_s)^2 \tag{5B.6}$$

in which $A_f=A_{tf}+A_{bf}$ is the area of the two flanges, where $A_{tf}=b_t t_f$ is the area of the top flange, $A_{bf}=b_b t_f$ is the area of the bottom flange, and $A_w=Ht_w$ is the web area.

Appendix (5C): Closed Form Solution of Coupled Transverse-Torsional Equations for Monosymmetric Thin-walled Vlasov Beam

5C.1 General

This appendix formulates the general closed-form solutions for thin-walled Vlasov beams of monosymmetric cross-sections subjected to general harmonic forces. Based on the Vlasov beam theory in which the shear deformation is not captured, the coupled field equations presented by equations (3.43) to (3.46) in Chapter 3 (Section 3.7.1) for asymmetric cross-sections are simplified by setting $y_s = 0$ (i.e., X is the axis of symmetry) to govern the coupling transverse-torsional response of thin-walled monosymmetric sections as:

$$EI_{xx}v^{iv} - \rho I_{xx}\ddot{v}'' + \rho A\left(\ddot{v} - x_s\ddot{\phi}\right) = q_y(z,t) \tag{5C.1}$$

$$EC_w\phi^{iv} - \rho C_w\ddot{\phi}'' - GJ\phi'' - \rho A\left(x_s\ddot{v} - r_o^2\ddot{\phi}\right) = m_z(z,t) \tag{5C.2}$$

The associated boundary conditions are:

$$\left[EI_{xx}v''' - V_y(z,t)\right]\delta v(z,t)\Big|_0^\ell = 0 \tag{5C.3}$$

$$\left[EC_w\phi''' - GJ\phi' - M_z(z,t)\right]\delta\phi(z,t)\Big|_0^\ell = 0 \tag{5C.4}$$

$$\left[EI_{xx}v'' - M_x(z,t)\right]\delta v'(z,t)\Big|_0^\ell = 0 \tag{5C.5}$$

$$\left[EC_w\phi'' - M_w(z,t)\right]\delta\phi'(z,t)\Big|_0^\ell = 0 \tag{5C.6}$$

5C.2 Field Equations for Harmonic Loading

The member is assumed to be subjected to applied harmonic forces within the member

$$\left[q_y(z,t), m_z(z,t)\right] = \left[\bar{q}_y(z), \bar{m}_z(z)\right]e^{i\Omega t} \tag{5C.7}$$

and the end harmonic forces

$$\left[V_y(z,t), M_z(z,t), M_w(z,t)\right] = \left[\bar{V}_y(z), \bar{M}_z(z), \bar{M}_w(z)\right]e^{i\Omega t} \tag{5C.8}$$

where Ω is the circular frequency of the applied forces, $i = \sqrt{-1}$ is the imaginary constant, $q_y(z,t)$ is the distributed transverse harmonic force, $m_z(z,t)$ is the distributed harmonic twisting moment, $V_y(z,t)$ is the concentrated transverse harmonic force,

$M_z(z,t)$ is the concentrated harmonic twisting moment and $M_w(z,t)$ is the concentrated harmonic bimoment.

Under the above applied harmonic forces, the steady state components $v(z,t)$ and $\phi(z,t)$ of the response are assumed to take the form:

$$\left[v(z,t),\phi(z,t)\right]=\left[\bar{v}(z),\bar{\phi}(z)\right]e^{i\Omega t} \tag{5C.9}$$

where $\bar{v}(z)$ and $\bar{\phi}(z)$ are unknown space functions for transverse deflection and torsional rotation, respectively. By substituting the displacement and forces expressions presented by equations (5C.7) to (5C.9) into the governing differential equations (5C.1) and (5C.2) and boundary conditions (5C.3) to (5C.6), yields:

$$EI_{xx}\bar{v}^{iv}+\rho I_{xx}\Omega^2\bar{v}''-\rho A\Omega^2\bar{v}+\rho Ax_s\Omega^2\bar{\phi}=\bar{q}_y(z) \tag{5C.10}$$

$$\rho Ax_s\Omega^2\bar{v}+EC_w\bar{\phi}^{iv}+\left(\rho C_w\Omega^2-GJ\right)\bar{\phi}''+\rho Ar_o^2\Omega^2\bar{\phi}=\bar{m}_z(z) \tag{5C.11}$$

the relevant boundary conditions are:

$$\left[EI_{xx}\bar{v}'''-\bar{V}_y(z)\right]\delta\bar{v}(z)\Big|_0^\ell=0 \tag{5C.12}$$

$$\left[EC_w\bar{\phi}'''-GJ\bar{\phi}'-\bar{M}_z(z)\right]\delta\bar{\phi}(z)\Big|_0^\ell=0 \tag{5C.13}$$

$$\left[EI_{xx}\bar{v}''-\bar{M}_x(z)\right]\delta\bar{v}'(z)\Big|_0^\ell=0 \tag{5C.14}$$

$$\left[EC_w\bar{\phi}''-\bar{M}_w(z)\right]\delta\bar{\phi}'(z)\Big|_0^\ell=0 \tag{5C.15}$$

5C.3 Homogeneous Solution of Field Equations

The solution of the homogeneous part of the governing coupled transverse-torsional equations is obtained by setting the right hand of the differential equations (5C.10) and (5C.11) to zero, i.e., $q_y(z,t)=m_z(z,t)=0$. The homogeneous solution of the unknown space displacement functions $\left\langle\bar{V}(z)\right\rangle_{1\times2}^T=\left\langle\bar{v}(z)\quad\bar{\phi}(z)\right\rangle_{1\times2}^T$ is assumed to take the following form:

$$\left\langle\bar{V}(z)\right\rangle_{1\times2}^T=\left\langle A_i\right\rangle_{1\times2}^T e^{m_i z}\text{, for } i=1,2 \tag{5.C16}$$

in which $\left\langle A_i\right\rangle_{1\times2}^T=\left\langle A_1\quad A_2\right\rangle_{1\times2}^T$.

Substituting the space displacement functions in (5C.16) into equations (5C.10) and (5C.11), one obtains:

$$\begin{bmatrix} \left(EI_{xx}\, m_i^4 + \rho\Omega^2 I_{xx}\, m_i^2 - \rho\Omega^2 A\right) & \rho A\Omega^2 x_s \\ \rho A\Omega^2 x_s & \left(EC_w\, m_i^4 - GJm_i^2 + \rho A\Omega^2 r_o^2\right) \end{bmatrix}_{2\times 2} \begin{bmatrix} e^{m_i z} & 0 \\ 0 & e^{m_i z} \end{bmatrix}_{2\times 2} \begin{Bmatrix} A_1 \\ A_2 \end{Bmatrix}_{2\times 1} = \{0\}_{2\times 1} \tag{5C.17}$$

The non-trivial solution of equation (5C.17) can be obtained by setting the determinant of the unknown amplitude coefficients A_1 and A_2 to zero, yielding

$$m_i^8 + q_1 m_i^6 + q_2 m_i^4 + q_3 m_i^2 + q_4 = 0 \tag{5C.18}$$

where $q_1 = \dfrac{1}{EC_w}\left[\rho\Omega^2 C_w - GJ\right]$, $q_2 = \dfrac{\rho\Omega^2}{E^2 I_{xx} C_w}\left[EA\left(I_{xx} r_o^2 - C_w\right) - GJI_{xx}\right]$,

$q_3 = \dfrac{\rho A\Omega^2}{E^2 C_w I_{xx}}\left[\rho\Omega^2 I_{xx} r_o^2 + GJ\right]$, and $q_4 = -\dfrac{-\rho^2 A^2 \Omega^4}{E^2 C_w I_{xx}}\left[r_o^2 + x_s^2\right]$.

Equation (5C.18) is analytically solved to determine the eight roots m_i (for $i = 1,2,3,....,8$) of the equation. The homogeneous solutions for the transverse displacement $\bar{v}(z)$ and angle of twist $\bar{\phi}(z)$ are:

$$\left\{\bar{V}_h(z)\right\}_{2\times 1} = [A]_{2\times 8}\left\{E(z)\right\}_{8\times 1} \tag{5C.19}$$

where $[A]_{2\times 8} = \left[\begin{array}{c:c:c:c:c:c:c:c} A_{1,1} & A_{1,2} & A_{1,3} & A_{1,4} & A_{1,5} & A_{1,6} & A_{1,7} & A_{1,8} \\ \hdashline A_{2,1} & A_{2,2} & A_{2,3} & A_{2,4} & A_{2,5} & A_{2,6} & A_{2,7} & A_{2,8} \end{array}\right]_{2\times 8}$, and

$$\left\langle E(z)\right\rangle_{1\times 8}^T = \left\langle e^{m_1 z} \;\vdots\; e^{m_2 z} \;\vdots\; e^{m_3 z} \;\vdots\; e^{m_4 z} \;\vdots\; e^{m_5 z} \;\vdots\; e^{m_6 z} \;\vdots\; e^{m_7 z} \;\vdots\; e^{m_8 z}\right\rangle_{1\times 8}^T.$$

In Equation (5C.19), 16 integration constants appear in the homogenous solution of $\bar{v}_h(z)$ and $\bar{\phi}_h(z)$, namely $A_{1,i}$ and $A_{2,i}$ for $i = 1,2,3,....,8$, but only eight boundary conditions are provided in Equations (5C.12) to (5C.15). It is thus necessary to reduce the two sets of unknown integration constants $A_{1,i}$ and $A_{2,i}$ to eight independent boundary conditions by writing one set of constants in terms of the constants of the other set

Substituting displacement functions in equation (5C.12) into the homogeneous form of equation (5C.10), yields

$$A_{1,i}=\frac{-\rho A x_s \Omega^2}{\left(EI_{xx}\, m_i^4+\rho I_{xx}\,\Omega^2 m_i^2-\rho A\Omega^2\right)}A_{2,i}\ ,\quad \text{for}\ \ i=1,2,3,...,8 \tag{5C.20}$$

By performing a similar substitution into Equation (5C.11) to check the expression obtained for $A_{1,i}$, given by Equation (5C.20). Another expression for $A_{1,i}$ is obtained as:

$$A_{1,i}=\frac{-\left[EC_w\, m_i^2+\left(\rho C_w\,\Omega^2\text{-}GJ\right)m_i^2+\rho A r_o^2\Omega^2\right]}{\rho A x_s\,\Omega^2}A_{2,i}\ ,\ \text{for}\ i=1,2,3,....,8 \tag{5C.21}$$

Thus, both expressions in equations (5C.20) and (5C.21) are valid relationships between $A_{1,i}$ and $A_{2,i}$ for $i=1,2,3,.....,8$, i.e., the two expressions are identical, and

$$\bar{A}_i=\frac{-\rho A x_s\,\Omega^2}{\left(EI_{xx}\, m_i^4+\rho I_{xx}\,\Omega^2 m_i^2-\rho A\Omega^2\right)}=\frac{-\left[EC_w\, m_i^4+\left(\rho C_w\,\Omega^2\text{-}GJ\right)m_i^2+\rho A r_o^2\Omega^2\right]}{\rho A x_s\,\Omega^2} \tag{5C.22}$$

The homogeneous solutions for transverse displacement $\bar{v}_h(z)$ and twist angle $\bar{\phi}_h(z)$ presented in equation (5C.12) are reduced to the following matrix form:

$$\left\{\bar{V}_h(z)\right\}_{2\times1}=\left[\bar{F}\right]_{2\times8}\left[E(z)\right]_{8\times8}\left\{A_{2,i}\right\}_{8\times1} \tag{5C.23}$$

where

$$\left[\bar{F}\right]_{2\times8}=\left[\begin{array}{c|c|c|c|c|c|c|c} \bar{A}_1 & \bar{A}_2 & \bar{A}_3 & \bar{A}_4 & \bar{A}_5 & \bar{A}_6 & \bar{A}_7 & \bar{A}_8 \\ \hline 1 & 1 & 1 & 1 & 1 & 1 & 1 & 1 \end{array}\right],$$

$$\left[E_8(z)\right]_{8\times8}=diag\left[\begin{array}{c|c|c|c|c|c|c|c} e^{m_1 z} & e^{m_2 z} & e^{m_3 z} & e^{m_4 z} & e^{m_5 z} & e^{m_6 z} & e^{m_7 z} & e^{m_8 z} \end{array}\right]_{8\times8}\text{, and}$$

$$\left\langle A_{2,i}\right\rangle_{1\times8}^{\mathrm{T}}=\left\langle\begin{array}{c|c|c|c|c|c|c|c} A_{2,1} & A_{2,2} & A_{2,3} & A_{2,4} & A_{2,5} & A_{2,6} & A_{2,7} & A_{2,8} \end{array}\right\rangle_{1\times8}^{\mathrm{T}}.$$

5C.4 Particular Solution of Field Equations

For constant $\bar{m}_z$ and $\bar{q}_y$, the particular solution for Equations (5C.10) and (5C.11) can be determined by assuming the functions for transverse displacement $\bar{v}_p(z)$ and angle of twist $\bar{\phi}_p(z)$ to take the form

$$\bar{v}_p(z)=C_1+C_2\,z\quad\text{and}\quad\bar{\phi}_p(z)=C_3+C_4\,z \tag{5C.24}$$

Substituting the expressions for $\bar{v}_p(z)$ and $\bar{\phi}_p(z)$ into equations (5C.10) and (5C.11), the unknown constants are obtained as:

$$C_2 = C_4 = 0,\ C_1 = \frac{1}{\rho A \Omega^2 \left(x_s^2 + r_o^2\right)} \left[x_s \bar{m}_z - r_o^2 \bar{q}_y \right], \text{ and}$$

$$C_3 = \frac{1}{\rho A \Omega^2 \left(x_s^2 + r_o^2\right)} \left[\bar{m}_z + x_s \bar{q}_y \right]$$

and as a result, the particular solutions are given as:

$$\left\langle \bar{V}_p \right\rangle_{1\times 2}^{\mathrm{T}} = \left\langle \bar{v}_p \quad \bar{\phi}_p \right\rangle_{1\times 2}^{\mathrm{T}} = \left\langle \frac{x_s \bar{m}_z - r_o^2 \bar{q}_y}{\rho A \Omega^2 \left(x_s^2 + r_o^2\right)} \quad \frac{\bar{m}_z + x_s \bar{q}_y}{\rho A \Omega^2 \left(x_s^2 + r_o^2\right)} \right\rangle_{1\times 2}^{\mathrm{T}} \tag{5C.25}$$

5C.5 General Solution

The complete solution is obtained by adding the homogeneous solution in equation (5C.23) to the particular solution in equation (5C.25), leading to

$$\left\{ \bar{V}(z) \right\}_{2\times 1} = \left[\bar{F} \right]_{2\times 8} \left[E(z) \right]_{8\times 8} \left\{ A_{2,i} \right\}_{8\times 1} + \left\{ \bar{V}_p(z) \right\}_{2\times 1} \tag{5C.26}$$

Equation (5C.26) represents the complete steady state solution of coupled transverse-torsional vibration for thin-walled member of monosymmetric sections under harmonic forces, in which the related boundary conditions are used to obtain the of unknown constants $\left\{ A_{2,i} \right\}_{8\times 1}$.

5C.6 Example 1: Cantilever under Member and End Forces

A cantilever beam with monosymmetric cross-section subjected to concentrated or distributed harmonic forces; concentrated transverse force $\bar{P}_y(\ell)e^{i\Omega t}$, bending moment $\bar{M}_x(\ell)e^{i\Omega t}$, twisting moment $\bar{M}_z(\ell)e^{i\Omega t}$ and bimoment $\bar{M}_w(\ell)e^{i\Omega t}$ applied at the beam free end, uniformly distributed transverse force $\bar{q}_y(z)e^{i\Omega t}$ and twisting moment $\bar{m}_z(z)e^{i\Omega t}$ is considered for analysis as shown in Figure (5C.1).

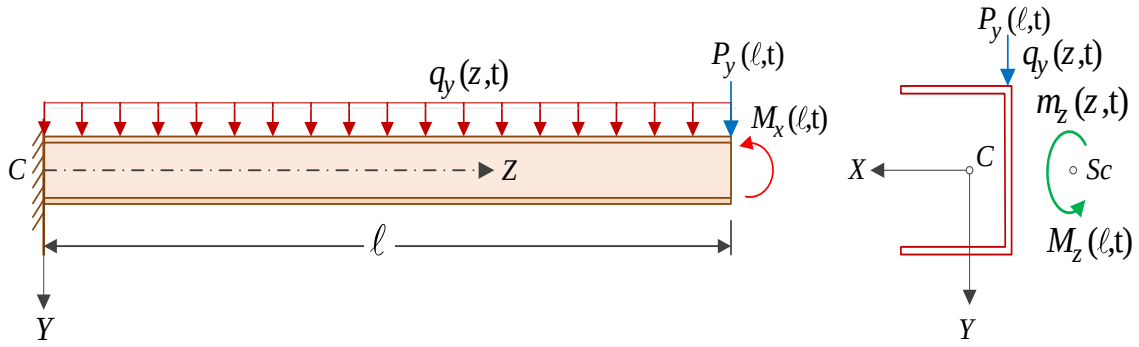

Figure (5C.1): Cantilever beam of monosymmetric C-section under harmonic forces

The cantilever boundary conditions at the fixed end $z=0$ are

$$\delta\bar{v}(0)=\delta\bar{\phi}(0)=\delta\bar{v}'(0)=\delta\bar{\phi}'(0)=0 \qquad (5C.27\text{-}30)$$

At the free end of the beam $z=\ell$, the boundary conditions are

$$EI_{xx}\bar{v}'''(\ell)=\bar{P}_y(\ell) \qquad (5C.31)$$

$$EC_w\bar{\phi}'''(\ell)-GJ\bar{\phi}'(\ell)=\bar{M}_z(\ell) \qquad (5C.32)$$

$$EI_{xx}\bar{v}''(\ell)=\bar{M}_x(\ell) \qquad (5C.33)$$

$$EC_w\bar{\phi}''(\ell)=\bar{M}_w(\ell) \qquad (5C.34)$$

Substituting the expressions for displacement functions presented in equations (5C.26) into above boundary conditions (5C.27) to (5C.30), one obtains:

$$\{\bar{V}_c(z)\}_{2\times1}=[\bar{F}]_{2\times8}[E(z)]_{8\times8}[\bar{\Phi}_c(z)]^{-1}_{8\times8}\{\bar{Q}_c\}_{8\times1}+\{\bar{V}_p(z)\}_{2\times1} \qquad (5C.35)$$

where $[\bar{\Phi}_c]_{8\times8}=$

$$\begin{bmatrix}
\bar{A}_1 & \bar{A}_2 & \bar{A}_3 & \bar{A}_4 & \bar{A}_5 & \bar{A}_6 & \bar{A}_7 & \bar{A}_8 \\
1 & 1 & 1 & 1 & 1 & 1 & 1 & 1 \\
m_1\bar{A}_1 & m_2\bar{A}_2 & m_3\bar{A}_3 & m_4\bar{A}_4 & m_5\bar{A}_5 & m_6\bar{A}_6 & m_7\bar{A}_7 & m_8\bar{A}_8 \\
m_1 & m_2 & m_3 & m_4 & m_5 & m_6 & m_7 & m_8 \\
G_{1,1} & G_{1,2} & G_{1,3} & G_{1,4} & G_{1,5} & G_{1,6} & G_{1,7} & G_{1,8} \\
G_{2,1} & G_{2,2} & G_{2,3} & G_{2,4} & G_{2,5} & G_{2,6} & G_{2,7} & G_{2,8} \\
G_{3,1} & G_{3,2} & G_{3,3} & G_{3,4} & G_{3,5} & G_{3,6} & G_{3,7} & G_{3,8} \\
G_{4,1} & G_{4,2} & G_{4,3} & G_{4,4} & G_{4,5} & G_{4,6} & G_{4,7} & G_{4,8}
\end{bmatrix}_{8\times8}$$

$$\left\{\bar{Q}_c\right\}_{8\times1}=\begin{Bmatrix}\left[r_o^2\bar{q}_y-x_s\bar{m}_z\right]\Big/\rho A\Omega^2\left(x_s^2+r_o^2\right)\\ -\left[\bar{m}_z+x_s\bar{q}_y\right]\Big/\rho A\Omega^2\left(x_s^2+r_o^2\right)\\ 0\\ 0\\ \bar{P}_y(\ell)/EI_{xx}\\ \bar{M}_z(\ell)/EC_w\\ \bar{M}_x(\ell)/EI_{xx}\\ \bar{M}_w(\ell)/EC_w\end{Bmatrix}_{8\times1},\quad G_{1,i}=\bar{A}_i m_i^3 e^{m_i\ell},$$

$G_{2,i}=\left[m_i^2-\left(\dfrac{GJ}{EC_w}\right)\right]m_i e^{m_i\ell}$, $G_{3,i}=\bar{A}_i m_i^2 e^{m_i\ell}$ and $G_{4,i}=m_i^2 e^{m_i\ell}$, for $i=1,2,3,...,8$.

5C.7 Example 2: Simply-supported under member and end forces

Consider a simply-supported beam with monosymmetric cross-section under distributed harmonic forces; transverse force $q_y(z,t)=\bar{q}_y e^{i\Omega t}$, bending moment $m_x(z,t)=\bar{m}_x e^{i\Omega t}$ and twisting moment $m_z(z,t)=\bar{m}_z e^{i\Omega t}$, and concentrated bending moment $M_x(z_e,t)=\bar{M}_x e^{i\Omega t}$ and bimoment $M_w(z_e,t)=\bar{M}_w e^{i\Omega t}$ applied at both ends $(z_e=0,\ell)$ as illustrated Figure (5C.2). The fork end supports allow the end-sections free to warp and rotate about X and Y axes.

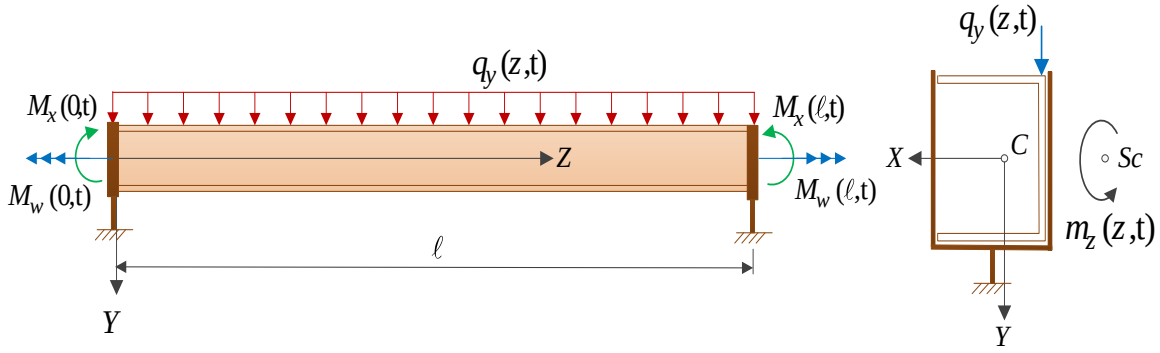

Figure (5C.2): Cantilever beam of monosymmetric C-section under harmonic forces

The boundary conditions at both ends $z=0$ and $z=\ell$ are

$$\delta\bar{v}(0)=\delta\bar{\phi}(0)=0 \qquad \text{(5C.36-37)}$$

$$\delta\bar{v}''(0)=-\bar{M}_x(0)/EI_{xx} \qquad \text{(5C.38)}$$

$$\delta\bar{\phi}''(0)=-\bar{M}_w(0)/EC_w \qquad \text{(5C.39)}$$

$$\delta\bar{v}(\ell)=\delta\bar{\phi}(\ell)=0 \qquad \text{(5C.40-41)}$$

$$\delta\bar{v}''(\ell)=\bar{M}_x(\ell)/EI_{xx} \qquad \text{(5C.42)}$$

$$\delta\bar{\phi}''(\ell)=\bar{M}_w(\ell)/EC_w \qquad \text{(5C.43)}$$

Then, the general closed-form solution is then

$$\{\bar{V}_s(z)\}_{2\times1}=[\bar{F}]_{2\times8}[E(z)]_{8\times8}[\bar{\Phi}_s(z)]^{-1}_{8\times8}\{\bar{Q}_s\}_{8\times1}+\{\bar{V}_p(z)\}_{2\times1} \qquad \text{(5C.44)}$$

in which the unknown integration constants $\{A_{2,i}\}_{8\times1}$ are obtained from the above boundary conditions (5C.36) to (5C.43). In Equation (5C.44), one has

$$\left[\bar{\Phi}_s\right]_{8\times 8} =$$

$$\begin{bmatrix}
\bar{A}_1 & \bar{A}_2 & \bar{A}_3 & \bar{A}_4 & \bar{A}_5 & \bar{A}_6 & \bar{A}_7 & \bar{A}_8 \\
1 & 1 & 1 & 1 & 1 & 1 & 1 & 1 \\
m_1^2\bar{A}_1 & m_2^2\bar{A}_2 & m_3^2\bar{A}_3 & m_4^2\bar{A}_4 & m_5^2\bar{A}_5 & m_6^2\bar{A}_6 & m_7^2\bar{A}_7 & m_8^2\bar{A}_8 \\
m_1^2 & m_2^2 & m_3^2 & m_4^2 & m_5^2 & m_6^2 & m_7^2 & m_8^2 \\
\bar{A}_1 e^{m_1\ell} & \bar{A}_2 e^{m_2\ell} & \bar{A}_3 e^{m_3\ell} & \bar{A}_4 e^{m_4\ell} & \bar{A}_5 e^{m_5\ell} & \bar{A}_6 e^{m_6\ell} & \bar{A}_7 e^{m_7\ell} & \bar{A}_8 e^{m_8\ell} \\
e^{m_1\ell} & e^{m_2\ell} & e^{m_3\ell} & e^{m_4\ell} & e^{m_5\ell} & e^{m_6\ell} & e^{m_7\ell} & e^{m_8\ell} \\
m_1^2\bar{A}_1 e^{m_1\ell} & m_2^2\bar{A}_2 e^{m_2\ell} & m_3^2\bar{A}_3 e^{m_3\ell} & m_4^2\bar{A}_4 e^{m_4\ell} & m_5^2\bar{A}_5 e^{m_5\ell} & m_6^2\bar{A}_6 e^{m_6\ell} & m_7^2\bar{A}_7 e^{m_7\ell} & m_8^2\bar{A}_8 e^{m_8\ell} \\
m_1^2 e^{m_1\ell} & m_2^2 e^{m_2\ell} & m_3^2 e^{m_3\ell} & m_4^2 e^{m_4\ell} & m_5^2 e^{m_5\ell} & m_6^2 e^{m_6\ell} & m_7^2 e^{m_7\ell} & m_8^2 e^{m_8\ell}
\end{bmatrix}_{8\times 8}$$

and

$$\left\{\bar{Q}_s\right\}_{8\times 1} = \begin{Bmatrix}
\left[r_o^2\bar{q}_y - x_s\bar{m}_z\right] \Big/ \rho A\Omega^2\left(x_s^2 + r_o^2\right) \\
-\left[\bar{m}_z + x_s\bar{q}_y\right] \Big/ \rho A\Omega^2\left(x_s^2 + r_o^2\right) \\
-\bar{M}_x(0)/EI_{xx} \\
-\bar{M}_w(0)/EC_w \\
\left[r_o^2\bar{q}_y - x_s\bar{m}_z\right] \Big/ \rho A\Omega^2\left(x_s^2 + r_o^2\right) \\
-\left[\bar{m}_z + x_s\bar{q}_y\right] \Big/ \rho A\Omega^2\left(x_s^2 + r_o^2\right) \\
\bar{M}_x(\ell)/EI_{xx} \\
\bar{M}_w(\ell)/EC_w
\end{Bmatrix}_{8\times 1} .$$

List of Symbols

A	Cross-sectional area
b	Flange width
C	Centroid of the cross-section
C_x, C_y	Coordinates of centroid along the principal X, Y axes
C_w	Warping constant
d	Height of beam cross-section
D_{xx}, D_{yy}, D_{xy} $D_{hx}, D_{hy}, D_{\omega\omega}$	Section properties defined in Equations (5.2-5.7)
E	Modulus of elasticity
G	Shear modulus
$h(s)$	Normal distance between the shear centre and the tangent to mid-surface
H	Height of beam cross-section from the flanges mid-surfaces
I_{xx}, I_{yy}	Moment of inertias of the cross-section about the principal X, Y axes
J	Saint-Venant torsional constant
ℓ	Member span
$M_j(z,t)$	Concentrated harmonic moment about X, Y, Z direction (for $j = x, y, z$)
$M_w(z,t)$	Concentrated bimoment
$m_j(z,t)$	Distributed harmonic moments about X, Y, Z direction (for $j = x, y, z$)
$m_w(z,t)$	Distributed harmonic bimoment
n	Axis along the normal direction at a point on the mid-surface
n, s, z	Local curvilinear coordinate system
$N_z(z,t)$	Concentrated end forces along longitudinal axis
$q_j(z,t)$	Distributed harmonic forces along X, Y, Z directions (for $j = x, y, z$)
$r(s)$	Normal distance between the shear centre S_c to the normal to mid-surface
s	Curvilinear coordinate along mid-surface of the section
S_c	Shear centre of the cross-section
t	Time in seconds
t_1, t_2	Time intervals

T^*	Kinetic energy
$\bar{u},\bar{v}$	Displacements of the shear centre S_c along the principal X ,Y axes
u_p,v_p,w_p	Displacements of a point p on the mid-surface along X ,Y ,Z axes
U^*	Internal strain energy
$V_j(z,t)$	Shear forces along X ,Y axes (for $j=x,y$)
$\bar{w}$	Average longitudinal displacement along the z axis
W^*	Work done by applied forces
x,y,z	Cartesian coordinate system
X ,Y ,Z	Principal coordinate system
$x(s),y(s)$	Coordinate of arbitrary point on mid-surface of the section along X ,Y axes
x_s	Coordinate of the shear centre S_c along the axis of symmetry
ρ	Density of the material
r_o	Polar radius of gyration
ξ,η	Tangential and normal displacements of a point p along X and Y axes
θ_j	Rotations angles around the X ,Y ,Z axes (for $j=x,y,z$)
$\hat{\alpha}(s)$	Angle between the tangent to the cross-section and the principal X axis
$\psi(z,t)$	Warping deformation function
Ω	Exciting frequency
$\omega(s)$	Warping function of the cross-section

CHAPTER (6)

DYNAMIC ANALYSIS OF ASYMMETRIC THIN-WALLED MEMBERS UNDER HARMONIC FORCES

Analytical Solution and Finite Element Formulation

Chapter (6) - Dynamic Analysis of Asymmetric Thin-walled Members under Harmonic Forces

Abstract

In this study, the closed-form solution and a finite element formulation are developed for the dynamic analysis of thin-walled members with asymmetric open sections subjected to harmonic forces. The dynamic equations of motion and associated boundary conditions are derived from Hamilton's principle. The formulation is based on a generalized Vlasov-Timoshenko beam theory and accounts for the effects of shear deformation due to bending and warping, translational and rotary inertia effects, and also captures the effects of flexural–torsional coupling due to cross section asymmetry. Closed-form solutions are obtained for cantilever and simply-supported boundary conditions. A family of shape functions is then developed based on the exact solution of the coupled field equations and then used to formulate a beam finite element. The new element has two nodes and six degrees of freedom per node and captures the coupled bending-torsional static and dynamic responses of asymmetric thin-walled members under harmonic forces. Results based on the closed-form solution and finite element formulation are assessed and validated against other well established finite element solutions.

6.1 Introduction and Scope

Thin-walled members are used widely in the design of many structural components in aerospace structures, steel building construction, steel bridges, ship and marine structural frames, etc. In some application, thin-walled members are subjected to harmonic excitations caused by machinery, aerodynamic forces, traffic loads, wave motion, etc. Also, harmonic forces can be induced from unbalance in rotating machinery and propellants and reciprocating machines. Under harmonic forces, the steady state component of the response of the structural member is sustained for a long time and is thus of particular importance in fatigue design. In contrast, the transient component response of the system which is induced at the beginning of the excitation tends to dampen out quickly and is thus of little or no importance in fatigue design. Within this context, the present study aims at developing an accurate and efficient solution which

captures the steady state response component of thin-walled members of asymmetric sections subjected to general harmonic forces.

6.2 Literature Review

6.2.1 General

The classical thin-walled beam theory developed by Vlasov (1961) is widely used for the analysis of members with open cross-sections. The theory was based on two kinematics assumptions: (i) the beam cross-section is assumed to be rigid (undeformed) in its own plane, and (ii) the transverse shear deformations within the section mid-surface are considered negligible. The second assumption signifies that, within the Vlasov theory, warping deformation is captured while shear deformations are omitted. Given the vast literature on the subject, the present literature survey focuses on the dynamic analysis of thin-walled members with asymmetric cross-sections, i.e., members with doubly symmetric and monosymmetric cross-sections are not included in the present survey. The interested reader is referred to our previous work in Chapters 4 and 5 for a review on doubly symmetric and monosymmetric sections.

6.2.2 Review of Analytical Solutions

6.2.2.1 Formulations Excluding Shear Deformation Effects

Friberg (1985) numerically developed the exact dynamic stiffness matrix for a thin-walled beam in coupled flexural and torsion vibrations. Leung (1991) numerically developed the exact dynamic stiffness matrix of a thin-walled beam based on Vlasov theory. His solution incorporates coupling effects due to axial force. In a subsequent study, Leung (1992) developed the dynamic stiffness matrix solution which incorporated coupling effects due to axial compressive force and strong-axis moments. Frequency-dependent shape functions based on the exact solutions of the governing differential equations were obtained and then used to formulate the dynamic stiffness matrix. Using the principle of virtual work, Chen and Tamma (1994) employed the finite element method in conjunction with an implicit-starting unconditionally stable numeric integration methodology for vibration analysis of thin-walled members subjected to constant axial force. Tanaka and Bercin (1997) investigated the coupled flexural-torsional free vibration analysis of thin-walled beams of asymmetric open cross-section using finite

element method. Based on d'Alembert principle, Tanaka and Bercin (1999) formulated the governing differential equations of motion for triply coupled vibrations based on non-orthogonal coordinates. The governing field equations were included the product of moment of inertia term. The system of equations was later on solved in an exact sense by Arpaci and Bozdag (2002). Arpaci et al. (2003) extended their work to include the effect of rotary inertia and developed an analytical solution for predicting the undamped natural frequencies. Kim et al. (2003a) conducted a free vibration analysis for the flexural–torsional behaviour of thin-walled beams with asymmetric sections under eccentric axial loads. The displacement functions were obtained and the exact dynamic stiffness matrices evaluated using force-deformation relationships. Voros (2004) analyzed the free coupled vibration of thin-walled beams with asymmetric open cross sections in which the warping deformation effect is incorporated. Using d'Alembert's principle, Li et al (2004c) formulated the equations of motions and the dynamic transfer matrix to compute the natural frequencies and mode shapes of axially loaded thin-walled beams. Using Hamilton's principle, Mohri et al. (2004) formulated the governing equations for pre-buckling and post-buckling dynamic behaviors in thin-walled composite members under compressive forces and transverse forces. Their solution captures non-linear warping and bending-torsion coupling. Based on Galerkin's approach, the governing partial differential equations were reduced to non-linear coupled differential equation system only in time. Using the principle of virtual work, Prokic (2005) derived a system of equations for triply coupled free vibrations of thin-walled beams. Closed-form solutions were obtained for the natural frequencies of simply-supported thin-walled of asymmetric cross-sections. Bin and Leung (2006) formulated the dynamic stiffness matrix for open thin-walled beams by employing frequency dependent shape functions which exactly satisfy the governing differential equations for free vibration. Based on Hamilton's principle, Vo et al. (2010) studied the coupled flexural-torsional free vibration for thin-walled open composite beams with arbitrary lay-ups subjected to constant axial compressive force. The theory was based on classical lamination theory and accounts for material anisotropy couplings.

The majority of the above studies were based on Vlasov beam theory and thus account for warping, rotary inertia and axial force effects except for the studies of Chen and Tamma (1994), Tanaka and Bercin (1997, 1999), Arpaci et al. (2003), Kim et al. (2003a), Voros

(2004), Prokic (2005) and Vo et al. (2010) who omitted the axial force effects and Li et al. (2004a) who omitted the rotary inertia effects.

Using d'Alembert's principle and the principle of virtual work, Chen and Hsiao (2007) formulated the governing equations for the coupled axial-torsional vibration response of the thin-walled beam of Z cross-sections. The coupled axial-torsional natural frequencies were obtained by solving the equations of motion. Kim et al. (2007) developed the static and dynamic stiffness matrices for coupled flexural-torsional stability and free vibration analyses for thin-walled beam subjected to linearly varying axial force. Their solution was based on Vlasov's kinematics and the static and dynamic stiffness matrices were derived based on the power series method. In their equations of motion and force-deformation relations they retained second order terms of the rotations. Explicit expressions for displacement fields were obtained in the form of power series. Using the principle of virtual work, Voros (2008 and 2009) formulated the governing field equations for bending-torsional coupled vibration of thin-walled beams subjected to longitudinal loads. The formulations account for large rotations. Using d'Alembert principle, Altintas (2010) derived the governing equations of motion for axially loaded thin-walled members. The field equations were discretized using the finite difference method. Their solution investigated the effects of material properties and axial force level on the natural frequencies.

6.2.2.2 Formulations Including Shear Deformation Effects

Shear deformation plays an important factor in dynamic problems where higher modes of vibrations are required or where the beam is subjected to harmonic forces with high frequencies. Therefore, modified versions of the Vlasov theory were developed by many researchers in order to capture the transverse shear deformation effects. Laudiero and Savoia (1991) studied the flexural-torsional vibrations of thin-walled beams with open and closed cross-sections. Secondary warping and shear lag effects were also included in their formulation. Bercin and Tanaka (1997) studied the coupled flexural-torsional free vibrations of thin-walled members of asymmetric open C-sections. Kollar (2001) developed a theory of free vibration analysis of thin-walled open section composite beams. He developed closed-form solutions for the coupled flexural-torsional natural frequencies for simply-supported beams. Cortinez and Piovan (2002) developed an

analytical solution for the free vibration analysis of composite thin-walled beams of open and closed cross-sections. Kim et al. (2003) formulated the exact dynamic and static stiffness matrices for the free vibration and stability analysis of thin-walled shear-deformable beams. Also, they incorporated flexural-torsional coupling effects due to the asymmetry of the cross-sections. In a subsequent study, Kim and Kim (2005) adopted the theory in Kim et al. (2003) to formulate the dynamic stiffness matrix element for the flexural-torsional free vibration of asymmetric shear-deformable thin-walled beams. By applying the Hellinger-Reissner variational principle, the governing equations of motion were derived for the coupled vibration response as well as the force-deformation relations. Using the virtual work principle, Prokic (2006) derived the differential equations for the coupled vibrations for thin-walled beams capturing shear deformation effects due to bending. The closed-form solution for the natural frequencies was derived for the case of simply supported beams. Vo and Lee (2009) presented a general analytical solution based on shear deformable beam theory for the study of flexural-torsional buckling and vibration analysis of open thin-walled composite beams. Ambrosini (2009) developed a general theory for coupled flexural-torsional free vibrations for thin-walled beams of open cross-sections. De Borbon and Ambrosini (2010) extended the theory for coupled flexure and torsion vibrations of thin-walled beams to incorporating the influence of the axial forces. In Ambrosini (2010), an experimental study for the free vibration of thin-walled beams with asymmetric open cross section was conducted and the results were used to assess the accuracy of various theoretical solutions. The above studies accounts for the effects of shear deformation, warping and rotary inertia.

6.2.3 Literature Review on Finite Element Formulations

This part of literature focuses on finite element formulations for the dynamic analysis of open thin-walled members. In general, finite element are based one on three types of shape functions; (1) approximate polynomial interpolation functions, (2) shape functions based on the exact solution of the static equilibrium equations, and (3) shape functions based on exact solution of the dynamic equations of motion. Formulations based on the approximate shape functions are most common and include the in work of Chen and Tamma (1994), Hashemi and Richard (2000a and 2000b), Lee and Kim (2002a and b), Kim and Kim (2005), Voros (2008, 2009), Vo and Lee (2009a, 2009b, 2010) and Vo et al. (2009, 2010, 2011). Solutions based on the exact solution for static equilibrium

equations include the work of Mei (1970) and Hu et al. (1996). They have the advantage of avoiding locking problems which could arise in some of the solutions based on polynomial interpolation. Finite element solutions based on exact solution of the dynamic equations of motion include the work of Hjaji and Mohareb (2011b) and offer two advantages: (1) they eliminate discretization errors arising in conventional interpolation schemes and they thus converge to the solution using a minimum number of degrees of freedom, and (2) they lead to elements that are free from shear locking arising from the approximate interpolation functions.

Within the above context, this chapter aims at developing a closed-form solution and finite element formulation for dynamic steady state analysis of thin-walled open members with asymmetric open sections. The finite element formulation sought is based on exact shape functions which exactly satisfy the homogeneous solution of the couple field equations, and captures shear deformation effects due to bending and warping, translational and rotary inertias and bending-torsional coupling effects due to the cross-section asymmetry.

6.3 Dynamic Equilibrium Equations for Asymmetric Cross-sections

According to the theory developed in chapter 3, the governing equations for a thin-walled beam with asymmetric section under harmonic forces are given in terms of space displacement functions $\bar{w}(z),\bar{u}(z),\bar{v}(z),\bar{\theta}_x(z),\bar{\theta}_y(z),\bar{\theta}_z(z),\bar{\psi}(z)$ as:

$$\left(\rho A\,\Omega^2 + EA\,\mathcal{D}^2\right)\bar{w}(z) = -\bar{q}_z(z) \tag{6.1}$$

$$\begin{aligned}-\left(\rho A\,\Omega^2 + GD_{xx}\mathcal{D}^2\right)\bar{u}(z) - \left(GD_{xy}\mathcal{D}^2\right)\bar{v}(z) - \left(GD_{xy}\mathcal{D}\right)\bar{\theta}_x(z) + \left(GD_{xx}\mathcal{D}\right)\bar{\theta}_y(z)\\ -\left(\rho A y_s\,\Omega^2 + GD_{hx}\mathcal{D}^2\right)\bar{\theta}_z(z) - \left(GD_{hx}\mathcal{D}\right)\bar{\psi}(z) = \bar{q}_x(z)\end{aligned} \tag{6.2}$$

$$\begin{aligned}-\left(GD_{xy}\mathcal{D}^2\right)\bar{u}(z) - \left(\rho A\,\Omega^2 + GD_{yy}\mathcal{D}^2\right)\bar{v}(z) - \left(GD_{yy}\mathcal{D}\right)\bar{\theta}_x(z) + \left(GD_{xy}\mathcal{D}\right)\bar{\theta}_y(z)\\ +\left(\rho A x_s\,\Omega^2 - GD_{hy}\mathcal{D}^2\right)\bar{\theta}_z(z) - \left(GD_{hy}\mathcal{D}\right)\bar{\psi}(z) = \bar{q}_y(z)\end{aligned} \tag{6.3}$$

$$\begin{aligned}-\left(GD_{xy}\mathcal{D}\right)\bar{u}(z) - \left(GD_{yy}\mathcal{D}\right)\bar{v}(z) + \left(\rho I_{xx}\,\Omega^2 - GD_{yy} + EI_{xx}\mathcal{D}^2\right)\bar{\theta}_x(z)\\ +GD_{xy}\bar{\theta}_y(z) - \left(GD_{hy}\mathcal{D}\right)\bar{\theta}_z(z) - D_{hy}\bar{\psi}(z) = \bar{m}_x(z)\end{aligned} \tag{6.4}$$

$$\begin{aligned}\left(GD_{xx}\mathcal{D}\right)\bar{u}(z) + \left(GD_{xy}\mathcal{D}\right)\bar{v}(z) + GD_{xy}\bar{\theta}_x(z) - \left(GD_{xx} - \rho I_{yy}\,\Omega^2 - EI_{yy}\mathcal{D}^2\right)\bar{\theta}_y(z)\\ +\left(GD_{hx}\mathcal{D}\right)\bar{\theta}_z(z) + GD_{hx}\bar{\psi}(z) = \bar{m}_y(z)\end{aligned} \tag{6.5}$$

$$-\left(\rho A\, y_s \Omega^2 + GD_{hx}\mathcal{D}^2\right)\bar{u}(z)+\left(\rho A x_s \Omega^2 - GD_{hy}\mathcal{D}^2\right)\bar{v}(z)-\left(GD_{hy}\mathcal{D}\right)\bar{\theta}_x(z) +\left(GD_{hx}\mathcal{D}\right)\bar{\theta}_y(z)-\left(\rho A\, r_o^2\,\Omega^2 + G(J+D_{\omega\omega})\mathcal{D}^2\right)\bar{\theta}_z(z)-\left(GD_{\omega\omega}\mathcal{D}\right)\bar{\psi}(z)=\bar{m}_z(z) \tag{6.6}$$

$$-\left(GD_{hx}\mathcal{D}\right)\bar{u}(z)-\left(GD_{hy}\mathcal{D}\right)\bar{v}(z)-GD_{hy}\bar{\theta}_x(z)+GD_{hx}\bar{\theta}_y(z)-\left(GD_{\omega\omega}\mathcal{D}\right)\bar{\theta}_z(z) +\left(\rho C_w\Omega^2 - GD_{\omega\omega}+EC_w\mathcal{D}^2\right)\bar{\psi}(z)=\bar{m}_w(z) \tag{6.7}$$

The associated boundary condition terms for asymmetric sections are:

$$\left[EA\bar{w}'-\bar{N}_z(z)\right]\delta\bar{w}(z)\Big|_0^\ell=0 \tag{6.8}$$

$$\left[\left(GD_{xx}\left[\bar{u}'-\bar{\theta}_y\right]+GD_{xy}\left[\bar{v}'+\bar{\theta}_x\right]+GD_{hx}\left[\bar{\theta}_z+\bar{\psi}\right]-\bar{V}_x(z)\right)\delta\bar{u}(z)\right]_0^\ell=0 \tag{6.9}$$

$$\left[\left(GD_{xy}\left[\bar{u}'-\bar{\theta}_y\right]+GD_{yy}\left[\bar{v}'+\bar{\theta}_x\right]+GD_{hy}\left[\bar{\theta}_z+\bar{\psi}\right]-\bar{V}_y(z)\right)\delta\bar{v}(z)\right]_0^\ell=0 \tag{6.10}$$

$$\left[\left(EI_{xx}\bar{\theta}_x'+\bar{M}_x(z)\right)\delta\bar{\theta}_x(z)\right]_0^\ell=0 \tag{6.11}$$

$$\left[\left(EI_{yy}\bar{\theta}_y'-\bar{M}_y(z)\right)\delta\bar{\theta}_y(z)\right]_0^\ell=0 \tag{6.12}$$

$$\left[\left(GD_{hx}\left[\bar{u}'-\bar{\theta}_y\right]+GD_{hy}\left[\bar{v}'+\bar{\theta}_x\right]+GD_{\omega\omega}\left[\bar{\theta}_z+\bar{\psi}\right]+GJ\bar{\theta}_z'-\bar{M}_z(z)\right)\delta\bar{\theta}_z(z)\right]_0^\ell=0 \tag{6.13}$$

$$\left[\left(EC_w\bar{\psi}'+\bar{M}_w(z)\right)\delta\bar{\psi}(z)\right]_0^\ell=0 \tag{6.14}$$

Equations (6.1) to (6.7) can be rewritten in matrix form as:

$$\left[\begin{array}{c|c} \bar{Z}_{11} & \langle 0\rangle_{6\times1}^T \\ \hline [0]_{1\times6} & [\bar{Z}_S] \end{array}\right]_{7\times7}\left\{\begin{array}{c} \bar{U}_1(z) \\ \hline \{\bar{U}_S(z)\}_{6\times1} \end{array}\right\}_{7\times1}=\left\{\begin{array}{c} \bar{Q}_1(z) \\ \hline \{\bar{Q}_S(z)\}_{6\times1} \end{array}\right\}_{7\times1} \tag{6.15}$$

in which

$\bar{Z}_{11}=\rho A\Omega^2+EA\mathcal{D}^2$,

$\left\langle \bar{U}_1(z)\,\middle|\,\langle\bar{U}_S(z)\rangle_{1\times6}^T\right\rangle_{1\times7}^T=\left\langle \bar{w}(z)\,\middle|\,\bar{u}(z)\;\;\bar{v}(z)\;\;\bar{\theta}_x(z)\;\;\bar{\theta}_y(z)\;\;\bar{\theta}_z(z)\;\;\bar{\psi}(z)\right\rangle_{1\times7}^T$,

$\left\langle \bar{Q}_1(z)\,\middle|\,\langle\bar{Q}_S(z)\rangle_{1\times6}^T\right\rangle_{1\times7}^T=\left\langle \bar{q}_z(z)\,\middle|\,\bar{q}_x(z)\;\;\bar{q}_y(z)\;\;\bar{m}_x(z)\;\;\bar{m}_y(z)\;\;\bar{m}_z(z)\;\;\bar{m}_w(z)\right\rangle_{1\times7}^T$,

and

$$\left[\bar{Z}_S\right]_{6\times6}=\begin{bmatrix}
-\left(\rho A\Omega^2+GD_{xx}\mathcal{D}^2\right) & -GD_{xy}\mathcal{D}^2 & -GD_{xy}\mathcal{D} & GD_{xx}\mathcal{D} & -\left(\rho A\Omega^2 y_s+GD_{hx}\mathcal{D}^2\right) & -GD_{hx}\mathcal{D} \\
 & -\left(\rho A\Omega^2+GD_{yy}\mathcal{D}^2\right) & -GD_{yy}\mathcal{D} & GD_{xy}\mathcal{D} & \left(\rho A\Omega^2 x_s-GD_{hy}\mathcal{D}^2\right) & -GD_{hy}\mathcal{D} \\
 & & \left(\rho I_{xx}\Omega^2-GD_{yy}+EI_{xx}\mathcal{D}^2\right) & GD_{xy} & -GD_{hy}\mathcal{D} & -GD_{hy} \\
 & & & \left(\rho I_{yy}\Omega^2-GD_{xx}+EI_{yy}\mathcal{D}^2\right) & GD_{hx}\mathcal{D} & GD_{hx} \\
 & Symm & & & -\left[\rho A\Omega^2 r_o^2+G\left(D_{\omega\omega}+J\right)\mathcal{D}^2\right] & -GD_{ww}\mathcal{D} \\
 & & & & & \left(\rho C_w\Omega^2-GD_{\omega\omega}+EC_w\mathcal{D}^2\right)
\end{bmatrix}_{6\times6}$$

where $r_o^2=(1/A)\int_A\left(h^2+r^2\right)dA=x_s^2+y_s^2+\left(I_{xx}+I_{yy}\right)/A$ is the polar radius of gyration. The first partition in Equation (6.15) and related boundary conditions (6.8) provides the governing equation for longitudinal deformation of the member, which is uncoupled from the remaining field equations and was solved independently in chapter 4. The second partition with associated boundary conditions (6.9) to (6.14) governs the solution for the coupled system biaxial bending-torsional response of the member. Due to the shear deformation effects and the nonsymmetry of the cross-section, the system of equations in space variables $\bar{u}(z),\bar{v}(z),\bar{\theta}_x(z),\bar{\theta}_y(z),\bar{\theta}_z(z),\bar{\psi}(z)$ is fully coupled. The present study thus focuses only on the solution of the coupled system of equations:

$$\left[\bar{Z}_S\right]_{6\times6}\left\{\bar{U}_S(z)\right\}_{6\times1}=\left\{\bar{Q}_S(z)\right\}_{6\times1} \tag{6.16}$$

in which $\left\langle\bar{Q}_S(z)\right\rangle_{1\times6}^{\mathrm{T}}=\left\langle\bar{q}_x(z)\quad\bar{q}_y(z)\quad\bar{m}_x(z)\quad\bar{m}_y(z)\quad\bar{m}_z(z)\quad\bar{m}_w(z)\right\rangle_{1\times6}^{\mathrm{T}}$, and $\left\langle\bar{U}_S(z,t)\right\rangle_{1\times6}^{\mathrm{T}}=\left\langle\bar{u}(z)\quad\bar{v}(z)\quad\bar{\theta}_x(z)\quad\bar{\theta}_y(z)\quad\bar{\theta}_z(z)\quad\bar{\psi}(z)\right\rangle_{1\times6}^{\mathrm{T}}$.

Section Properties for Asymmetric Channel and J-Sections

The section properties $D_{xx}, D_{yy}, D_{xy}, D_{hx}, D_{hy}, D_{\omega\omega}$ for asymmetric channel and J-sections illustrated in Figure (6.1) are provided in Table (6.1).

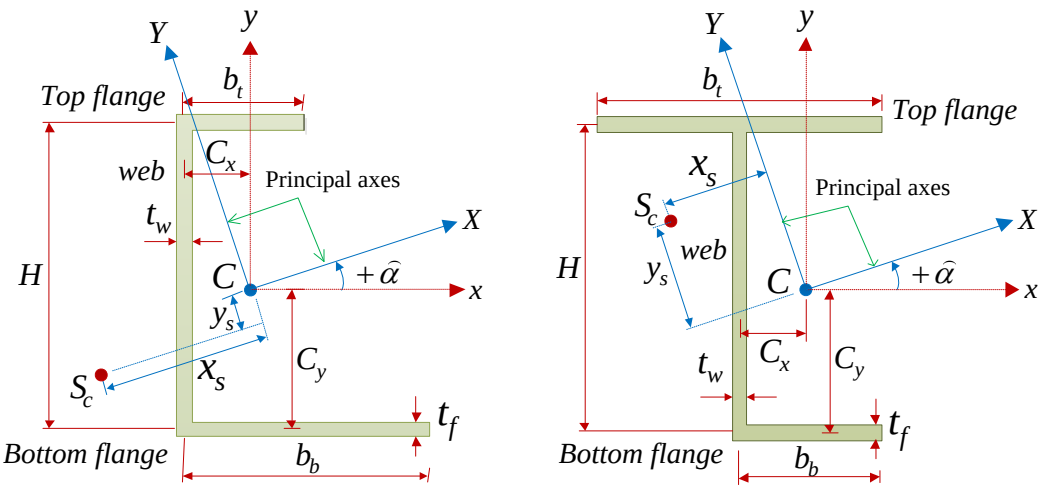

Figure (6.1): Asymmetric channel and J-sections

Table (6.1): Section properties for asymmetric C and J cross-sections

Expression	**Asymmetric C and J-sections**
$D_{xx} = \sum_{i=3} \int_{A_i} \left(\cos\hat{\alpha}_i(s)\right)^2 dA_i$	$A_t \cos\hat{\alpha}_t + A_w \cos\hat{\alpha}_w + A_b \cos\hat{\alpha}_b$
$D_{yy} = \sum_{i=3} \int_{A_i} \left(\sin\hat{\alpha}_i(s)\right)^2 dA_i$	$A_t \sin\hat{\alpha}_t + A_w \sin\hat{\alpha}_w + A_b \sin\hat{\alpha}_b$
$D_{xy} = \sum_{i=3} \int_{A_i} \cos\hat{\alpha}_i(s) \sin\hat{\alpha}_i(s) dA_i$	$A_t \sin\hat{\alpha}_t \cos\hat{\alpha}_t + A_w \sin\hat{\alpha}_w \cos\hat{\alpha}_w + A_b \sin\hat{\alpha}_b \cos\hat{\alpha}_b$
$D_{hx} = \sum_{i=3} \int_{A_i} h_i(s) \cos\hat{\alpha}_i(s) dA_i$	$A_t h_t \cos\hat{\alpha}_t + A_w h_w \cos\hat{\alpha}_w + A_b h_b \cos\hat{\alpha}_b$
$D_{hy} = \sum_{i=3} \int_{A_i} h_i(s) \sin\hat{\alpha}_i(s) dA_i$	$A_t h_t \sin\hat{\alpha}_t + A_w h_w \sin\hat{\alpha}_w + A_b h_b \sin\hat{\alpha}_b$
$D_{\omega\omega} = \sum_{i=3} \int_{A_i} \left[h_i(s)\right]^2 dA_i$	$h_t^2 A_t + h_w^2 A_w + h_b^2 A_b$

in which the areas are $A_t = b_t t_f$, $A_b = b_b t_f$, $A_w = Ht_w$, the angles are $\bar{\alpha}_t = 180^o - \bar{\alpha}$, $\bar{\alpha}_w = 270^o - \bar{\alpha}$, $\bar{\alpha}_b = -\bar{\alpha}$, while the distances h_t, h_w, h_b can be obtained for each section from the Figure (6.2).

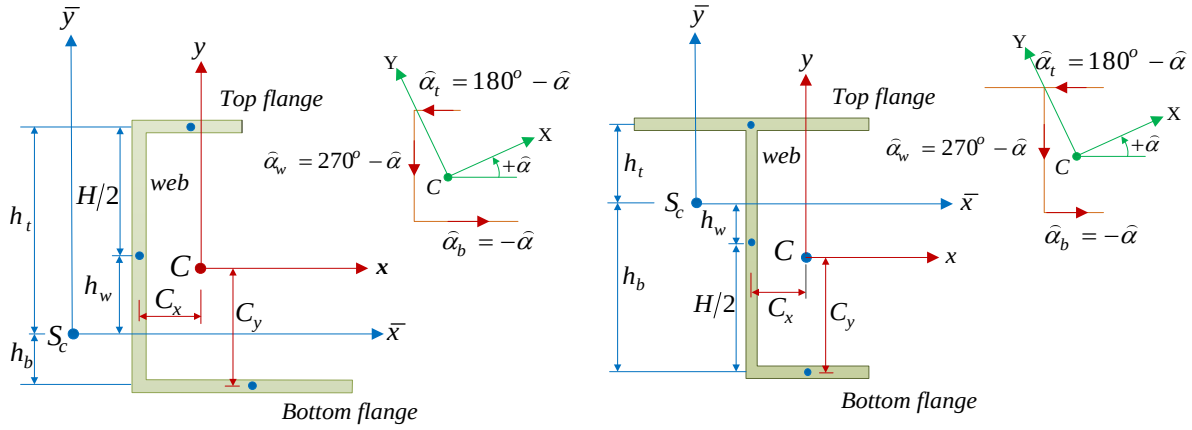

Figure (6.2): Dimensions of asymmetric channel and J-sections

6.4 Closed-form Solution for Coupled Field Equations

The total solution of the governing field equations is the summation of the homogeneous solution and particular solution, i.e.,

$$\left\{\bar{U}_S(z)\right\}_{6\times1} = \left\{\bar{U}_{S_H}(z)\right\}_{6\times1} + \left\{\bar{U}_{S_P}(z)\right\}_{6\times1} \tag{6.17}$$

where $\left\{\bar{U}_{S_H}(z)\right\}_{6\times1}$ is the homogeneous solution and $\left\{\bar{U}_{S_P}(z)\right\}_{6\times1}$ is the particular solution.

6.4.1 Homogeneous Solution for Coupled Field Equations

The exact solution of the homogeneous part of the governing field equations $\left[\bar{Z}_S\right]_{6\times6}\left\{\bar{U}_S(z)\right\}_{6\times1} = \left\{\bar{Q}_S(z)\right\}_{6\times1}$ is obtained by setting the loading terms in the field equations to zero, i.e., $\left\{\bar{Q}_S(z)\right\}_{6\times1} = 0$. The homogeneous solution of the displacement functions $\left\{\bar{U}_{S_H}(z)\right\}_{6\times1}$ is then assumed to take the following exponential form:

$$\begin{aligned}\left\langle\bar{U}_{S_H}(z)\right\rangle_{1\times6}^T &= \left\langle\bar{u}(z)\;\bar{v}(z)\;\bar{\theta}_x(z)\;\bar{\theta}_y(z)\;\bar{\theta}_z(z)\;\bar{\psi}(z)\right\rangle_{1\times6}^T \\ &= \sum_{i=1}^{6}\left\langle a_1\;a_2\;a_3\;a_4\;a_5\;a_6\right\rangle_{i,1\times6}^T e^{m_i z}\end{aligned} \tag{6.18}$$

From the space displacements postulated in Equation (6.18), by substituting into Equation (6.16), one obtains:

$$\left[\bar{Y}_S\right]_{i,6\times6}\left[\bar{E}_S\right]_{6\times6}\{a\}_{i,6\times1}=\{0\}_{6\times1} \tag{6.19}$$

in which $\langle a\rangle^T_{i,1\times6}=\langle a_1 \;\vdots\; a_2 \;\vdots\; a_3 \;\vdots\; a_4 \;\vdots\; a_5 \;\vdots\; a_6\rangle^T_{i,1\times6}$ is the vector of unknown integration constants, $\left[\bar{E}_S\right]_{6\times6}=diag\left[e^{m_1 z} \;\vdots\; e^{m_2 z} \;\vdots\; e^{m_3 z} \;\vdots\; e^{m_4 z} \;\vdots\; e^{m_5 z} \;\vdots\; e^{m_6 z}\right]_{6\times6}$ and $\left[\bar{Y}_S\right]_{6\times6}$ is a symmetric matrix given by:

$$\left[\bar{Y}_S\right]_{6\times6}=\begin{bmatrix}
-\left(\rho A\Omega^2+GD_{xx}m_i^2\right) & -GD_{xy}m_i^2 & -GD_{xy}m_i & GD_{xx}m_i & -\left(\rho A\Omega^2 y_s+GD_{hx}m_i^2\right) & -GD_{hx}m_i \\
 & -\left(\rho A\Omega^2+GD_{yy}m_i^2\right) & -GD_{yy}m_i & GD_{xy}m_i & \left(\rho A\Omega^2 x_s-GD_{hy}m_i^2\right) & -GD_{hy}m_i \\
 & & \left(\rho I_{xx}\Omega^2-GD_{yy}+EI_{xx}m_i^2\right) & GD_{xy} & -GD_{hy}m_i & -GD_{hy} \\
 & & & \left(\rho I_{yy}\Omega^2-GD_{xx}+EI_{yy}m_i^2\right) & GD_{hx}m_i & GD_{hx} \\
 & Symm & & & -\left[\rho A\Omega^2 r_o^2+G\left(D_{\omega\omega}+J\right)m_i^2\right] & -GD_{\omega\omega}m_i \\
 & & & & & \left(\rho C_w\Omega^2-GD_{\omega\omega}+EC_w m_i^2\right)
\end{bmatrix}_{6\times6}$$

The nontrivial solution of Equation (6.19) is obtained by setting the determinant of matrix $\left[\bar{Y}_S\right]_{6\times6}$ to zero. One obtains the quadratic eigen-value problem:

$$\left(m_i^2\left[\bar{M}\right]_{6\times6}+m_i\left[\bar{C}\right]_{6\times6}+\left[\bar{K}\right]_{6\times6}\right)\{a\}_{i,6\times1}=0 \tag{6.20}$$

where vectors $\{a\}_{i,6\times1}$ are the eigenvectors corresponding to eigenvalues m_i, and the matrices $\left[\bar{M}\right]_{6\times6}$, $\left[\bar{C}\right]_{6\times6}$ and $\left[\bar{K}\right]_{6\times6}$ are defined by:

$$\left[\bar{M}\right]_{6\times6}=\begin{bmatrix} -GD_{xx} & -GD_{xy} & 0 & 0 & -GD_{hx} & 0 \\ & -GD_{yy} & 0 & 0 & -GD_{hy} & 0 \\ & & EI_{xx} & 0 & 0 & 0 \\ & & & EI_{yy} & 0 & 0 \\ & Symm & & & -G\left(D_{\omega\omega}+J\right) & 0 \\ & & & & & EC_w \end{bmatrix}_{6\times6},$$

$$\left[\bar{C}\right]_{6\times6}=\begin{bmatrix} 0 & 0 & -GD_{xy} & GD_{xx} & 0 & -GD_{hx} \\ & 0 & -GD_{yy} & GD_{xy} & 0 & -GD_{hy} \\ & & 0 & 0 & -GD_{hy} & 0 \\ & & & 0 & GD_{hx} & 0 \\ & Symm & & & 0 & -GD_{\omega\omega} \\ & & & & & 0 \end{bmatrix}_{6\times6}, \text{ and}$$

$$\left[\bar{K}\right]_{6\times6}=\begin{bmatrix} -\rho A\Omega^2 & 0 & 0 & 0 & -\rho A\Omega^2 y_s & 0 \\ & -\rho A\Omega^2 & 0 & 0 & \rho A\Omega^2 x_s & 0 \\ & & \left(\rho I_{xx}\Omega^2-GD_{yy}\right) & GD_{xy} & 0 & -GD_{hy} \\ & & & \left(\rho I_{yy}\Omega^2 & 0 & -GD_{hx} \\ & & & -GD_{xx}\right) & & \\ & Symm & & & -\rho A\Omega^2 r_o^2 & 0 \\ & & & & & \left(\rho C_w\Omega^2 \\ & & & & & -GD_{\omega\omega}\right) \end{bmatrix}_{6\times6}$$

The quadratic 6×6 eigenvalue problem in Equation (6.20) can be transformed into the equivalent 12×12 unsymmetric linear right-handed eigenvalue form [e.g., Saad 1992] as:

$$\left(m_i\begin{bmatrix}\left[I_n\right]_{6\times6} & \left[0\right]_{6\times6}\\ \left[0\right]_{6\times6} & \left[\bar{M}\right]_{6\times6}\end{bmatrix}-\begin{bmatrix}\left[0\right]_{6\times6} & \left[I_n\right]_{6\times6}\\ \left[-\bar{K}\right]_{6\times6} & \left[-\bar{C}\right]_{6\times6}\end{bmatrix}\right)_{12\times12}\begin{Bmatrix}\left\{a\right\}_{i,6\times1}\\ m_i\left\{a\right\}_{i,6\times1}\end{Bmatrix}_{12\times1}=\left\{0\right\}_{12\times1} \tag{6.21}$$

which is then solved for the 12 eigen-pairs m_i and $\left\{a\right\}_{i,6\times1}$.

The eigen-solution of Eq. (6.21) gives the eigenvalues and the corresponding eigenvectors of the system. The solution of Equation (6.21) is to be numerically determined. For an asymmetric section, it is observed that all twelve roots are non-zero and distinct. Thus, the homogeneous solution of system of Equation (6.20) takes the form:

$$\begin{aligned}\left\{\bar{U}_{S_H}(z)\right\}_{6\times1}&=\left[\bar{A}\right]_{6\times12}\left\{\bar{S}(z)\right\}_{12\times1}\\ &=\begin{bmatrix}\left\{a\right\}_1 & \left\{a\right\}_2 & \left\{a\right\}_3 & \left\{a\right\}_4 & \cdots\cdots & \left\{a\right\}_{12}\end{bmatrix}_{6\times12}\left\{\bar{S}(z)\right\}_{12\times1}\end{aligned} \tag{6.22}$$

where $\left\langle \bar{S}(z) \right\rangle^T = \left\langle e^{m_1 z} \;\vdots\; e^{m_2 z} \;\vdots\; e^{m_3 z} \;\vdots\; e^{m_4 z} \;\vdots\; \ldots\ldots \;\vdots\; e^{m_{12} z} \right\rangle^T$ and matrix $\left[\bar{A}\right]_{6\times 12}$ contains the eigen vectors $\{a\}_i$ (for $i = 1,2,3,\ldots..,12$) of the eigenvalue problem defined by Equation (6.21). In Equation (6.22), matrix $\left[\bar{A}\right]_{6\times 12}$ has 72 unknown integration constants of which only twelve should be independent. The reduction of the number of constants is accomplished by relating the five terms of the eigenvector $\langle a_1 \;\; a_2 \;\; a_3 \;\; a_4 \;\; a_5 \rangle_i$ to the sixth term $\langle a_6 \rangle_i$. In a partitioned form, Equation (6.16) can be re-written as:

$$\begin{bmatrix} [T_5]_{i,5\times 5} & \{T_2\}_{i,5\times 1} \\ \hdashline \langle T_2 \rangle^T_{i,1\times 5} & [T_1]_{i,1\times 1} \end{bmatrix}_{i,6\times 6} \begin{Bmatrix} a_1 \\ \hdashline a_2 \\ \hdashline a_3 \\ \hdashline a_4 \\ \hdashline a_5 \\ \hdashline a_6 \end{Bmatrix}_{i,6\times 1} = \{0\}_{6\times 1} \tag{6.23}$$

where

$$[T_5]_{i,5\times 5} = \begin{bmatrix} -\left[\rho A\Omega^2 + GD_{xx} m_i^2\right] & -GD_{xy} m_i^2 & -GD_{xx} m_i & GD_{xx} m_i & -\left[\rho A\Omega^2 y_s + GD_{hx} m_i^2\right] \\ & -\left[\rho A\Omega^2 + GD_{yy} m_i^2\right] & -GD_{yy} m_i & GD_{xy} m_i & \left[\rho A\Omega^2 x_s - GD_{hy} m_i^2\right] \\ & & \left[\rho I_{xx}\Omega^2 - GD_{yy} + EI_{xx} m_i^2\right] & GD_{xy} & -GD_{hx} m_i \\ & Symm & & \left[\rho I_{yy}\Omega^2 - GD_{xx} + EI_{yy} m_i^2\right] & \\ & & & & -\left[\rho A\Omega^2 r_o^2 + G(D_{\omega\omega} + J) m_i^2\right] \end{bmatrix}_{i,5\times 5}$$

$[T_1]_{i,1\times 1} = \left[\rho C_w \Omega^2 - GD_{\omega\omega} + EC_w m_i^2\right]_{i,1\times 1}$, and

$\langle T_2 \rangle^T_{i,1\times 5} = \left\langle -GD_{hx} m_i \;\vdots\; -GD_{hy} m_i \;\vdots\; -GD_{hy} \;\vdots\; GD_{hx} \;\vdots\; -GD_{\omega\omega} m_i \right\rangle^T_{i,1\times 5}$.

By expanding the upper portion of the partitioned system in Equation (6.23), the five sets of unknown integration constants $\{a_1\}_i, \{a_2\}_i, \{a_3\}_i, \{a_4\}_i, \{a_5\}_i$ are expressed in terms of the set $\{a_6\}_i$ as:

$$\begin{Bmatrix} a_1 \\ a_2 \\ a_3 \\ a_4 \\ a_5 \end{Bmatrix}_{i,5\times1} = -\left[T_5\right]^{-1}_{i,5\times5}\left\{T_2\right\}_{i,5\times1} a_{6,i} = \begin{bmatrix} q_{11} & q_{12} & q_{13} & q_{14} & q_{15} \\ & q_{22} & q_{23} & q_{24} & q_{25} \\ & & q_{33} & q_{34} & q_{35} \\ & Symm & & q_{44} & q_{45} \\ & & & & q_{55} \end{bmatrix}_{i,5\times5} \left\{T_2\right\}_{i,5\times1} a_{6,i} = \begin{Bmatrix} \bar{F}_{1,i} \\ \bar{F}_{2,i} \\ \bar{F}_{3,i} \\ \bar{F}_{4,i} \\ \bar{F}_{5,i} \end{Bmatrix}_{i,5\times1} a_{6,i} \tag{6.24}$$

where

$\bar{F}_{k,i} = \dfrac{\left\langle q_{k1} \;\; q_{k2} \;\; q_{k3} \;\; q_{k4} \;\; q_{k5} \right\rangle^T_{i,1\times5}}{\left|\left[q\right]_{i,5\times5}\right|}\left\{T_2\right\}_{i,5\times1}$, for $k = 1,2,3,4,5$ and $\left[q\right]_{i,5\times5} = -\left[T_5\right]^{-1}_{i,5\times5}$.

From Equation (6.24), by substituting into Equation (6.26), the homogeneous solution is then given by:

$$\begin{aligned} \left\{\bar{U}_{S_H}(z)\right\}_{6\times1} &= \left[\begin{Bmatrix} \bar{F}_{1,1} \\ \bar{F}_{2,1} \\ \bar{F}_{3,1} \\ \bar{F}_{4,1} \\ \bar{F}_{5,1} \\ 1 \end{Bmatrix}_{6\times1} a_{6,1} \;\vdots\; \begin{Bmatrix} \bar{F}_{1,2} \\ \bar{F}_{2,2} \\ \bar{F}_{3,2} \\ \bar{F}_{4,2} \\ \bar{F}_{5,2} \\ 1 \end{Bmatrix}_{6\times1} a_{6,2} \;\vdots\; \begin{Bmatrix} \bar{F}_{1,3} \\ \bar{F}_{2,3} \\ \bar{F}_{3,3} \\ \bar{F}_{4,3} \\ \bar{F}_{5,3} \\ 1 \end{Bmatrix}_{6\times1} a_{6,3} \;\vdots\; \cdots\cdots \;\vdots\; \begin{Bmatrix} \bar{F}_{1,12} \\ \bar{F}_{2,12} \\ \bar{F}_{3,12} \\ \bar{F}_{4,12} \\ \bar{F}_{5,12} \\ 1 \end{Bmatrix}_{6\times1} a_{6,12} \right]_{6\times12} \left\{\bar{S}(z)\right\}_{12\times1} \\ &= \left[\bar{F}\right]_{6\times12}\left[diag\left\langle A_{6,i}\right\rangle^T \right]_{12\times12}\left\{\bar{S}(z)\right\}_{12\times1} \\ &= \left[\bar{F}\right]_{6\times12}\left[diag\left\langle \bar{S}(z)\right\rangle^T \right]_{12\times12}\left\{A_{6,i}\right\}_{12\times1} = \left[\bar{\chi}(z)\right]_{6\times12}\left\{A_{6,i}\right\}_{12\times1} \end{aligned} \tag{6.25}$$

in which $\left[\bar{F}\right]_{6\times12} = \left[\begin{Bmatrix} \bar{F}_{1,1} \\ \bar{F}_{2,1} \\ \bar{F}_{3,1} \\ \bar{F}_{4,1} \\ \bar{F}_{5,1} \\ 1 \end{Bmatrix} \;\vdots\; \begin{Bmatrix} \bar{F}_{1,2} \\ \bar{F}_{2,2} \\ \bar{F}_{3,2} \\ \bar{F}_{4,2} \\ \bar{F}_{5,2} \\ 1 \end{Bmatrix} \;\vdots\; \begin{Bmatrix} \bar{F}_{1,3} \\ \bar{F}_{2,3} \\ \bar{F}_{3,3} \\ \bar{F}_{4,3} \\ \bar{F}_{5,3} \\ 1 \end{Bmatrix} \;\vdots\; \cdots\cdots \;\vdots\; \begin{Bmatrix} \bar{F}_{1,12} \\ \bar{F}_{2,12} \\ \bar{F}_{3,12} \\ \bar{F}_{4,12} \\ \bar{F}_{5,12} \\ 1 \end{Bmatrix} \right]_{6\times12}$, and

$\left[\bar{\chi}(z)\right]_{6\times12} = \left[\bar{F}\right]_{6\times12}\left[diag\left\langle \bar{S}(z)\right\rangle^T \right]_{12\times12}$ and $\left\langle A_{6,i}\right\rangle^T_{1\times12} = \left\langle a_{6,1} \;\vdots\; a_{6,2} \;\vdots\; a_{6,3} \;\vdots\; \cdots\cdots \;\vdots\; a_{6,12}\right\rangle^T_{1\times12}$.

Equation (6.25) provides the homogeneous solution for the space displacement functions $\bar{u}(z), \bar{v}(z), \bar{\theta}_x(z), \bar{\theta}_y(z), \bar{\theta}_z(z), \bar{\psi}(z)$ of the coupled system of equations in (6.26), which contain only twelve independent integration constants $\left\{A_{6,i}\right\}_{12\times1}$. For a given problem, these constants are determined from the related boundary conditions.

6.4.2 Particular Solution for Uniform Member Forces

Consider a member under uniform distributed forces

$$\begin{aligned}\left[q_x(z),q_y(z),q_z(z),m_x(z),m_y(z),m_z(z),m_w(z)\right]\mathrm{e}^{i\Omega t}\\ =\left[\bar{q}_x,\bar{q}_y,\bar{q}_z,\bar{m}_x,\bar{m}_y,\bar{m}_z,\bar{m}_w\right]\mathrm{e}^{i\Omega t}\end{aligned} \tag{6.26}$$

the corresponding particular solution $\left\{\bar{U}_{S_p}(z)\right\}_{6\times1}$ of the field equations is assumed as:

$$\begin{aligned}\left\langle\bar{U}_{S_p}(z)\right\rangle_{1\times6}^{T}&=\left\langle\bar{u}_p\ \ \bar{v}_p\ \ \bar{\theta}_{x_p}\ \ \bar{\theta}_{y_p}\ \ \bar{\theta}_{z_p}\ \ \bar{\psi}_p\right\rangle_{1\times6}^{T}\\&=\left\langle\hat{A}_1+\hat{B}_1z\ \ \hat{A}_2+\hat{B}_2z\ \ \hat{A}_3+\hat{B}_3z\ \ \hat{A}_4+\hat{B}_4z\ \ \hat{A}_5+\hat{B}_5z\ \ \hat{A}_6+\hat{B}_6z\right\rangle_{1\times6}^{T}\end{aligned} \tag{6.27}$$

From Equations (6.26) and (6.27), by substituting into Equation (6.16), yields:

$$\begin{aligned}&\left[\bar{S}_1\right]_{6\times6}\left\{\hat{A}\right\}_{6\times1}+\left[\bar{S}_2\right]_{6\times6}\left[diag\left[z\right]\right]_{6\times6}\left\{\hat{B}\right\}_{6\times1}\\&\quad=\left[\bar{S}_1\right]_{6\times6}\left\{\hat{A}\right\}_{6\times1}+\left[\bar{S}_2\right]_{6\times6}\left[diag\left[\hat{B}\right]\right]_{6\times6}\left\{\bar{Z}_o\right\}_{6\times1}=\left\{\bar{Q}_f\right\}_{6\times1}\end{aligned} \tag{6.28}$$

where $\left[\bar{S}_1\right]_{6\times6}=$

$$\begin{bmatrix}-\rho A\Omega^2 & 0 & 0 & 0 & -\rho A\Omega^2 y_s & 0\\ & -\rho A\Omega^2 & 0 & 0 & \rho A\Omega^2 x_s & 0\\ & & \left(\rho I_{xx}\Omega^2-GD_{yy}\right) & GD_{xy} & 0 & -GD_{hy}\\ & & & \left(\rho I_{yy}\Omega^2-GD_{xx}\right) & 0 & GD_{hx}\\ & Symm & & & -\rho A\Omega^2 r_o^2 & 0\\ & & & & & \left(\rho C_w\Omega^2-GD_{\omega\omega}\right)\end{bmatrix}_{6\times6}$$

$$\left[\bar{S}_2\right]_{6\times6}=\begin{bmatrix}-\rho A\Omega^2 & 0 & -GD_{xy} & GD_{xx} & -\rho A\Omega^2 y_s & -GD_{hx}\\ & -\rho A\Omega^2 & -GD_{yy} & GD_{xy} & \rho A\Omega^2 x_s & -GD_{hy}\\ & & \left(\rho I_{xx}\Omega^2-GD_{yy}\right) & GD_{xy} & -GD_{hy} & -GD_{hy}\\ & & & \left(\rho I_{yy}\Omega^2-GD_{xx}\right) & GD_{hx} & GD_{hx}\\ & Symm & & & -\rho A\Omega^2 r_o^2 & -GD_{\omega\omega}\\ & & & & & \left(\rho C_w\Omega^2-GD_{\omega\omega}\right)\end{bmatrix}_{6\times6}$$

in which $\left\langle \hat{A} \right\rangle_{1\times 6}^{T} = \left\langle \hat{A}_1 \;\middle|\; \hat{A}_2 \;\middle|\; \hat{A}_3 \;\middle|\; \hat{A}_4 \;\middle|\; \hat{A}_5 \;\middle|\; \hat{A}_6 \right\rangle_{1\times 6}^{T}$, $\left\langle \hat{B} \right\rangle_{1\times 6}^{T} = \left\langle \hat{B}_1 \;\middle|\; \hat{B}_2 \;\middle|\; \hat{B}_3 \;\middle|\; \hat{B}_4 \;\middle|\; \hat{B}_5 \;\middle|\; \hat{B}_6 \right\rangle_{1\times 6}^{T}$,

$\left\langle \bar{Q}_f \right\rangle_{1\times 6}^{T} = \left\langle \bar{q}_x \;\middle|\; \bar{q}_y \;\middle|\; \bar{m}_x \;\middle|\; \bar{m}_y \;\middle|\; \bar{m}_z \;\middle|\; \bar{m}_w \right\rangle_{1\times 6}^{T}$, and

$\left\langle \bar{Z}_o \right\rangle_{1\times 6}^{\mathrm{T}} = \left\langle z \;\middle|\; z \;\middle|\; z \;\middle|\; z \;\middle|\; z \;\middle|\; z \right\rangle_{1\times 6}^{\mathrm{T}}$.

From Eq. (6.28), coefficients are equal, yielding:

$$\left\{\bar{B}\right\}_{6\times 1} = \left\{0\right\}_{6\times 1} \quad \text{and} \quad \left[\bar{S}_1\right]_{6\times 6}\left\{\bar{A}\right\}_{6\times 1} = \left\{\bar{Q}_f\right\}_{6\times 1} \tag{6.29}$$

From Eq. (6.29), by substituting into Eq. (6.27), one obtains:

$$\left\langle \bar{U}_{S_p}(z) \right\rangle_{1\times 6}^{T} = \left\langle \bar{u}_p \;\middle|\; \bar{v}_p \;\middle|\; \bar{\theta}_{x_p} \;\middle|\; \bar{\theta}_{y_p} \;\middle|\; \bar{\theta}_{z_p} \;\middle|\; \bar{\psi}_p \right\rangle_{1\times 6}^{T} = \left\langle \left[\bar{S}_1\right]_{6\times 6}^{-1}\left\{\bar{Q}_f\right\}_{6\times 1} \right\rangle_{1\times 6}^{T} \tag{6.30}$$

By adding the homogeneous solution in Eq. (6.25) to the particular solution in Eq. (6.30), the total steady state solution is then obtained:

$$\left\{\bar{U}_S(z)\right\}_{6\times 1} = \left\{\bar{U}_{S_h}(z)\right\}_{6\times 1} + \left\{\bar{U}_{S_p}(z)\right\}_{6\times 1} = \left[\bar{\chi}(z)\right]_{6\times 12}\left\{A_{6,i}\right\}_{12\times 1} + \left[\bar{S}_1\right]_{6\times 6}^{-1}\left\{\bar{Q}_f\right\}_{6\times 1} \tag{6.31}$$

In Equation (6.31), the unknown integration constants $\left\{A_{6,i}\right\}_{12\times 1}$ (for $i = 1,2,3,.....,12$) are to be determined from the boundary conditions. Equation (6.31) presents the total closed-form solution for thin-walled members of asymmetric open section subjected to general harmonic forces.

6.4.3 Example- Solution for Cantilever under Member and End Forces

A cantilever beam with asymmetric cross-section subjected to (1) member harmonic forces; distributed transverse force $\bar{q}_y(z)e^{i\Omega t}$, distributed lateral force $\bar{q}_x(z)e^{i\Omega t}$, distributed bending moments $\bar{m}_x(z)e^{i\Omega t}$ and $\bar{m}_y(z)e^{i\Omega t}$ about X and Y axes, distributed torsional moment $\bar{m}_z(z)e^{i\Omega t}$ and distributed bimoment $\bar{m}_w(z)e^{i\Omega t}$, and (2) end harmonic forces; transverse force $\bar{P}_y(\ell)e^{i\Omega t}$, lateral force $\bar{P}_x(\ell)e^{i\Omega t}$, bending moments $\bar{M}_x(\ell)e^{i\Omega t}$, $\bar{M}_y(\ell)e^{i\Omega t}$, twisting moment $\bar{M}_z(\ell)e^{i\Omega t}$ and bimoment $\bar{M}_w(\ell)e^{i\Omega t}$ is considered as shown in Figure (6.3).

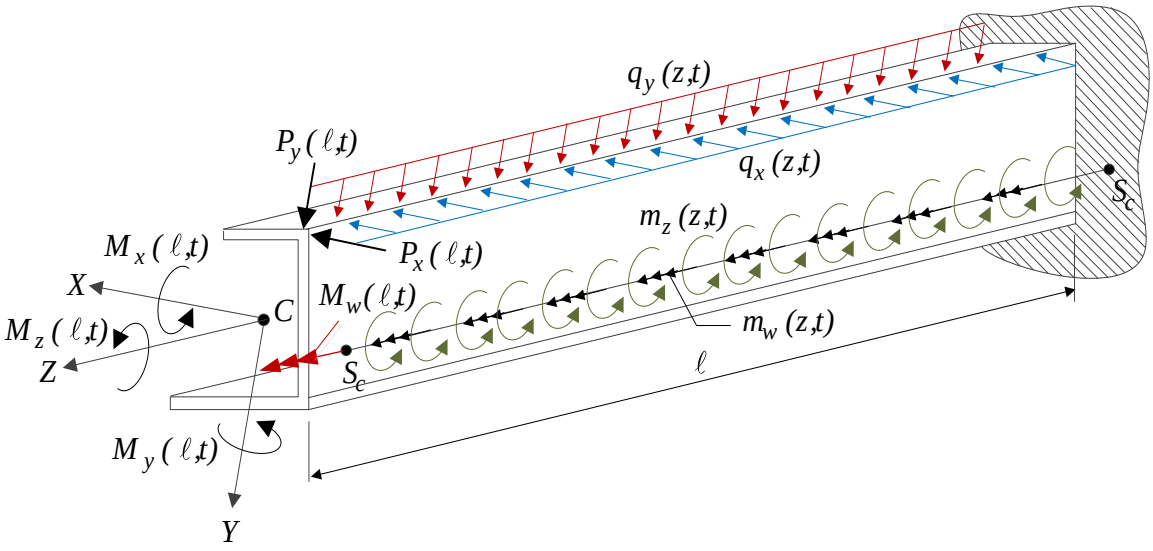

Figure (6.3): Cantilever of asymmetric section under general harmonic forces

It is required to obtain the unknown integration constants $\{A_{6,i}\}_{12\times1}$ from the boundary conditions presented in Equations (6.9-6.14). At the fixed end $z=0$, the boundary conditions for this problem are given as:

$$\delta\bar{u}(0)=\delta\bar{v}(0)=\delta\bar{\theta}_x(0)=\delta\bar{\theta}_y(0)=\delta\bar{\theta}_z(0)=\delta\bar{\psi}(0)=0 \tag{6.32-37}$$

and at free end $z=\ell$:

$$GD_{xx}\left[\bar{u}'(\ell)-\bar{\theta}_y(\ell)\right]+GD_{xy}\left[\bar{v}'(\ell)+\bar{\theta}_x(\ell)\right]+GD_{hx}\left[\bar{\theta}_z'(\ell)+\bar{\psi}(\ell)\right]=\bar{V}_x(\ell) \tag{6.38}$$

$$GD_{xy}\left[\bar{u}'(\ell)-\bar{\theta}_y(\ell)\right]+GD_{yy}\left[\bar{v}'(\ell)+\bar{\theta}_x(\ell)\right]+GD_{hy}\left[\bar{\theta}_z'(\ell)+\bar{\psi}(\ell)\right]=\bar{V}_y(\ell) \tag{6.39}$$

$$EI_{xx}\bar{\theta}_x'(\ell)=-\bar{M}_x(\ell) \tag{6.40}$$

$$EI_{yy}\bar{\theta}_y'(\ell)=\bar{M}_y(\ell) \tag{6.41}$$

$$GD_{hx}\left[\bar{u}'(\ell)-\bar{\theta}_y(\ell)\right]+GD_{hy}\left[\bar{v}'(\ell)+\bar{\theta}_x(\ell)\right]+GD_{\omega\omega}\left[\bar{\theta}_z'(\ell)+\bar{\psi}(\ell)\right]+GJ\bar{\theta}_z'(\ell)=\bar{M}_z(\ell) \tag{6.42}$$

$$EC_w\bar{\psi}'(\ell)=-\bar{M}_w(\ell) \tag{6.43}$$

Substituting Equation (6.31) into Equations (6.32-6.43), the resulting equations are written in matrix form:

$$\left[\Phi_C\right]_{12\times12}\left\{A_{6,i}\right\}_{12\times1}=\left\{\bar{Q}_C\right\}_{12\times1} \tag{6.44}$$

in which

$$[\Phi_C]^T_{12\times12} = \Big[\{\bar{F}_{1,\mathrm{j}}\}_{12\times1} \;\Big|\; \{\bar{F}_{2,\mathrm{j}}\}_{12\times1} \;\Big|\; \{\bar{F}_{3,\mathrm{j}}\}_{12\times1} \;\Big|\; \{\bar{F}_{4,\mathrm{j}}\}_{12\times1} \;\Big|\; \{\bar{F}_{5,\mathrm{j}}\}_{12\times1} \;\Big|\; \{1\}_{12\times1} \;\Big|\; \{\bar{G}_{1,\mathrm{j}}\}_{12\times1} \;\Big|\; \{\bar{G}_{2,\mathrm{j}}\}_{12\times1} \;\Big|\; \{\bar{G}_{3,\mathrm{j}}\}_{12\times1} \;\Big|\; \{\bar{G}_{4,\mathrm{j}}\}_{12\times1} \;\Big|\; \{\bar{G}_{5,\mathrm{j}}\}_{12\times1} \;\Big|\; \{\bar{G}_{6,\mathrm{j}}\}_{12\times1}\Big]^T_{12\times12}$$

$$\langle \bar{Q}_C \rangle^T_{1\times12} = \Big\langle -\bar{u}_p \;\Big|\; -\bar{v}_p \;\Big|\; -\bar{\theta}_{x_p} \;\Big|\; -\bar{\theta}_{y_p} \;\Big|\; -\bar{\theta}_{z_p} \;\Big|\; -\bar{\psi}_p \;\Big|\; \Big[\bar{P}_x(\ell) - G\left(D_{xy}\bar{\theta}_{x_p} - D_{xx}\bar{\theta}_{y_p} + D_{hx}\bar{\psi}_p\right)\Big] \;\Big|\; \Big[\bar{P}_y(\ell) - G\left(D_{yy}\bar{\theta}_{x_p} - D_{xy}\bar{\theta}_{y_p} + D_{hy}\bar{\psi}_p\right)\Big] \;\Big|\; -\bar{M}_x(\ell) \;\Big|\; \bar{M}_y(\ell) \;\Big|\; \Big[\bar{M}_z(\ell) - G\left(D_{hy}\bar{\theta}_{x_p} - D_{hx}\bar{\theta}_{y_p} + D_{\omega\omega}\bar{\psi}_p\right)\Big] \;\Big|\; -\bar{M}_w(\ell)\Big\rangle^T_{1\times12}$$

where

$$\bar{G}_{1,j} = G\left(D_{xx}\left[\bar{F}_{1,\mathrm{j}}m_j - \bar{F}_{4,\mathrm{j}}\right] + D_{xy}\left[\bar{F}_{2,\mathrm{j}}m_j + \bar{F}_{3,\mathrm{j}}\right] + D_{hx}\left[\bar{F}_{5,\mathrm{j}}m_j + 1\right]\right)e^{m_i\ell},$$

$$\bar{G}_{2,j} = G\left(D_{xy}\left[\bar{F}_{1,\mathrm{j}}m_j - \bar{F}_{4,\mathrm{j}}\right] + D_{yy}\left[\bar{F}_{2,\mathrm{j}}m_j + \bar{F}_{3,\mathrm{j}}\right] + D_{hy}\left[\bar{F}_{5,\mathrm{j}}m_j + 1\right]\right)e^{m_i\ell},$$

$$\bar{G}_{3,\mathrm{j}} = EI_{xx}\bar{F}_{3,\mathrm{j}}m_j\,e^{m_i\ell}, \quad \bar{G}_{4,\mathrm{j}} = EI_{yy}\bar{F}_{4,\mathrm{j}}m_j\,e^{m_i\ell},$$

$$\bar{G}_{5,\mathrm{j}} = G\left(D_{hx}\left[\bar{F}_{1,\mathrm{j}}m_j - \bar{F}_{4,\mathrm{j}}\right] + D_{hy}\left[\bar{F}_{2,\mathrm{j}}m_j + \bar{F}_{3,\mathrm{j}}\right] + D_{\omega\omega}\left[\bar{F}_{5,\mathrm{j}}m_j + 1\right] + J\,\bar{F}_{5,\mathrm{j}}m_j\right)e^{m_i\ell},$$

and $\bar{G}_{6,i} = EC_w m_i\,e^{m_i\ell}$, for $i = 1,2,3,4,.....,12$.

From Equation (6.44), by substituting into Equation (6.31), the solution for the bending-torsional coupled response is obtained as:

$$\left\{\bar{U}_{S_C}(z)\right\}_{6\times1} = \left[\bar{\chi}(z)\right]_{6\times12}\left[\bar{\Phi}_C(z)\right]^{-1}_{12\times12}\left\{\bar{Q}_C\right\}_{12\times1} + \left[\bar{S}_1\right]^{-1}_{6\times6}\left\{\bar{Q}_f\right\}_{6\times1} \tag{6.45}$$

Equation (6.45) represents the general steady state dynamic response for cantilever thin-walled members of asymmetric sections under general harmonic forces.

6.4.4 Example- Solution for Simply-Supported Beam under Harmonic Forces

A simply supported beam with asymmetric section under general (1) distributed harmonic forces; lateral and transverse forces $\bar{q}_j(z)\mathrm{e}^{i\Omega t}$, bending moments $\bar{m}_j(z)\mathrm{e}^{i\Omega t}$, (for $j = x, y$) about X and Y axes, respectively, twisting moment $\bar{m}_z(z)\mathrm{e}^{i\Omega t}$, and bimoment $\bar{m}_w(z)\mathrm{e}^{i\Omega t}$, (2) end harmonic forces: bending moments $\bar{M}_x(z_e)\mathrm{e}^{i\Omega t}$ and $\bar{M}_y(z_e)\mathrm{e}^{i\Omega t}$ about X and Y axes, and bimoments $\bar{M}_w(z_e)\mathrm{e}^{i\Omega t}$ at both ends $(z_e = 0, \ell)$ is considered as illustrated in Figure (6.4).

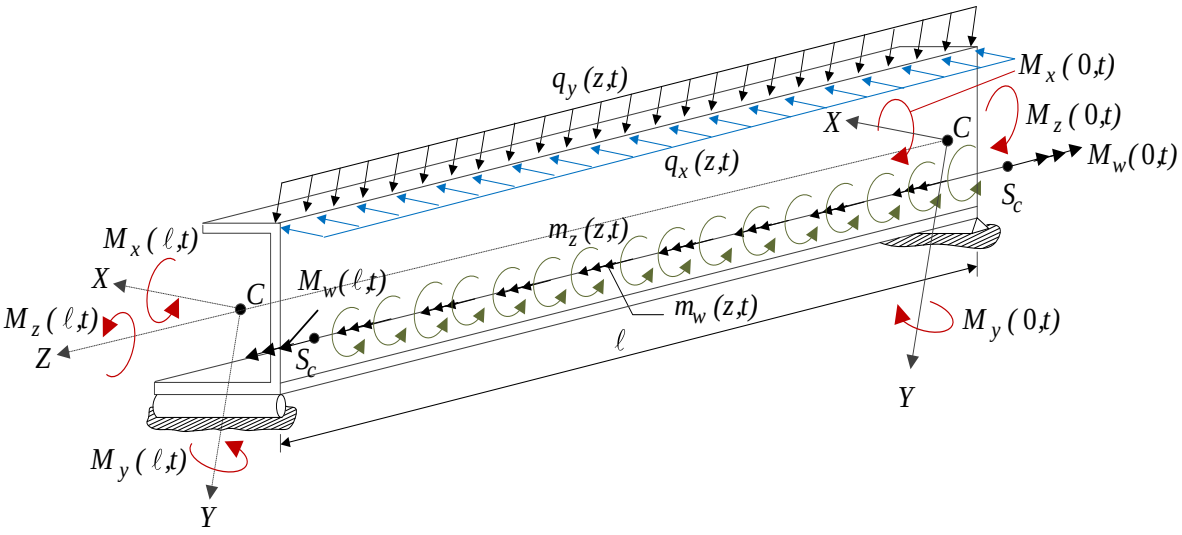

Figure (6.4): Simply-supported member of asymmetric cross-section under general harmonic forces

The restraints leave the end-sections free to warp and to rotate about X and Y axes. Imposing the following simply supported boundary conditions at both member ends $z=0$ and $z=\ell$:

$$\bar{u}(0)=0,\ \bar{v}(0)=0,\quad EI_{xx}\bar{\theta}_x'(0)=\bar{M}_x(0) \tag{6.46-48}$$

$$EI_{yy}\bar{\theta}_y'(0)=-\bar{M}_y(0),\quad \bar{\theta}_z(0)=0,\quad EC_w\bar{\psi}'(0)=\bar{M}_w(0) \tag{6.49-51}$$

$$\bar{u}(\ell)=0,\quad \bar{v}(\ell)=0,\quad EI_{xx}\bar{\theta}_x'(\ell)=-\bar{M}_x(\ell) \tag{6.52-54}$$

$$EI_{yy}\bar{\theta}_y'(\ell)=\bar{M}_y(\ell),\ \bar{\theta}_z(\ell)=0,\quad EC_w\bar{\psi}'(\ell)=-\bar{M}_w(\ell) \tag{6.55-57}$$

Substituting the expressions for displacement functions (6.31) into the above boundary conditions (6.46) to (6.57), the obtained expressions are provided in matrix form as:

$$[\Phi_S]_{12\times12}\{A_{6,i}\}_{12\times1}=\{\bar{Q}_S\}_{12\times1} \tag{6.58}$$

in which

$$[\Phi_S]^T_{12\times12}=\Big[\{\bar{F}_{1,j}\}_{12\times1}\ \{\bar{F}_{2,j}\}_{12\times1}\ \{\bar{F}_{3,j}m_j\}_{12\times1}\ \{\bar{F}_{4,j}m_j\}_{12\times1}\ \{\bar{F}_{5,j}\}_{12\times1}\ \{m_j\}_{12\times1}\ \{\bar{E}_{1,j}\}_{12\times1}\ \{\bar{E}_{2,j}\}_{12\times1}\ \{\bar{E}_{3,j}m_j\}_{12\times1}\ \{\bar{E}_{4,j}m_j\}_{12\times1}\ \{\bar{E}_{5,j}\}_{12\times1}\ \{\bar{E}_{6,j}\}_{12\times1}\Big]^T_{12\times12}$$

$$\langle\bar{Q}_S\rangle^T_{1\times12}=\Big\langle-\bar{u}_p\ -\bar{v}_p\ \bar{M}_x(0)/EI_{xx}\ -\bar{M}_y(0)/EI_{yy}\ -\bar{\theta}_{z_p}\ \bar{M}_w(0)/EC_w\ -\bar{u}_p\ -\bar{v}_p\ -\bar{M}_x(\ell)/EI_{xx}\ \bar{M}_y(\ell)/EI_{yy}\ -\bar{\theta}_{z_p}\ -\bar{M}_w(\ell)/EC_w\Big\rangle^T_{1\times12}$$

where $\bar{E}_{k,j}=\bar{F}_{k,j}e^{m_i\ell}$, $\bar{E}_{6,j}=m_j e^{m_j\ell}$, for $k=1,2,3,4,5$ and $j=1,2,3,....,12$.

From Equation (6.58), by substituting into Equation (6.46), the solution for the bending-torsional coupled deformation is obtained as:

$$\left\{\bar{U}_{S_s}(z)\right\}_{6\times1} = \left[\bar{\chi}(z)\right]_{6\times12}\left[\Phi_S\right]^T_{12\times12}\left\{\bar{Q}_S\right\}_{12\times1} + \left[\bar{S}_1\right]^{-1}_{6\times6}\left\{\bar{Q}_f\right\}_{6\times1} \tag{6.59}$$

The above formulation represents the general steady state dynamic response solution of simply-supported asymmetric members under general harmonic excitations.

6.5 Finite Element Solution

This section formulates a two-noded finite element with six degrees of freedom per node. The element is based on a family of shape functions which exactly satisfy the dynamic equilibrium equations. Figure (6.5) shows a two-noded finite asymmetric channel-beam element with six degrees of freedom at each node.

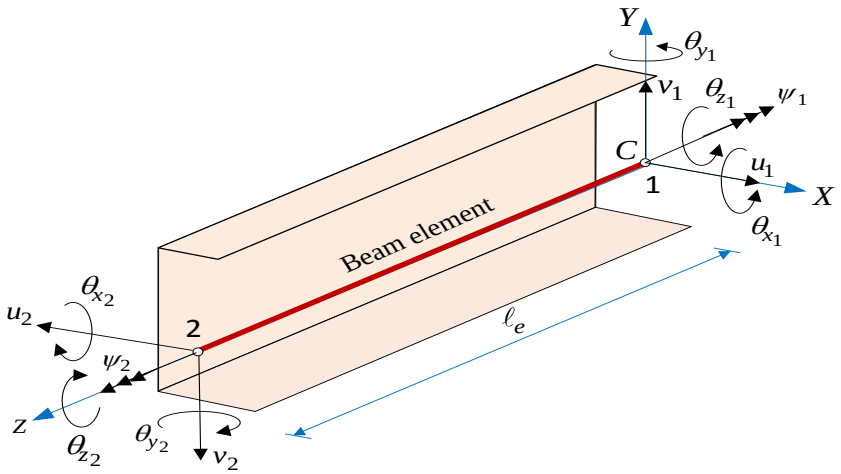

Figure (6.5): Thin-walled two-noded asymmetric channel-beam element

6.5.1 Variational Formulation

From the Hamilton's variational principle expressed by $\int_{t_1}^{t_2}\delta\left(T^* - U^*\right)dt + \int_{t_1}^{t_2}\delta W^* dt = 0$, by substituting the displacements and forces expressions presented in Equations (3.79) to (3.81) into kinetic energy expression T^*, internal strain energy U^* and the external work of the applied forces on the system W^* presented by Equations (3.13), (3.21) and (3.35), and by enforcing the orthogonality conditions; performing integration by parts with respect to time t; and noting that all the variations of the coefficients at time limits t_1 and t_2 are zero, i.e., $\delta\bar{u}(t_1) = \delta\bar{u}(t_2) = 0$, $\delta\bar{v}(t_1) = \delta\bar{v}(t_2) = 0$, $\delta\bar{\theta}_x(t_1) = \delta\bar{\theta}_x(t_2) = 0$,

$\delta\bar{\theta}_y(t_1)=\delta\bar{\theta}_y(t_2)=0$, $\delta\bar{\theta}_z(t_1)=\delta\bar{\theta}_z(t_2)=0$, and $\delta\bar{\psi}(t_1)=\delta\bar{\psi}(t_2)=0$, the variations of the energy expressions are then obtained in terms of nodal degrees of freedom, in which the variation of kinetic energy δT^* is given as:

$$\int_{t_1}^{t_2}\delta T^* dt=\int_{t_1}^{t_2}\left[-\Omega^2\int_0^{\ell}\left(\left\langle\delta\bar{U}_S(z)\right\rangle_{1\times6}^T\left[\bar{X}_S\right]_{6\times6}\left\{\bar{U}_S(z)\right\}_{6\times1}+\left\langle\delta\bar{U}_r(z)\right\rangle_{1\times3}^T\left\{\bar{X}_r(z)\right\}_{3\times1}\right)dz\right]e^{i\Omega t}dt \quad (6.60)$$

in which $\left[\bar{X}_S\right]_{6\times6}=diag\left[\rho A \;\vdots\; \rho A \;\vdots\; \rho I_{xx} \;\vdots\; \rho I_{yy} \;\vdots\; \rho A r_o^2 \;\vdots\; \rho C_w\right]_{6\times6}$,

$\left\langle\bar{U}_r(z)\right\rangle_{1\times3}^T=\left\langle\bar{u}(z) \quad \bar{v}(z) \quad \bar{\theta}_z(z)\right\rangle_{1\times3}^T$ and

$\left\langle\bar{X}_r(z)\right\rangle_{1\times3}^T=\left\langle\rho A y_s\bar{\theta}_z(z) \quad -\rho A x_s\bar{\theta}_z(z) \quad \rho A\left[y_s\bar{u}(z)-x_s\bar{v}(z)\right]\right\rangle_{1\times3}^T$

The variation of the internal strain energy δU^* is:

$$\int_{t_1}^{t_2}\delta U^* dt=\int_{t_1}^{t_2}\left[\int_0^{\ell}\left(\left\langle\delta\bar{U}_S'(z)\right\rangle_{1\times6}^T\left[\bar{X}_a\right]_{6\times6}\left\{\bar{U}_S'(z)\right\}_{6\times1}+\left\langle\delta\bar{U}_d'(z)\right\rangle_{1\times6}^T\left\{\bar{X}_b(z)\right\}_{6\times6}\left\{\bar{U}_d(z)\right\}_{6\times1}\right)dz\right]e^{i\Omega t}dt \quad (6.61)$$

in which $\left[\bar{X}_a\right]_{6\times6}=diag\left[0 \;\vdots\; 0 \;\vdots\; EI_{xx} \;\vdots\; EI_{yy} \;\vdots\; GJ \;\vdots\; EC_w\right]_{6\times6}$,

$$\left[\bar{X}_b\right]_{6\times6}=\begin{bmatrix} GD_{xx} & GD_{xy} & GD_{xy} & -GD_{xx} & GD_{hx} & GD_{hx} \\ & GD_{yy} & GD_{yy} & -GD_{xy} & GD_{hy} & GD_{hy} \\ & & GD_{yy} & -GD_{xy} & GD_{hy} & GD_{hy} \\ & & & GD_{xx} & -GD_{hx} & -GD_{hx} \\ & Symm & & & GD_{\omega\omega} & GD_{\omega\omega} \\ & & & & & GD_{\omega\omega} \end{bmatrix}_{6\times6}$$

and $\left\langle\bar{U}_d(z)\right\rangle_{1\times6}^T=\left\langle\bar{u}'(z) \;\vdots\; \bar{v}'(z) \;\vdots\; \bar{\theta}_x(z) \;\vdots\; \bar{\theta}_y(z) \;\vdots\; \bar{\theta}_z'(z) \;\vdots\; \bar{\psi}(z)\right\rangle_{1\times6}^T$.

and the work done δW^* by the applied harmonic forces is:

$$\int_{t_1}^{t_2}\delta W^* dt=\int_{t_1}^{t_2}\left[\int_0^{\ell}\left\langle\delta\bar{U}_S(z)\right\rangle_{1\times6}^T\left\{\bar{P}(z)\right\}_{6\times1}dz\right]e^{i\Omega t}dt \quad (6.62)$$

in which $\left\langle\bar{P}(z)\right\rangle_{1\times6}^T=\left\langle\bar{q}_x(z) \;\vdots\; \bar{q}_y(z) \;\vdots\; \bar{m}_x(z) \;\vdots\; \bar{m}_y(z) \;\vdots\; \bar{m}_z(z) \;\vdots\; \bar{m}_w(z)\right\rangle_{1\times6}^T$.

From Equations (6.60) to (6.62), by substituting into variational form of Hamilton's principle, one recovers:

$$\int_0^{\ell}\Big[\Omega^2\left(\left\langle\delta\bar{U}_S(z)\right\rangle_{1\times6}^T\left[\bar{X}_S\right]_{6\times6}\left\{\bar{U}_S(z)\right\}_{6\times1}+\left\langle\delta\bar{U}_r(z)\right\rangle_{1\times3}^T\left\{\bar{X}_r(z)\right\}_{3\times1}\right)-\left(\left\langle\delta\bar{U}_S'(z)\right\rangle_{1\times6}^T\left[\bar{X}_a\right]_{6\times6}\left\{\bar{U}_S'(z)\right\}_{6\times1}+\left\langle\delta\bar{U}_d'(z)\right\rangle_{1\times6}^T\left[\bar{X}_b\right]_{6\times6}\left\{\bar{U}_d(z)\right\}_{6\times1}-\left\langle\delta\bar{U}_S(z)\right\rangle_{1\times6}^T\left\{\bar{P}(z)\right\}_{6\times1}\right)\Big]dz=0 \quad (6.63)$$

6.5.3 Formulating Exact Shape Functions

In the present study, the vector of unknown integration constants $\{A_{6,i}\}_{12\times1}$ is expressed in terms of the nodal displacements by enforcing the conditions: $\bar{u}(0)=u_1$, $\bar{v}(0)=v_1$, $\bar{\theta}_x(0)=\theta_{x_1}$, $\bar{\theta}_y(0)=\theta_{y_1}$, $\bar{\theta}_z(0)=\theta_{z_1}$, $\bar{\psi}(0)=\psi_1$ and $\bar{u}(\ell)=u_2$, $\bar{v}(\ell)=v_2$, $\bar{\theta}_x(\ell)=\theta_{x_2}$, $\bar{\theta}_y(\ell)=\theta_{y_2}$, $\bar{\theta}_z(\ell)=\theta_{z_2}$, $\bar{\psi}(\ell)=\psi_2$. The displacement field functions $\langle\bar{U}_S(z)\rangle^T_{1\times6}$ are expressed in terms of nodal displacements

$\langle\bar{U}_N(z)\rangle^T_{1\times12}=\langle u_1 \mid v_1 \mid \theta_{x_1} \mid \theta_{y_1} \mid \theta_{z_1} \mid \psi_1 \mid u_2 \mid v_2 \mid \theta_{x_2} \mid \theta_{y_2} \mid \theta_{z_2} \mid \psi_2\rangle^T_{1\times12}$, yielding:

$$\{\bar{U}_N(z)\}_{12\times1}=\begin{Bmatrix}\{\bar{U}_S(0)\}_{6\times1}\\ \{\bar{U}_S(\ell)\}_{6\times1}\end{Bmatrix}=\begin{bmatrix}[\bar{\chi}(0)]_{6\times12}\\ [\bar{\chi}(\ell)]_{6\times12}\end{bmatrix}\{A_{6,i}\}_{12\times1}=[R]_{12\times12}\{A_{6,i}\}_{12\times1} \tag{6.64}$$

From Eq. (6.64), by substituting into the homogeneous part of Eq. (6.31), noting that the particular part is vanished in the finite element formulation, one obtains:

$$\{\bar{U}_S(z)\}_{6\times1}=[\bar{\chi}(z)]_{6\times12}[R]^{-1}_{12\times12}\{\bar{U}_N(z)\}_{12\times1}=[H(z)]_{6\times12}\{\bar{U}_N(z)\}_{12\times1} \tag{6.65}$$

in which matrix $[H(z)]_{6\times12}=[\bar{\chi}(z)]_{6\times12}[R]^{-1}_{12\times12}$ is a matrix of shape functions. It is noted that the interpolation shape functions provided in Equation (6.65) exactly satisfy the homogeneous solution of the field coupled equations.

6.5.4 Finite element formulation

From Equation (6.65), by substituting into the vectors for space displacements and forces represented in the governing differential equation (6.63), one obtains:

$$\left([K_e]_{12\times12}-\Omega^2[M_e]_{12\times12}\right)_{12\times12}\{\bar{U}_N\}_{12\times1}=\{\bar{F}_e\}_{12\times1} \tag{6.66}$$

where $[K_e]_{12\times12}=\int_0^\ell\left([H'(z)]^T_{12\times6}[\bar{X}_a]_{6\times6}[H'(z)]_{6\times12}+[H_d(z)]^T_{12\times6}[\bar{X}_b]_{6\times6}[H_d(z)]_{6\times12}\right)dz$ is the element stiffness matrix, $[M_e]_{12\times12}=\int_0^\ell\left([H(z)]^T_{12\times6}[\bar{X}_S]_{6\times6}[H(z)]_{6\times12}+[H_r(z)]_{12\times12}\right)dz$ is the element mass matrix and the element load vector of applied harmonic forces is given by: $\{F_e(z)\}_{12\times1}=\int_0^\ell[H(z)]^T_{12\times6}\{\bar{P}(z)\}_{6\times1}dz$, where

$$\left[H_d(z)\right]^T_{12\times 6}=\left[\left\{H'_{1,\mathrm{j}}(z)\right\}_{12\times 1}\ \left\{H'_{2,\mathrm{j}}(z)\right\}_{12\times 1}\ \left\{H_{3,\mathrm{j}}(z)\right\}_{12\times 1}\ \left\{H_{4,\mathrm{j}}(z)\right\}_{12\times 1}\ \left\{H'_{5,\mathrm{j}}(z)\right\}_{12\times 1}\ \left\{H_{6,\mathrm{j}}(z)\right\}_{12\times 1}\right]^T_{12\times 6},$$

$$\left[H_r(z)\right]_{12\times 12}=\left[\left\{H_{1,\mathrm{j}}(z)\right\}_{12\times 1}\ \left\{H_{2,\mathrm{j}}(z)\right\}_{12\times 1}\ \left\{H_{5,\mathrm{j}}(z)\right\}_{12\times 1}\right]_{12\times 3}\begin{bmatrix} y_s\rho A\left\langle H_{5,\mathrm{j}}(z)\right\rangle^T_{1\times 12} \\ \cdots\cdots \\ -x_s\rho A\left\langle H_{5,\mathrm{j}}(z)\right\rangle^T_{1\times 12} \\ \cdots\cdots \\ \rho A\left[y_s\left\langle H_{1,\mathrm{j}}(z)\right\rangle^T_{1\times 12}-x_s\left\langle H_{2,\mathrm{j}}(z)\right\rangle^T_{1\times 12}\right] \end{bmatrix}_{3\times 12}.$$

The present finite element formulation is used to capture the coupled bending-torsional-warping dynamic response for asymmetric cross-sections under general harmonic forces. The stiffness, mass matrices and the load vector are obtained by using the exact shape functions developed in this formulation.

6.6 Examples and Discussion

In this section, a set of examples for thin-walled open beams of asymmetric cross-sections subjected to general harmonic forces and various boundary conditions are presented to assess the validity, accuracy and applicability of the present closed-form and finite element solutions (using a single two-noded beam element having twelve degrees of freedom). Provided are comparisons with results based on other established available solutions for static and steady state responses. The static response can be approached by using very low exciting frequency Ω compared to the first natural frequency $\bar{\omega}_1$ of the system, i.e., $\Omega=0.01\bar{\omega}_1$. The material properties used in all examples are $E=200GPa$, $G=77GPa$ and $\rho=7850.0\,kg/m^3$. Three solutions are provided for comparison. These are:

(i) A solution based on the Vlasov beam theory (appendix 6B provides the closed-form solution of coupled bending-torsional response for thin-walled Vlasov beam) which neglects shear deformation and distortional effects,

(ii) A solution based on Abaqus two-noded B31OS beam element with seven degrees of freedom per node (i.e., three translations, three rotations and warping deformation) which accounts for shear deformation only for bending but ignores (a) shear deformation due to warping deformation and (b) distortional effects, and

(iii) A solution based on Abaqus S4R shell element (four-noded doubly curved shell element with six degrees of freedom per node, i.e., three translations and three

rotations) which captures shear deformation and distortional effects of the cross-section.

6.6.1 Example 1- Long cantilever under member twisting moment

A 4.0m span cantilever has a thin-walled asymmetric channel-section of unequal flanges as shown in Figure (6.6), and it is subjected to uniformly distributed twisting moment $0.40\mathrm{e}^{i\Omega t}\,kNm/m$. The channel-section has an upper flange width $b_t=40mm$, lower flange width $b_b=80mm$, and mid-surface height $H=100mm$, flange thicknesses are $t_f=10mm$ and web thickness is $t_w=8mm$.

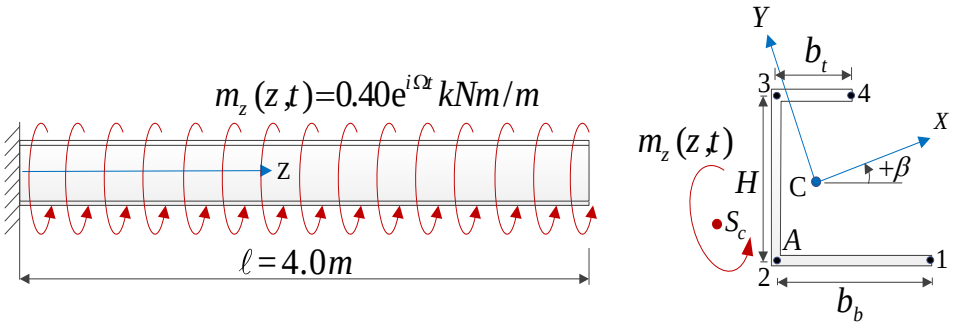

Figure (6.6): Cantilever asymmetric C-section under distributed twisting moment

It is required to (1) extract the natural frequencies from a steady state dynamic analysis, and (2) determine the quasi-static response by adopting a very low exciting frequency, i.e., $\Omega=0.01\bar{\omega}_1\approx 0.2312rad/\sec$, and (3) determine the steady state dynamic response for an exciting frequency $\Omega=1.356\omega_1\approx 31.42rad/\sec$. (As observed under the results of item 1, the first natural frequency is $\bar{\omega}_1=23.12rad/\sec$).

The sectional properties for the channel-section with respect to the XCY principal coordinate system through the centroid C are $A=0.20\times10^4\,mm^2$, $I_{xx}=3.723\times10^6\,mm^4$, $I_{yy}=0.878\times10^6\,mm^4$, $J=0.571\times10^5\,mm^4$, $C_w=0.861\times10^9\,mm^6$. The principal coordinates are inclined through an angle $\beta=17.14^o$ (Fig. 6.4). The centroidal coordinates in the global coordinate system are $(C_x,C_y)=(20mm,60mm)$ while the coordinates of the shear centre S_c in the principal direction are $(X_s,Y_s)=(-42.83mm,-10.29mm)$.

In the Abaqus shell model, the cantilever is subdivided into 200 S4R shell elements along the longitudinal axis of the member, four elements along the top flange, eight elements along the bottom flange, and ten elements along the web height, i.e., the Abaqus shell model consists of 4,400 S4R-elements (Figure 6.7) with approximately 27,740 degrees of freedom. In the case of the Abaqus beam model, a total of 200 B31OS-beam elements with 1,400 degrees of freedom were needed to achieve convergence, while the finite element solution developed in the present study is based on exact shape functions and are conducted using a single finite element with two nodes and six degrees of freedom per node and was observed to give results exactly matching those based on the closed-form solution developed in this study up to five significant digits.

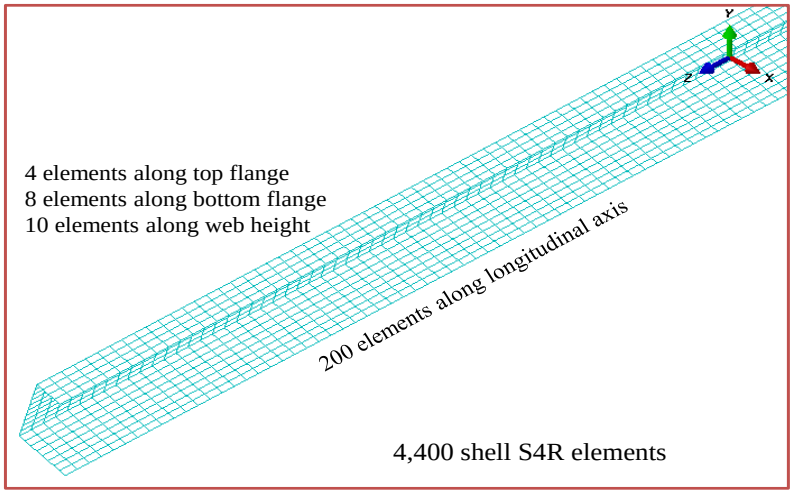

Figure (6.7): Shell S4R meshing of long cantilever asymmetric channel-section

6.6.1.1 Steady state dynamic analysis

The steady state response analysis under distributed twisting moments $0.40\mathrm{e}^{i\Omega t}\ kNm/m$ is performed multiple times for an exciting frequency Ω varying from nearly zero to 100Hz. The natural frequencies are then extracted from the peaks of the displacement-frequency relationships. The lateral displacement $\bar{u}_A$, transverse displacement $\bar{v}_A$, bending rotations $\bar{\theta}_x$, $\bar{\theta}_y$, twist angle $\bar{\theta}_z$ and warping deformation $\bar{\psi}$ at the cantilever tip (Fig. 6.6) against the exciting frequency Ω are depicted in Figures (6.8*a*, 6.8*c*, 6.8*e*, 6.8*g*, 6.8*i* and 6.8*k*), respectively. The solutions based on Vlasov beam theory, Abaqus B31OS and Abaqus shell solutions are overlaid on the same diagrams for comparison. Each peak indicates resonance and thus identifies natural frequencies of the beam. Thus, the first

seven natural frequencies were extracted from the peaks of Figures (6.8*b*, 6.8*d*, 6.8*f*, 6.8*h*, 6.8 *j* and 6.8*l*).

In the shell FEA model, the rotation angles $\bar{\theta}_x$, $\bar{\theta}_y$ and warping deformation $\bar{\psi}$ for a given section z_i are determined from the Abaqus shell model by extracting the longitudinal displacements at section z_i at the four corner points of the cross-sections (Fig. 6.6). Equation (3.3) is then used to express the longitudinal displacements leading to four equations of the form $\bar{w}(z,s_i)=\bar{w}(z)+y(s_i)\bar{\theta}_x(z)-x(s_i)\bar{\theta}_y(z)+\omega(s_i)\bar{\psi}(z)$, where x_i, y_i (for $i=1,2,3,4$) are the coordinates of the four corner points along the principal directions (X,Y), and ω_i (for $i=1,2,3,4$) are the corresponding warping function values. This leads to the system of equations:

$$\begin{Bmatrix} \bar{w}(z,s_1) \\ \bar{w}(z,s_2) \\ \bar{w}(z,s_3) \\ \bar{w}(z,s_4) \end{Bmatrix}_{4\times1} = \begin{bmatrix} 1 & y(s_1) & -x(s_1) & \omega(s_1) \\ 1 & y(s_2) & -x(s_2) & \omega(s_2) \\ 1 & y(s_3) & -x(s_3) & \omega(s_3) \\ 1 & y(s_4) & -x(s_4) & \omega(s_4) \end{bmatrix}_{4\times4} \begin{Bmatrix} \bar{w}(z) \\ \bar{\theta}_x(z) \\ \bar{\theta}_y(z) \\ \bar{\psi}(z) \end{Bmatrix}_{4\times1} \tag{6.67}$$

which is then solved for the vector of generalized space displacements $\langle \bar{w}(z) \;\; \bar{\theta}_x(z) \;\; \bar{\theta}_y(z) \;\; \bar{\psi}(z) \rangle^T_{1\times4}$. The resulting warping values for $\bar{\psi}(z)$ are depicted in Figures (6.8k and 6.8*l*).

Table (6.2) provides the first eight natural frequencies as extracted from the steady state response analyses based on all four solutions. As a general observation, the present solution predicts frequencies in excellent agreement with those based on Vlasov closed-form and Abaqus beam and shell solutions. This is particularly the case for the lower eigen-frequencies. The agreement is observed to slightly deteriorate for higher frequency modes, although remaining close. At the eighth eigen-frequency predictions of all four solutions agree within a few percents.

Frequencies predicted by the Vlasov solution are the highest (since the solution neglects shear deformation and distortion effects, and thus provides the stiffest representation of the structure) while Abaqus shell solution has the lowest values (since it incorporates shear deformation and distortional effects, and thus provides the most flexible and most

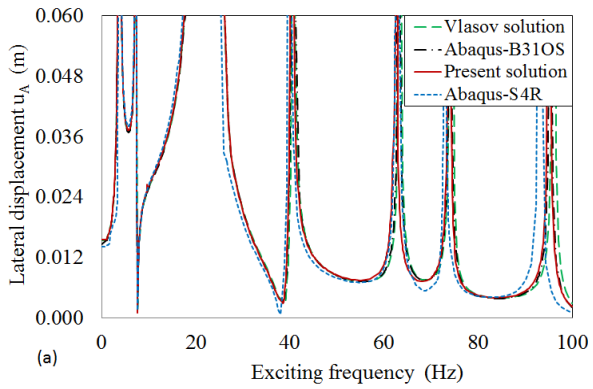
Vlasov solution
Abaqus-B31OS
Present solution
Abaqus-S4R
Lateral displacement u_A (m)
Exciting frequency (Hz)
(a)

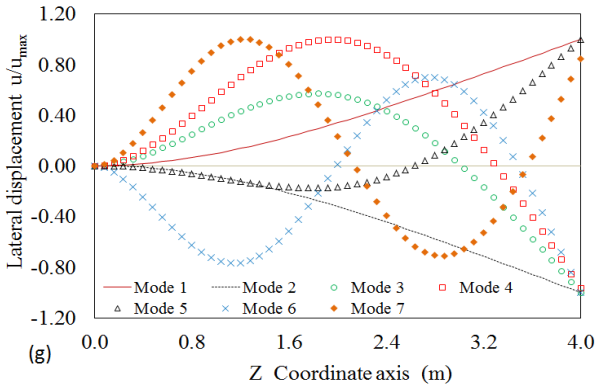
Lateral displacement u/u_{max}
Mode 1
Mode 2
Mode 3
Mode 4
Mode 5
Mode 6
Mode 7
Z Coordinate axis (m)
(g)

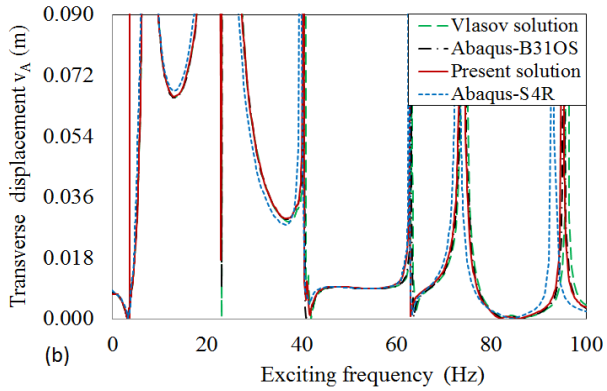
Vlasov solution
Abaqus-B31OS
Present solution
Abaqus-S4R
Transverse displacement v_A (m)
Exciting frequency (Hz)
(b)

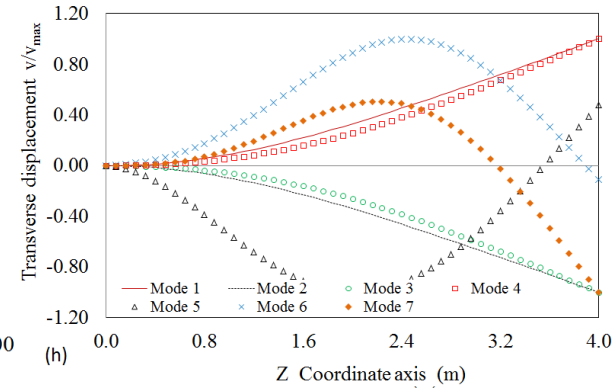
Transverse displacement v/v_{max}
Mode 1
Mode 2
Mode 3
Mode 4
Mode 5
Mode 6
Mode 7
Z Coordinate axis (m)
(h)

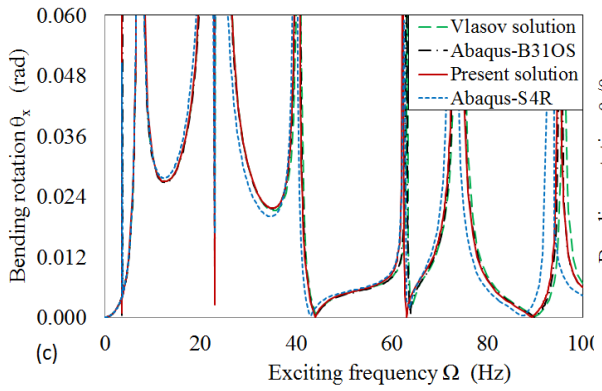
Vlasov solution
Abaqus-B31OS
Present solution
Abaqus-S4R
Bending rotation θ_x (rad)
Exciting frequency Ω (Hz)
(c)

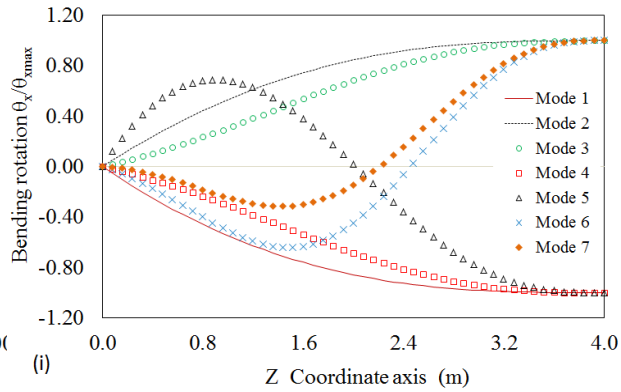
Bending rotation θ_x/θ_{xmax}
Mode 1
Mode 2
Mode 3
Mode 4
Mode 5
Mode 6
Mode 7
Z Coordinate axis (m)
(i)

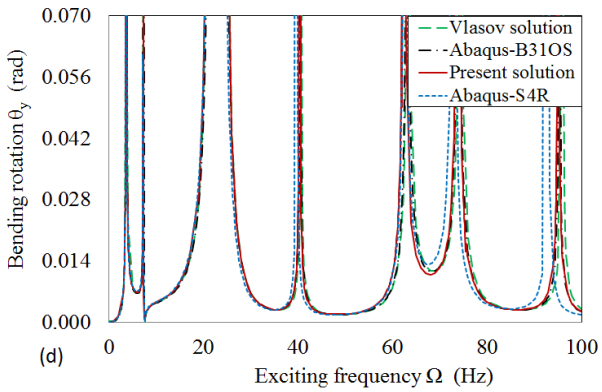
Vlasov solution
Abaqus-B31OS
Present solution
Abaqus-S4R
Bending rotation θ_y (rad)
Exciting frequency Ω (Hz)
(d)

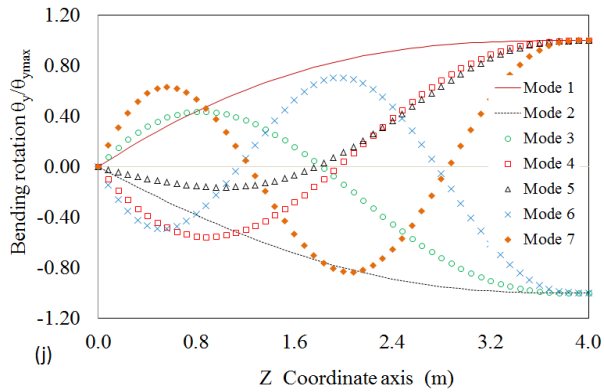
Bending rotation θ_y/θ_{ymax}
Mode 1
Mode 2
Mode 3
Mode 4
Mode 5
Mode 6
Mode 7
Z Coordinate axis (m)
(j)

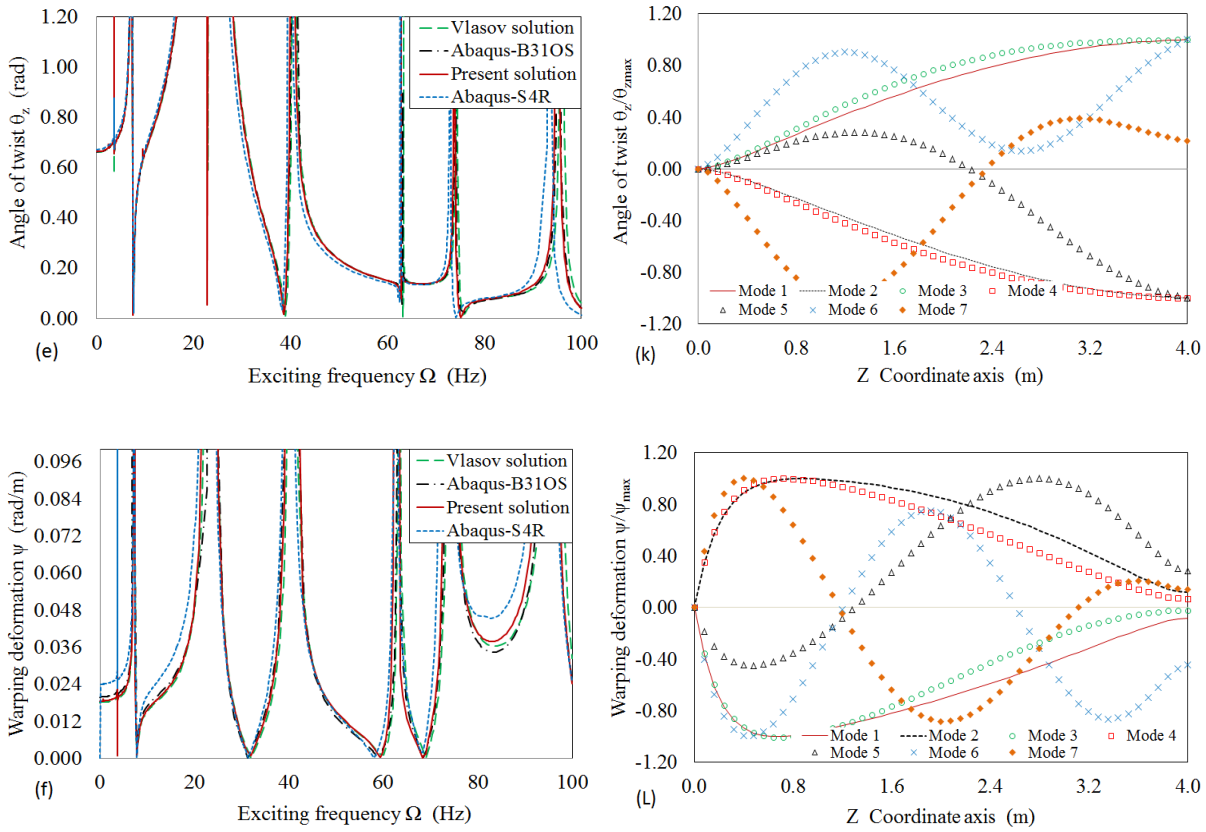

Figure (6.8): Natural frequencies and modes extracted from steady state response of cantilever asymmetric C-section under distributed harmonic torsion.

Table (6.2): Bending-torsional coupled natural frequencies for cantilever asymmetric channel-section under distributed harmonic torsion

No.	Abaqus S4R [1] (≈27,750 DOF)	Present Solution [2] (12DOF)	Abaqus B31OS [3] (1,400 DOF)	Vlasov Solution [4] (closed-form)	Present Difference =[1-2]/1	B31OS Difference =[1-3]/1	Vlasov Difference =[1-4]/1
1	3.679	3.680	3.686	3.687	-0.03%	-0.19%	-0.22%
2	7.251	7.265	7.269	7.280	-0.19%	-0.25%	-0.40%
3	22.05	22.35	22.46	22.48	-1.36%	-1.86%	-1.95%
4	23.45	23.75	23.78	23.81	-1.28%	-1.41%	-1.54%
5	39.82	40.37	40.45	40.68	-1.38%	-1.58%	-2.16%
6	62.59	62.82	63.11	63.32	-0.29%	-0.75%	-1.09%
7	72.83	73.86	74.03	74.32	-1.41%	-1.65%	-2.05%
8	92.91	95.07	95.31	95.78	-2.32%	-2.58%	-3.09%

accurate representation of the structure). The eigen-frequencies predicted by the Abaqus shell model differ from those based on the present finite element solution by 2.32%, from the B31OS solution by 2.58%, and from the Vlasov solution by 3.09%. In other words, the present theory provides the best agreement with the shell solution. From a computational viewpoint, the present solution provides by far the most efficient solution. Using a single finite element with twelve degrees of freedom gives results in excellent agreement with Abaqus shell model with 27,750 degrees of freedom and Abaqus B31OS model with 1,400 degrees of freedom.

6.6.1.2 Quasi-static analysis

The quasi-static coupled response is approached by setting a very low value for the exciting frequency $\Omega=0.01\bar{\omega}_1\approx 0.2312$ rad/sec. Given the non-symmetry of the cross-section, the entries in the matrix of coefficients in Equation (6.16) suggest that, in general, all six displacement fields are fully coupled. However, in the quasi-static results of the present problem, it is observed that the rotation angles $\bar{\theta}_x(z_i)$ and $\bar{\theta}_y(z_i)$ for all values of z_i vanish in all four solutions. Appendix (6-A) provides a mathematical proof that indeed this should be the case under the present formulation. The lateral displacement $\bar{u}_A$, transverse displacement $\bar{v}_A$, angle of twist $\bar{\theta}_z$ and warping deformation $\bar{\psi}$ are presented in Table (6.3) along with comparisons with other solutions. A comparison of the deformed configurations is presented in Figures (6.9*a*-*d*). The present closed-form and finite element solutions are observed to be in excellent agreement with those obtained by Vlasov beam theory, Abaqus B31OS-beam and S4R-shell models. At the cantilever tip,

Table (6.3): Comparison of deformation values at cantilever tip

Variable	Abaqus S4R [1]	Present Solution [2]	Abaqus B31OS [3]	Vlasov Solution [4]	Present Difference =[1-2]/1	B31OS Difference =[1-3]/1	Vlasov Difference =[1-4]/1
u_A (mm)	-14.82	-14.62	-14.56	-14.55	1.35%	1.75%	1.82%
v_A (mm)	7.933	7.918	7.887	7.877	0.19%	0.58%	0.71%
θ_z (10^{-3}rad)	673.3	662.1	661.1	660.4	1.66%	1.81%	1.92%
ψ (10^{-6} rad/mm)	-23.96	-19.25	-19.00	-18.07	19.66%	20.70%	24.58%

the warping deformation $\bar{\psi}$ deviates from the results based on the Abaqus shell model by 19.66%. This is slightly better than the B31OS solution which differs by 20.70% and the Vlasov theory by 24.58%. The differences are predominantly due to distortional effects which are only captured in the shell element model but not in the other three solutions. In spite of this difference at the cantilever tip, the warping deformation within the span is found to be in excellent agreement with the shell FEA solution as evidenced by the comparison provided in Figure (6.9d).

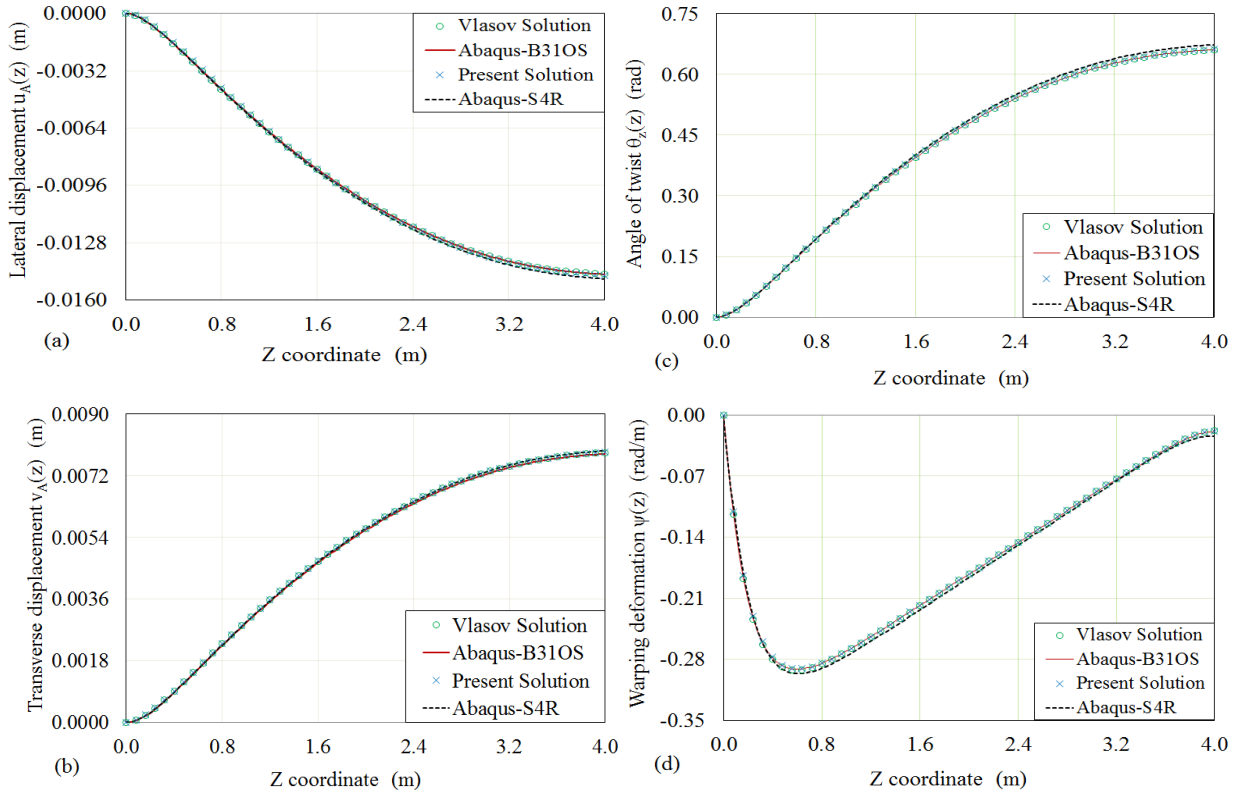

Figure (6.9): Static response of cantilever asymmetric C-section under harmonic torsion

6.6.1.3 Steady state dynamic response

The steady state results for an exciting frequency $\Omega=1.356\bar{\omega}_1 \approx 31.42$ rad/sec are illustrated in Figure (6.10*a-f*). It is observed that the steady state amplitudes for the lateral displacement $\bar{u}_A(z)$, transverse displacement $\bar{v}_A(z)$, bending rotations $\bar{\theta}_x(z), \bar{\theta}_y(z)$, angle of twist $\bar{\theta}_z(z)$ and warping deformation $\bar{\psi}(z)$ based on the present formulations are in excellent agreement with the results obtained by Vlasov beam theory and Abaqus beam

and shell models. This signifies that shear deformation and distortional effects play a rather minor role on the steady state response for such a long-span cantilever.

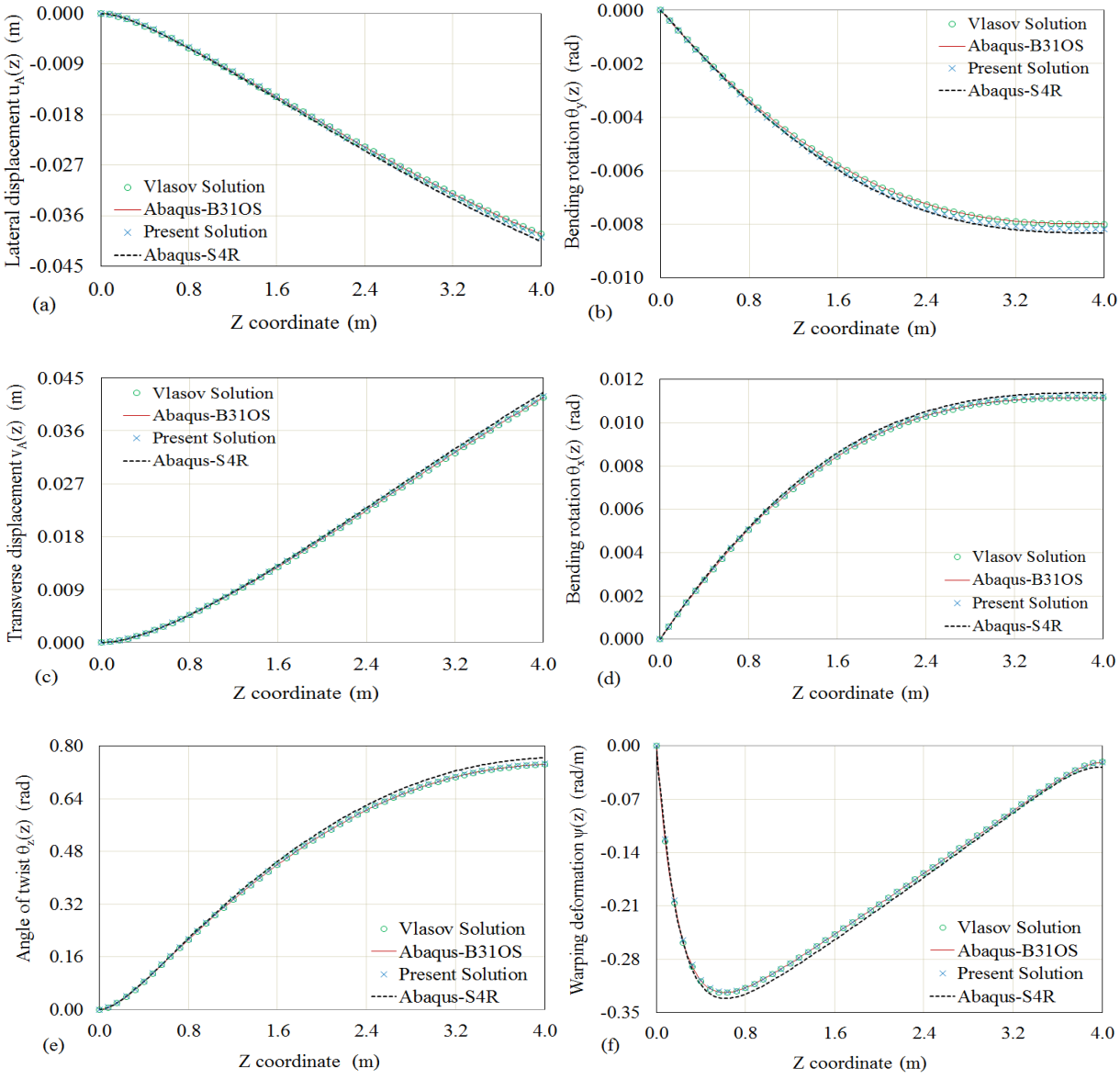

Figure (6.10): Steady state responses for cantilever asymmetric C-section under torsion

The steady state amplitude responses for lateral displacement $\bar{u}_A(z)$, transverse displacement $\bar{v}_A(z)$, bending rotations $\bar{\theta}_x(z)$ and $\bar{\theta}_y(z)$, twist angle $\bar{\theta}_z(z)$ and warping deformation function $\bar{\psi}(z)$ for the given cantilever beam are illustrated in Figures (6.11) for four values of the exciting frequency; $\Omega_1 = 1.10\bar{\omega}_1$, $\Omega_2 = (\bar{\omega}_1 + \bar{\omega}_2)/2$, $\Omega_3 = 1.10\bar{\omega}_2$ and $\Omega_4 = (\bar{\omega}_2 + \bar{\omega}_3)/2$, where $\bar{\omega}_1, \bar{\omega}_2, \bar{\omega}_3$ are the first three natural frequencies.

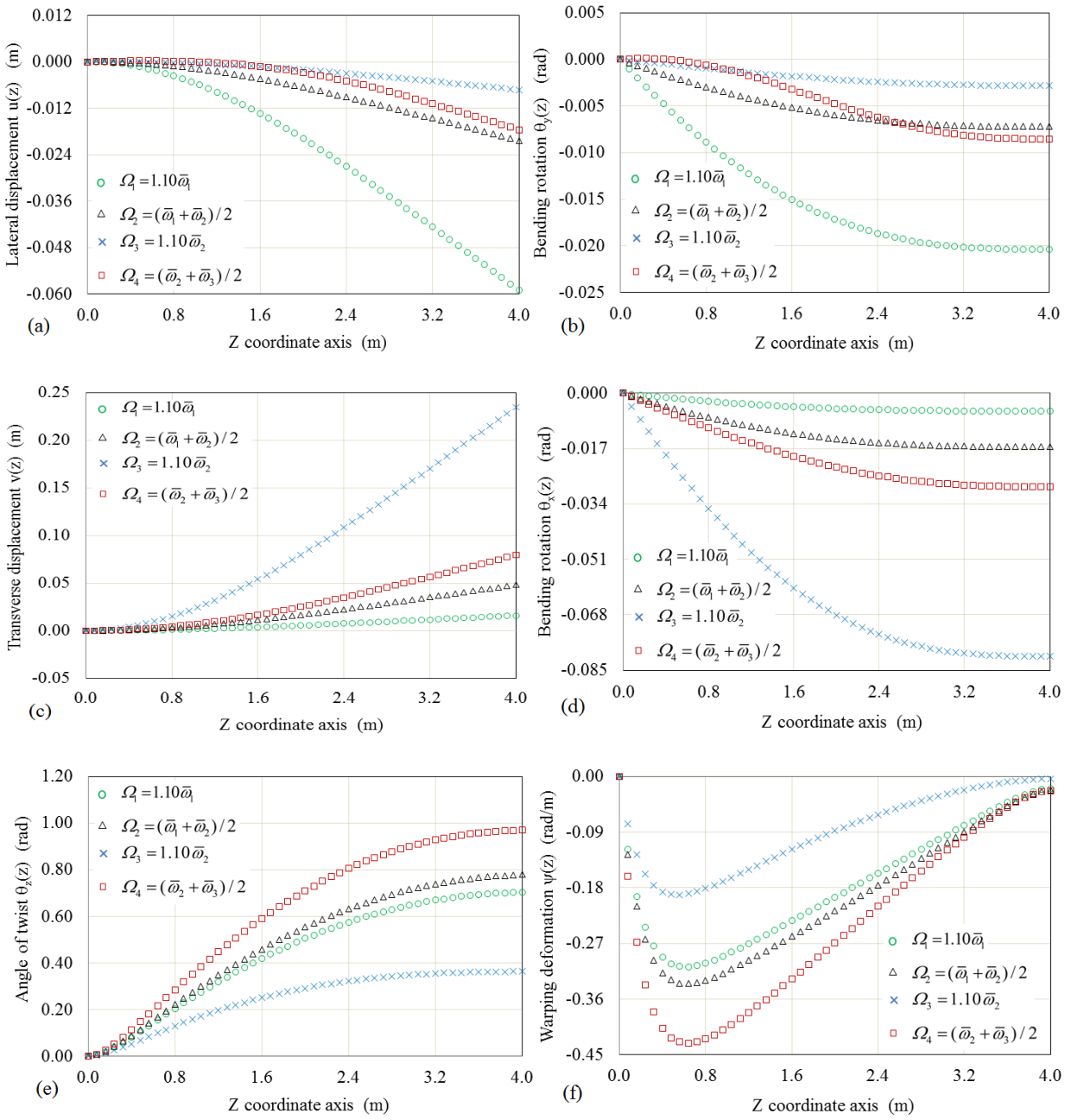

Figure (6.11): Steady state response for cantilever asymmetric channel-section under distributed harmonic torsion

6.6.2 Example 2 – Shear deformation effect

To illustrate the shear deformation effects, a short 1.0m span cantilever is considered. Cross-section is taken identical to Example 1. The member is subjected to a uniformly distributed harmonic twisting moment $8.0e^{i\Omega t}\ kNm/m$ as illustrated in Figure (6.12). It is required to (1) conduct a steady state dynamic analysis and extract the natural frequencies of the beam, (2) capture the quasi-static response by applying a very low exciting

frequency $\Omega=0.001\bar{\omega}_1\approx 0.3594$ rad/sec, and (3) determine the steady state dynamic response of the cantilever under the given load with exciting frequency $\Omega=0.84\bar{\omega}_1\approx 31.42$ rad/sec, (the first natural frequency of the cantilever is $\bar{\omega}_1=57.20Hz$). For comparison, the Vlasov closed-form solution, Abaqus B31OS beam solution and S4R shell element models, are provided.

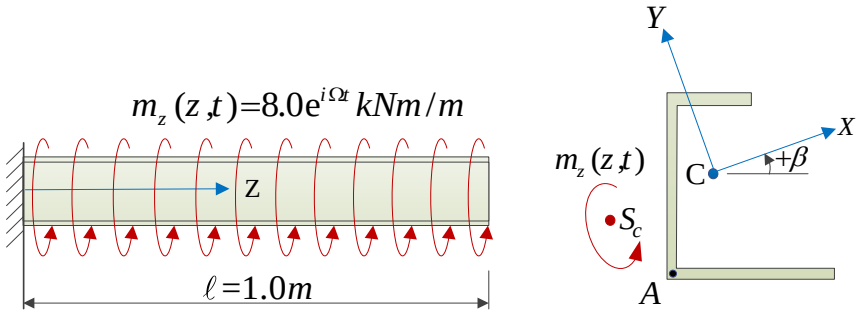

Figure (6.12): Short cantilever asymmetric C-section under member harmonic torsion

In the Abaqus shell solution (Figure 6.13), the cantilever is subdivided into 100 elements in the longitudinal direction, and like Example 1, eight and four elements along the width of top and bottom flanges, and ten elements through the web height. The Abaqus shell model thus consists of 2,200 S4R shell elements. For the B31OS solution model, a total of 100 beam elements are used.

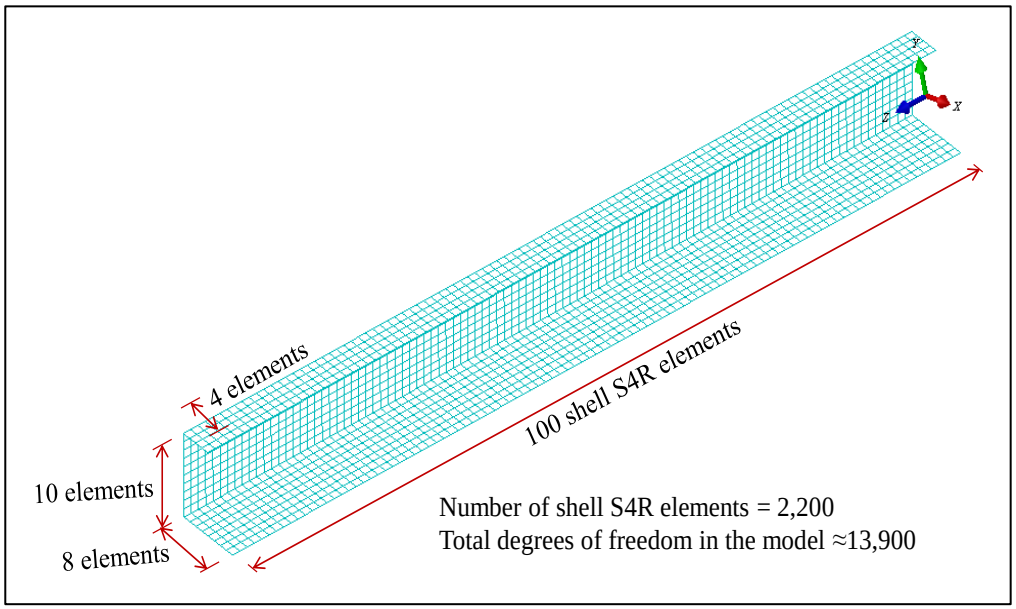

Figure (6.13): Shell S4R meshing of short cantilever asymmetric channel-section

6.6.2.1 Shear Deformation Effects on Natural Frequencies

The steady state response is illustrated in Figures (6.14*a*-*b*) over an exciting frequency range from nearly zero to $700Hz$. To illustrate the influence of shear deformation on the natural frequencies, plots representing the amplitudes of the lateral displacement $\bar{u}_A$ and angle of twist $\bar{\theta}_z$ at the cantilever tip versus the exciting frequency are provided in (Fig. 6.14*a*-*b*). These curves exhibit six peaks which correspond to the first six natural frequencies of the member. For the lower frequencies, all four solutions closely predict the location of peaks associated with the first three natural frequencies. For higher frequencies, deviations in the locations of the peaks are observed between all four solutions. The Abaqus shell model predicts the lowest values of eigen-frequencies while the Vlasov beam theory predicts the highest values. The present solution yields slightly higher values than those based on the shell model. This suggests that for the present beam, the effects of distortion are minor while the shear deformation effects gain significance for higher frequencies. A similar observation was reported in the work of Bercin and Tanaka (1997).

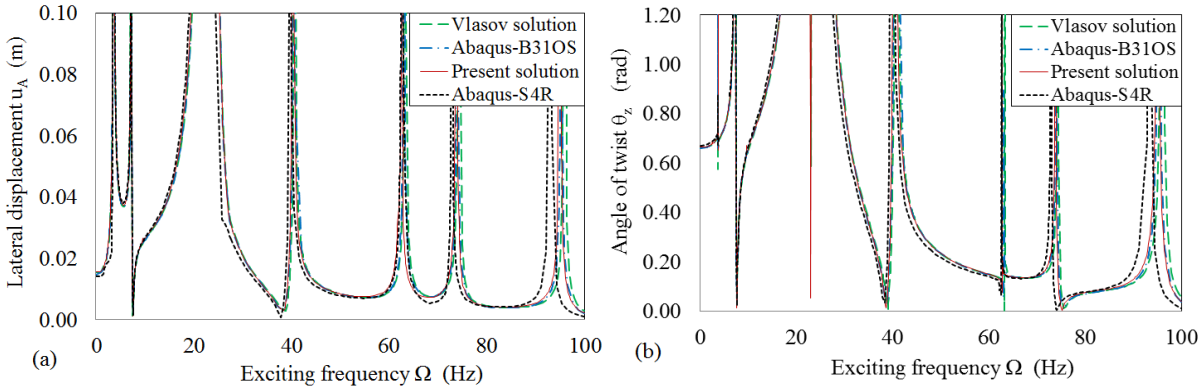

Figure (6.14): Natural frequency analysis of short cantilever asymmetric C-section (a) lateral displacement $\bar{u}_A$, and (b) angle of twist $\bar{\theta}_z$.

Table (6.4) shows the comparison of the first six natural frequencies. As a general observation, the results show very good agreement between all four solutions. For higher frequencies, the present formulation (capturing the shear deformation effects) over-predicts the frequencies by less than 2.0% while the Vlasov beam theory which does not capture the shear deformation effects over-predicts the corresponding frequencies by

5.28-8.44% compared to the Abaqus shell element model. It is observed that shear deformation effects are prominent in short span beams and for higher eigen-frequencies.

Table (6.4): Coupled bending-torsional natural frequencies for short cantilever asymmetric channel-section under member harmonic torsion

No.	Abaqus S4R [1] (≈13,900 DOF)	Present Solution [2] (12DOF)	Abaqus B31OS [3] (700DOF)	Vlasov Solution [4] (closed-form)	Present Difference =[1-2]/1	B31OS Difference =[1-3]/1	Vlasov Difference =[1-4]/1
1	57.20	57.34	57.96	58.18	-0.24%	-1.33%	-1.71%
2	72.32	73.76	74.23	74.60	-1.99%	-2.64%	-3.15%
3	172.9	174.8	175.5	180.3	-1.10%	-1.50%	-4.28%
4	264.1	265.9	276.6	278.7	-0.68%	-4.73%	-5.53%
5	358.2	361.8	368.8	377.1	-1.01%	-2.96%	-5.28%
6	550.7	559.4	592.3	597.2	-1.58%	-7.55%	-8.44%

6.6.2.2 Shear deformation effects on displacement responses

The quasi-static and steady state displacement amplitudes at the cantilever tip subjected to exciting frequency $\Omega=0.001\bar{\omega}_1\approx 0.3594$ rad/sec and $\Omega=0.84\bar{\omega}_1\approx 31.42$ rad/sec are provided in Table (6.5) and Table (6.6), respectively. In both cases, the displacements and rotations predicted by the present study are in excellent agreement with those of Abaqus S4R shell element model. For quasi-static loading (Table 6.5), the warping deformation $\bar{\psi}$ at the cantilever tip as predicted by the Abaqus shell element model is observed to depart from the present solution by 18.12%, by 19.01% from the B31OS solution, and by 19.51% from the Vlasov solution. For the steady state response, it departs from the present solution by 18.12% from the present solution, by 19.01% from the B31OS solution (Table 6.6), and by 19.51% from the Vlasov solution. Again, the difference is attributed to the localized distortion effects at the cantilever tip, which are captured only in the shell model (Fig. 6.15).

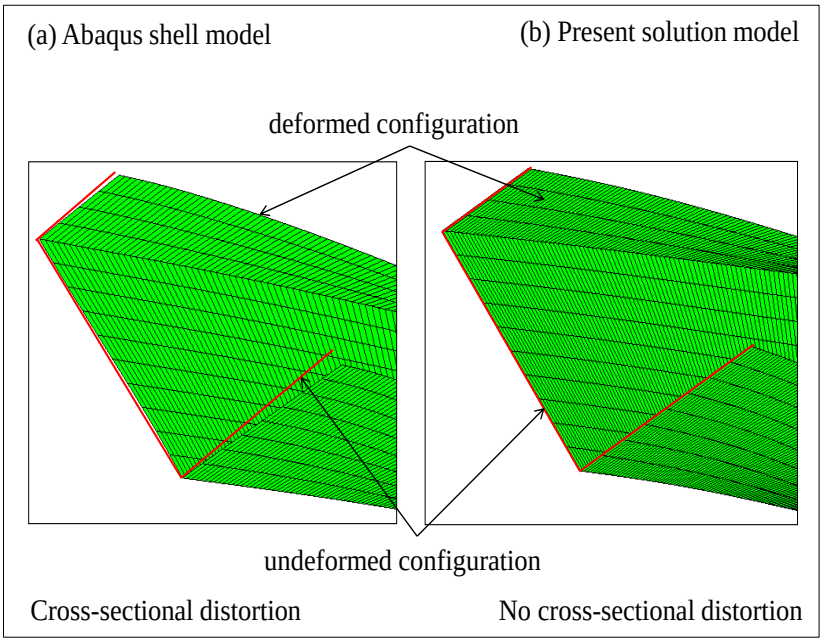

Figure (6.15): Cross-sectional distortional comparison of finite shell model and present solution model for cantilever asymmetric C-section under member torsion

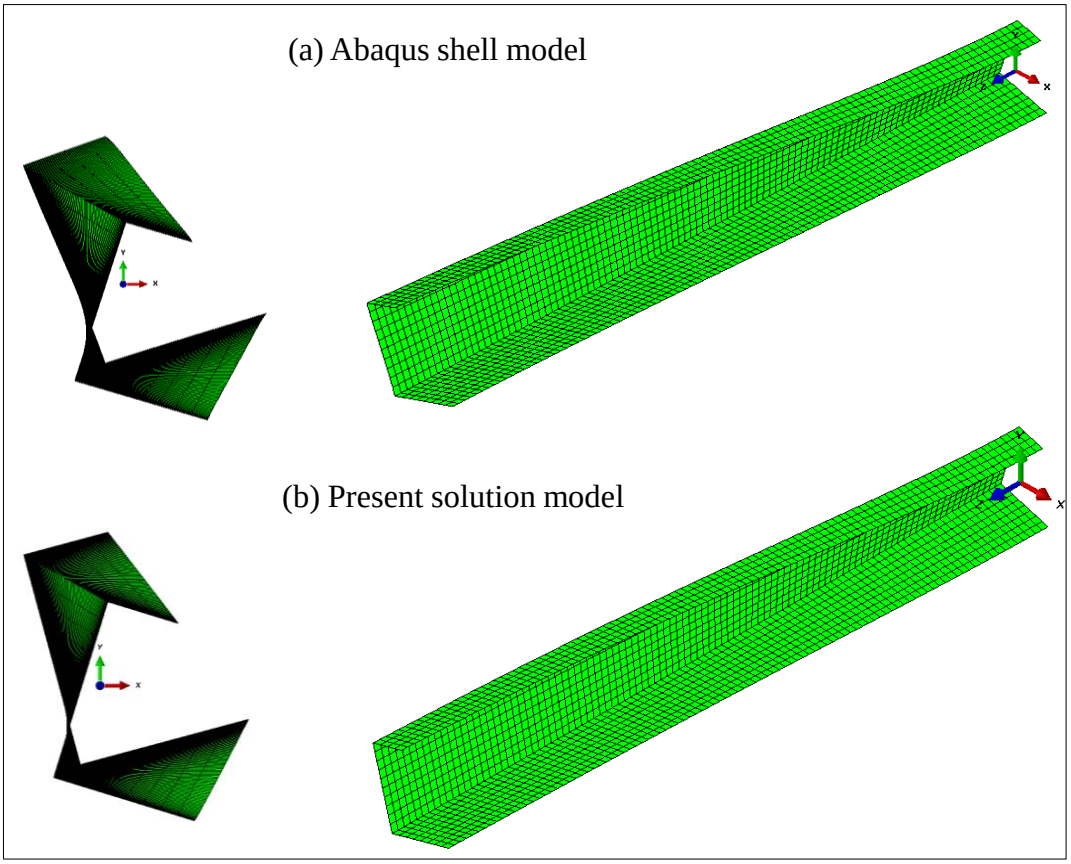

Figure (6.16): Comparison of Abaqus shell model and present model

Table (6.5): Static response of short cantilever asymmetric C-section under distributed harmonic twisting moment

Variable	Abaqus S4R [1] (≈13,900 DOF)	Present Solution [2] (12DOF)	Abaqus B31OS [3] (700DOF)	Vlasov Solution [4] (Closed-Form)	Present Difference =[1-2]/1	B31OS Difference =[1-3]/1	Vlasov Difference =[1-4]/1
$\bar{u}_A$ (mm)	-14.44	-14.25	-14.16	-13.57	1.32%	1.94%	6.02%
$\bar{v}_A$ (mm)	7.635	7.591	7.647	7.348	0.58%	-0.16%	3.76%
$\bar{\theta}_z$ (10^{-3}rad)	635.5	629.6	624.7	615.9	0.93%	1.70%	3.08%
$\bar{\psi}$ (10^{-6} rad/mm)	-417.3	-348.8	-345.0	-342.9	18.12%	19.01%	19.51%

Table (6.6): Steady state response of short cantilever asymmetric C-section under distributed harmonic twisting moment

Variable	Abaqus S4R [1] (≈13,900 DOF)	Present Solution [2] (12DOF)	Abaqus B31OS [3] (700DOF)	Vlasov Solution [4] (Closed-Form)	Present Difference =[1-2]/1	B31OS Difference =[1-3]/1	Vlasov Difference =[1-4]/1
$\bar{u}_A$ (mm)	4.315	4.170	3.111	2.728	3.36%	27.90%	36.78%
$\bar{v}_A$ (mm)	24.73	23.47	22.48	21.87	5.10%	9.10%	11.56%
$\bar{\theta}_x$ (10^{-3}rad)	-14.84	-14.17	-13.59	-13.23	4.51%	8.42%	10.85%
$\bar{\theta}_y$ (10^{-3}rad)	39.70	38.91	36.79	35.32	1.99%	7.33%	11.03%
$\bar{\theta}_z$ (10^{-3}rad)	1121	1076	1043	1020	4.01%	6.96%	9.01%
$\bar{\psi}$ (10^{-6} rad/mm)	-755.8	-620.2	-611.7	-603.1	17.94%	19.07%	20.20%

The amplitude responses for lateral displacement $\bar{u}_A(z)$, transverse displacement $\bar{v}_A(z)$, angles of rotations $\bar{\theta}_x(z)$, $\bar{\theta}_y(z)$, angle of twist $\bar{\theta}_z(z)$ and warping deformation $\bar{\psi}(z)$ are plotted in Figures (6.17*a-f*), respectively under the exciting frequency $\Omega = 0.84\bar{\omega}_1 \approx 31.42$ rad/sec. Results based on the present solution are observed to be in excellent agreement with those of the Abaqus shell element solution. Due to the omission of the shear deformation fully in Vlasov beam theory and partially in Abaqus beam model (since B31OS does not capture shear deformation due to warping), the predicted results obtained by these two solutions show some deviation from the Abaqus shell model results. This leads to conclude that the shear deformation effects become important for short beams under harmonic forces. In contrast, the present solution provides very good agreement with shell model results.

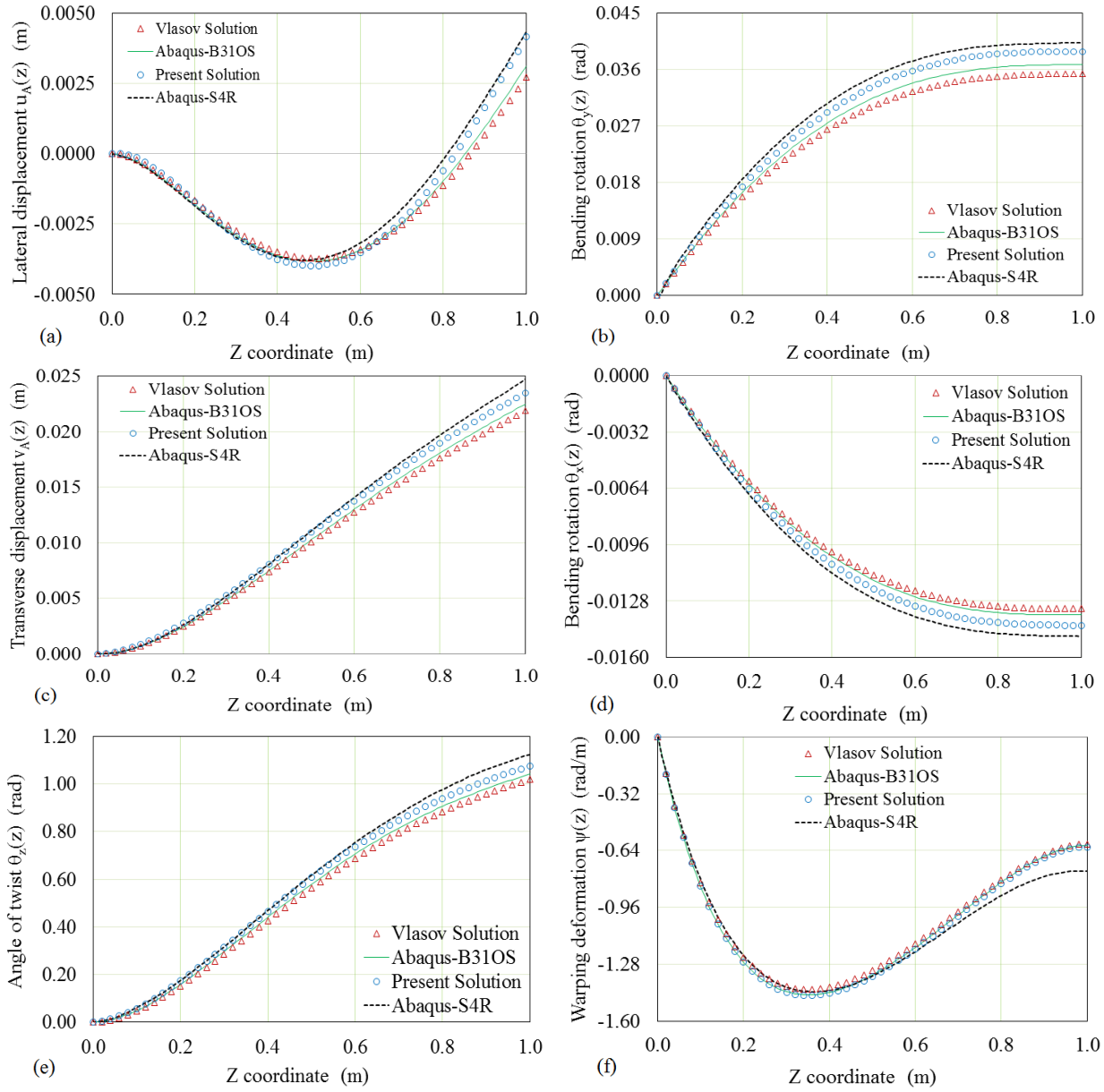

Figure (6.17): Steady state response for cantilever asymmetric C-section under distributed harmonic twisting moment

6.6.3 Example 3 – Three-Span Continuous beam

A three-span continuous beam has an asymmetric section (Fig. 6.18) is subjected to three harmonic forces; uniformly distributed transverse force $12.0\,e^{i\Omega t}\ kN/m$, concentrated twisting moment $8.0\,e^{i\Omega t}\ kNm$ and concentrated transverse force $24.0\,e^{i\Omega t}\ kN$. Section dimensions are $b_u = 160mm$, $b_\ell = 80mm$, $t_f = 20mm$, $t_w = 15mm$ and $H = 200mm$. The coordinates of the centroid C are $C_x = 8.205mm$, $C_y = 120.5mm$ and the coordinates of

the shear centre S_c along the principal coordinates are $X_s = -23.89mm$, $Y_s = 42.24mm$, the orientation of principal direction is $\beta = 9.46^o$, and the properties of cross-section are;

$A = 0.78\times10^4 mm^2$, $I_{xx} = 56.16\times10^6 mm^4$, $I_{yy} = 8.489\times10^6 mm^4$, $J = 0.8650\times10^6 mm^4$,

$C_w = 57.0\times10^9 mm^6$, $D_{xx} = 47.51\times10^4 mm^2$, $D_{yy} = 30.49\times10^4 mm^2$, $D_{xy} = -2.918\times10^4 mm^2$,

$D_{hy} = 1.296\times10^4 mm^3$, $D_{hx} = -3.705\times10^4 mm^3$, $D_{\omega\omega} = 47.14\times10^6 mm^4$.

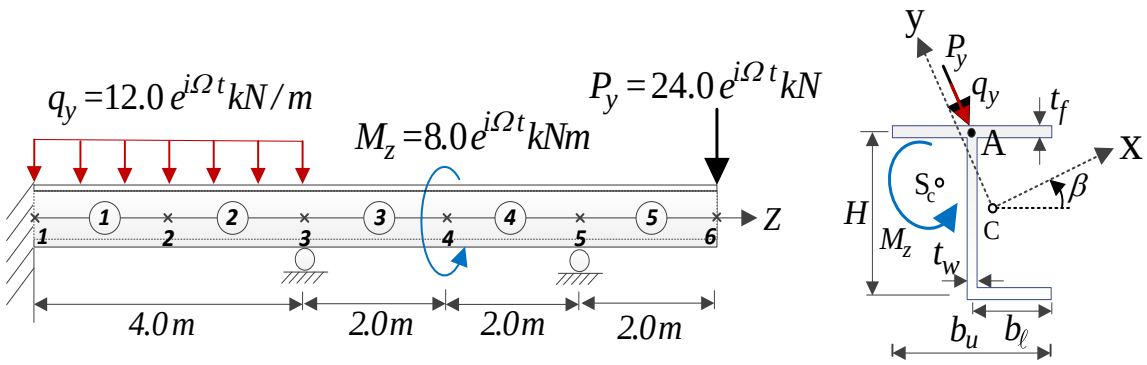

Figure (6.18): Three-span continuous beam with asymmetric J-section

It is required to assess the accuracy and efficiency of the present finite element formulation, in (1) predicting the quasi-static response corresponding to exciting frequency $\Omega = 0.01\bar{\omega}_1 \approx 0.7138$ rad/sec, and (2) determining the steady state dynamic response under an exciting frequency $\Omega = 1.74\omega_1 \approx 124.2$ rad/sec, where the first natural frequency of the three-span beam is $\bar{\omega}_1 = 11.36Hz$.

Three solutions are provided for the problem. These are:

(1) In the Abaqus shell model, the three-span beam is subdivided into 400 shell S4R elements along the longitudinal direction, 10 elements along height of the web, 8 and 4 elements along the width of the upper and lower flanges, respectively. The model thus consists of 8,800 shell S4R elements with six degrees of freedom per node which leads to about 55,000 degrees of freedom.

(2) In the case of Abaqus finite beam model, 200 beam B31OS elements in which a total of 1,400 degrees of freedom were needed to attain the required accuracy.

(3) In the present solution, the member is subdivided into only five beam elements along the member span, i.e., the model has only thirty degrees of freedom.

6.6.3.1 Comparison of displacement responses

The displacement functions $\bar{u}(z), \bar{v}(z), \bar{\theta}_x(z), \bar{\theta}_y(z), \bar{\theta}_z(z)$ and $\bar{\psi}(z)$ are provided in Figures (6.19) and (6.20), for quasi-static analysis case ($\Omega = 0.01\omega_1 \approx 0.714$ rad/sec), and steady state dynamic response case ($\Omega = 1.74\omega_1 \approx 124.2$ rad/sec), respectively. The two sets of figures show excellent agreement between the nodal displacement functions predicted by the present finite element model (using 30 degrees of freedom) and the Abaqus finite element models, shell model (using 55,000 degrees of freedom) and beam

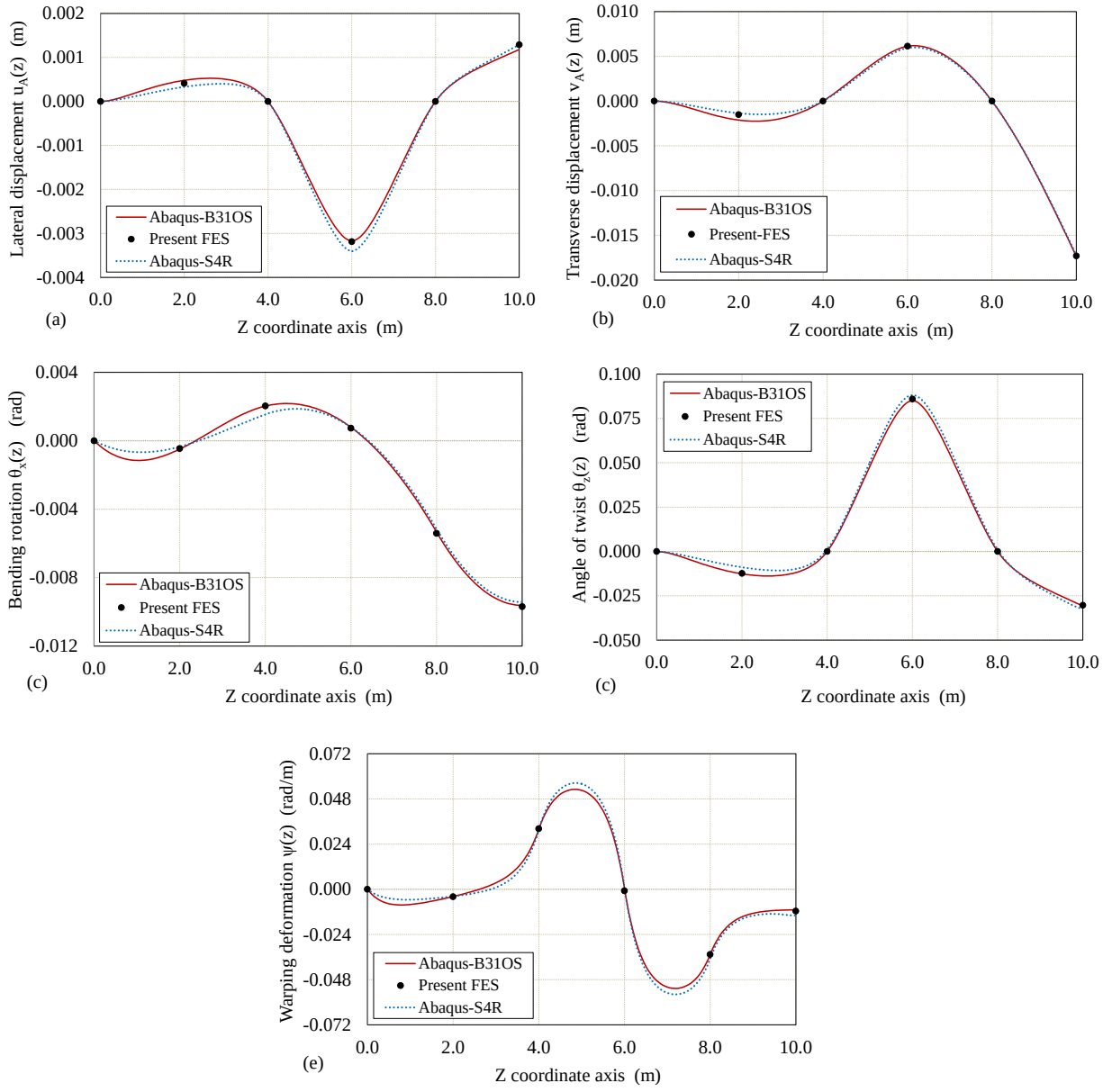

Figure (6.19): Quasi-static analysis of three-span continuous beam under harmonic forces

model (using 1,400 degrees of freedom). In the quasi-static case, it is also observed that the angle of rotation $\bar{\theta}_y(z)$ vanishes in all three solutions. The computational effort in the present solution is several orders of magnitudes less than that of other solutions. This is a natural outcome of the fact that the present finite element is based on the shape functions which exactly satisfy the homogeneous form of the equations of motion, which in turn eliminates discretization errors encountered in finite element formulations.

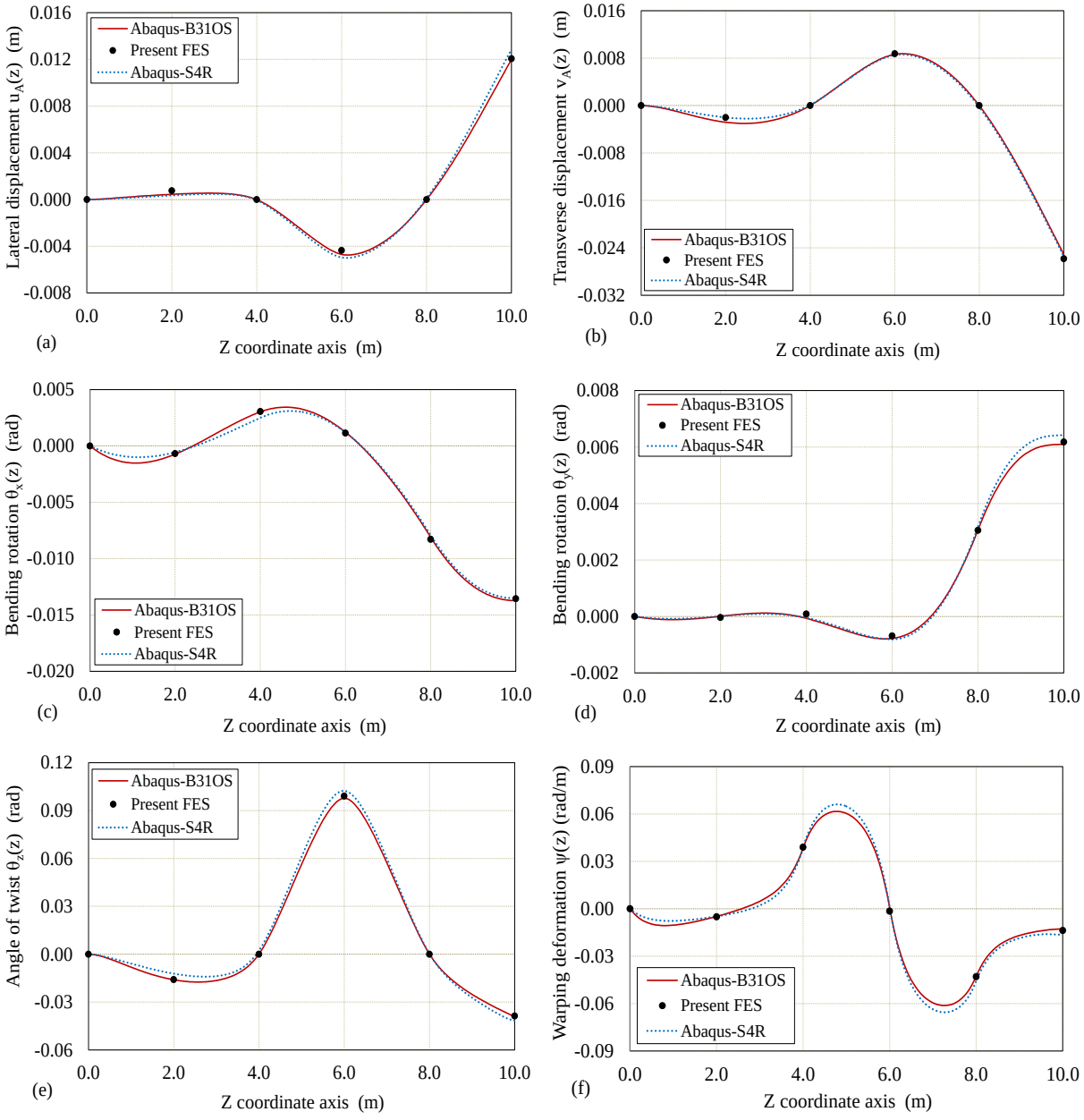

Figure (6.20): Steady state analysis of three-span beam under general harmonic forces

6.7 Summary and Conclusions

1. The equations of motion and related boundary conditions are derived for thin-walled members with asymmetric open cross-sections under general harmonic forces. The formulation captures shear deformation effects due to bending and warping, translational and rotary inertia effects and the bending-torsional coupling effects due to the nonsymmetry of the cross-section.
2. Closed-form solutions are formulated for the resulting coupled system of equations.
3. A family of shape functions is derived based on the exact homogeneous solution of the governing field equations.
4. A super-convergent finite element based on the exact shape functions is then formulated.
5. The new element involves no discretization errors and generally provides excellent results with a minimal number of degrees of freedom.
6. The present solution is capable of efficiently capturing the static and steady state responses of members under harmonic forces. It is also able to predict the natural frequencies and mode-shapes of the system.
7. The solution successfully captures the coupled bending-torsional response of asymmetric cross-sections under harmonic forces.
8. Comparisons with Vlasov beam theory solution demonstrates the importance of shear deformation effects on short-span thin-walled members under higher exciting frequencies.
9. Comparisons with shell element solutions show that the distortional effects are more pronounced in cantilevers with shorter spans rather than longer spans.

6.8 References

[6.1] Vlasov, V. (1961), Thin-walled elastic beams, second edition, Jerusalem, Israel Prog. for Scientific Translation.

[6.2] Hjaji, M. A. and Mohareb, M. (2011a), Steady state response of doubly symmetric thin-walled members under harmonic excitations- Closed-Form solution, second International Engineering Mechanics and Materials Specialty Conference, Ottawa, Ontario, Canada.

[6.3] Hjaji, M. A. and Mohareb, M. (2011b), Steady state response of doubly symmetric thin-walled members under harmonic excitations–Finite element formulation,

second International Engineering Mechanics and Materials Specialty Conference, Ottawa, Ontario, Canada.

[6.4] Friberg, P.O. (1985), Beam element matrices derived from Vlasov's theory of open thin-walled elastic beams. International Journal for Numerical Methods in Engineering, 21:1205-28.

[6.5] Leung, A. Y. T. (1991), Natural shape functions of a compressed Vlasov element, Thin-walled Structures, 11: 431-38.

[6.6] Leung, A. Y. T. (1992), Dynamic stiffness analysis of thin-walled structures, Thin-walled Structures, 14: 209-222.

[6.7] Chen, X. and Tamma, K. (1994), Dynamic response of elastic thin-walled structures influenced by coupling effects, Computers and Structures, 51(1): 91-105.

[6.8] Tanaka, M. and Bercin, A. N. (1999), Free vibration solution for uniform beams of non-symmetrical cross section using Mathematica, Computes and Structures, 71:1–8.

[6.9] Arpaci, A. and Bozdag, E. (2002), On free vibration analysis of thin-walled beams with non-symmetrical open cross-sections, Computers and Structures, 80: 691–695.

[6.10] Arpaci, A. et al. (2003), Triply coupled vibrations of thin-walled open cross-section beams including rotary inertia effects, Journal of Sound and Vibration, 260: 889-900.

[6.11] Kim, N. et al. (2003a), Exact dynamic and static stiffness matrices of nonsymmetric thin-walled beam-columns, Computers and Structures, 81: 1425-1448.

[6.12] Voros, G. M. (2004), Free vibration of thin-walled beams, Periodica Polytechnica Ser. Mech. Eng., 48(1): 99–110.

[6.13] Li, J, Li, et al. (2004), Coupled bending and torsional vibration of nonsymmetrical axially loaded thin-walled Bernoulli-Euler beams, Mechanics Research Communications, 31: 697-711.

[6.14] Mohri, F. et al. (2004), Vibration analysis of buckled thin-walled beams with open sections, Journal of Sound and Vibration, 275: 434-446.

[6.15] Prokic, A. (2005), On fivefold coupled vibrations of Timoshenko thin-walled beams, Engineering Structures, 28: 54-62.

[6.16] Bin, Z. and Leung, A. Y. T. (2005), Dynamic stiffness for thin-walled structures by power series, Journal of Zhejiang University SCIENCE A, 7(8): 1351-1357.

[6.17] Chen, H. H. and Hsiao, K. M. (2007), Coupled Axial-torsional Vibration of Thin-walled Z-section Beam Induced by Boundary Conditions, Thin-Walled Structures, 45(6): 573-583.

[6.18] Kim, N. et al. (2007), Stiffness matrices for flexural-torsional/lateral buckling and vibration analysis of thin-walled beam, Journal of Sound and Vibration, 299: 739-756.

[6.19] Voros, G. M. (2008), On Coupled Vibrations of Beams with Lateral Loads, Journal of computational and Applied Mechanics, 9 (2): 1-14.

[6.20] Voros, G. M. (2009), On Coupled bending-torsional vibrations of beams with initial loads, Mechanics Research Communications, 36: 603-611.

[6.21] Altintas, G. (2010), Effect of material properties on vibrations of non-symmetrical axially loaded thin-walled Euler-Bernoulli beams, Mathematical and Computational Applications, 15: 96-107.

[6.22] Vo, T. P. et al. (2010), On triply coupled vibrations of axially loaded thin-walled composite beams, Computers and Structures, 88(3-4): 144-153.

[6.23] Laudiero, F. and Savoia, M. (1991), The shear strain influence on the dynamics of thin-walled beams, Thin-walled Structures, 11: 375-407.

[6.24] Bercin, A. N. and Tanaka, M. (1997), Finite element modeling of the coupled bending and torsional free vibration of uniform beams with an arbitrary cross-section, Applied Mathematical Modelling, 21(6): 339-344.

[6.25] Kollar, J. P. (2001), Flexural-torsional vibration of open section composite columns with shear deformation, International Journal of Solids and Structures, 38 (42-43):7543-7558.

[6.26] Cortinez, V. H. and Piovan, M. T. (2002), Vibration and buckling of composite thin-walled beams with shear deformability, Journal of Sound and Vibration, 258(4-5): 701–723.

[6.27] Kim, M. Y. et al. (2003), Exact dynamic and static stiffness matrices of shear deformable thin-walled beam-columns, Journal of Sound and Vibration, 267: 29–55.

[6.28] Kim, N. I. and Kim, M. N. (2005), Exact Dynamic/Static Stiffness Matrices of Non-Symmetric Thin-Walled Beams considering coupled shear deformation effects, Thin-walled Structures, 43: 701-734.

[6.29] Prokic, A. (2006), On fivefold coupled vibrations of Timoshenko thin-walled beams, Engineering Structures, 28: 54-62.

[6.30] Vo, T.P. and Lee, J. (2009), On six-fold coupled buckling of thin-walled composite beams, Composite Structures, 90: 295-303.

[6.31] Ambrosini, D. (2009), On free vibration of nonsymmetrical thin-walled beams, Thin-Walled Structures, 47(6-7): 629-636.

[6.32] De Bordon, F. and Ambrosini, D. (2010), On free vibration analysis of thin-walled beams axially loaded, Thin-Walled Structures, 48(12): 915-920.

[6.33] Ambrosini, D. (2010), Experimental validation of free vibrations from nonsymmetrical thin walled beams, Engineering Structures, 32(5): 1324-1332.

[6.34] Hashemi S. M., Richard M. J. (2000a), A Dynamic Finite Element Method for Free Vibrations of Bending -Torsion Coupled Beams, Aerospace Sci. Technology, 4: 41-55.

[6.35] Hashemi S. M., and Richard M. J. (2000b), Free vibrational analysis of axially Bending-Torsion Coupled Beams-A dynamic finite element, Computers and structures, 77: 711-724.

[6.36] Lee, J. and Kim, S. E. (2002a), Free Vibration of Thin-walled Composite Beams with I-Shaped cross-sections, Composite Structures, 55(2): 205-215.

[6.37] Lee, J. and Kim, S. E. (2002b), Flexural–torsional coupled vibration of thin-walled composite beams with channel sections, Computers and Structures, 80: 133–144.

[6.38] Vo, T. P. and Lee, J. (2009a), Flexural-torsional coupled vibration and buckling of thin-walled open section composite beams using shear-deformable beam theory, International Journal of Mechanics Sciences, 51: 631-641.

[6.39] Vo, T. P. and Lee, J. (2009b), Free vibration of axially thin-walled composite box beams, Composite Structures, 90: 233-241.

[6.40] Vo, T. P. and Lee, J. (2010a), Interaction curves for vibration and buckling of thin-walled composite box beams under axial loads and end moments, Applied Mathematical Modelling, 34: 3142-3157.

[6.41] Vo, T. P. et al. (2009), On six-fold coupled vibrations of thin-walled composite box beams, Composite Structures, 89: 524-535.

[6.42] Vo, T. P. and Lee, J. (2010b), Free vibration of axially thin-walled composite Timoshenko beams, Archive of Applied Mechanics, 81 (9):1165-1180.

[6.43] Vo, T. P. et al. (2011), Vibration analysis of thin-walled composite beams with I-shaped cross-sections, Composite Structures, 93(3-4): 812-820.

[6.44] Mei, C. (1970), Coupled Vibrations of Thin-walled Beams of Open Section Using the Finite Element Method, International journal of mechanical science, 12: 883-891.

[6.45] Hu, Y. et al. (1996), A Finite Element Model for Static and Dynamic Analysis of Thin-walled Beams with Asymmetric Cross-Sections, Computers and Structures, 61: 897-908.

[6.46] Back, S.Y. and Will, K.M. (1998), A shear-flexible element with warping for thin-walled open beams, Int. J Numerical Methods in Engineering, 43:1173–1191.

[6.47] Li, J, et al. (2004), Coupled bending and torsional vibration of nonsymmetrical axially loaded thin-walled Bernoulli-Euler beams, Mechanics Research Communications, 31: 697-711.

[6.48] Kim, N. et al. (2003), Exact dynamic and static stiffness matrices of nonsymmetric thin-walled beam-columns, Computers and Structures, 2003: 81: 1425-1448.

[6.49] Machado, S. P. and Cortinez, V. H. (2007), Free vibration of thin-walled composite beams with static initial stresses and deformations, Engineering Structures, 29(3): 372-382.

[6.50] Machado, S. P. (2007), Geometrically non-linear approximations on stability and free vibration of composite beams, Engineering Structures, 29(12): 3567-3578.

[6.51] Wu, L. and Mohareb, M. (2011), Buckling of shear deformable thin-walled members – I. Variational principle and analytical solutions, Thin-walled Structures, 9(1): 197-207.

[6.52] Librescu, L and Song, O. (2006), Thin-walled composite beams: theory and application, Springer, The Netherlands.

[6.53] Saad, Y. (1992), Numerical methods for large eigenvalue problems, John Wiley and Sons Inc., New York, USA.

Appendix (6A): Proof that bending rotations $\theta_x(z)$ and $\theta_y(z)$ vanish for a cantilever with no external forces

It is required to formulate the expression for the rotation angles $\theta_x(z)$ and $\theta_y(z)$ for a cantilever beam with no externally distributed lateral force $q_x(z)$ and bending moment $m_y(z)$. By setting the right hand side of the static equilibrium equations related to lateral response (Equations 3.55 and 3.59, chapter 3) equal to zero, one obtains:

$$-G\left[D_{xx}\left(u'-\theta_y\right)+D_{xy}\left(v'+\theta_x\right)+D_{hx}\left(\theta_z'+\psi\right)\right]'=0 \tag{6A.1}$$

$$-EI_{yy}\theta_y''-G\left[D_{xx}\left(u'-\theta_y\right)+D_{xy}\left(v'+\theta_x\right)+D_{hx}\left(\theta_z'+\psi\right)\right]=0 \tag{6A.2}$$

and the related boundary conditions are:

$$\left[G\left\{D_{xx}\left(u'-\theta_y\right)+D_{xy}\left(v'+\theta_x\right)+D_{hx}\left(\theta_z'+\psi\right)\right\}-V_x(z)\right]\delta u(z)\Big|_0^{\ell}=0 \tag{6A.3}$$

$$\left[EI_{yy}\theta_y'-M_y(z)\right]\delta\theta_y(z)\Big|_0^{\ell}=0 \tag{6A.4}$$

For simplicity, Eq. (6A.1) can be re-write as:

$$\chi'(z)=-G\left[D_{xx}\left(u'-\theta_y\right)+D_{xy}\left(v'+\theta_x\right)+D_{hx}\left(\theta_z'+\psi\right)\right]'=0 \tag{6A.5}$$

Integrating Eq. (6A.5) with respect to z, leads to:

$$\chi(z)=-G\left[D_{xx}\left(u'-\theta_y\right)+D_{xy}\left(v'+\theta_x\right)+D_{hx}\left(\theta_z'+\psi\right)\right]=C_1 \tag{6A.6}$$

From Eq. (6A.6), by substituting into Eq. (6A.2), one obtains:

$$-EI_{yy}\theta_y''(z)-\chi(z)=0 \tag{6A.7}$$

For the cantilever beam, the boundary conditions at the fixed end $z=0$:

$$u(0)=0 \quad \text{and} \quad \theta_y(0)=0 \tag{6A.8}$$

and at the cantilever free end $z=\ell$, noting that no external bending moment $M_y(\ell)$ nor shear force $V_x(\ell)$ are applied, Eqs. (6A.3) and (6A.4) are:

$$EI_{yy}\theta_y'(\ell)=0 \tag{6A.9}$$

$$G\left[D_{xx}\left(u'-\theta_y\right)+D_{xy}\left(v'+\theta_x\right)+D_{hx}\left(\theta_z'+\psi\right)\right]_{z=\ell}=0 \tag{6A.10}$$

From Eq. (6A.6), by substituting into Eq. (6A.10), one obtains:

$$\chi(\ell)=0 \tag{6A.11}$$

From Equation (6A.6), one obtains

$$\chi(z)=\chi(\ell)=0 \tag{6A.12}$$

or $C_1=0$. From Eq. (6A.12) by substituting into Eq. (6A.7), and by integrating the resulting equation, one obtains

$$\theta_y(z)=C_2 z+C_3 \tag{6A.13}$$

Imposing the boundary conditions in Equations (6A.8) and (6A.9) into Eq. (6A.13), yields

$$C_2=C_3=0 \tag{6A.14}$$

From Eq. (6A.14), by substituting into Eq. (6A.13), leads to conclude that the bending rotation about Y axis is vanished, i.e.,

$$\theta_y(z)=0 \tag{6A.15}$$

In a similar manner, the other rotation angle $\theta_x(z)$ is also found to vanish, i.e.,

$$\theta_x(z)=0 \tag{6A.16}$$

In summary, for the special case of quasi-static response of a cantilever beam with asymmetric section, the bending rotations $\theta_x(z)$ and $\theta_y(z)$ for the member are shown to vanish.

Appendix (6B): Closed-Form Solutions for Governing Field Equations of thin-walled asymmetric Vlasov beam

6B.1 General

This appendix derives the general closed-form solution for the thin-walled Vlasov beams with asymmetric cross-sections subjected to general harmonic excitations. When one ignores the shear deformation which is not captured by Vlasov beam theory, the field equations governing the coupled lateral-transverse-torsional-warping response presented in equations (3.44) to (3.46) become

$$EI_{yy}u^{\mathrm{iv}}-\rho I_{yy}\ddot{u}''+\rho A\left(\ddot{u}+y_s\ddot{\phi}\right)=q_x(z,t) \tag{6B.1}$$

$$EI_{xx}v^{\mathrm{iv}}-\rho I_{xx}\ddot{v}''+\rho A\left(\ddot{v}-x_s\ddot{\phi}\right)=q_y(z,t) \tag{6B.2}$$

$$EC_w\phi^{iv}-\rho C_w\ddot{\phi}''-GJ\phi''+\rho A\left(y_s\ddot{u}-x_s\ddot{v}+r_o^2\ddot{\phi}\right)=m_z(z,t) \tag{6B.3}$$

The related boundary conditions are

$$\left[EI_{yy}u''-M_y(z,t)\right]\delta u'(z,t)\Big|_0^\ell=0 \tag{6B.4}$$

$$\left[EI_{xx}v''-M_x(z,t)\right]\delta v'(z,t)\Big|_0^\ell=0 \tag{6B.5}$$

$$\left[EI_{yy}u'''-V_x(z,t)\right]\delta u(z,t)\Big|_0^\ell=0 \tag{6B.6}$$

$$\left[EI_{xx}v'''-V_y(z,t)\right]\delta v(z,t)\Big|_0^\ell=0 \tag{6B.7}$$

$$\left[EC_w\phi'''-GJ\phi'-M_z(z,t)\right]\delta\phi(z,t)\Big|_0^\ell=0 \tag{6B.8}$$

$$\left[EC_w\phi''-M_w(z,t)\right]\delta\phi'(z,t)\Big|_0^\ell=0 \tag{6B.9}$$

6B.2 Field Equations for Harmonic Forces

The asymmetric thin-walled member is assumed to be subjected to general harmonic forces within the member

$$q_x(z,t),q_y(z,t),m_x(z,t),m_y(z,t),m_z(z,t),m_w(z,t)=\left[\bar{q}_x,\bar{q}_y,\bar{m}_x,\bar{m}_y,\bar{m}_z,\bar{m}_w\right]e^{i\Omega t} \tag{6B.10}$$

and end harmonic forces

$$\begin{aligned}V_x(z_e,t),V_y(z_e,t),M_x(z_e,t),M_y(z_e,t),M_z(z_e,t),M_w(z_e,t)\\ =\left[\bar{V}_x(z_e),\bar{V}_y(z_e),\bar{M}_x(z_e),\bar{M}_y(z_e),\bar{M}_z(z_e),\bar{M}_w(z_e)\right]e^{i\Omega t}\end{aligned} \tag{6B.11}$$

in which $q_x(z,t), q_y(z,t)$ are the distributed harmonic forces, $m_x(z,t), m_y(z,t), m_z(z,t)$ are the distributed harmonic moments, $m_w(z,t)$ is the distributed harmonic bimoment, $V_x(z_e,t), V_y(z_e,t)$ are the transverse and lateral forces applied at the member ends $(z_e = 0,\ell)$, $M_x(z_e,t), M_y(z_e,t), M_z(z_e,t)$ are the harmonic end moments and $M_w(z_e,t)$ is the harmonic end bimoments, Ω is the circular frequency of the applied forces and $i = \sqrt{-1}$ is the imaginary constant.

Under the above harmonic forces, the displacement fields corresponding to the steady state response are also harmonic, i.e.,

$$v(z,t), u(z,t), \phi(z,t) = \left[\bar{v}(z), \bar{u}(z), \bar{\phi}(z)\right] e^{i\Omega t} \tag{6B.12}$$

in which $\bar{u}(z), \bar{v}(z)$ and $\bar{\phi}(z)$ are space functions for lateral, transverse and torsional rotation. By substituting the force and displacement expressions in equations (6B.10) to (6B.12) into coupled field equations (6B.1) to (6B.3) and boundary conditions (6B.4) to (6B.9), leads to

$$\begin{bmatrix} \left[EI_{yy}\mathcal{D}^4 + \rho I_{yy}\Omega^2\mathcal{D}^2 - \rho A\Omega^2\right] & 0 & -\rho A\Omega^2 y_s \\ & \left[EI_{xx}\mathcal{D}^4 + \rho I_{xx}\Omega^2\mathcal{D}^2 - \rho A\Omega^2\right] & \rho A\Omega^2 x_s \\ Symm & & \left[EC_w\mathcal{D}^4 - \rho A\Omega^2 r_o^2 + \left(\rho C_w\Omega^2 - GJ\right)\mathcal{D}^2\right] \end{bmatrix}_{3\times 3} \begin{Bmatrix} \bar{u} \\ \bar{v} \\ \bar{\phi} \end{Bmatrix}_{3\times 1} = \begin{Bmatrix} \bar{q}_x \\ \bar{q}_y \\ \bar{m}_z \end{Bmatrix}_{3\times 1} \tag{6B.13}$$

and the associated boundary conditions are:

$$\left[EI_{yy}\bar{u}'' - \bar{M}_y(z)\right]\delta\bar{u}'(z)\Big|_0^\ell = 0 \tag{6B.14}$$

$$\left[EI_{xx}\bar{v}'' - \bar{M}_x(z)\right]\delta\bar{v}'(z)\Big|_0^\ell = 0 \tag{6B.15}$$

$$\left[EI_{yy}\bar{u}''' - \bar{V}_x(z)\right]\delta\bar{u}(z)\Big|_0^\ell = 0 \tag{6B.16}$$

$$\left[EI_{xx}\bar{v}''' - \bar{V}_y(z)\right]\delta\bar{v}(z)\Big|_0^\ell = 0 \tag{6B.17}$$

$$\left[EC_w\bar{\phi}''' - GJ\bar{\phi}' - \bar{M}_z(z)\right]\delta\bar{\phi}(z)\Big|_0^\ell = 0 \tag{6B.18}$$

$$\left[EC_w\bar{\phi}''-\bar{M}_w\left(z\right)\right]\delta\bar{\phi}'\left(z\right)\Big|_0^{\ell}=0 \tag{6B.19}$$

6B.3 Homogeneous Solution of Coupled Field Equations

The homogeneous solution of the system of equations in (6B.13) is obtained by setting the right hand side to zero, i.e., $\bar{q}_x=\bar{q}_y=\bar{m}_z=0$. The unknown displacement functions $\bar{u}_h\left(z\right),\bar{v}_h\left(z\right),\bar{\phi}_h\left(z\right)$ are then assumed to take the following form:

$$\left\langle\bar{U}_h\left(z\right)\right\rangle_{1\times3}^{\mathrm{T}}=\left\langle\bar{u}_h\left(z\right)\quad\bar{v}_h\left(z\right)\quad\bar{\phi}_h\left(z\right)\right\rangle_{1\times3}^{\mathrm{T}}=\sum_{\mathrm{i}=1}^{6}\left\langle C_{1,\mathrm{i}}\quad C_{2,\mathrm{i}}\quad C_{3,\mathrm{i}}\right\rangle_{1\times3}^{\mathrm{T}}e^{m_iz} \tag{6B.20}$$

Substituting equation (6B.20) into homogeneous part of equations (6B.13), one obtains

$$\begin{bmatrix}\left[EI_{yy}m_i^4+\rho I_{yy}\Omega^2m_i^2-\rho A\Omega^2\right] & 0 & -\rho A\Omega^2y_s\\ & \left[EI_{xx}m_i^4+\rho I_{xx}\Omega^2m_i^2-\rho A\Omega^2\right] & \rho A\Omega^2x_s\\ Symm & & \left[EC_wm_i^4-\rho A\Omega^2r_o^2+\left(\rho C_w\Omega^2-GJ\right)m_i^2\right]\end{bmatrix}_{3\times3}\begin{bmatrix}e^{m_iz} & 0 & 0\\ 0 & e^{m_iz} & 0\\ 0 & 0 & e^{m_iz}\end{bmatrix}_{3\times3}\begin{Bmatrix}C_{1,i}\\C_{2,i}\\C_{3,i}\end{Bmatrix}_{3\times1}=\left\{0\right\}_{3\times1} \tag{6B.21}$$

A non-trivial solution of resulting equation (6B.21) is can be determined by setting the determinant of the unknown coefficients $C_{1,i},C_{2,i},C_{3,i}$ to zero, one obtains

$$q_1m_{\mathrm{i}}^{12}+q_2m_{\mathrm{i}}^{10}+q_3m_{\mathrm{i}}^8+q_4m_{\mathrm{i}}^6+q_5m_{\mathrm{i}}^4+q_6m_{\mathrm{i}}^2+q_7=0 \tag{6B.22}$$

in which $q_1=E^3C_wI_{xx}I_{yy}$, $q_2=E^2I_{xx}I_{yy}\left(3\rho\Omega^2C_w-GJ\right)$

$$q_3=\rho\Omega^2E\left[I_{xx}I_{yy}\left(3\rho\Omega^2C_w-2GJ\right)-EA\left(C_w\left[I_{yy}+I_{xx}\right]+I_{xx}I_{yy}r_o^2\right)\right]$$

$$q_4=\rho\Omega^2\left[\left(\rho\Omega^2C_w-GJ\right)\left\{\rho\Omega^2I_{xx}I_{yy}-EA\left(I_{xx}+I_{yy}\right)\right\}-\rho A\Omega^2E\left\{2I_{xx}I_{yy}r_o^2+C_w\left(I_{xx}+I_{yy}\right)\right\}\right]$$

$$q_5 = \rho A\Omega^2\Big[A\Omega^2 r_o^2\left(EI_{yy} - \rho^2\Omega^2 I_{xx}I_{yy}\right) + E\,\rho A\Omega^2\left\{C_w - I_{yy}x_s^2 + I_{xx}\left(r_o^2 - y_s^2\right)\right\} - \rho\Omega^2\left(\rho\Omega^2 C_w - GJ\right)\left(I_{xx} + I_{yy}\right)\Big]$$

$$q_6 = \left(\rho A\Omega^2\right)^2\left[\rho\Omega^2 r_o^2\left(I_{xx} + I_{yy}\right) - \rho\Omega^2\left(I_{yy}x_s^2 + I_{xx}y_s^2\right) + \left(\rho\Omega^2 C_w - GJ\right)\right], \text{ and}$$

$$q_7 = \left(\rho A\,\Omega^2\right)^3\left[x_s^2 + y_s^2 - r_o^2\right].$$

Equation (6B.22) is solved analytically to obtain the roots (m_i for i =1,2,3,....,12) of the equation. When all twelve roots are distinct (i.e., $m_i \neq m_j$ for $i \neq j$), the homogenous solution for the space functions takes the form

$$\left\{\bar{U}_h(z)\right\}_{3\times1} = \left[\bar{C}\right]_{3\times12}\left\{E_{12}(z)\right\}_{12\times1} \tag{6B.23}$$

in which $\left\langle E_{12}(z)\right\rangle_{1\times12}^{\mathrm{T}} = \left\langle e^{m_1 z} \;\; e^{m_2 z} \;\; e^{m_3 z} \;\; e^{m_4 z} \;\; e^{m_5 z} \;\; \ldots\ldots \;\; e^{m_{12} z}\right\rangle_{1\times12}^{\mathrm{T}}$ and

$$\left[\bar{C}\right]_{12\times3}^{\mathrm{T}} = \left[\left\{C_{1,\mathrm{i}}\right\}_{12\times1} \;\; \left\{C_{2,\mathrm{i}}\right\}_{12\times1} \;\; \left\{C_{3,\mathrm{i}}\right\}_{12\times1}\right]_{12\times3}^{\mathrm{T}}, \text{ for } i = 1,2,3,4,....,12.$$

In equation (6B.23), thirty six integration constants appear in the homogenous solution of space functions $\bar{u}_h(z)$, $\bar{v}_h(z)$ and $\bar{\phi}(z)$, namely $C_{1,\mathrm{i}}$, $C_{2,\mathrm{i}}$ and $C_{3,\mathrm{i}}$ for i =1,2,3,...,12, but only twelve boundary conditions related to the displacements $\bar{u}_h(z)$, $\bar{v}_h(z)$ and $\bar{\phi}(z)$ are provided in Equations (6B.14) to (6B.19). It is thus required to reduce the three sets of unknown integration constants $C_{1,\mathrm{i}}$, $C_{2,\mathrm{i}}$ and $C_{3,\mathrm{i}}$ to twelve independent boundary conditions by writing two sets of constants in terms of the constants of the other set.

Equations (6B.23) are substituted into homogeneous form of equations in (6B.13). The resulting equations must be applicable for any value of variable z, leads to

$$\left(EI_{yy}m_{\mathrm{i}}^4 + \rho\Omega^2 I_{yy}m_{\mathrm{i}}^2 - \rho A\Omega^2\right)C_{1,\mathrm{i}} - \left(\rho A\Omega^2 y_s\right)C_{3,\mathrm{i}} = 0 \tag{6B.24}$$

$$\left(EI_{xx}m_{\mathrm{i}}^4 + \rho\Omega^2 I_{xx}m_{\mathrm{i}}^2 - \rho A\Omega^2\right)C_{2,\mathrm{i}} - \left(\rho A\Omega^2 x_s\right)C_{3,\mathrm{i}} = 0 \tag{6B.25}$$

$$\left(\rho A\Omega^2 y_s\right)C_{1,\mathrm{i}} - \left(\rho A\Omega^2 x_s\right)C_{2,\mathrm{i}} - \left[EC_w m_i^4 + \left(\rho\Omega^2 C_w - GJ\right)m_i^2 - \rho A\Omega^2 r_o^2\right]C_{3,\mathrm{i}} = 0 \tag{6B.26}$$

From equations (6B.24) and (6B.24), obtains

$$C_{1,\mathrm{i}}=\frac{\left(\rho A\Omega^2 y_s\right)}{\left(EI_{yy}m_{\mathrm{i}}^4+\rho\Omega^2 I_{yy}m_{\mathrm{i}}^2-\rho A\Omega^2\right)}C_{3,\mathrm{i}}=\bar{G}_{1,\mathrm{i}}C_{3,\mathrm{i}}\ ,\quad \text{for } i=1,2,3,....,12\,. \tag{6B.27}$$

$$C_{2,\mathrm{i}}=\frac{\left(\rho A\Omega^2 x_s\right)}{\left(EI_{xx}m_{\mathrm{i}}^4+\rho\Omega^2 I_{xx}m_{\mathrm{i}}^2-\rho A\Omega^2\right)}C_{3,\mathrm{i}}=\bar{G}_{2,\mathrm{i}}C_{3,\mathrm{i}}\ ,\quad \text{for } i=1,2,3,....,12\,. \tag{6B.28}$$

From equations (6B.27) and (6B.28), by substituting into equation (6B.23), the homogeneous solution for $\bar{u}_h(z),\bar{v}_h(z),\bar{\phi}_h(z)$ is then reduced to the following form

$$\left\{\bar{U}_h(z)\right\}_{3\times1}=\left[\bar{G}\right]_{3\times12}\left[E(z)\right]_{12\times12}\left\{C_{3,i}\right\}_{12\times1} \tag{6B.29}$$

in which $\left[\bar{G}\right]_{12\times3}^{\mathrm{T}}=\left[\left\{\bar{G}_{1,\mathrm{i}}\right\}_{12\times1}\ \vdots\ \left\{\bar{G}_{2,\mathrm{i}}\right\}_{12\times1}\ \vdots\ \{1\}_{12\times1}\right]_{12\times3}^{\mathrm{T}}$, for $i=1,2,3,....,12$

$\left\langle C_{3,i}\right\rangle_{1\times12}^{T}=\left\langle C_{3,1}\ \vdots\ C_{3,2}\ \vdots\ C_{3,3}\ \vdots\ C_{3,4}\ \vdots\ C_{3,5}\ \vdots\ .....\ \vdots\ C_{3,12}\right\rangle_{1\times12}^{T}$ and

$\left[E(z)\right]_{12\times12}=diag\left[e^{m_1z}\ \vdots\ e^{m_2z}\ \vdots\ e^{m_3z}\ \vdots\ e^{m_4z}\ \vdots\ e^{m_5z}\ \vdots\ .....\ \vdots\ e^{m_{12}z}\right]_{12\times12}$.

6B.4 Particular Solution for Uniform Member Forces

For a thin-walled member under uniform distributed forces

$$\left[\bar{q}_x(z),\bar{q}_y(z),\bar{m}_x(z),\bar{m}_y(z),\bar{m}_z(z),\bar{m}_w(z)\right]e^{i\Omega t}=\left[\bar{q}_x,\bar{q}_y,\bar{m}_x,\bar{m}_y,\bar{m}_z,\bar{m}_w\right]e^{i\Omega t},$$

the corresponding particular solution $\left\{\bar{U}_P(z)\right\}_{3\times1}$ of the field coupled equations (6B.13) is assumed to take the form

$$\left\langle\bar{U}_p(z)\right\rangle_{1\times3}^{\mathrm{T}}=\left\langle\bar{u}_p\ \vdots\ \bar{v}_p\ \vdots\ \bar{\phi}_p\right\rangle_{1\times3}^{T}=\left\langle A_1+B_1z\ \vdots\ A_2+B_2z\ \vdots\ A_3+B_3z\right\rangle_{1\times3}^{\mathrm{T}} \tag{6B.30}$$

From expressions in equation (6B.30), by substituting into equation (6B.13), leads to

$$\left\{\bar{U}_P\right\}_{3\times1}=\begin{Bmatrix}\bar{u}_p\\ \bar{v}_p\\ \bar{\phi}_p\end{Bmatrix}_{3\times1}=\begin{Bmatrix}\dfrac{y_s\left(x_s\bar{q}_y+\bar{m}_z\right)-\bar{q}_x\left(r_{\mathrm{o}}^2-x_{\mathrm{s}}^2\right)}{\rho\Omega^2\left(I_{xx}+I_{yy}\right)}\\ \dfrac{x_s\left(y_s\bar{q}_x-\bar{m}_z\right)-\bar{q}_y\left(r_{\mathrm{o}}^2-y_{\mathrm{s}}^2\right)}{\rho\Omega^2\left(I_{xx}+I_{yy}\right)}\\ \dfrac{\left[y_s\bar{q}_x-x_s\bar{q}_y-\bar{m}_z\right]}{\rho\Omega^2\left(I_{xx}+I_{yy}\right)}\end{Bmatrix}_{3\times1} \tag{6B.31}$$

6B.5 General Solution

The complete solution for the system of coupled equations is then obtained by adding the homogeneous part in equation (6B.30) to particular part in equation (6B.31), one obtains

$$\left\{\bar{U}(z)\right\}_{3\times1} = \left[\bar{G}\right]_{3\times12}\left[E(z)\right]_{12\times12}\left\{C_{3,i}\right\}_{12\times1} + \left\{\bar{U}_p(z)\right\}_{3\times1} \tag{6B.32}$$

where the unknown integration constants $\left\{C_{3,i}\right\}_{12\times1}$ (for i =1,2,3,....,12) in equation (6B.32) are determined from the related boundary conditions leading to closed-form solution.

6B.6 Solution for cantilever member under member harmonic forces

A cantilever beam of asymmetric cross-section subjected to (i) concentrated end harmonic forces; lateral force $\bar{P}_x(\ell)e^{i\Omega t}$, transverse force $\bar{P}_y(\ell)e^{i\Omega t}$, end moments $\bar{M}_x(\ell)e^{i\Omega t}$, $\bar{M}_y(\ell)e^{i\Omega t}$, twisting moment $\bar{M}_z(\ell)e^{i\Omega t}$, bimoment $\bar{M}_w(\ell)e^{i\Omega t}$, and (ii) distributed harmonic forces; lateral force $\bar{q}_x e^{i\Omega t}$, transverse force $\bar{q}_y e^{i\Omega t}$, bending moments $\bar{m}_x e^{i\Omega t}$ and $\bar{m}_y e^{i\Omega t}$, twisting moment $\bar{m}_z e^{i\Omega t}$ and bimoment $\bar{m}_w e^{i\Omega t}$ is considered as shown in Figure (6B.1). Note that, the forces are applied in the direction of the principal axes.

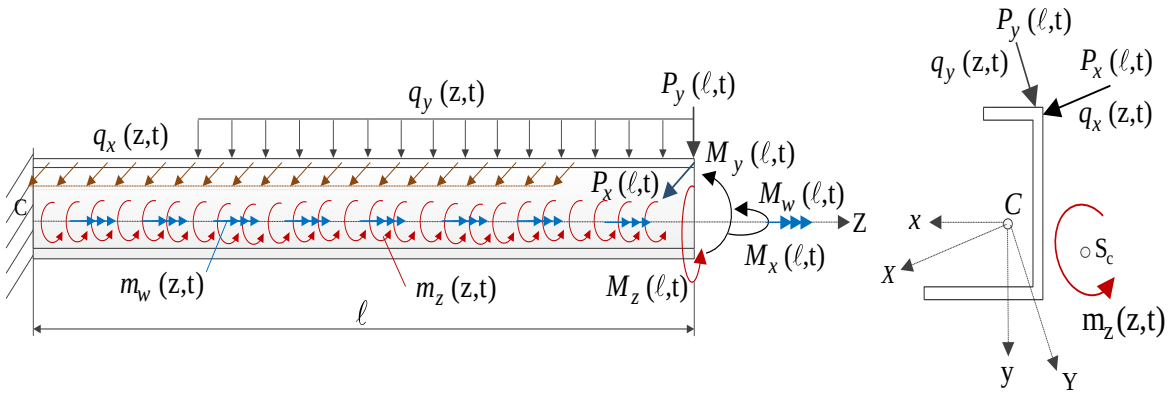

Figure (6B.1): Cantilever of asymmetric section under general harmonic forces

Imposing the following cantilever boundary conditions at beam both ends, i.e., $z=0$ and $z=\ell$

$$\delta\bar{u}(0) = \delta\bar{v}(0) = \delta\bar{\phi}(0) = \delta\bar{u}'(0) = \delta\bar{v}'(0) = \delta\bar{\phi}'(0) = 0 \tag{6B.32-37}$$

$$EI_{yy}\bar{u}''(\ell) = \bar{M}_y(\ell), \quad EI_{xx}\bar{v}''(\ell) = \bar{M}_x(\ell), \quad EI_{yy}\bar{u}'''(\ell) = \bar{P}_x(\ell) \tag{6B.38-40}$$

$$EI_{yy}\bar{v}'''(\ell)=\bar{P}_y(\ell),\ EC_w\bar{\phi}'''(\ell)-GJ\bar{\phi}'(\ell)=\bar{M}_z(\ell)\ \text{and}\ EC_w\bar{\phi}''(\ell)=\bar{M}_w(\ell) \qquad \text{(6B.40-43)}$$

Substituting the expressions for displacement functions in Equations (6B.36) into above boundary conditions (6B.32) to (6B.43), one obtains

$$\left\{\bar{U}_C(z)\right\}_{3\times1}=\left[\bar{G}\right]_{3\times12}\left[E(z)\right]_{12\times12}\left[\chi_C\right]^{-1}_{12\times12}\left\{\bar{Q}_f\right\}_{12\times1}+\left\{\bar{U}_p(z)\right\}_{3\times1} \qquad \text{(6B.44)}$$

in which

$$\left[\chi_C\right]^{\mathrm{T}}_{12\times12}=\Big[\left\{\bar{G}_{1,\mathrm{i}}\right\}_{12\times1}\ \left\{\bar{G}_{2,\mathrm{i}}\right\}_{12\times1}\ \left\{1\right\}_{12\times1}\ \left\{m_i\bar{G}_{1,\mathrm{i}}\right\}_{12\times1}\ \left\{m_i\bar{G}_{2,\mathrm{i}}\right\}_{12\times1}\ \left\{m_i\right\}_{12\times1}$$
$$\left\{m_{\mathrm{i}}^2\bar{G}_{1,\mathrm{i}}e^{m_i\ell}\right\}_{12\times1}\ \left\{m_i^2\bar{G}_{2,\mathrm{i}}e^{m_i\ell}\right\}_{12\times1}\ \left\{m_{\mathrm{i}}^2e^{m_i\ell}\right\}_{12\times1}\ \left\{m_{\mathrm{i}}^3\bar{G}_{1,\mathrm{i}}e^{m_i\ell}\right\}_{12\times1}\ ,\ \text{and}$$
$$\left\{m_{\mathrm{i}}^3\bar{G}_{2,\mathrm{i}}e^{m_i\ell}\right\}_{12\times1}\ \left\{\left[m_{\mathrm{i}}^2-(GJ/EC_w)\right]m_{\mathrm{i}}e^{m_i\ell}\right\}_{12\times1}\Big]^T_{12\times12}$$

$$\left\langle\bar{Q}_f\right\rangle^{\mathrm{T}}_{1\times12}=\Bigg\langle\left(\frac{\bar{q}_x\left(r_{\mathrm{o}}^2-x_{\mathrm{s}}^2\right)-y_s\left(x_s\bar{q}_y+\bar{m}_z\right)}{\rho\Omega^2\left(I_{xx}+I_{yy}\right)}\right)\left(\frac{\bar{q}_y\left(r_{\mathrm{o}}^2-y_{\mathrm{s}}^2\right)-x_s\left(y_s\bar{q}_x-\bar{m}_z\right)}{\rho\Omega^2\left(I_{xx}+I_{yy}\right)}\right)$$
$$\frac{\left[x_s\bar{q}_y+\bar{m}_z-y_s\bar{q}_x\right]}{\rho\Omega^2\left(I_{xx}+I_{yy}\right)}\ 0\ 0\ 0\ \frac{\bar{M}_y(\ell)}{EI_{yy}}\ \frac{\bar{M}_x(\ell)}{EI_{xx}}\ \frac{\bar{M}_w(\ell)}{EC_w}\ \frac{\bar{P}_x(\ell)}{EI_{yy}}\ \frac{\bar{P}_y(\ell)}{EI_{xx}}\ \frac{\bar{M}_z(\ell)}{EC_w}\Bigg\rangle^{\mathrm{T}}_{1\times12}.$$

6B.7 Solution for Simply-supported Beam under Member Harmonic Forces

A simply supported beam with asymmetric section subjected to (1) distributed harmonic forces: lateral force $\bar{q}_x e^{i\Omega t}$, transverse force $\bar{q}_y e^{i\Omega t}$, bending moments $\bar{m}_y e^{i\Omega t}$, $\bar{m}_x e^{i\Omega t}$, twisting moment $\bar{m}_z e^{i\Omega t}$ and bimoment $\bar{m}_w e^{i\Omega t}$, and (2) end harmonic forces: bending moments $\bar{M}_x(z_e)e^{i\Omega t}$, $\bar{M}_y(z_e)e^{i\Omega t}$ and bimoment $\bar{M}_w(z_e)e^{i\Omega t}$ at beam both ends $(z_e=0,\ell)$ is considered as shown in Figure (6B.2). Knowing that, all the forces are applied in the direction of the principal axes.

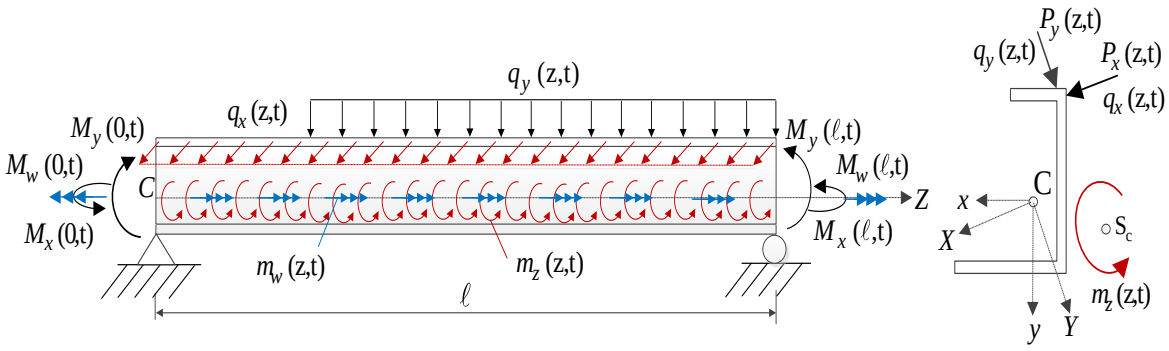

Figure (6B.2): Simply-supported beam of asymmetric section under harmonic forces

The members are restrained at their ends by fork supports in which the boundary conditions are the same as for a simply supported beams, i.e., the fork end restraints allow the end-sections free to warp and to rotate about x and y axes. The boundary conditions of the member at end $z=0$ are

$$\delta\bar{u}(0)=\delta\bar{v}(0)=\delta\bar{\phi}(0)=0 \tag{6B.45-47}$$

$$EI_{yy}\bar{u}''(0)=-\bar{M}_y(0),\quad EI_{xx}\bar{v}''(0)=-\bar{M}_x(0),\quad EC_w\bar{\phi}''(0)=-\bar{M}_w(0) \tag{6B.48-50}$$

and at the end $z=\ell$

$$\delta\bar{u}(\ell)=\delta\bar{v}(\ell)=\delta\bar{\phi}(\ell)=0 \tag{6B.51-53}$$

$$EI_{yy}\bar{u}''(\ell)=\bar{M}_y(\ell),\ EI_{xx}\bar{v}''(\ell)=\bar{M}_x(\ell) \text{ and } EC_w\bar{\phi}''(\ell)=\bar{M}_w(\ell) \tag{6B.54-56}$$

From equation (6B.32), by substituting into the above boundary conditions (6B.45) to (6B.56), the general solution is obtained as:

$$\left\{\bar{U}_S(z)\right\}_{3\times1}=\left[\bar{G}\right]_{3\times12}\left[E(z)\right]_{12\times12}\left[\chi_S\right]^{-1}_{12\times12}\left\{\bar{Q}_S\right\}_{12\times1}+\left\{\bar{U}_P\right\}_{3\times1} \tag{6B.57}$$

in which

$$\left[\chi_S\right]^{\mathrm{T}}_{12\times12}=\Big[\left\{\bar{G}_{1,\mathrm{i}}\right\}_{12\times1}\left\{\bar{G}_{2,\mathrm{i}}\right\}_{12\times1}\left\{1\right\}_{12\times1}\left\{m_i^2\bar{G}_{1,\mathrm{i}}\right\}_{12\times1}\left\{m_i^2\bar{G}_{2,\mathrm{i}}\right\}_{12\times1}\left\{m_i^2\right\}_{12\times1}\left\{\bar{G}_{1,\mathrm{i}}e^{m_i l}\right\}_{12\times1}$$
$$\left\{\bar{G}_{2,\mathrm{i}}e^{m_i\ell}\right\}_{12\times1}\left\{e^{m_i\ell}\right\}_{12\times1}\left\{m_i^2\bar{G}_{1,\mathrm{i}}e^{m_i\ell}\right\}_{12\times1}\left\{m_i^2\bar{G}_{2,\mathrm{i}}e^{m_i\ell}\right\}_{12\times1}\left\{m_i^2e^{m_i\ell}\right\}_{12\times1}\Big]^{\mathrm{T}}_{12\times12},$$

$$\left\langle\bar{Q}_S\right\rangle^{\mathrm{T}}_{1\times12}=\Bigg\langle\frac{\bar{q}_x\left(r_o^2-x_s^2\right)-y_s\left(x_s\bar{q}_y+\bar{m}_z\right)}{\rho\Omega^2\left(I_{xx}+I_{yy}\right)}\ \frac{\bar{q}_y\left(r_o^2-y_s^2\right)-x_s\left(y_s\bar{q}_x-\bar{m}_z\right)}{\rho\Omega^2\left(I_{xx}+I_{yy}\right)}$$
$$\frac{-\bar{M}_y(0)}{EI_{yy}}\ \frac{-\bar{M}_x(0)}{EI_{xx}}\ \frac{-\bar{M}_x(0)}{EI_{xx}}\ \frac{\bar{q}_x\left(r_o^2-x_s^2\right)-y_s\left(x_s\bar{q}_y+\bar{m}_z\right)}{\rho\Omega^2\left(I_{xx}+I_{yy}\right)}$$
$$\frac{\bar{q}_y\left(r_o^2-y_s^2\right)-x_s\left(y_s\bar{q}_x-\bar{m}_z\right)}{\rho\Omega^2\left(I_{xx}+I_{yy}\right)}\ \frac{\left[x_s\bar{q}_y+\bar{m}_z-y_s\bar{q}_x\right]}{\rho\Omega^2\left(I_{xx}+I_{yy}\right)}\ \frac{\bar{M}_y(\ell)}{EI_{yy}}\ \frac{\bar{M}_x(\ell)}{EI_{xx}}\ \frac{\bar{M}_w(\ell)}{EC_w}\Bigg\rangle^{\mathrm{T}}_{1\times12}.$$

List of Symbols

The following list of symbols are given

A	Cross-sectional area
b	Length of the flange
C	Centroid of the cross-section
C_w	Warping constant
d	Height of beam cross-section
D_{xx} ,D_{yy} D_{xy} ,D_{hx} D_{hy} ,$D_{\omega\omega}$	Section properties
E	Modulus of elasticity
G	Shear modulus
$h(s)$	Normal distance between the shear centre and the tangent to mid-surface
H	Height of beam cross-section from the flanges mid-surfaces
I_{xx} ,I_{yy}	Moment of inertias of the cross-section about the principal X and Y axes
J	Torsional constant
ℓ	Length of the member
$\bar{M}_j(z)$	Concentrated moment about j-th direction (for $j = x, y, z$)
$\bar{M}_w(z)$	Concentrated bimoment
$\bar{m}_j(z)$	Distributed moments about j-th direction (for $j = x, y, z$)
$\bar{m}_w(z)$	Distributed bimoment
n, s, z	Local curvilinear coordinate system
$\bar{N}_z$	Concentrated end forces along longitudinal axis
$\bar{q}_j(z)$	Distributed forces along x, y, z directions (for $j = x, y, z$)
s	Curvilinear coordinate along mid-surface of the section
S_c	Shear centre of the cross-section
t	Time in seconds
t_1,t_2	Time intervals

T^*	Kinetic energy
$\bar{u},\bar{v}$	Displacements of the shear centre along the principal X ,Y axes
U^*	Internal strain energy
$\bar{V}_j(z)$	Shear forces along x ,y axes (for $j = x, y$)
$\bar{w}$	Average longitudinal displacement along the Z axis
W^*	Work done by applied forces
x, y, z	Cartesian coordinate system
X, Y, Z	Principal coordinate system
$x(s), y(s)$	Coordinates of arbitrary point on mid-surface of the section along X and Y axes
X_s, Y_s	Coordinates of the shear centre along the principal directions
Z	Longitudinal coordinate
ρ	Density of the material
r_o	Polar radius of gyration
$\bar{\theta}_x, \bar{\theta}_y, \bar{\theta}_z$	Rotations angles around the X ,Y ,Z axes, respectively
$\hat{\alpha}(s)$	Angle between the tangent to the cross-section and the principal X axis
$\bar{\psi}$	Warping deformation function
Ω	Exciting frequency
$\omega(s)$	Warping function of the cross-section

CHAPTER (7)

FATIGUE ANALYSIS AND DESIGN OF THIN-WALLED MEMBERS UNDER MULTIPLE HARMONIC FORCES

Chapter (7) - Fatigue Analysis and Design of Thin-walled Members under Multiple Harmonic Forces

7.1 Introduction and Scope

A key objective of the present study was to provide an effective tool to predict the fatigue life of thin walled members subject to harmonic forces. The mechanistic aspects of the solutions including closed form and finite element solutions have already been discussed in Chapters 3-6. The present chapter complements the previous work by

(a) Devising a technique to predict the stresses within thin walled members under multiple harmonic forces with different exciting frequencies (Section 7.3),

(b) Reviewing present design methodologies for predicting fatigue life (Section 7.4), and

(c) Combining the stress histories generated from steps (a) and (b) with established design methodologies to predict the lifespan of thin-walled members under the effect of multiple harmonic forces (Section 7.6).

7.2 Response under Multiple Harmonic Forces with Distinct Frequencies

Closed form and finite element solutions were developed for members subject to harmonic forces applied with identical exciting frequencies. The adoption of this assumption has successfully eliminated the need for time discretization in the solution of the governing equations. In real life applications, it is conceivable to have multiple exciting forces with different exciting frequencies. It is thus desirable to extend the capabilities of the model to accommodate such cases. Within this context, this section proposes a methodology for constructing the response of a member under multiple harmonic forces with different exciting frequencies, starting with the individual steady state responses for each individual harmonic force.

7.3 Formulating Expressions for Stresses

A thin-walled member of general cross-section (Fig. 7.1a) is assumed to be subjected to concentrated and distributed harmonic excitations as

$$q_z(z,t),q_x(z,t),q_y(z,t),m_x(z,t),m_y(z,t),m_z(z,t),m_w(z,t)$$
$$=\left[\bar{q}_z(z),\bar{q}_x(z),\bar{q}_y(z),\bar{m}_x(z),\bar{m}_y(z),\bar{m}_z(z),\bar{m}_w(z)\right]\sin\Omega t$$

$$N_z(z,t),V_x(z,t),V_y(z,t),M_x(z,t),M_y(z,t),M_z(z,t),M_w(z,t)$$
$$=\left[\bar{N}_z(z),\bar{V}_x(z),\bar{V}_y(z),\bar{M}_x(z),\bar{M}_y(z),\bar{M}_z(z),\bar{M}_w(z)\right]\sin\Omega t \quad (7.1)$$

where $q_z(z,t), N_z(z,t)$ are the longitudinal member and point force, distributed and concentrated shear forces $q_x(z,t)$, $q_y(z,t)$ and $V_x(z,t)$, $V_y(z,t)$, applied along the principal axes X and Y, $m_x(z,t)$, $m_y(z,t)$ and $M_x(z,t)$, $M_y(z,t)$ are distributed and concentrated bending moments, respectively, $m_z(z,t), M_z(z,t)$ are the distributed and point torsion, and $m_w(z,t), M_w(z,t)$ are the member and concentrated bimoments.

Under the above applied harmonic forces, the response is assumed to take the following form

$$w(z,t),u(z,t),v(z,t),\theta_x(z,t),\theta_y(z,t),\theta_z(z,t),\psi(z,t)$$
$$=\left[\bar{w}(z),\bar{u}(z),\bar{v}(z),\bar{\theta}_x(z),\bar{\theta}_y(z),\bar{\theta}_z(z),\bar{\psi}(z)\right]\sin\Omega t \quad (7.2)$$

It is required to derive an expression for normal and shear stresses in terms of stress resultants.

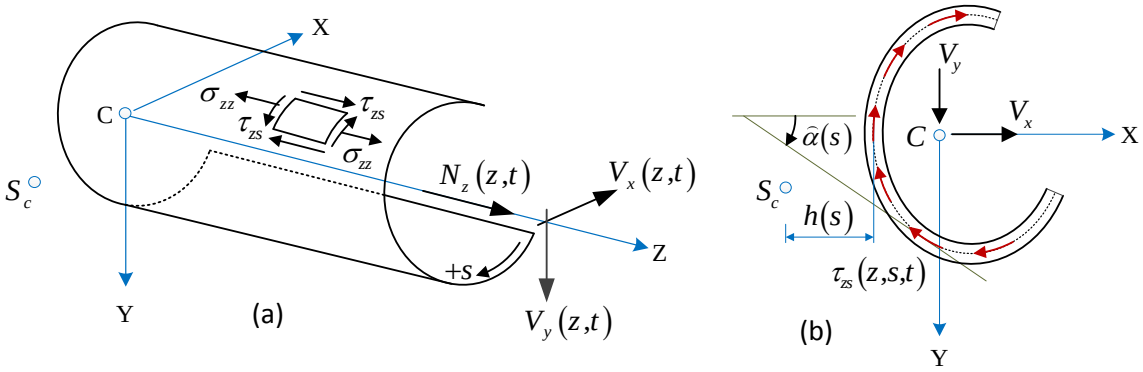

Figure (7.1): An arbitrary thin-walled member under longitudinal and shear forces

7.3.1 Normal Stresses

The normal stress $\sigma_{zz}(z,s,t)$ is related to the longitudinal strain $\varepsilon_{zz}(z,s,t)$ through the Hook's law as

$$\sigma_{zz}\left(z,s,t\right)=E\,\varepsilon_{zz}\left(z,s,t\right) \tag{7.3}$$

in which the longitudinal strain $\varepsilon_{zz}\left(z,s,t\right)$ is expressed in terms of the longitudinal displacement $w\left(z,s,t\right)$. Substituting the longitudinal displacement expression given in Equation (3.3) and Equation (7.2) into Equation (3.7), yields

$$\begin{aligned}\varepsilon_{zz} &= w'\left(z,t\right)+y\left(s\right)\theta_x'\left(z,t\right)-x\left(s\right)\theta_y'\left(z,t\right)+\omega\left(z\right)\psi'\left(z,t\right)\\ &=\left\langle 1 \quad y\left(s\right) \quad -x\left(s\right) \quad \omega\left(s\right)\right\rangle_{1\times 4}^{T}\left\{\hat{U}_d\left(z\right)\right\}_{4\times 1}\sin\Omega t=\left\langle \hat{X}_s\right\rangle_{1\times 4}^{T}\left\{\hat{U}_d\left(z\right)\right\}_{4\times 1}\sin\Omega t\end{aligned} \tag{7.4}$$

where $\left\langle \hat{U}_d\left(z\right)\right\rangle_{1\times 4}^{T}=\left\langle \bar{w}'\left(z\right) \quad \bar{\theta}_x'\left(z\right) \quad \bar{\theta}_y'\left(z\right) \quad \bar{\psi}'\left(z\right)\right\rangle_{1\times 4}^{T}$, and

$\left\langle \hat{X}_s\right\rangle_{1\times 4}^{T}=\left\langle 1 \quad y\left(s\right) \quad -x\left(s\right) \quad \omega\left(s\right)\right\rangle_{1\times 4}^{T}$

From Equation (7.4), substituting into Equation (7.3), yields

$$\sigma_{zz}\left(z,s,t\right)=E\,\varepsilon_{zz}=E\left\langle \hat{X}_s\right\rangle_{1\times 4}^{T}\left\{\hat{U}_d\left(z\right)\right\}_{4\times 1}\sin\Omega t \tag{7.5}$$

7.3.2 Normal Stresses in terms of Stress Resultants

The internal forces induced by the normal stresses at a given arbitrary cross-section are given by

$$\begin{aligned}&\left\langle N_z\left(z,t\right) \mid M_x\left(z,t\right) \mid M_y\left(z,t\right) \mid M_w\left(z,t\right)\right\rangle_{1\times 4}^{T}\\ &=\int_A\left\langle \sigma_{zz}\left(z,s,t\right) \mid -y\left(s\right)\sigma_{zz}\left(z,s,t\right) \mid -x\left(s\right)\sigma_{zz}\left(z,s,t\right) \mid \omega\left(s\right)\sigma_{zz}\left(z,s,t\right)\right\rangle_{1\times 4}^{T}dA\end{aligned} \tag{7.6}$$

From Equation (7.5), by substituting into Equation (7.6) and enforcing the orthogonality conditions, $\int_A\left[x\left(s\right),y\left(s\right),x\left(s\right)y\left(s\right),x\left(s\right)\omega\left(s\right),y\left(s\right)\omega\left(s\right),\omega\left(s\right)\right]dA=\left(0,0,0,0,0,0\right)$, one obtains

$$\begin{Bmatrix} N_z\left(z,t\right)\\ M_x\left(z,t\right)\\ M_y\left(z,t\right)\\ M_w\left(z,t\right)\end{Bmatrix}_{4\times 1}=\begin{Bmatrix} \bar{N}_z\left(z\right)\\ \bar{M}_x\left(z\right)\\ \bar{M}_y\left(z\right)\\ \bar{M}_w\left(z\right)\end{Bmatrix}_{4\times 1}\sin\Omega t=E\begin{bmatrix} A & 0 & 0 & 0\\ 0 & -I_{xx} & 0 & 0\\ 0 & 0 & I_{yy} & 0\\ 0 & 0 & 0 & C_w\end{bmatrix}_{4\times 4}\begin{Bmatrix} \bar{w}'\left(z\right)\\ \bar{\theta}_x'\left(z\right)\\ \bar{\theta}_y'\left(z\right)\\ \bar{\psi}'\left(z\right)\end{Bmatrix}_{4\times 1}\sin\Omega t \tag{7.7}$$

in which the section properties $\left(A,I_{xx},I_{yy},C_w\right)=\int_A\left(1,y^2,x^2,\omega^2\right)dA$ were defined.

Equation (7.7) is inverted to relate the derivatives of the displacement expressions as

$$\left\{\hat{U}_d\left(z\right)\right\}_{4\times1}=\begin{Bmatrix}\bar{w}'\left(z\right)\\ \bar{\theta}_x'\left(z\right)\\ \bar{\theta}_y'\left(z\right)\\ \bar{\psi}'\left(z\right)\end{Bmatrix}_{4\times1}=\frac{1}{E}\begin{bmatrix}A & 0 & 0 & 0\\ 0 & -I_{xx} & 0 & 0\\ 0 & 0 & I_{yy} & 0\\ 0 & 0 & 0 & C_w\end{bmatrix}^{-1}_{4\times4}\begin{Bmatrix}\bar{N}_z\left(z\right)\\ \bar{M}_x\left(z\right)\\ \bar{M}_y\left(z\right)\\ \bar{M}_w\left(z\right)\end{Bmatrix}_{4\times1} \tag{7.8}$$

From Equation (7.8), by substituting into Equation (7.5), the normal stresses

$$\sigma_{zz}\left(z,s,t\right)=\left\langle\hat{X}_s\right\rangle^T_{1\times4}\begin{bmatrix}A & 0 & 0 & 0\\ 0 & I_{yy} & 0 & 0\\ 0 & 0 & I_{xx} & 0\\ 0 & 0 & 0 & C_w\end{bmatrix}^{-1}_{4\times4}\begin{Bmatrix}\bar{N}_z\left(z\right)\\ \bar{M}_x\left(z\right)\\ \bar{M}_y\left(z\right)\\ \bar{M}_w\left(z\right)\end{Bmatrix}_{4\times1}\sin\Omega t \tag{7.9}$$

The normal stress expression given by Equation (7.9) is simplified to

$$\sigma_{zz}\left(z,s,t\right)=\left(\frac{\bar{N}_z\left(z\right)}{A}-\frac{\bar{M}_x\left(z\right)}{I_{xx}}y\left(s\right)+\frac{\bar{M}_y\left(z\right)}{I_{yy}}x\left(s\right)+\frac{\bar{M}_w\left(z\right)}{C_w}\omega\left(s\right)\right)\sin\Omega t \tag{7.10}$$

Equation (7.10) presents the total normal stresses caused by longitudinal, shear forces, bending moments about the principal axes and bimoment.

The stress resultants, $\bar{N}_z\left(z\right),\bar{M}_x\left(z\right),\bar{M}_y\left(z\right),\bar{M}_w\left(z\right)$ at a given section $z=z_e$ are determined by conducting a steady state analysis for the problem, extracting the nodal displacements for one of the two elements connected to the section of interest, $z=z_e$, and pre-multiplying the element dynamic stiffness matrix by the nodal displacements as extracted from the finite element solution. This yields 14 stress resultants $\bar{N}_z\left(z\right)$, $\bar{V}_x\left(z\right),\bar{V}_y\left(z\right)$, $\bar{M}_x\left(z\right)$, $\bar{M}_y\left(z\right),\bar{M}_z\left(z\right)$ and $\bar{M}_w\left(z\right)$ at both ends of the element.

7.3.3 Shear Stresses

The shear stress distribution in a thin-walled arbitrary section is illustrated in Figure (7.1b). The shear stress $\tau_{zs}\left(z,s,t\right)$ can be determined as

$$\tau_{zs}\left(z,s,t\right)\approx G\gamma_{zs}=G\left(\frac{\partial\xi}{\partial z}+\frac{\partial w}{\partial s}\right) \tag{7.11}$$

Substituting Equations (3.10) and (7.2) into Equation (7.11), yields

$$\tau_{zs}(z,s,t)=G\left\langle \cos\hat{\alpha}(s)\ \ \sin\hat{\alpha}(s)\ \ h(s)\right\rangle_{1\times 3}^{T}\begin{Bmatrix}(\bar{u}'-\bar{\theta}_y)\\(\bar{v}'+\bar{\theta}_x)\\(\bar{\theta}_z'+\bar{\psi})\end{Bmatrix}_{3\times 1}\sin\Omega t \tag{7.12}$$

7.3.4 Stress Resultants in terms of Shear Stresses

The shear forces $V_x(z,t)$, $V_y(z,t)$ in the direction of principal X and Y axes and the warping torsion $M_{zw}(z,t)$ are determined as

$$\begin{Bmatrix}V_x(z,t)\\V_y(z,t)\\M_{zw}(z,t)\end{Bmatrix}_{3\times 1}=\int_A\begin{Bmatrix}\cos\hat{\alpha}(s)\\\sin\hat{\alpha}(s)\\h(s)\end{Bmatrix}_{3\times 1}\tau_{zs}\,dA$$

$$=G\int_A\begin{bmatrix}\left[\cos\hat{\alpha}(s)\right]^2 & \sin\hat{\alpha}(s)\cos\hat{\alpha}(s) & h(s)\cos\hat{\alpha}(s)\\ \sin\hat{\alpha}(s)\cos\hat{\alpha}(s) & \left[\sin\hat{\alpha}(s)\right]^2 & h(s)\sin\hat{\alpha}(s)\\ h(s)\cos\hat{\alpha}(s) & h(s)\sin\hat{\alpha}(s) & \left[h(s)\right]^2\end{bmatrix}_{3\times 3}dA\begin{Bmatrix}(\bar{u}'-\bar{\theta}_y)\\(\bar{v}'+\bar{\theta}_x)\\(\bar{\theta}_z'+\bar{\psi})\end{Bmatrix}_{3\times 1}\sin\Omega t$$

$$=G\begin{bmatrix}D_{xx} & D_{xy} & D_{hx}\\ D_{xy} & D_{yy} & D_{hy}\\ D_{hx} & D_{hy} & D_{\omega\omega}\end{bmatrix}_{3\times 3}\begin{Bmatrix}(\bar{u}'-\bar{\theta}_y)\\(\bar{v}'+\bar{\theta}_x)\\(\bar{\theta}_z'+\bar{\psi})\end{Bmatrix}_{3\times 1}\sin\Omega t \tag{7.13}$$

in which the cross-sectional properties $D_{xx}=\int_A\left[\cos\hat{\alpha}(s)\right]^2dA$, $D_{yy}=\int_A\left[\sin\hat{\alpha}(s)\right]^2dA$, $D_{xy}=\int_A\sin\hat{\alpha}(s)\cos\hat{\alpha}(s)dA$, $D_{hx}=\int_A h(s)\cos\hat{\alpha}(s)dA$, $D_{hy}=\int_A h(s)\sin\hat{\alpha}(s)dA$ and $D_{\omega\omega}=\int_A\left[h(s)\right]^2dA$ were defined.

From Equation (7.13), by substituting into Equation (7.12), the new expression of the transverse shear stress $\tau_{zs}(z,s,t)$ in terms of force resultants and section properties is determined as

$$\tau_{zs}(z,s,t)=\left\langle \cos\hat{\alpha}(s)\ \ \sin\hat{\alpha}(s)\ \ h(s)\right\rangle_{1\times 3}^{T}\begin{bmatrix}D_{xx} & D_{xy} & D_{hx}\\ D_{xy} & D_{yy} & D_{hy}\\ D_{hx} & D_{hy} & D_{\omega\omega}\end{bmatrix}_{3\times 3}^{-1}\begin{Bmatrix}\bar{V}_x(z)\\\bar{V}_y(z)\\\bar{M}_{zw}(z)\end{Bmatrix}_{3\times 1}\sin\Omega t \tag{7.14}$$

7.3.5 Shear Stress Due to Saint-Venant Torsion

When the thin-walled member is subjected to uniform twisting moment, i.e., Saint Venant torsion $M_{zsv}(z,t)$, the cross-section rotates through an angle $\theta_z(z,t)$ as shown in Figure (7.2). If the warping is completely unrestrained, the St. Venant torsional moment $M_{zsv}(z,t)$ resisted by the cross-section is given by

$$M_{zsv}(z,t) = GJ\theta_z'(z,t) = GJ\bar{\theta}_z'(z)\sin\Omega t \tag{7.15}$$

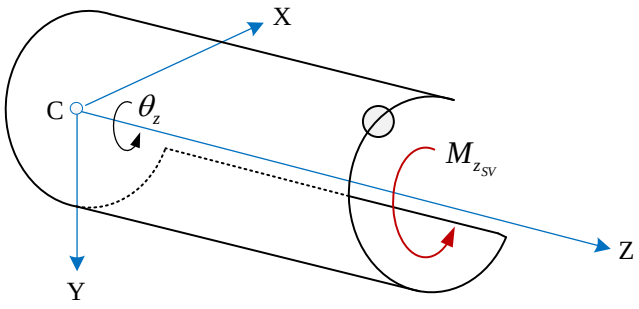

(a) Thin-walled beam under St. Venant Torsion

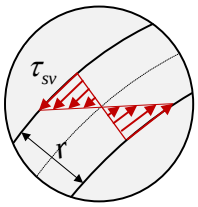

(b) St Venant Shear Stress distribution

Figure (7.2): Thin-walled member under St. Venant Torsion

The shear stress $\tau_{sv}(z,r,t)$ due to Saint Venant torsion is given as

$$\tau_{sv}(z,r,t) = M_{zsv}(z,t)\frac{r}{J} = Gr\bar{\theta}_z'(z)\sin\Omega t \tag{7.16}$$

where r is the wall thickness and $J = \frac{1}{3}\sum_{i=1} b_i t_i^3$ is the Saint-Venant torsional constant.

The total shear stress $\tau_{sv}(z,s,t)$ is obtained by adding the expression in Equation (7.14) to the St. Venant torsion shear stress given in Equation (7.16) which varies linearly through the wall thickness (Fig. 7.2b) as

$$\tau_{zs} = \left(\left\langle \cos\hat{\alpha}(s) \;\; \sin\hat{\alpha}(s) \;\; h(s) \right\rangle_{1\times 3}^{T} \begin{bmatrix} D_{xx} & D_{xy} & D_{hx} \\ D_{xy} & D_{yy} & D_{hy} \\ D_{hx} & D_{hy} & D_{\omega\omega} \end{bmatrix}_{3\times 3}^{-1} \begin{Bmatrix} \bar{V}_x \\ \bar{V}_y \\ \bar{M}_{zw} \end{Bmatrix}_{3\times 1} + Gr\bar{\theta}_z'(z) \right) \sin\Omega t \tag{7.17}$$

In Equation (7.17), $\bar{V}_x(z)$ and $\bar{V}_y(z)$ are known from the end force reactions as described at the end of Section (7.2.2), while the terms $\bar{M}_{zw}$ and $\bar{\theta}_z'(z)$ are not directly available. The following procedure outlines a procedure to determine $\bar{M}_{zw}$ and $\bar{\theta}_z'(z)$. The total torsion $\bar{M}_z$ (known from the end reactions) is the sum of the warping torsion and St. Venant torsion, i.e., $\bar{M}_z = \bar{M}_{zw} + \bar{M}_{zsv}$. Also, the St. Venant torsion is related to the derivative of the angle of twist through $\bar{M}_{zsv} = GJ\,\bar{\theta}_z'$. These relations allow the expression of the warping torsion as $\bar{M}_{zw} = \bar{M}_z - GJ\,\bar{\theta}_z'$. By substituting into Equation (7.13), one obtains

$$\begin{Bmatrix} \bar{V}_x \\ \bar{V}_y \\ \bar{M}_z - GJ\,\bar{\theta}_z' \end{Bmatrix}_{3\times1} = G \begin{bmatrix} D_{xx} & D_{xy} & D_{hx} \\ D_{xy} & D_{yy} & D_{hy} \\ D_{hx} & D_{hy} & D_{\omega\omega} \end{bmatrix}_{3\times3} \begin{Bmatrix} (\bar{u}' - \bar{\theta}_y) \\ (\bar{v}' + \bar{\theta}_x) \\ (\bar{\theta}_z' + \bar{\psi}) \end{Bmatrix}_{3\times1} \tag{7.18}$$

In Equation (7.18), one recalls that the stress resultants $\bar{V}_x$, $\bar{V}_y$ and $\bar{M}_z$ are determined from the member end reaction (as described in Section 7.2.5) and $\bar{\theta}_x$, $\bar{\theta}_y$ and $\bar{\psi}$ are known from the nodal displacements. The system of equations can be solved for the three unknowns $\bar{u}'$, $\bar{v}'$ and $\bar{\theta}_z'$. Once $\bar{\theta}_z'$ is known, the St. Venant torsion is determined from $\bar{M}_{zsv} = GJ\,\bar{\theta}_z'$ and the warping torsion can be determined from $\bar{M}_{zw} = \bar{M}_z - GJ\,\bar{\theta}_z'$.

7.3.6 Shear Stresses for Doubly symmetric cross-section

For doubly symmetric sections, the section properties D_{xy}, D_{hx}, D_{hy} are vanished. Then the shear resultants given by Equation (7.13) are simplified to

$$\begin{Bmatrix} V_x(z,t) \\ V_y(z,t) \\ \bar{M}_z(z,t) - GJ\,\bar{\theta}_z' \end{Bmatrix}_{3\times1} = G \begin{bmatrix} D_{xx} & 0 & 0 \\ 0 & D_{yy} & 0 \\ 0 & 0 & D_{\omega\omega} \end{bmatrix}_{3\times3} \begin{Bmatrix} (\bar{u}' - \bar{\theta}_y) \\ (\bar{v}' + \bar{\theta}_x) \\ (\bar{\theta}_z' + \bar{\psi}) \end{Bmatrix}_{3\times1} \sin\Omega t \tag{7.19}$$

From Equation (7.17), the shear stress $\tau_{zs}(z,s,t)$ is given as

$$\tau_{zs}=\left(\left\langle\cos\hat{\alpha}(s)\ \sin\hat{\alpha}(s)\ h(s)\right\rangle_{1\times3}^{T}\begin{bmatrix}\frac{1}{D_{xx}} & 0 & 0\\ 0 & \frac{1}{D_{yy}} & 0\\ 0 & 0 & \frac{1}{D_{\omega\omega}}\end{bmatrix}_{3\times3}\begin{Bmatrix}\bar{V}_x(z)\\ \bar{V}_y(z)\\ \bar{M}_z(z)-GJ\,\bar{\theta}_z'(z)\end{Bmatrix}_{3\times1}+Gr\theta_z'(z)\right)\sin\Omega t \tag{7.20}$$

7.3.7 Shear Stresses for Mono-symmetric cross-section

In the case of mono-symmetric cross-sections, in which the X axis is the axis of symmetry, the section properties D_{xy}, D_{hx} are zero. Substituting the sectional properties $D_{xy}=D_{hx}=0$ into Equation (7.13), yields

$$\begin{Bmatrix}V_x(z,t)\\ V_y(z,t)\\ M_z(z,t)-GJ\,\theta_z'\end{Bmatrix}_{3\times1}=G\begin{bmatrix}D_{xx} & 0 & 0\\ 0 & D_{yy} & D_{hy}\\ 0 & D_{hy} & D_{\omega\omega}\end{bmatrix}_{3\times3}\begin{Bmatrix}\left(\bar{u}'-\bar{\theta}_y\right)\\ \left(\bar{v}'+\bar{\theta}_x\right)\\ \left(\bar{\theta}_z'+\bar{\psi}\right)\end{Bmatrix}_{3\times1}\sin\Omega t \tag{7.21}$$

and the shear stress expression in (7.17) is reduced to:

$$\tau_{zs}=\left(\left\langle\cos\hat{\alpha}(s)\ \sin\hat{\alpha}(s)\ h(s)\right\rangle_{1\times3}^{T}\begin{bmatrix}D_{xx} & 0 & 0\\ 0 & D_{yy} & D_{hy}\\ 0 & D_{hy} & D_{\omega\omega}\end{bmatrix}_{3\times3}^{-1}\begin{Bmatrix}\bar{V}_x(z)\\ \bar{V}_y(z)\\ \bar{M}_z(z)-GJ\,\bar{\theta}_z'\end{Bmatrix}_{3\times1}+Gr\theta_z'(z)\right)\sin\Omega t \tag{7.22}$$

When the structural member is subjected to k sets of harmonic loads, each set with a harmonic frequency Ω_i, (for $i=1,k$), a number of k steady state problems can be solved for each set of exciting frequencies Ω_i separately and the corresponding normal $\sigma_{zz_i}(z,s,t)$ and shearing stresses $\tau_{zs_i}(z,s,t)$ can be obtained from Equations (7.10) and (7.17).

The total stresses $\sigma_{zz}(z,s,t)$ and $\tau_{sz}(z,s,t)$ is given by summation, i.e.,

$$\begin{Bmatrix}\sigma_{zz}(z,s,t)\\ \tau_{zs}(z,s,t)\end{Bmatrix}=\sum_{i=1}^{k}\begin{Bmatrix}\bar{\sigma}_{zz_i}(z,s)\\ \bar{\tau}_{zs_i}(z,s)\end{Bmatrix}\sin\Omega_i t \tag{7.23}$$

7.4 Review of Key Concepts in Fatigue Design

7.4.1 Classification of Fatigue Failures

Fatigue failures are generally classified into two types; (1) low-cycle fatigue (LCF) and (2) high-cycle fatigue (HCF). During low-cycle fatigue, the number of loading cycles is small $\left(1 < N < 10^3 cycles\right)$ and the level of stress is high, i.e., the stresses are commonly high enough to induce plastic deformation. In the high cyclic fatigue, a large number of cycles $\left(N > 10^5 cycles\right)$ at low applied stress levels take place and the deformation is primarily elastic [Liu 2005]. A comparison between low-cycle and high-cycle fatigue is provided in Table (7.1).

Table (7.1): A comparison between fatigue types

Subject	**Low-Cycle Fatigue (LCF)**	**High-Cycle Fatigue (HCF)**
Service life	Short	Long
Number of cycles	Low number of cycles $1 < N < 10^5 cycles$	High number of cycles $N > 10^5 cycles$
Loading	High cyclic loads	Low cyclic loads
Deformation	Plastic range	Elastic range
Approach	Strain-based method	Stress-based method

7.4.2 Fatigue Life Analysis

Generally, there are three main methods to predict fatigue life: stress-life, strain-life and linear elastic fracture mechanics. Stress-based analysis is based on stress levels in which the stresses always remain elastic. Under this approach, the stress-life (S-N curves, i.e., magnitude of a cyclic stress against the number of cycles to failure) is mainly applicable for long fatigue life estimation (i.e., high-cycle fatigue typically involving millions of cycles). The strain-life method is widely used for fatigue crack initiation life calculation in which plastic deformations that may occur at localized regions is considered. This method is used for low-cycle fatigue applications in which the stresses are high enough to induce plastic deformation [Bhandari 2010]. The linear elastic fracture mechanics approach is based on the

existence of an initial crack. In other words, this approach is used to predict the crack growth under repeated or cyclic loading [Tawancy et al 2004]. Since the main focus of this study is to estimate the fatigue life of the structural steel members in which the stresses must be based on elastic analysis, the stress-based approach is used in this study of fatigue life predictions.

7.4.3 Types of Fatigue Loading

Structural members are subjected to two kinds of fatigue loading cycles; constant-amplitude and variable amplitude loading. In reality, very few structural members are actually subjected to constant amplitude loading during their service life. Figure (7.3a) shows the constant-amplitude cyclic stress. This type of loading normally occurs in machinery parts under harmonic excitations. Constant amplitude loading is defined by the following terms [Liu 2005]:

1. The stress range $\Delta\sigma$ is the algebraic difference between the maximum stress $\sigma_{\max}$ and minimum stress $\sigma_{\min}$ in a cycle, i.e.,

$$\Delta\sigma = \sigma_{\max} - \sigma_{\min} \tag{7.24}$$

2. The mean stress σ_m is the algebraic average of maximum and minimum stresses in the cycle, i.e.,

$$\sigma_m = \frac{1}{2}\left(\sigma_{\max} + \sigma_{\min}\right) \tag{7.25}$$

3. The stress amplitude σ_a is the one-half the stress range in the cycle, i.e.,

$$\sigma_a = \frac{\Delta\sigma}{2} = \frac{\left(\sigma_{\max} - \sigma_{\min}\right)}{2} \tag{7.26}$$

4. Stress ratio R is defined as the ratio of the minimum stress $\sigma_{\min}$ to maximum stress $\sigma_{\max}$ in a cycle, i.e.,

$$R = \frac{\sigma_{\min}}{\sigma_{\max}} \tag{7.27}$$

The above parameters are important for fatigue life prediction.

In practice, structural members or components subjected to variable cyclic loading exhibit complex variable amplitude stress cycles (Figure 7.3b). This type of response is experienced

by many structural members, such as aircraft structural wings under aerodynamic forces, wave loading on ship and marine structures, and truck loading on steel bridges.

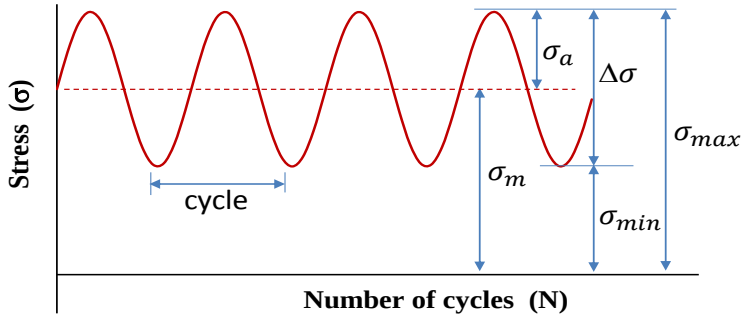

(a) Constant amplitude loading

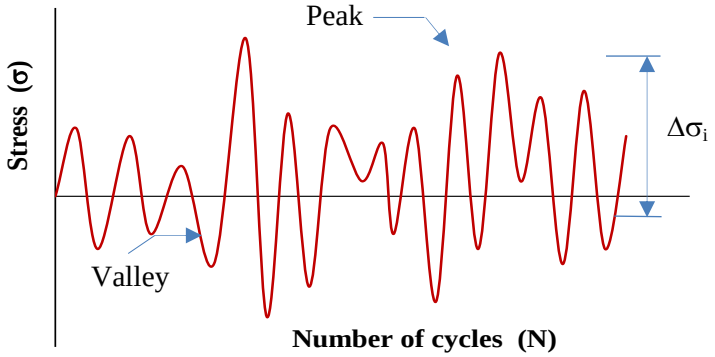

(b) Variable amplitude loading

Figure (7.3): Types of fatigue loading cycles [Liu 2005]: (a) Constant amplitude cycles of loading, (b) Variable amplitude loading cycles

The design fatigue life of structural members under complex stress histories can be evaluated by using the following steps [Collins et al 2010]:

(1) Using the rainflow cycle counting method to reduce the complex loading to a series of equivalent constant amplitude cycles.

(2) Creating a histogram of stress cycles from the rainflow analysis to form a fatigue damage spectrum,

(3) Calculating the fatigue damage for each stress range level $\Delta\sigma_i$ in the loading history, and

(4) Combining the fatigue damage for all the cycles in loading history using Palmgren-Miners linear cumulative-damage rule in order to obtain the fatigue damage D_{total} of the whole loading history [Collins et al 2010].

Figure (7.4) shows the main procedure used to predict the fatigue life of the structural member under variable amplitude loading.

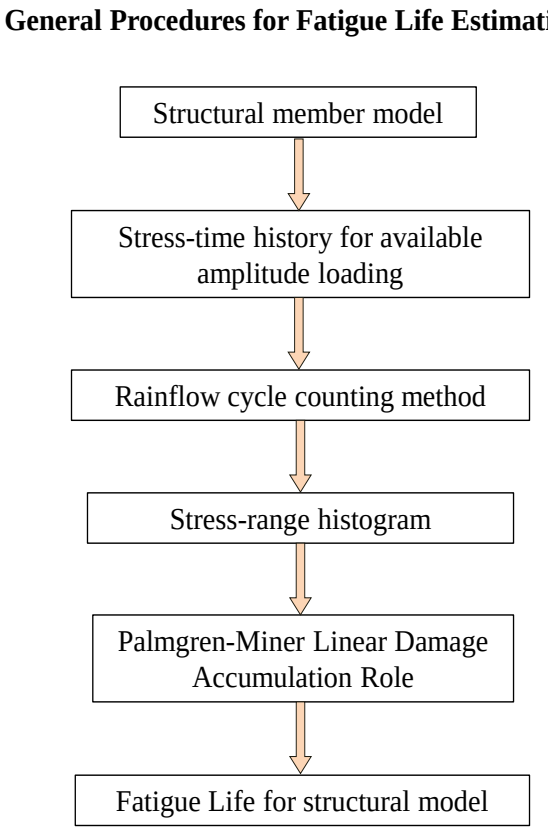

Figure (7.4): Flow chart for general procedures used for fatigue life estimation of structural member under variable amplitude loading (adapted from [Collins 1993])

7.4.4 The Rainflow cycles counting method

The rainflow cycle counting approach is commonly used to identify and count the fatigue cycles from the stress-time history. Using rainflow counting, the stress-time history is used to convert complex variable stress-time history into equivalent stress sets of constant amplitude blocks.

The irregular stress cycles are transformed to a set of peaks (tensile stresses) and valleys (compressive stresses) as illustrated in Figure (7.5a). In the rain-flow counting method, the peaks and valleys in the stress-time history are numbered and then plotted such that the time

axis is oriented downward (Fig.7.5b). At peaks and valleys, a rain-flow is assumed to drop down the resulting pagoda roof based on the following three rules [Suresh 1998]:

(i) the rain-flow initiates at each peak (or valley), but a new rain-flow does not start while the present rain-flow is flowing down,

(ii) a rain-flow starts down from a peak (or valley), continues to flow down and stops at the valley (or peak) when the magnitude of the following opposite peak (or valley) has a higher magnitude than the one from which it starts. For example, a rain-flow started from valley 1 stopped at peak 4 because the magnitude of the following opposite peak 5 is greater than that of peak 1, and

(iii) a new rain-flow must stop when it encounters a previous rain-flow trajectory. For example, during the rain-flow from valley 3 to peak 4, the rain-flow starts from valley 3 and stops at point 2a, since it encounters the previous rain-flow at that point.

Note that, (1) every part of the stress-time history is counted once and only once, and (2) every rain-flow stress range, from its start (such as peak 8) to its finish (valley 9) is counted as a half stress cycle.

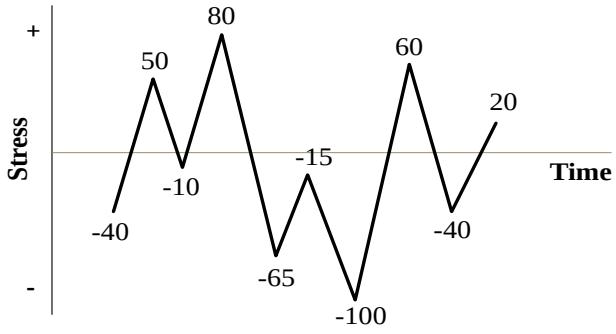

(a) Variable amplitude stress

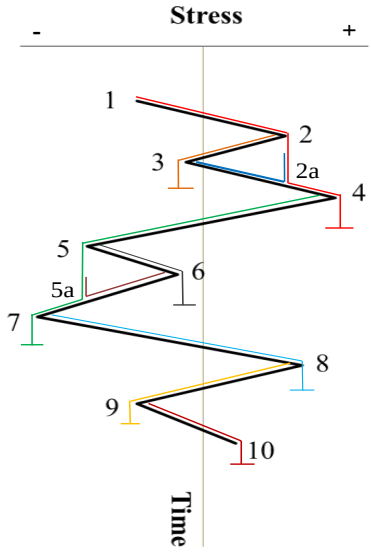

(b) Rainflow counting cycles

Figure (7.5): Rainflow counting cycles Method [adapted from Ref. Suresh 1998]

The rain-flow counting analysis for the stress-time history in Figure (7.5a) is provided in Table (7.2).

Table (7.2): Rainflow counting data for one block of stress-time pattern

Peak/Valley number	Stress value σ_1 At initial point (MPa)	Stress value σ_2 At the end of trajectory (MPa)	Half cycle stress range $\Delta\sigma_i = \sigma_1 - \sigma_2$ (MPa)
1	-40	80	-120
2	50	-10	60
3	-10	50	-60
4	80	-100	180
5	-65	-15	-50
6	-15	-65	50
7	-100	60	-160
8	60	-40	100
9	-40	20	-60
10	20	-	-

Table (7.3) provides the stress ranges for a single stress-time history event which pairs the positive and negative half-cycles of identical magnitudes to count the number of complete cycles.

Table (7.3): Number of cycles and half cycles for one stress event

Stress range $\lvert\sigma_1 - \sigma_2\rvert$ in (MPa)	Whole cycles	Half cycles
50	1	0
60	1	1
100	0	1
120	0	1
160	0	1
180	0	1

If the stress event described in Figure (7.5) is repeated 5×10^5 times, a stress range histogram can be calculated by multiplying the number of cycles and half cycles by 5×10^5 and a stress range histogram is generated. Therefore, the stress range histogram in Figure (7.6) consists of six constant stress range blocks in which each block is characterized by its stress range $\Delta\sigma_i$

and number of cycles n_i. In Figure (7.6), the stress histogram having stress range blocks $\Delta\sigma_1 = 180MPa$, $\Delta\sigma_2 = 160MPa$, $\Delta\sigma_3 = 120MPa$, $\Delta\sigma_4 = 100MPa$, $\Delta\sigma_5 = 60MPa$, $\Delta\sigma_6 = 50MPa$ and the corresponding number of cycles $n_1 = n_2 = n_3 = n_4 = 250\times10^3 cycles$, $n_5 = 750\times10^3 cycles$ and $n_6 = 1{,}250\times10^3 cycles$ are ranked in decreasing magnitudes of the stress range. It is noted that the ordering of the different stress range blocks does not make a difference since the damage calculations are based on the linear cumulative damage Palmgren-Miner method.

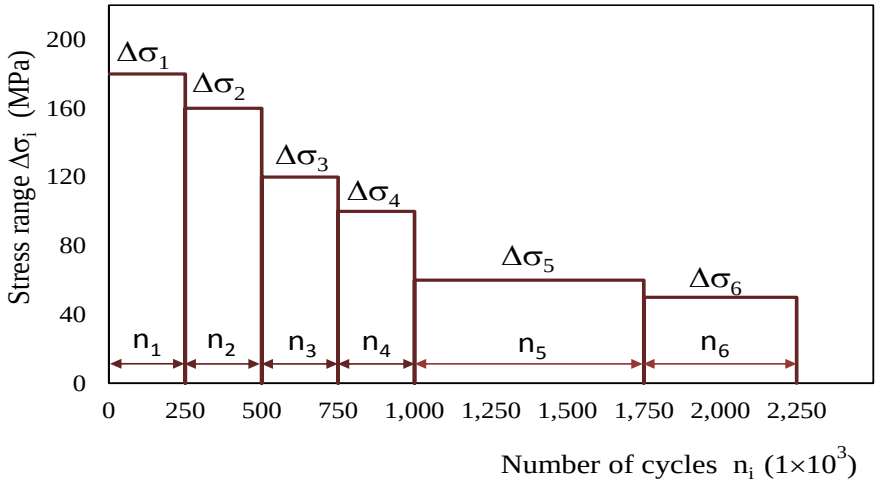

Figure (7.6): Stress range histogram

The fatigue strength of a structural member can be provided from the S-N curves (defined as Wohler S-N curve). These curves are based on experimental investigations applying to a typical detail category. Each curve is a plot of alternating stresses σ versus number of cycles to failure N (a log scale is used for N).

7.4.5 Palmgren-Miner's Rule

The cumulative damage fatigue life analysis is generally based on Palmgren-Miner's method. Under variable amplitude loading, the fatigue life can be estimated by (1) calculating the partial damage by each stress range loading block in the stress histogram, and (2) determining the total cumulative fatigue damage by linearly summing the damage cyclic ratios for the different stress range blocks. According to Palmgren-Miner's Rule, total

damage D_{total} will occur when the sum of partial damages D_i reaches unity [Collins et al 2010] i.e.,

$$D_{total} = \sum_{i=1}^{k} D_i = 1.0 \tag{7.28}$$

in which $D_i = \left(n_i / N_i\right)$ is the partial damage ratio at i -th stress range level $\Delta\sigma_i$, n_i is the number of cycles at constant stress range $\Delta\sigma_i$. For a number β of repeated stress events, each containing m_i stress cycles, the total number of stress cycles is $n_i = \beta m_i$. Also, in Equation (7.27), N_i is the total number of cycles to failure corresponding to constant stress range $\Delta\sigma_i$. Figure (7.7) shows the total number of cycles to failure for each stress range level $\Delta\sigma_i$ plotted for the previous example.

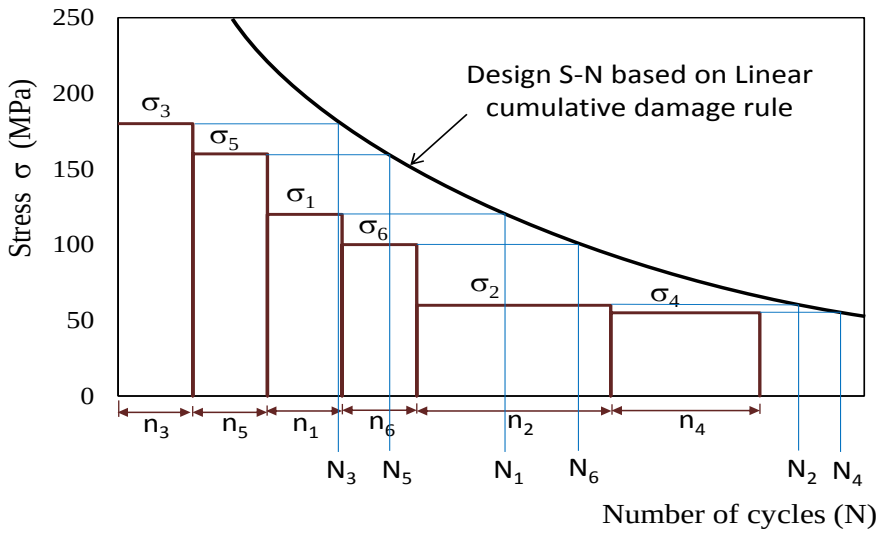

Figure (7.7): Design S-N curve based on linear cumulative fatigue rule

7.5 Fatigue Design Criteria in the Canadian Code CSA S16-09

In general, structural steel members subjected to fatigue loads need to be designed and fabricated in order to minimize stress concentrations in the cross-sections. In most cases, the elastic analysis based on principles of mechanics of materials is applicable to evaluate the stresses in the member. For the present problem, this task has been accomplished from the formulations developed in Chapters 3-6 and the associated stress expressions for multiple

harmonic forces that were developed in Section (7.2). Fatigue life calculations are required only in the locations of applied tensile stress while stress ranges that are completely associated with compressive stresses are not accounted for in fatigue analysis [Kulak and Grondin 2010].

The number of cycles to failure corresponding to a stress range $\Delta\sigma_i$ is given by:

$$N_i = \begin{cases} \gamma \Delta\sigma_i^{-3} & \text{for } \Delta\sigma_i \geq \Delta\sigma_{ti} \\ \gamma' \Delta\sigma_i^{-5} & \text{for } \Delta\sigma_i < \Delta\sigma_{ti} \end{cases} \tag{7.29}$$

in which γ, γ' are the fatigue life constants, and $\Delta\sigma_{ti}$ is the constant amplitude threshold stress range (endurance limit for constant amplitude stress ranges only), which is stress range below which a crack will not grow. In other words, when the stress range is always less than this value, it can be expected that growth of the fatigue crack will not take place. When the stress ranges $\Delta\sigma_i$ are less than the constant amplitude fatigue limit $\Delta\sigma_{ti}$, the fatigue life constant γ' is used [Kulak and Grondin 2010]. Fatigue constants γ, γ' and $\Delta\sigma_{ti}$ are defined in Table (7.4) and illustrated in Figure (7.8) for different detail categories in the Canadian Standards. The detail categories are described and tabulated in Clause 26 of CSA S16-09 [Ref. 7.2].

The values given in Table (7.4) can be graphically determined from a series of straight lines in S-N curves presented in Figure (7.8). Each line in the S-N curves is established from a series of constant amplitude fatigue tests for different detail categories.

7.6 Numerical Examples

The aim of fatigue life calculations is to ensure that the thin-walled steel members under effect of multiple harmonic forces with different exciting frequencies have sufficient fatigue life. Two examples, simply-supported and cantilever members of doubly symmetric cross-sections, are investigated for fatigue life analysis in order to demonstrate the application of the finite element formulation developed in this study. In both examples, the material is 350W, i.e., the yielding strength is $F_y = 350MPa$. The modulus of elasticity is $E = 200GPa$, the Poisson's ratio is $\upsilon = 0.3$ and the corresponding shear modulus is $G = 77GPa$.

Table (7.4): Fatigue constants for various detail categories [Ref. 7.2]

Detail Category	Fatigue life Constant γ (MPa)	Fatigue life constant γ' (MPa)	Constant amplitude threshold stress range $\Delta\sigma_{ti}$ (MPa)
A	8190×10^{9}	223×10^{15}	165
B	3930×10^{9}	47.6×10^{15}	110
B1	2000×10^{9}	13.8×10^{15}	83
C	1440×10^{9}	6.86×10^{15}	69
C1	1440×10^{9}	9.92×10^{15}	83
D	721×10^{9}	1.66×10^{15}	48
E	361×10^{9}	0.347×10^{15}	31
E1	128×10^{9}	0.0415×10^{15}	18

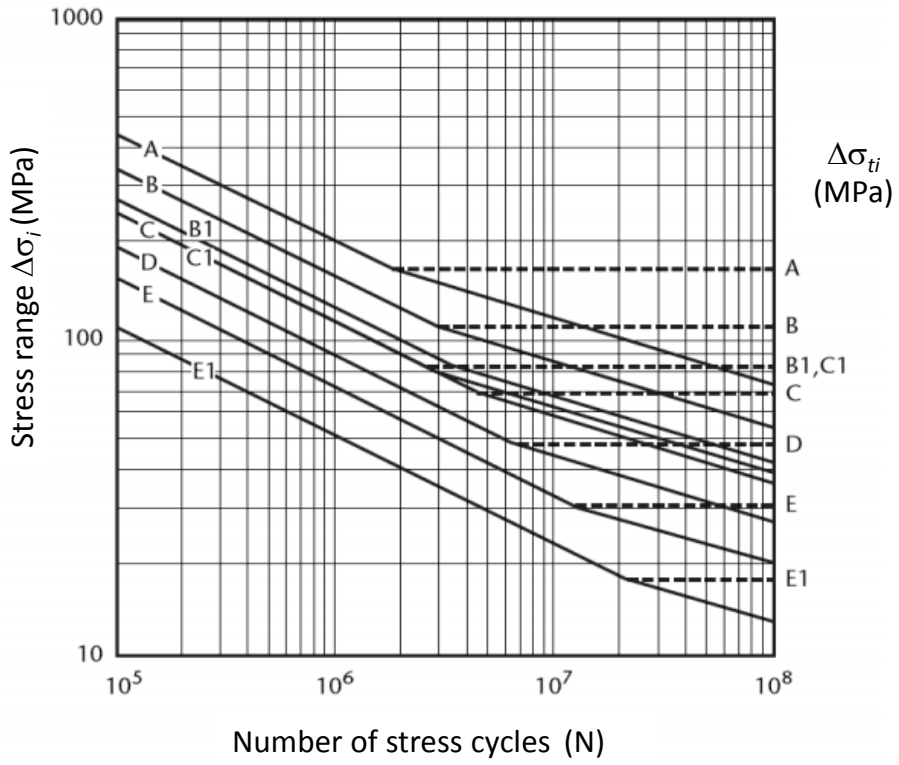

Figure (7.8): Characteristics S-N curves for various detail categories

According to CAN/CSA S16-06 [Ref. 7.2]

7.6.1 Example (1) – Stress Calculations

A cantilever beam has a span 2.0m and a monosymmetric channel section. The cantilever is subjected to a transverse harmonic load $P_y\left(2.0m,t\right)=5.0e^{i\Omega t}kN$ acting at the corner point at the tip as illustrated in Figure (7.9). The dimensions of the channel section are; flange thickness $t_f=20.0mm$, web thickness $t_w=15.0mm$, flange width $b=80.0mm$ and the middle surface height $h=200.0mm$. The exciting frequency of value $\Omega=24Hz$ is considered in order to calculate the normal and shear stresses distributions over the cross-section. The first natural frequency for the cantilever channel-section is $\bar{\omega}_1=18.38Hz$.

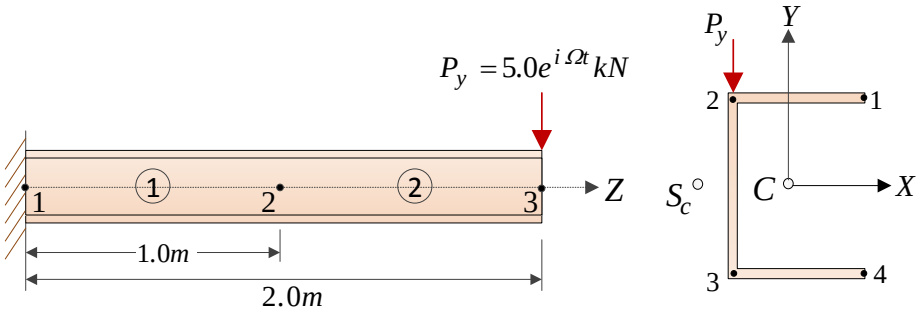

Figure (7.9): Cantilever C-beam under concentrated end harmonic force

The coordinate of the centroid in the direction of principle axis of symmetry is $C_x=20.65mm$ and the shear centre coordinate along the axis of symmetry is $x_s=-51.12mm$. The section properties are $A=6.20\times10^3mm^2$, $I_{xx}=42.0\times10^6mm^4$, $I_{yy}=4.184\times10^6mm^4$, $J=0.650\times10^6mm^4$, $C_w=29.26\times10^9mm^6$, $D_{xx}=0.32\times10^4mm^2$, $D_{yy}=0.30\times10^4mm^2$, $D_{hy}=9.143\times10^4mm^3$ and $D_{\omega\omega}=34.79\times10^6mm^4$. This example aims at verifying the accuracy of the present formulations. It is required to conduct the steady state dynamic analysis (exciting frequency $\Omega=24.0Hz$) in order to calculate the normal and shear stresses distributions over the cross-section. The results obtained based on the present formulations are compared with the Abaqus shell element and Vlasov beam solutions.

For an orthogonal system of coordinates, (i) the original O of the coordinate system is located at the centroid C of the section and the axes OX and OY are the principal axes, i.e.,

$\int_A [x, y, xy]\, dA = 0$, and (ii) the pole and the sectorial origin S_o are placed at the shear centre S_c, i.e., $\int_A [x\,\omega, y\,\omega, \omega]\, dA = 0$. The y principal coordinate and ω sectorial coordinate distributions on the channel cross-section are illustrated in Figure (7.10).

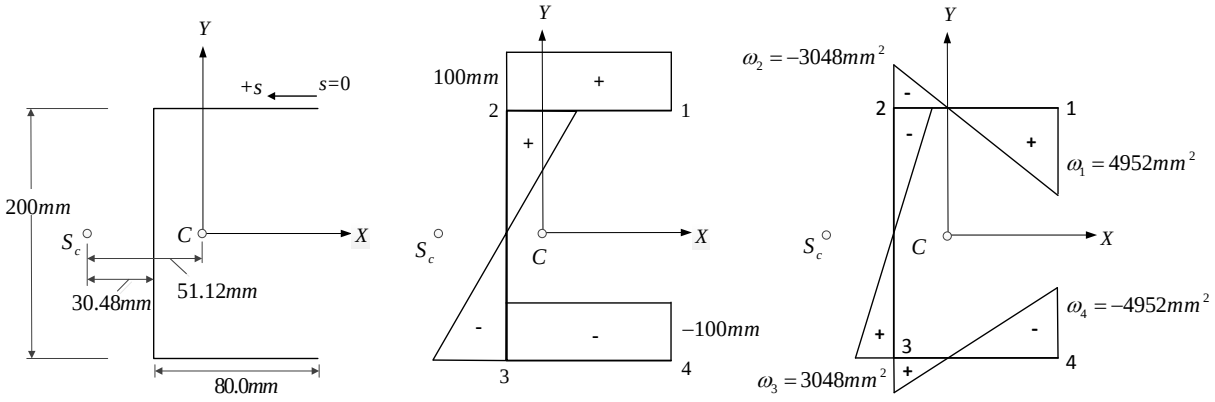

(a) Cross-section (b) y coordinate diagram (b) ω coordinate diagram

Figure (7.10): Diagrams for y principal coordinate and ω sectorial coordinate Distributions over the channel-section

7.6.1.1 Finite Element Meshing

In the Abaqus shell model, the cantilever beam is subdivided into 200 shell S4R elements along the longitudinal direction, 10 elements along height of the web, and 5 elements along the width of the flange. The model thus consists of 4,000 shell S4R elements with six degrees of freedom per node which leads to about 50,650 degrees of freedom. In the present solution, the member is divided into only two beam elements along the beam span, i.e., the model has only twelve degrees of freedom. It is evident that the stress results obtained based on the present closed-form solution are found identical to those obtained from the present finite element formulation using only two noded-beam elements.

7.6.1.2 Calculation of Normal and Shear Stresses

The normal $\sigma_{zz}(z,t)$ and shear stresses $\tau_{zs}(z,t)$ for a monosymmetric channel-section are determined using the expressions derived in Equations (7.10) and (7.22), respectively, where the vector of the nodal internal forces $\langle F_e \rangle_{1\times 8}^T$ is obtained from Equation (5.67) by pre-

multiplying the nodal displacement vector $\langle U_N \rangle_{1\times 8}^T$ by the element dynamic stiffness matrix $\left[D(\Omega)\right]_{8\times 8}$, i.e., $\{F_e\}_{8\times 1} = \left[D(\Omega)\right]_{8\times 8}\{U_e\}_{8\times 1} = \left(\left[K_e\right]_{8\times 8} - \Omega^2\left[M_e\right]_{8\times 8}\right)\{U_e\}_{8\times 1}$, in which the nodal displacement vector $\langle U_N \rangle_{1\times 8}^T$, element stiffness matrix $\left[K_e\right]_{8\times 8}$, element mass matrix $\left[M_e\right]_{8\times 8}$ and the nodal internal forces vector $\langle F_e \rangle_{1\times 8}^T$ are defined previously in section (5.5.3) in Chapter 5. The nodal internal forces $\langle F_e \rangle_{1\times 8}^T$ are then substituted into the stress-stress resultant expressions. Then, the distributions of the normal stress (at the mid-surface) caused by the shearing force and non-uniform torsional moment are shown in Figures (7.11). Based on the

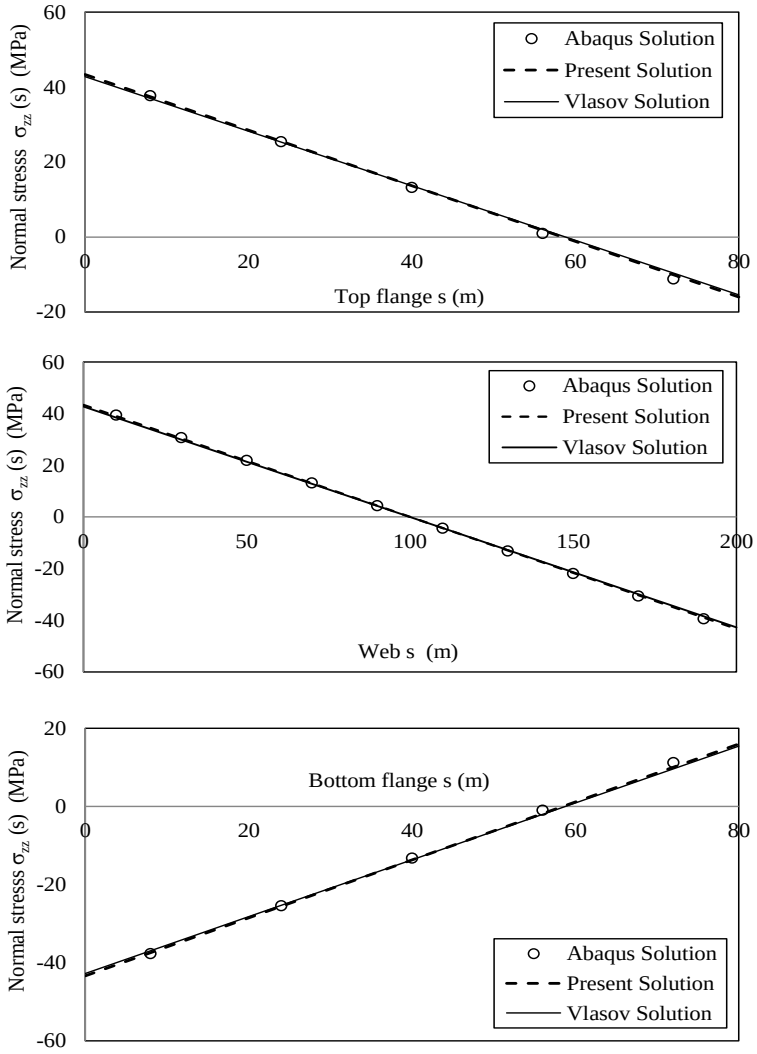

Figure (7.11): Normal stress distributions at the mid-surface over channel-section

present formulations, the stress values determined at the joints (1,2,3,4) are obtained from Equation (7.10), while the normal stresses between the joints are computed by considering the linear distribution of the normal stresses at each segment.

Table (7.5): Comparisons of Normal Stresses at the joints (corner points)

Joint	Abaqus Solution [1] σ_{zz} (MPa)	Present Solution [2] σ_{zz} (MPa)	Vlasov Solution [3] σ_{zz} (MPa)	Difference =[1-2]/1	Difference =[1-3]/1
1	-17.39	-15.98	-15.43	8.11%	11.27%
2	43.82	43.35	42.79	1.07%	2.35%
3	-43.82	-43.35	-42.79	1.07%	2.35%
4	17.39	15.98	15.43	8.11%	11.27%

The shear stress expression according to Vlasov beam theory is given as [Erkmen 2006]:

$$\tau_k(s,z)t(s)=\tau_k(s_{1k},z)t(s_{1k})-\frac{\bar{S}_{xk}(s_{1k},s)}{I_{xx}}\bar{V}_y(z)-\frac{\bar{S}_{\omega k}(s_o,s_{1k},s)}{C_w}\bar{M}_{zw}(z) \tag{7.30}$$

in which $\tau_k(s,z)$ is the shear stress at a point s and $\tau_k(s_{1k},z)$ is the shear stresses at the beginning point s_{1k} of segment k, $t(s_{1k}),t(s)$ are the thickness at the beginning of the plate and at location s respectively, $\bar{S}_{xk}$ and $\bar{S}_{\omega k}$ are the first moments of area of coordinates y and ω for segments $k=1,2,3$ at a the section of interest denoted by coordinate $\bar{S}_k$ are given by

$$\begin{aligned}\bar{S}_{xk}(s)&=\int_{s_{1k}}^{s}y(s)t_k(s)ds=t_k(s)\int_{s_{1k}}^{s}y(s)ds\\&=t_k\int_{s_{1k}}^{s}\left[y_{1k}\left(1-\frac{s}{h_k}\right)+y_{2k}\left(\frac{s}{h_k}\right)\right]ds\\&=t_k\left[y_{1k}s+\left(\frac{y_{2k}-y_{1k}}{h_k}\right)\frac{s^2}{2}\right]-t_k\underline{\left[y_{1k}s_{1k}+\left(\frac{y_{2k}-y_{1k}}{h_k}\right)\frac{s_{1k}^2}{2}\right]}\end{aligned} \tag{7.31}$$

$$\begin{aligned}\bar{S}_{\omega k}(s) &= \int_{s_{1k}}^{s} \omega(s_o,s)t_k(s)ds = t_k(s)\int_{s_{1k}}^{s} \omega(s_o,s)ds \\ &= t_k \int_{s_{1k}}^{s} \left[\omega_{1k}\left(1-\frac{s}{h_k}\right)+\omega_{2k}\left(\frac{s}{h_k}\right)\right]ds \\ &= t_k\left[\omega_{1k}s+\left(\frac{\omega_{2k}-\omega_{1k}}{h_k}\right)\frac{s^2}{2}\right]-\underline{t_k\left[\omega_{1k}s_{1k}+\left(\frac{\omega_{2k}-\omega_{1k}}{h_k}\right)\frac{s_{1k}^2}{2}\right]}\end{aligned} \tag{7.32}$$

in which y_{1k}, y_{2k} and ω_{1k}, ω_{2k} (for $k=1,2,3$) are obtained from the y and ω coordinate diagrams at the beginning and end points of the segments (e.g., Fig. 7.10), and h_k are the segments widths. For the top flange segment (s=0 for top right corner point, Fig. 7.10a), the underlined terms vanishes, while for the web segment, the underlined terms come from $\bar{S}_{xk}$ and $\bar{S}_{\omega k}$ values at the end point of the previous segment (left point of the top flange, Fig. 7.10a) given the continuity of shear flow across the joint. Based on the y principal coordinate and ω sectorial coordinate diagrams as illustrated in Figure (7.12), the first moments of area for flanges and web segments are provided in Table (7.6).

Table (7.6): Expressions for moment of areas $\bar{S}_{xk}, \bar{S}_{\omega k}$ for flanges and web segments

Segment	Domain of applicability	$\bar{S}_{xk}$ expression	$\bar{S}_{\omega k}$ expression
Top flange	$0 \le s_1 \le h_1$	$t_1\left[y_{11}s_1+\left(\frac{y_{21}-y_{11}}{h_1}\right)\frac{s_1^2}{2}\right]$	$t_1\left[\omega_{11}s_1+\left(\frac{\omega_{21}-\omega_{11}}{h_1}\right)\frac{s_1^2}{2}\right]$
Web	$0 \le s_2 \le h_2$	$t_2\left[y_{12}s_2+\left(\frac{y_{22}-y_{12}}{h_2}\right)\frac{s_2^2}{2}\right]$ $-t_2\left[y_{12}h_1+\left(\frac{y_{22}-y_{12}}{h_2}\right)\frac{h_1^2}{2}\right]$	$t_2\left[\omega_{12}s_2+\left(\frac{\omega_{22}-\omega_{12}}{h_2}\right)\frac{s_2^2}{2}\right]$ $-t_2\left[\omega_{12}h_1+\left(\frac{\omega_{22}-\omega_{12}}{h_2}\right)\frac{h_1^2}{2}\right]$
Bottom flange	$0 \le s_3 \le h_3$	$t_3\left[y_{13}s_3+\left(\frac{y_{23}-y_{13}}{h_3}\right)\frac{s_3^2}{2}\right]$ $-t_3\left[y_{13}(h_1+h_2)\right.$ $\left.+\left(\frac{y_{23}-y_{13}}{h_3}\right)\frac{(h_1+h_2)^2}{2}\right]$	$t_3\left[\omega_{13}s_3+\left(\frac{\omega_{23}-\omega_{13}}{h_3}\right)\frac{s_3^2}{2}\right]$ $-t_3\left[\omega_{13}(h_1+h_2)\right.$ $\left.+\left(\frac{\omega_{23}-\omega_{13}}{h_3}\right)\frac{(h_1+h_2)^2}{2}\right]$

For the given section, the distributions of the functions $\bar{S}_{xk}$,$\bar{S}_{\omega k}$ over the channel-section are displayed in Figure (7.12), where the $\bar{S}_{xk}$,$\bar{S}_{\omega k}$ (for $k=1,2,3$) values at the joints (1,2,3,4) are also provided in the diagrams.

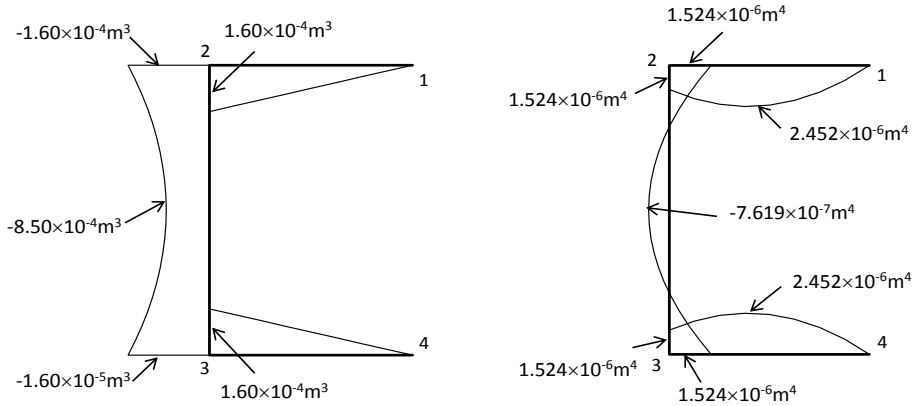

(a) $\bar{S}_x(s)$ diagram (b) $\bar{S}_\omega(s)$ diagram

Figure (7.12): Moments of the area $\bar{S}_x(s)$ and $\bar{S}_\omega(s)$ diagrams

The internal forces $\bar{V}_y(z=0)$ and $\bar{M}_{zw}(z=0)$ as obtained from the present finite element solution and the values of $\bar{S}_{xk}$,$\bar{S}_{\omega k}$ (provided in Fig. 7.12) into Equation (7.30) in order to obtain the shear stress based on the Vlasov theory. Figure (7.13) shows the resulting shear stresses at the middle surface of the cross section. The shear stresses due to Saint-Venant torsion vanishes at the cantilever fixed end.

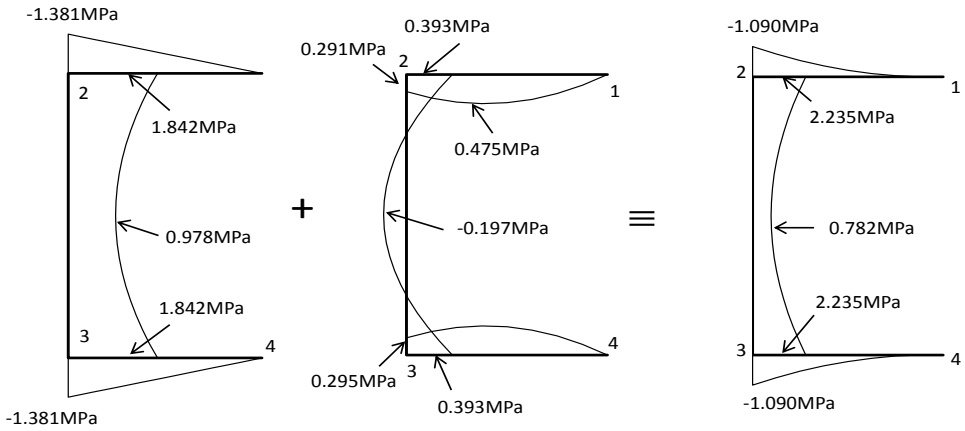

(a) Shear stress due to shear force τ_{zsb} (b) Shear stress due to warping τ_{zsw} (c) Total shear stress τ_{zs}

Figure (7.13): Shear stress distributions over the C-section (Vlasov shear stress equations)

Figure (7.14) provides comparisons of the shear stress distributions over the given cross-section for the three solutions; (i) Abaqus shell S4R element model extracted at the Gauss points, (ii) based on the present solution as described in (section 7.3.7) and (iii) Vlasov solution as provided by Equation (7.30). It is observed that, the shear stress values obtained are very small (i.e., $\tau_{zs\,max} < 2.5MPa$) compared to the normal stresses (i.e., $\sigma_{zz\,max} \approx 44.0MPa$).

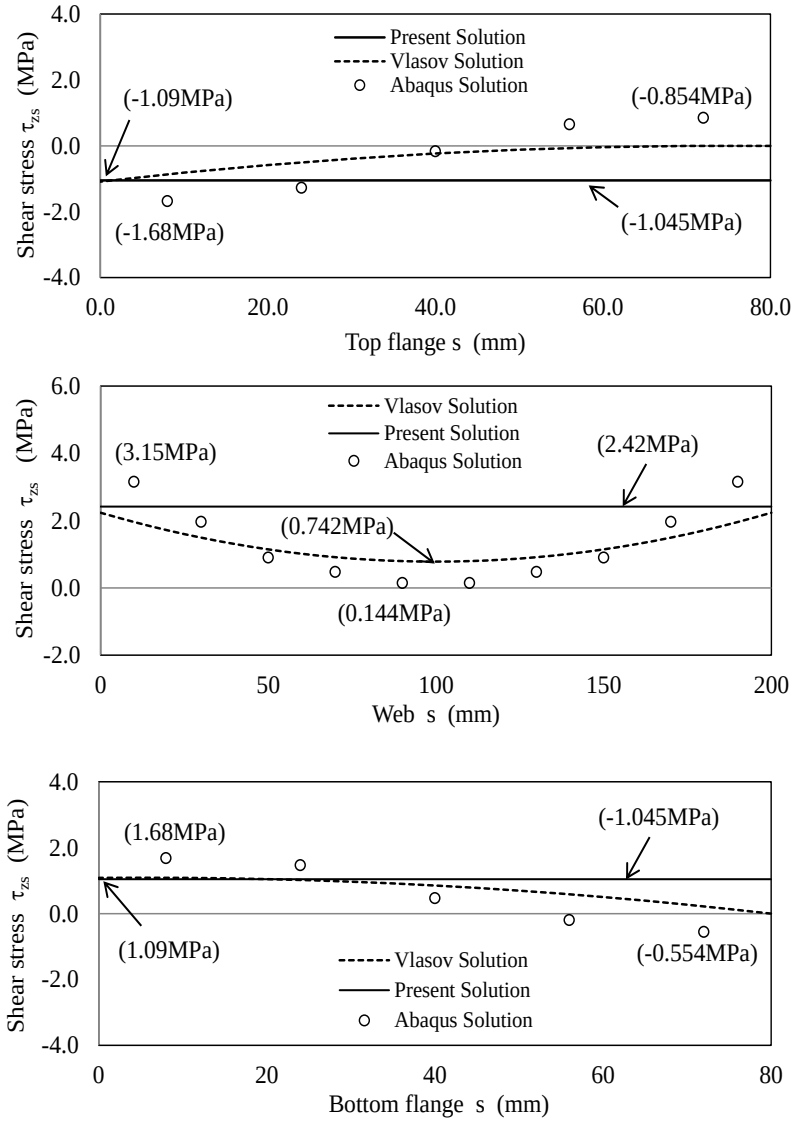

Figure (7.14): Total shear stresses distributions

It is observed that both methods for calculating shear stresses deviate from the stresses obtained based on the shell finite element. Possible reasons include the fact the shell solution is the only solution that captures distortional effects. It is noted that the shear stresses

calculated based on Equation (7.22) provides an average value of the shear stress within each of the flanges and the web. Equation (7.30) provides a closer trend to the shear distribution as predicted by FEA.

7.6.2 Example (2): Simply support I-beam under transverse harmonic forces

A cantilever beam is made of a symmetric I-section and has 7.0m span. The selected cross-section is W200×27 (depth $d=207mm$, flange width $b=133mm$, flange thickness $t_f=8.4mm$, web thickness $t_w=5.8mm$, elastic section modulus $S_x=249\times10^3 mm^3$, strong-axis moment of inertia $I_{xx}=25.8\times10^6 mm^4$, Saint-Venant torsional constant $J=71.3\times10^6 mm^4$, and warping constant $C_w=32.5\times10^9 mm^6$). The cantilever is subjected to two concentrated transverse harmonic forces; (1) $P_{y_1}=4.0e^{i\Omega_1 t}kN$ ($\Omega_1=8.0Hz$) applied at $z=1.4m$ from the left support and (2) $P_{y_2}=5.0e^{i\Omega_2 t}kN$ ($\Omega_2=18.0Hz$) applied at $z=2.8m$ from the right support as illustrated in Figure (7.15). The first transverse natural frequency of the simply supported beam is $\bar{\omega}_1=14.03Hz$. It is required to estimate the fatigue life of the given steel member subjected to variable amplitude stresses induced from the application of given harmonic forces.

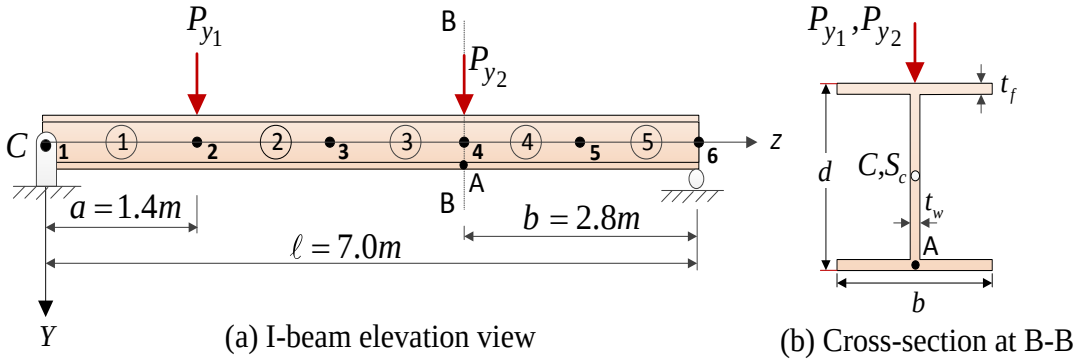

(a) I-beam elevation view (b) Cross-section at B-B

Figure (7.15): Simply supported I-beam under concentrated transverse harmonic forces

A preliminary static analysis and design is conducted for the given structural member according to Canadian standard CSA S16-09 as presented in Appendix (7.A).

7.6.2.1 Dynamic Analysis

Two types of analysis are conducted. The first one is based on a modification of the present formulation to account for multiple loads with distinct exciting frequencies and the other one is based on ABAQUS shell model. Both methods are then compared to establish the validity of the modification proposed to account for loads with distinct exciting frequencies.

Since the beam is subjected to two harmonic forces $P_{y_1}=4.0e^{i\Omega_1}kN$ and $P_{y_2}=5.0e^{i\Omega_2}kN$ with different exciting frequencies and the formulation is restricted to harmonic forces with a single frequency, the principle of superposition is evoked to separate the problem into two separate problems, each with a single frequency Ω_i (where $i=1,2$) as shown in Fig. (7.16).

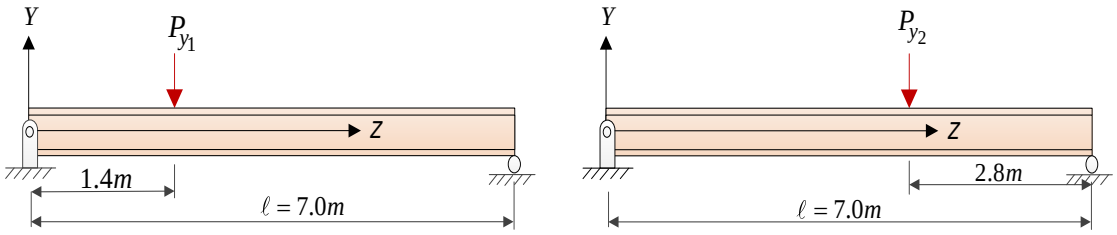

Figure (7.16): Simply supported I-beams under single harmonic force

Under the present formulation, the problem was analyzed based on five finite elements as shown in Figure (7.15). Assuming section B-B to correspond to the maximum normal stresses, the stresses at section B-B can be determined by obtaining the internal forces of member 3 by post-multiplying the stiffness matrix of element 3 by the element nodal displacement.

The superposition method is then used to evaluate the stresses at the point of interest $A(s_A,z_A)$ (where s_A denotes the tangential coordinate at the bottom flange) induced due to both harmonic forces from the equation

$$\sigma_{zz}(s_A,z_A,t)=-\left(\bar{M}_{x_1}(z_A)/I_{xx}\right)y(s_A)\sin(\Omega_1 t)-\left(\bar{M}_{x_2}(z_A)/I_{xx}\right)y(s_A)\sin(\Omega_2 t)$$

in which $\bar{M}_{x_1}(z_A)$ and $\bar{M}_{x_2}(z_A)$ are the steady state bending moments corresponding to the two problems identified in Figure (7.16).

In the Abaqus shell S4R model, the beam is subdivided into 160 elements in the longitudinal direction, 10 elements along height of the web, and 10 elements along the width of each flange. The beam is then modeled using 4,800 S4R shell elements corresponding to a total of 52,450DOFs.

In the Abaqus shell model solution, the implicit dynamic direct integration analysis was used to calculate the total time history response, i.e., the transient and the sum of the steady state responses were obtained and depicted on Figure (7.17). The implicit dynamic analysis procedure is performed for a total time of 2.0 sec and a time increments $\Delta t = 0.0001\,\text{sec}$. A damping ratio of 5.0% is used in the analysis. The present solution takes a few seconds to perform the analysis. Using the Abaqus implicit solver, the total CPU time takes over 19 hours on a Pentium Dual-Core CPU T4400 @ 2.20GHz.

The numerical results for the longitudinal stresses at the bottom flange at section $\sigma_{zz}\left(s_A, z_A, t\right)$ at section B-B (Fig. 7.15) obtained from the present solution are then compared with those based on the Abaqus S4R shell model solution. It is emphasized that the shell analysis in Abaqus captures the initial transient and steady state response, while the present solution based on the summation of the steady state responses of the problems defined in Figure (7.17) captures only the steady state response. This difference is responsible for the discrepancy between both solutions in the initial response (Fig. 7.17). After the initial stage however, the transient component of the response dampens out and both solutions show excellent agreement. This is illustrated by the block termed “typical stress event” in Figure (7.17). The initial part of the response which is missed in the present formulation occurs only once and does not influence the fatigue life of the structure. Conversely, the typical stress events which are efficiently captured by the present formulation are repeated frequently and dictate the fatigue life of the structure.

7.6.2.2 Fatigue Life Calculation

Under the action of the two harmonic loads applied, stress magnitudes $\bar{\sigma}_{zzA}$ were determined at point A located at section B-B. The maximum shear stresses are found negligible compared to normal stresses, and thus they are omitted. The stress-time history corresponding to normal stresses based on the present calculations is presented in Fig. (7.18).

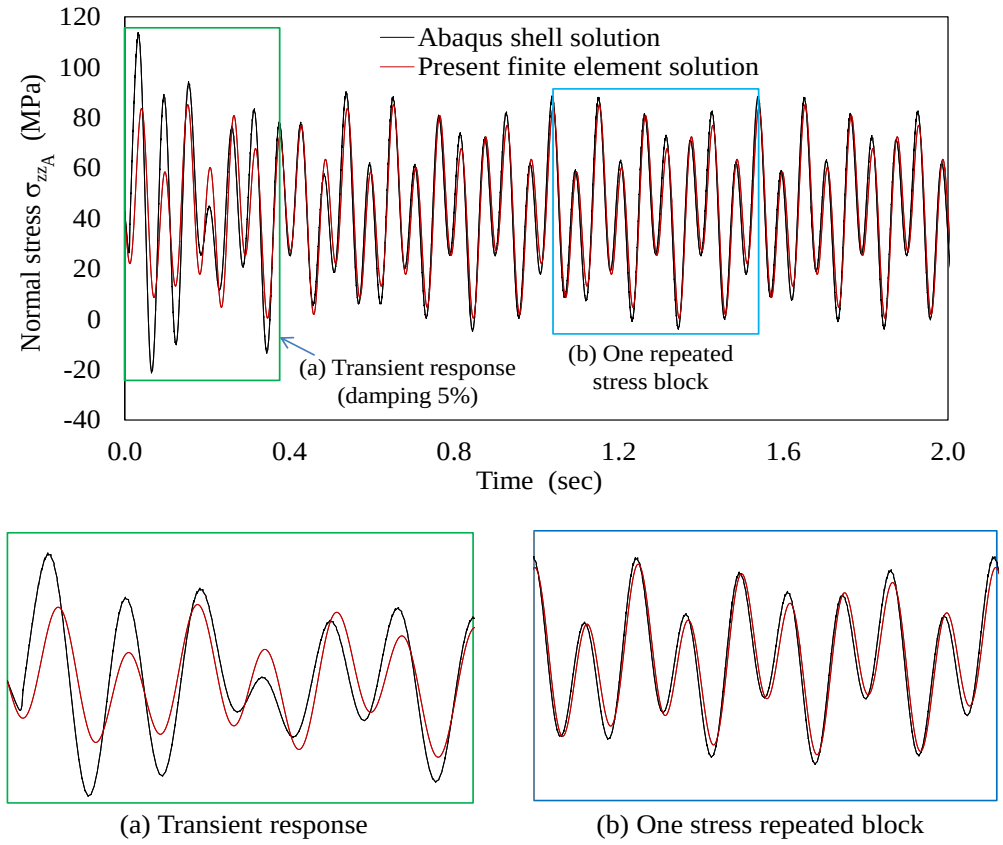

Figure (7.17): A comparison of normal bending stresses

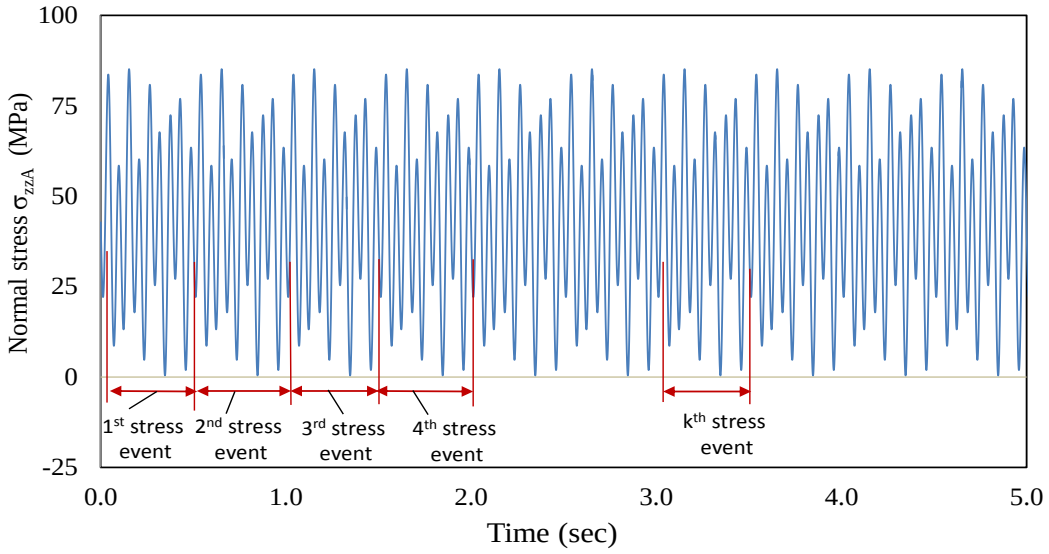

Figure (7.18): Stress-time history of simply-supported beam under harmonic forces

It is observed that the stresses due to the loading event has a repetitive stress pattern, i.e., the block of stress cycles for one stress event is repeated periodically. Figure (7.19) presents the stress values at the peaks for one stress cycles block based on a single stress event.

In order to perform a rain-flow counting analysis, the stress peaks and valleys for a single stress event (i.e., one typical stress range event) illustrated in Figure (7.19a) are numbered and then rotated 90 degrees as illustrated in Figure (7.19b). The stress values of these peaks and valleys are provided in Table (7.4a).

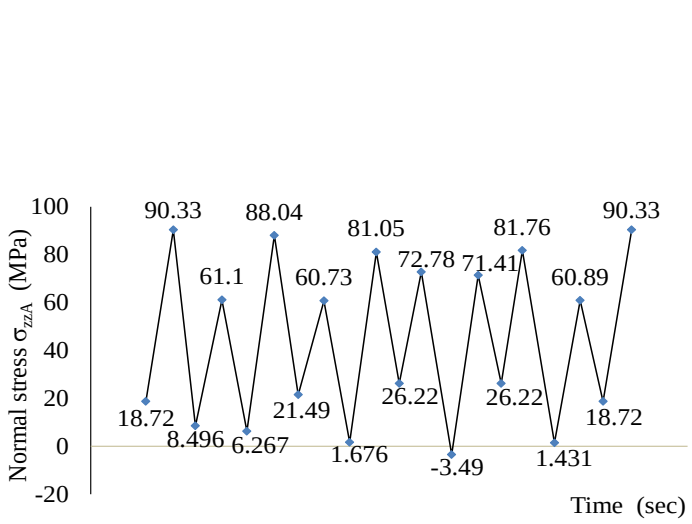

(a) Stress-peak and valley values for A single stress event

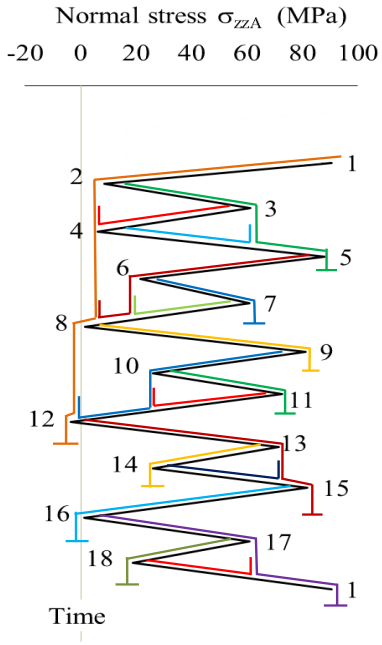

(b) Peaks and valleys numbered for a single stress event

Figure (7.19): Stress peaks and valleys numbered for a single repeated stress event

The rain-flow counting method is then used to count the half cycles in the single repeated stress-time event plotted in Figure (7.19b). The results of cycles and half cycles obtained are presented in Table (7.7).

According to the S16-09 Standard, the present simply-supported beam is classified as a detail category B [Ref. 7.2]. For Category B detail, the threshold stress as read from Figure (7.8) or obtained directly from Table (7.4) is $\Delta\sigma_{ti} = 110MPa$. It is noted that, all the stress ranges given in the last column of Table (7.7) are smaller than the constant amplitude fatigue limit

$\Delta\sigma_{ti} = 110MPa$ for detail category B. Therefore, Equation (7.29) is used (with an exponent $1/5$ and a fatigue life constant $\gamma' = 47.6\times10^{15}$ as provided in Table (7.4) to evaluate the number of fatigue stress cycles N_i values as tabulated in the third column of Table (7.8).

Table (7.7): Values of stress peaks and valleys for single typical stress block event

Peak/Valley number	Stress value σ_1 at initial point (MPa)	Stress value σ_2 at the end of trajectory (MPa)	Half cycle stress range $\Delta\sigma_i = \sigma_1 - \sigma_2$ (MPa)
1	90.33	-3.490	93.82
2	8.496	88.04	-79.54
3	61.10	8.496	52.60
4	6.267	61.10	-54.83
5	88.04	6.267	81.77
6	21.49	60.73	-39.24
7	60.73	21.49	39.24
8	1.676	81.05	-79.37
9	81.05	1.676	79.37
10	26.22	72.78	-46.56
11	72.78	26.22	46.56
12	-3.490	81.76	-85.25
13	71.41	26.22	45.19
14	26.22	71.41	-45.19
15	81.76	1.431	80.33
16	1.431	90.33	-88.90
17	60.89	18.72	42.17
18	18.72	60.89	-42.17

The fatigue damage due to a single stress event results in the third column are obtained from the fact that, the stress block event is repeated as observed in Figure (7.18) due to the application of multiple harmonic forces, i.e.,

$$D_{total} = \sum_{i=1}^{k}\left(n_i / N_i\right) = \beta \sum_{i=1}^{k}\left(m_i / N_i\right) = 1 \tag{7.33}$$

in which β is the total number of stress events.

Table (7.8): Fatigue damage estimation for a single stress event

stress range $\lvert\Delta\sigma_i\rvert$ (MPa)	Number of cycles per stress event m_i	Fatigue Resistance $N_i = \gamma'\left(\Delta\sigma_i\right)^{-5}$ (number of cycles)	Damage due to a single stress event $\left(\frac{m_i}{N_i}\right)$
93.82	0.5	6.548×10^{6}	7.636×10^{-8}
79.54	0.5	1.495×10^{7}	3.344×10^{-8}
52.6	0.5	1.182×10^{8}	4.230×10^{-9}
54.83	0.5	9.605×10^{7}	5.205×10^{-9}
81.77	0.5	1.302×10^{7}	3.840×10^{-8}
39.24	1.0	5.116×10^{8}	1.955×10^{-9}
79.37	1.0	1.511×10^{7}	6.617×10^{-8}
46.56	1.0	2.175×10^{8}	4.597×10^{-9}
85.25	0.5	1.057×10^{7}	4.730×10^{-8}
45.19	1.0	2.526×10^{8}	3.959×10^{-9}
80.33	0.5	1.423×10^{7}	3.514×10^{-8}
88.90	0.5	8.572×10^{6}	5.833×10^{-8}
42.17	1.0	3.569×10^{8}	2.802×10^{-9}
Sum	-	$\sum_{i=1}^{k} N_i = 1.636\times10^{9}$	$\sum_{i=1}^{k}\left(m_i / N_i\right) = 3.779\times10^{-7}$

The fatigue damage results due to a single stress event (i.e., stress block) provided in the above table are obtained. Based on linear cumulative Palmgren-Miner's rule, the total number of stress events β that would induce fatigue failure can be determined from Equation (7.33) as:

$$\beta = 1 \Big/ \sum_{i=1}^{k}\left(m_i / N_i\right) = 2.65\times10^{6} \text{ events}$$

Therefore, the total number of stress events β that can be safely applied to the beam is $\beta = 2.65\times10^{6}$ prior the beam undergoing a fatigue failure.

7.6.3 Example 3: Cantilever I-beam under lateral harmonic forces

A cantilever beam of a doubly symmetric I-cross section (W200×22) has a span $\ell = 2{,}500mm$ as illustrated in Figure (7.20). The beam is subjected to two concentrated lateral harmonic forces; $P_{x_1} = 0.15e^{i\Omega_1 t}\,kN$ with exciting frequency $\Omega_1 = 7.0Hz$ applied at $z = 1.5m$ from the fixed end and $P_{x_2} = 0.20e^{i\Omega_2 t}\,kN$ with exciting frequency $\Omega_2 = 15.0Hz$ acting at the cantilever tip. The dimensions of the cross-section are as follows: flange thickness $t_f = 8.0mm$, web thickness $t_w = 6.2mm$, flange width $b = 102mm$ and a middle surface height $H = 198.0mm$, while the properties of the doubly symmetric cross section are given in Table (7.9). The first lateral natural frequency for the cantilever is $\bar{\omega}_1 = 9.928Hz$. It is required to determine the service life of the beam.

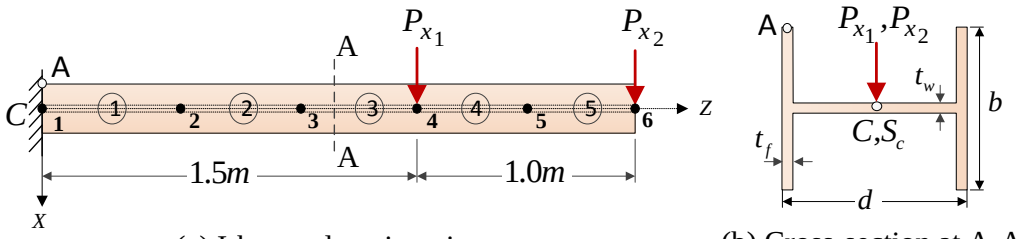

(a) I-beam elevation view (b) Cross-section at A-A

Figure (7.20): Cantilever I-beam under lateral harmonic forces

Table (7.9): Cross-sectional properties for Cross-section W200×27

$A = 2680\times10^4\,mm^2$	$I_{yy} = 1.420\times10^6\,mm^4$	$J = 56.60\times10^9\,mm^4$
$C_w = 13.90\times10^9\,mm^6$	$S_y = 27.80\times10^3\,mm^3$	$Z_y = 43.70\times10^3\,mm^3$
$D_{xx} = 0.1632\times10^4\,mm^2$	$D_{yy} = 0.1278\times10^4\,mm^2$	$D_{\omega\omega} = 16.00\times10^6\,mm^4$

A preliminary static analysis and design for the given cantilever beam of doubly symmetric section (W200×22) according to Canadian standard CSA S16-09 is provided in Appendix (7B).

In the shell finite element model, the cantilever beam is subdivided into 100 elements along the longitudinal direction, 6 elements along the width of each flange, and 8 elements along

height of the web. The model thus consists of 2,000 S4R elements. The fixed end is modeled by restraining all six degrees of freedom at all nodes at the fixed end of the cantilever. In the present finite element solution, five beam elements along the member are taken (Fig. 7.20).

Fatigue life Calculation

In the Abaqus shell model, the implicit dynamic analysis response of the cantilever is performed for 5.0 sec using time increment as 0.00025 and by using damping ratio of 5%. It is noted from Figure (7.21) that, Abaqus model captures the transient and steady state components of the response while the present solution captures only the steady state response. The maximum tensile stress-time history (at point A located at the fixed end as shown in Fig. 7.20) induced due to the given lateral harmonic forces is displayed in Fig. (7.21).

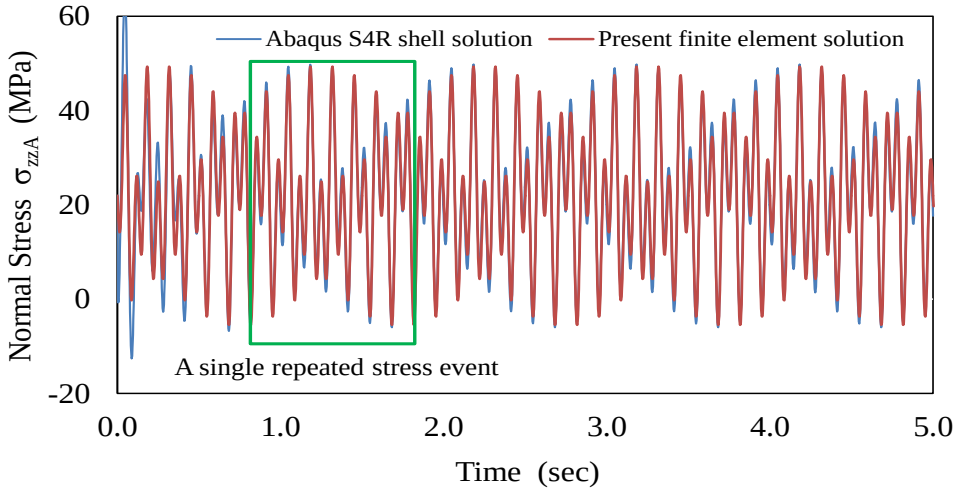

(a) Stress-time history

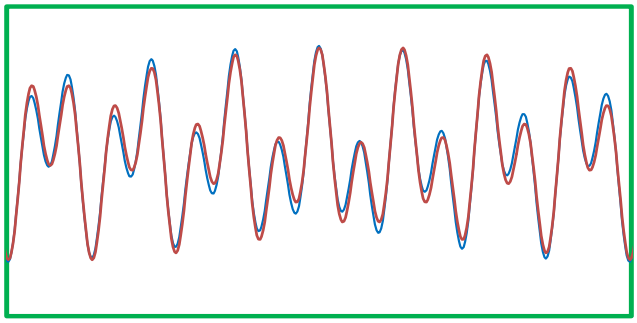

(b) A single repeated stress block event

Figure (7.21): Stress-time history for cantilever I-beam under multiple lateral forces

The stress results associated with steady state response obtained using the present finite element formulation show excellent agreement with those results obtained by the Abaqus shell model. Noting that the shear stresses are very small compared to the normal stresses, the analysis focuses on normal stresses.

It is noted that the normal stresses exhibit a repeated pattern of stress range blocks as observed in Figure (7.22a). The rainfall counting approach is used to count the number of cycles and half cycles in one repeated stress block event (Fig. 7.22a).

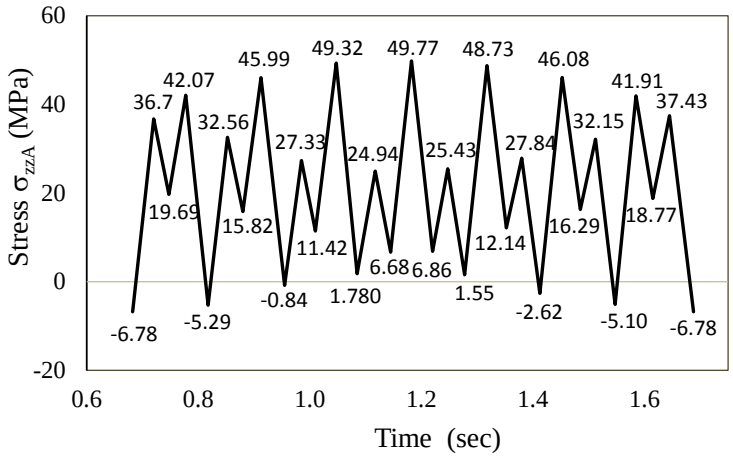

(a) Stress-time history of a single repeated stress block event

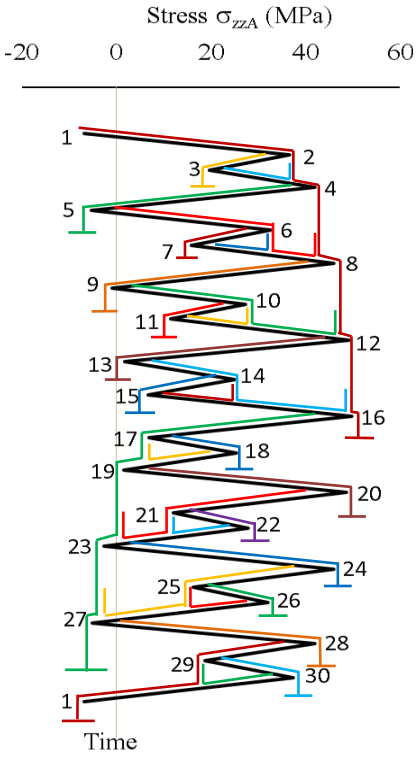

(b) Peaks and valleys numbered for a single stress block event

Figure (7.22): Peaks and valleys numbered for one stress block event

The half-cycle calculations due to a single repeated stress event illustrated in Figure (7.22b) are provided in Table (7.10).

According to the S16-09 Standard, the cantilever beam is a detail category B, in which the threshold stress is $\Delta\sigma_{ti} = 110MPa$. It is noted that all the stress ranges $\Delta\sigma_i$ presented in the last column of Table (7.10) fall below the constant amplitude fatigue $\Delta\sigma_{ti} = 110MPa$ for

detail category B. Therefore, the number of fatigue stress cycles N_i given in Table (7.11) is obtained using Eq. (7.29) with an exponent $1/5$ and a fatigue life constant $\gamma' = 47.6\times10^{15}$ as provided in Table (7.4). The fatigue damage calculations due to a single repeated stress event (as illustrated in Fig. 7.21) are provided in Table (7.11).

Table (7.10): Rainflow counting cycles for a single repeated stress event

Peak/Valley number	Stress value σ_1 at initial point (MPa)	Stress value σ_2 at the end of the trajectory (MPa)	Half Cycle stress $\Delta\sigma_i = \sigma_1 - \sigma_2$ (MPa)
1	-6.78	49.77	-56.55
2	36.70	19.69	17.01
3	19.69	36.70	-17.01
4	42.07	-5.29	47.36
5	-5.29	42.07	-47.36
6	32.56	15.82	16.74
7	15.82	32.56	-16.74
8	45.99	-0.840	46.83
9	-0.840	45.99	-46.83
10	27.33	11.42	15.91
11	11.42	27.33	-15.91
12	49.32	1.780	47.54
13	1.780	49.32	-47.54
14	24.94	6.68	18.26
15	6.680	24.94	-18.26
16	49.77	-5.100	54.87
17	6.860	25.43	-18.57
18	25.43	6.860	18.57
19	1.550	48.73	-47.18
20	48.73	1.550	47.18
21	12.14	27.84	-15.70
22	27.84	12.14	15.70
23	-2.62	46.08	-48.70
24	46.08	-2.620	48.70
25	16.29	32.15	-15.86
26	32.15	16.29	15.86
27	-5.100	41.91	-47.01
28	41.91	-6.780	48.69
29	18.77	37.43	-18.66
30	37.43	18.77	18.66

Table (7.11): Fatigue damage estimation for one repeated stress block event

Half-cycle stress range $\lvert\Delta\sigma_i\rvert$ (MPa)	Number of cycles per stress event m_i	Fatigue resistance $N_i = \gamma'\left(\Delta\sigma_i\right)^{-5}$ (cycles)	Damage due to a single repeated stress event $\left(\frac{m_i}{N_i}\right)$
56.55	0.5	8.231×10^{7}	6.075×10^{-9}
17.01	1.0	3.343×10^{10}	2.992×10^{-11}
47.36	1.0	1.998×10^{8}	5.006×10^{-9}
16.74	1.0	3.621×10^{10}	2.762×10^{-11}
46.83	1.0	2.113×10^{8}	4.732×10^{-9}
15.91	1.0	4.669×10^{10}	2.142×10^{-11}
47.54	1.0	1.960×10^{8}	5.101×10^{-9}
18.26	1.0	2.345×10^{10}	4.265×10^{-11}
54.87	0.5	9.570×10^{7}	5.224×10^{-9}
18.57	1.0	2.155×10^{10}	4.639×10^{-11}
47.18	1.0	2.036×10^{8}	4.911×10^{-9}
15.70	1.0	4.990×10^{10}	2.004×10^{-11}
48.70	1.0	1.738×10^{8}	5.755×10^{-9}
15.86	1.0	4.743×10^{10}	2.108×10^{-11}
47.01	0.5	2.073×10^{8}	2.412×10^{-9}
48.69	0.5	1.739×10^{8}	2.874×10^{-9}
18.66	1.0	2.104×10^{10}	4.753×10^{-11}
Sum	-	$\sum_{i=1}^{k} N_i = 2.813\times10^{11}$	$\sum_{i=1}^{k}\left(m_i/N_i\right) = 4.235\times10^{-8}$

The total number of stress events β is evaluated from Equation (7.33) as:

$$\beta = 1\Big/\sum_{i=1}^{k}\left(m_i/N_i\right) = 2.36\times10^{7} \text{ events}$$

Therefore, the total number of stress block events β that can be safely applied to the cantilever beam is $\beta = 2.36\times10^{7}$ events prior the cantilever undergoing a fatigue failure. Given that the duration of a single event as determined in Figure (7.22a) is 1.14sec, this corresponds to a service life of 7,400 hours.

7.7 Conclusion

This chapter has provided a technique to generalize the solutions developed in Chapters 3-6 for problems with multiple harmonic loads with distinct exciting frequencies. A general expression for extracting the resulting stresses from the present formulation was proposed and assessed against shell finite element solutions. Established fatigue design procedures were reviewed and the present formulation was used in conjunction with fatigue design procedures to establish the fatigue life in practical design situations.

7.8 References

[7.1] Bhandari, V. B., (2010), Design of Machine Elements, third edition, Tata McGraw Hill Education Private Limited, New Delhi, India.

[7.2] Canadian Institute of Steel Construction, Handbook of Steel Construction, Tenth edition, Canada, (2010).

[7.3] Collins, J. A., (1993), Failure of Materials in Mechanical Design: Analysis, Prediction, Prevention, Second edition, John Wiley and Sons, Inc., Canada.

[7.4] Collins, J. A., Busby, H. R. and Staab, G. H., (2010), Mechanical Design of Machine Elements and Machines, second edition, John Wiley and Sons Inc., USA.

[7.5] Kulak, G. L. and Grondin, G. Y., (2010), Limit States Design in Structural Steel, Ninth edition, Canadian Institute of steel construction, Canada.

[7.6] Lee, Y. L., Pan, J., Hathaway, R., and Barkey, M. (2005), Fatigue Testing and Analysis: Theory and Practice, Elsevier Butterworth-Heinemann, USA.

[7.7] Liu, A. (2005), Mechanics and Mechanisms of Fracture: An Introduction, ASM International, USA.

[7.8] Milne, I., Ritchie, R.O. and Murakami, Y., (2003), Comprehensive Structural Integrity, Volume 4, cyclic loading and fatigue, Elsevier, Amsterdam.

[7.9] Nussbaumer, A., Borges, L. and Davaine, L. (2011), Fatigue Design of Steel and Composite Structures, ECCS - European Convention for Constructional Steelwork, Portugal.

[7.10] Rothbert, H. A. and Brown, T. H., (2006), Mechanical Design Handbook, Second edition, McGraw-Hill Companies, Inc., USA.

[7.11] Suresh, S., (1998), Fatigue of materials, second edition, Cambridge University Press, Cambridge, UK.

[7.12] Tawancy, H. M., Ul-Hamid, A. and Abbas, N. M., (2004), Practical Engineering Failure Analysis, Marcel Dekker, Inc., USA.

Appendix (7A): Preliminary Static Analysis and Design for Example 2

This appendix performs a preliminary analysis and design for Example 1 which omits inertia effects. A more thorough analysis which incorporates dynamic effects is given in Chapter 7.

7A.1 Cross-Section Classification Limits

The flange slenderness is calculated by

$$\frac{b}{2t_f} = \frac{133}{2(8.4)} = 7.92$$

The threshold for class 1 flanges is

$$\frac{145}{\sqrt{F_y}} = \frac{145}{\sqrt{350}} = 7.75$$

The threshold for class 2 flanges is

$$\frac{170}{\sqrt{F_y}} = 9.09$$

Since

$$\frac{145}{\sqrt{F_y}} < \frac{b}{2t_f} < \frac{170}{\sqrt{F_y}}$$

Flange class is 2.

The web slenderness is calculated by

$$\frac{h}{t_w} = \frac{190.2}{5.8} = 32.79$$

Threshold for class 2 web

$$\frac{1,700}{\sqrt{350}} = 90.87$$

Based on the above calculations, the web meets class 2 requirements and section class is 2.

7A.2 Check of Member Capacity

Although member is Class 2, the yield moment will be calculated as M_y :

$$M_y = S_x F_y = 249.0 \times 10^{-6} \times 350 \times 10^6 = 87.15 kN.m$$

The factored moment resistance is then given by:

$$M_r = \phi M_y = 78.44 kNm$$

where the resistance factor is taken as 0.9.

Omitting dynamic effects, the maximum bending moment can be calculated from Figure (7A.1) as:

$$M_{x_{\max}} = R_2 b = \frac{P_{y_1} ab + P_{y_2} b(\ell - b)}{\ell} = 10.6 MNm$$

The maximum moment in the beam is significantly lower than the yield moment. This margin of safety provides some room of dynamic amplification caused by the proximity of the exciting frequency to the natural frequency of the structure.

The corresponding maximum bending stress $\sigma_{zz\,\max}$ is:

$$\sigma_{zz\,\max} = \frac{M_{x_{\max}} y}{I_{xx}} = 40.95 MPa$$

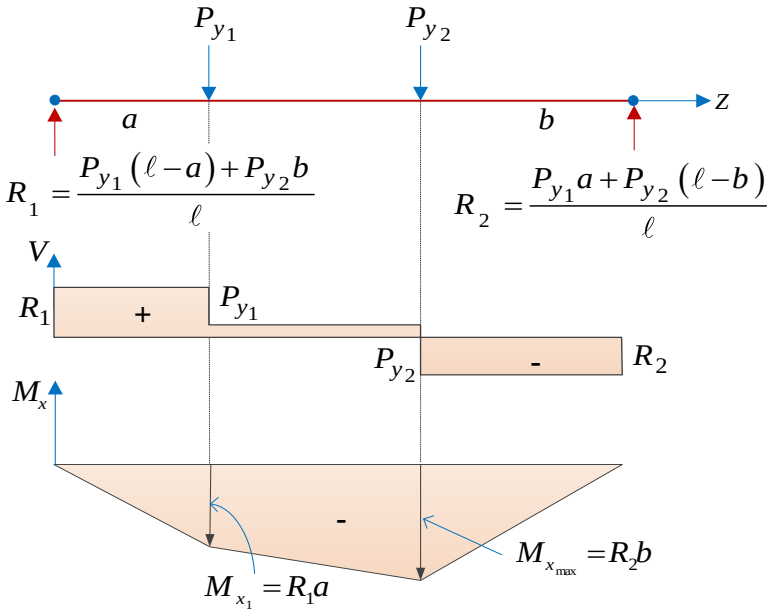

Figure (7A.1): Bending moment diagram for the simply supported beam

7A.3 Deflection Calculations

The vertical deflection $v(z)$ of the simply supported is given by:

$$v(z)=\frac{1}{EI_{xx}}\left[\left\{\frac{P_{y_1}(\ell-a)+P_{y_2}b}{\ell}\right\}\frac{z^3}{6}-\frac{P_{y_1}(z-a)^3}{6}+\left\{\frac{P_{y_1}}{6\ell}\left[(\ell-a)^3-\ell^2(\ell-a)\right]+\frac{P_{y_2}b}{6\ell}\left(b^2-\ell^2\right)\right\}z\right]\quad,\ for\ \ a\le z\le(\ell-b) \tag{7A.1}$$

The maximum deflection $v(z)$ can be evaluated when the slope is zero, i.e., $v'(z)=0$. Differentiating Equation (7A.1) with respect to z and then solving for z, the location of the maximum deflection is obtained as

$$z_m=-\frac{P_{y_1}a}{(R_1-P_{y_1})}+\frac{\sqrt{\left(2aP_{y_1}\right)^2-4\left(R_1-P_{y_1}\right)\left(2C_3-P_{y_1}a^2\right)}}{2\left(R_1-P_{y_1}\right)}=3.510m \tag{7A.2}$$

The maximum deflection $v_{\max}$ is then determined as

$$v_{\max}=v\big|_{z=z_m}=9.68mm$$

The corresponding span to deflection ratio is

$$\frac{\ell}{\Delta}=\frac{7000.0}{9.68}=723$$

The above ratio is high and suggests there is enough margin for dynamic amplification once inertia effects are incorporated into the analysis.

7A.4 Normal and Shear Stresses distribution

The expressions for the normal and shear stresses in terms of stresses resultants as derived in Section (7.2) are

$$\sigma_{zz}(z,s)=-\frac{M_x(z)}{I_{xx}}y(s)\quad\text{and}\quad\tau_{zs}(z,s,t)=\frac{V_y(z)}{D_{yy}}\sin\hat{\alpha}(s) \tag{7A.3}$$

The normal and shear stress distributions displayed in Figure (7A.2) are obtained at maximum bending moment and shear stress distributions illustrated in Figure (7A.1). In generating the stress distributions in Figure (7A.2), the maximum bending moment $M_{x\max}=10.64kNm$ and the maximum shear force $V_y=R_1=5.20kN$ were used. It is noted shear stresses are one order of magnitude less than the normal stresses. Therefore, focus in the dynamic analysis will be placed on normal stresses.

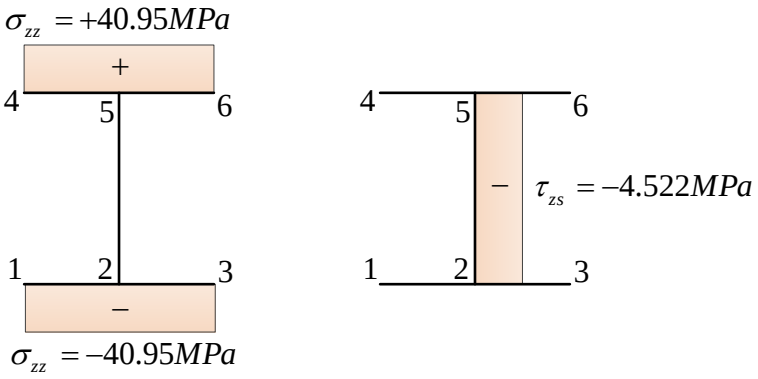

(a) Normal Stress (MPa) (b) Shear Stress (MPa)

Figure (7A.2): Normal and shear stresses distribution

Appendix (7B): Preliminary Static Analysis and Design for Example 3

In this appendix, the preliminary static analysis and design for example 2 which ignores the inertia force effects. A more detailed analysis of the cantilever beam under dynamic forces is investigated in Chapter 7.

7B.1 Determination of the Cross-section Class

In a similar manner to Example 1, the flange slenderness is evaluated as

$$\frac{b}{2t_f} = \frac{102}{2(8)} = 6.40$$

The threshold for class 1 flanges is

$$\frac{145}{\sqrt{F_y}} = \frac{145}{\sqrt{350}} = 7.80$$

The threshold for class 2 flanges is

$$\frac{170}{\sqrt{F_y}} = \frac{170}{\sqrt{350}} = 9.09$$

Since $\frac{145}{\sqrt{F_y}} < \frac{b}{2t_f} < \frac{170}{\sqrt{F_y}}$

The flange class is1.

The web slenderness is obtained by

$$\frac{h}{t_w} = \frac{190}{6.2} = 30.6$$

Threshold for class 2 web

$$\frac{1,700}{\sqrt{F_y}} = \frac{1,700}{\sqrt{350}} = 90.87$$

Based on the above calculation, the web meets class 2 requirements and the section class is 1.

7B.2 Weak-axis Bending Strength

Although the proposed cross-section is class 1, the design of the cantilever beam requires to be based on elastic response. The yield moment M_y about the weak-axis is obtained as:

$$M_y = S_y F_y = 27.8\times10^{-6}\times350 = 9.730\,kNm$$

The corresponding maximum weak-axis bending stress can be evaluated as:

$$\sigma_{zz} = \frac{M_y c}{I_{yy}} = \frac{9.730\times10^{3}\times51\times10^{-3}}{1.42\times10^{-6}} = 349.5MPa$$

The factored moment resistance M_{r_y} is then given by:

$$M_r = \phi M_y = 0.9\times9.730 = 8.757kNm$$

Ignoring the inertia forces, the maximum weak-axis bending moment can be evaluated from Figure (7B.1) as:

$$M_{y_{\max}} = P_{x_1} a + P_{x_2}\ell = 150\times1.5 + 200\times2.5 = 0.725kNm$$

It is noted that the maximum bending moment in the cantilever beam is significantly smaller than the yield bending moment. This margin of safety suggests enough space of dynamic amplification caused by inertia effects incorporated in the analysis.

The corresponding maximum bending stress $\sigma_{zz\,\max}$ is obtained as:

$$\sigma_{zz\,\max} = \frac{M_{y_{\max}} c}{I_{yy}} = \frac{0.725\times10^{3}\times51\times10^{-3}}{1.42\times10^{-6}} = 26.04MPa$$

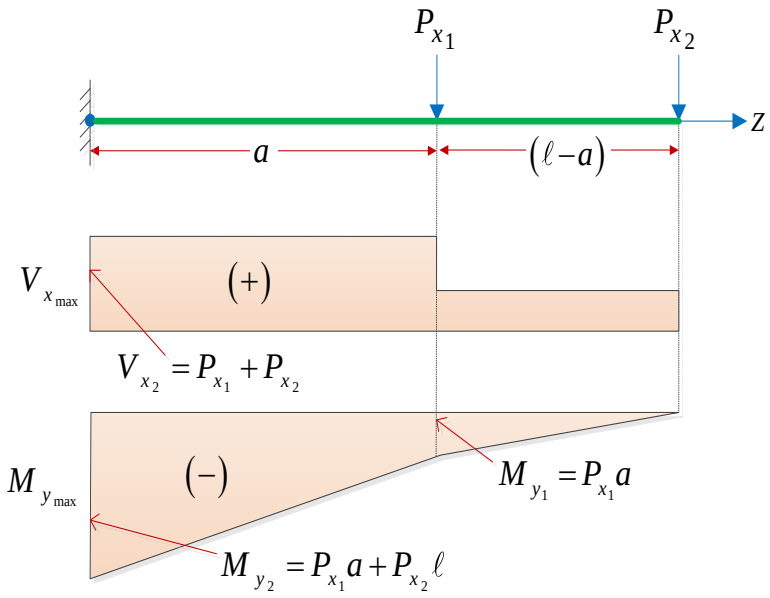

Figure (7B.1): Shear force and bending moment diagrams for the cantilever I-beam

7B.3 Lateral Deflection Limit

Using $\ell/200$ as the criterion limit, the maximum allowable lateral deflection of the cantilever under given static lateral forces is 12.5mm.

The maximum lateral deflection of the cantilever beam is obtained as:

$$u_{\max} = \frac{\ell^3}{48EI_{yy}}\left(5P_{x_1} + 16P_{x_2}\right) = \frac{2.5^3}{48\times 200\times 10^9 \times 1.42\times 10^{-6}}\left[5\times 150 + 16\times 200\right] = 4.527mm$$

The corresponding span to deflection ratio is

$$\frac{\ell}{u_{\max}} = \frac{2{,}500}{4.527} = 552$$

The above ratio is significantly high and provides there is enough margin of safety for dynamic amplification once inertia force effects are included into the analysis.

7B.4 Normal and Shear Stresses Distribution

Due to the given applied forces, the normal and shear stresses expressions in terms of stress resultants for doubly symmetric sections are presented by Equations (7.10) and (7.20) as:

$$\sigma_{zz}\left(z,s\right) = \frac{M_y\left(z\right)}{I_{yy}}x\left(s\right) \quad \text{, and}$$

$$\tau_{zs}\left(z,s\right) = \frac{V_y\left(z\right)}{D_{yy}}\cos\hat{\alpha}\left(s\right)$$

The maximum normal and shear stresses results, at the fixed end of the cantilever ($z=0$), obtained from the above stress expressions are provided in Table (7B.1) and illustrated in Figure (7B.1). Knowing that the maximum bending moment is $M_{y\max} = 0.725MPa$ and the maximum shear force is $V_{x\max} = 0.350kN$, and the angles $\hat{\alpha}\left(s\right) = 0^o, 90^o, 180^o$ for lower flange, web and upper flange, respectively. It is observed that the shear stresses are significantly lower than the normal stresses. Therefore, the shear stresses will be neglected in the fatigue life calculation.

Table (7B.1): Results of normal and shear stresses

Point number	Normal stress σ_{zz} (MPa)	Shear stress τ_{zs} (MPa)
1	-26.04	-0.2145
2	0.0	-0.2145
3	26.04	-0.2145
4	-26.04	+0.2145
5	0.0	+0.2145
6	26.04	+0.2145

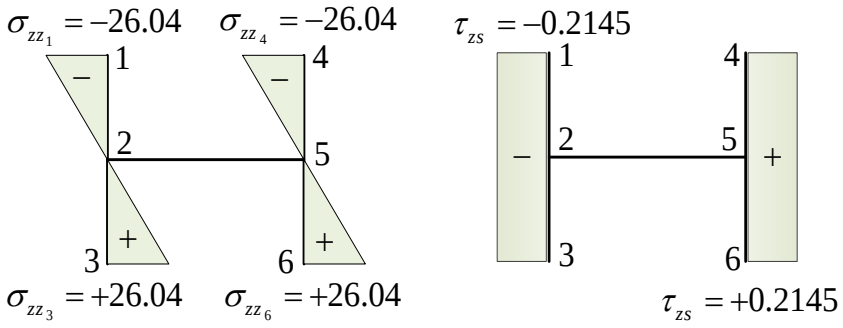

(a) Normal Stress (MPa) (b) Shear Stress (MPa)

Figure (7B.2): Normal and shear stresses distribution

List of Symbols

The following list of symbols is given:

A	Cross-sectional area
b	Flange width
C_w	Warping constant
d	Cross-section height
D_i	Partial damage ratio at i - th stress range level
D_{total}	Total fatigue damage
D_{xx} ,D_{yy} D_{xy} D_{hx} ,D_{hy} ,$D_{\omega\omega}$	Cross-section properties
E	Modulus of elasticity
$\Delta\sigma_i$	Fatigue stress range
$\Delta\sigma_{ti}$	Constant amplitude threshold stress range
G	Shear modulus
$h(s)$	Normal distance between the shear centre and the tangent to mid-surface
I_{xx} ,I_{yy}	Moment of inertias of the cross-section about the principal X and Y axes
J	Saint-Venant torsional constant
ℓ	Member span
$\bar{M}_j$	Concentrated moment about j-th direction (for $j = x, y, z$)
$\bar{M}_w$	Concentrated bimoment
$\bar{m}_j(z)$	Member moments about j-th direction (for $j = x, y, z$)
$\bar{m}_w(z)$	Member bimoment
$\bar{N}_z$	Concentrated end forces along longitudinal axis
N_i	Number of cycles to failure
n_i	Number of stress cycles at constant stress range
m_i	Number of stress cycles per stress event

β	Total number of stress events
$\bar{q}_j(z)$	Member forces along x, y, z directions (for $j = x, y, z$)
S_c	Shear centre of the cross-section
t	Time in seconds
$\bar{u}, \bar{v}$	Displacements of the shear centre along the principal X, Y axes
$\bar{V}_j(z)$	Shear forces along x, y axes (for $j = x, y$)
$\bar{w}$	Average longitudinal displacement along the Z axis
x, y, z	Cartesian coordinate system
X, Y, Z	Principal coordinate system
$x(s), y(s)$	Coordinates of a point on mid-surface of the section along X and Y axes
x_s, y_s	Coordinates of the shear centre along the principal directions
ρ	Density of the material
r_o	Polar radius of gyration
$\bar{\theta}_x, \bar{\theta}_y, \bar{\theta}_z$	Rotations angles around the X, Y, Z axes, respectively
$\hat{\alpha}(s)$	Angle between the tangent to the cross-section and the principal X axis
$\bar{\psi}(z)$	Warping deformation
Ω_i	Exciting frequency
$\omega(s)$	Warping function of the cross-section
$\Delta\sigma_i$	Stress range level
σ_{zz}	Normal stress
τ_{sv}	Shear stress due to Saint-Venant torsion
τ_{sz}	Total transverse shear stress
γ, γ'	Fatigue life constants

CHAPTER (8)

SUMMARY AND CONCLUSIONS

Chapter (8) - Summary and Conclusions

8.1 Summary

Starting with the variational form of the Hamiltonian functional, the governing differential equations of motion and the corresponding boundary conditions were formulated for thin-walled members of arbitrary open cross-sections under general harmonic forces (Chapter 3). The various aspects of the study are summarized in the following;

(1) The behaviour of thin-walled members subjected to various harmonic excitations was investigated. The general closed-form solutions and finite element formulations for the steady state dynamic analyses of thin-walled members with doubly symmetric, monosymmetric and asymmetric cross-sections were developed.

(2) The present formulations efficiently and accurately capture the shear deformation effects due to bending and non-uniform warping and translational and rotary inertia effects. Also the formulations incorporate the coupling flexural–torsional effects due to the non-symmetry of the cross-sections.

(3) The analytical closed-form solutions derived were successfully used to formulate a family of exact shape functions. These shape functions were derived based on the exact homogeneous solution of the governing coupled field equations and then used to formulate a series of super-convergent finite element for the cases of doubly symmetric, mono-symmetric, and asymmetric cross-sections. The resulting elements have two nodes and seven degrees of freedom per node.

(4) The finite element formulation was successfully in capturing the coupled bending-torsional dynamic response of thin-walled members under a variety of harmonic forces and boundary conditions.

(5) Several programs were coded under FORTRAN and MAPLE platforms in order to implement the formulations developed in this study, for the following analyses:

(a) The static and steady state dynamic analyses for thin-walled members of doubly symmetric cross-sections under harmonic forces based on the formulations in Chapter 4.

(b) The coupled bending-torsional static and steady state responses for monosymmetric thin-walled members based on the finite element formulations developed in Chapter 5.

(c) The static and steady state dynamic responses were implemented for thin-walled members of asymmetric cross-sections which coupled flexural-lateral-torsional-warping response formulations derived in Chapter 6.

(d) Closed form solutions of non-shear deformable thin-walled members (classical Vlasov and Euler-Bernoulli beam theories) for doubly symmetric, monosymmetric and asymmetric cross sections (for comparison to those based on the present theory).

(6) Generalized expressions for predicting normal and shear stresses based on the theories developed in this study were formulated and used for predicting the fatigue life of thin-walled members under multiple harmonic forces with distinct frequencies.

8.2 Conclusions

From the various examples conducted throughout the thesis, the following remarks can be made:

(1) The present analytical closed-form and finite element formulations are capable to efficiently capture the static and steady state responses of thin-walled beams under harmonic forces. Furthermore, they are able to extract the eigen-frequencies and eigen-modes of the system from the steady state response analyses.

(2) Shear deformation effects are important when predicting the response for short span cantilevers under higher exciting frequencies.

(3) With only a few degrees of freedom, the solutions developed in the present study reliably predict the response of thin walled members under harmonic forces when compared to (a) Abaqus shell element model with thousands of degrees o freedom and (b) Abaqus beam element model with hundreds of B31OS beam elements.

(4) The finite element formulations based on this study achieve computational efficiency on two fronts: (a) on the use of exact shape functions keeps the number of degrees of freedom to a minimum, and (b) the elimination of time discretization eliminates the need to conduct incremental analysis.

Further, the procedure attains the steady state response of the structure without the need to extract eigenmodes as in other methods based on mode superposition.

(5) Comparisons with Abaqus shell element solutions demonstrate that distortional effects captured by the shell element model, but not in the present study, were more pronounced in cantilevers with shorter spans.

(6) The formulation isolates the steady state response, a desirable feature when conducting fatigue analysis (since the transient response occurs rarely throughout the life time of the structure and thus plays no role in the fatigue life of the structure). Thus the present formulation is recommended for fatigue life computations.

8.3 Proposed Future Developments

(1) The proposed generalized Vlasov-Timoshenko beam theory can be modified to capture the distortional effects of the cross-sections.

(2) Possible extension of the analysis to include the effect of adding static forces, bending and twisting moments on the steady state response of thin-walled members under harmonic forces.

(3) The methodology developed can be extended to capture the static and dynamic analyses of composite thin-walled open members under harmonic loads.

(4) The proposed formulations can be extended to capture the static and steady state responses of thin-walled curved members.